Distribution, Mineralogy And Provenance Of Heavy Minerals In Cainozoic Sediments Of The Namaqua Mines Area, West Coast Of South Africa

by

Carlo Philander

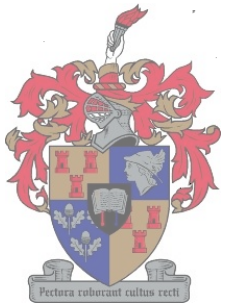

Thesis presented in partial fulfilment
of the requirements for the degree of
Master of Science
in the Department of Geology
University of Stellenbosch

December 1999

Study leader: Prof. A. Rozendaal

Stellenbosch
December 1999

DECLARATION

I, the undersigned, hereby declare that the work contained in this thesis is my own original work and has not previously in its entirety or in part been submitted at any university for a degree. Where use was made of the work of others, it has been duly acknowledged in the text.

24/11/1999

C. Philander Date

ABSTRACT

In view of the recent developments in heavy mineral exploration, a sampling programme was initiated to determine the economic potential of heavy mineral occurrences in the Kleinzee mining area. The primary objectives were to record the concentration and mineralogy of the heavy mineral population and also to determine their provenance.

The heavy mineral occurrences are hosted by high maturity Miocene fluvial sediments and unconsolidated Plio-Pleistocene marine sediments overlying basement rocks of the Mid-Proterozoic Namaqua Metamorphic Complex and Pan-African Gariep Supergroup. The development of the fluvial palaeochannels is linked to a major regression during the Late Oligocene whereas the marine deposits are genetically related to wave-cut, raised marine terraces between 0 and 90m *amsl*

Quartz, followed by feldspar are the dominant light minerals. The total heavy fraction (>2.9 g/cm^3 density) averages 6.4%, but concentrations are extremely variable and ranges from a few per cent in the fluvial sediments to as much as 60 per cent in particular marine successions. The mechanism anticipated for these anomalous accumulations is believed to be a powerful wave-regime with favourable burial conditions considered essential in preserving the mineralisation.

Heavy mineral suites are diverse and consist of various proportions of ilmenite and its related alteration products, hematite, magnetite, rutile, zircon, garnet, amphibole, pyroxene, epidote, aluminosilicates, titanite, monazite, staurolite, collophane and glauconite. The economically valuable minerals, ilmenite, rutile and zircon constitute a very large portion of the total heavy mineral suite, often an order of magnitude greater than the gangue. Generally the total heavy mineral suite in the Kleinzee area is dominated by ilmenite (50-73 wt%), with zircon (6-12 wt%) and rutile (1%) constituting the remainder of the economic fraction.

The titanium-bearing minerals comprise in addition to pure ilmenite, a complex suite of Fe-Ti oxides often intimately intergrown. Single grain analyses indicate that ilmenites contain on average 51% TiO_2 with only trace amounts of impurities. Only a small proportion (~8%) of the ilmenite fraction is altered and in most cases alteration was insufficient to enhance the titanium content of the ilmenite fraction. These results are remarkably consistent with previous studies conducted at other west coast localities, which indicates that climatic

conditions during the Plio-Pleistocene were uniform along the entire west coast of South Africa.

Zircon populations were found to be heterogeneous, displaying contrasting physical, geochemical, cathodoluminescent and radiometric properties. It is demonstrated that the heterogeneity of various zircon populations reflects the compositional maturity of their host sediments. As a result, zircon properties will allow conclusions about the evolutionary path of its host sediment. Similarly, zircon chemistry and radiometry can be useful to fingerprint and discriminate stratigraphic successions.

Heavy mineral suites are qualitatively similar, indicating a uniform source area for the Kleinzee sediments. Heavy mineral assemblages indicate contributions from igneous and metamorphic as well as reworked sedimentary sources. Garnet, epidote, augite, hornblende, staurolite, titanite, rutile and aluminosilicates were demonstrated to be ultimately derived from metamorphic rocks. Other minerals such as the iron-titanium oxides, monazite and zircon were derived from igneous or metamorphic rocks. The striking similarity of mineral chemistry from Kleinzee sediments and lithologies from the NMC, unambiguously indicate the NMC as primary source terrain for the Kleinzee sediments. Mineralogical and textural evidence suggests that the majority of heavy minerals were eroded and transported from a nearby area, indicating a relative proximal source for the heavy minerals as well as their host sediments.

The present appraisal of the economic importance of heavy mineral occurrences in the study area indicates that it does not compare favourably with Quaternary megadeposits such as Richards Bay Minerals or Graauwduinen. The economic viability of the area is greatly impaired by the generally low heavy mineral content as well as the composition of the economic fraction which is dominated by less valuable ilmenite. Bulk chemistry as well as single grain analysis also indicate that the TiO_2 content is low (<50%). However, a few target areas have been delineated which indicate limited economic potential and deserves a follow-up study in order to calculate their potential resources.

OPSOMMING

In die lig van die huidige ontwikkeling in swaarmineraal eksplorasie is 'n monsteringsprogram geloods om die ekonomiese potensiaal van die swaarmineraal voorkomste in die Kleinzee mynbougebied te evalueer. Die primêre doelwitte was om die konsentrasie, mineralogie en provenans van die swaarmineraal populasie te bepaal.

Swaarmineraal konsentrasies in die studiegebied kom voor in volwasse Mioseen fluviale sedimente en ongekonsolideerde Plio-Pleistoseen mariene sedimente wat vloergesteentes oorlê van die Mid-Proterosoïese Namakwa Metamorfe Kompleks en Pan-Afrikaanse Gariep Supergroep. Die ontwikkeling van prominente fluviale palaeokanale word verbind met 'n massiewe regressie tydens die Laat Oligoseen, terwyl die mariene sedimente geneties verwant is aan brandergekerfde, verhewe mariene terrasse wat geleë is tussen 0 en 90m bo gemiddelde seevlak.

Kwarts, gevolg deur veldspaat is die dominante ligte minerale. Die totale swaarmineraal-fraksie (digtheid >2.9 g/cm^3) beloop gemiddeld 6.4%, maar konsentrasies is hoogs wisselend en is selde meer as 'n paar persent in die fluviale sedimente, maar kan so hoog as 60% wees in sekere mariene opeenvolgings. Anomale konsentrasies van swaarminerale was die gevolg van 'n kragtige golfregime en gunstige begrawings kondisies wat mineralisasie gepreserveer het.

Swaarmineraal suites verskil in 'n hoë mate deurdat dit bestaan uit verskillende proporsies van ilmeniet en geassosieërde veranderingsprodukte, hematiet, magnetiet, rutiel, sirkoon, granaat, amfibool, pirokseen, epidoot, aluminiumsilikate, titaniet, monasiet, stauroliet, kollofaan en glaukoniet. Die ekonomies waardevolle minerale nl. ilmeniet, sirkoon en rutiel vorm 'n groot gedeelte van die totale swaarmineraal suite en in sommige gevalle in rangordes groter as die nie-ekonomiese fraksie. Die totale swaarmineraal suite van die Kleinzee area word oor die algemeen gedomineer deur ilmeniet (5-73%) met sirkoon (6-12%) en rutiel (1%) wat die res van die ekonomiese fraksie opmaak.

Die titaan-bevattende minerale sluit in suiwer ilmeniet asook 'n komplekse suite van tussen vergroeide -en veranderde Fe-Ti oksiedes. Enkelkorrel analises dui aan dat die ilmeniete gemiddeld 51% TiO_2 en spoorhoeveelhede van onsuiwerhede bevat. Slegs 'n baie klein gedeelte (~8%) van die ilmeniet fraksie is veranderd en in die meeste gevalle was

verandering onvoldoende om die titaan-inhoud van die ilmeniet fraksie te verhoog. Hierdie resultate is merkwaardig in ooreenstemming met vorige studies wat uitgevoer was by ander weskus lokaliteite en dui daarop dat klimatiese toestande tydens die Cenosoïkum konstant was langs die hele weskus van Suid-Afrika.

Sirkoonpopulasies is heterogeen met betrekking tot fisiese, geochemiese, katodeluminisente en radiometriese eienskappe. Daar is gedemonstreer dat die heterogeniteit van die verskeie sirkoonpopulasies die samestellings rypheid van hulle gasheer sedimente reflekteer. Sirkoon eienskappe sal dit dus moontlik maak om afleidings te maak omtrent die evolusie van die gasheer sedimente. Soortgelyk kan sirkoon chemie -en radiometrie ook van waarde wees om stratigrafiese opeenvolgings te korreleer.

Swaarmineraal suites is kwalitatief dieselfde en dui dus op 'n uniforme brongebied vir die Kleinzee sedimente. Swaarmineraal versamelings dui aan dat die swaarminerale afkomstig is van stollings -en metamorfe gesteentes sowel as herwerkte sedimente. Daar is getoon dat granaat, epidoot, ougiet, horingblende, stauroliet, titaniet, rutiel en aluminiumsilikate primêr afkomstig is van metamorfe gesteentes. Die yster-titaanoksiedes, monasiet en sirkoon kon egter van stollings of metamorfe rotse kom. Mineraalchemie van Kleinzee sedimente en rotse van die Namakwa Metamorfe Kompleks (NMK) stem merkwaardig ooreenkom, wat onteenseglik daarop dui dat die NMK die primêre brongebied vir die Kleinzee sedimente was. Mineralogiese en teksturele bewyse suggereer dat die oorgrote meerderheid van die swaarminerale ge-erodeer en vervoer was van 'n nabye gebied, wat moontlik aandui dat die swaarminerale sowel as hul gasheer sedimente afkomstig is van 'n relatiewe proksimale bron.

Die huidige ekonomiese evaluering van swaamineraal konsentrasies in die studiegebied toon dat dit nie gunstelik vergelyk met Kwarternêre mega-afsettings soos Richard Bay Minerals of Graauwduinen nie. Die ekonomiese vatbaarheid van die area word grotendeels aan bande gelê deur die baie lae swaarmineraal konsentrasie asook die samestelling van die ekonomiese fraksie wat gedomineer word deur minder waardevolle ilmeniet. Verder dui grootmaat-chemie sowel as enkelkorrel analises daarop dat die TiO_2 inhoud (50%) van ilmeniet laag is. Nietemin is verskeie teiken-areas afgepen wat beperkte ekonomiese potentiaal aantoon.

ACKNOWLEDGEMENTS

I am deeply grateful to The Creator for whom nothing is impossible and who turns dreams into reality.

My sincere appreciation goes to the De Beers mining company, who financed this project. Special thanks to the Kleinzee Geology staff who provided accommodation and technical support.

Additional funding were granted by the FRD, University of Stellenbosch, Kagiso and the Harry Crossley Trust.

Christa deserves special mentioning for her continuous support and unconditional love.

I am extremely grateful for close family and friends who kept my spirit high during this study.

Prof. A. Rozendaal, my supervisor, is acknowledged for his continuous encouragement and constructive criticism.

Prof. J.P. Le Roux, J. Pether, L.M. Cilliers and G. Nicholas are thanked for numerous discussions.

The assistance of the technical staff of the Geology Department of Stellenbosch is gratefully acknowledged.

I am indebted to a large number of individuals and institutions who provided high quality analytical data.

TABLE OF CONTENTS

CHAPTER 1

INTRODUCTION

1.1. Location

This thesis presents the first quantitative data on the heavy mineral concentrations that occur in Pliocene to Pleistocene marine and non-marine sediments in the Koingnaas, Kleinzee and inland mining areas owned by De Beers Consolidated Ltd., known as Namaqua-Mines. The small town of Kleinzee is situated on the west coast of South Africa, approximately 102km northwest of Springbok (Fig. 1.1). Koingnaas, a smaller settlement, lies approximately 60 km to the south of Kleinzee. The three mining areas are referred to as the Buffels Marine Complex (BMC), Koingnaas Complex (KNC) and Buffels Inland Complex (BIC), simply after their geographical setting. The BMC include the coastal farms Annex Kleinzee, Dreyers Pan, Kareedoornvlei, Tweepad and Oubeep and extends for almost 45 km in a northerly direction (Fig. 1.2). The KNC consists of the mining areas Somnaas, Koingnaas, Swartlintjies River and Langklip, stretching nearly 80 km to the south of Koingnaas. The Hondeklip Bay mine, owned by Transhex Pty (Ltd.), which is situated between the Langklip and the Swartlintjies River mining area, interrupts it. The Nuttabooi and Langhoogte mining areas, which are, part of the BIC and is situated 31km east of Kleinzee. The ephemeral Buffels River debauches just north of Kleinzee and the smaller Swartlintjies River has its mouth approximately 35km south of Koingnaas.

1.2 Previous work

The discovery of diamonds at the beginning of the century drew considerable interest to the west coast of South Africa, in particular to the Namaqualand area. Since then, mining along that stretch of the coast has been dominated by the successful exploitation of onshore and offshore diamond deposits. During the last two decades however, emphasis has shifted from exclusively diamond mining and exploration to include heavy mineral exploration.

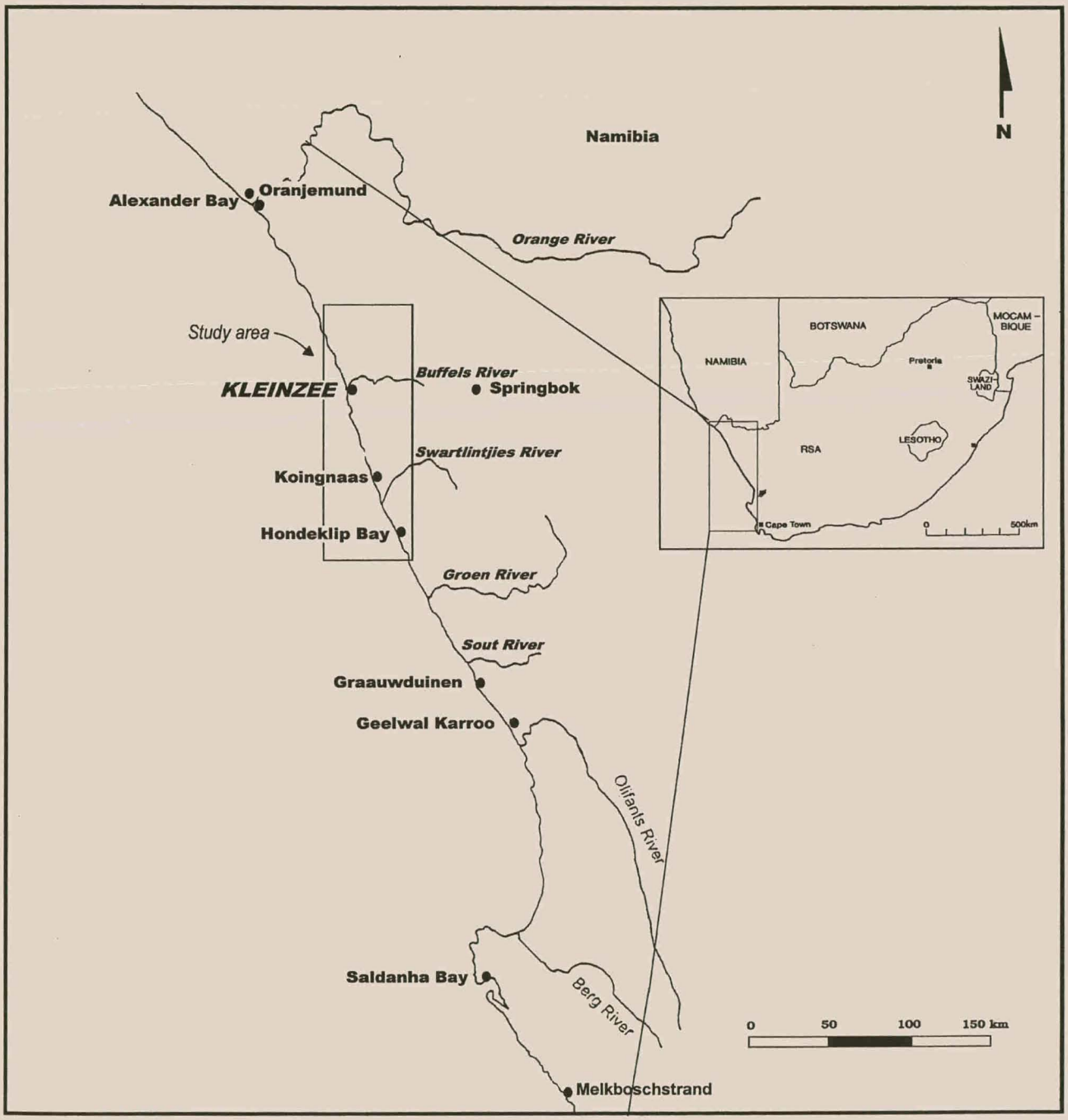

Figure 1.1. Locality map of the study area.

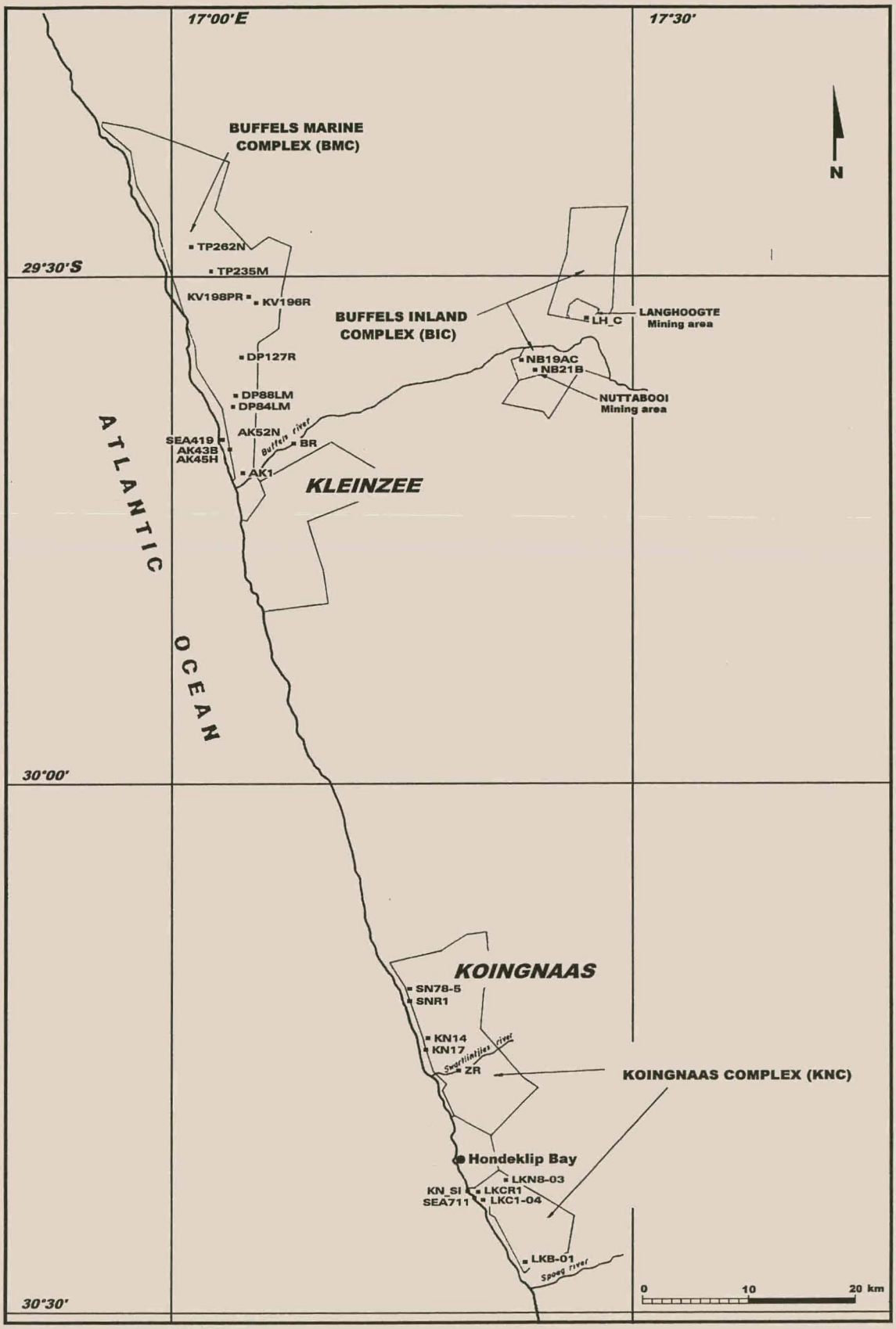

Figure 1.2. Detailed map of the study area showing the locality of sample sites. Site names conform to mining blocks.

Heavy mineral occurrences have been known since the discovery of diamonds and Toerien and Groeneveld (1957) carried out the first comprehensive study. These workers reported on the mineralogy and economic potential of the deposit situated between the Sout River and Strandfontein. In follow-up studies, Herzberg (1969, 1970) described sampling and prospecting results of a radiometric survey performed by the Geological Survey in the area between the Olifants River and Hondeklip Bay.

Renewed interest in heavy mineral sands during the 1980's consequently led to exploration programs, which located several significant concentrations along the Namaqualand coast. One of these, known as the Graauwduinen deposit, resulted in the establishment of Namakwa Sands Ltd., which currently is a significant producer of high quality zircon, ilmenite and rutile by world standards. Total resources for the deposit are quoted at 500Mt with a grade of 10% total heavy minerals (THM) and the production rate is a nominal 10Mt per annum (Palmer, 1994).

Cilliers (1995) and Macdonald (1996) have documented the results of systematic research on heavy minerals along the west coast. Cilliers (1995) studied the Graauwduinen heavy mineral deposit that occurs in a set of raised beach terraces. He focused on the genesis, mineralogy and provenance characteristics of the deposit. Macdonald (1996) provided a detailed description of the mineralogy and mineral chemistry of the Geelwal Karoo heavy mineral deposit, 20 km south of Graauwduinen. He characterised the Geelwal present-day placer and proposed a similar depositional environment for the Graauwduinen deposit. Using a unique approach, Macdonald *et al.* (1997) and De Meijer *et al.* (1997) applied radiometry to fingerprint heavy mineral sands from various west coast localities. A series of integrated studies on west coast heavy minerals (Macdonald and Rozendaal, 1995; Rozendaal *et al.*, 1995; Philander *et al.*, 1998; Rozendaal, 1998; Rozendaal *et al.*, 1999), furnished invaluable information on their complex petrography and chemistry.

1.3. Aims and objectives

The aims of this study are to:

- record the distribution of heavy mineral concentration with respect to their depositional environment and sediment type
- determine the degree of concentration and the mineralogy of the heavy mineral population for economic reasons
- deduce the provenance of the heavy mineral population from mineral petrography and mineral chemistry

The objectives are:

- Collecting representative heavy mineral suites from a variety of sedimentary units at different elevations (terraces).
- A petrographic study of samples to determine the type and percentage of heavy minerals present.
- Establishing the proportional and spatial distribution of the various heavy mineral species vertically among units and laterally over the study area.
- To delineate areas of probable economic heavy mineral concentration.
- Implementation of analytical and statistical techniques to identify representative and distinctive heavy mineral populations and assemblages within a sedimentary facies.
- Discrimination and correlation of sedimentary facies by means of these typical mineral assemblages and ratios.
- Application of these data to postulate provenance/source models for the heavy mineral population.

CHAPTER 2
METHODOLOGY

2.1. Sampling

2.1.1. Sample locality

The sample strategy was designed to establish a general picture of the heavy mineral distribution in the study area. In order to obtain a representative sample group, it was decided to sample sediments from:

- wave-cut terraces in the Buffels Marine Complex (BMC)
- marine packages in the Koingnaas Complex (KNC)
- fluvial lithologies in the Buffels Inland Complex (BIC)
- fluvial lithologies from palaeochannels located in the KNC.

Emphasis was placed on sites that showed visible heavy mineral concentration. Within the above constraints, excavated mining blocks provided an excellent opportunity for both sampling and window mapping. Sample sites were consequently named after the corresponding mining block. Samples were taken from each lithological unit and sample names coincide with the unit designation, for example sample AK1_1 was sampled from unit AK1_1 at sample site AK1. The approximate positions of the sample sites are shown in Fig. 1.2.

Additional samples were taken from the present-day beaches as well as the Buffels and Swartlintjies Rivers. Non-geological samples were gathered from heaped tailings at the three mining areas. In total 111 samples were taken: 35 from the BMC, 32 from the KNC, 14 from the BIC, 10 from the palaeochannels, 2 from present-day beaches, 2 from rivers and 16 from the mine heaps and slimes dams. Sample sites, their XYZ co-ordinates, sample names and types are listed in Appendix A.

2.1.2. Sampling method

Samples were collected using a garden trowel to make a clean vertical cut in the exposure. A bucket with a plastic bag inside was put in the recess and the sediment was collapsed in the bag moving the trowel from the top to the bottom of the unit. Where compacted sediments were encountered a hammer and chisel was utilised in a similar manner. A different approach was followed to obtain samples from the rivers, present-day beaches and tailings dumps. In this case, a hole was dug and an *in situ* sample taken approximately one meter below the surface.

2.2. Analytical techniques

A series of laboratory techniques were employed to investigate the chemical and physical characteristics of the sediments and their associated heavy minerals. Details of selective techniques are given in Appendix B.

The gravel (>4 mm) component was removed from the raw sample and retained for classification. A rotary splitter was used to split the <4 mm fraction into three parts, of which one portion was stored as a reference. A second portion was pre-treated as explained in Appendix B, before it was subjected to sieve-analysis. The <63μm fraction of palaeochannel samples obtained from sieving was separated into a silt and clay fraction. XRD analysis was performed on both fractions for mineralogical identification. The third portion of the initial split was separated using bromoform as a heavy medium. The light minerals were discarded and the heavy fraction weighed to determine the total heavy mineral content. The heavy fraction was subsequently split into three using a riffle mini-splitter. One split was stored whereas a polished section was made from the second split. The thin sections were studied to identify, describe and point-count the heavy minerals. These sections were also used for SEM-EDS, cathodoluminescence and electron microprobe investigations. A series of separation techniques, which include dense media separation, panning and electromagnetic separation, were employed to obtain monomineralic fractions of garnet and zircon from selective samples. Garnet and zircon fractions were subjected to REE analysis whereas the zircon fractions were radiometrically analysed.

2.2.1. *Polarised light microscopy*

A Leitz polarising microscope was used to identify and describe the heavy minerals from polished thin sections. Non-opaque minerals were observed in transmitted light whilst opaque minerals were studied in reflected light using both air and oil immersion lenses.

2.2.2. *Point-counting*

Point-counting 400-600 grains using the polarised microscope determined heavy mineral compositions of samples. By counting 400-600 grains, the probable error for a mineral that constitutes 10% of the sample is within the limit of ±1%; the probable error however becomes significant for minerals that constitute less than 1%. To minimise the counting error and the risk of missing smaller grains, point-counting was performed using a modified ribbon method as suggested by Carver (1971). Non-opaques and opaques were counted together using oil immersion lenses; transmitted light was used for the non-opaques and reflected light for the opaques.

2.2.3. *Scanning electron microscopy (SEM)*

Selected carbon-coated grains were examined by a SEM coupled to an energy dispersive X-ray analyser (EDS) to semi-quantify geochemistry and verify optical observations. The SEM also provided a means of studying textural relationships among minerals and within single grains. Backscattered electron (BSE) images made it possible to locate chemical zones within grains that would otherwise display a homogeneous optical character. BSE images reveal contrasts in average atomic number (Z) of a phase: the higher the number, the more electrons an area will "reflect" and the brighter it will appear. SEM-EDS studies were carried out at the University of Cape Town Electron Microscope Unit on a Leica Stereoscan S440. Operating conditions and detection limits of the apparatus are given in Appendix C.

2.2.4. *Cathodoluminescence (CL)*

CL images were acquired using an Oxfords Instruments MonoCL system attached to the Leica Stereoscan S440 SEM.

2.2.5. *X-ray diffraction analysis*

XRD analysis was used to identify and semi-quantify the mineral components of the matrix of the palaeochannel sediments. The samples were run on a Philips 1030/00 system that is managed by Diffraction Technology® software. Phase identification was accomplished using Trace® software in conjunction with the JCPDS-ICDD database (Joint Committee of Powder Diffraction International Committee on Diffraction Data). Quantification of the different phases was calculated using Siroquant® software. Operating conditions and detection limits are given in Appendix C.

2.2.6. *X-ray fluorescence (XRF) analysis*

Major and trace elements in ilmenite fractions were analysed by X-ray fluorescence with a Philips 1130/00 diffractometer. To avoid contamination by tungsten carbide, all samples were ground with silica grinding equipment. Major elements were determined on fused glass and trace elements from pressed powder pellets following the method of Norrish and Hutton (1969). Operating conditions are given in Appendix C.

2.2.7. *Microprobe analysis*

Quantitative chemical analysis of the heavy minerals was performed using two electron microprobes: a Cameca Camebax Electron Probe Microanalyser at the University of Cape Town and a JEOL Superprobe 733 at the Council for Geoscience. Standard operating conditions, standards used and detection limits are given in Appendix C. Raw count data was converted to oxide weight percentages. Generally, two points per grain were analysed and the average thereof calculated to reduce the effects of chemical variability.

2.2.8. *Radiometric analysis*

Selected zircon and ilmenite fractions were forwarded to the Kernfysisch Versneller Instituut at the Rÿksuniversiteit, Groningen, Netherlands for radiometric analysis. The radiometric technique is fully discussed by De Meijer *et al.* (1990) and De Meijer *et*

al. (1994) and only a brief description of the method is given below. The system utilises a high sensitivity gamma-ray detector using a bismuth germinate scintillator crystal (Macdonald *et al.*, 1996; Macdonald, 1996). In this method of analysis ^{40}K and gamma-ray emitting nuclei in the ^{238}U and ^{232}Th decay series are of relevance. In a closed radiogenic system, such as in zircon, the activity concentration of one member reveals information on the presence of the rest of the members in the specific decay series (Greenfield *et al.*, 1989; De Meijer *et al.*, 1990; De Meijer *et al.*, 1994). For instance ^{214}Bi and ^{214}Po, yield information on ^{238}U in the ^{238}U decay series (Macdonald *et al.*, 1996; Macdonald, 1996). Therefore, the activity concentrations in the ^{238}U decay series are expressed as ^{214}Bi. From the equation $N=t_{½}A/\ln 2$ where N is the number of atoms present, $t_{½}$ the half-life of the radionucleus, the activity A in $Bq.kg^{-1}$ can be calculated.

2.2.9. Inductively coupled plasma atomic emission spectroscopy (ICP-AES)

Zircon and garnet fractions were analysed for their rare earth element content by means of ICP-AES at the Physics Department, University of Stellenbosch. Operating conditions are given in Appendix C. Inductively coupled plasma atomic emission spectroscopy (ICP-AES) is an analytical method used for the determination of all elements except argon (Barnes, 1981). Pre-selected elements are selectively leached from the sample where its atoms are plamasised in the ICP apparatus to an unstable ionised state. When the atoms return to their semi-stable state, it is accompanied by a loss of energy through emission of radiation. Each element has a characteristic emission spectrum making it possible to distinguish between specific elements.

CHAPTER 3
GEOLOGICAL SETTING

3.1. Regional geology

The west coast of southern Africa between Saldanha Bay and Oranjemund is rocky and generally straight with only a few local embayments and prominent headlands. It is backed by the "Great Escarpment", a topographical feature that runs for 100km parallel to the coast and a 3-6 km wide coastal plain that rises gently to a maximum height of 100m (Heydorn and Tinley, 1980). The arid Namaqualand coastal plain is drained by numerous rivers, which are not all major contributors of sediment to the continental margin. The seasonal Orange River is the largest river along the west coast and is classified together with the Berg and Olifants River as major rivers. The Orange River and the Krom River, a tributary of the Olifants River, are the only to cross the escarpment. Minor rivers include the perennial Sout, Groen, Spoeg, Swartlintjies, Buffels and Holgat Rivers (Fig. 1.1).

The regional geology of the Namaqualand coast consists of Cainozoic to Recent deposits superimposed on Precambrian and Palaeozoic rocks (De Villiers and Söhnge, 1959; Hallam, 1964; Kensley and Pether, 1986; Woodborne, 1991; Pether, 1994). The latter include diverse lithologies from the Mid-Proterozoic Namaqua Metamorphic Complex, Late Proterozoic Gariep Group and Palaeozoic Cape Supergroup. Early Miocene, clay-filled fluvial channels, occur along the west coast and are locally associated with high concentrations of diamonds (Carrington and Kensley, 1969; Siesser and Dingle, 1981; Rogers *et al.*, 1990). Pleistocene to Pliocene diamondiferous marine deposits overlie the coastal channels and occur as a number of wave-cut, raised marine terraces consisting of basal gravels, overlain by a sequence of marine and aeolian sands (Dingle *et al.*, 1983; Pether, 1994; Corbett, 1996).

Southwards from the Orange River to Port Nolloth the coastal rocks belong to the metasedimentary sequence of the Gariep Supergroup (Rogers, 1977; De Decker, 1986; 1987; Woodborne 1986, 1991; Rogers *et al.*, 1990). The coast between Port Nolloth and Kleinzee comprises mainly rocks of the Lower Stinkfontein Formation of the Gariep Complex (Joubert and Kröner, 1971) intercalated with gneiss, schist and quartzites, localised amphibolite bands and occasional pegmatite veins pertaining to the Namaqua Metamorphic Complex (Coward, 1981; Saggerson and Turner, 1995).

South of Kleinzee to the Brak River granitic gneiss, schist and quartzite of the Namaqua Metamorphic Complex are prevalent (Coward 1981; Jack 1980; Pether, 1994). The Malmesbury Group, comprising limestone, phyllites and quartzites occurs as fringes between the Brak River and the Olifants River. At Geelwal Karoo the basement rocks are dominated by limestone, dolomite and phyllite of the Neoproterozoic Vanrhynsdorp Group (Germs and Gresse, 1991; Gresse 1992; Macdonald and Rozendaal, 1995; Macdonald, 1996). Occasionally, gneissic outcrops of the Namaqua Metamorphic Complex are observed. Table Mountain Group sediments comprising quartzite, shale and tillite, has its northernmost boundary with the Gariep Complex metamorphites at Graauwduinen (Cilliers, 1995) and stretches southwards to Elands Bay. Basement rocks of Namaqualand exhibit multiphase deformation and intrusional events. The intrusion of dolerite dykes and sills are the youngest evidence of this event (Siesser and Dingle, 1981; Tankard *et al.*, 1982).

Neogene deposits occur northwards from Kleinzee to Oranjemund on a series of raised wave-cut terraces at various elevations, but from Koingnaas southwards, the *en echelon* arrangement of marine terraces is less noticeable due to a more rugged bedrock relief. Progressive downwarping around a hinge line between the Olifants River mouth and Cape Agulhas has lowered the palaeostrandlines in the south (Tankard, 1976). The marine deposits commonly consist of basal marine gravels, overlain by a sequence of marine sands associated with abundant shells. Specific shells often characterise a unique marine sequence with faunal assemblages facilitating correlations of the west coast Neogene deposits (Krige, 1927; Haughton

1928; Carrington and Kensley, 1969; Hendey, 1976, 1981, 1982; Pether, 1983, 1986, 1994; Kensley and Pether, 1986; Gresse, 1988). Pleistocene aeolianites and Holocene sheetwash and alluvium cover marine sands.

Although lithologically very similar, the current terminology for the marine sediments along the west coast of South Africa is confusing and no general nomenclature has been accepted to date. A discussion on the Namaqualand coastal deposits highlights the differences in the present terminology. In the Langebaan-Saldanha area, the upper part of the Elandsfontyn Formation (Fig. 3.1.) contains a suite of intercalated fluviatile clays and peat that are dated as Mid-Miocene by Coetzee and Rogers (1982). The quartzose phosphorite of the locally developed Saldanha Formation was deposited during the Mid-to Late Miocene and remnants of contemporary phosphorites occur widely along the west coast (Gresse, 1988; Hendey, 1978; Pether, 1994; Cilliers, 1995; Nicholas, 1995; Macdonald, 1996; Rogers *et al.*, 1990). Pether (1986, 1994) regards these phosphorites to be near-shelf deposits of his 90m Package. Hendey (1981) suggested that the Late Pliocene Varswater Formation that overlies the Saldanha Formation could be correlated with the 75-90m Complex (Carrington and Kensley, 1969).

Pether (1983, 1986, and 1994) has made detailed investigations in the Hondeklip Bay area and his studies of the Hondeklip Bay sequence led to his marine package terminology, which is well known among west coast geologists. Pether (1986) defines a marine package to be "a group of sedimentary facies deposited during individual oscillations of sea-level." The nomenclature is related to the maximum sea-level elevation reached during transgression as correlated with local and global sea-level fluctuations (Fig. 3.2). Pether recognised progressively younger marine packages that truncate its antecedent. Based on the Hondeklip exposures (Fig. 3.4.), Pether (1986, 1994) reviewed the work of Carrington & Kensley (1969), reclassified their nomenclature, and amended relative ages of the marine terraces (Fig. 3.4). He described the 75-90m Complex as the 90m Package and referred to the 45-50m Complex as the 50m Package since it contains the zone fossil *Donax haughtoni*.

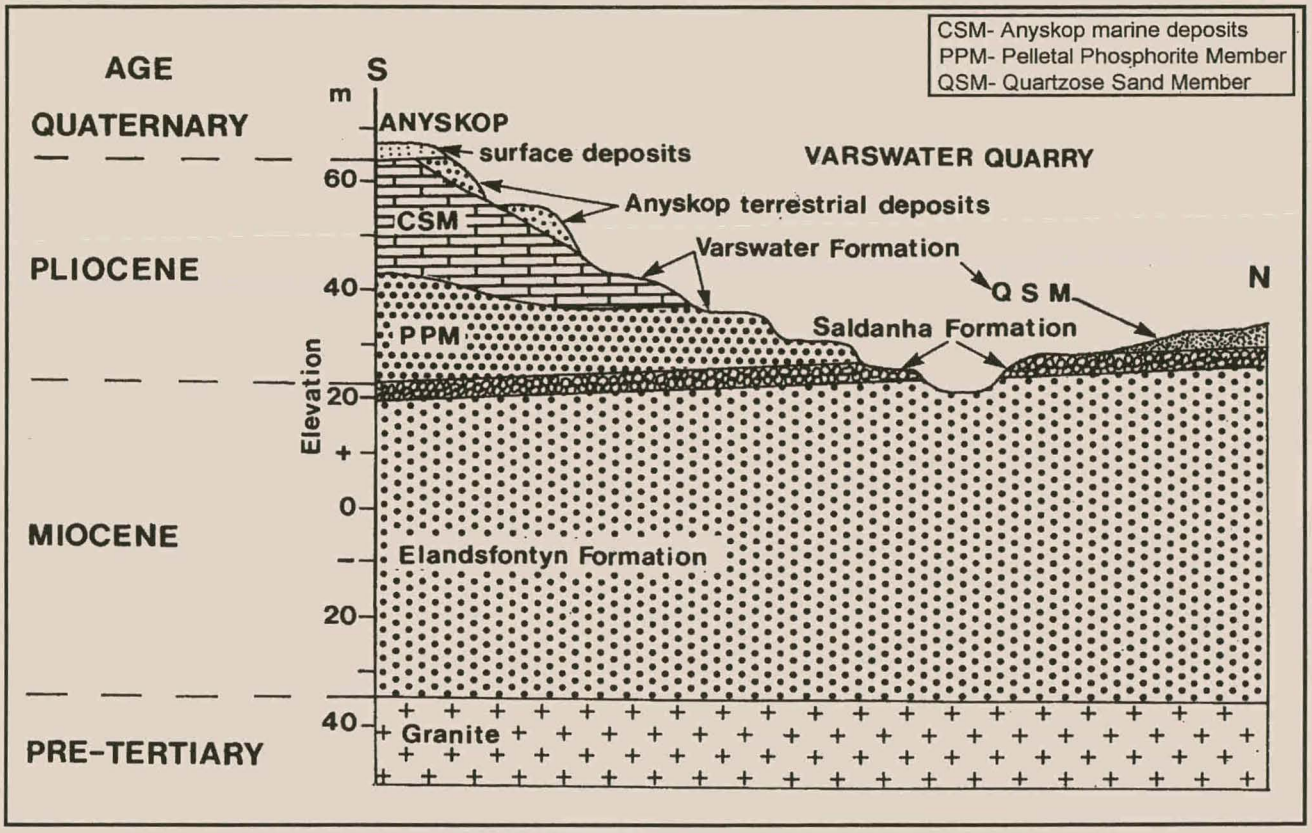

Figure 3.1. Stratigraphic profile across the Varswater Quarry (Rogers *et al.*, 1990).

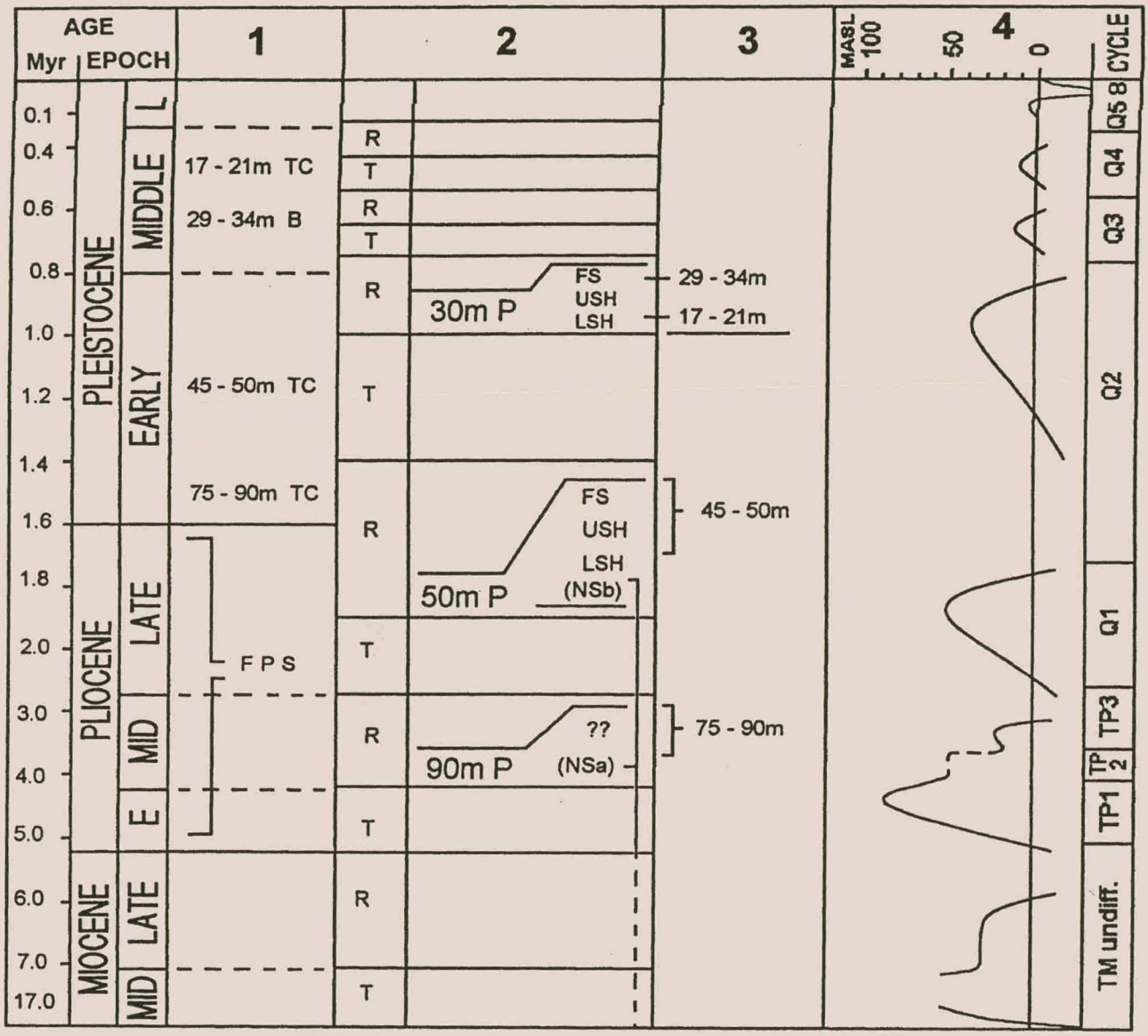

Figure 3.2. West Coast stratigraphy: summary of previous work (from Pether, 1986).
Column1: succession after Carrington and Kensley (1969); TC, transgression complex; B, beach; FPS, fossiliferous phosphatic siltstones. Column 2: succession after Pether (1986); R, regression; T, transgression; 30m P, 30 metre Complex; 50m P, 50 metre Complex; 90m P, 90 metre Complex; FS, foreshore facies; USH, upper shoreface; LSH, lower shoreface; NSb, 50m Complex nearshore shelf; NSa, 90m Complex nearshore shelf. Column 3: correlation between Carrington and Kensley (1969; Col. 1) and Pether (1986; Col. 2). Column 4: Neogene and Quaternary sea-level cycles modified from Vail and Hardenbol (1979).

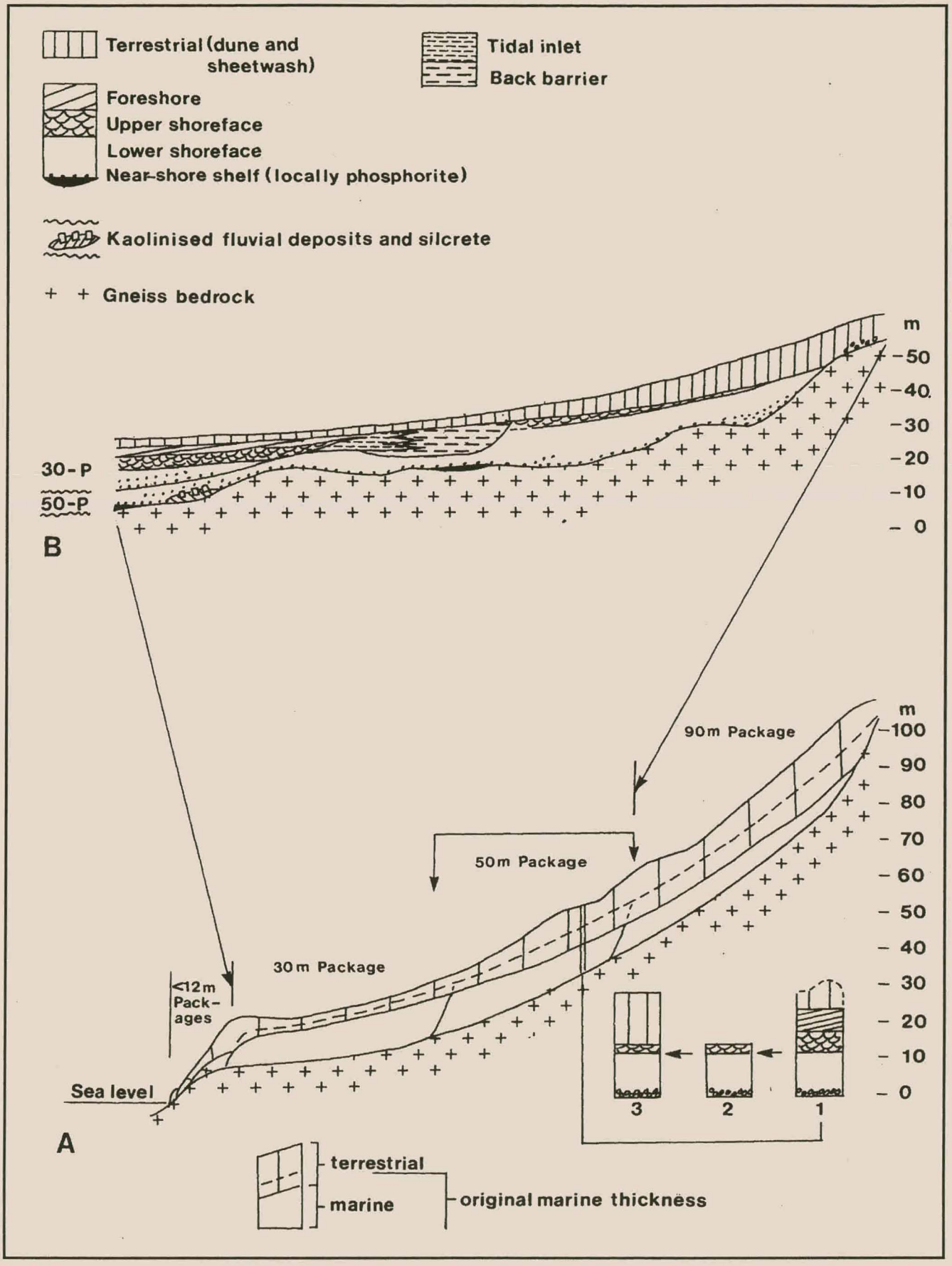

Figure 3.3. Illustration of the Hondeklip succession (from Rogers *et al.*, 1990).

The 17-21m and 29-34m Complexes were grouped together as the 30m Package since the zone fossil *Donax rogersi* is abundant in both these complexes. From the local sea-level history, Pether (1986) deduced an Early Pliocene age for the 90m Package. In a similar manner the age of the 50m Package and 30m Package respectively is inferred as Late Pliocene and Early Pleistocene. Late Pleistocene to Holocene low elevation (< 10m *amsl*) palaeo-shorelines provide the youngest Cainozoic marine sedimentation at Hondeklip Bay. Pether (*op. cit.*) considers that all the marine packages were deposited as regressive units as the sea-level dropped from its transgressive maxima. Using faunal assemblages and sedimentary features, he showed that the 30m, 50m and 90m Packages occur along the entire Namaqualand coastal plain. Pether (1994) concluded that the 30m Package shows remarkably linear continuity over 1500km along the South African west coast, in contrast with the 50m Package that is locally preserved and the 90m Package that is only present as remnants.

Pether (1994) also gives detailed descriptions of basal kaolinitic deposits. These sediments consist of a basal quartz gravel in a clay matrix deposited in a fluvial channel incised into bedrock and were reported by earlier workers (Carrington and Kensley 1969; Tankard 1966, 1975). Similar channels occur infrequently along the west coast and their appearance becomes prominent in the Koingnaas area (Rogers *et al.*, 1990; Nicholas, 1995). The age of the channels is estimated to be Early Miocene (Siesser and Dingle, 1981; Rogers *et al.*, 1990) and they could be correlated with the Elandsfontyn Formation in the Langebaan-Saldanha area. Cole and Roberts (1996) reported lignite-enriched clays associated with the Elandsfontyn Formation within similar palaeochannels at Koekenaap, Bergrivier and Kraaifontein.

North of the Olifants River, at Geelwal Karoo, Macdonald (1996) recorded marine sediments on elevated terraces (35-45m *amsl*) conforming to the 50m Package (Fig. 3.5). Cilliers (1995) reported the presence of four strandlines namely 20m, 35m, 65m, and 110m *amsl* near Graauwduinen (Fig. 3.6.) overlying clay-filled fluvial channels of Quaternary age (Rozendaal and Gresse, 1995). Cilliers (1995) correlates the sediments associated with the 35m strandline with the 30m Package,

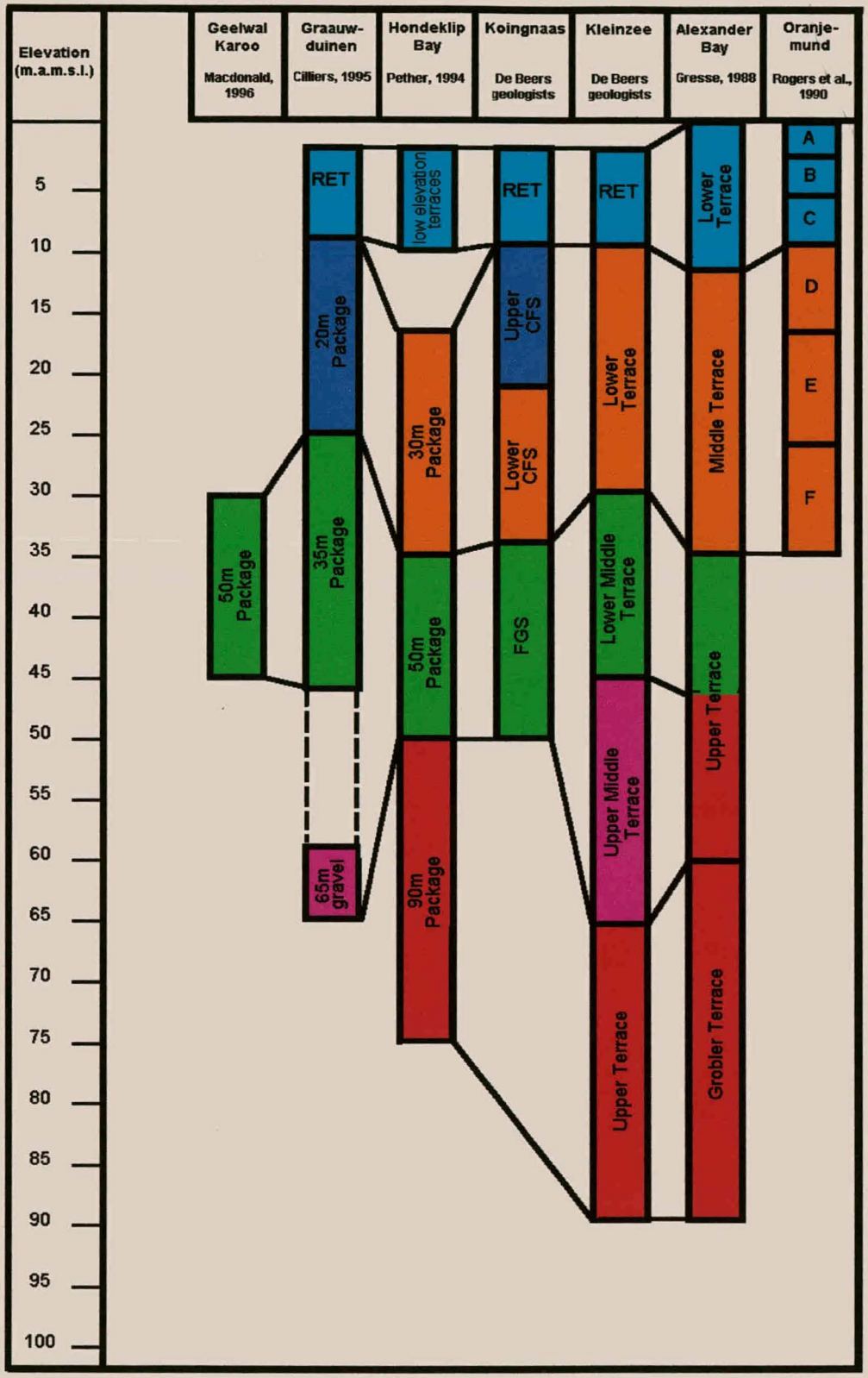

Figure 3.4. Stratigraphic correlation of the Cainozoic marine sediments along the west coast of South Africa.

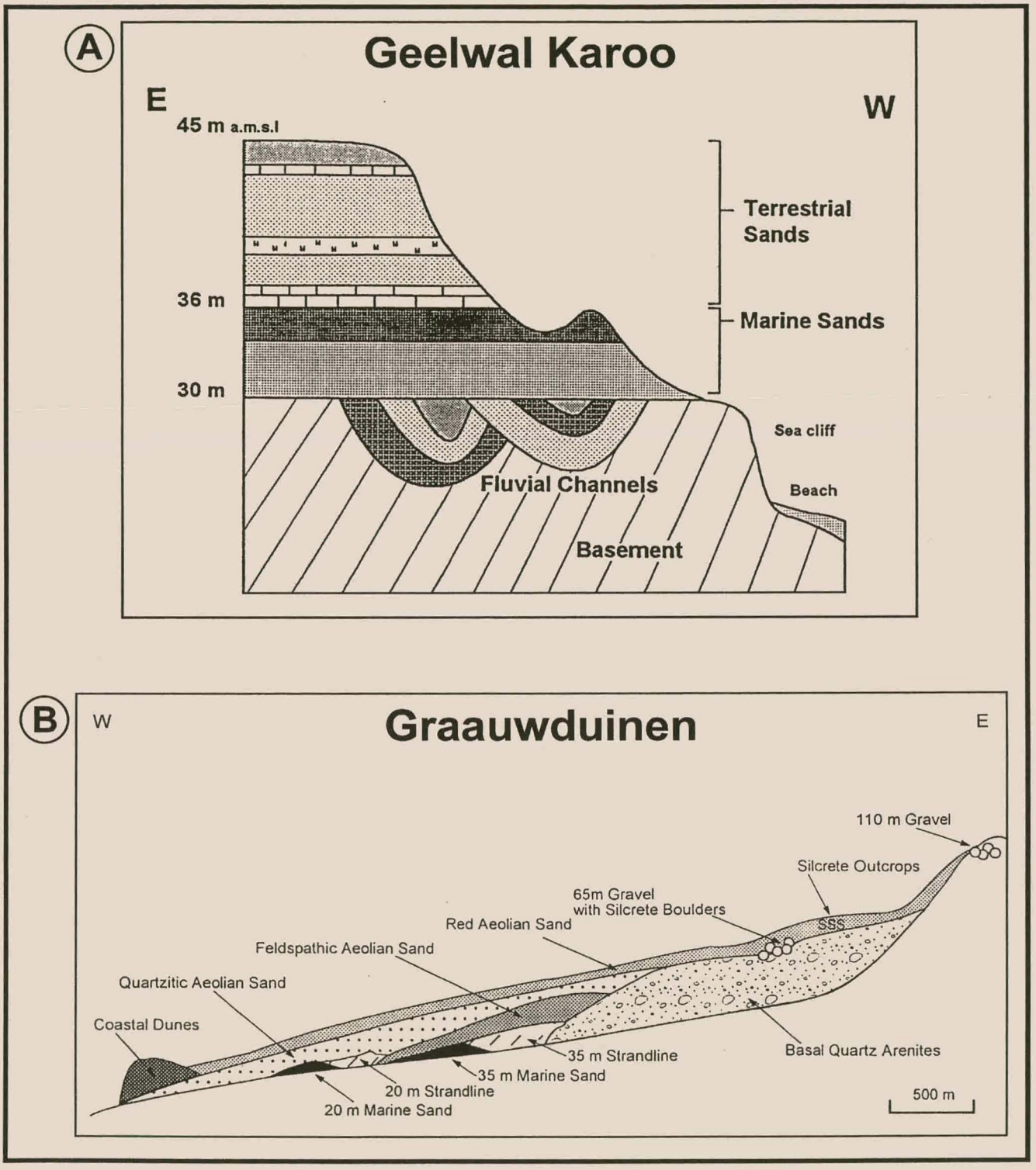

Figure 3.5. Geological cross-section of the A) Geelwal Karoo beach deposit (from Macdonald, 1996) and B) Graauwduinen heavy mineral deposit (after Cilliers, 1995).

the 65m strandline with both the 50m Package and Kleinzee's Upper Middle Terrace and the 110m strandline with the 90m Package (Fig. 3.4). Cilliers (1995) disagrees with Pether's (1986) view that the 17-21m Complex and 29-34m Complex of Carrington and Kensley (1969) should be grouped together as the 30m Package. Instead, he argued that mineralogical studies of Graauwduinen sediments proved that there is substantial evidence to support the existence of a separate 20m Package.

In the Koingnaas area, Nicholas (1995) observed marine sequences locally known as the Fine Green Sands (FGS) and Coarse Feldspathic Sands (CFS) that shows remarkable correlation with beach complexes identified by Carrington and Kensley (1969). To some extent these sequences also coincide with sediments characteristic of the 30m and 50m Package (Fig. 3.4). The marine packages are overlain by younger heavy mineral-enriched, elevated beaches at 3, 6 and 10-14m *amsl*, collectively labelled as the Recent Emergence Terrace (RET). Nicholas (1994) opposes Pether's grouping of the 17-21 and 29-34 Complex of Carrington and Kensley (1969) into his 30m Package and based on sedimentological evidence suggest that a separate 20m Package identity be reserved for 17-21m Complex sediments, supporting Cilliers (1995).

At Kleinzee, three characteristic wave-cut terraces, namely the Upper, Middle and Lower Terraces occur at different elevations, (Rogers *et al.*, 1990; Fig. 3.6). The Upper Terrace occurs at an elevation of 75-90m *amsl* and is correlated with the Early Pliocene Varswater Formation in the Langebaan area. The Late Pliocene, Middle Terrace is subdivided into an Upper Middle Terrace situated between 45-65m *amsl* and the Lower Middle Terrace is observed between 30-45m *amsl* The Lower Terrace occurring between 10-30m *amsl* is locally associated with the 30m Package for which an Early Pleistocene age is suggested.

Keyser (1972) recognised four distinct terraces (Fig. 3.6.) in the area that stretches from Alexander Bay to Port Nolloth and his work has subsequently been revised by Rogers *et al.* (1990). The oldest wave-cut terrace is the Miocene Grobler Terrace

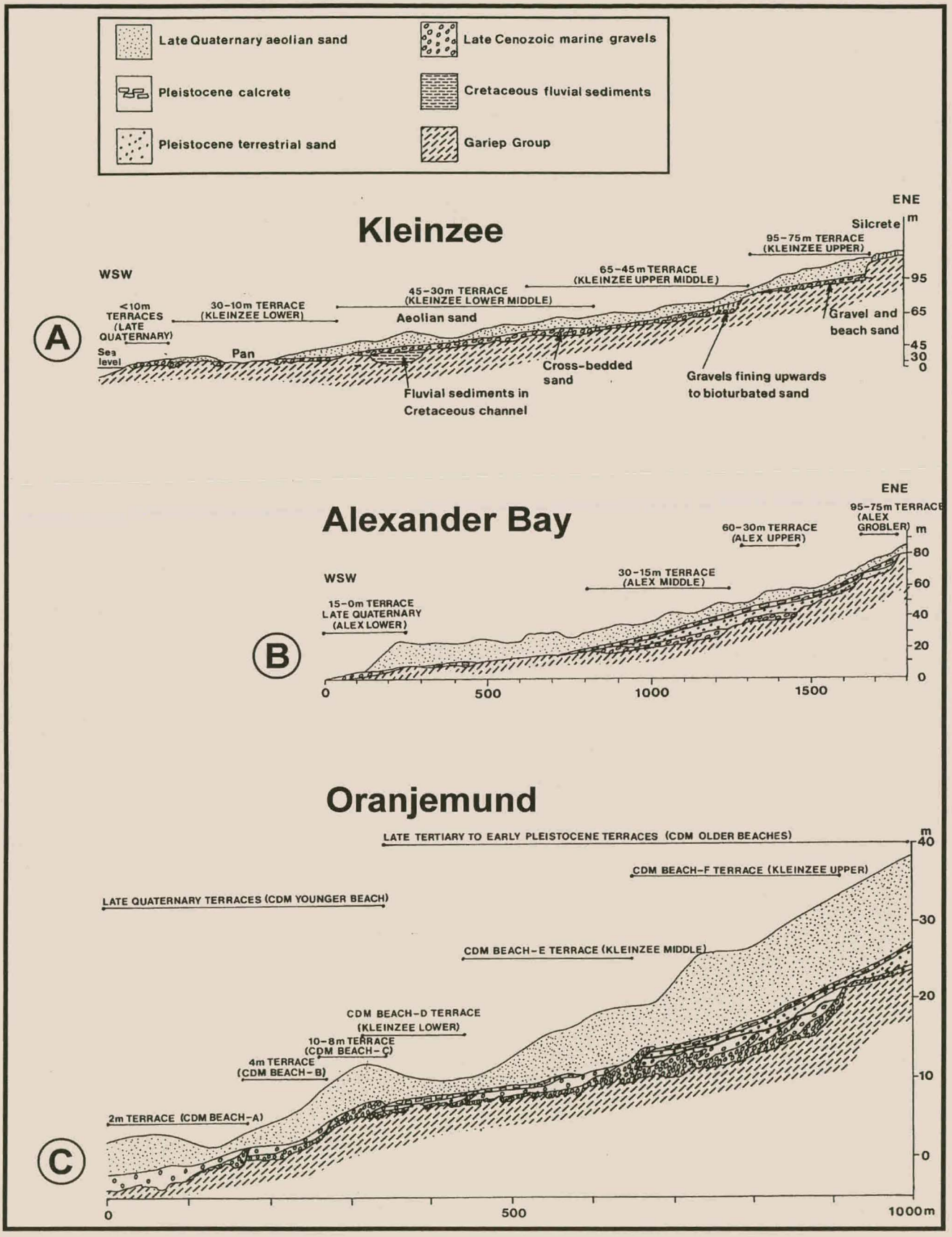

Figure 3.6. Illustration of the marine terraces at A) Kleinzee and B) Alexander Bay and C) Oranjemund (from Rogers *et al.*, 1990).

that lies between 75-90m *amsl* The Pliocene-Pleistocene Upper Terrace occurs between 35-60m *amsl*, the Pleistocene Middle Terrace between 15-35m *amsl* and the Lower Terrace between 0-15m *amsl* Gresse (1988) proposes a correlation between Alexander Bay's Grobler Terrace, the upper part of the Upper Terrace, Kleinzee's Upper and Upper Middle Terraces and the 90m Package. He matches the lower part of the Alexander Bay's Upper Terrace (Kleinzee's Lower Middle Terrace) with the 50m Package and the Alexander Bay's Middle Terrace (Kleinzee's Lower Terrace) with the 30m Package (Fig. 3.4).

Six raised beaches are evident at Oranjemund (Fig. 3.6.) and are divided into the Late Miocene, Upper Terrace Group comprising the D, E and F beaches and a Quaternary, Lower Terrace Group consisting of the A, B and C beaches (Hallam, 1964; Hendey, 1981; Rogers *et al.*, 1990). Crustal movement during the Miocene to Pleistocene was effective in downwarping the Upper Terrace Group beaches to the north while the younger beaches maintained constant elevations (Hallam, 1964; Dingle *et al.*, 1983; Rogers *et al.*, 1990). The D, E, and F beaches occur at elevations from 14-35m *amsl* while the A, B and C beaches occur at elevations 2-10m *amsl* (Hallam, 1964; Rogers *et al.*, 1990). Rogers, *et al.* (1990) postulated that the D, E and F beaches correlate with the Upper, Middle and Lower Terraces of Kleinzee, but Pether (1986) claimed that these beaches are more likely to be 30m Package correlates since they contain the zone fossil *Donax rogersi*.

3.2. Local geology

Stratigraphically the oldest sediments in the study area coincide with the Late Precambrian Gariep Supergroup that overlies the Namaqua Metamorphic Complex. Unconsolidated Miocene fluvial and Pliocene-Pleistocene marine sequences that are commonly associated with diamond mineralisation unconformably overlie basement rocks. Recent aeolian dunes ultimately blanket the marine sequences. The mining area to the north of Kleinzee, known as the Buffels Marine Complex (BMC) is marked by a series of elevated beaches, which are commonly associated with diamond occurrences. The Koingnaas Complex (KNC), located between Hondeklip Bay and Kleinzee, contain two types of deposits. The older of these constitutes what

is known as the channel sediments, which consist of fluvial sediments deposited in channel-like features cut into bedrock. These are overlain by younger, marine sequences which were not deposited on raised terraces as found in the BMC, but instead are associated with characteristic sea-level elevations during their deposition. Inland, the area known as the Buffels Inland Complex (BIC) comprises sediments that are remnants of a typical fluvial sequence deposited in a meandering proto-Buffels River.

3.2.1. Buffels Marine Complex (BMC)

In this area, a series of Plio-Pleistocene raised beaches, which are labelled locally as the Upper, Middle, and Lower Terraces are cut into the bedrock. Overlying bedrock is a series of diamondiferous unconsolidated marine gravels and sands that were deposited in nearshore, foreshore and upper-shoreface environments. Terrigenous and aeolian sands that vary considerably in thickness, mainly overlie the marine sediments.

Bedrock geology

Basement rocks in the BMC conform to the Mid-Proterozoic Namaqua Metamorphic Complex as well as tectonic slices of the Neoproterozoic metasedimentary Stinkfontein "Formation" of the Gariep Belt (Kirtley, 1985). Observed rock types include arkoses, quartzites, phyllites, quartz-mica schists, quartzo-feldspathic gneisses and minor volcanics. Amphibolite bands, quartz and epidote veins as well as small pegmatitic intrusions are also recognised. The variable competence of the basement rocks led to differences in the bedrock profile; gullies and deep potholes are cut into the more resistant rocks which form ideal trapsites where high concentrations of diamonds have accumulated (Rogers *et al.*, 1990). Where the rocks are foliated, the bedrock was eroded to a more evenly surface which prevents good trapsite development.

Upper Terrace

The Upper Terrace was cut on a wave platform when the sea maintained a eustatic level of 75-90m above present sea-level (Fig. 3.7). Regionally, the platform runs almost parallel to the existing coastline and is terminated in a well-defined cliff in the east (Rogers *et al.,* 1990; Fig. 3.8.) Locally, the platform can be extremely irregular depending on the competence of the bedrock. Marine sediments on the Upper and Middle Terraces were deposited mainly during regressional stages as successive deposits and were reworked during subsequent minor transgressions. Typically, the Upper Terrace sediments consist of a basal gravel overlain by a medium to coarse-grained brown quartzo-feldspathic sand (Fig 3.9). The gravels are usually clast-supported, poorly sorted and either display chaotic fabric or in rare cases show some imbrication. Clasts are predominantly subrounded to rounded and consist mainly of quartzite, schist and gneiss.

The overlying orange-brown quartzo-feldspathic sands usually consist of two units separated by a gradational contact. A coarser, moderately sorted, gritty sand, displaying a fining upward gradation, directly overlies the gravel. This unit is often marked by swash-deposited heavy mineral laminae that dip slightly seaward, indicating deposition in a foreshore environment (Plate 3.1A). The overlying unit has better sorting and displays large scale cross-bedding, which could be a combination of younger sheetwash and aeolian sand. Brown, semi-compacted terrigenous sand, often calcretized, comprises the top unit. Correlation with the 90m Complex in the Hondeklip area (Pether, 1986) as well as with the Varswater Formation in the Langebaan-Saldanha area (Hendey, 1981) suggests an Early to Mid-Pliocene age for the Upper Terrace sediments.

Middle Terrace

The Middle Terrace originated when there were sea-level stillstands between 45-65 meters (Fig. 3.7.) and is divided into an Upper and Lower division, with the boundary between them delineated by a significant break in the bedrock slope at approximately 45m *amsl* (Fig. 3.9). Both terraces occur on well-developed wave-cut platforms with the Upper Middle Terrace defined in the east by a well defined 65

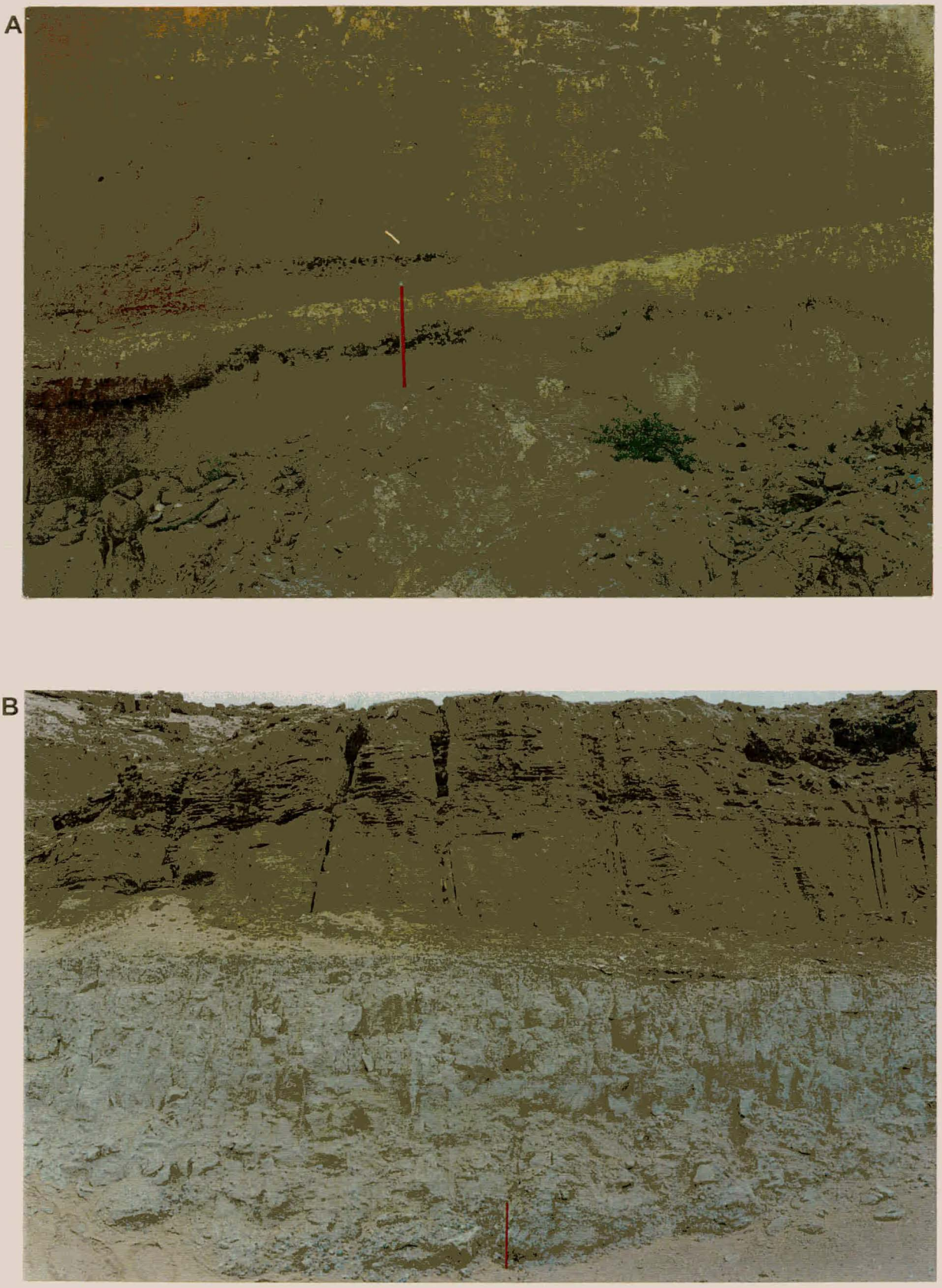

Plate 3.1.

A) Typical configuration of an Upper Terrace sequence in the Buffels Marine Complex. A basal quartzitic gravel is overlain by swash-deposited heavy mineral sands.

B) Lower CFS sediments unconformably overlie much older channel sediments in the Koingnaas area. Length of ruler is 1m.

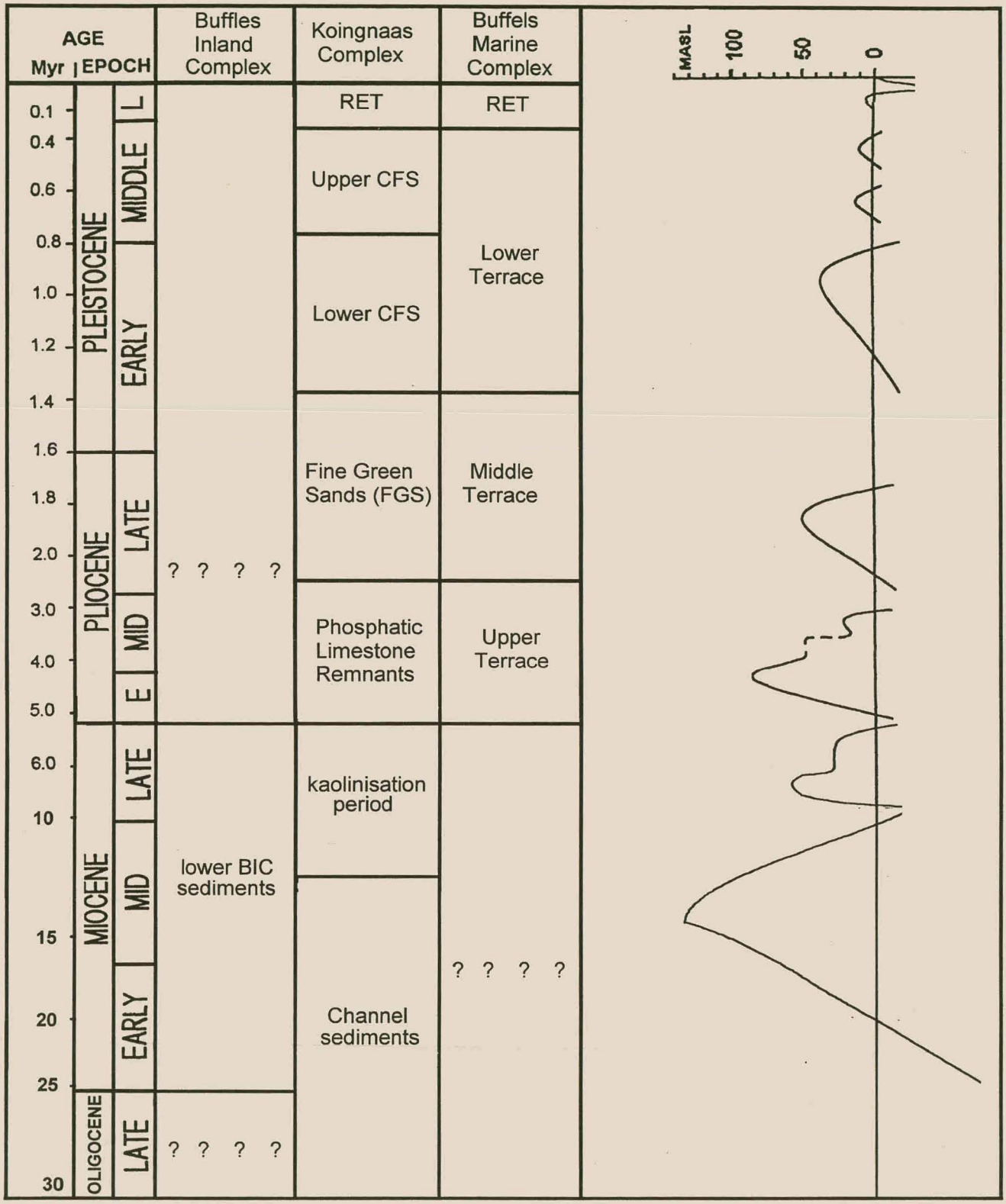

Figure 3.7. Stratigraphy and relative sea-level curves for Cainozoic sediments in the study area.

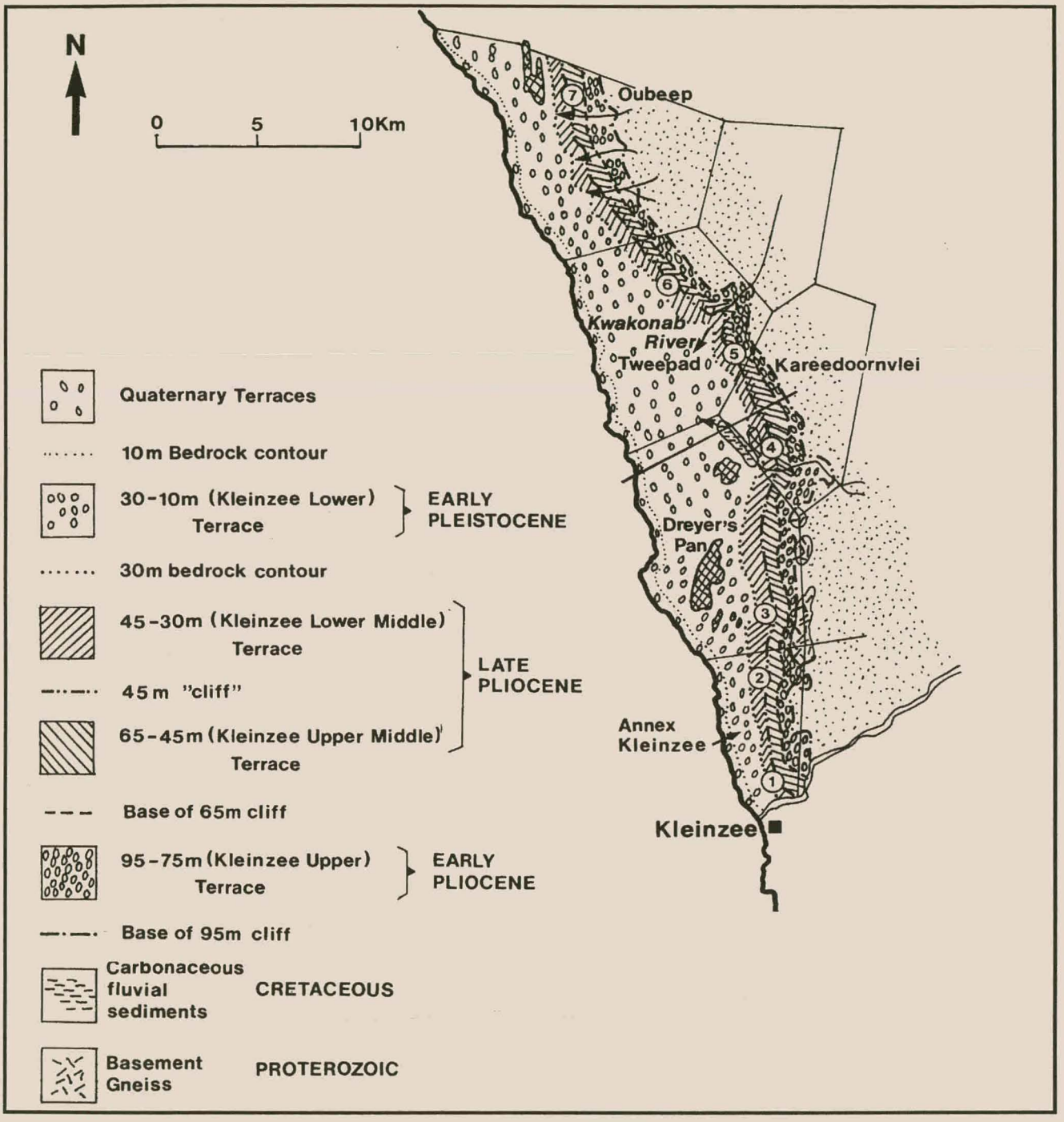

Figure 3.8. Distribution of wave-cut terraces in the Kleinzee area (after Rogers *et al.*, 1990).

meter cliff and the Lower Middle Terrace by a 45 meter cliff that becomes more diffuse to the south. The Upper Middle Terrace has considerable lateral continuity and is only occasionally breached by relative younger fluvial channels (Fig. 3.8).

Marine sediments on the Middle Terrace are compositionally and texturally quite similar to those of the Upper Terrace. The former are however, relatively more complex, as the transgressional phase becomes more significant. The oldest sediments comprise a basal gravel overlain by low angle, swash-bedded heavy mineral sands, which were presumably deposited under foreshore conditions (Fig. 3.9). Remnants of lower shoreface facies are frequently preserved in a seaward (westerly) direction and are characterised by hummocky cross-bedding, herringbone cross-bedding, trough cross-bedding and extensive bioturbation. Back-beach gravels interbedded with heavy mineral sands are also relatively common and were possibly deposited during storm conditions. Using the basal gravel of the Upper Terrace as a chronostratigraphic marker, the age of the Middle Terrace sediments is estimated to be Late Pliocene.

Lower Terrace

In comparison with the Upper and Middle Terraces, the wave-cut platform of the Lower Terrace is poorly developed and considering the absence of cliff features and significant breaks in the bedrock profile, there is no distinctive boundary between the Lower Terrace and the 45 meter cliff of the Lower Middle Terrace (Fig. 3.9). De Beers's geologists proposed a division at 30 meters that is based on a minor break in bedrock slope and correlation with the 30m Package in the Koingnaas-Hondeklip Bay area. The Lower Terrace is characterised by a sequence of sediments that are generally more massive than those of the Middle and Upper Terraces (Fig. 3.9). Generally, the sequence comprises a basal gravel overlain by coarse to medium-grained dark brown quartzo-feldspathic sand. Heavy mineral laminae are generally absent and sedimentary structures are well preserved due to prominent bedrock ridges parallel to the coast. The top part of the sequence is often calcretized. Based on a correlation with the 30m Complex in the Hondeklip Bay area an Early to Mid-Pleistocene age is inferred for the Lower Terrace.

A

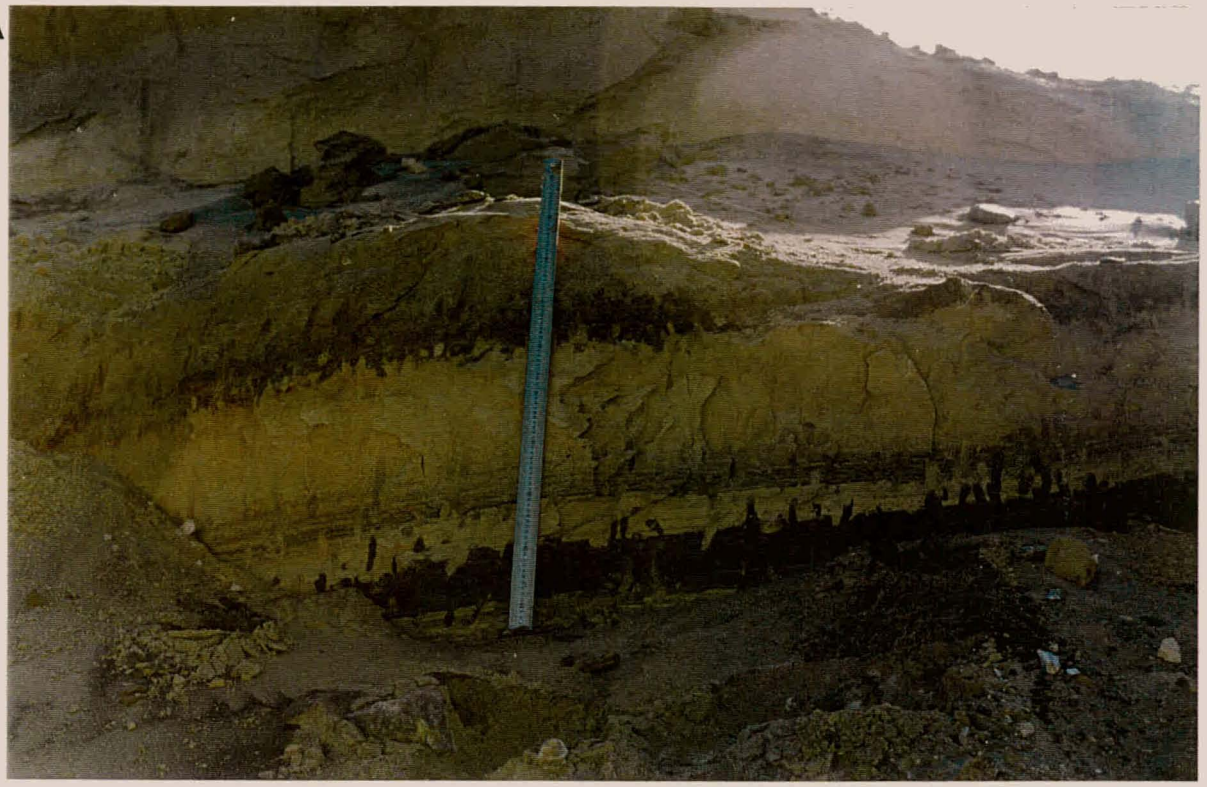

B

Plate 3.2.

A) Low elevation heavy mineral beaches of the Recent Emergence Terrace (RET) consist almost exclusively of quartz, garnet and Fe-Ti oxides.

B) Basal indurated gravel overlain by a series of cross-bedded sandstones (Langhoogte deposit, Buffels Inland Complex).

Length of ruler is 1m.

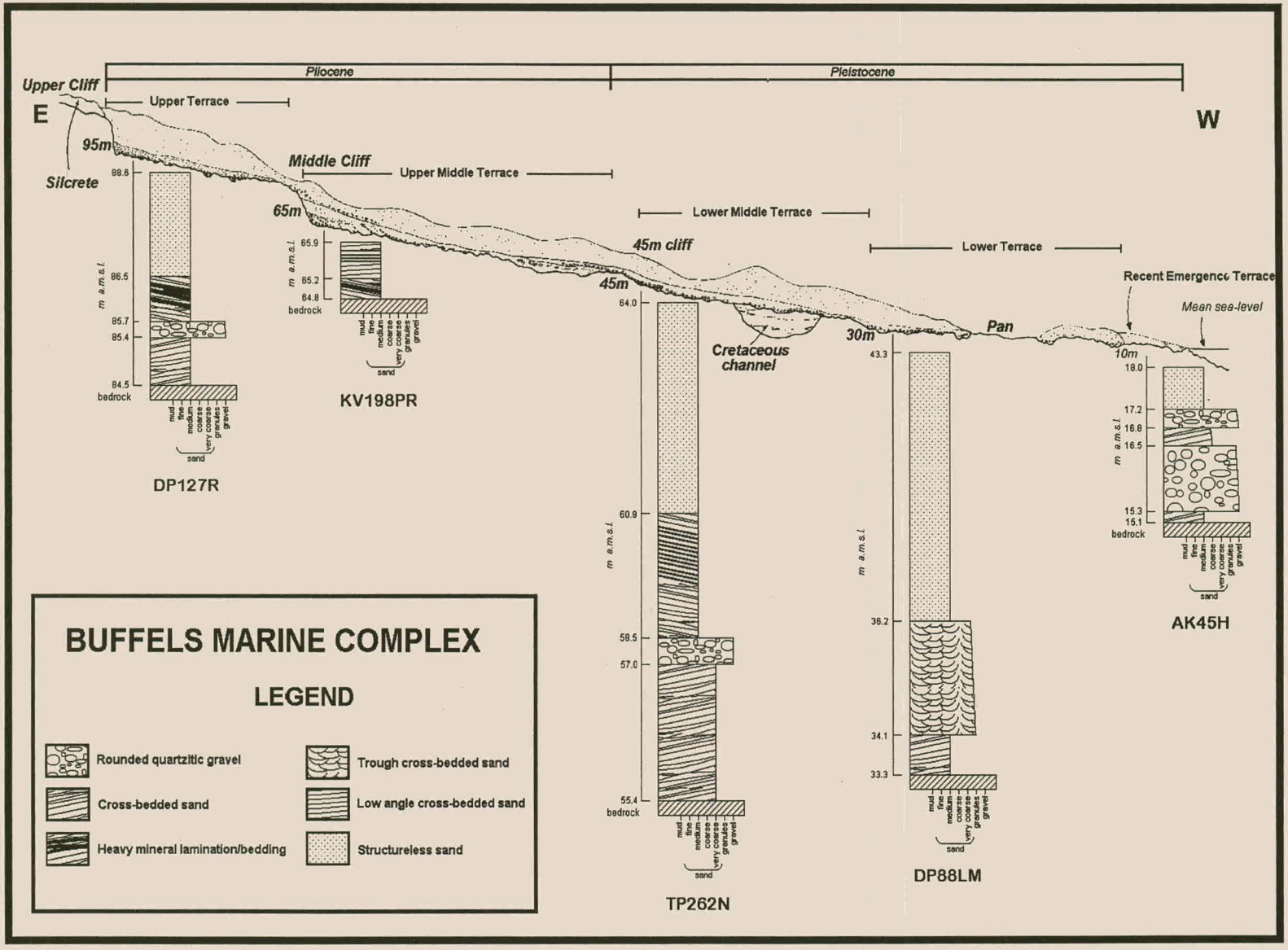

Figure 3.9. Cross section of the stratigraphy and representative sections from the Buffels Marine Complex.

Recent Emergence Terrace (RET)

The Recent Emergence Terrace (RET) is widely developed along the Namaqualand coast and beaches at 2, 5 and 8m *amsl* have been recognised at Koingnaas. A distinctive feature of the RET beaches is the presence of abundant shell remains of mostly modern or living species characteristic of the cold water fauna found along the west coast. Minor regressional phases during the Mid-to Late Pleistocene (Fig. 3.7.) resulted in the origin of the RET. The RET in the BMC comprise a series of raised beaches at lower elevations that reaches a maximum elevation of 10m *amsl* These deposits are characterised by a well-developed basal gravel and localised gravels and are overlain by a sequence of fine, moderately sorted clayey quartzo-feldspathic sand with substantial shellbanks (Fig. 3.9). These particular sediments truncate the older Lower Terrace sediments including the calcretized upper portion.

Cretaceous channel

L.M. Cilliers (*pers. comm.*) reported the presence of a remnant fluvial channel in the BMC (Fig. 3.9). The channel was thought to be analogous with the Koingnaas palaeochannels, but palynology dating on spores indicates a much older, Early Cretaceous age (Rogers *et al.*, 1990). Presently no other channel on the West Coast could be positively linked to this, but it is possible that it can be connected to the Cretaceous post-Gondwana erosional event that was effective in creating similar channel features.

3.1.2. Koingnaas Complex (KNC)

In contrast with the raised beach terraces present in the BMC, similar linear terraces are absent in the Koingnaas Complex (KNC). Instead, unconsolidated marine sequences, which directly overlie bedrock or palaeo-fluvial sediments, are associated with periods of lower sea-level stillstands. Although marine sequences from both the KNC and Hondeklip Bay areas are remarkably similar, it was not decided to use Pether's (1986) interpretation of the 30m Package in the Koingnaas area. The terminology of De Beers is used (Rogers *et al.,* 1990) for the KNC sediments, but with clear reference to the "package" nomenclature of Pether (1986, 1994).

Bedrock geology

The bedrock geology of the KNC is relatively simple with the granite-gneiss of the Namaqua Metamorphic Complex forming the bulk of the basement in this area (Theart, 1980; Jack, 1980; Zelt, 1980). These may be unweathered and competent, thereby forming prominent ridges and bedrock highs, or weathered and kaolinised, forming depressions where diamond concentration occurs. The complicated local bedrock morphology of the basement also accounts for the absence of raised terraces in the Koingnaas-Hondeklip Bay area (Rogers *et al.,* 1990).

Palaeochannels

The oldest known sediments in the KNC are the palaeochannel sediments, which are associated with a series of fluvial channels incised into the bedrock. The incision is thought to have occurred during the major Oligocene regression with subsequent rapid infilling of these channels during the Late Oligocene to the Mid-Miocene (De Decker, 1986; Rogers *et al.,* 1990; Fig. 3.7). These channel sediments can therefore be correlated with the Elandsfontyn Formation in the Langebaan-Saldanha area. A suggested Oligocene-Miocene age for these deposits is also confirmed by age determination derived from analysis of peat deposits (Rogers *et al.,* 1990; Cole and Roberts, 1996).

Ideally, a matrix-supported, subrounded vein-quartz gravel within a greenish-grey clay matrix and intercalated poorly sorted quartzose sands form the basal unit (Plate 3.1B). The clay gravels normally grade into grey clays and gritty quartzose silts and sands (Fig. 3.10). The mutual presence of poorly sorted angular granitic fragments and mica, quartz and feldspar grains suggests that this sediment was initially a locally derived arkose which was severely kaolinised by post-depositional processes. The deep weathering profile and kaolinisation of the palaeochannels can be related to the post-African erosional surfaces that formed during the Miocene when climatic conditions were close to tropical (De Wit, 1993). Several workers (Dixey, 1955; King, 1959; Partridge and Maud, 1987; De Wit, 1993) stress that these erosional surfaces

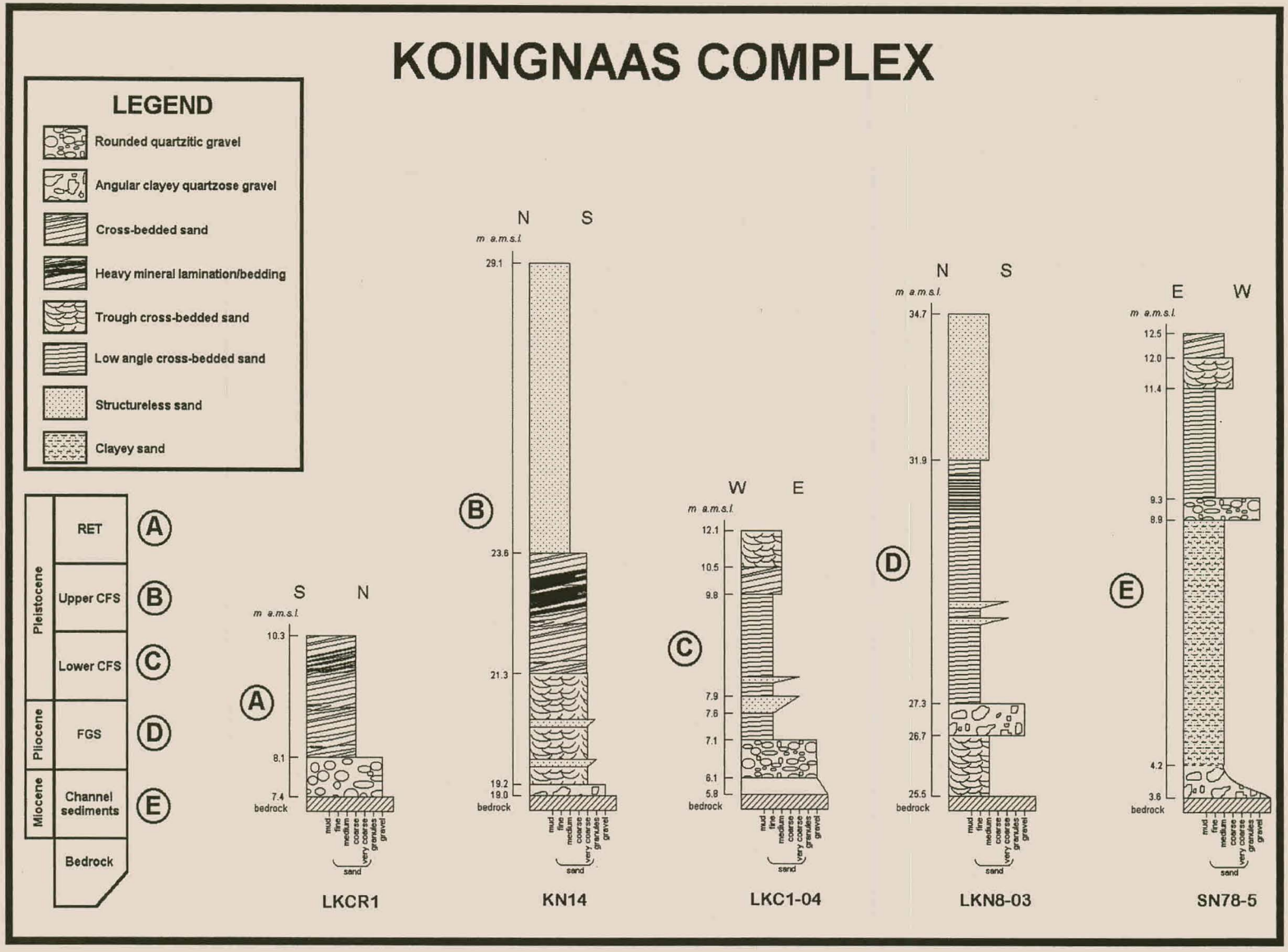

Figure 3.10. General stratigraphy and representative sections of the Koingnaas Complex.

were probably induced or influenced by repeated continental movement and corresponding sea-level fluctuations.

The basal channel gravels host anomalous concentrations of diamonds and represents the richest deposits in the area. During numerous trangressive-regressive events since the Miocene, the channel sediments were extensively reworked so that the diamonds were incorporated into the basal marine deposits, which because of the original channel morphology, were preserved in bedrock depressions (Rogers *et al.*, 1990).

Fine Green Sands (FGS)

Sediments that are locally known as the Fine Green Sands (FGS) unconformably overlie the channel sediments. These sediments are locally correlated with the 50m Package (Pether, 1994) and were deposited when a sea-level stillstand was attained around 50m *amsl*, after the sea regressed from 90m *amsl* (Fig 3.7.; Pether, 1986). Generally, a well-developed basal gravel or granular sand directly overlies bedrock (Fig. 3.9). Clasts comprise poorly sorted subrounded quartz pebbles and cobbles with minor quantities of phosphorite and silcrete. A well-sorted, pale-green or yellow sand occurring with planar-laminated heavy minerals overlies the basal unit. Occasionally clay units are intersected at the base of this uniform FGS sequence. Overlying these sands are well-developed shell banks exhibiting a diverse faunal assemblage including the zone fossil *Donax haughtoni* that typifies the 50m Package. A greenish, highly bioturbated sand with no sedimentary structures, characterises the overlying unit. The sequence is vertically terminated by poorly sorted, brown, terrigenous topsoil.

Nicholas (1995) interpreted the FGS to be a regressive sequence set in a shoreface environment. The basal gravels however, were considered to represent a transgressive lag or storm event. The sequence (or part) of the fine heavy mineral laminated sands, extensive shell beds and highly bioturbated sands of the FGS could also be linked to a low-energy depositional environment. The presence of clay within the heavy mineral laminated sands and the unstable heavy mineral

assemblage reinforce the possibility that deposition took place in a protected area such as a backbarrier environment where periodic influx of sediments was storm-related. G. Nicholas (*pers. comm.*) agreed that prominent bedrock highs would form a barrier to the sea so that the FGS would be sheltered and preserved in depressions. Likewise, Pether (1994) states that the preservation of FGS in a backbarrier environment might suggest minor transgressional events. It appears that there are probably both transgressive and regressive aspects of the FGS preserved as backbarrier deposits. Fragments of phosphatic fossils in the basal FGS gravel correlate with Hendey's (1982) phosphorites which are dated as Mid-Pliocene, implying a Late Pliocene age for the FGS (Rogers *et al.*, 1990).

Coarse Feldspathic Sands (CFS)

The FGS deposits are unconformably overlain by the Early to Mid-Pleistocene Coarse Feldspathic Sands (CFS) which are divided into a Lower and Upper succession. The Lower CFS sediments were presumably deposited during a sea-level stillstand at 29-34m *amsl* (Fig. 3.7.), whereas the Upper CFS correlates with the 17-21m Complex of Carrington and Kensley (1969). The classic regressive (prograding) succession of the Lower CFS, exemplified by its typical wedge shape, provides excellent correlation with part of the 30m Package found in the Hondeklip Bay area. Characteristically, the Lower CFS deposits comprises a poorly developed basal gravel (Fig. 3.10.), which include polished quartzite pebbles, cobbles and some boulders, that have been reworked from the underlying FGS and deposited during storm events (Nicholas, 1995).

Overlying the gravels is a series of moderately sorted quartzo-feldspathic sands, which display sedimentary structures that are commonly associated with a lower shoreface to upper shoreface environment (Plate 3.1B). The deposition of these particular sands can be connected to re-working of the FGS Package following deposition over the unconsolidated FGS strata or directly over bedrock (Nicholas, 1995). The influence of storm conditions is observed as tapered, coarse sand layers within massive fine sand. Remnants of shells and in rare cases shell banks of the

zone fossil *Donax rogersi* found in the exposures, represents regressive phases (Nicholas, 1995) and reaffirms a proposed correlation with the 30m Package.

Lithologically, the sediments of the locally known Upper CFS, alternatively suggested to represent the 20m Package (Nicholas, 1995), consists of a range of coarse-grained to granular muddy, dark brown, poorly sorted, quartzo-feldspathic sands (Fig. 3.10). These sediments are generally massive and are marked by trough cross-bedding passing upward into swash cross-bedding. Seaward-dipping heavy mineral layers are prominent and were preserved as the sea retreated. Muddy, medium-grained, semi-consolidated terrestrial sediments overlie the Upper CFS on an obtuse contact.

Donax rogersi, the zone fossil that characterises the 30m Package, is notably absent from the Upper CFS. The total absence of the zone fossil might indicate that the Upper CFS is in fact not part of the 30m Package, but should be considered as a separate sequence. Pether (*pers. comm.*) contests this view, stating that a high-energy marine environment inferred as the foreshore would be effective in destroying any shell fragments present. Sedimentological and mineralogical data from this study however, overwhelmingly supports Nicholas' (1995) interpretation of the Upper CFS as a separate marine package.

Recent Emergence Terrace (RET)

The youngest marine sediments in the KNC, pertaining to the Recent Emergence Terrace (RET) were deposited and preserved under transgressive-regressive conditions during the Late Pleistocene (Nicholas, 1995; Fig. 3.7). The RET in the KNC is characterised by a basal gravel overlain by shelly, well-sorted, white or orange, medium-grained sands. Unlike their BMC equivalents, these sands are marked by distinct heavy mineral bands that dip with a low angle seawards and wedge upwards against the older sediments of the Upper CFS (Fig. 3.10; Plate 3.2A). The RET sediments were also effective in truncating and reworking both the underlying Upper CFS and terrestrial cover.

3.2.3. *Buffels Inland Complex (BIC)*

Along the Buffels River, below the Great Escarpment, the Buffels Inland Complex (BIC) comprises a group of small mines identified by farm names such as Nuttabooi and Langhoogte. In these deposits, the diamondiferous ore comprises remnants of fluvial gravels, which are preserved as isolated patches in bedrock depressions and channels above the present-day bed of the Buffels River. The formation of the BIC deposits is generally accepted to be related to a meandering proto-Buffels River during the Miocene (McCormick, 1988; Farrow, 1988), but recently an alternative alluvial model has been suggested (Rogers *et al.*, 1990).

Bedrock geology

The Central Zone of the NMC constituting granites, gneisses and quartz-mica schists represents the basement rocks in this area (McCormick, 1988; Farrow, 1988). The bedrock is typically irregular and undulating with localised gullies and hollows. Localised bedrock depressions are apparently the result of varying degrees of weathering. Extensive bedrock weathering was also effective in destroying the rock fabric and creating an undulating weathered surface.

Nuttabooi

McCormick (1988) recognised six distinctive lithological units in the Nuttabooi area namely: bedrock lithologies, gravels and conglomerates, hard sandstone beds, clay and silt layers, channel sandstones and terrigenous topsoil (Fig. 3.11). Basal gravels or conglomerates vary in thickness and form the main orebodies. Generally, the gravels are matrix-supported, displaying poor and often chaotic sorting. Clast lithology comprises predominantly vein quartz with lesser quantities of bedrock and occasionally clay clasts. The majority of clasts vary randomly from pebbles to cobbles with a limited occurrence of large boulders. Clast shapes vary from sub-angular to subrounded and their distribution seems erratic. The matrix consists of argillaceous quartzo-feldspathic sand, apparently derived from the bedrock and occasionally tends to be exclusively quartzose. White quartzose sandstone overlies the basal gravels and is confined to channel thalweg. The sandstone consists of well-cemented sub-angular quartz grains in a fine calcareous matrix. A prograding

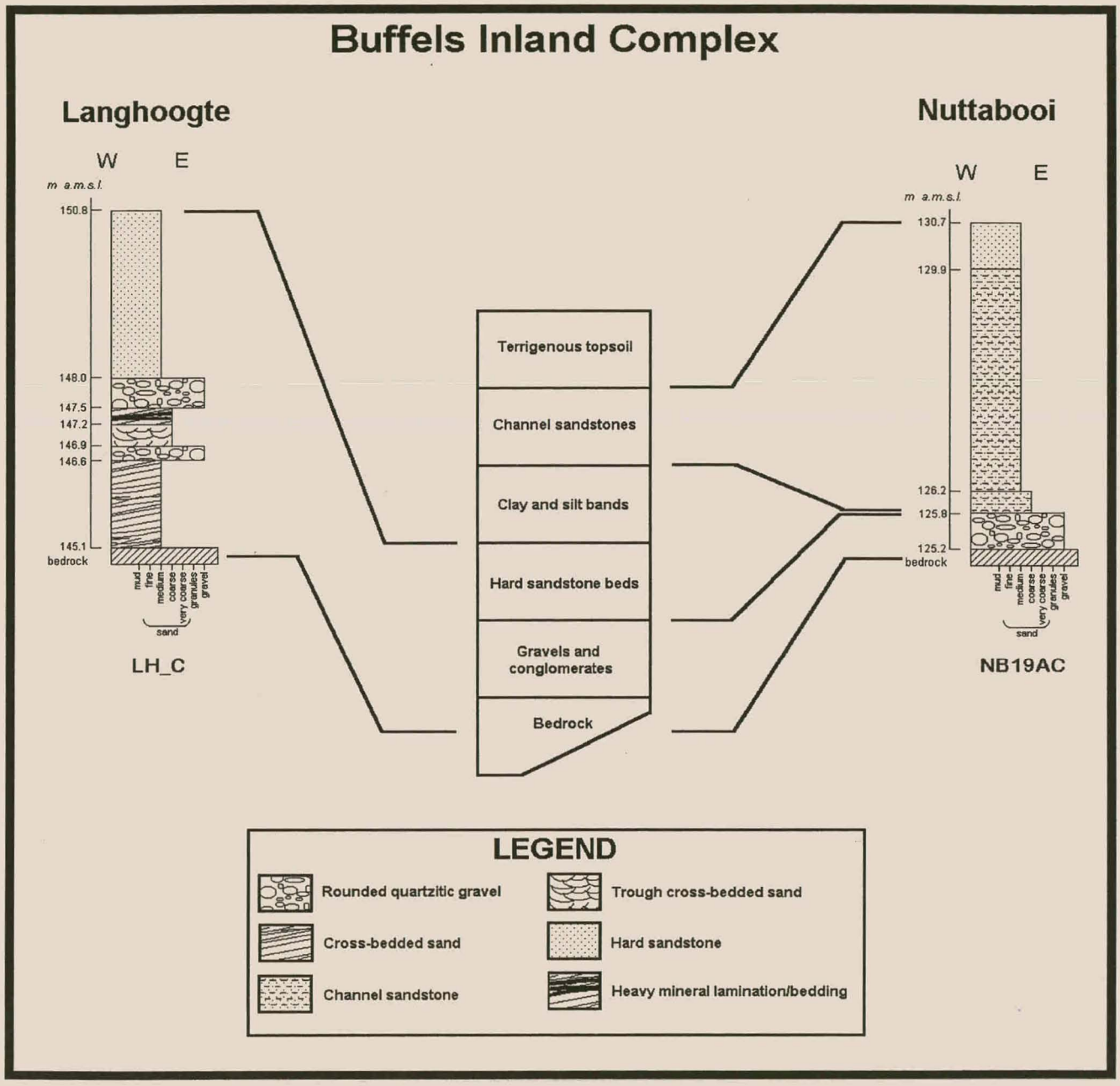

Figure 3.11. Summary of the Buffels Inland Complex stratigraphy and schematic logs of the Nuttabooi and Langhoogte deposits.

succession of clays, silts and channel sands with varying thickness overlies the sandstone. McCormick (1988) interpreted these sedimentary deposits as overbank deposits.

Channel sandstones are present as an upward fining cycle, of a coarse, poorly sorted quartzo-feldspathic nature. The sandstone is poorly cemented; being senso stricto, a sand layer in some cases. Sedimentary structures either are absent or obliterated. Manganese and iron staining occur in well-developed laminations. Channel sandstones are restricted to the lower parts of the channel-fill succession and are ultimately covered by a well-sorted aeolian sand that is occasionally calcretized. McCormick (1988) considers the Nuttabooi deposit to be a fluvial channel system that originated on a southerly meander of the proto-Buffels River. Basal gravels were deposited under high-energy conditions, after channel erosion. Stream velocity decreased, creating a system of braided, smaller channels that deposited the channel sandstones, clays and silts. The age of the lower BIC deposits is estimated to be Miocene (Rogers *et al.*, 1990; Fig. 3.7.) and implies a possible correlation with the Elandsfontyn Formation as well as with the palaeochannels at Hondeklip Bay and Koingnaas.

Langhoogte

Sediments of the Langhoogte orebody were supposedly deposited in a tributary of the meandering proto-Buffels River and its lithostratigraphy is very similar to that of Nuttabooi (Fig 3.11). Ideally, the sequence begins with a basal indurated gravel overlain by a succession of sandstones, siltstones and clays that fill bedrock channels (Plate 3.2B). Localised gravels interbedded with the sandstones are closely associated with oblique bar and longitudinal bar facies. The complete succession is seldom observed and is only preserved in the deeper depressions where little or no erosion has taken place. In most cases only remnants of the original gravel remain where complete reworking have taken place. In contrast to the Nuttabooi deposit the Langhoogte sediments are marked by prominent heavy mineral laminae and are severely hydrated and oxidised, imparting a dark orange brown colour to the sediments.

CHAPTER 4

SEDIMENT CHARACTERISTICS

4.1. Granulometry

A conventional sieve method was employed to perform grain-size analysis on 95 sand samples. Sieves with a range from -2→ 4ϕ at 0.5 ϕ intervals were used and the technique is fully discussed in Appendix B. The sand samples were grouped into four major sets which relate to their locality and origin. All Buffels Marine Complex (BMC) and Koingnaas Complex (KNC) samples are marine in origin, in contrast with samples from the Buffels Inland Complex (BIC) that are derived from a fluvial environment. The fourth group of samples comprises fluvial sediments from the palaeochannels.

Grain-size distributions of the dataset represented in phi (ϕ) units are plotted as barcharts (Addendum A). Textural parameters (mean diameter, sorting, skewness, kurtosis) were calculated using the formulas of Folk and Ward (1957) and are presented in Appendix D. A brief definition of each parameter and its relevant formula is given below.

Mean (Mz) is a measure of average grain-size and is calculated by the formula

$$Mz = \frac{(\phi_{16} + \phi_{50} + \phi_{86})}{3}$$ where ϕ_{16} conforms to the phi diameter at the 16th percentile of the distribution.

Inclusive graphic deviation (σ_I) describes the measure of dispersion around the median; also better known as sorting.

$$\sigma_I(\text{sorting}) = \frac{(\phi_{84} - \phi_{16})}{4} + \frac{(\phi_{95} - \phi_5)}{6.6}$$

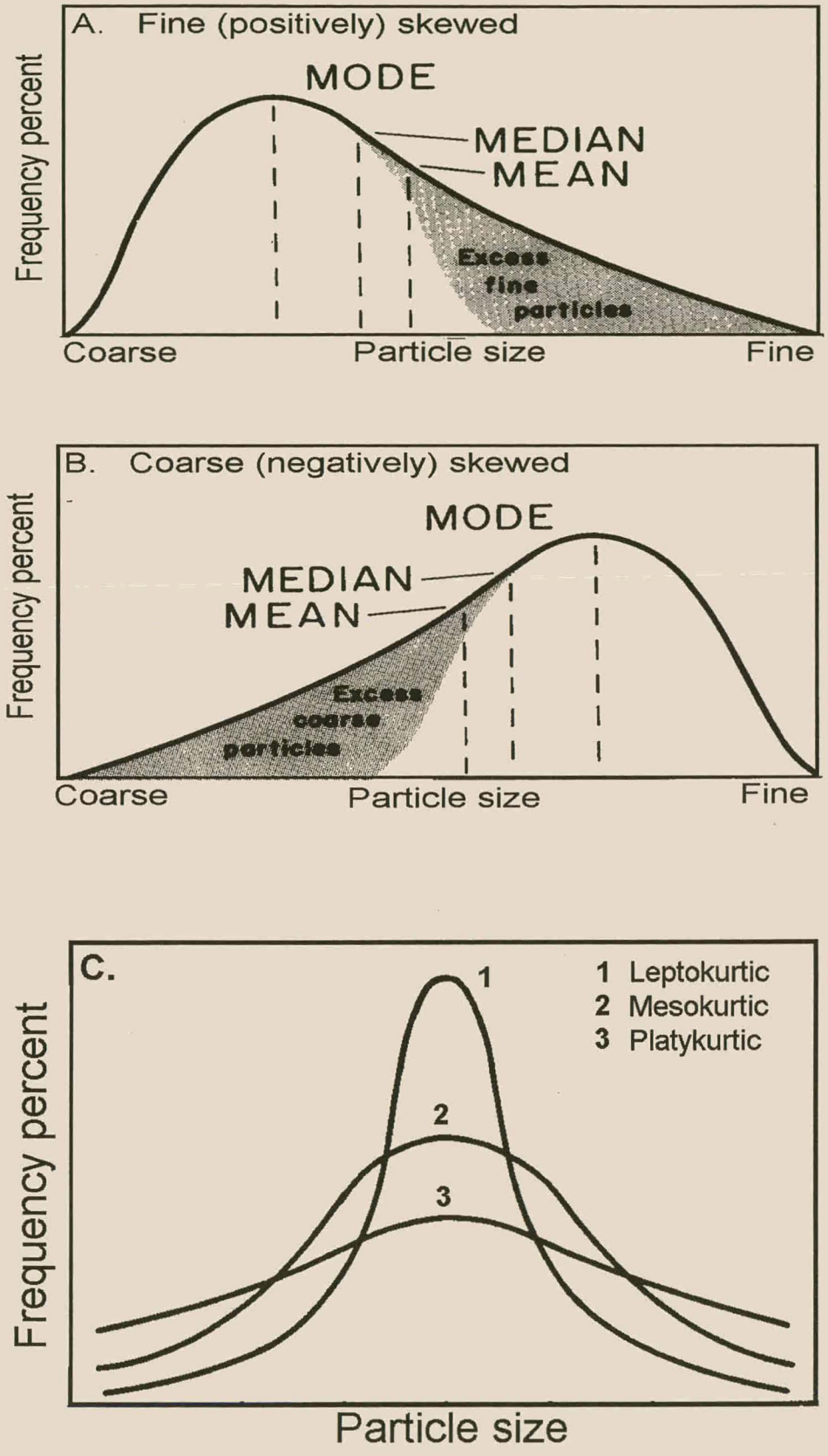

Figure 4.1. A) Fine-skewed and B) coarse-skewed, grain size distributions. C) Examples of grain size distributions of different kurtosis.

Inclusive graphic skewness **(Sk_I)** measures the departure of the mean from the median. If the skewness is negative, more coarse material is present, displayed as a tail in the coarser grades (Fig. 4.1A). If the skewness is positive, the grain-size distribution has a tail in the finer grades (Fig. 4.1B).

$$Sk_I = \frac{(\phi_{16} + \phi_{84} - 2\phi_{50})}{2(\phi_{84} - \phi_{16})} + \frac{(\phi_5 + \phi_{95} - 2\phi_{50})}{2(\phi_{95} - \phi_5)}$$

Inclusive graphic kurtosis **(K_G)** measures the sorting in the central and extreme parts of the distribution. The contrast between two symmetrical distributions that differ in kurtosis is illustrated in Fig. 4.1C.

$$K_G = \frac{(\phi_{95} - \phi_5)}{2.44(\phi_{75} - \phi_{25})}$$

The mean grain-size of a sample was compared with the Udden-Wentworth scale (Lewis, 1984, p.59) to classify the sand texturally. Folk and Ward (1957) devised a series of verbal scales for use with their grain-size parameters (Table 4.1).

Table 4.1. Descriptive terms applied to the grain-size parameters as defined by Folk and Ward (1957).

Sorting (σ_I)		Skewness (Sk_I)		Kurtosis (K_G)	
<0.35	very well sorted	+0.3→ +1	very positively skewed	<0.67	very platykurtic
0.35→0.5	well sorted	+0.1→ +0.3	positively skewed	0.67→0.90	platykurtic
0.5→1.0	moderately sorted	+0.1→ -0.1	symmetrical	0.90→1.11	mesokurtic
1.0→2.0	poorly sorted	-0.1→ -0.3	negatively skewed	1.11→1.50	leptokurtic
2.0→4.0	very poorly sorted	-0.3→ -1	very negatively skewed	1.50→3.00	very leptokurtic
>4.0	extremely poorly sorted			>3.00	extremely leptokurtic

Smoothed frequency curves were compiled from individual values for the mean grain-size and sorting for each of the four sample sets and are presented in Fig. 4.2. The frequency distribution curve of mean grain diameters for the BIC sediments (Fig. 4.2.) is bimodal; most of the mean values occur around 0.25ϕ with a secondary mode of 1.28ϕ. BIC sediments are therefore classified as generally coarse-grained, with a subordinate quantity of samples being medium-grained. The sand-size fraction of the palaeochannel sediments plots as a unimodal frequency distribution with a

mode at 1.67ϕ classifying these sediments as medium-grained. Mean grain-sizes of beach sediments from respectively the BMC and KNC generate frequency distribution curves that are quite different in shape. The frequency distribution curve of the BMC sediments is practically unimodal (mode at 1.67ϕ), characterising most of the sand as medium-grained and the rest as coarser grained. By contrast, the frequency distribution curve of the KNC sediments spreads over a wide range and is weakly bimodal with modes at 0.40ϕ and 1.61ϕ. Consequently, similar proportions of sediments are characterised as coarse-and medium-grained. Fine-grained sediments constitute a very small part.

The frequency distribution curve reflecting sorting of the BIC sediments is bimodal (Fig. 4.2.) with a major mode at 1.29ϕ and a lesser mode at 0.92ϕ. BIC sediments are generally poorly sorted (σ_I > 1.0) although selective samples are moderately sorted. Palaeochannel sediments display similar sorting values compared to BIC sediments. Sediments from the two marine groups (BMC and KNC) generally exhibit better sorting than sediments from the BIC and palaeochannels. Both the frequency distribution curves of sorting values of the BMC and KNC sediments are polymodal, but the KNC sediments are slightly better sorted than those from the BMC. KNC samples are mainly moderately sorted with the rest of the sediments either well or poorly sorted. By contrast, equal proportions of the BMC sediments are poorly and moderately sorted.

Fig. 4.2. clearly shows that the KNC area was supplied with a wider range in grain-sizes in comparison with the BMC area that feature a more restricted grain-size range. This implies differences in the grain-size of the source material, competence of the transporting agent as well as contrasting sedimentological processes during and after deposition in the two areas (Folk and Ward, 1957; Friedman; 1961, 1967; Gale and Hoare, 1991). It is also clear that the BMC sediments either had a uniform source or significant recycling of detritus amongst stratigraphic successions has taken place. Fig 4.2. also indicates that more than one source contributed detritus to sediments in the KNC. Close inspection of individual mean-grain sizes shows that the sediments from the younger successions (RET and Upper CFS) are much

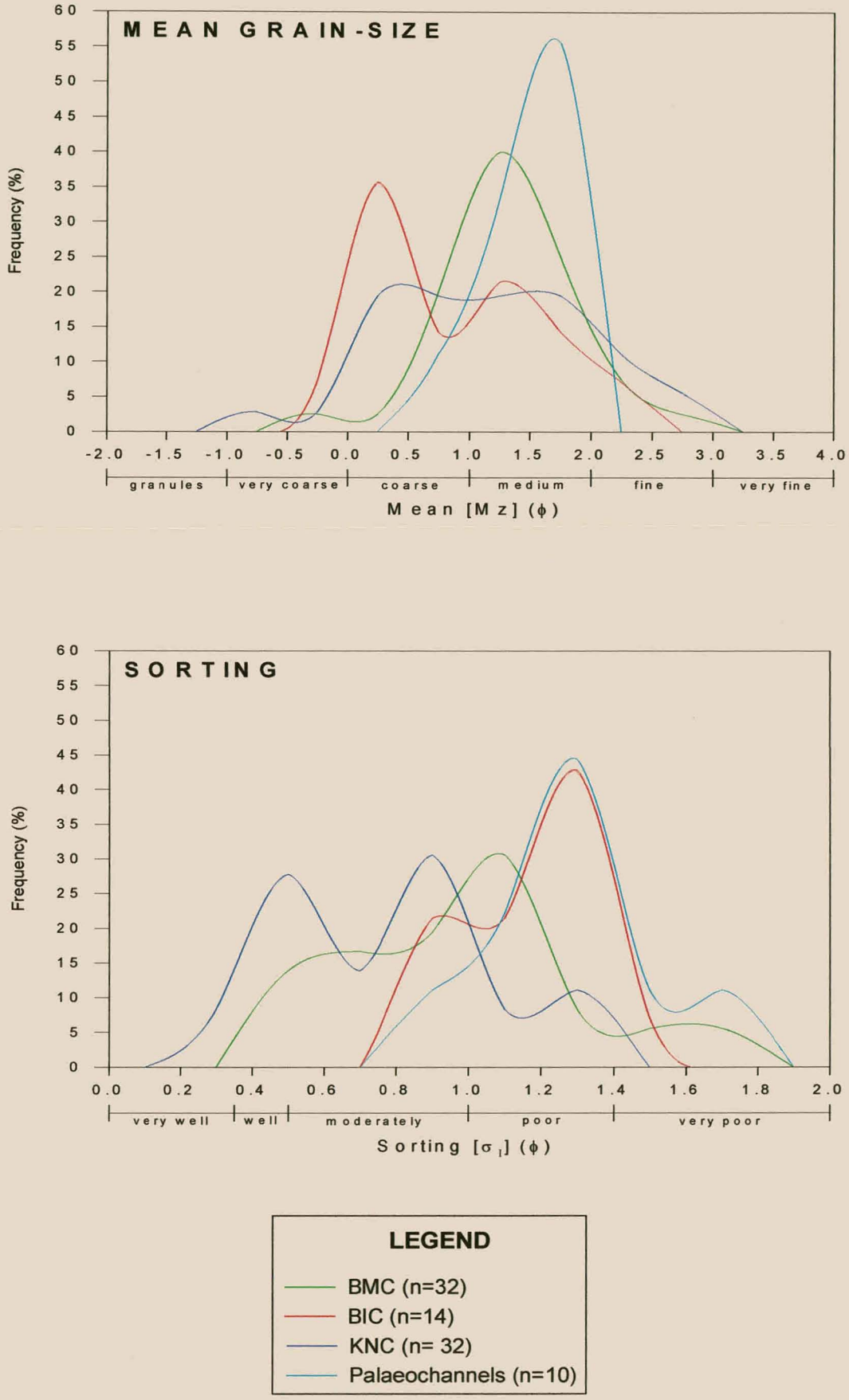

Figure 4.2. Frequency distribution of mean grain-size and sorting values for the studied sediments.

coarser than those from the older successions (Lower CFS and FGS); accounting for the bimodal distribution of grain-sizes in the KNC area.

Different sorting mechanisms were active during deposition among stratigraphic sequences as indicated by the polymodality of the frequency distribution curves of sorting (Folk and Ward, 1957; Mason and Folk, 1958). Individual grain size distributions support the opinion that both fluvial and marine deposition took place in several contrasting environments. A correlation analysis was performed to determine whether mean grain-size and sorting are interrelated. Fig. 4.3. shows there is no apparent trend between mean grain-size and sorting i.e., finer sediments are not necessarily better sorted than coarser sediments. This could indicate that factors other than normal hydraulic sorting controlled the observed grain-sizes. Such processes for instance would be active during storm deposition.

Previous investigations have shown that fluvial sediments are poorly sorted and fine-skewed in contrast with beach sediments that tend to be negatively skewed and well sorted (Folk and Ward, 1957; Friedman, 1961, 1967; Mason and Folk, 1958). In this study, the sorting and skewness characteristics of fluvial sediments are consistent with earlier studies, but most beach sediments of the KNC and BMC are poorly sorted and fine-skewed. Poor sorting and positive skewness of beach sediments could have been the result of post-depositional processes such as diagenetic alteration (Gale and Hoare, 1991; Lewis, 1984), where unstable minerals are preferentially removed. Original sorting characteristics of a sediment could also have been altered during high energy conditions such as during a storm period where different grain-size populations are mixed that are not necessarily in equilibrium with their environment (King, 1966; Martins, 1964; J.P. Le Roux, *pers. comm*). The relatively uncommon positive skewness values for marine samples are easily explained by the concentration of considerable amounts of heavy minerals in the finer grades (2.5-3.5ϕ) which shifts the skewness of the grain-size distribution to a positive value (Elsner, 1992; Ghosh and Chatterjee, 1994).

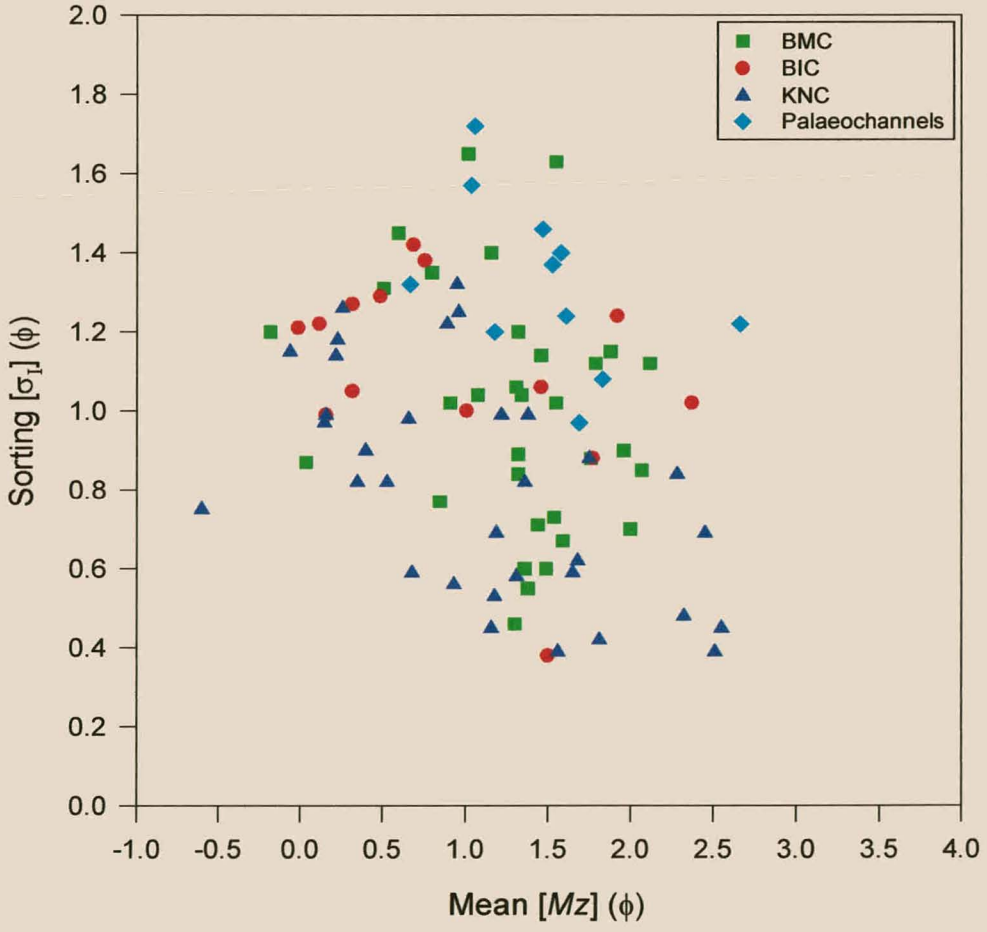

Figure 4.3. Bivariate plot of mean grain size against sorting for the studied sediments.

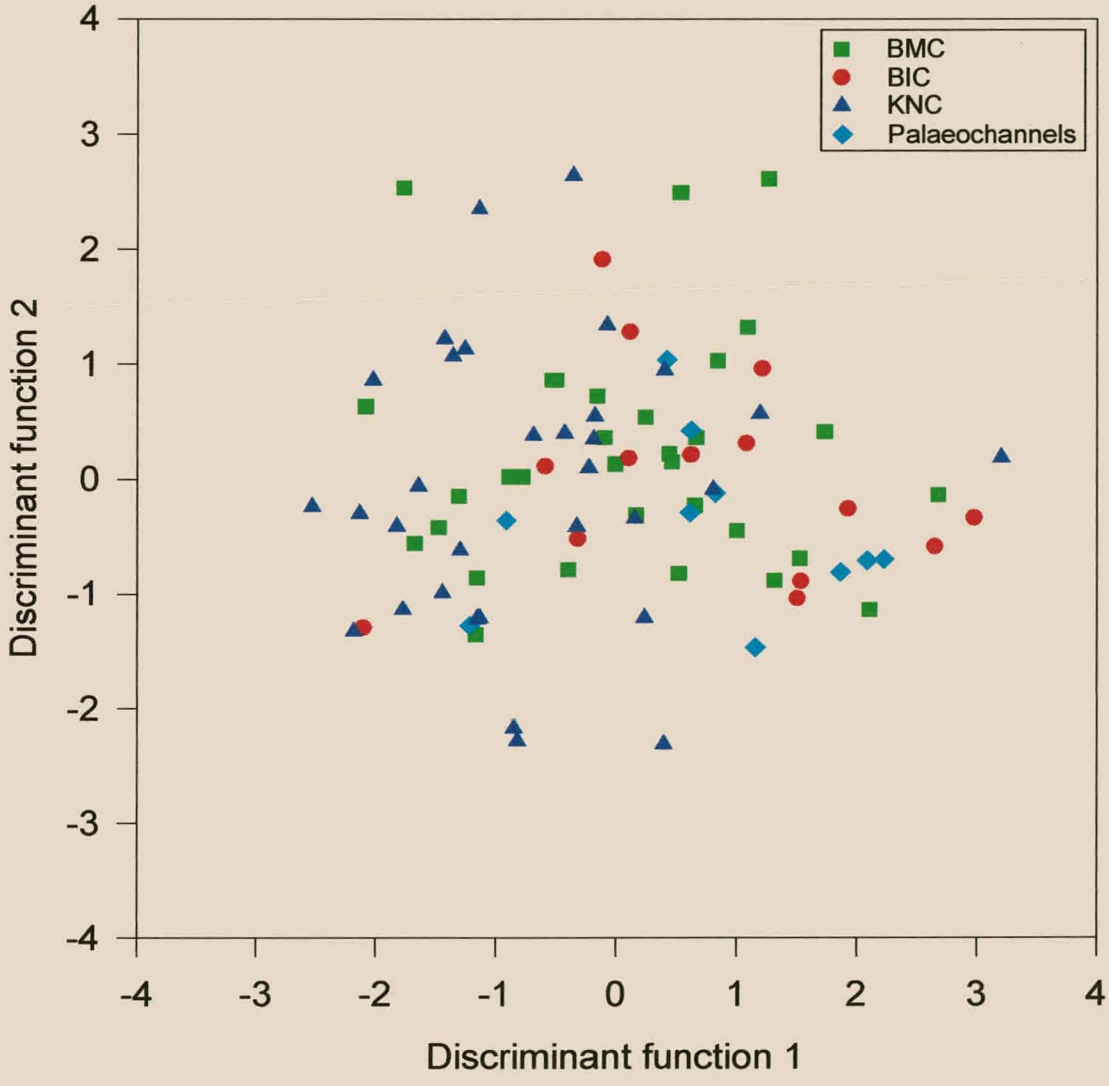

Figure 4.4. Discriminative plot based on the graphic approach with mean, sorting, skewness and kurtosis as the discriminant functions.

Numerous authors (Friedman, 1961, 1967; Martins, 1964; Mason and Folk, 1958; Carranza-Edwards and Rosalez, 1994) have shown that the interrelationship of grain-size parameters is useful in demarcating and classifying depositional environments. These authors made use of scattergrams of the grain-size parameters to discriminate between sediments derived from different environments. Constructing the boundaries that define each depositional field was unfortunately subjective and results differ greatly among studies. Consequently this method of discrimination was rejected and it was decided to rely on discriminant analysis using the grain-size parameters as variables.

Discriminant analysis performed with Statistica® shows that the fields associated with sediments from fluvial and marine environments overlap greatly (Fig. 4.4). Although this could signify similar hydraulic conditions and grain-sizes, it clearly reflects the poor sensitivity of this method in discriminating depositional environments. In similar studies, Klovan (1966), Sutherland and Lee (1994) and Ghosh and Chatterjee (1994) also acknowledged limited success in employing this technique to discriminate sedimentological environments. In conclusion, although individual textural attributes clearly indicate contrasting depositional environments, current discriminant statistics failed to verify this.

4.2. Grain roundness

The roundness of individual ilmenite and garnet populations from selective thin sections representative of each stratigraphic sequence of the BMC, BIC and KNC were investigated. Grains from palaeochannel sediments comprise the fourth group. Mineral grains were compared to the visual roundness scale of Shepard and Young (1961) where roundness is expressed by six classes ranging from very angular to well-rounded (Fig. 4.5A). About 200 grains from each thin section were chosen to satisfy statistical confidence levels and the results are shown in Appendix E and presented as barcharts in Fig. 4.5B.

In all the samples studied, garnets display some degree of angularity in contrast with ilmenites that are more rounded (Fig. 4.5B). There is no significant variation in the

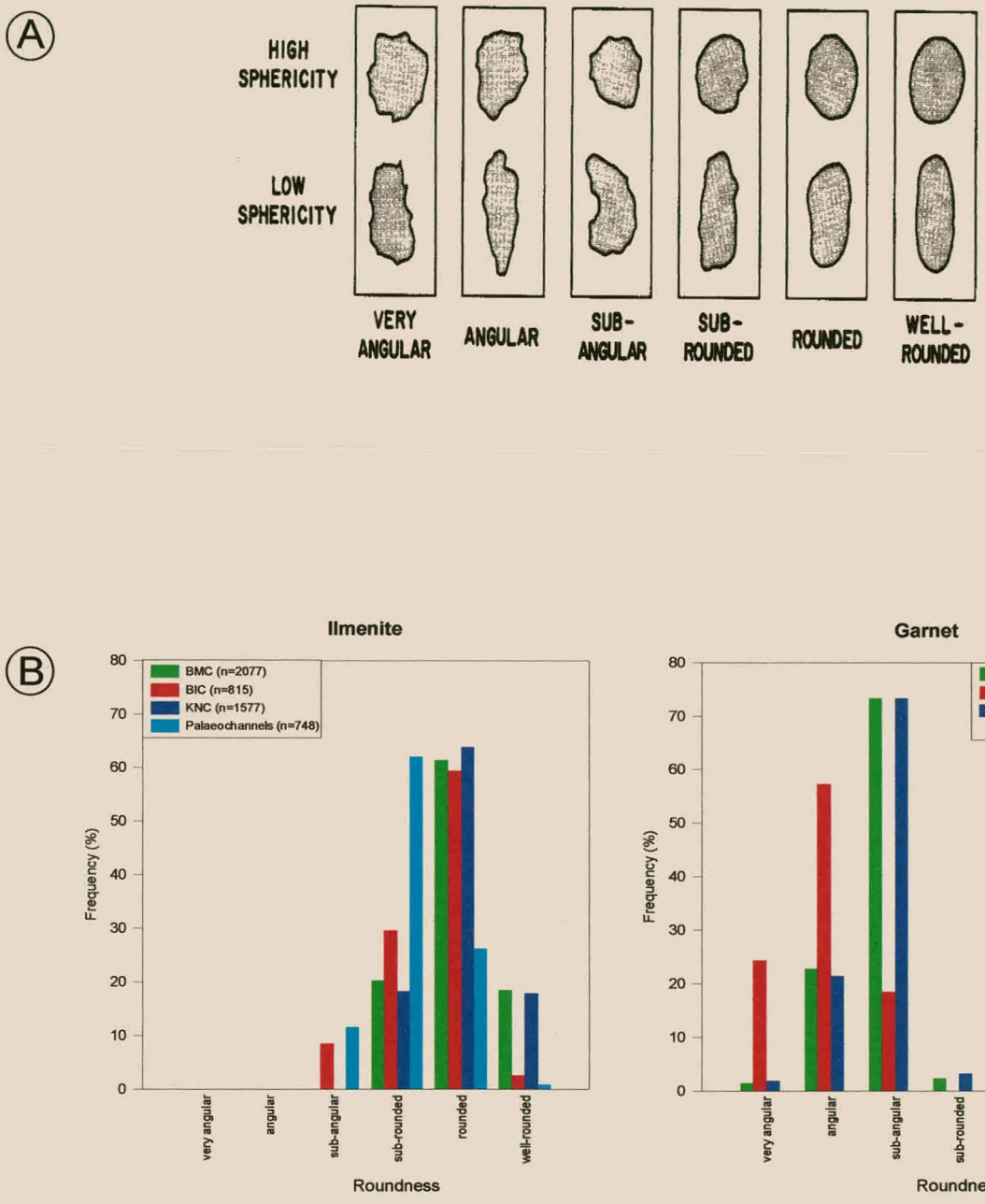

Figure 4.5. A) Diagram for visual comparison of roundness for sand grains (after Shepard and Young, 1961). B) Roundness class-frequency histograms of ilmenite and garnet grains from the BMC, BIC, KNC and palaeochannels.

roundness of the garnets and ilmenites from the BMC and KNC. Both the KNC and BMC are marked by rounded to well-rounded ilmenites and angular to sub-angular garnet populations. By comparison, garnets and ilmenites from the BIC are slightly more angular. The same trend is evident for ilmenites from the palaeochannels.

Semi-quantitatively, monazite and the ultrastable zircon and rutile are well rounded to rounded in all environments. In a similar manner, beach environments contain major amounts of sub-angular and minor quantities of subrounded minerals while the fluvial environments contain considerable amounts of angular and subangular grains. It is interpreted that the ilmenite, zircon, rutile and monazite and to a lesser degree the unstable minerals, were recycled from pre-existing sedimentary sources.

4.3. Clay mineralogy

The mud fraction of the palaeochannel samples were separated into 5-63μm (silt) and <5μm (clay) fractions that were subjected to XRD analysis. The samples were subjected to a series of dissolution techniques prior to separation, which are fully discussed in Appendix B. Semi-quantitative mineralogical results and representative diffractograms are presented in Appendix F.

Peak identification in correspondence with the JCPDS database established the presence of two major phases as kaolinite-1A (PDFno. 14-0164) and quartz (PDFno. 33-1161; Fig. 4.6). All eight samples have the same mineralogical composition in both the 5-63 μm and 5 μm fractions. The 5 μm fraction consists exclusively of kaolinite, whereas the 5-63 μm fraction is a mixture of kaolinite and other clay minerals. Kaolinite ranges in abundance from 60-99%. Analyses furthermore reveal lower intensity peaks at d-spacings of 7.25, 10 and 14 Å. These peaks suggest the minor presence of illite, montmorillonite and chlorite, but this could not be verified without detailed XRD analysis or differential thermal analysis (DTA), which was not done.

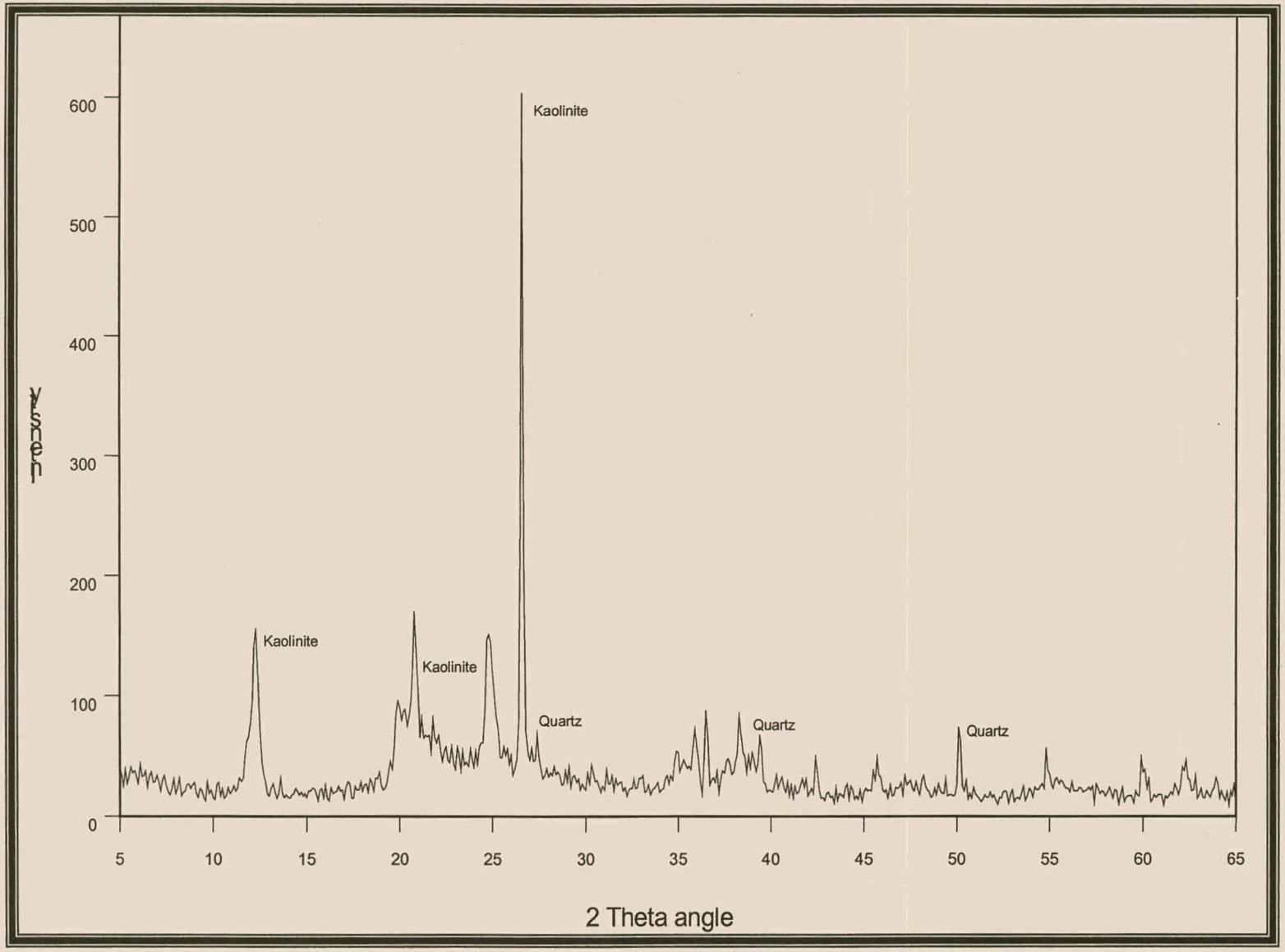

Figure 4.6. X-ray diffractogram of a clay sample representative of the palaeochannel sediments.

Millot (1970) presents the following transformational series of clay minerals during diagenesis and/or weathering in a soil profile:

feldspars ⇒ micas\sericite ⇒ kaolinite

This series suggests that the kaolinite was derived from a feldspathic source. Millot (*op. cit.*) states that the presence of massive kaolinite as encountered in the palaeochannels at Kleinzee suggests strong weathering of feldspars in a well drained, acidic environment, which persisted in a humid and/or tropical climate. Relicts of partly kaolinised feldspar pieces, support the idea that the parent rock contained a significant feldspathic component. The data are in general agreement with the work of Pether (1994) who identified kaolinite as the major clay mineral in the channel sediments in the Hondeklip Bay area. In a similar fashion, Pether (*op. cit.*) regards the kaolinite to be derived from the decomposition of feldspars.

4.4. Sediment composition

4.4.1. Heavy mineral content

Bromoform with a density of 2.82 g/cm^3 was used to separate the light and heavy fractions of samples. The technique is summarised in Appendix B. The total heavy mineral (THM) content of samples expressed as weight percentages is tabulated in Appendix G and is also depicted in geological cross-sections (Addendum A). The THM content refers to the fraction that has a density greater than 2.82 and includes ore minerals (ilmenite, rutile, hematite, magnetite), silicate minerals (zircon, pyroxenes, amphiboles, garnet), rock fragments and accessory minerals such as aluminosilicates, staurolite, titanite, certain feldspars and shell fragments.

The total heavy mineral (THM) content of the sediments is variable and averages 6% for both the BMC (n=32) and KNC (n=32); 5% for the BIC (n=14) and 1% by weight for the palaeochannels (n=10). These figures are however deceptive, since more than 70% of the studied sediments have a THM content of less than 2.5% (Fig. 4.7.), which is considerably lower than the THM content of ~5% of an average modern sand (Pettijohn, 1975). The rest of the sediments in each mining area have a wide and variable THM content (5-60%) as seen in the scattered anomalies on the

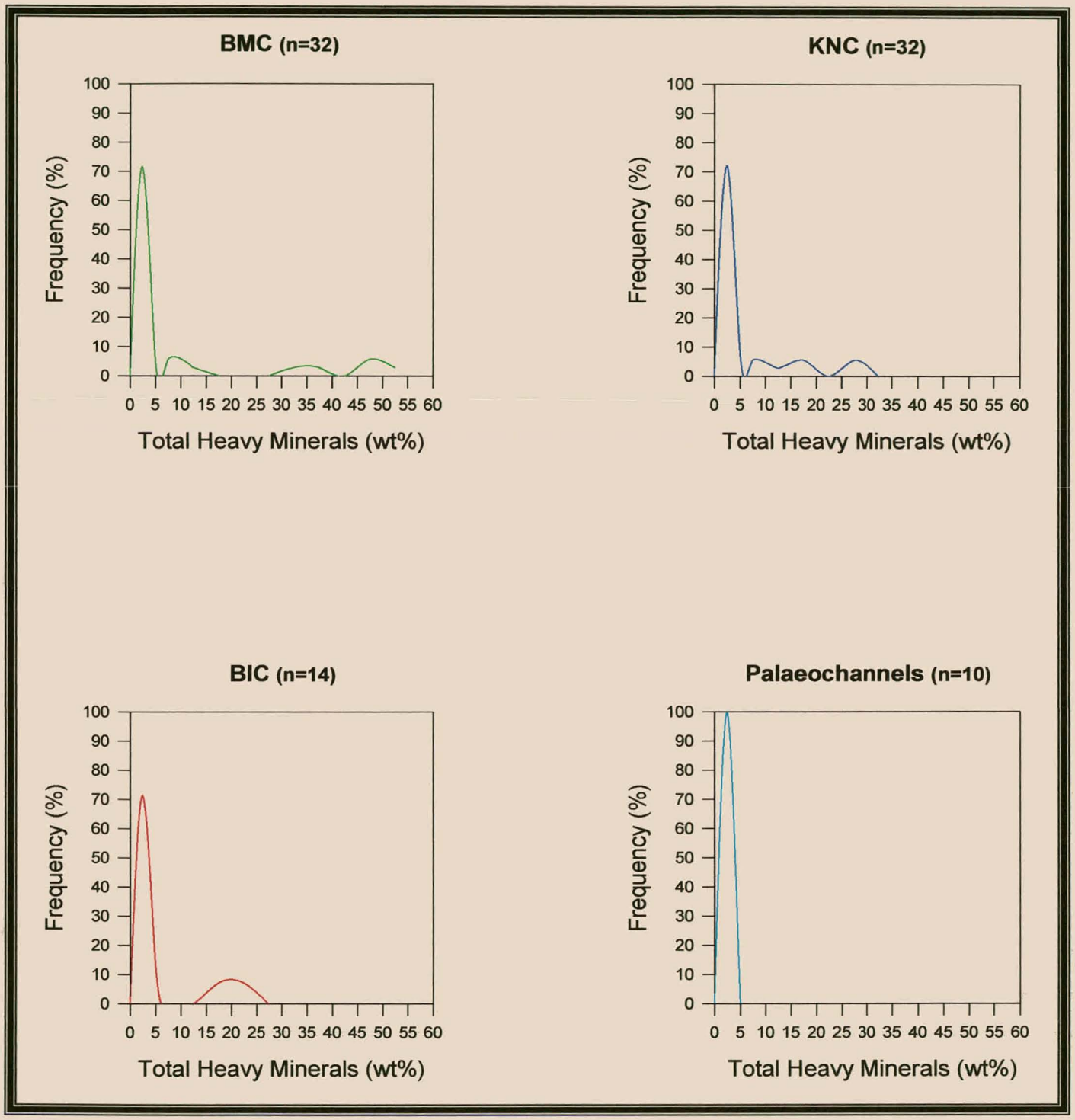

Figure 4.7. Frequency distribution diagrams of the total heavy mineral content (THM) expressed as weight percentage, for the BMC, BIC, KNC and palaeochannels.

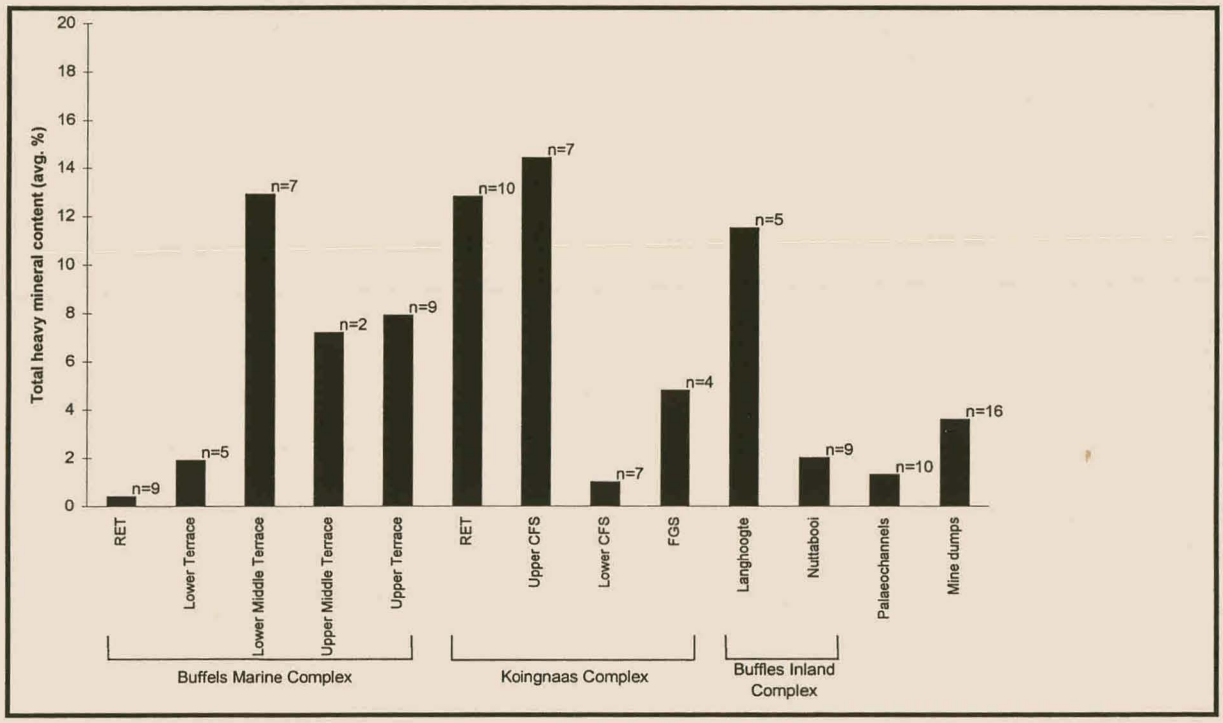

Figure 4.8. Average total heavy mineral content of the studied successions.

frequency plot. Localised heavy mineral concentrations are portrayed by these infrequent anomalies. Mine heap samples average 3.6% THM (n=16). Although no quantitative method was followed, the studied heavy minerals generally concentrate in the 2-3 ϕ fractions. The exception however is heavy mineral-enriched sediments where the heavy minerals are concentrated over a wider grain-size range.

The relative older sediments of the Upper and Middle Terraces (45-90m *amsl*) of the BMC are marked by higher THM values (Fig. 4.8.) compared to the much younger Lower Terrace and RET sediments that show no significant mineralisation. Conversely, the younger sediments from the RET and Upper CFS in the KNC area feature high THM values. The older, Pliocene FGS and Early Pleistocene Lower CFS sediments are generally depleted in heavy minerals. The economic importance of the heavy mineral occurrences will be discussed in a later chapter.

Fig. 4.9A illustrates that there is no apparent relationship between median grain diameter and THM content within a lithological unit. However, it is notable that samples with a high THM content show a clustering of median grain diameters around 0.5-1.5 ϕ. Correspondingly, no clear correlation between sorting and THM content is apparent; i.e., samples that are better sorted do not necessarily display the highest THM content (Fig. 4.9B). This anticipates that processes other than hydraulic sorting were responsible for the anomalous accumulation of heavy minerals in certain lithological units.

The expected mechanism for the heavy mineral concentration in the marine deposits is believed to be a powerful wave-regime prevailing during high-energy conditions with favourable burial conditions considered essential in preserving the mineralisation (Force, *op. cit*). Normal wave action combined with the swash and backwash motion facilitates deposition of heavy minerals as thin swash lamellae in the foreshore (Plate 4A), whereas thick heavy mineral layers are the result of powerful waves in the foreshore (Plate 4B). High waves produced during stormy weather erode a significant part of the foreshore and emerged backshore and this material of mixed sand is kept in suspension by an agitated sea. The panning action

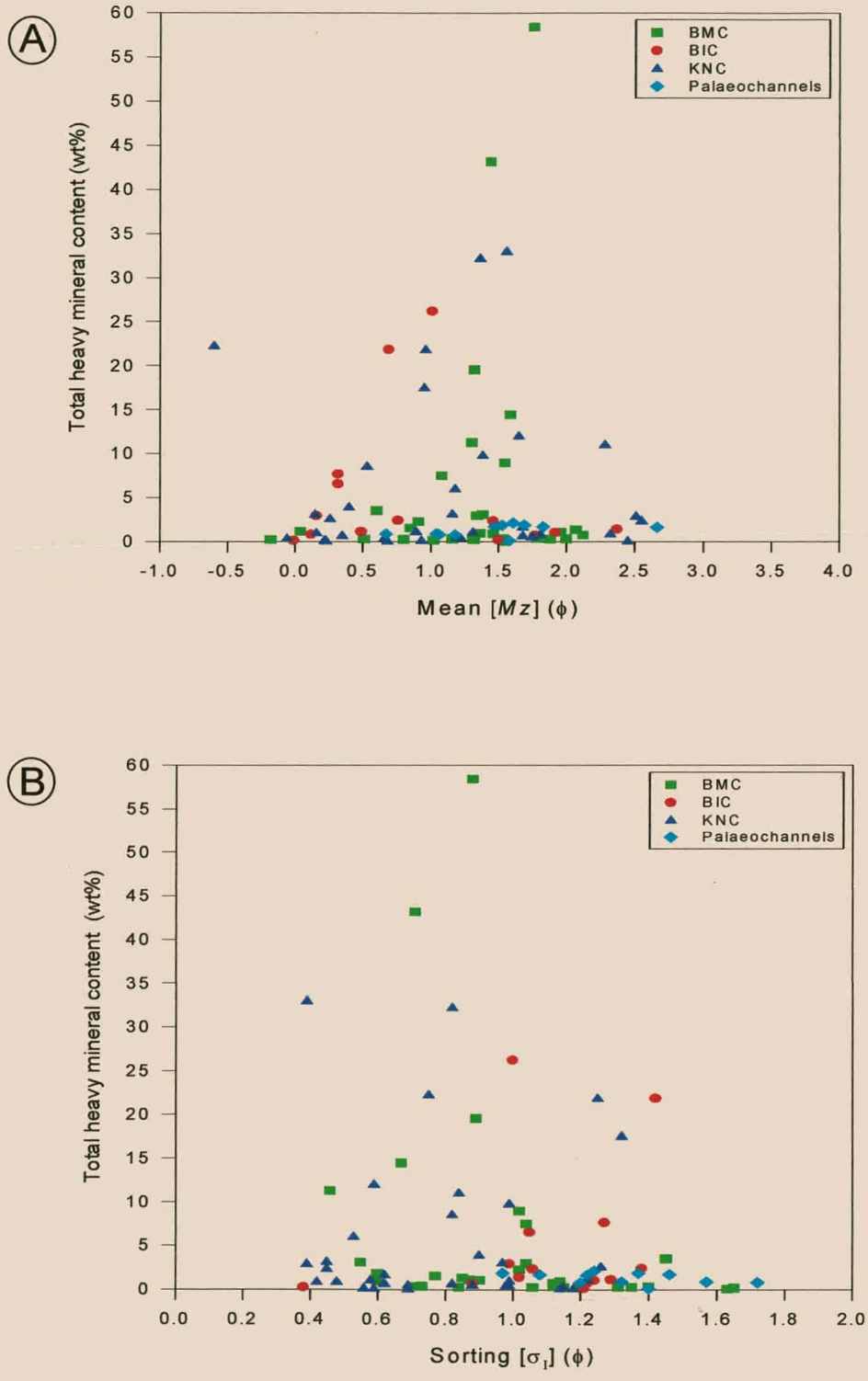

Figure 4.9. Bivariate plots of A) mean grain size and B) sorting against total heavy minerals present.

A

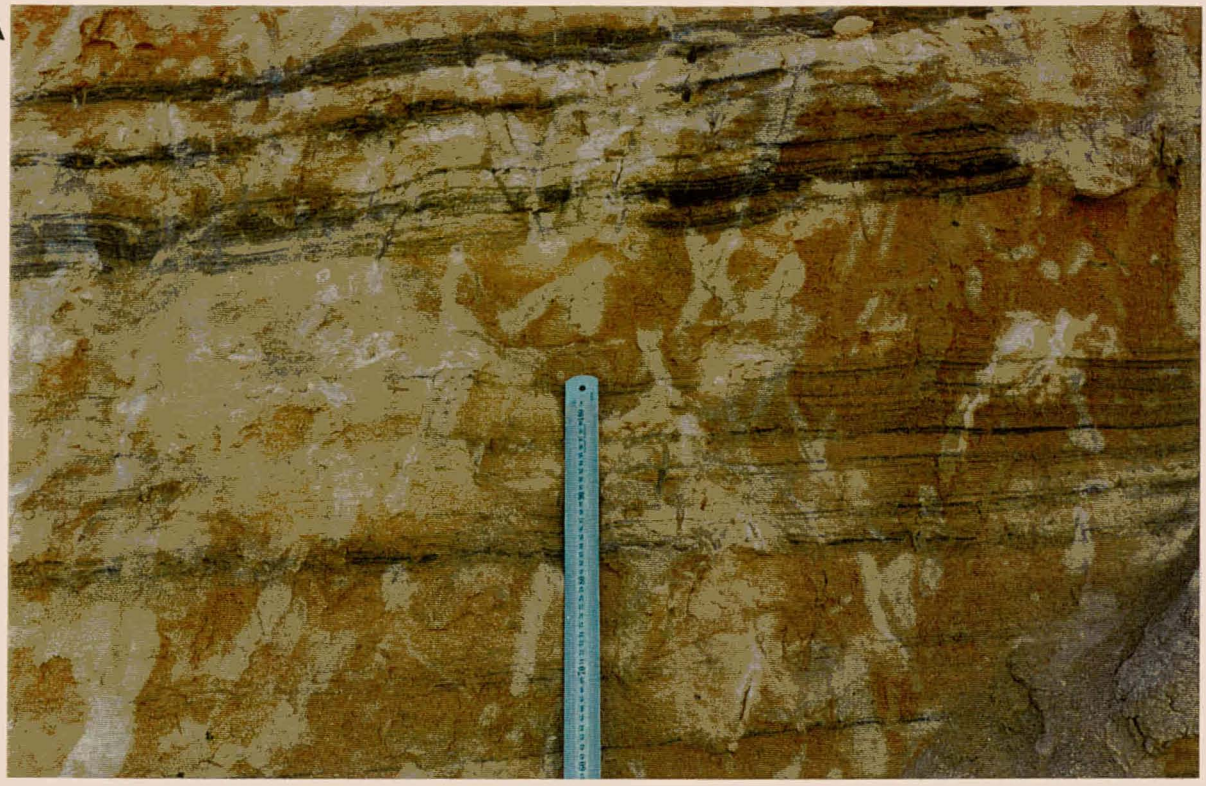

B

Plate 4.

A) Low angle, swash-laminated heavy minerals indicate a foreshore environment.

B) Thick heavy mineral layers overlying boulder beaches are associated with storm deposits in the foreshore.

Length of ruler is 1m.

of the waves carries the lighter minerals away for deposition at a lower location along the beach, leaving the heavy minerals behind to form thick residual concentrates. When the sea reaches its original lower position these placer accumulations on the backshore are sheltered and remain inaccessible until the next storm period. A low concentration of heavy minerals possibly reflects the reduction of source material or the absence of suitable concentrating mechanisms within contrasting depositional environments (McLane, 1995).

High concentrations of heavy minerals in the BIC sediments are associated with sedimentation on point bars (L.M. Cilliers, *pers. comm*). In the KNC, heavy minerals are concentrated at 6-14m *amsl*, but the most significant occurrence is between 20-32m *amsl* Field observations support the speculation that these strandlines with higher than average heavy mineral grades correlate with local sea-level stillstands (De Decker, *op. cit*). It is interesting to note that the Namakwa Sands heavy mineral deposit has high-grade strandlines at similar elevations. In the BMC, heavy minerals were concentrated during the Pliocene on well-developed wave-cut platforms during similar sea-level stillstands, but at much higher elevations (45-90 m.a.m.s.l). Major deposits that are considered to have formed during world-wide, Pliocene transgressive-regressive events include Trail Ridge, Florida; Eneabba, Western Australia; Lakehurst, New Jersey; and deposits from the western Murray basin, Victoria, Australia. The majority of heavy minerals in these deposits are typically concentrated between equivalent elevations of 46 to 96m *amsl* (Carpenter and Carpenter, 1991; Pirkle *et al.*, 1991; Puffer and Cousminer, 1982; Elsner, 1992; Williams, 1990).

4.4.2. Heavy mineral composition

Visual inspection of the studied sediments indicates that they are mature, containing quartz as a major constituent accompanied by minor quantities of feldspar. Shell debris often contributes significant amounts (0-12%) to the light fraction. A whole range of heavy minerals present in minor to trace amounts constitutes the rest of the mineral assemblage. These heavy minerals include Fe-Ti oxides, hematite,

magnetite, garnet, zircon, pyroxene, amphibole, staurolite, apatite, aluminosilicates, titanite, epidote, monazite, rutile and glauconite.

Heavy mineral proportions of individual samples have been calculated from point-count data and are presented in Appendix G. Marcasite and glauconite were noted, but not counted. The heavy mineral data are presented in barcharts for each of the stratigraphic successions (Fig. 4.10). In addition, these mineral frequencies were also transferred to the geological cross-sections (Addendum A). The opaque fraction incorporates all the Fe-Ti minerals as well as magnetite and hematite. The term ilmenite refers to the fraction that contains primary ilmenite and all its alteration products, but excludes hemo-ilmenite, which is grouped with ilmo-hematite and other complex Fe-Ti phases as Fe-Ti intergrowths. Terminology has been adopted from Carver (1971) to describe mineral abundance: predominant or abundant: >>20%; fairly abundant: 10-20%; minor: 5-10%; accessory: 1-5%; trace: <1%.

Generally, a similar suite of heavy minerals marks the studied sediments, the only difference being the proportion of each mineral present. Apart from the palaeochannels, heavy mineral populations are generally diverse and in every single case are dominated by Fe-Ti oxides of which ilmenite constitutes the greatest part. The remainder of the heavy mineral suites comprises variable amounts of hematite, zircon, garnet, hornblende, pyroxene and epidote whereas magnetite aluminosilicates, monazite, titanite, staurolite, rutile and apatite are always present as traces or accessories. Palaeochannel samples are unique since they almost exclusively host zircon and opaque minerals in similar quantities. Zircon predominates, followed by opaques (Fig. 4.10). The two fluvial deposits of the BIC also have distinctive heavy mineral suites. Langhoogte samples are characterised by almost 95% opaques and in comparison, Nuttabooi heavy mineral suites comprise around 75% opaques and abundant zircon.

Heavy mineral ratios for the marine sediments from the Lower Middle, Upper Middle and Upper Terraces of the BMC are similar; the associated suites contain ~80% opaques and minor amounts of garnet and zircon as well as accessory pyroxene,

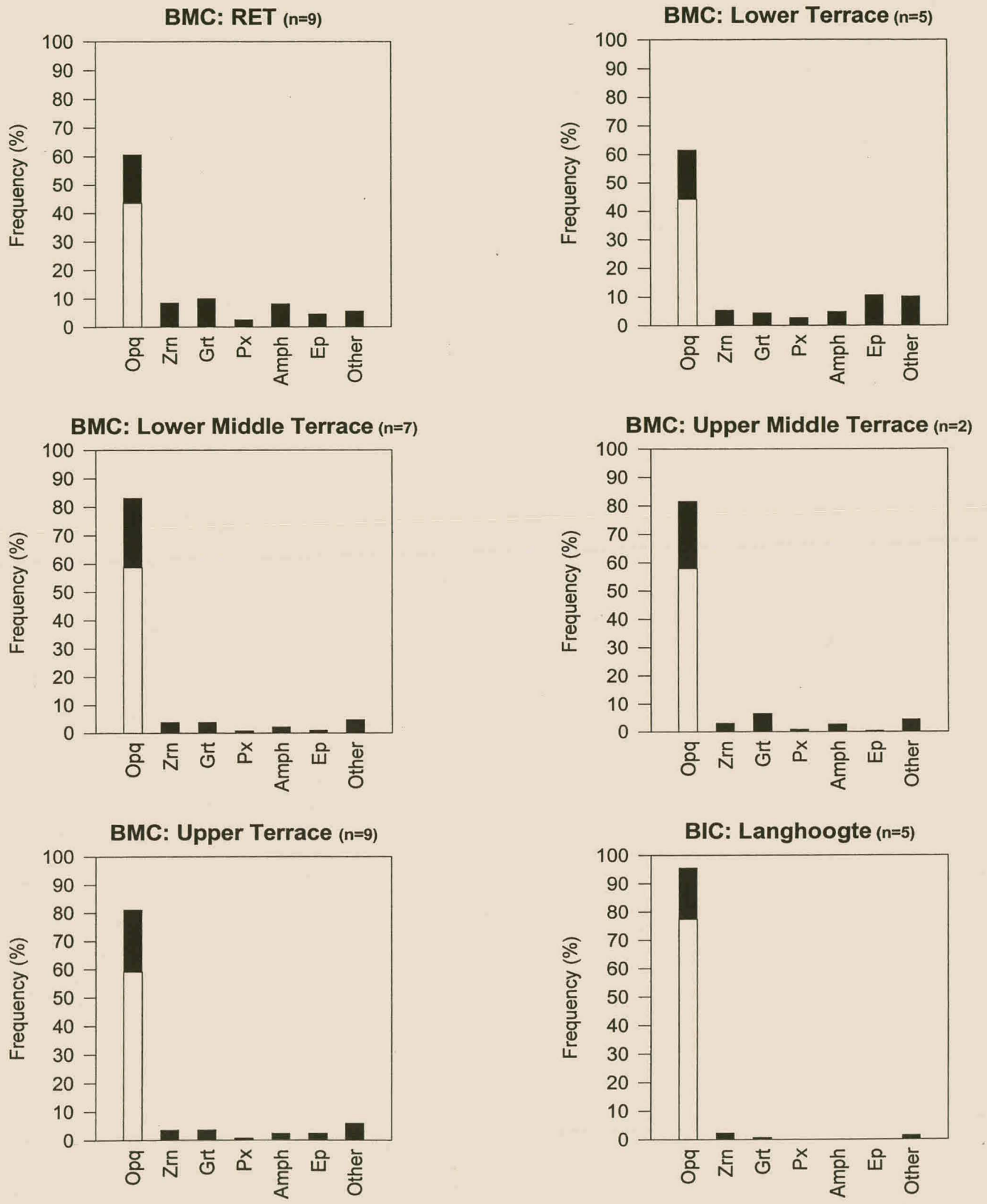

Figure 4.10. Mineral abundance histograms of the most important minerals in the sedimentary units. Mineral fractions were compiled from point count data. Mineral fractions are indicated by: Opq= opaque minerals; the ilmenite proportion of the opaque fraction is represented by the unshaded area; shaded area represents Fe-Ti intergrowths, magnetite and hematite. Grt=garnet; Zrn=zircon, Px=pyroxene; Amph=amphibole; Ep=epidote; Other= apatite, staurolite, kyanite, titanite, rutile, monazite.

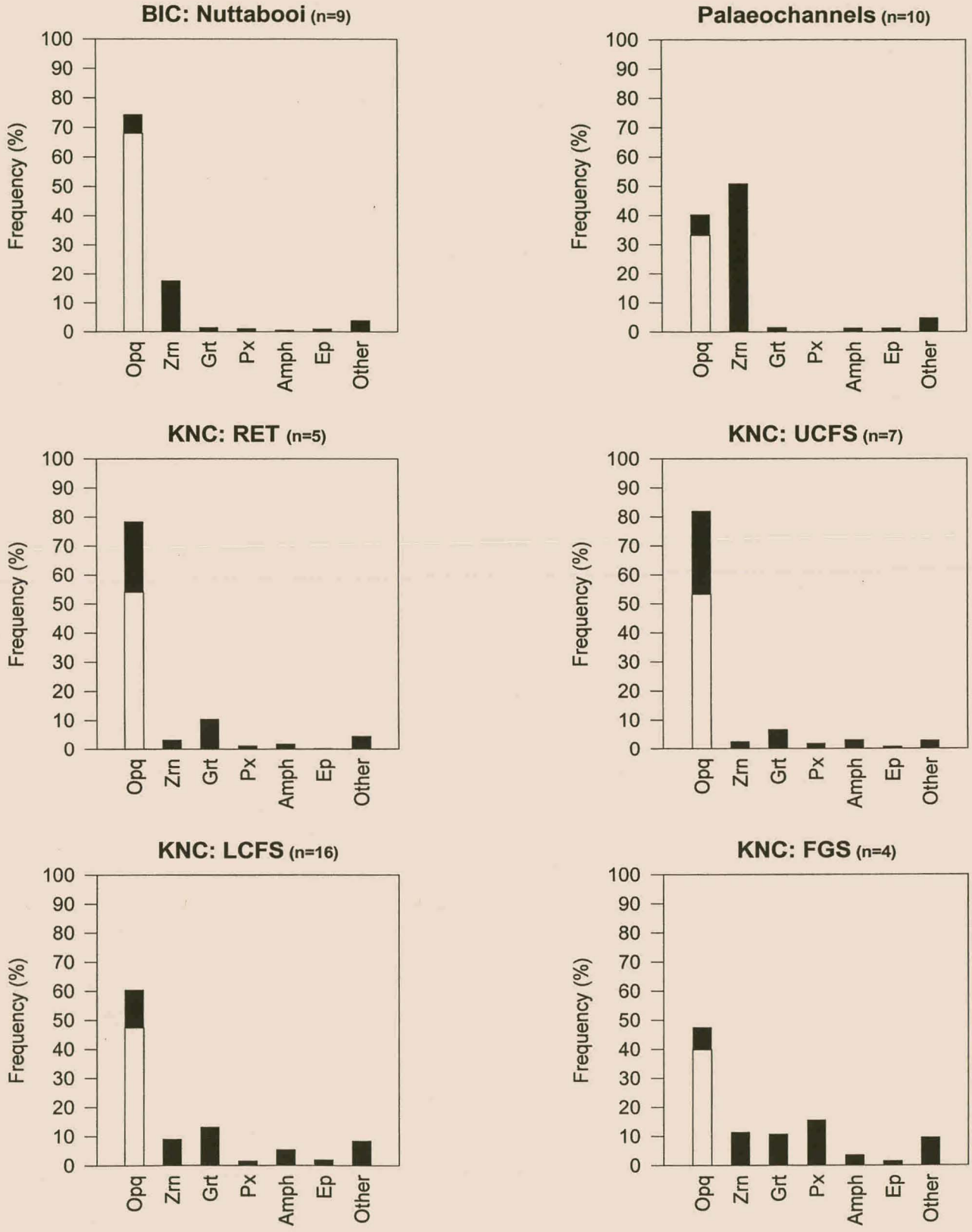

Figure 4.10. (Cont.) Mineral abundance histograms of the most important minerals in the sedimentary units. Mineral fractions were compiled from point count data. Mineral fractions are indicated by: Opq= opaque minerals; the ilmenite proportion of the opaque fraction is represented by the unshaded area; shaded area represents Fe-Ti intergrowths, magnetite and hematite. Grt=garnet; Zrn=zircon, Px=pyroxene; Amph=amphibole; Ep=epidote; Other= apatite, staurolite, kyanite, titanite, rutile, monazite.

amphibole and apatite. Other minerals such as aluminosilicates, staurolite, titanite, rutile and monazite rarely exceed trace quantities. In comparison with these older terraces, the heavy mineral suites of the younger RET and Lower Terrace sediments are made up of lesser amounts of opaques (60%), but correspondingly contain greater amounts of zircon and garnet (Fig. 4.10). A significant increase in the unstable minerals such as hornblende, epidote, pyroxene and apatite is also apparent. The THM composition of the youngest marine sediments in the KNC which belong to the RET and Upper CFS, resemble those pertaining to the Lower Middle, Upper Middle and Upper Terraces of the BMC. In general, heavy mineral suites of the Upper CFS and RET consist of comparable quantities of opaques (~80%) and zircon abundance is also comparable, but garnet shows a relative increase (Fig. 4.10). Accessory pyroxene and hornblende together with trace minerals makes up the rest of the heavy fraction.

The oldest sequence in the KNC, namely the FGS has heavy mineral suites that are characterised by a low abundance of opaques (48%; Fig. 4.10). The FGS heavy mineral suites characteristically contain on average, the highest clinopyroxene content in the KNC and in the entire study area. A noticeable aspect is also the considerable increase in garnet and zircon. Apatite and hornblende are distributed as accessories along with a range of trace minerals. In comparison with the FGS, the Lower CFS sediments have similar zircon and garnet abundance, but the opaque mineral content (60%) is significantly higher (Fig. 4.10). Unlike the FGS, heavy mineral suites of the Lower CFS are depleted in clinopyroxene, but are richer in hornblende. Variable amounts of trace minerals are also present.

The present-day Buffels River contains 59% opaques, abundant hornblende and fairly abundant garnet. Zircon, clinopyroxene and epidote occur in accessory quantities. By contrast, the present-day Swartlintjies River contains a lower amount of ilmenite (32%), with appreciable amounts of zircon, hornblende, epidote and apatite. Heavy mineral fractions of the mine heaps are dominated by opaques (66%). The rest of their heavy mineral suites are composed of fairly abundant zircon,

abundant hornblende and accessory quantities of epidote, garnet and apatite (Fig. 4.10).

Heavy mineral data indicate that the valuable minerals ilmenite, zircon and rutile vary (increase) with the maturity of the heavy mineral assemblage and generally comprise a large part (42-100%) thereof. Ratios of ore minerals to gangue vary for individual samples and the most favourable ratios are associated with samples that contain appreciable amounts of total heavy minerals. It is apparent that the heavy fractions of those sands with the greatest THM contain the greatest percentage of ilmenite and zircon, which are the heaviest of valuable minerals. On the contrary, minerals of intermediate specific gravity which are also economically less important, such as hornblende, pyroxene and epidote, are much more abundant in those sands with a small heavy mineral content. Throughout the entire study area, rutile uniformly constitutes only 1% of the valuable fraction. Heavy mineral populations of the BMC and KNC comprise on average equal amounts of ilmenite (51% of the THM) together with 6 and 8% zircon respectively. Ilmenite accounts for a much lower proportion (33%) of the palaeochannel samples, but zircon abundance on average is the highest (51%) of the entire study area. Heavy mineral suites in the BIC are relatively enriched in ilmenite averaging 72% of the THM and zircon comprises 8% of the heavy fraction.

4.4.3. Heavy mineral assemblages

The character of the heavy mineral suites is qualitatively uniform throughout the study area, but the relative abundance of mineral species and groups vary temporally and spatially. Principal component and factor analysis of heavy mineral abundance using Statistica® were utilised to establish the best combination of mineral variables that explain the variance between samples. The opaque minerals, zircon, garnet, pyroxene, hornblende and epidote were recognised as the prime contributors to variance of mineral abundance. Other minerals such as aluminosilicates, monazite, staurolite, titanite and apatite are considered insignificant factors because of their relatively lower abundance and inconsistent distribution. The single extracted factor loads heavily (+) on the opaque minerals, zircon and garnet,

whereas pyroxene, amphibole and epidote loads negatively (Fig. 4.11). The relevant factors were utilised to construct the most significant heavy mineral assemblages for the stratigraphic sequences. The results are summarised in Table 4.2.

Visual inspection of the heavy mineral data and principal component analysis suggests that the sediments of the study area have mineral assemblages typified by two components (Fig. 4.11). These components are marked by a difference in mineral density and chemical stability. The dense and chemical stable mineral component is represented by the opaque minerals, garnet and zircon, while hornblende, clinopyroxene and epidote depict the chemically less stable and less dense mineral component. The stable mineral component is present and predominant in all the stratigraphic successions, whereas the unstable component is present in particular stratigraphic successions. Consequently, the relative magnitude of these components within a heavy mineral suite has a direct relationship with the maturity of the heavy mineral assemblage and host sediments.

Compared to the immature heavy mineral assemblages of the RET and Lower Terrace sediments, the older Middle and Upper Terraces sediments are marked by distinctive mature heavy mineral assemblages (Table 4.2). Equivalent mature heavy mineral assemblages are typical of the RET and Upper CFS sediments in the KNC area. FGS sediments feature a diagnostic heavy mineral assemblage which is the most diverse (immature) in the whole study area (Table 4.2). Apart for an increase of hornblende at the expense of pyroxene, the younger Lower CFS sediments have similar heavy mineral assemblages.

In comparison with sediments from the BMC and KNC, both the BIC deposits (Nuttabooi and Langhoogte) are marked by a very mature mineral assemblage (opaques-zircon). Similarly, the palaeochannels are characterised by a simple suite of resistant heavy minerals such as zircon and ilmenite. The heavy mineral assemblages of the Buffels and the Swartlintjies Rivers are similar, except that garnet is significantly present in the Buffels River.

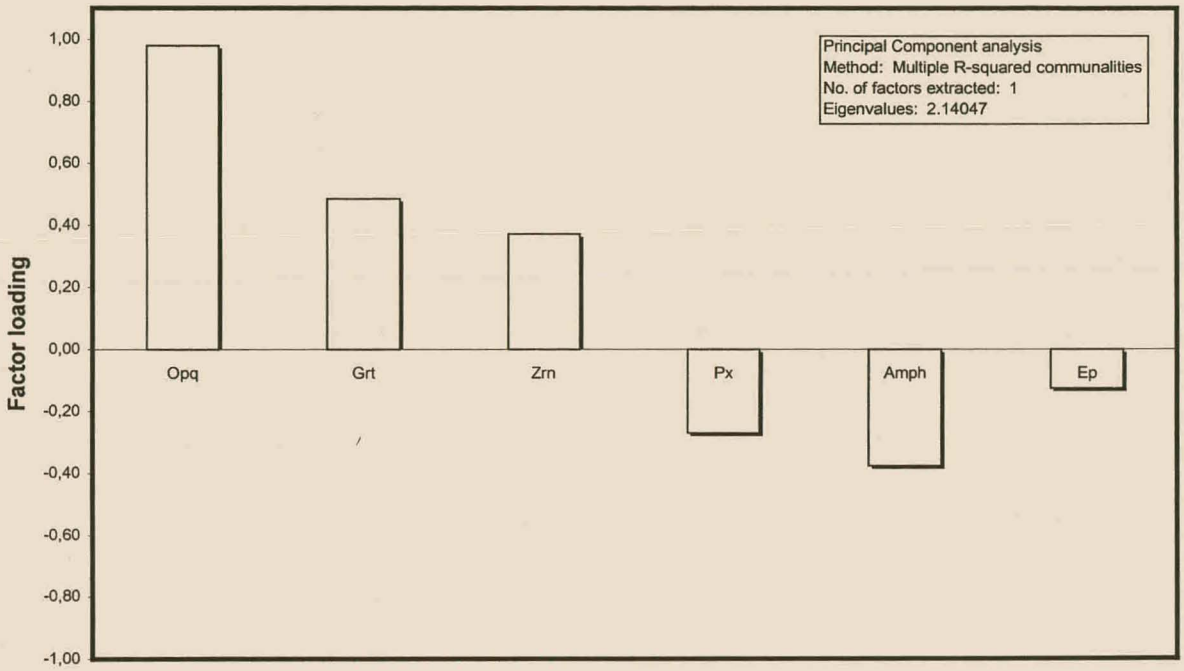

Figure 4.11. Factor loadings obtained from principal component analysis for the significant minerals. Opq=opaques; Grt=garnet; Zrn=zircon, Px=pyroxene; Amph=amphibole; Ep=epidote.

Table 4.2. Heavy mineral assemblages of stratigraphic successions in the three mining areas.

Stratigraphic succession	Heavy mineral assemblage
BMC	
RET	opaques-garnet-zircon-hornblende-epidote
Lower Terrace	opaques-hornblende-zircon-garnet-epidote
Lower Middle Terrace	opaques-garnet-zircon
Upper Middle Terrace	opaques-garnet-zircon
Upper Terrace	opaques-garnet-zircon
KNC	
RET	opaques-garnet-zircon
Upper CFS	opaques-garnet-zircon
Lower CFS	opaques-garnet-zircon-hornblende
FGS	opaques-garnet-zircon-clinopyroxene-hornblende
BIC	
Nuttabooi	opaques-zircon
Langhoogte	opaques-zircon
Palaeochannels & rivers	
Palaeochannels	opaques-zircon
Buffels River	opaques-garnet-zircon-epidote-hornblende-clinopyroxene
Swartlintjies River	opaques-zircon-epidote-hornblende-clinopyroxene

A discriminant analysis using the significant factors obtained from factor analysis, was performed to evaluate the differentiation of stratigraphic sequences based on their heavy mineral assemblage. Despite the similar mineral assemblages proposed for the palaeochannels and the BIC sediments, the latter are well discriminated from the fluvial sediments of the palaeochannels (Fig. 4.12). This could be attributed to the presence of trace amounts of minerals other than zircon and opaques in the BIC sediments. Discriminatory function analysis confirm that sediments from the RET and Lower Terrace are marked by a slightly different heavy mineral assemblage, which is well distinguished from sediments from the Upper and Middle Terraces for which a similar heavy mineral assemblage has been determined. Sediments from the FGS and Lower CFS in the KNC seem to be well discriminated from the Upper CFS and RET sediments that have a strikingly similar compositional character (Fig. 4.12).

Sediments from the marine environments exhibit similar mineral assemblages as can be seen from partial overlap of their respective fields (Fig. 4.12). This is best explained by interdependent geological factors such as source rock mineralogy, hydraulic conditions in the depositional environment during deposition and diagenetic processes (Stapor, 1973; Pettijohn, 1975; Morton and Smale, 1990). The effect of these factors on heavy mineral assemblages in the study area was investigated and will be discussed in a Chapter 6.

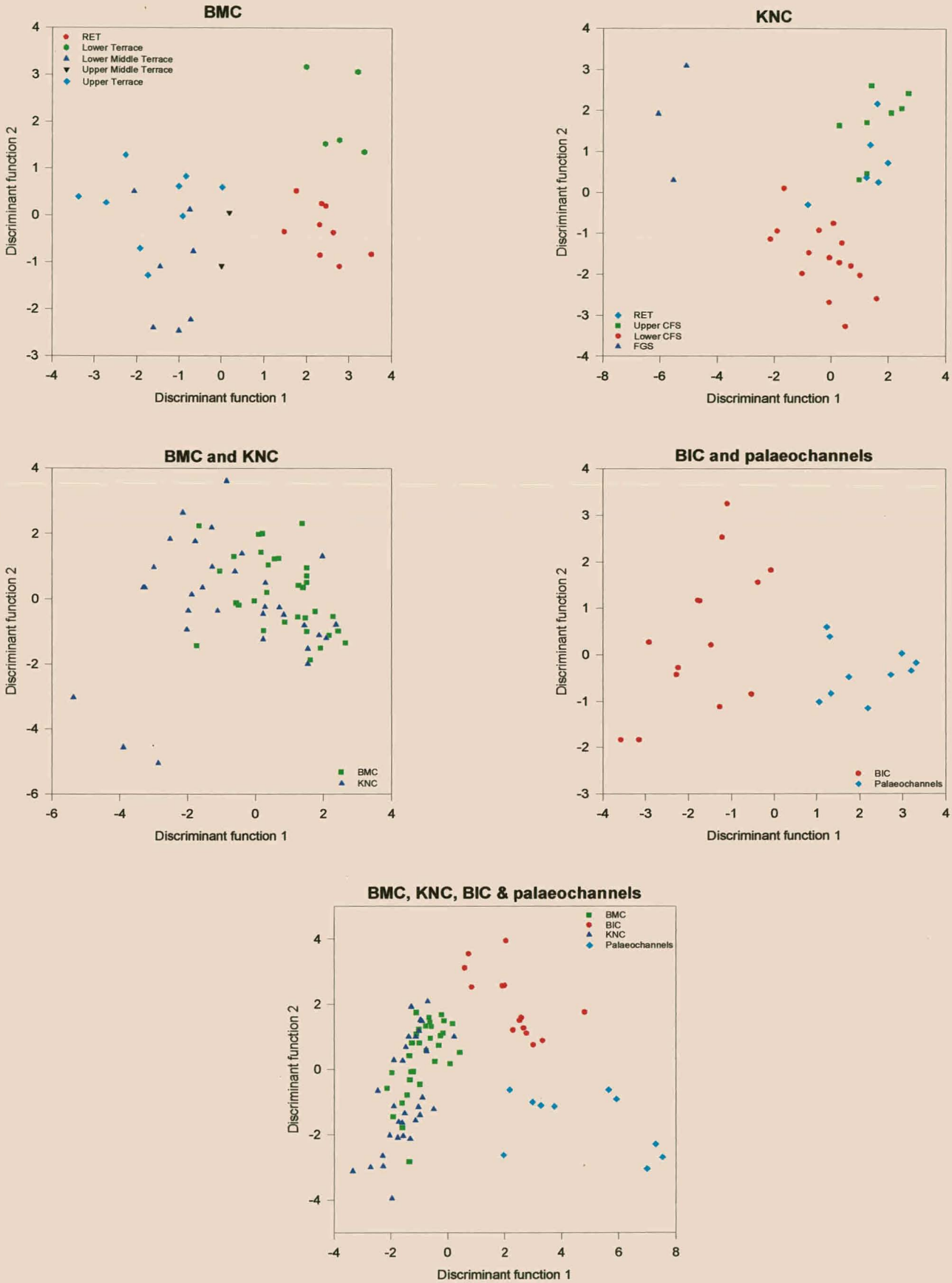

Figure 4.12. Discriminatory diagrams based on heavy mineral assemblages of the various stratigraphic successions.

CHAPTER 5

MINERALOGY

5.1. Nomenclature of the Fe-Ti oxides and their derivatives

No general accepted terminology exists for the nomenclature of minerals in the TiO_2-FeO-Fe_2O_3 system and most of the workers follow Buddington and Lindsley's (1964) classification (Fig 5.1). The nomenclature used in this study is concurrent with the classification systems of Buddington and Lindsley (1964) and Hugo (1993).

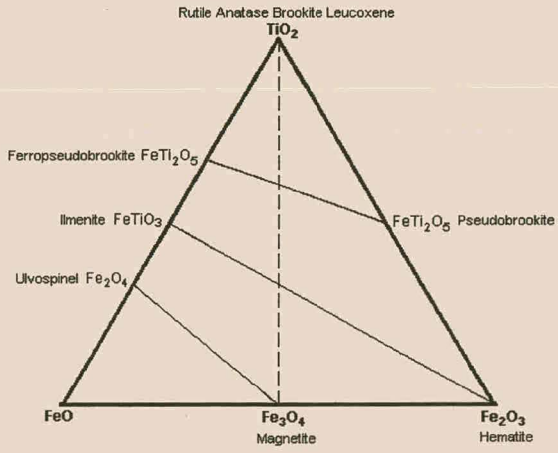

Figure 5.1. Illustration of the relation of the iron-titanium oxides in the TiO_2-FeO-Fe_2O_3 system (simplified from Battey, 1981).

- *Rutile:* A tetragonal phase, consisting of TiO_2 with minor impurities.
- *Anatase:* A tetragonal phase, essentially pure TiO_2.
- *Brookite:* An orthorhombic phase, essentially pure TiO_2.
- *Ilmenite:* A trigonal phase consisting of FeO-TiO_2, with >45 wt% TiO_2 and up to 6% Fe_2O_3 in solid solution.
- *Ferrian-ilmenite:* A rhombohedral ilmenite phase that contains >6 wt% Fe_2O_3 and 3-4 wt% excess TiO_2 in solid solution.
- *Hematite:* A trigonal phase with a stoichiometry approaching Fe_2O_3 and <5 wt% TiO_2
- *Titanohematite:* A Fe-Ti phase with a stoichiometry of at least 50 wt% hematite and >5 wt% TiO_2 usually as FeO-TiO_2 in solid solution.

- *Hemo-ilmenite:* A Fe-rich ilmenite that contains a mixture of ferrian-ilmenite and titano-hematite and/or ilmeno-hematite intergrowths.
- *Ilmo-hematite:* A Fe-rich hematite that consists of a mixture of titanohematite and/or hematite with intergrowths of ferrian-ilmenite or hemo-ilmenite.
- *Magnetite:* A cubic phase with a stoichiometry approaching Fe_3O_4 containing less than 5 % TiO_2.
- *Titanomagnetite:* A phase with an oxide stoichiometry of approximately R_3O_4, which can be recalculated in terms of Fe_3O_4, $2FeOTiO_2$ or $FeOTiO_2$, or both, with Fe_3O_4 as the dominant phase (Buddington and Lindsley, 1964).
- *Ulvöspinel:* Spinel structure with a stoichiometry approaching Fe_2TiO_4.
- *Pseudobrookite:* An orthorhombic phase with a > 50 mol% Fe_2TiO_5.
- *Ferropseudobrookite:* Similar to pseudobrookite, but with less than 50 mol% Fe_2TiO_5.
- *Titanite (sphene):* A monoclinic mineral with the general formula $CaTiSiO_5$.
- *Alteration products of ilmenite*

The nomenclature of the alteration products of ilmenite is often confusing and the combined classifications of Dyadchenko and Khatunseva (1960), Bailey *et al.* (1964), Temple (1966) and Frost *et al.* (1983) are used.

Hydrated ilmenite: altered ilmenite containing a small quantity of crystalline water. These areas of alteration usually contain 53-60 % TiO_2 and are microscopically distinguished from unaltered ilmenite by their grey-blue colour and weaker anisotropism.

Pseudorutile: an ilmenite alteration product with a stoichiometry approaching $Fe_2Ti_3O_9$ and a TiO_2 content of 61-70%. This phase is also lesser known as arizonite (Palmer, 1909). Pseudorutile indistinctly exhibits a blue-grey colour (nearly isotropic) with a slightly higher reflectance than ilmenite.

Leucoxene: altered ilmenite that has >70 wt% TiO_2 content. Leucoxene is optically distinguished by its white to yellow internal reflections and characteristic sugary texture. Temple (1966) and Hugo (1993) suggest that leucoxene may form from the alteration of almost any titanium-bearing mineral. Grouping these different leucoxene

grains with markedly different compositions is impractical from a petrographic point of view and hence the broader use of the term leucoxene is used in this study.

- *Composite grains*

Composite grains are often encountered either as two or more minerals interlocked or as exsolution features in each other. Macdonald (1995) refers to these grains as complex grains, but excludes ilmo-hematite and hemo-ilmenite, which he classifies separately. Although Hugo (1993) proposed a comprehensive classification for composite grains, it is not applied in this study due to the low abundance of these particular grains. Instead ilmo-hematite and hemo-ilmenite were counted separately during point-counting, but were classified together as Fe-Ti intergrowths. Composite grains consisting of unaltered ilmenite and one or more of its alteration products are simply referred to as altered ilmenites.

5.2. Ilmenite-Hematite series

Since ilmenite and hematite form a solid solution series and usually co-exist the characteristics of these minerals are collectively discussed.

5.2.1. Petrography

The opaque fraction is dominated by a diverse assemblage of Fe-Ti oxides, which generally varies in size between 75-250 μm, although grain sizes as large as 500 μm have been noted in certain stratigraphic successions. Ilmenites occurring as subrounded to rounded grains are the most abundant; platy fragments are less common, but well-rounded grains are rare. The Fe-Ti oxides rarely either display embayed outlines or irregular crystal boundaries and are interlocked with other minerals such as garnet, feldspar and quartz along ilmenite peripheries.

Unaltered ilmenite (Plate 5.1A) is usually pinkish brown (in oil immersion under reflected light) while ferrian-ilmenite sometimes displays a darker pink colour and stronger pleochroism (Plate 5.1B). Inclusions normally show no preferred orientation and phases positively identified by SEM-EDS include pyrite, sphene, pyroxene, feldspar, biotite, apatite and other silicates (Plate 5.1C). These inclusions formed during ilmenite growth in the melt or by reaction of the growing ilmenite crystals with

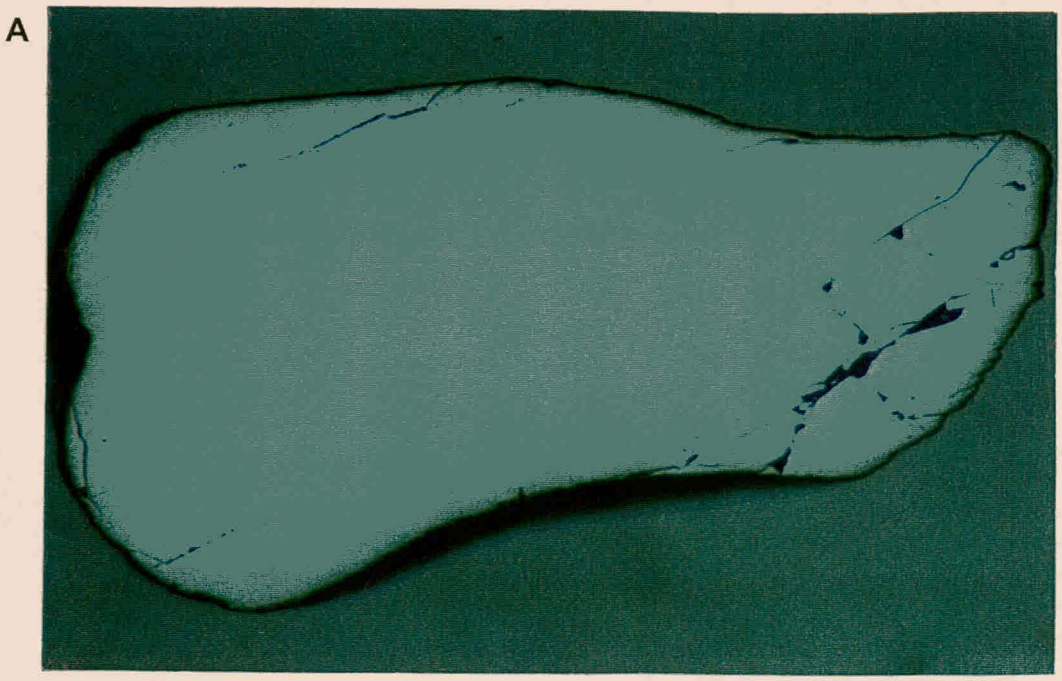

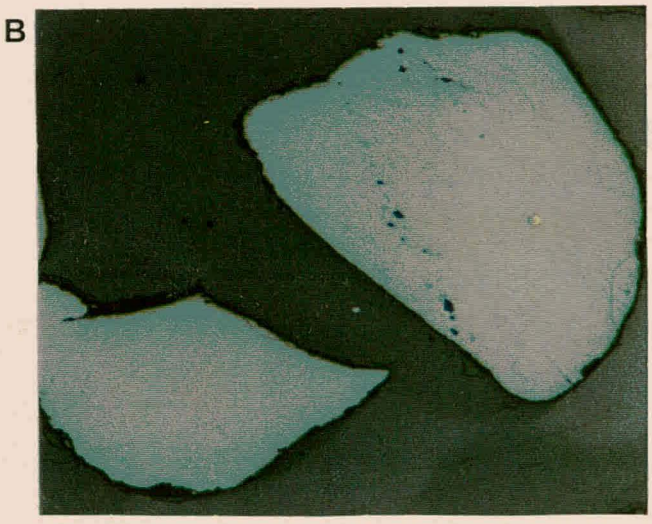

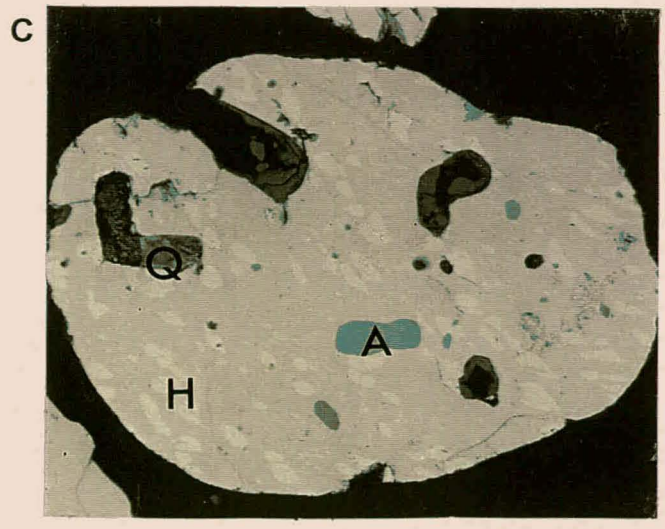

Plate 5.1. Selected ilmenite grains from the study area.

A) Sub-rounded, homogeneous unaltered ilmenite.

B) Grains of ferrian ilmenite, displaying a more pinkish tint compared to common ilmenite.

C) Backscatter scanning electron (BSE) image of ilmenite showing mineral inclusions of different types. Hematite (H), apatite (A) and quartz (Q).

Scale: 200X

a silica melt and indicate their magmatic parentage (Hugo, 1993). Authigenic red-brown dustclouds, presumably of iron-oxide, are often recognised along grain boundaries.

Hematite (Plate 5.2A) has similar physical characteristics to ilmenite and is present as discrete, altered or pitted, angular to occasionally subrounded grains. The mineral exhibits a distinctive bright white colour under reflected light, occasionally marked by red internal reflections. Most of the ilmenite grains are generally free from exsolution lamellae. Exsolved phases in ilmenite become less abundant in the older stratigraphic successions, probably due to the low stability of these phases. Hemo-ilmenite is characterised by abundant fine hematite exsolution lamellae invariably orientated parallel to (0001), the ilmenite host (Plate 5.2B). When the grains are cut perpendicular to (0001), the exsolution lamellae generally exhibit irregular, lense-shaped forms (Plate 5.2C).

Often more than one generation of exsolution are present as small blebs of hematite in ilmenite or hematite blebs in ilmenite. An almost complete gradation between hemo-ilmenite and ilmo-hematite is found in the studied samples. Complex grains include ilmenite grains that contain large aeras of apparently exsolved hematite (or titanohematite) that in turn contains a finer series of ilmenite and vice versa. Fine rutile exsolution lamellae are occasionally developed in the hematite-rich areas. Complex grains, consisting of approximately equal proportions of ilmenite and hematite, from which it is difficult to distinguish between host and intergrown phase were also detected (Plate 5.2D).

Hematite containing essentially similar Fe-Ti intergrowths to ilmenite, is also found, but far less common (Plate 5.2E). Exsolution lamellae are however more common in titanohematite. These grains are generally heterogeneous, containing lenses of ilmenite or with exsolved z-shaped rutile forming Ramdohr's (1980) "blitz" texture (Plate 5.2F). Complex grains of intimately, sympletic intergrowths of hematite, titanohematite and rutile were also noted. Such grains containing the association of

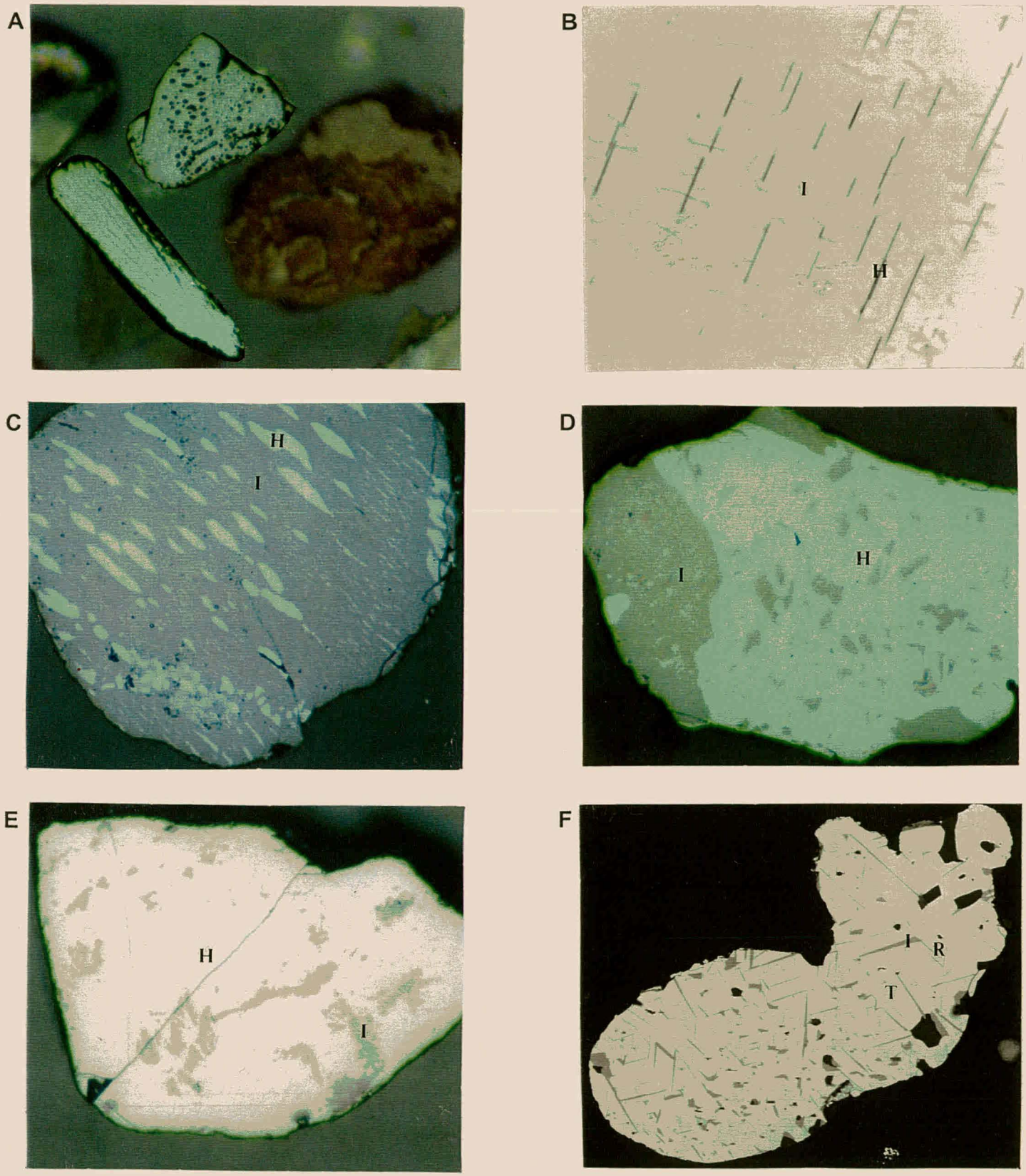

Plate 5.2. Representative grains from the ilmenite-hematite solid-solution series.

A) Altered, pitted hematite grains.

B) BSE image of hemo-ilmenite containing parallel lamellae of hematite (H) in the ilmenite matrix.

C) Hemo-ilmenite, containing two generations of exsolved hematite (H) within an ilmenite (I) host.

D) Complex grain consisting of hematite (H) and ilmenite (I).

E) Ilmo-hematite with unorientated, irregular-shaped ilmenite exsolution lamellae in hematite host (white).

F) Titanohematite displays the "blitz" texture of Ramdohr (1980). The darker grey lenses are ilmenite (I); the lighter grey z-shaped lamellae are rutile (R).

Scale: 200X

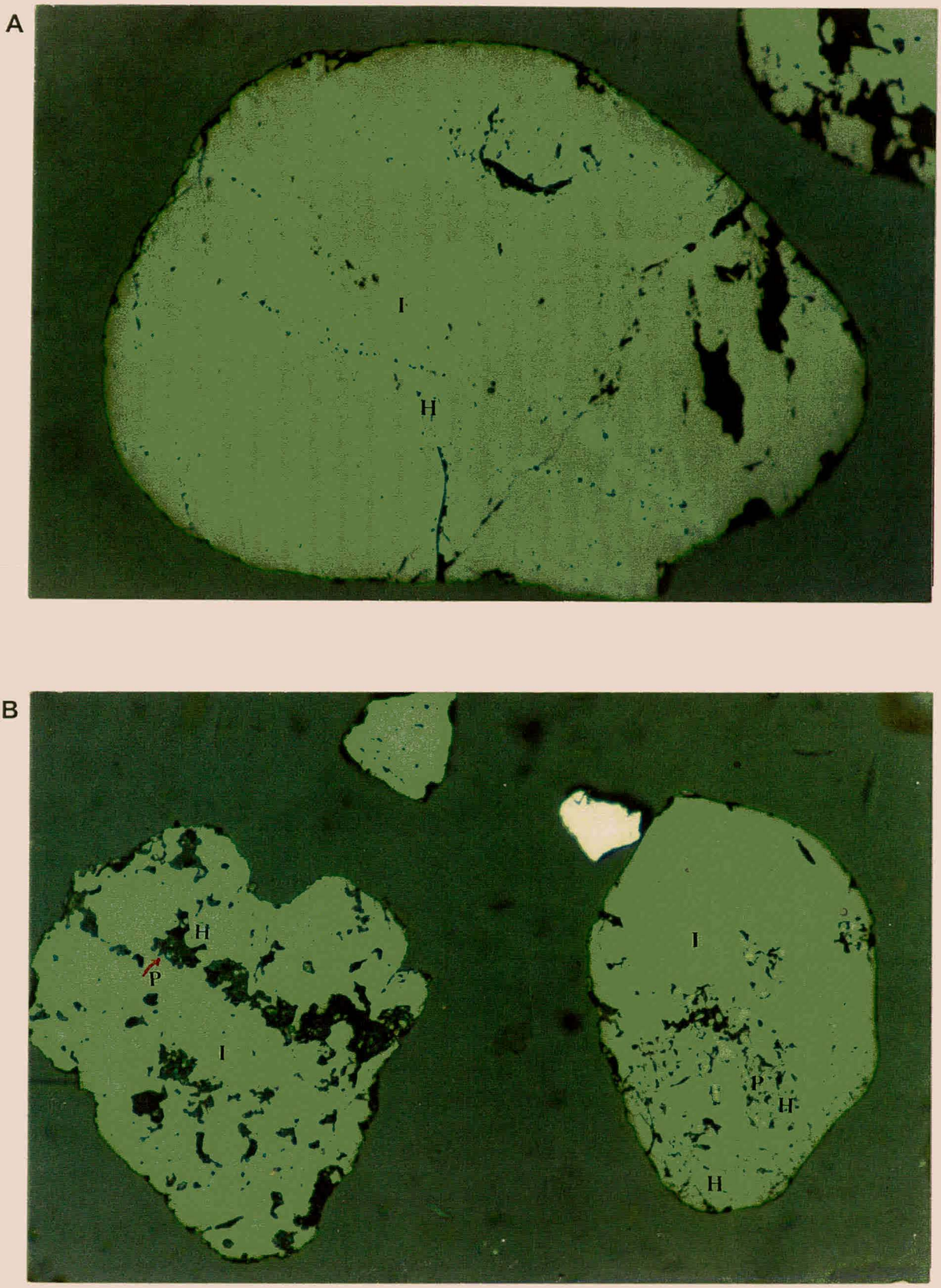

Plate 5.3. Typical altered ilmenites.

A) Hydrated ilmenite. This microphotograph clearly illustrates the patchy development of hydrated ilmenite (H) in an unaltered ilmenite (I) grain. Note how alteration is concentrated along structurally weak zones.

B) Pseudorutile. Ilmenite (I) altered to pseudorutile (P) via hydrated ilmenite (H).

Scale: 200X

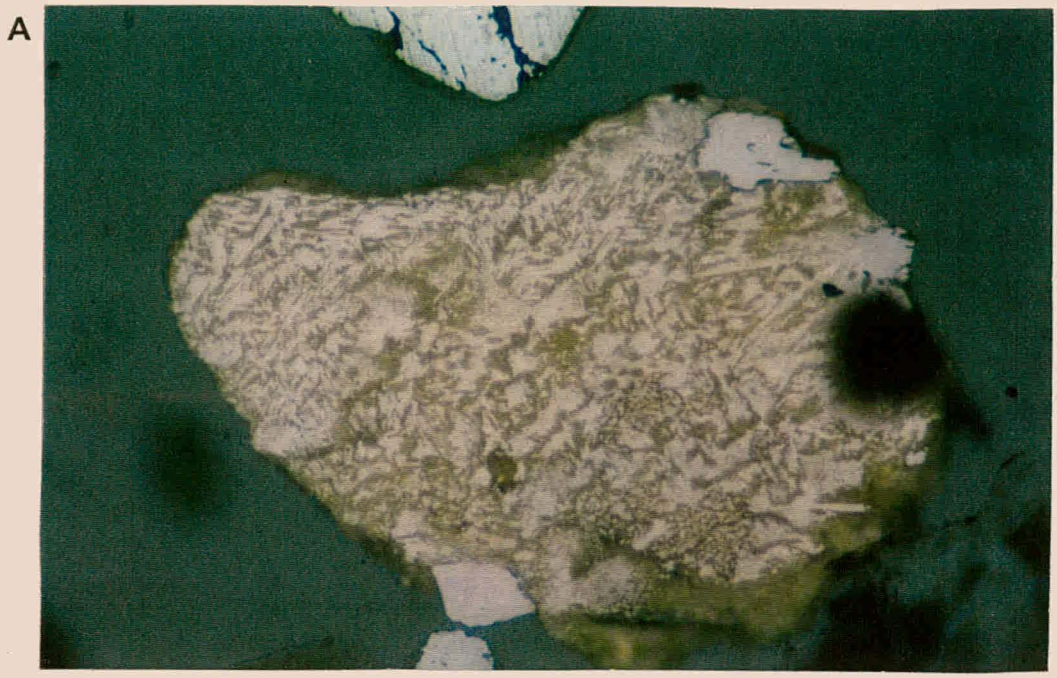

Plate 5.4. Leucoxene grains from the study area.

A) Leucoxene consisting of thin, prismatic microcrystals, resembling rutile in habit.

B) Well-rounded leucoxene displaying a porous, cellular habit.

C) BSE image of highly siliceous, inhomogeneous leucoxene. The titaniferous and siliceous areas display a symplectic texture.

Scale: 200X

A

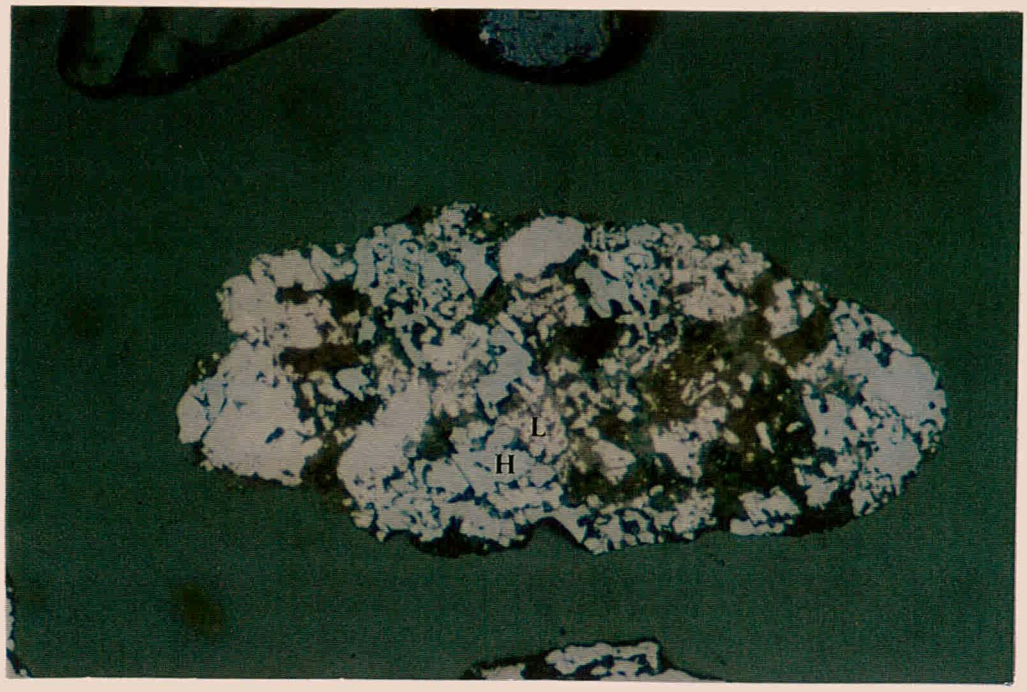

B

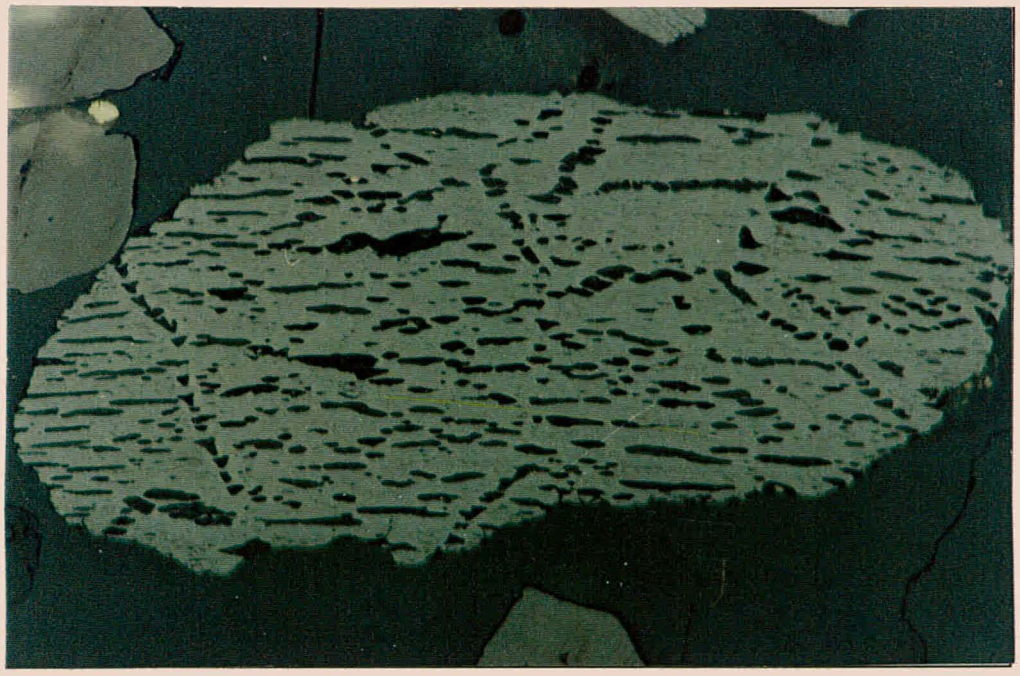

Plate 5.5. Alteration products of complex ilmenite grains.

A) A complex grain containing hematite (H) and leucoxene (L). The pristine grain was an ilmenite-hematite composite. The ilmenite was altered to leucoxene whilst some of the hematite was removed by chemical dissolution.

B) Altered ilmenite showing relics of possibly hematite lamellae. Hematite was completely leached from the primary hemo-ilmenite grain resulting in the pitted texture.

Scale: 200X

ilmenite, titanohematite and titanite were also recognised. Due to their low abundance, no particular attention was given to the study of these complex grains.

With increasing alteration, altered ilmenites, change colour from pinkish brown (in oil immersion under reflected light to bluish-grey when altered to hydrated ilmenite (Plate 5.3A). The colour changes to a brighter grey when pseudorutile is formed (Plate 5.3B) and finally yellow-white when leucoxene is formed (Plate 5.4A). Pseudorutile commonly displays isotropism. Leucoxene is recognised by its characteristic sugary texture and its bright yellow-white internal reflections (Plate 5.4B). Some leucoxenes appear to have a porous character, where SiO_2 and Al_2O_3 fill the porous cavities (Plate 5.4C).

The majority of studied ilmenites show no sign of alteration. Ilmenite generally displays varying degrees of alteration, mostly to hydrated ilmenite and to a lesser extent to pseudorutile and leucoxene. Complex grains containing Fe-Ti exsolutions such as hemo-ilmenite, titanohematite and ilmo-hematite may be altered in different ways. Ilmenite may be differentially altered, whereas the hematite is unaltered (Plate 5.5A) or the hematite is partially or completely removed from the grain, resulting in a pitted grain surface (Plate 5.5B).

5.2.2. Chemistry

Representative mineral grains of the hematite-ilmenite series including titanohematite, ilmenite and hematite, were analysed for Ti, Fe, Al, Mn, Mg, Cr, Ca and Si. The results are presented as oxide weight percentages in Appendix H. The FeO and Fe_2O_3 content were calculated from stoichiometry as outlined by Droop (1987).

Unaltered ilmenite

The chemical formula for ilmenite is $FeTiO_3$, but Mn, Mg and Fe^{3+} commonly substitutes Fe^{2+} in the crystal structure and in addition ilmenite can contain minor or trace amounts of Ca, Al, Cr, Si, V, Cu, and Zn. A total of 212 representative, unaltered ilmenites were analysed and the analyses indicate that the ilmenite in the

study area contains on average 50.3 wt% TiO_2, 41.5 wt% FeO, less than 3 wt% Fe_2O_3 and MnO and trace amounts of Al_2O_3, Cr_2O_3, SiO_2 and MgO.

The ilmenite compositions are illustrated by frequency histograms of TiO_2, FeO, Fe_2O_3, and MnO (Fig. 5.2-5.5). In addition, X-Y scatterdiagrams of selected elements versus TiO_2 are presented in Fig. 5.6.

The following observations are evident from these diagrams:

- The TiO_2 content ranges from 46.0 to 53.9 wt%. Several grains with a TiO_2 content greater than 53.5 wt% (which is the proposed lower limit of altered ilmenites) show optically no signs of alteration and are therefore considered as unaltered ilmenites. Except for the BMC, all the other ilmenites display a negatively skewed frequency distribution. The majority of ilmenites in the study area contain between 50-52 wt% TiO_2, averaging 50.4 wt% TiO_2 (n=236).
- The FeO content ranges between 33.1-46.5 wt% and all the frequency distributions are skewed towards the higher values. Most of the BMC and BIC ilmenites have between 40 and 42 wt% FeO which is slightly lower than the ilmenites from the palaeochannels and KNC. The lower FeO content of BMC and BIC ilmenites is explained by a greater degree of substitution of Mn^{2+} for Fe^{2+}.
- Both the frequency distributions of the Fe_2O_3 and MnO content of the unaltered ilmenite population are highly variable (0-12 wt%) and strongly positively skewed with most of the ilmenites containing less than 4 wt% Fe_2O_3 and MnO.
- The antipathetic relationship between the Fe_2O_3 and TiO_2 content is clearly illustrated in Fig. 5.6, emphasising the solid solution series that exists between the hematite and ilmenite. Similarly, a direct relationship is evident between MnO and FeO content illustrating Mn^{2+} substitution for Fe^{2+} in the ilmenite lattice.
- Most of the ilmenites contain Al_2O_3, Cr_2O_3, SiO_2, CaO and MgO in amounts very near to the detection limit of the microprobe. Scatterplots of Al_2O_3, Cr_2O_3, SiO_2, CaO and MgO against TiO_2 indicate no noteworthy trends except that these trace elements show some small increase when the TiO_2 content is greater than 50 wt% (Fig. 5.6).

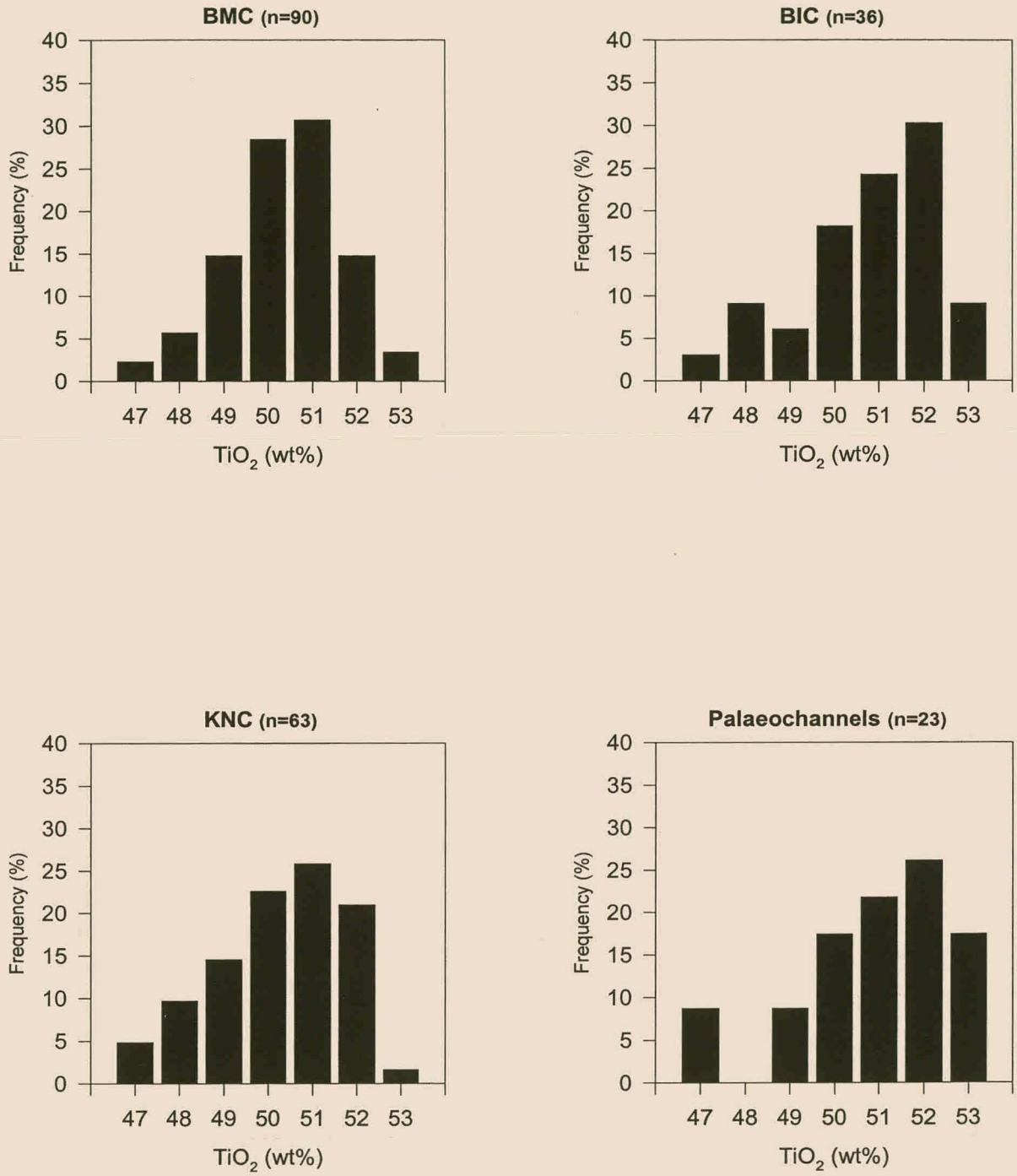

Figure 5.2. Frequency histograms of TiO_2 content of individual unaltered ilmenite analyses in the study area.

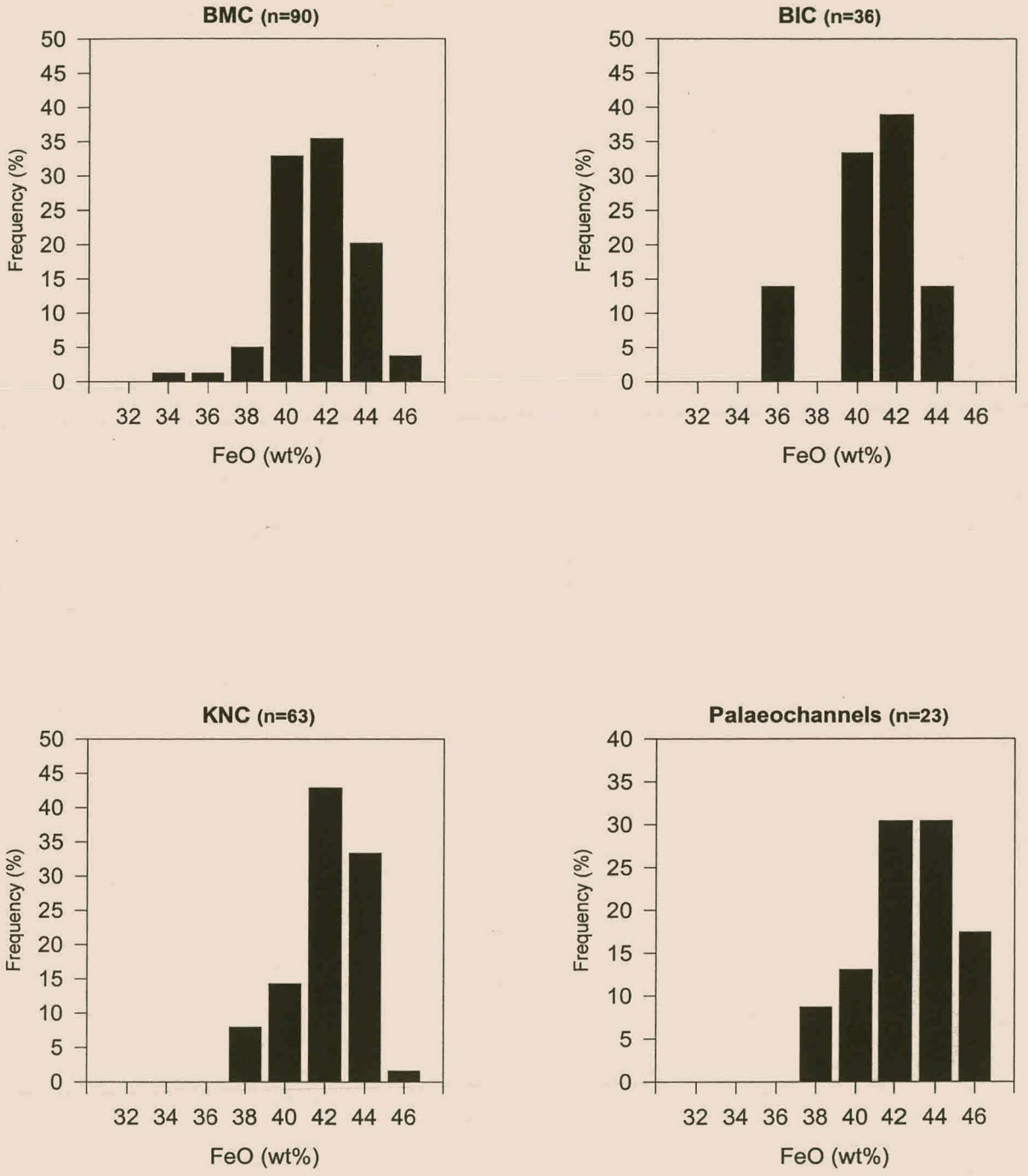

Figure 5.3. Frequency histograms of FeO content of individual unaltered ilmenite analyses in the study area.

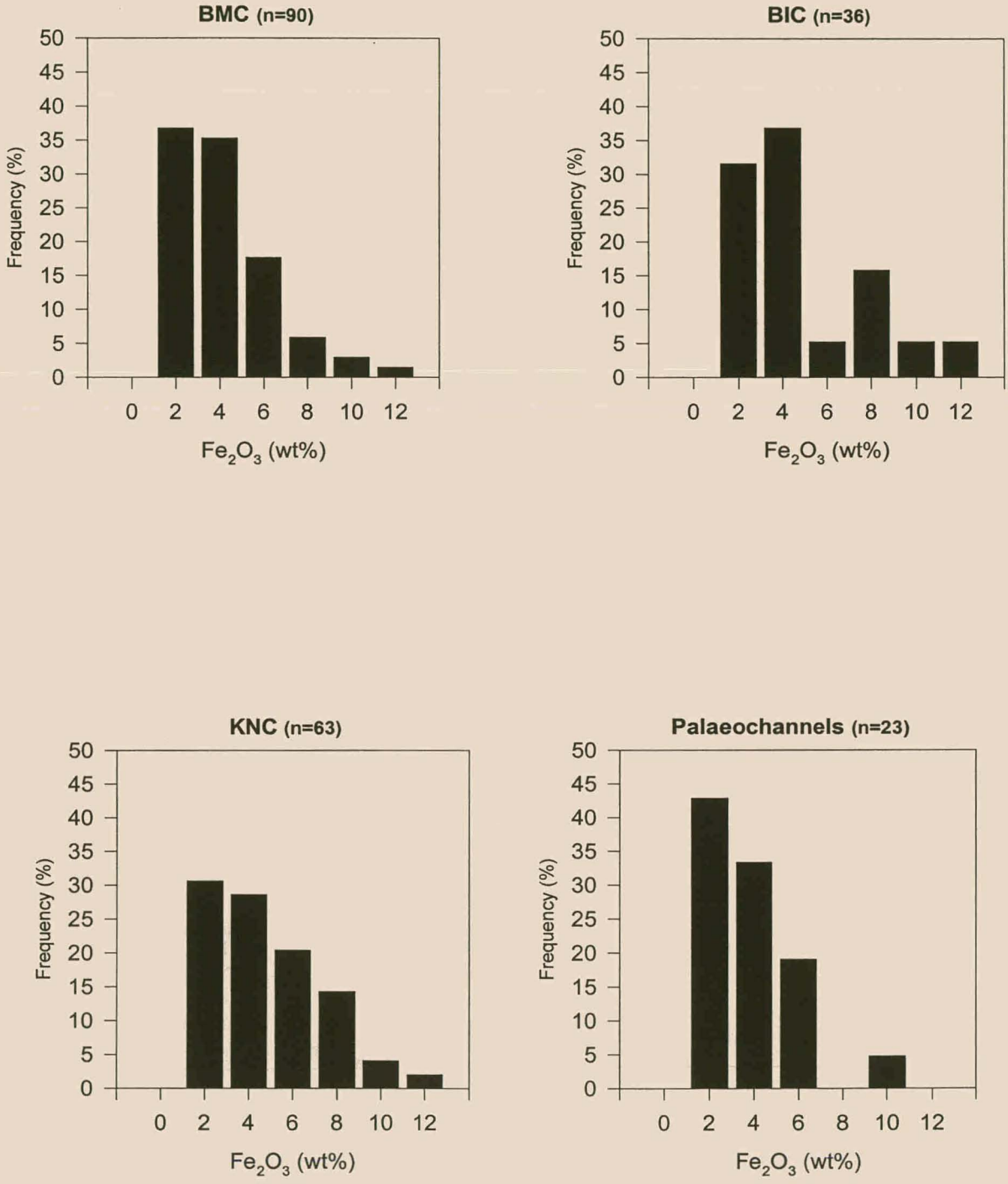

Figure 5.4. Frequency histograms of Fe_2O_3 content of individual unaltered ilmenite analyses in the study area.

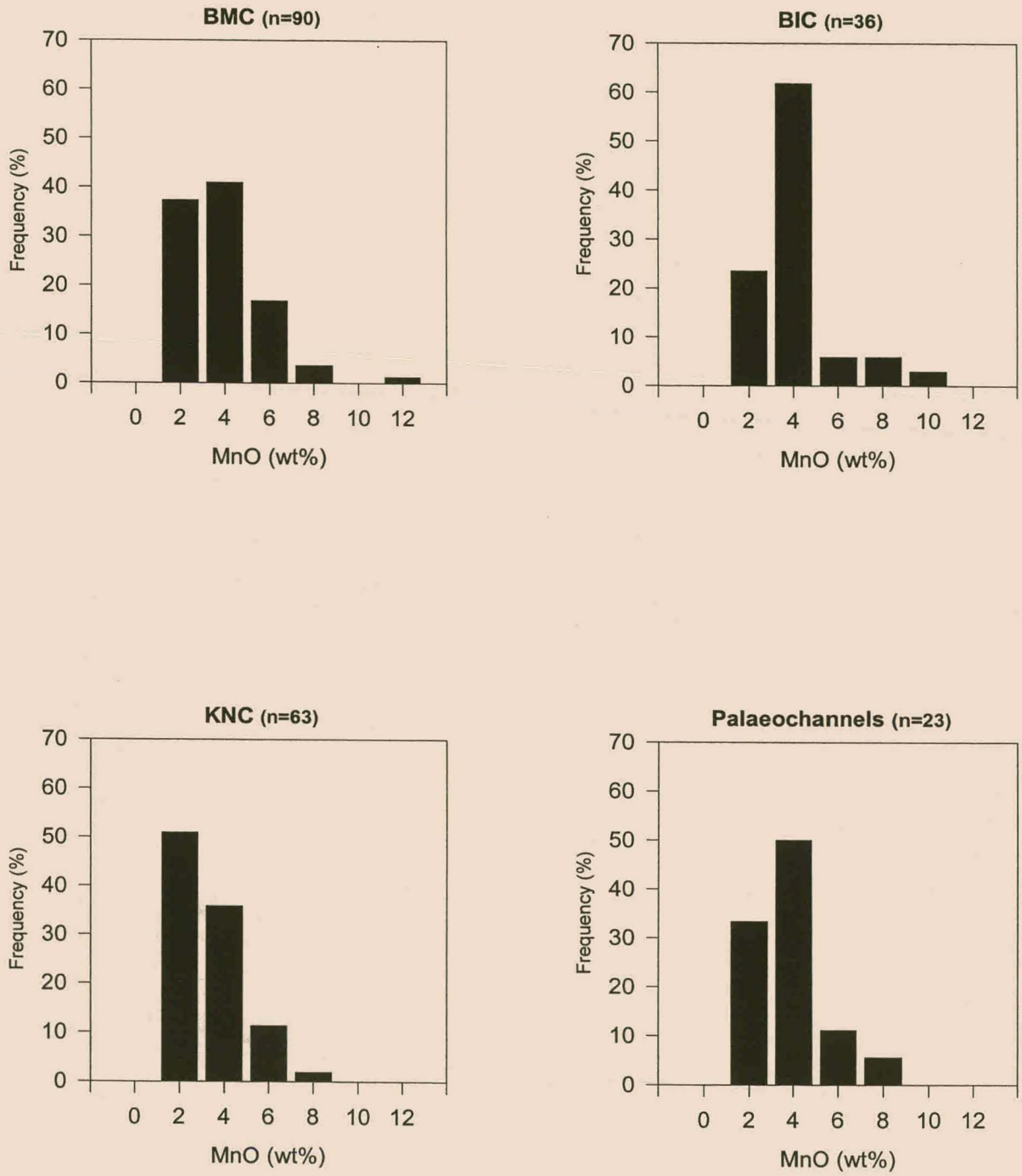

Figure 5.5. Frequency histograms of MnO content of individual unaltered ilmenite analyses in the study area.

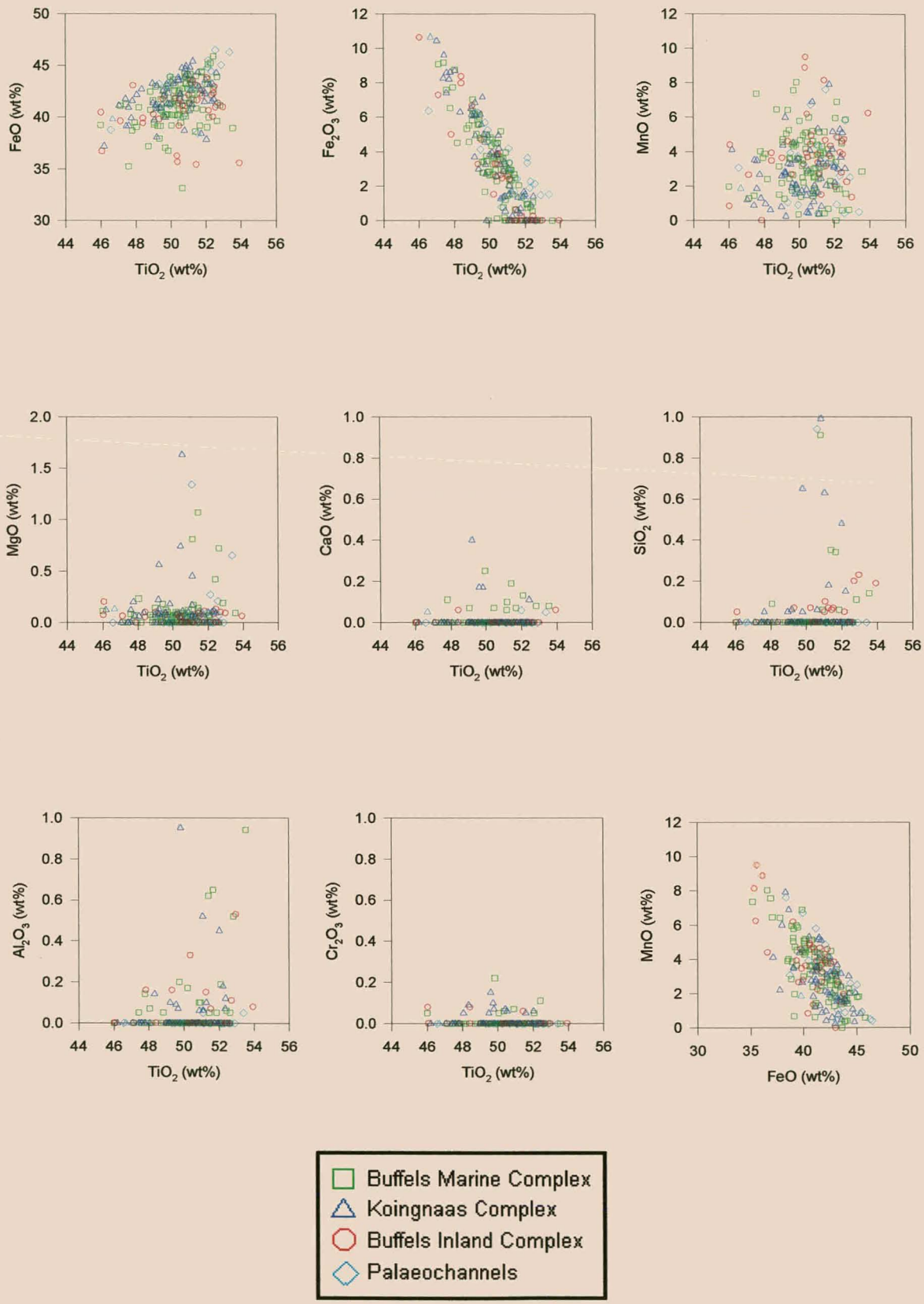

Figure 5.6. X-Y scatterdiagrams of selected elements against TiO_2 contents for unaltered ilmenite analyses in the study area.

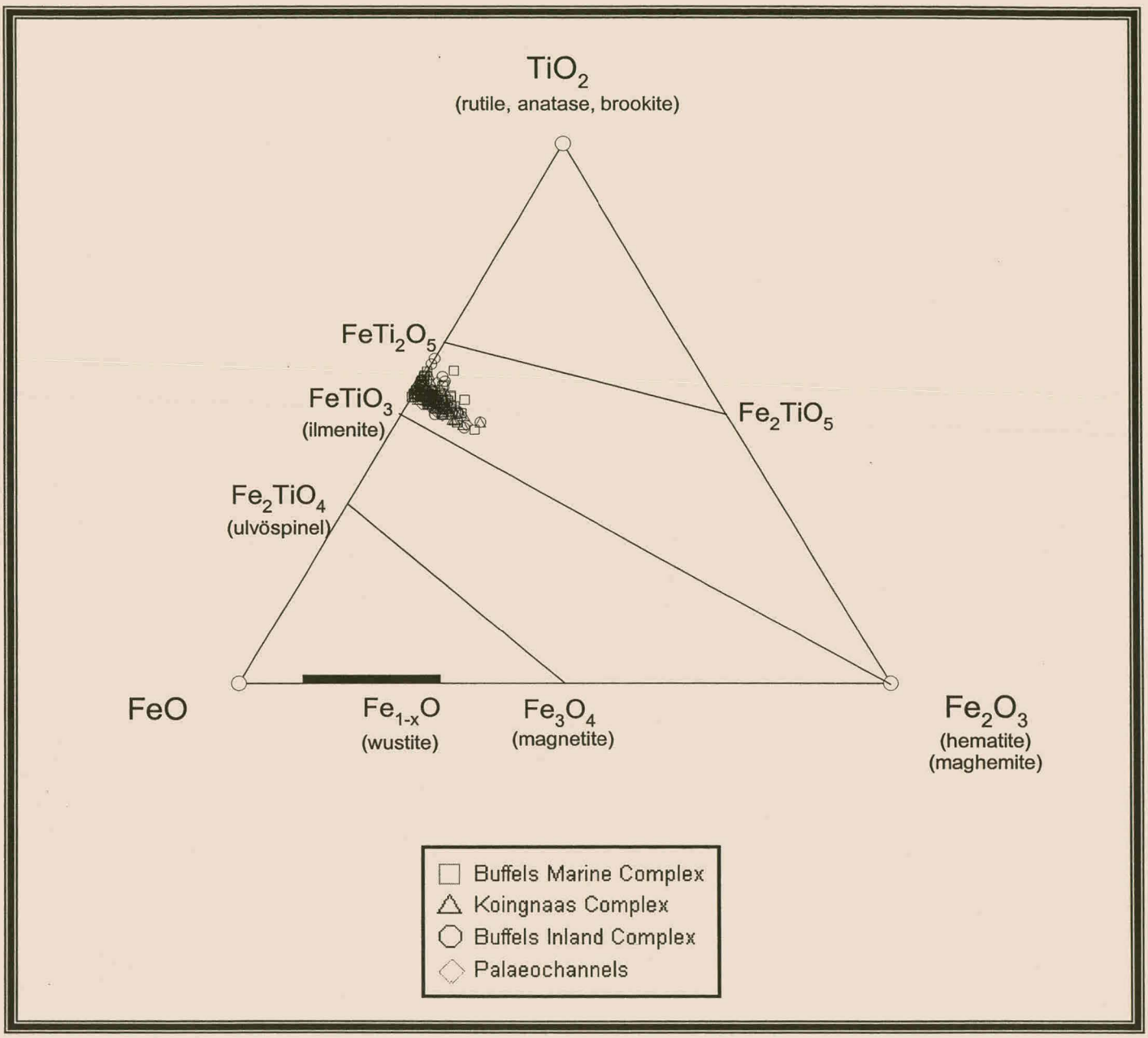

Figure 5.7. Ternary plot of ilmenite chemistry in the FeO-TiO_2-Fe_2O_3 system of unaltered ilmenites from the study area (after Buddington and Lindsley, 1964).

Ilmenite chemistry is illustrated on a ternary plot in the TiO_2-FeO-Fe_2O_3 system (Fig. 5.7). All the analyses plot in a tight field near, but not on the $FeTiO_3$ end-member which indicates relative TiO_2 enrichment. This trend however, is probably the result of significant Fe^{2+}-Mn^{2+} substitution, where the FeO component is significantly reduced.

Altered ilmenite

The results of microprobe analysis performed on altered ilmenites are presented in Appendix H. The same set of elements analysed was used as in the case of the unaltered ilmenites. Many analyses show low totals, in particular those from the BIC and palaeochannels. Ilmenite degradation under the beam is probably indicative of hydration and resultant low totals.

Comparison of chemical compositions of altered and unaltered ilmenites show that the altered ilmenites have a greater TiO_2 content. TiO_2 frequency histograms show that the altered ilmenite population is dominated by hydrated ilmenites (53-61 wt% TiO_2) and that a very low percentage of altered ilmenites consist of pseudorutile or leucoxene (Fig. 5.8). It is also clear that the degree of alteration is greater for ilmenites from the palaeochannels compared to those from the BMC, BIC and KNC. Altered ilmenites range in chemical composition from the pure ilmenite end-member to a point between pseudobrookite (Fig. 5.9).

The variation of selected elements with increasing alteration is presented on crossplots (Fig. 5.10). The following observations are apparent:

- FeO and MnO decrease with increasing alteration (greater TiO_2 content). FeO and MnO tend to decrease very sharply when the TiO_2 content ranges between 53 and 61 wt% and beyond this point these elements occur only in trace amounts. This trend suggests that during increased alteration, Fe^{2+} is oxidised to Fe^{3+} whilst Mn^{2+} is preferentially removed from the structure.
- Fe_2O_3 increases with alteration up to point of 61-62 wt% TiO_2 after which its abundance decreases, as it is believed to be leached from the ilmenite structure.

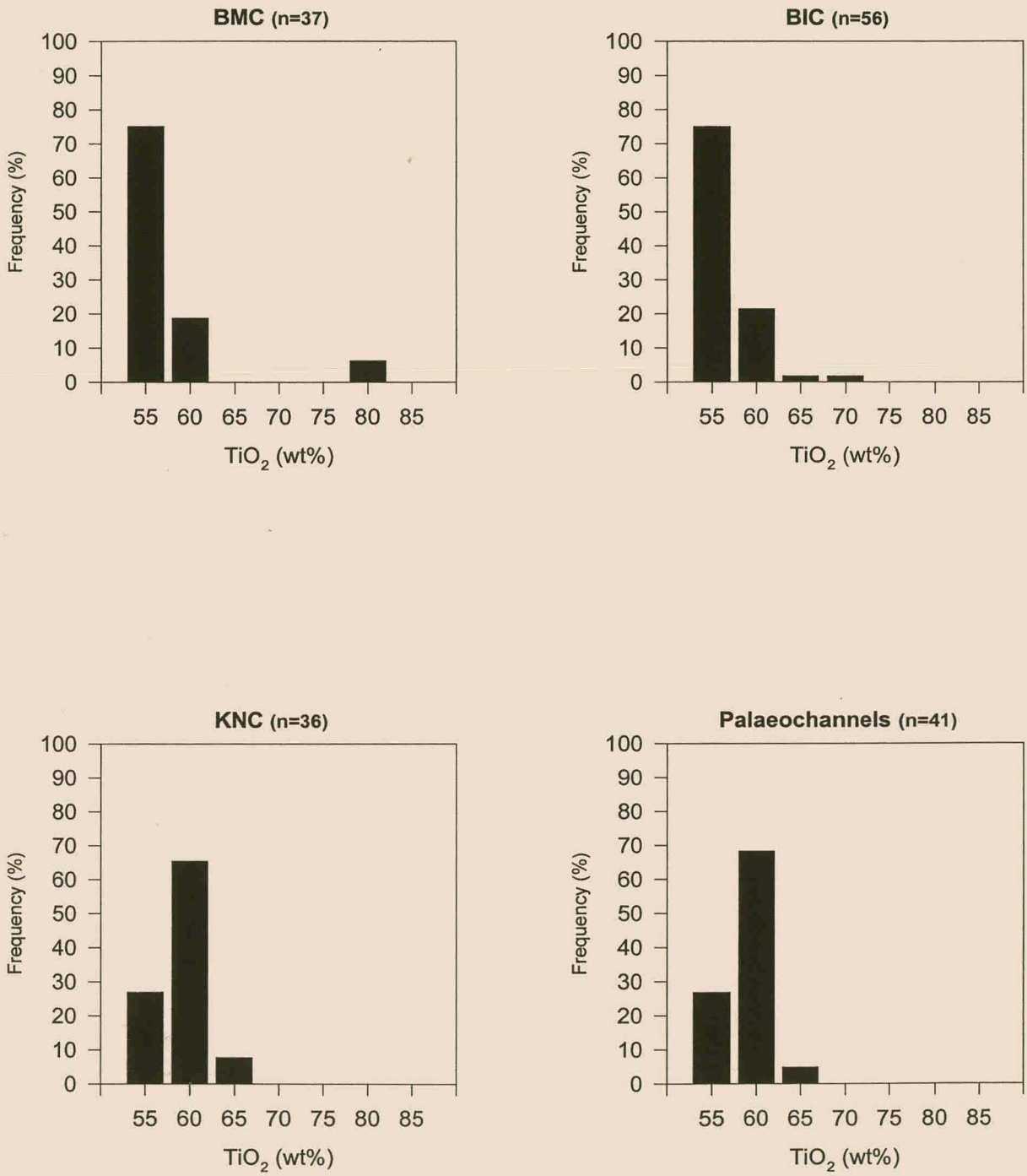

Figure 5.8. Frequency histograms of TiO_2 content of individual altered ilmenite analyses in the study area.

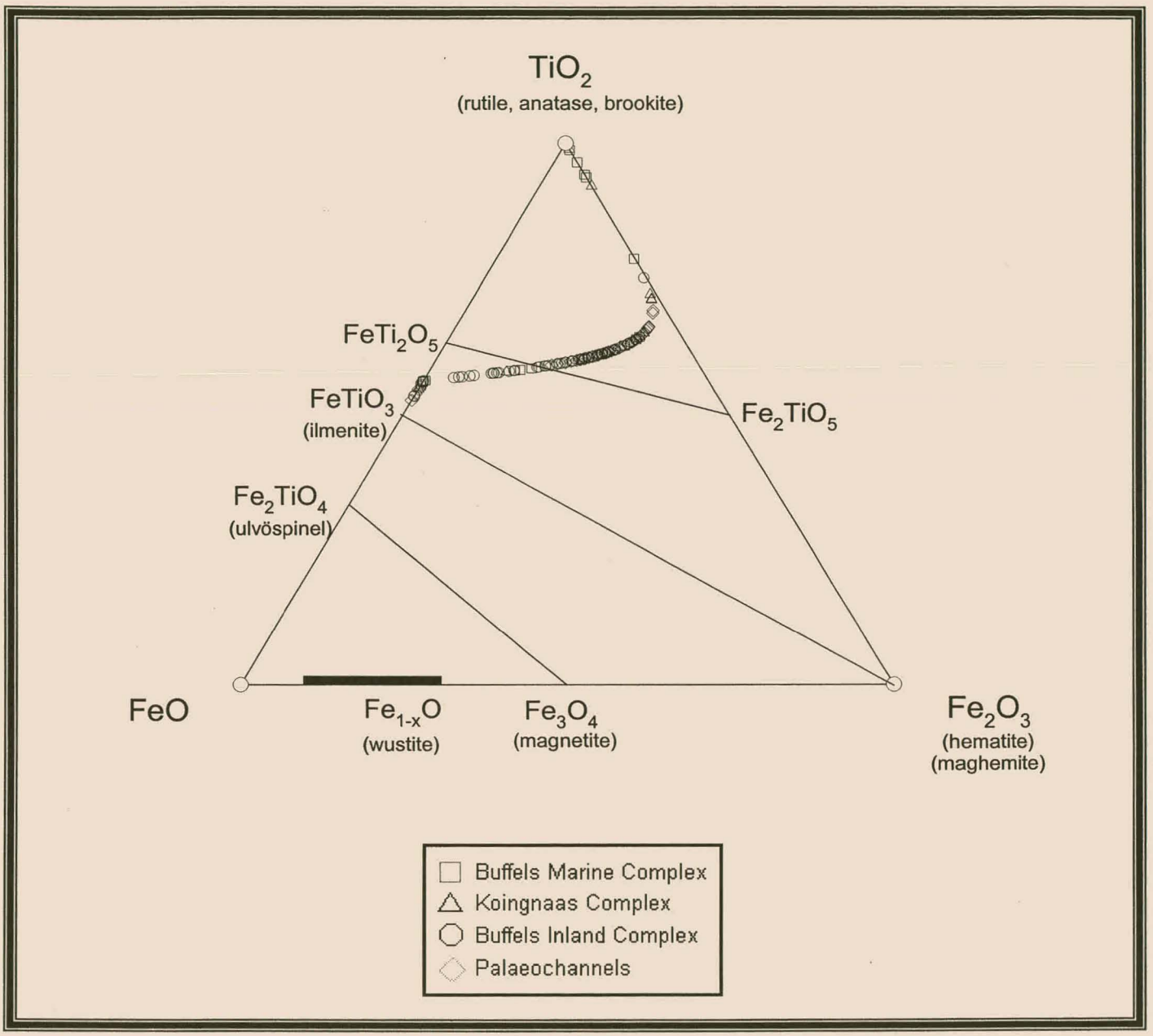

Figure 5.9. Ternary plot of ilmenite chemistry in the FeO-TiO_2-Fe_2O_3 system of altered ilmenites from the study area (after Buddington and Lindsley, 1964).

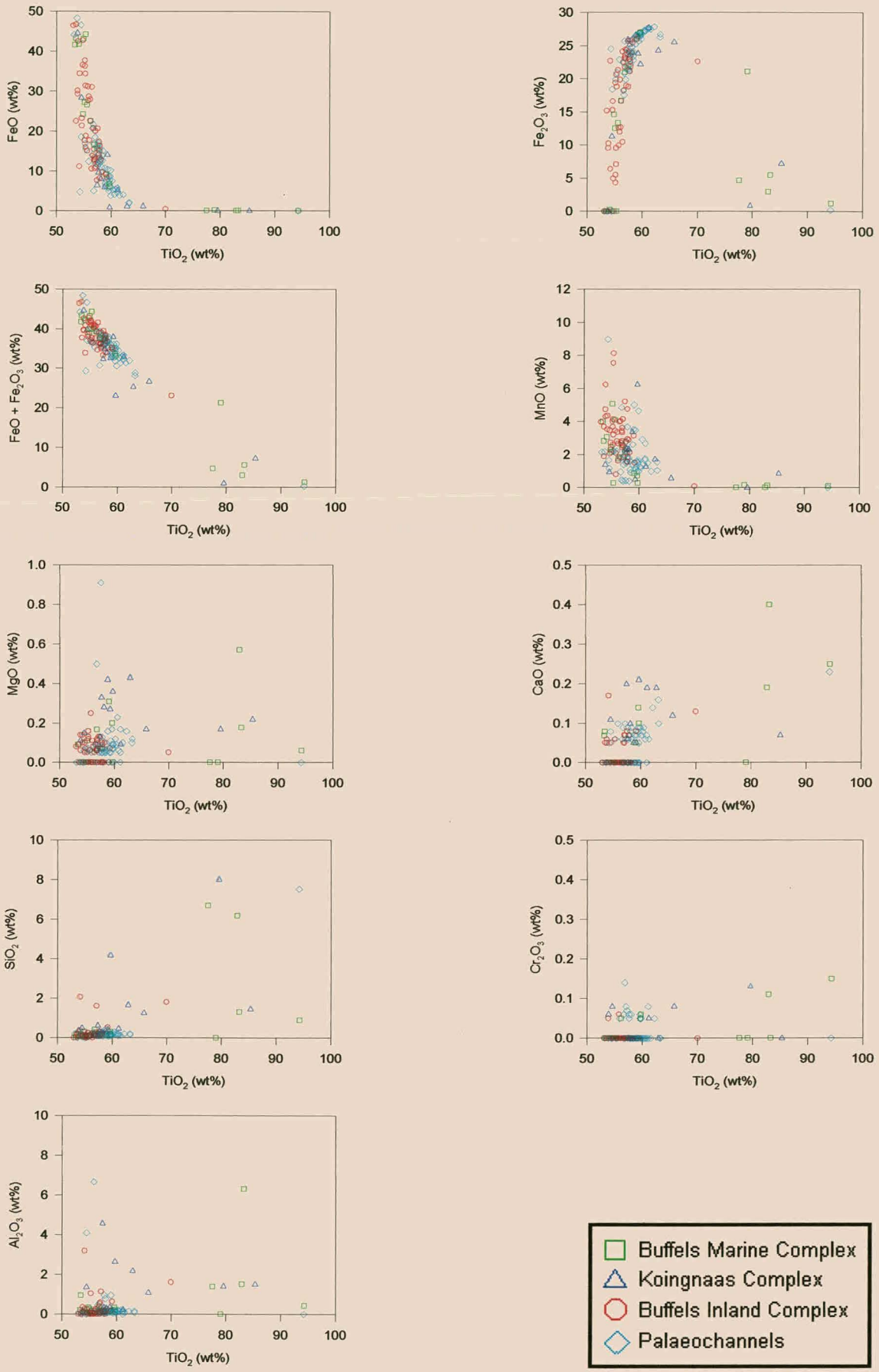

Figure 5.10. Variation of selected elements with ilmenite alteration from particular analyses in the study area.

Collectively, there is a dramatic decrease in total iron ($FeO+Fe_2O_3$) with increasing alteration.

- Similarly to unaltered ilmenites, CaO and MgO are present in altered ilmenites in amounts very near to the detection limits of the microprobe and in addition trace amounts of Al_2O_3 and SiO_2 are also present.
- No consistent trend of Cr_2O_3, Al_2O_3 and MgO abundance with increasing alteration is evident whilst CaO and SiO_2 content shows a tendency to increase slightly with increasing alteration.

The ilmenite chemistry of the altered population indicates that no distinction between the various samples is possible, but that palaeochannel ilmenites display a greater degree of alteration in contrast with those from the KNC, BIC and BMC. This could be attributed to the strong weathering profile in the palaeochannels.

Hematite and titanohematite

Microprobe analyses show that hematite is essentially pure Fe_2O_3, whereas the titanohematite contains variable amounts of TiO_2 (25-44 wt%). In addition to TiO_2 and Fe_2O_3, titanohematite contains appreciable amounts of FeO (24-50 wt%) and trace amounts of MnO, Al_2O_3, Cr_2O_3 and SiO_2. On the TiO_2-FeO-Fe_2O_3 ternary plot, titanohematite analyses plot in a straight line parallel to the $FeTiO_3$-TiO_2 line, illustrating the continuous solid solution series that exists between ilmenite and hematite (Figs. 5.11; 5.12).

5.2.3. Ilmenite alteration

Although theories concerning the mechanism of ilmenite alteration differ, it is generally accepted that ilmenite alteration is the result of iron oxidation and its removal from the ilmenite lattice procuring relative TiO_2 enrichment. There is also general agreement that the degree (but not necessarily the extent) of ilmenite alteration in a sedimentary environment is mainly a function of soil conditions and duration of exposure. Ilmenite alteration is promoted under elevated temperatures and in addition, corrosive fluids are known to enhance alteration. The period of

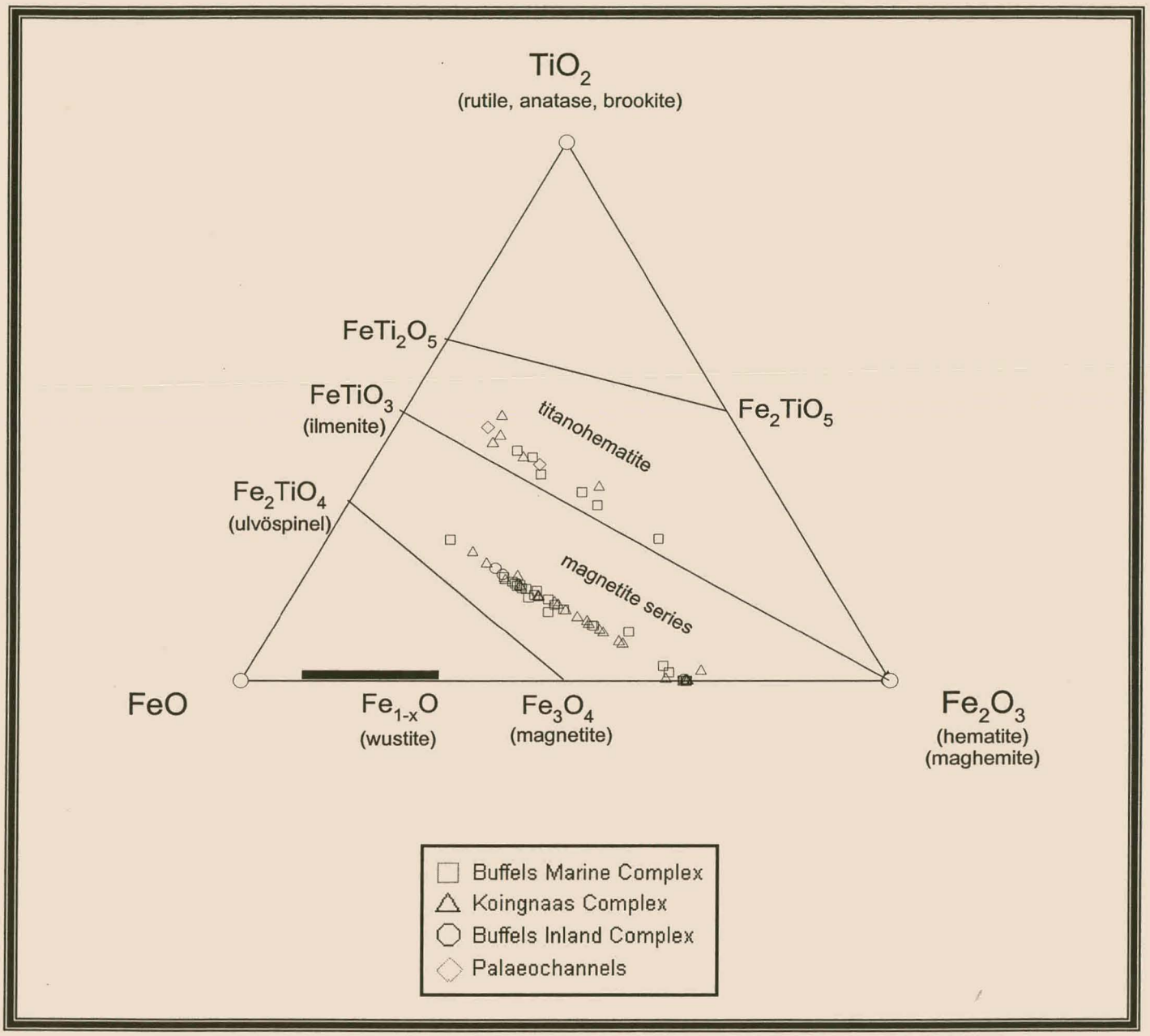

Figure 5.11. Ternary plot illustrating the chemistry of titanohematite and magnetite from the study area in the FeO-TiO_2-Fe_2O_3 system (after Buddington and Lindsley, 1964).

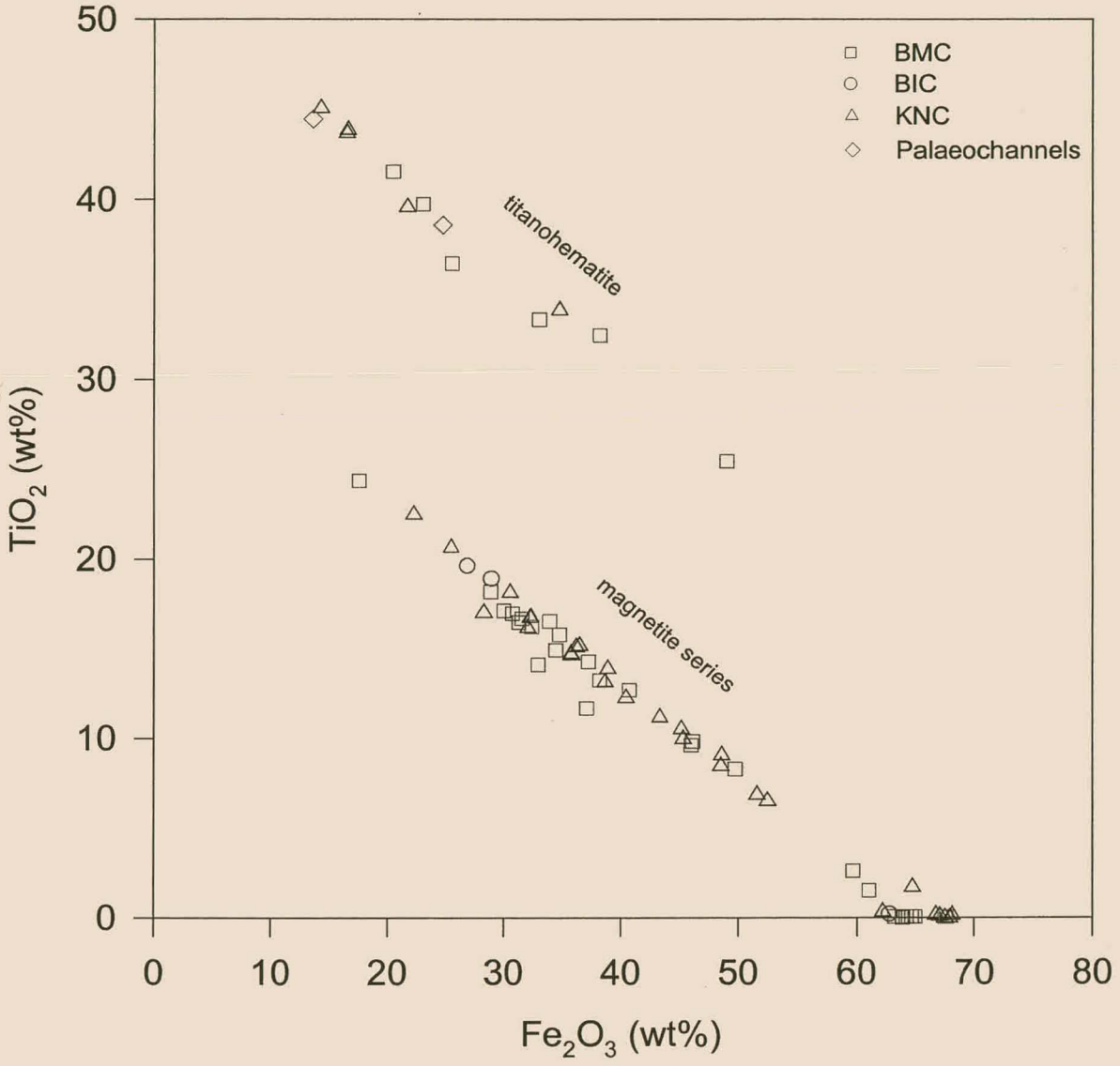

Figure 5.12. Variation diagram illustrating the TiO_2 versus Fe_2O_3 content of titanohematites and magnetites in the study area.

exposure to these conditions is a very important factor and many older ilmenite deposits such as those along the west coast of Australia are economically enhanced by their age.

Several authors (Bailey *et al.*, 1956; Hugo, 1988; Macdonald, 1993; Babu *et al.*, 1994) found that the physical and chemical characteristics of the mineral are modified during ilmenite alteration, that will unquestionably effect the quality and recoverability of ilmenite. Generally, as alteration (or the TiO_2 content) increases, FeO decreases due to oxidation to Fe_2O_3, that in turn increases up to a point between ~65-70 wt% TiO_2 where after which it is believed to be removed. Likewise, the Al_2O_3 and SiO_2 contents are significantly enhanced, compared to the MnO and MgO contents that decrease very sharply with increasing alteration (Nassef, 1981; Morad and Aldaham, 1986). Corresponding physical changes include crystallographic re-configuration as well as a decrease in magnetic susceptibility and density (Wort and Jones, 1980; Hugo and Cornell, 1991; Brown *et al.*, 1993).

Bailey *et al.* (1956) provided a three-stage model for ilmenite alteration based on distinct petrographic observations. According to this model, the first stage described as "patchy ilmenite" is accompanied by "elongated stringers, rims and round patches" of bluish-grey material. Stage two is marked by the development of an essentially amorphous, bright grey, isotropic iron-titanium oxide, but by using detailed scanning transmission electron studies Hugo (1993) discredited the existence of an amorphous titanium phase. During the final stage of the Bailey' *et al.* (1956) model, leucoxene is thought to form at the expense of this "amorphous" phase.

Several workers (Karkhanavala and Momin, 1959; Temple 1966; Teufer and Temple, 1966; Dimanche and Bartolomé; Grey and Reid, 1975; Frost *et al.*, 1983; Mücke and Chaudhuri, 1991; Hugo and Cornell, 1991) recorded similar observations regarding ilmenite alteration; reporting that alteration is most prominent along grain boundaries, structural weaknesses and the basal plane of the ilmenite.

Teufer and Temple (1966) believed that although structural differences are evident across the entire compositional range, chemically the alteration products are transitional in composition from unaltered ilmenite to leucoxene. These workers advocated that the structural change occurs when the TiO_2 composition is 65-70%, where the removal of sufficient iron forces the trigonal ilmenite lattice to deform to the hexagonal structure of the mineral pseudorutile (Karkhanavala and Momin, 1959; Grey and Reid, 1975). Further removal of iron would result in the transformation to cryptocrystalline rutile (leucoxene).

Grey and Reid (1975) proposed a dual-stage model for ilmenite alteration, which is acclaimed by the majority of workers. The first stage involves the oxidation and removal of iron via an electrochemical process and comprises the first two stages of the Bailey *et al.* (1956) model. The first stage is described by the reaction:

$$3Fe^{2+}TiO_3 + H^+ + \tfrac{1}{2}O_2 \longrightarrow Fe_2^{3+}Ti_3O_9 + Fe^{2+}(OH)^-$$

ilmenite pseudorutile + dissolved iron

Approximately a third of the iron is removed in this manner and the model further suggests that when pseudorutile is formed all the iron is present in the ferric form. The reaction is considered to take place in mildly acidic conditions in areas below the water table (Grey and Reid, 1975; Dimanche and Bartolomé, 1976; Hugo and Cornell, 1991).

During the second stage, alteration beyond pseudorutile takes place via a leaching and reprecipitation process where both iron and titanium are dissolved, but the titanium is reprecipitated while the iron is leached from the grain.

Cryptocrystalline rutile (leucoxene) is the ultimate product of this process, which is described by the reaction:

$$Fe_2^{3+}Ti_3O_9 + 4H^+ \longrightarrow 3TiO_2 + 2Fe^{2+} + \tfrac{1}{2}O_2 + 2H_2O$$

This process is thought to occur in the near surface environment under acidic conditions which result from humic acids. Pseudorutile is believed to be unstable under these conditions and is readily transformed to leucoxene. It is envisaged that

temperate atmospheric conditions and ample fluid circulation would accelerate the alteration process. In a similar way, elevated ilmenite alteration is connected with a rising water table and humid or warm climate.

Hugo and Cornell (1991) and Hugo (1993) in their study of ilmenites from the east coast of South Africa, presented evidence that ilmenite alteration follows three distinct mechanisms:

Type I: gradual alteration of ilmenite, from hydrated ilmenite via pseudorutile to finally leucoxene.

Type II: direct alteration of ilmenite to leucoxene.

Type III: pre-depositional alteration of ilmenite in source rocks to ilmenite and hematite, followed by the leaching of hematite to form ilmenite consisting of porous TiO_2 microcrystallites.

Type I alteration conforms to identical observations noted by many workers (Temple, 1966; Teufer and Temple, 1966; Carpenter and Carpenter, 1991; Pirkle *et al.*, 1991) and is best accounted for by the model of Grey and Reid (1975), postulated to occur in regions below the water table. Type II represents a single step dissolution-reprecipitation process where ilmenite alters directly to leucoxene without the formation of pseudorutile (Hugo, 1993). Frost *et al.* (1983), and Hugo and Cornell (1991) found that this type of alteration is confined to near-surface regions where soil acids directly alter ilmenite.

Type III alteration is represented by the replacement of ilmenite by prismatic or vermiform TiO_2 microcrystallites. Characteristic of this type of alteration is that it is not prevalent along structural weaknesses, but occurs as irregular patches throughout the grain. These grains were initially altered in their metamorphic or igneous host rocks to ilmenite and hematite (Hugo, 1993) and subsequent alteration in a sedimentary environment leached the hematite resulting in an ilmenite containing essentially TiO_2 microcrystallites.

Ilmenite alteration in the Kleinzee area

Typical proportions of ilmenite and its alteration products in the study area are presented in Appendix G. It is evident that most of the ilmenite in the study area occurs as homogeneous unaltered grains. The percentage of altered grains from the BMC, BIC and KNC is almost uniform, averaging ~8% in contrast with the altered ilmenites from the palaeochannels that comprise more than 90% of the ilmenite population.

The amount of leucoxene increases almost invariable with elevation, attaining the greatest significance in the topmost sedimentary unit. This is supportive evidence that leucoxene preferably forms in the uppermost soil layers as postulated by the models of Grey and Reid (1975) and Hugo and Cornell (1991). However, the figures quoted for the proportion of the altered ilmenite population could be regarded as distorted since the extent of alteration was not considered. During point-counting grains that are volumetrically less altered were not distinguished from grains that show extensive alteration. In a similar manner, excluding leucoxene, all the altered ilmenites were recorded as a single altered population, regardless of their degree of alteration.

The ilmenite alteration spectrum contains grains that are characteristic of alteration mechanisms formulated by both Grey and Reid (1975) and Hugo and Cornell (1991). The majority of the altered ilmenite population displays only incipient alteration, which did not proceed beyond the hydrated ilmenite phase. This alteration type is mainly confined to cracks, grain boundaries and basal stringers, corresponding to the initial stages of models suggested by Grey and Reid (1975) and Hugo and Cornell (1991). A large percentage of hydrated ilmenites have a TiO_2 content less than the proposed constraint of 53%, despite possessing the optical properties of hydrated ilmenites TiO_2. These grains conspicuously show higher Fe_2O_3 and correspondingly lower FeO values, implying that although comprehensive oxidation has taken place, prevailing conditions were non-conducive in removing the ferric iron from the crystal.

Plate 5.3B shows an ilmenite that is in a more advanced stage of alteration where pseudorutile is partially replacing the hydrated ilmenite. This represents the second stage of Grey and Reid's (1975) model in which the pseudorutile is ultimately transformed to microcrystalline rutile (Plate 5.1A). Although Grey and Reid (1975) stated that the degree of ilmenite alteration could be associated with the water table, this could not be verified, because it was not studied.

Ilmenite typical of type II from the Hugo and Cornell (1991) model was rarely noted. These particular ilmenite grains (Plate 5.1B) are believed to alter directly to leucoxene, without the development of any pseudorutile. Particular leucoxenes often display a porous character and these areas contain significant quantities of SiO_2 and Al_2O_3. SEM analyses revealed that the siliceous phase occurs as infillings in cavities or as distinct highly siliceous areas in homogeneous areas (Plate 4C). Hugo (1993) and Frost *et al.* (1983) showed that this type of alteration is confined to the upper surface regions. In the study area this type of altered ilmenite is randomly distributed with respect to elevation (or depth) and is especially prevalent in the palaeochannels. Altered ilmenite that conforms to Hugo and Cornell's (1991) type III alteration, although very rare, has also been recognised in the study area. These grains are marked by vermiform rutile crystallites and are interpreted as having formed by alteration in the parent rocks. It was noted that other complex Fe-Ti oxides alter in a similar manner as discussed by the mechanisms of Grey and Reid (1975) and Hugo and Cornell (1991) suggesting that their models could hold merit in explaining general alteration in all titanium-bearing oxides.

Geochemical traverses across studied ilmenite grains (Fig. 5.13→5.15) confirms that these particular ilmenites alter to different stages as postulated by Grey and Reid (1975). Geochemistry indicates that as alteration progresses, the ferrous iron decreases as it is oxidised to the ferric state, only to be preferentially removed. Fig. 5.10. indicates that when the TiO_2 is 61-62 wt% (a phase which could be considered pseudorutile), virtually no ferrous iron is present. As alteration progresses to the final stage of Grey and Reid (1975), the ferric iron is removed and when the TiO_2 content reaches ~70 wt%, the other substitution elements Mn and Mg are totally

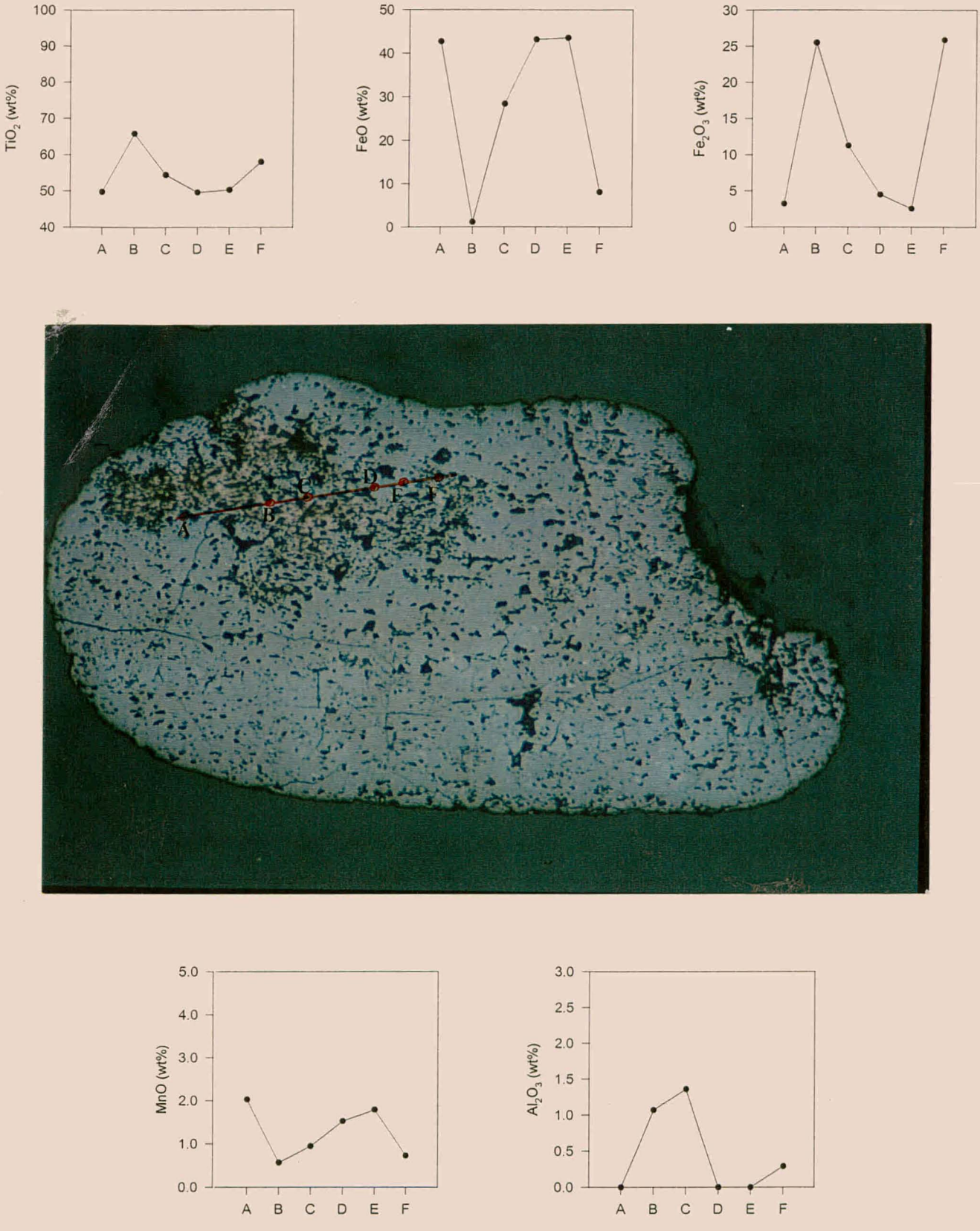

Figure 5.13. Chemical traverse across a moderately altered ilmenite grain.

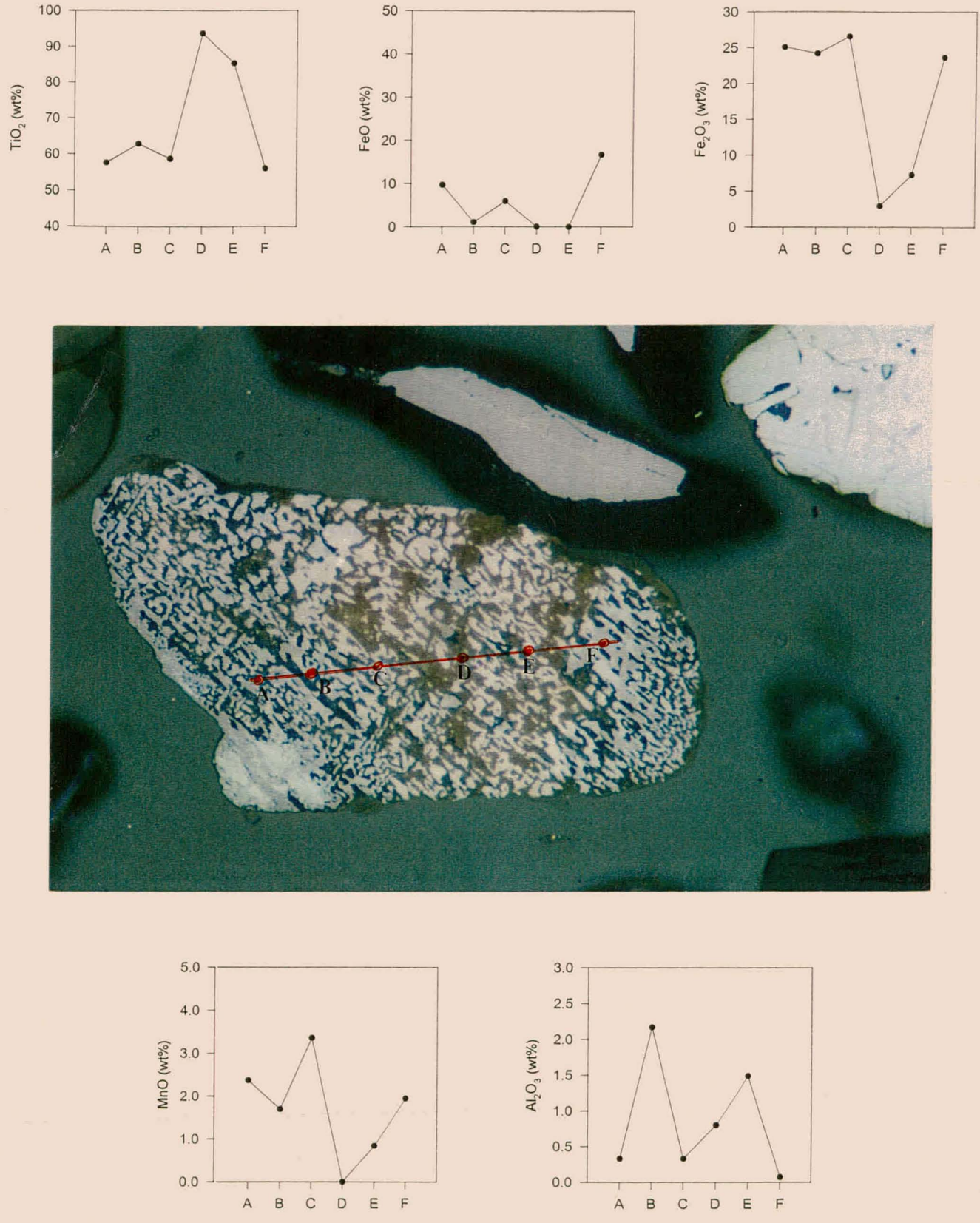

Figure 5.14. Chemical traverse across a highly altered ilmenite.

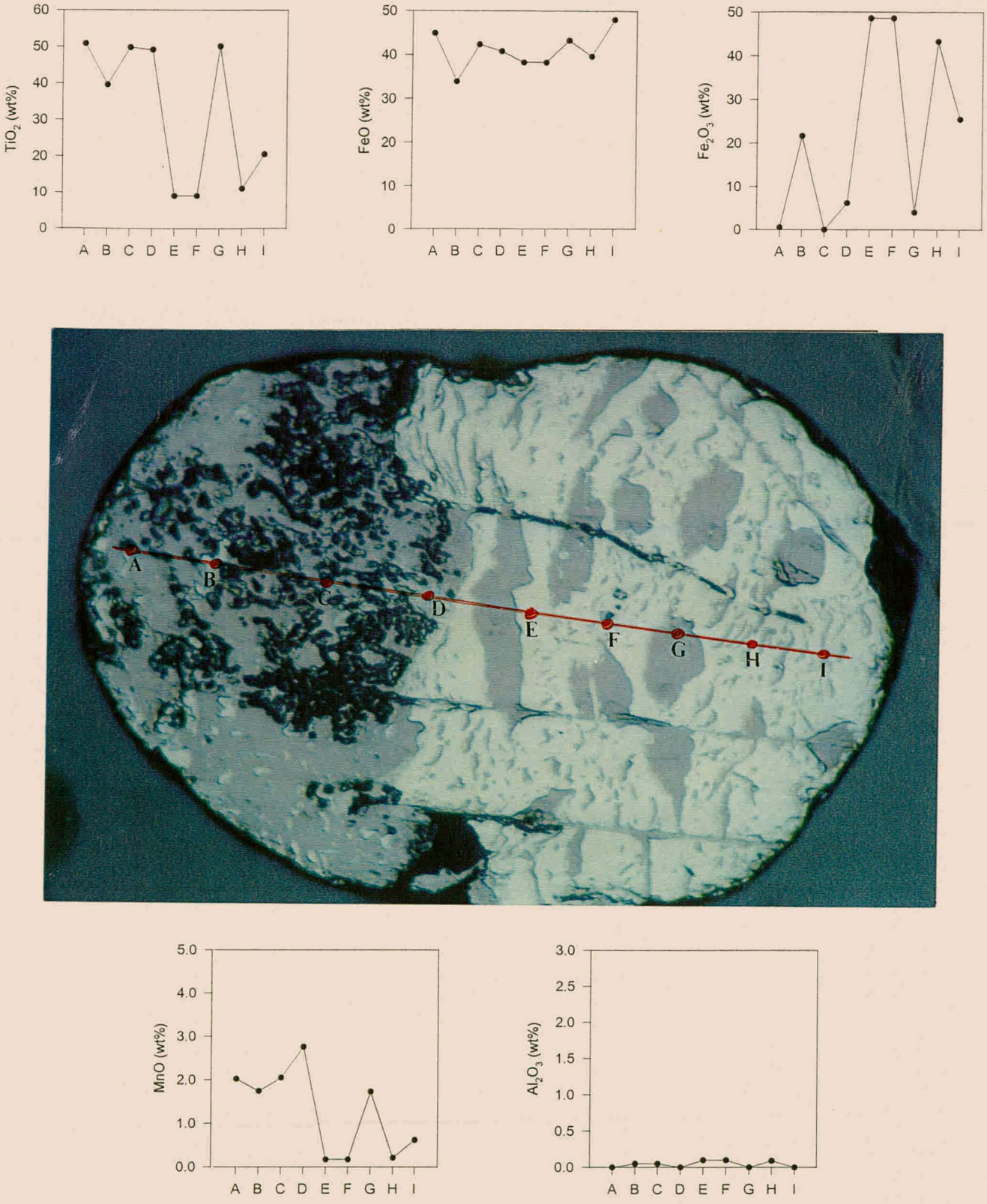

Figure 5.15. Chemical traverse across a complex iron-titanium oxide that consists of altered and unaltered ilmenite, hemo-ilmenite and titanohematite.

removed as the pseudorutile structure adjusts to that of rutile (Neumann, 1974). Al and Si, however seem to increase markedly during this stage. Frost *et al.* (1983) and Hugo (1993) postulate that it is possible that the Al and Si could co-precipitate with Ti or adsorb onto the surface when conditions are suitable, while other workers (Puffer and Cousminer, 1982; Anand and Gilkes, 1985; Babu *et al.*, 1994) argue that Al and Si are partially present as clay minerals in pore cavities. Golding (1961) stated that leucoxene high in Al and Si could probably be derived from the alteration of titanite.

It is concluded that although a complex suite of marks the Kleinzee sediments altered Fe-Ti oxides, nearly all the alteration products follow the mechanism suggested by Grey and Reid (1975). There is also overwhelming evidence that the majority of altered ilmenites were altered *in situ*. Hydrated ilmenite invariably dominates the altered population while pseudorutile in comparison with the low and high order altered product has a conspicuously low content. This discrepancy could be explained by the fact that pseudorutile is unstable under specific conditions and instead the conversion to leucoxene is promoted. Pseudorutile is furthermore mechanically less stable so that dominant wave-action could be responsible for its removal from the altered assemblage. A single model however, cannot satisfactorily explain ilmenite alteration in the Kleinzee area and is better explained by a model where differentially altered ilmenites have mixed during successive events of reworking.

It is interesting to note that compared to the Kleinzee area, Cilliers (1995) and Macdonald (1996) reported strikingly similar alteration products and proportions; both stating that ilmenite alteration in the respective areas follow the mechanism of Grey and Reid (1975) and in part correspond to a model suggested by Hugo and Cornell (1991). In perspective, this indicates that climatic conditions during the Pliocene-Pleistocene were uniform along the entire west coast of South Africa. It is envisaged that the climate during this period was semi-arid and surface vegetation minimal (Truswell, 1977; Tankard *et al.*, 1982; Partridge and Maud, 1987). Collectively, these factors limited advanced ilmenite alteration resulting in the poor TiO_2 grade of the west coast deposits. Ilmenite alteration in the palaeochannels deposits is significantly

enhanced because of their relatively older, Miocene age and the activity of a very strong leaching fluid.

5.3. Magnetite-ulvöspinel series

5.3.1. Petrography

Magnetite is a minor constituent, but is present in nearly every sample. Magnetite grains are often smaller than 150 μm, but larger grains have been observed in the younger (less mature) stratigraphic sequences. Magnetite is grey with varying tints of dark brown in reflected light using oil immersion lenses and is characteristically isotropic. It commonly occurs as angular to subrounded grains; very often fragmented grains with well-developed crystal forms are observed. Magnetite in this study is generally homogeneous and only some grains display sparsely distributed rutile or ilmenite lamellae.

Ilmenite exsolution lamellae parallel to the (111) plane were rarely observed (Plate 5.6A), but unorientated ilmenite inclusions within magnetite forming composite grains are more common. A few magnetite grains display Ramdohr's (1980) woven or cloth texture that represents ulvöspinel exsolution in magnetite. Pleonaste ($FeAl_2O_4$-$MgAl_2O_4$) exsolution manifesting as orientated blebs (Plate 5.6B) was confirmed by EDS. Such grains are commonly derived from metamorphosed gneissic or ultramafic rocks (Razjigaeva and Naumova, 1992).

The alteration of magnetite to hematite appears as lamellae parallel to (111) magnetite planes referred to as martitisation (Plate 5.7). The magnetite generally exhibits varying degrees of martitisation, which takes place directly along the octahedral planes. Although martitisation occurs primarily under higher fO_2 and above 550°C in the source rocks during late-stage metasomatism, Haggerty (1976) and Riezebos (1979) stated the possibility of martite development due to atmospheric weathering in a sedimentary environment. Characteristic of this process is the thin hematite lamellae that start to form from the outside of a magnetite grain (Plate 5.7). The development of goethite at the expense of martite occurs in the more weathered sequences, especially in the BIC sediments.

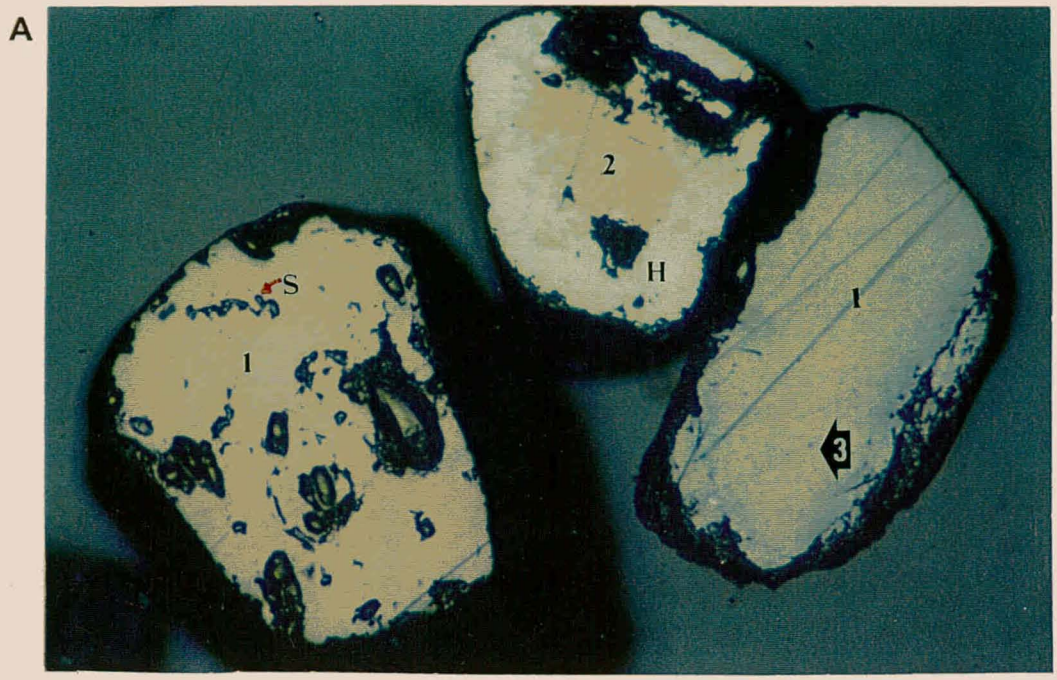

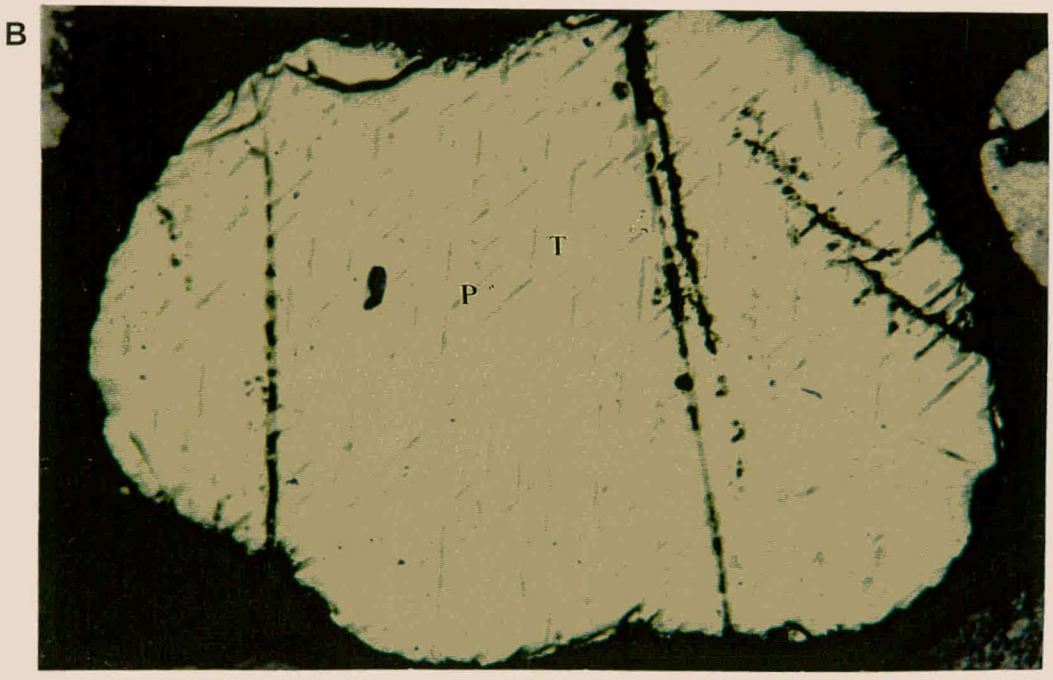

Plate 5.6. Selected magnetite grains.

A) 1- homogeneous magnetite with minute inclusions of spinel; 2- magnetite oxidized to hematite; 3- magnetite with prominent ilmenite (I) lamellae.

B) Titanomagnetite (T) with thin cross-cutting laminae of pleonaste (P).

Scale: 200X

Plate 5.7. Replacement of magnetite (M) by hematite (H), better known as martite. Note how martitasation advances from the outside of the grain.

Scale: 200X

5.3.2. Chemistry

Magnetite ($Fe^{3+}[Fe^{3+}Fe^{2+}]O_4$) forms a solid-solution series with the spinel group in particular with ulvöspinel (Fe_2O_4) and also accommodates variable amounts of Al, Cr, V, Mg, Mn and Ca (Deer *et al.,* 1992). Magnetites were analysed for Ti, Al, Si, Mn, Mg, Ca, Fe and the results are presented in Appendix H.

Microprobe results indicate that almost the entire compositional spectrum between ulvöspinel and magnetite is present (Fig. 5.11). The majority of the magnetites are Ti-rich and some of them contain sufficient TiO_2 to be classified as titaniferous magnetites (Reynolds, 1978). Many of the magnetites were not oxidised and have near stoichiometric compositions as indicated by the strong TiO_2 - Fe_2O_3 correlation (Fig. 5.12). Mn, Mg, Al, Cr, Si and Ca are invariably present in trace quantities.

5.4. Rutile

5.4.1. Petrography

Rutile is invariably present as a rare constituent and varies in size between 75-90 μm. It occurs as red, brown, black and yellow, well-rounded, sub-elongated prismatic forms often with terminated ends (Plate 5.8A, 8B and 8C). Very scarce opaque (black) rutile resembles ilmenite in appearance, but is easily distinguished from the latter by its brilliant internal reflections, in oil reflected light. Twinning displayed as oblique striations (Plate 5.8A), often intersecting each other and inclusions are common in particular grains. No distinction was possible between rutile and the other two TiO_2 polymorphs anatase and brookite due to their identical optical properties.

5.4.2. Chemistry

Rutile grains were analysed by electron microprobe for Ti, Si, Al, Cr, Fe, Mn, Mg and Ca and representative rutile compositions are given in Appendix H. Results show that no regional variation in the composition of the grains is evident. Representative rutiles are chemically very pure, containing near stoichiometric proportions of TiO_2 ranging from 96-99%. The only impurity to occur in trace amounts is FeO, which displays no particular correlation with the TiO_2 content (Fig. 5.16). The rest of the

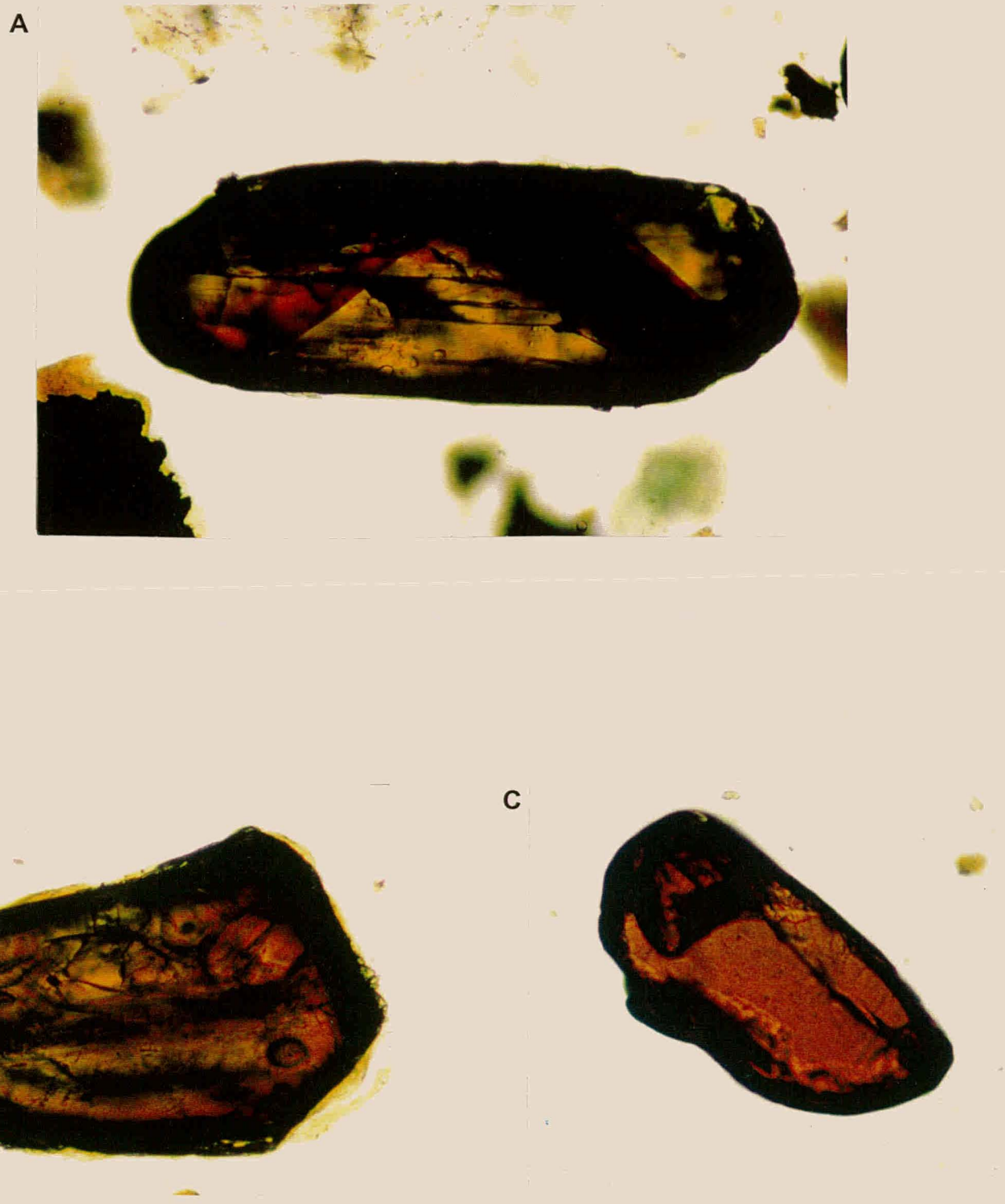

Plate 5.8. Selected primary rutile grains from the study area. Note the intersecting sets of twin lamellae (A).

Scale: 200X

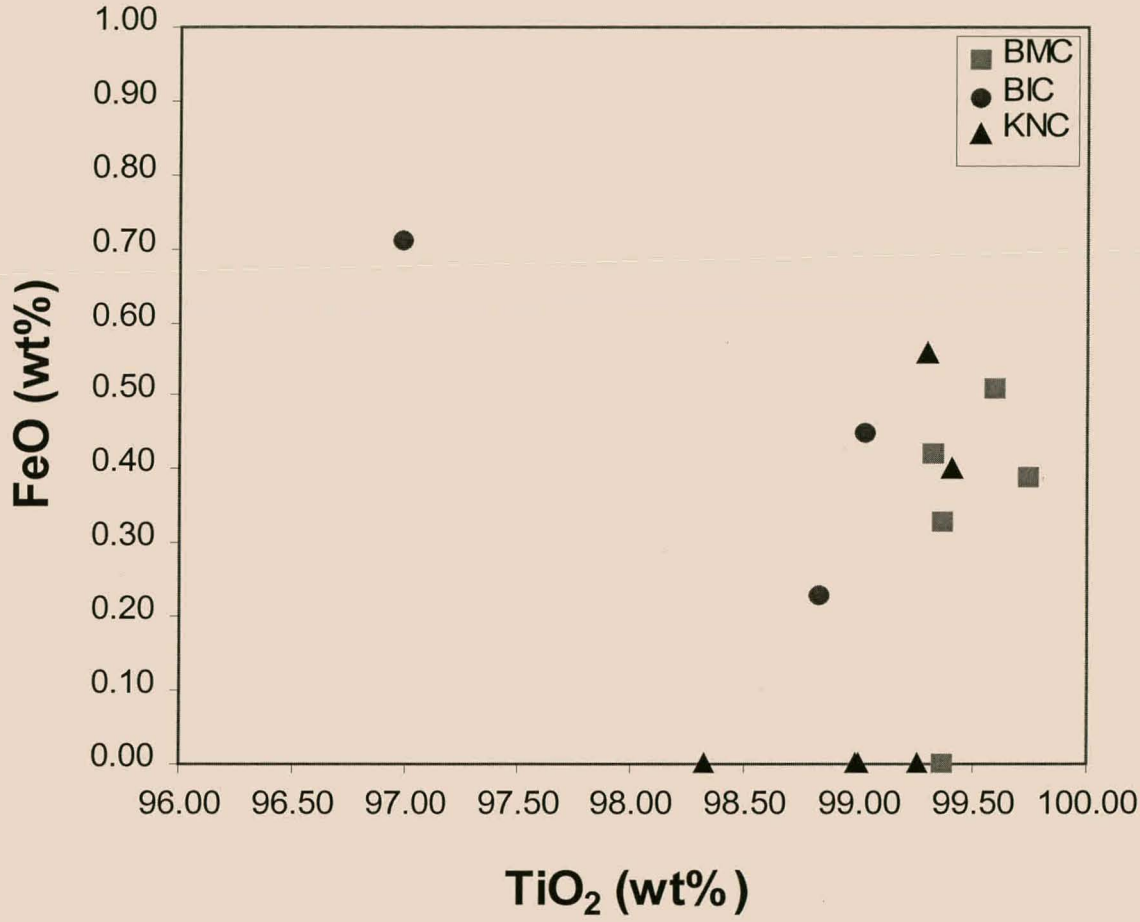

Figure 5.16. Variation of FeO with TiO_2 content for selected rutile grains from the study area.

elements generally occur in concentrations below the detection limit of the microprobe.

5.5. Zircon

5.5.1. Petrography

Zircon is ubiquitous in all samples and varies in size between 75 and 180 μm, although larger zircon grains of up to 250 μm occur in the palaeochannels. The colour of a given zircon population in the study area is generally heterogeneous and extremely variable. Although the colourless (Plate 5.9A) and pink (Plate 5.9B) variety dominates, some display shades of yellow (Plate 5.9C) of brown and also orange or purple. Metamict zircons in particular, show a range of colours from light grey to yellow and brown (Plate 5.10A).

The composition of the zircon population and consequently each coloured variety differ proportionately for sediments from the marine, palaeochannel and fluvial environments. Zircons of the palaeochannels are mainly pink with colourless, yellow varieties present in minor to trace amounts. Marine sediments host variable mixtures of pink, clear and yellow types. By contrast, zircons from the fluvial environments show a variety in colour with yellow to yellow-brown types dominating the population. Fielding (1970) suggested that strong colours are associated with the presence of U, supporting the conclusions of Matumura and Koga (1962) that colour centres were produced by radiation-induced reduction of Zr^{4+}.

Morphologically most zircons occur as rounded to spherical grains (Plate 5.10B) dominating over idiomorphic crystals (Plate 5.10C). Distinctly zoned grains with complex internal structures are also present. Fluvial zircons are mainly distinctive euhedral crystals including a variety of crystal forms and habit, whereas the BMC, KNC and palaeochannels contain more rounded zircon grains, with poorly preserved crystal faces. Irregularly shaped, angular fragments are more common in the fluvial environments. Many grains are frosted, grooved or pitted, a feature caused by abrasion and etching during transport.

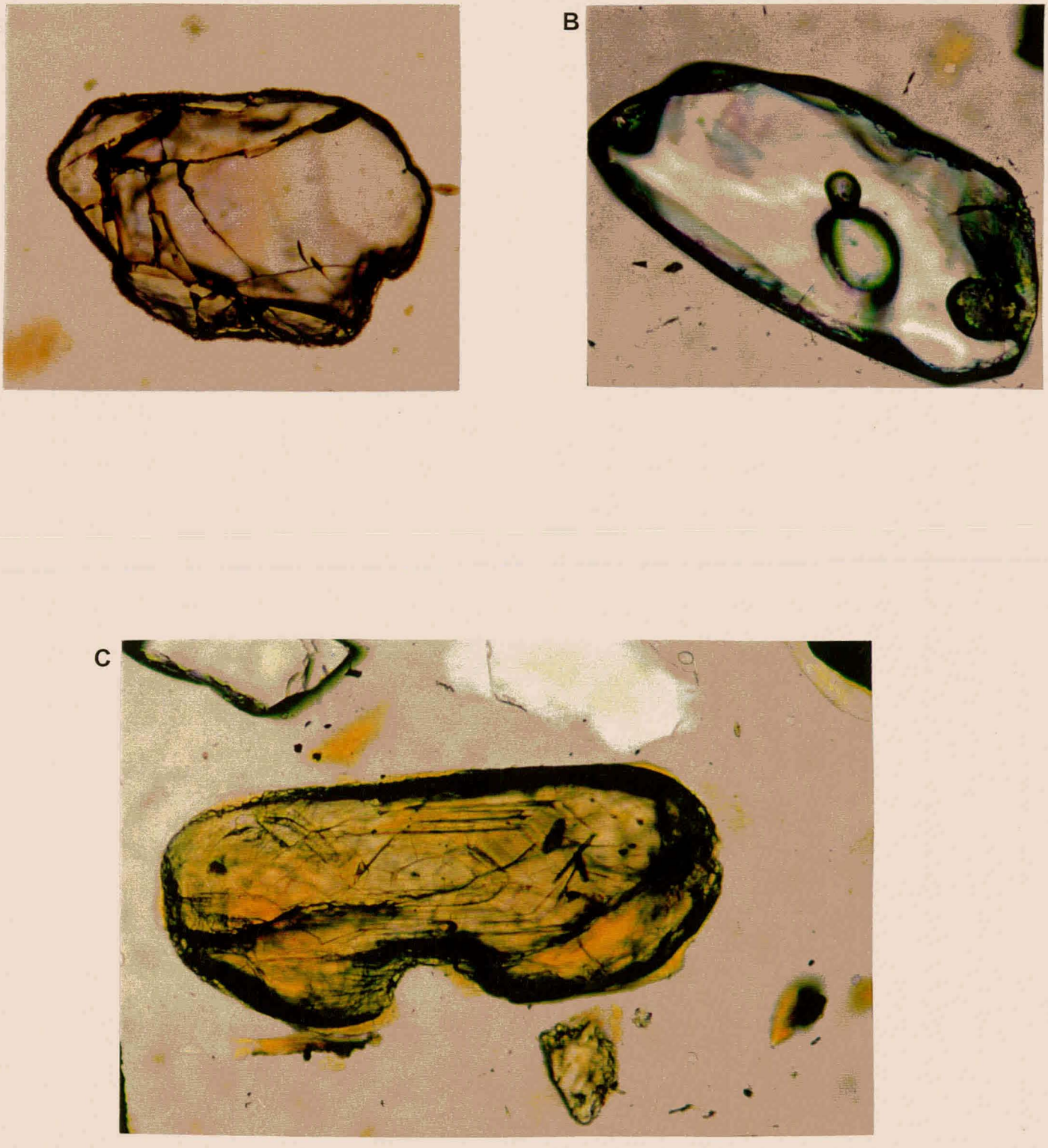

Plate 5.9. Typical zircons encountered in the study area.

A) Simple, pink zircon with outgrowth.

B) Common, clear-colourless zircon.

C) Yellow zircon, displaying fine oscillatory zoning.

Scale: 200X

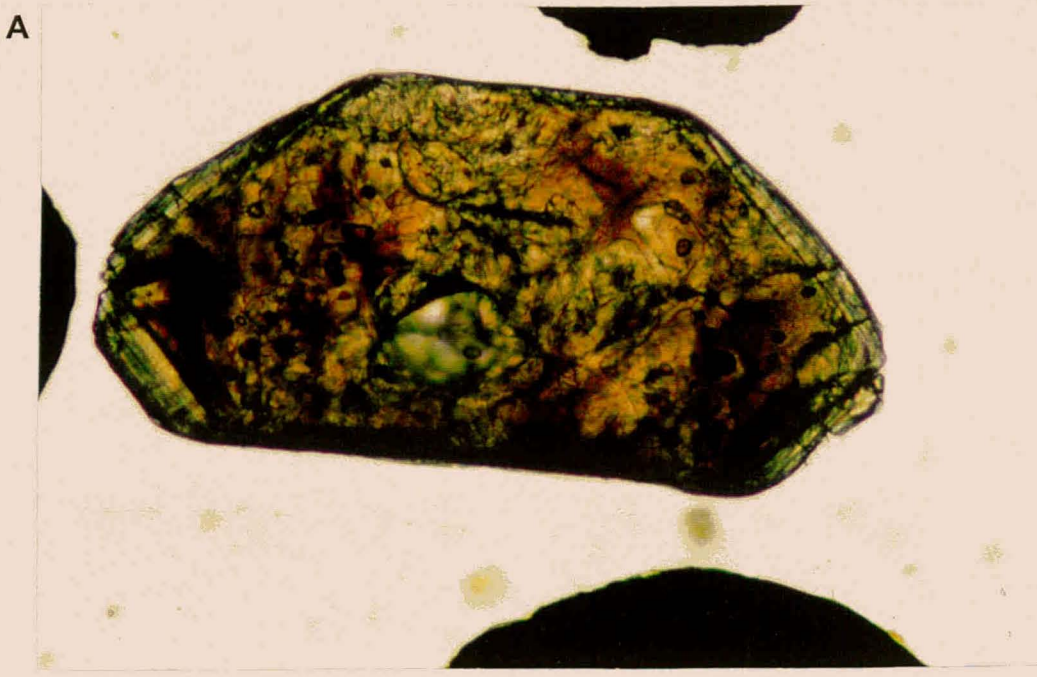

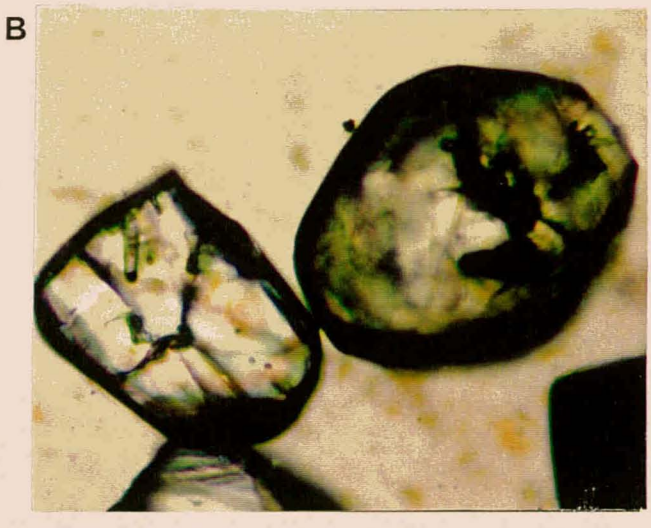

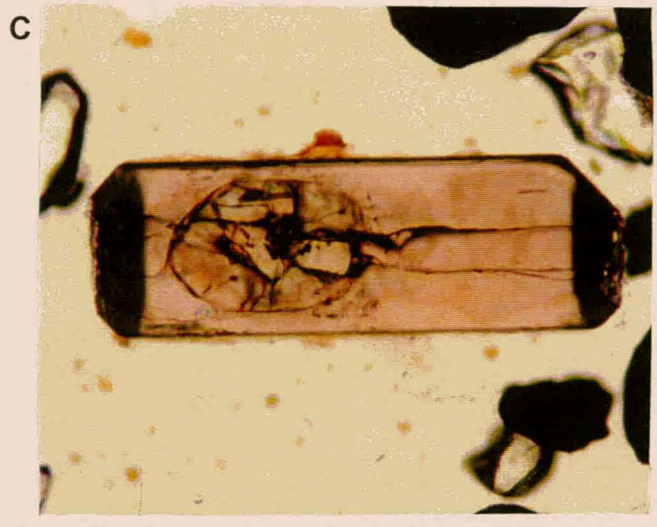

Plate 5.10. Selection of zircons in the study area.

A) Euhedral, metamict zircon.

B) Zircons displaying subrounded to rounded habit.

C) Euhedral zircon, with a core that has been damaged by intracrystalline radioactive emission.

Scale: 200X

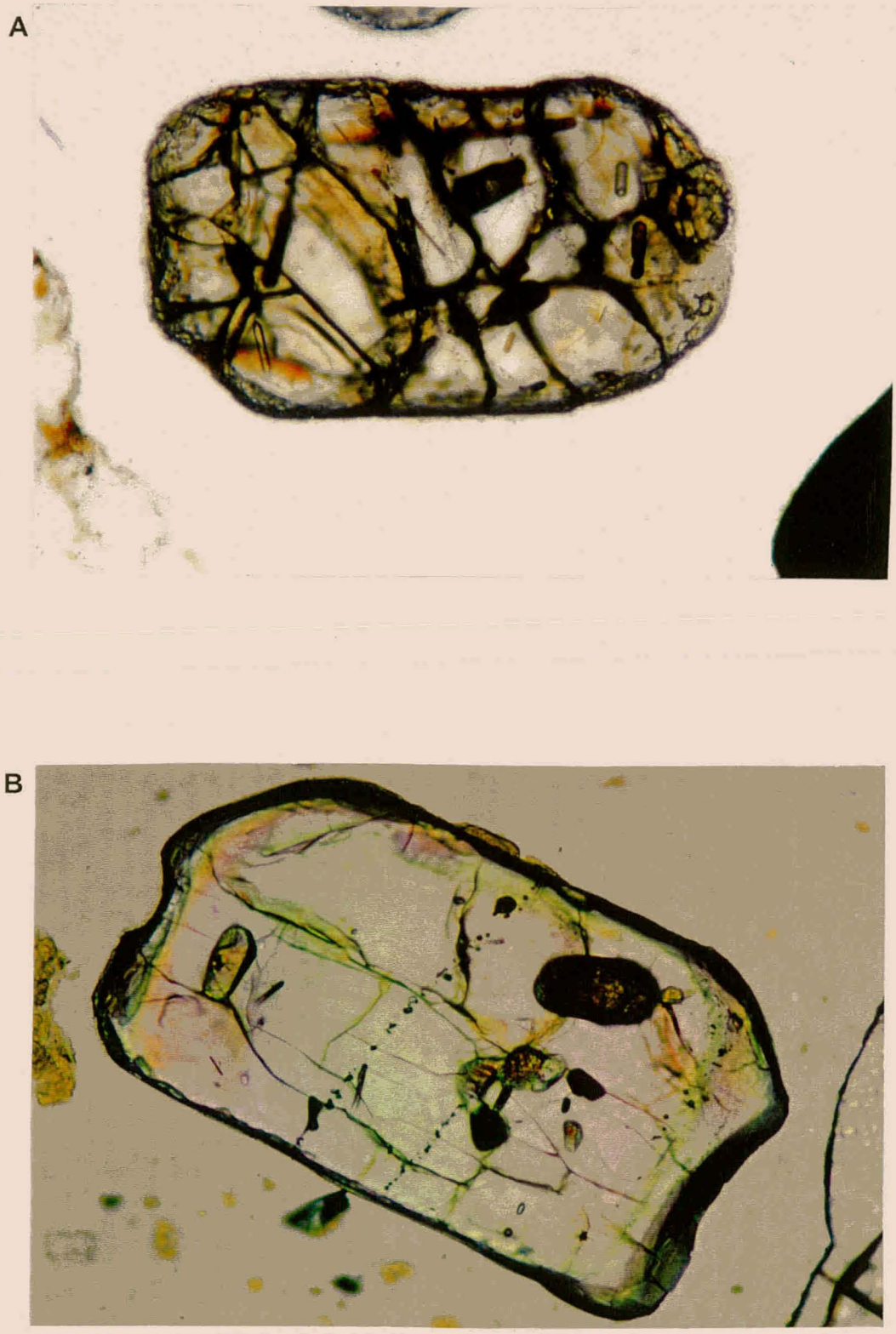

Plate 5.11. Typical studied zircons.

A) Zircon with a system of fractures. Fractures could be the result of extensive physical exposure or radioactive emissions.

B) Zircon hosting several types of inclusions of which apatite is the most common. Note the characteristic colour zoning of zircon.

Scale: 200X

Several zircons are marked by radiating or concentric fractures, often crossing an opaque inclusion originating from the middle (Plate 5.11A), and are a typical feature of metamict zircons, particularly common in the BIC and present-day rivers. Speer (1980) suggested that this feature is related to the radioactivity of Th and U present as substitution elements in the zircon crystal lattice. Observed opaque spots are believed to form when atoms are forced from the crystal by radiogenic emissions from U and Th, leaving vacant positions in the crystal lattice that subsequently leads to crystal shattering.

Fractures may be promoted during metamictisation (Hartmann *et al.*, 1997) as regions high in radiogenic nuclides create a high internal stress within the crystal (Lee and Tromp, 1995), causing the lattice to expand and shatter. Some fractures however, might be the result of external physical processes as these fractures sometimes cut across grains. SEM and BSE imaging revealed that growth regions enriched in Hf, U and Y commonly fill fractures.

Inclusions are frequently hosted by zircons (Plate 5.11B), comprising spherical and tabular gas/fluid inclusions, transparent crystals, opaque phases and combinations thereof. Tabular inclusions are often elongated parallel to the crystallographic axis while other inclusions show no preferred orientation. Solid inclusions confirmed by EDS include ilmenite, rutile, biotite, muscovite, titanite, apatite, monazite, xenotime, allanite, sillimanite, feldspar, quartz and several unidentified phases. Inclusions of earlier small, euhedral zircon crystals, often orientated parallel to the c-axis, were noted and confirmed by EDS. Larger zircons generally host the most inclusions. Ilmenite forms the largest and most common inclusions, closely followed by apatite.

5.2.2. Chemistry

The chemical formula of zircon is $ZrSiO_4$, but a whole range of trace elements can be incorporated in the crystal lattice through coupled substitution. Zr^{4+} is commonly replaced by Hf^{4+}, U^{4+}, Th^{4+}, Y^{3+}, REE^{3+} (La→Lu), Nb^{5+}, Ta^{5+}, Ti^{4+}, Pb^{4+}, Pb^{2+}, Fe^{3+}, Fe^{2+}, Ca^{2+}, Na^{+} and K^{+} and Si^{4+} by Al^{3+}, P^{5+} and S^{6+} (Speer, 1980). It is also possible that these trace elements are present as inclusions of separate mineral phases. Hf is

most closely related to Zr and is the major substitute for Zr in zircon. Typically, zircon contains on average 1 wt% Hf although individual growth zones might be significantly richer (Speer, 1980; Hinton and Upton, 1991; Deer *et al.*, 1982). Most zircons have a Hf/Zr ratio of 0.02 and this ratio apparently increases with differentiation and increasing alkalinity, volatile content and silica saturation of the parent liquid/melt (Brooks, 1970; Deer *et al.*, 1992). Some of the highest Hf/Zr ratios are found in metamict varieties (Speer, 1980). Of the Y-REE group, Y predominates in zircon and this can be related to the isostructural relationship between xenotime (YPO_4) and zircon. Zircons usually contain less than 1 wt% REE_2O_3, but in more differentiated igneous rocks, higher values are common (Speer, 1980).

Microprobe analyses were performed on a representative suite of zircons for Si, Zr, Hf, Al, Fe, K, Ca, Y, P, Th and U and the results are presented in Appendix H. Compositionally the differences between zircons from the different groups are slight. Zircons from the palaeochannels have on average 32.35 wt% Si, 65.06 wt% Zr and 1.31 wt% Hf. Zircons the from KNC, Buffels and Swartlintjies rivers show strikingly similar chemistry. BMC zircons display a similar, but slightly greater Hf content. By contrast, zircons from the BIC have higher Zr values of 66.36 wt% and a relatively elevated Hf content of 1.51 wt%. The Hf-Zr relationships of zircons from the various areas are clearly illustrated in Fig. 5.17. There is no linear correlation between the Hf and Zr content.

Elements in minor amounts include Y, P, Th and Fe and are not particular to any specific group. Most of the concentrations are very close to the detection limit of the instrument. Semi-quantitative SEM data showed that the strongly coloured zircons are relatively enriched in Fe and Al, particularly for zircons from the BIC and present-day rivers. Trace amounts of K, Ca and Mg have also been detected. Within the constraints of the electron microprobe, no consistent correlation between colour and chemistry could be established. In a follow-up operation however, Rozendaal *et al.*, (1999) have demonstrated in their analysis of single zircons grains by LA-ICP-MS that various zircon colour types are associated with specific trace element chemistry. Colourless-clear types were found to contain high Hf and very low U, Th and total

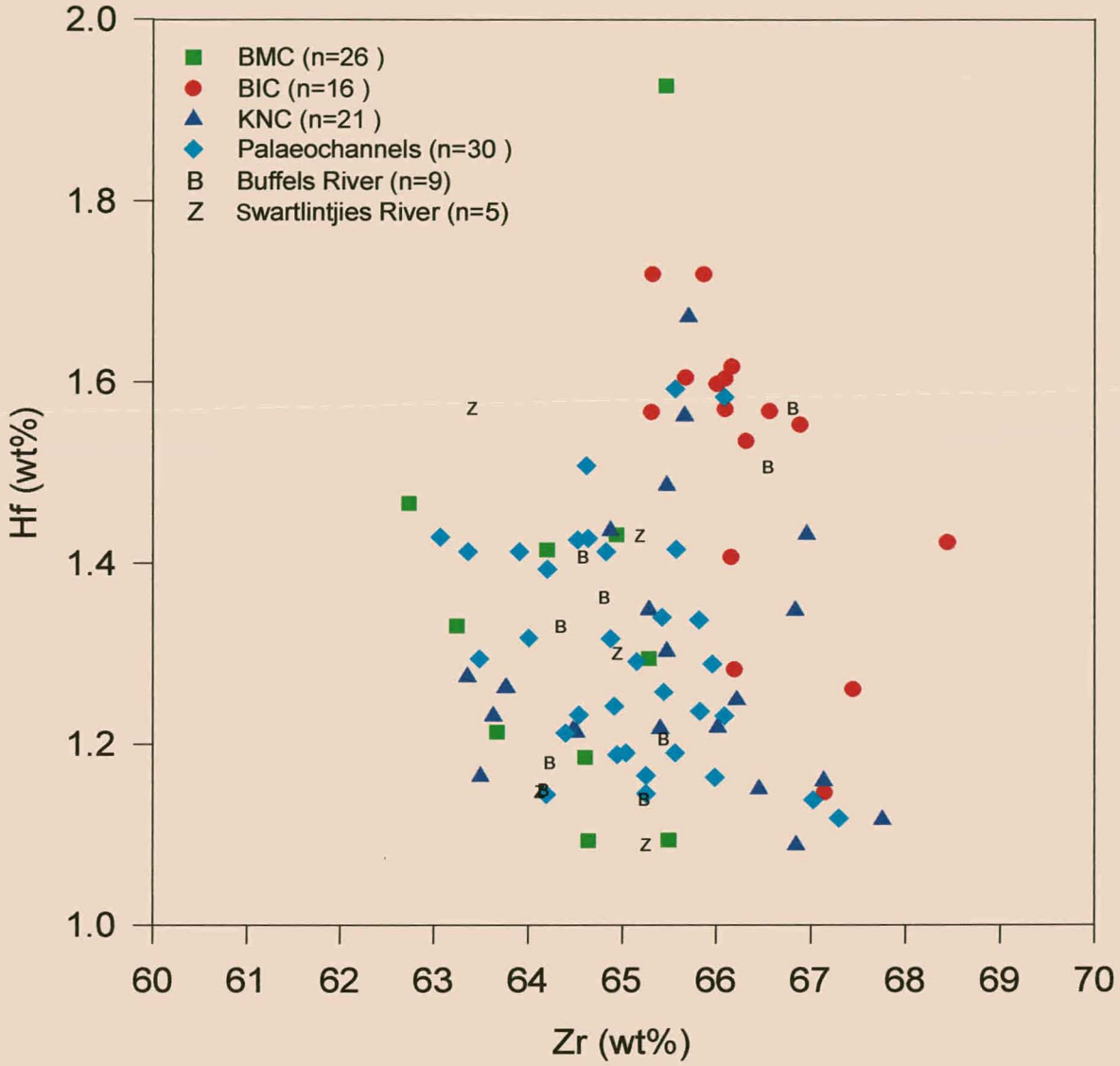

Figure 5.17. Binary diagram illustrating hafnium/zirconium relationship of zircons from the study area. Note the relative Hf enrichment of BIC zircons.

REE concentrations compared to the zoned, coloured and metamict varieties. Brown and metamict zircons are enriched in Y-REE and may host U and Th up to percentage levels. Compared to colourless zircons, pink types contain similar amounts of REE, but are marked by a greater abundance of U and Th. Yellow zircons host a diversity of elements including Y-REE, Al, Fe, P, U and Th in variable concentrations. Rozendaal *et al.* (1999) also illustrated that the HREE profiles are uniform for all zircon types, but that the LREE profiles vary extremely amongst types.

It is noted that the heavier REE predominate in zircon (Fielding, 1970; Romans *et al.*, 1975; Taylor and McLennan, 1985). Since the size of Zr^{4+} is closer to the heavier than to the light REE's it has a strong preference to fractionate the HREE. Semenov and Barinskii (1958) have however reported enrichment of LREE in zircon. Experimental studies have demonstrated that significant LREE partitioning into zircon is possible (Hinton and Upton, 1991). Unexpected LREE enrichments in zircons may also be due to inclusions that are enriched in the LREE such as allanite, apatite, sphene and monazite. Generally, zircons are characterised by a HREE dominated profile with a small to moderate LREE pattern and a well-defined negative Eu anomaly. In contrast, Hinton and Upton (1991), Pietersen (1993), Rozendaal et al. (1999) reported zircons with a positive Ce anomaly, while Schaltegger and Krahenbuhl (1990) described zircons with a negative Nd anomaly.

The relatively low abundance of zircon in the majority of studied sediments made it impractical to isolate adequate amounts of this mineral for REE and radiometric measurements. The only samples that yielded sufficient zircon for analysis were those from the palaeochannels and consequently discussion will centre on these zircons. The results obtained from REE analysis of pure zircon concentrates from the palaeochannels are listed in Appendix I and graphically represented as chondrite normalised values after Evensen (1978) in Fig. 5.18. In addition, a La/Yb index was calculated reflecting on which of the LREE and HREE dominates the REE profile. The La/Yb is calculated by the formula $\frac{La + Ce + Pr + Nd + Sm}{Gd + Dy + Ho + Er + Yb}$. The total REE content (ΣREE) of the palaeochannel zircons is quite variable, ranging from 886-2042 ppm.

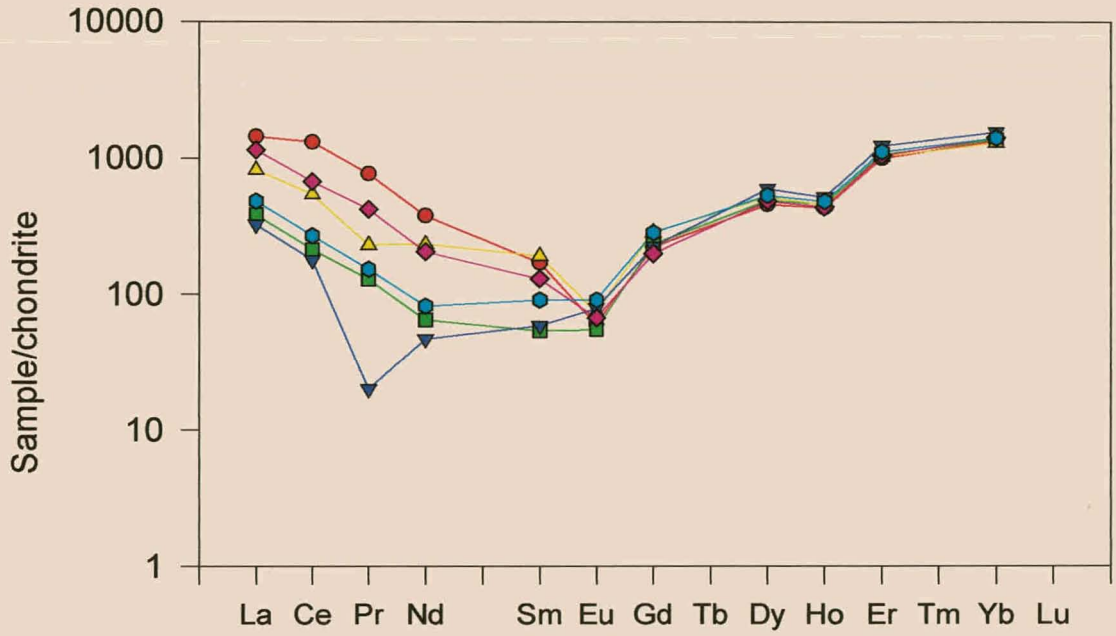

Figure 5.18. REE patterns for zircon separates from the palaeochannels.

Chondrite-normalised patterns appear to have a typical "birdwing" distribution and are characterised by a prominent LREE and HREE enriched profiles, well-defined Eu anomaly and the absence of a Ce anomaly. Suspect La values, which are the result of La contamination in the flux, are probably the reason for the absence of expected Ce anomalies. The HREE profiles are furthermore remarkably smooth with a minor change of slope at Ho. La/Yb values show that all the zircons of the palaeochannels are characteristically enriched in the HREE with respect to the LREE. HREE enrichment is strikingly similar, unlike the LREE profiles that are quite variable, resulting in the observed variance of ΣREE.

The difference in the LREE character between the various samples is related to the primary trace element chemistry of their respective zircon populations (Philander *et al.*, 1998; Rozendaal, 1998). Using high-resolution zircon chemistry, Rozendaal *et al.* (1999) confirmed that different colour zircon types have distinctive trace element characteristics. Those samples with dominantly coloured, zoned and metamict populations were found to have significantly higher LREE and resultant higher total REE concentrations. A variation in the individual mix of the various zircon types within a population will surely produce different LREE characters. Although zircon populations from the palaeochannels are dominated by the pink variety, yellow and zoned types were also observed, but to a lesser degree. Only a slight variation in the proportion of these yellow and zoned zircons among the studied populations would be sufficient to explain the shift of their respective LREE profiles.

Compared to bulk zircon chemistry, Rozendaal *et al.* (1999) also reported uniform HREE, but variable LREE profiles for single zircon grains, irrespective of colour type. This indicates that HREE is preferentially partitioned into zircon until the mineral structure is satisfied. It is inferred that after this, other trace elements such as the LREE, U, Th, Fe and Al are scavenged and incorporated to variable concentrations depending on their initial availability in the parent magma.

5.5.3. *Radiometry*

The concentration or activity of ^{40}K and gamma-ray emitting nuclei in the ^{238}U and ^{232}Th decay series are measured by the radiometric method. Only the activity concentrations of Bi and Th are reported and K activity values are omitted because of the high statistical uncertainties associated with it (De Meijer, *et al.*, 1990). Since most of the measured radiometric activity can be attributed to U of the bulk sample, it implies that there is a direct relationship between Bi activity and U content of the total zircon population.

Results from the radiometric analysis of zircon concentrates are given in Appendix J with the activity concentrations of bismuth (C_{Bi}) and thorium (C_{Th}) expressed in $Bq.kg^{1}$. Results show that activity of U exceeds Th by an order of a magnitude, a characteristic that was also noticed by Macdonald (1996) and Rozendaal (1998). Using the relevant transformation formula, radiometric measurements indicate that the zircon of the palaeochannels contain 200-300 ppm U and 100-250 ppm Th, compared to the single Buffels River zircon fraction which is enriched in U (670 ppm) and Th (580 ppm).

Zircons from the Buffels River are marked by C_{Bi} and C_{Th} values that are several orders of a magnitude greater than those for channel zircons (Fig. 5.19), reflecting their elevated U and Th content. Radiometry of the palaeochannel zircons discriminates two groups; one group has analyses with variable and elevated C_{Bi} and C_{Th} values, in contrast with the other group that is marked by more uniform C_{Bi} and C_{Th} values (Fig. 5.19). These groups are furthermore distinguished by anticipated lower and similar C_{Th}/C_{Bi} ratios. It is assumed that the two distinct groups signify a difference in the composition of a zircon population as propagated by Philander *et al.*, (1998) and Rozendaal (1998). As a result, the contrast in radiometric signatures of the studied populations is also explained by the difference in their respective LREE characters. Values of the group with the relatively elevated uniform Bi and Th activities are however slightly exaggerated, since close inspection revealed that these particular samples contain appreciable amounts of marcasite and rutile.

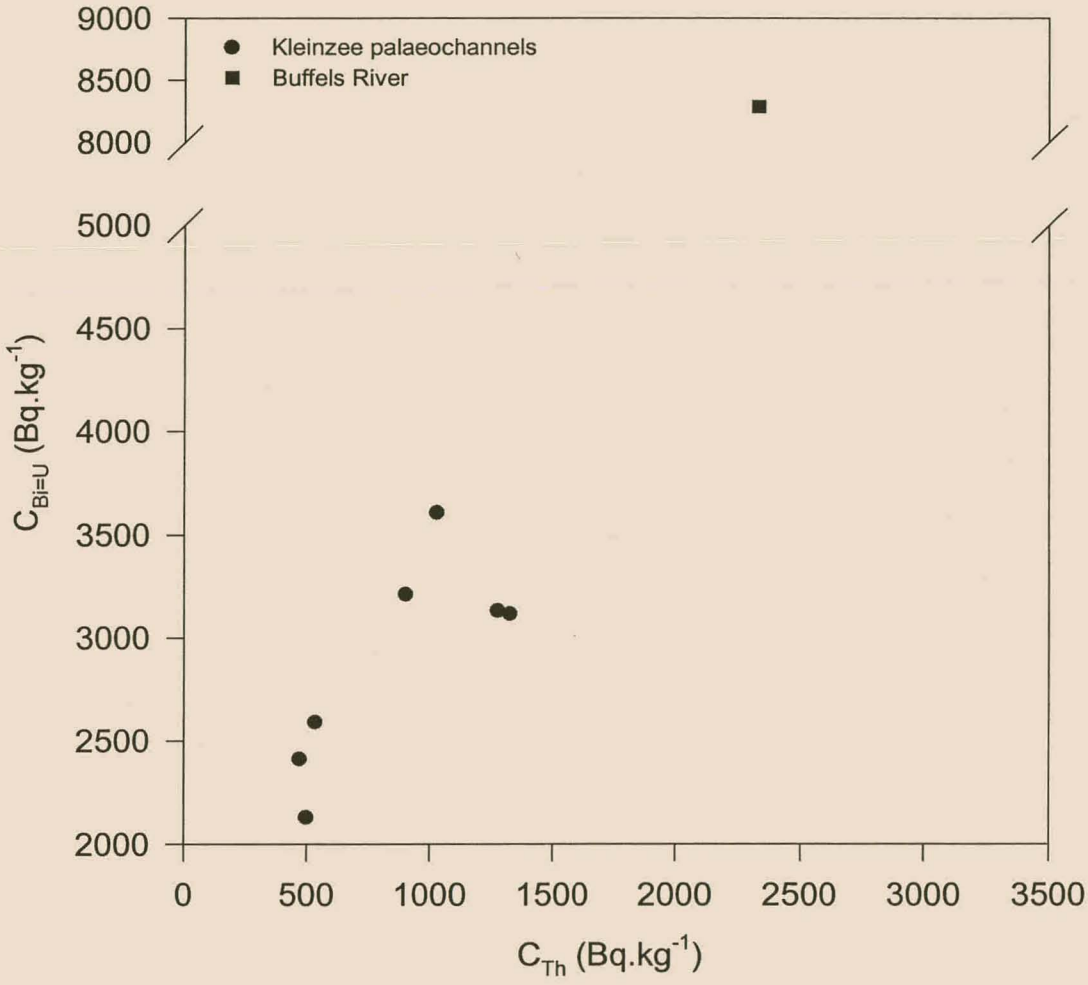

Figure 5.19. Radiometric activity of Th (C_{Th}) and U (C_{Bi}) of zircon separates from the study area.

Consequently, the effective weight of the zircon concentration is lowered which result in the measurement of relatively higher activity concentrations.

5.5.4. Cathodoluminescence

Cathodoluminescence (CL) displayed by zircons can be primarily attributed to transitions of Dy^{3+} ions, defects in the zircon crystal lattice (specifically by electron defects localised on the SiO_4 tetrahedron), but also by the presence of small amounts of Nd, Mn, Ho, Tm, Yb and Lu (Mariano, 1988, 1989; Remond *et al.*, 1990; Yang *et al.*, 1992; Vasconcellos *et al.*, 1996). Other elements such as Fe, Hf, Y, P and U act as quenchers and suppress cathodoluminescence (Hanchar and Miller, 1993; Hanchar and Rudnick, 1997). Therefore, the relative intensity of cathodoluminescence depends on the quantity and types of activators and quenchers (Koschek, 1993).

BSE images reveal contrasts in the average atomic number of a phase; the higher the number, the more electrons an area will "reflect" and the brighter it will appear. The element primarily responsible for these BSE variations in crustal zircons is Hf, with U having a secondary effect (Hanchar and Miller, 1993). Y, P and the HREEs also play a secondary role as activators in BSE imaging (Hanchar and Miller, 1993; Hanchar and Rudnick, 1997). As observed from the literature, bright areas in BSE images appear dark in CL spectroscopy and vice versa.

Excluding zoned zircons, nearly all the zircons appear structureless in plane polarised or reflected light. The zircons generally reveal no internal features in BSE, except for anomalous brighter cores and zones. It is inferred that the cores are inherited from igneous crystallisation and the brighter, very thin unzoned rims are to be sedimentary overgrowths. Although most zircons appear structureless in plane polarised or reflected light, CL spectroscopy reveals complex internal relationships (Fig. 5.20).

A variety of types were discriminated in the presently studied population:

I. Zircon that was either homogeneously weak or brightly luminescent and sometimes passes into a peripheral overgrowth with contrasting luminescence. Occasionally, no rim overgrowth was observed.

II. Zircon that showed a patchy distribution of non-uniform luminescence throughout the crystal. A thin bright overgrowth marked the rim. The patchy distribution of CL in this type may indicate fracture-controlled diffusive redistribution of trace atoms after zircon growth (Cherniak *et al.*, 1993; Hanchar and Rudnick, 1997).

III. Zircon that displayed narrowly spaced oscillatory growth zoning. Oscillatory zoning is ascribed to zircon growth in the initial melt (Rubatto *et al.*, 1998). Ortleva, *et al.* (1987) suggested that oscillatory zoning is the result of the differential rate of diffusion of spatially associated trace elements to the surface of the growing crystal. More than one region of oscillatory growth was commonly present and discriminated by a difference in luminescence (Fig. 5.20). The overall luminescence of the different regions decreased to the rim. Cores are rarely observed and the rims are marked by a bright overgrowth. Cracks radiating from the core indicated metamict zircons.

IV. Zircon similar to type III, but a well-defined core was present that overprints the surrounding oscillatory zones. Occasionally the different oscillatory zones replaced each other. A thin, very luminescent rim overgrowth was observed. The observed replacement of oscillatory zoning is the result of homogenisation by late-magmatic or younger metamorphic processes (Hanchar and Rudnick, 1997; Nasdala, 1998).

V. Zircons similar to type IV, but in addition contained secondary growth zones with differing luminescence that surrounded and replace the oscillatory zones from the outside of the crystal. A well-defined bright overgrowth marked the rim. The cores and growth zones were marked by a well-preserved resorption surface. Resorption surfaces are typical features related to metamorphism (Campbell *et al.*, 1993; Vavra *et al.*, 1996; Nemchin and Pidgeon, 1997).

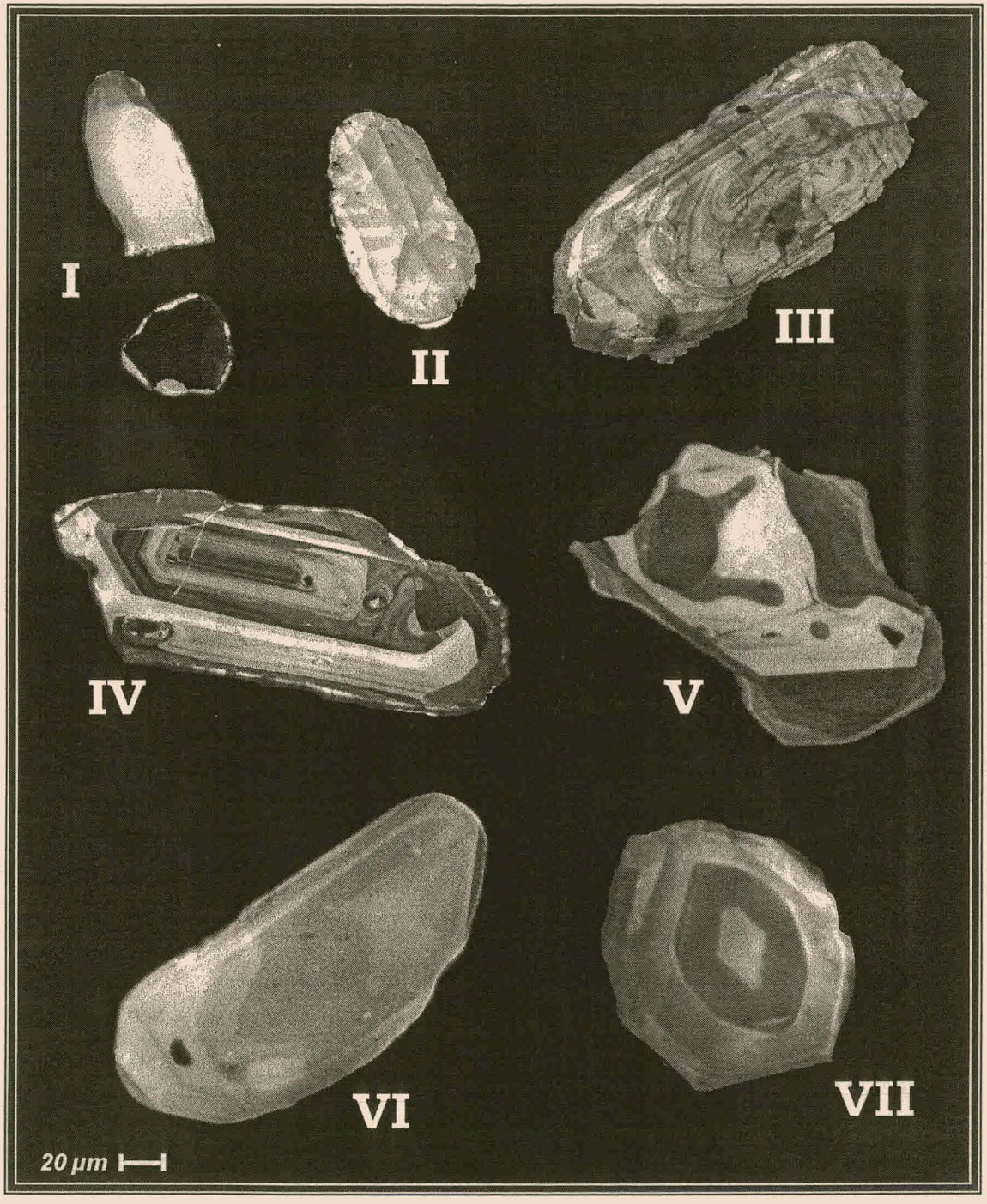

Figure 5.20. Cathodoluminescence spectra of selected zircons in the study area.

VI. Zircon with a prominent core, surrounded by one or more concentric growth zones of contrasting luminescence and, if present, a brighter rim. These zircons had a distinct boundary between the core and subsequent overgrowth; each region gave a distinctive CL emission. The rim overgrowth may be either present or absent.

VII. Zircon similar to type VI, but the core replaced the surrounding brighter phases of growth. A bright rim overgrowth was present.

In summary, the studied zircon population displays complex CL images demonstrating their variable trace element chemistry and protracted evolution. Investigated zircons show evidence of intricate growth-histories in the form of complex patterns of zoning and sedimentary overgrowths. Zircons with homogeneous cores (type I) and fine oscillatory zoning (type II) are typical of primary magmatic crystallisation (Vavra and Hansen, 1991; Hanchar and Miller, 1993; Hanchar and Rudnick, 1997). The rest of the population, marked by relics of inherited igneous cores and displaying complex secondary growth zoning, is the result of metamorphism (Vavra, 1999). These complex internal replacement structures do not occur in most of the amphibolite facies and start only near the transition to the granulite facies (Vavra *et al.,* 1999). These particular zircons were therefore supposedly subjected to high-grade metamorphism; type V is especially ascribed to high temperatures, possibly indicating anatexis of the host rock (Pidgeon *et al.*, 1998). It is concluded that CL demonstrated the studied zircon population to be representative of both igneous and metamorphic rocks.

5.4.5. Discussion

Zircon is chemically stable and is often resilient to abrasion due to its robustness. Taking these characteristics in account, Hubert (1962) used the abundance of zircon along with rutile and tourmaline to define his ZTR maturity index for sediments. The value of the index was a relative measure of the degree of maturity of the host sediments; high values mean that the sediments were highly evolved and low values *vice versa*. In unique studies, Philander *et al.* (1998) and Rozendaal (1998) made use of geochemistry and radiometry to conclusively prove that the composition of a

given zircon population records the maturity of its host sediment. Geochemical as well as radiometric characteristics of bulk zircon populations are therefore believed to indicate the relative degree of maturity of their host sediments. Alternatively, single grain zircon chemistry will provide invaluable information about their source rocks.

Philander *et al.* (1998) showed that various depositional environments along the west coast of South Africa are marked by distinct zircon populations that contain variable mixes of clear, coloured, zoned and metamict grains. These particular environments also contain sediments that display differences in their relative maturity. Sediments that host heterogeneous zircon populations are believed to be immature and very proximal to their source due to the high occurrence of cracked and unstable (U-Th enriched, metamict) grains. Marine sediments, which are more mature than their fluvial derivatives, contain zircon populations that are, marked by more stable zircon types. It is believed that as sediments evolve, the unstable zircons are preferentially removed by fluvial and/or marine processes, resulting in a zircon population that comparatively, is less heterogeneous.

It is concluded that the individual mix (heterogeneity) of various zircon populations reflects the evolution of their host sediments. The radiometric and geochemical contrast between the zircon populations from the Buffels River and palaeochannels confirms that the heterogeneity of the respective populations relates to the compositional maturity of the host sediment. Buffels River sediments are immature and contain zircon populations that are heterogeneous and often contain Hf, REE-enriched and uraniferous types, whereas palaeochannel sediments are very mature and host a virtual homogeneous stable zircon population. In agreement with Philander *et al.*, (1998) and Rozendaal (1998), marine sediments of Kleinzee host a lesser variety of zircon types, which is generally depleted in unstable grains.

Rozendaal (1998) argues that the ratio of the various zircon types constituting a particular population is not only constant for a depositional environment, but also is consistent for a given deposit. This conclusion has very important applications, which could prove to be very valuable in diamond exploration. Firstly, zircon chemistry and

radiometry can be useful to fingerprint different stratigraphic sequences. Geochemical and radiometric characteristics of zircon populations from known diamondiferous sediments can be used to locate sediments with similar zircon attributes, which in all probability will also be diamond bearing. A second application would be to direct zircon chemistry and radiometry towards the determination of source region characteristics. Zircon chemistry and radiometry of populations from diamondiferous sediments will indicate the relative maturity of their host sediments. From this information, the proximity of the precursors of these diamondiferous deposits can be tentatively determined.

5.6. Garnet

5.6.1. Petrography

All the studied garnets are characterised by high relief and isotropism, ranging in size from 300-1000 μm. The internal form of garnet is usually structureless with small haphazardly arranged quartz, feldspar, rutile and fluid/gas inclusions. Rarely observed anisotropism may be due to the presence of these inclusions. Based on colour, three distinct varieties of garnets are recognised. Colourless garnet (Plate 5.12A) is the predominant variety characterised by euhedral grain morphology. Pale pink garnet (Plate 5.12B) is the next important variety. It occurs mainly as angular fragments representing pieces of larger crystals, often showing one or two imperfect crystal faces. Grains are usually angular to subangular and bounded by conchoidal fracture surfaces. Orange coloured garnet, characterised by nearly perfect crystal faces, is relatively scarce. Some garnets display extremely irregular outlines, which may suggest intrastratal dissolution. Particular garnets also display distinct etchmarks seen under high magnification as triangular-shaped hollows (Plate 5.12C), often exhibiting crystallographic orientation.

5.6.2. Chemistry

A total of 64 garnet grains representative of the BMC, KNC and BIC were analysed with an electron microprobe for Si, Al, Fe, Mg, Ca, Mn, Cr, Ti, V, Zr, Y, Na and K (Appendix H). Additionally, the five most dominant garnet end-members were

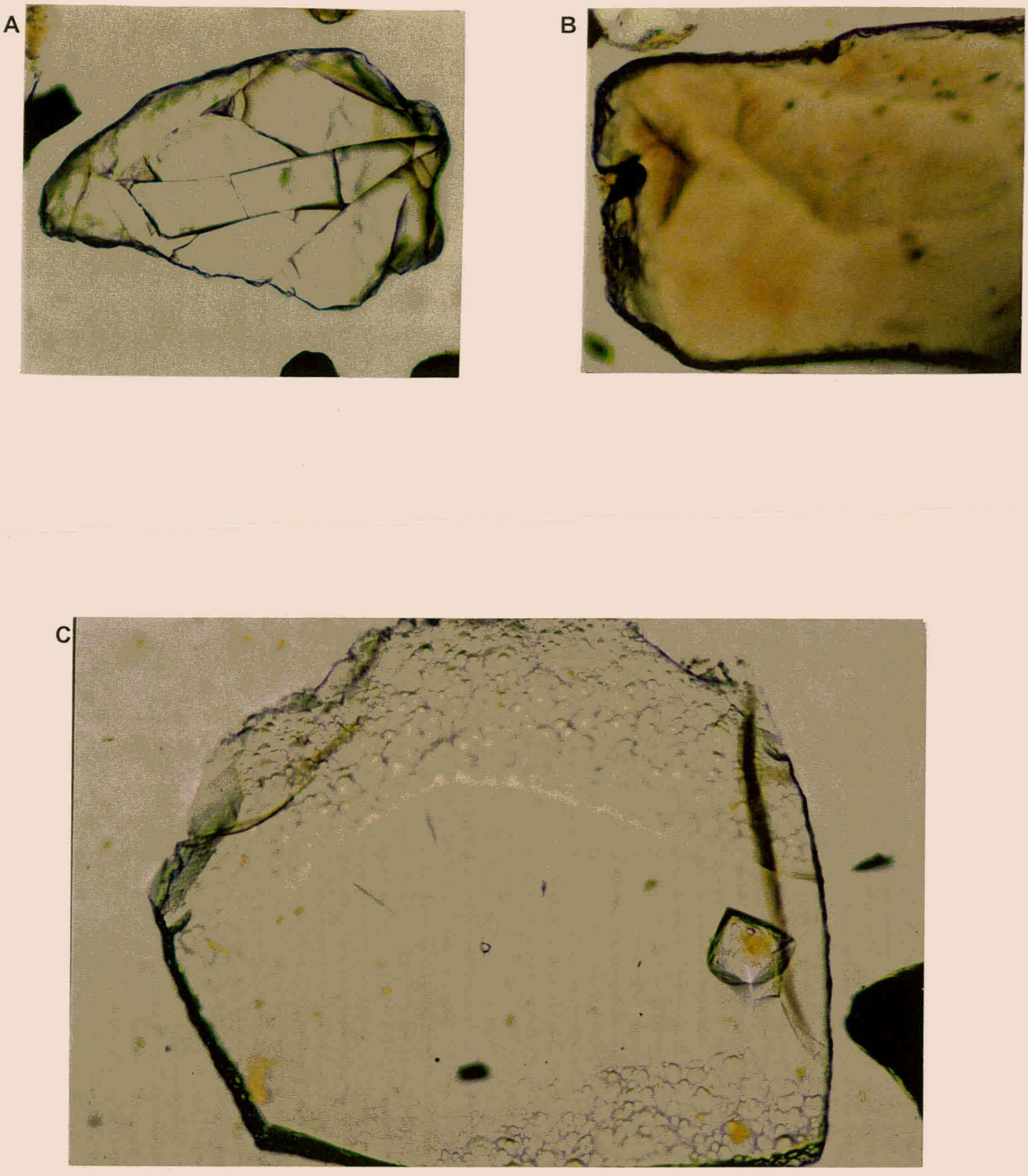

Plate 5.12. Garnets characteristic of the studied area.

A) Colourless, angular, cracked garnet.

B) Euhedral pink garnet.

C) Garnet showing etch pits on its surface, indicating severe chemical dissolution.

Scale: 200X

calculated for each grain. Results are graphically presented on a ternary diagram (Fig. 5.21).

Geochemistry shows that the garnets are generally enriched in Fe and Mg, illustrating that they belong to the broad almandine-pyrope group. One very rare Mn-containing garnet accentuates the compositional range that exists between spessartine and almandine in the pyralspite garnet group. The grossular, andradite and uvarovite end-members are present in trace amounts. Within the constraints of the electron microprobe, no consistent correlation between the different colour types and chemical composition could be established.

The whole garnet suite is compositionally similar and consists mainly of almandine (59-83 mol%), pyrope (15-35 mol%) and unequal amounts of grossular (0-6 mol%) and spessartine (0-9% mol%). The high almandine content is typical of garnets in peraluminous rocks (Sisson and Bacon, 1992). Although chemical zoning is very common in garnet and especially recognised in metamorphic garnets (Cygan and Lasaga, 1982; Hickmott *et al.*, 1987; Hickmott and Shimizu, 1990; Hickmott and Spear, 1992), no significant chemical zoning was detected by microprobe analysis.

REE analyses for handpicked garnet separates from the BMC, BIC and KNC are given in Appendix I and presented on chondrite normalised diagrams together with analyses from Graauwduinen and Geelwal Karoo (Fig. 5.22). All three garnet fractions from the study area have a narrow range in REE abundance ranging from 479-485 ppm. The normalised REE patterns are marked by a LREE depleted and HREE-enriched pattern with pronounced negative Eu and Nd anomalies, similarly to garnet analyses reported by Taylor and McLennan (1985). REE patterns furthermore show that garnet incorporates HREE more readily than LREE, which is concordant with comparative studies (Taylor and McLennan, 1985; Sorenson and Grossman, 1989). The garnets commonly exhibit very low LREE/HREE ratios (0.04-0.05) which are characteristic for igneous as well as metamorphic garnets (Irving and Frey, 1978; Hickmott *et al.*, 1987). Although the REE abundance is considerably lower for Graauwduinen and Geelwal Karoo garnets, REE patterns are identical, suggesting

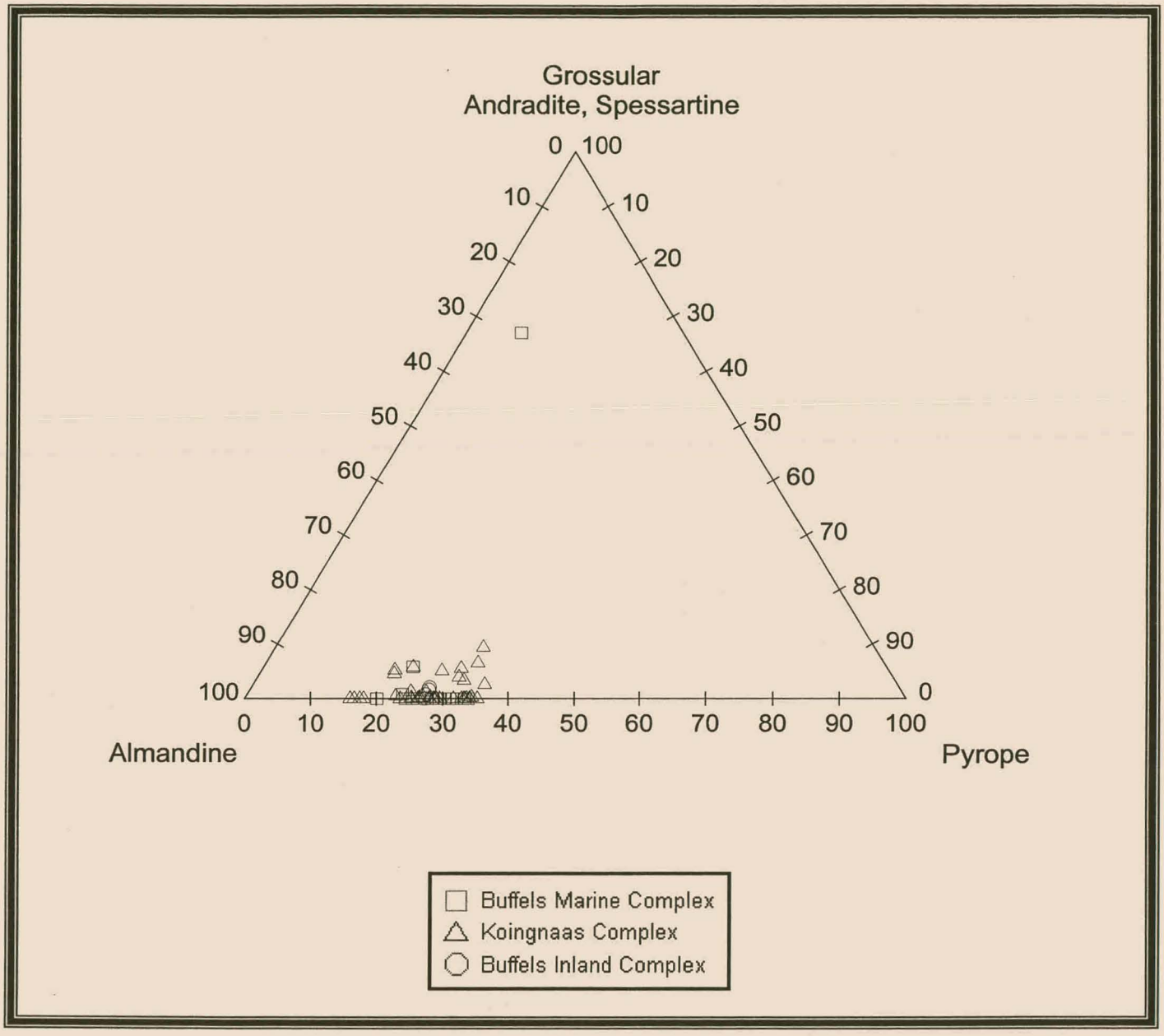

Figure 5.21. Garnet classification based on the garnet end members, pyrope, grossular + andradite + spessartine and almandine.

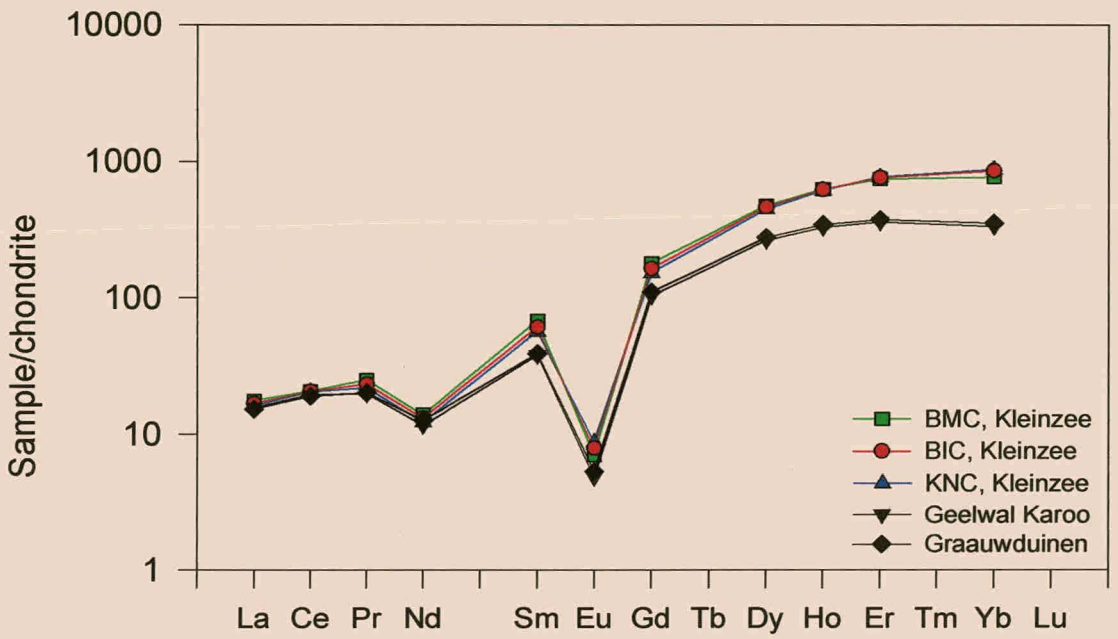

Figure 5.22. Chondrite-normalised REE plots for garnet separates from Kleinzee, Graauwduinen and Geelwal Karoo.

similar source rocks. Likewise, the similarity of the major and REE chemistry between individual garnets in the study area implies a common source.

5.7. Pyroxene

5.7.1. Petrography

Pyroxene grains are mainly colourless and non-pleochroic, although a weakly pleochroic, pale-green variety was occasionally noticed. Grains commonly display a rectangular, prismatic habit with sharp, angular or rounded corners (Plate 5.13). Etch patterns are frequent and are seen as hacksaw-terminated grain boundaries or grooves on their surface. Accessory mineral and fluid inclusions are fairly common. Parallel extinction on the (100) plane indicates that the studied pyroxenes belong to the clinopyroxene class. No orthopyroxenes have been identified.

The characteristic 90° cleavage was rarely observed; instead, most of the grains exhibit a distinct single cleavage trace on (100) or (010). Particular grains display close parting on (100), which is referred to as diallage (Philips and Griffen, 1981). Twinning, amplified under x-nichols, was rarely noticed, but zoning features are much more common. Deer *et al.* (1963, 1992) state that zoning in pyroxene could be related to chemical variation, but this was not investigated in this study. Alteration is abundant and is prominent along cracks and cleavage planes often creating a mesh-like structure. Iron staining, presumably the result of alteration, is concentrated along cleavage traces and cracks and sometimes becomes so extensive that little of the optical properties of the pyroxenes can be observed.

5.7.2. Chemistry

None of the pyroxene could with certainty be identified by optical properties alone. Instead, chemical analysis was used to classify the pyroxenes from the study area. Microprobe analysis for Si, Ti, Al, Cr, Fe, Mn, Mg, Ca, Na and K was performed on 53 representative pyroxene grains of the various areas and the results are reported as oxide weight percentages in Appendix H.

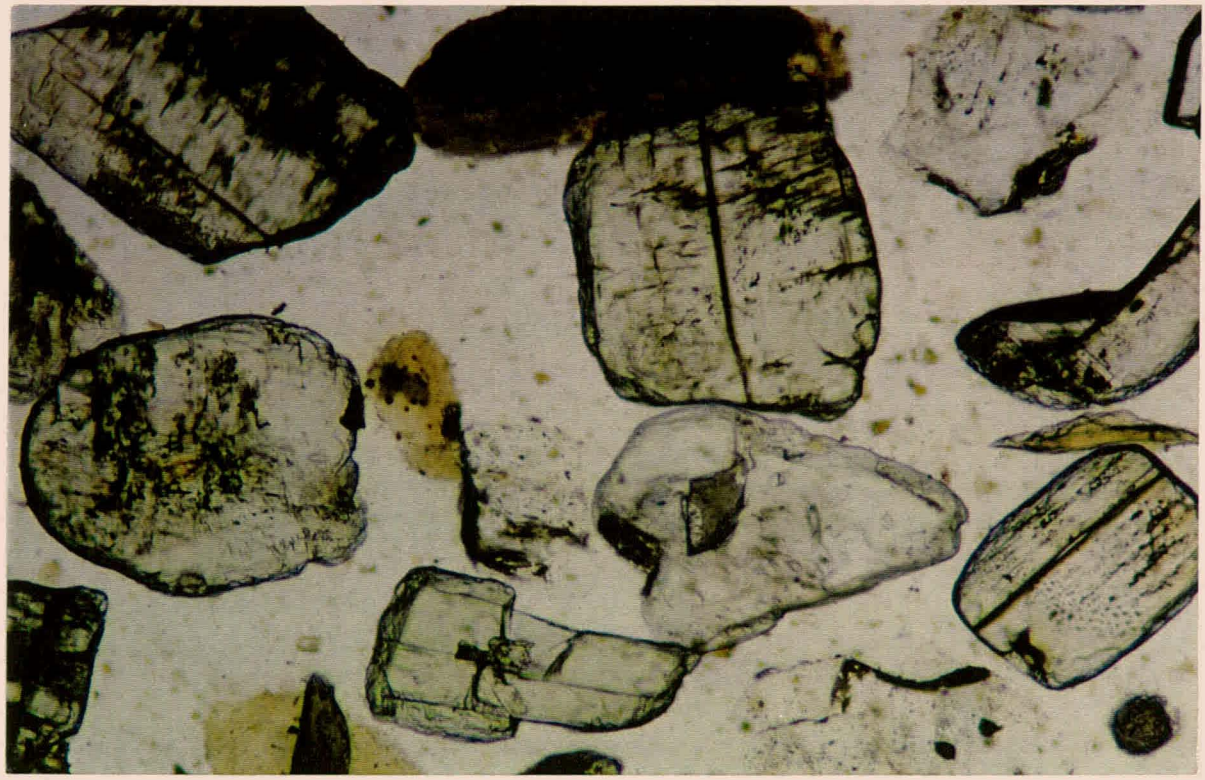

Plate 5.13. A collection of pyroxene grains from the study area. Prismatic cleavage and subangular habit are apparent.

Scale: 200X

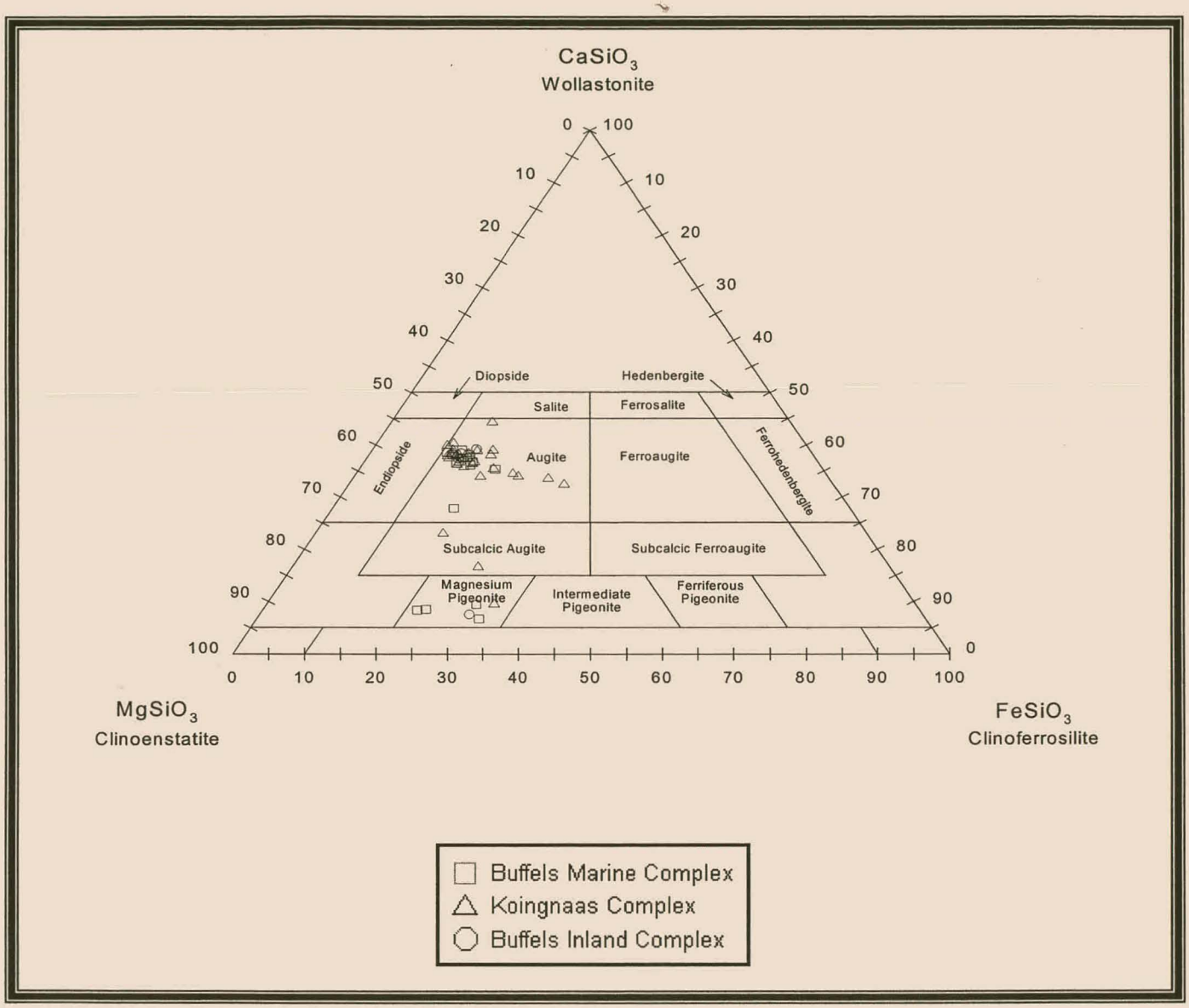

Figure 5.23. Chemical classification of pyroxenes from the study area (after Poldervaart and Hess, 1951).

Pyroxene analyses show that they are generally Ca-Mg rich and that two distinct groups can be discriminated. The majority of analyses plot well in the augite field, most of them close to the endiopside-augite boundary, while the rest of the analyses occupy the Mg-pigeonite field (Fig. 5.23). Two single analyses plot in the subcalcic augite field. Fig 5.23. shows that no pyroxene type is particular to any specific locality. In addition to the major elements, the pyroxenes have an Al_2O_3 content of less than 2%, with trace amounts of Ti, Cr, and Na.

5.8. Amphibole

5.8.1. Petrography

The amphiboles in the study area are highly coloured and two main varieties, green (Plate 5.14A, 14B and 14C) and brown (Plate 5.14D, 14E and 14F) have been observed. The green variety can be subdivided into various shades of green that incorporate light-green, blue-green, olive-green and brown-green varieties. Pleochroism is intense, is extremely variable in tints of green for the green variety and yellow, and browns for the brown type. Some grains display colour zoning that could indicate a contrast in chemical composition (Mange and Maurer, 1991).

Hornblende commonly occurs as prismatic, elongated crystals or angular fragments. Fibrous grains also occur, but less frequently. Grain edges are often rounded or ragged, but most grains commonly display the typical hacksaw structure (Plate 5.14A, 14C and 14F) that is a characteristic sign of chemical dissolution (Mange and Maurer, 1991; Morton and Smale, 1990). Prismatic cleavage on (010) is pronounced and rather common compared to the characteristic amphibole cleavage on (110). Etching of amphibole is recognised by the pitted and "bleached" character of the grains (Plate 5.14 A). Amphibole inclusions that were verified with the SEM-EDS include biotite, epidote and Fe-Ti opaques. Fluid and gas inclusions were less frequently noticed.

Although Deer *et al.* (1963), and Philips and Griffen (1981) provide diagnostic optical characteristics for the different amphibole members, precise classification of a

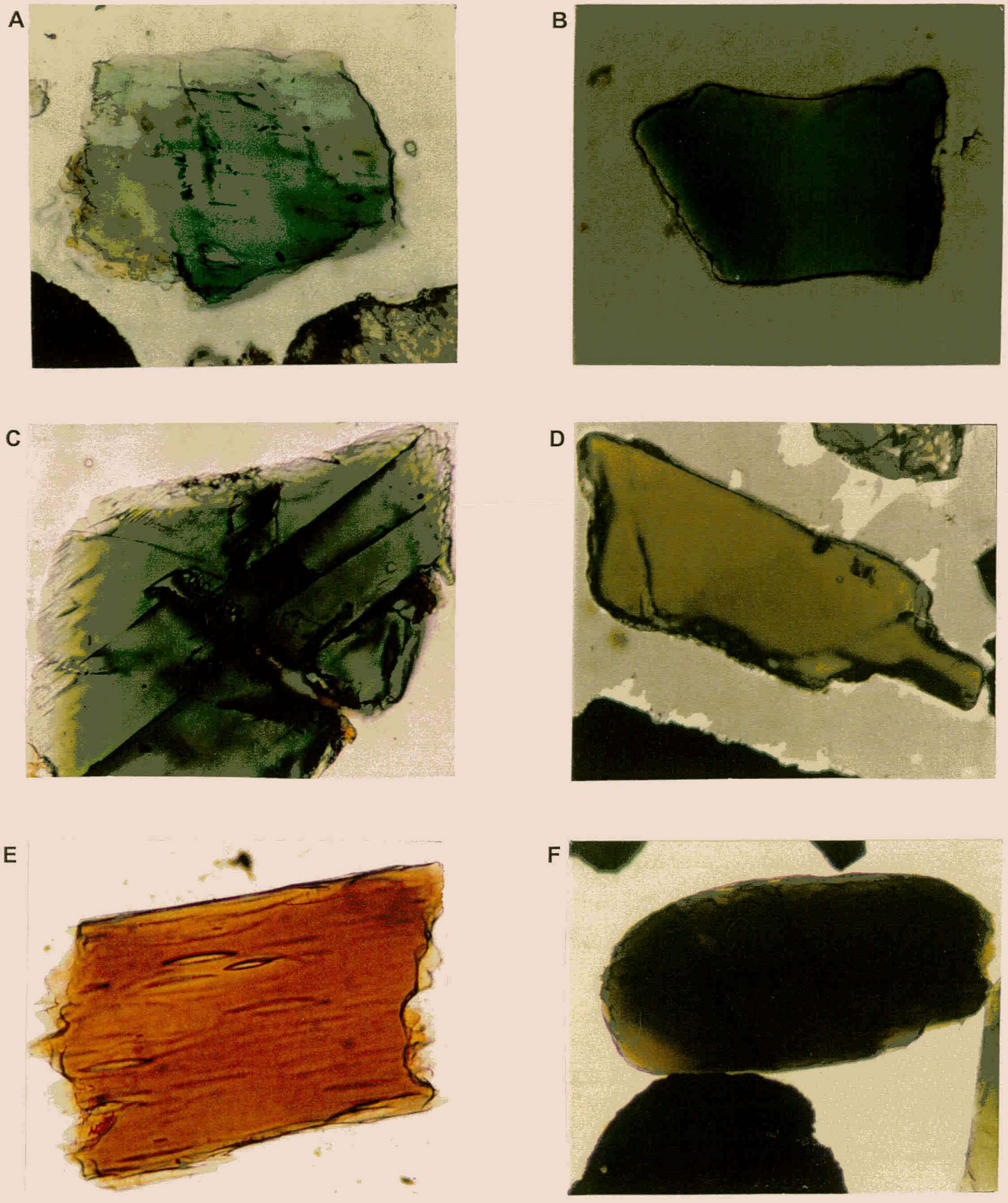

Plate 5.14. Amphiboles with different colour; green varieties (A, B and C) and brown (D, E and F) types. Proof of chemical dissolution is recognised by the bleached colour (A) of the mineral and typical hacksaw terminations (C and E).

Scale: 200X

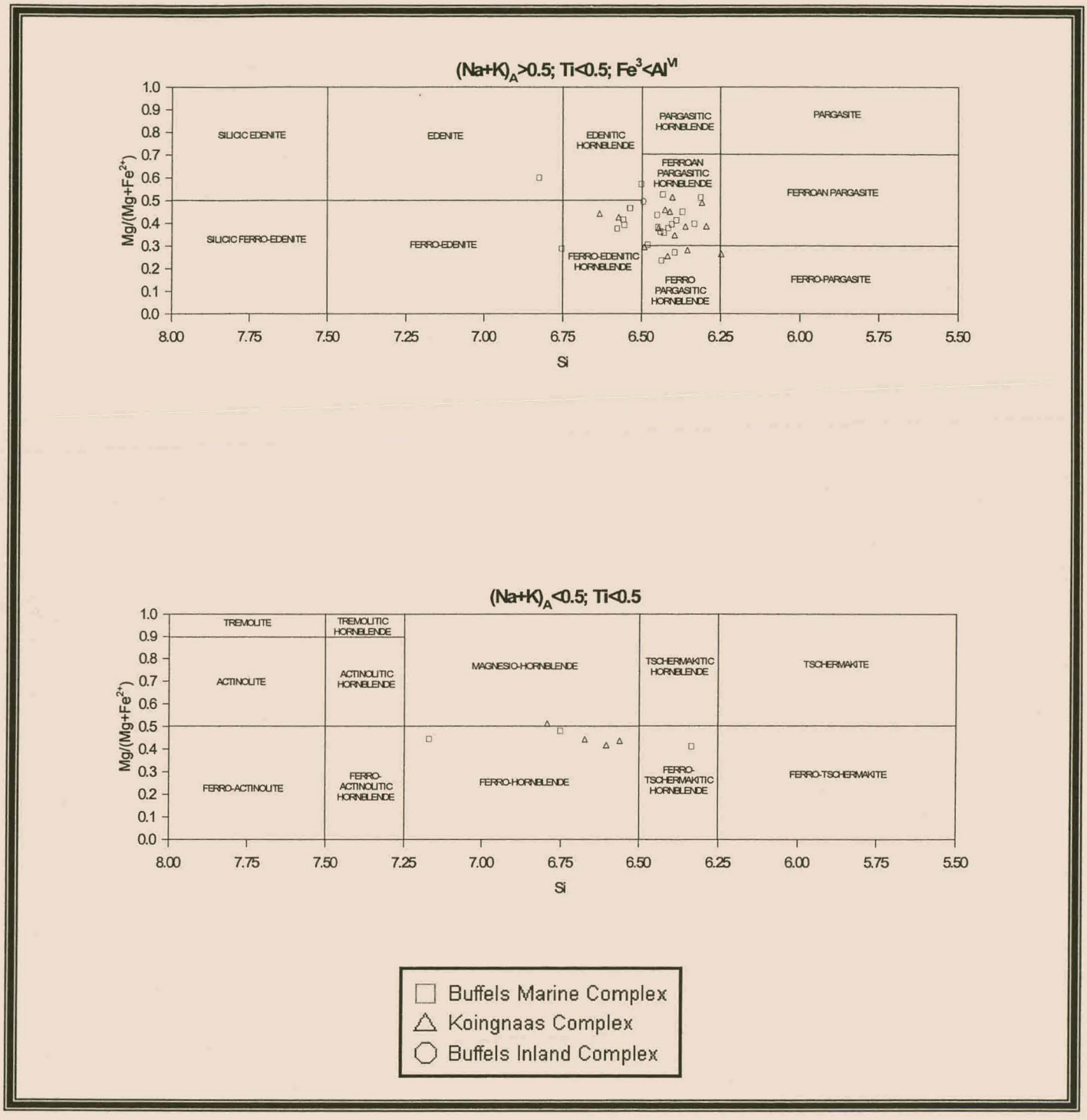

Figure 5.24. Classification of amphiboles in the study area (after Leake, 1978).

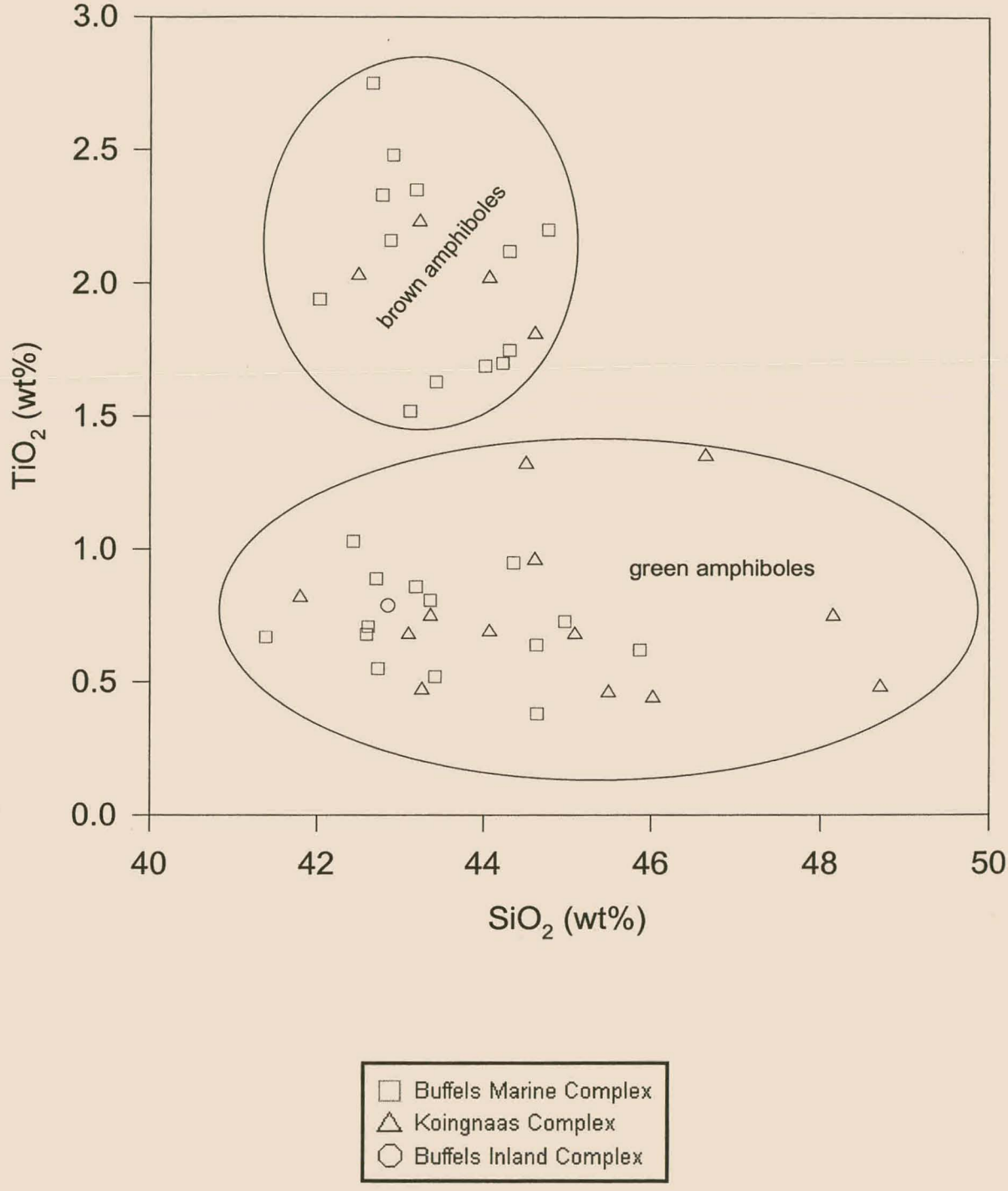

Figure 5.25. Compositional variations, illustrated in terms of TiO_2 and SiO_2 content, between the green and brown amphibole populations from the study area.

particular member requires chemical analysis and subsequently this method was used in classification.

5.8.2. Chemistry

Microprobe analysis for Si, Al, Fe, Ti, Cr, Mg, Mn, Ca, Na, K, was performed on 46 amphibole grains and the results are presented as oxide weight percentages in Appendix H. Leake's (1978) classification scheme indicates that all the amphiboles are members of the broad calcic amphibole group. The amphiboles fall into a number of different categories when classified according to the Leake scheme (1978), including magnesio-hornblende, ferro-hornblende, ferro-tschermakitic hornblende, edenite, ferro-edenitic hornblende, ferroan pargasitic hornblende and ferro-pargasitic hornblende. Fig. 5.24. illustrates that ferroan pargasitic hornblende is the dominant amphibole variety.

Microprobe analysis has confirmed that the optical distinction of the amphibole population into brown and green varieties is justified geochemically. The brown variety is Ti-rich (>1.5%) and relatively restricted in SiO_2 content, whereas the green population is Ti-poor and spans a greater SiO_2 range (Fig. 5.25). Brown amphiboles proved to be essentially ferroan pargasitic hornblende compared to the green amphibole population that falls into a number of different categories. No notable trends in colour or chemistry are apparent between amphiboles from the various stratigraphic sequences. The very high totals indicate low OH^- content, which suggests that the studied amphiboles be of a metamorphic origin.

5.9. Epidote Group

5.9.1. Petrography

The epidote group minerals have extremely similar chemical and mineralogical properties (Deer *et al.,* 1986) making distinction between species difficult and therefore the properties of the species of this mineral group are collectively discussed.

Clinozoisite and epidote were the only epidote group minerals identified in this study. Epidote is found mostly as subangular to subrounded, equant, often irregular grains of characteristically pale yellowish-green colour (Plate 5.15A, 15B and 15C). Grains rarely display cleavage. Pleochroism is usually very weak and the epidotes invariably exhibit irregular colour distribution. Interference colours are vivid in diagnostic tints of yellow-green. Epidote is biaxial negative compared to clinozoisite that is biaxial positive (Mange and Maurer, 1992), but due to the lack of suitable optic figures this is of little aid in distinguishing between the two species.

Clinozoisite occurs as subhedral, equidimensional or prismatic grains. The mineral is either colourless (Plate 5.10D) or pale yellow and displays a perfect cleavage on (001). Interference colours in tints of anomalous blue and yellow, often pronounced at grain boundaries, are characteristic of clinozoisite and aid in distinguishing clinozoisite from epidote. Zoning is very common and is expressed in changes of colour or other optical properties such as extinction angle or birefringence. The two epidote species frequently host fluid inclusions and solid phases of unknown composition. Etch patterns were often noticed and in conjunction with observed ragged grain boundaries suggest moderate chemical dissolution.

5.9.2. Chemistry

Microprobe results (Table 5) indicate that the variation in chemical composition of the entire epidote population is restricted to a very narrow range. Geochemistry further indicates no clear distinction between clinozoisite and epidote in this study area. Likewise, no difference can be recognised between samples from the different localities. Besides the major elements, Si, Al, Fe and Ca, the epidotes contain variable amounts of Ti, Mn and Mg which in total amount to less than 1%.

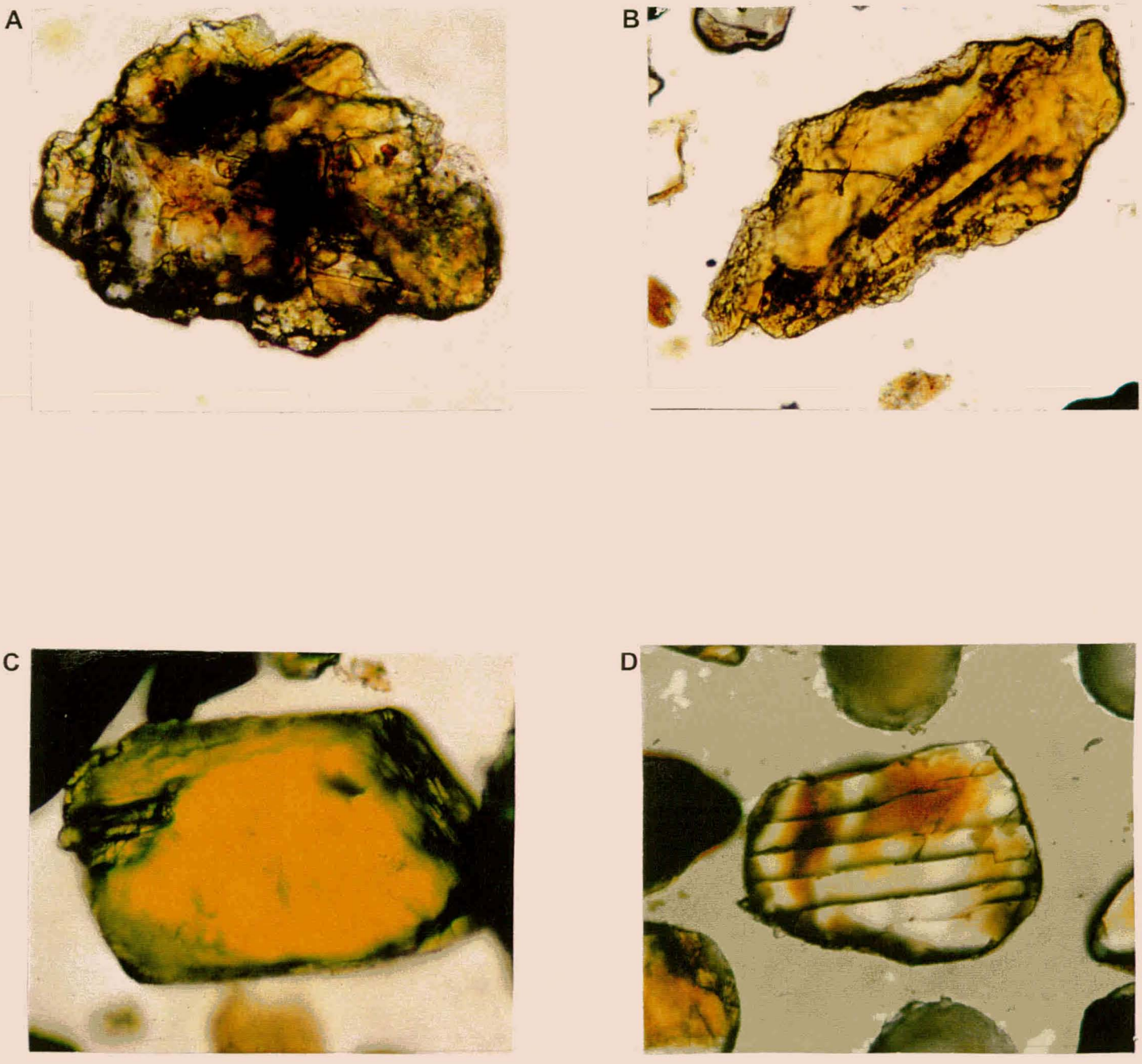

Plate 5.15. Typical, irregular shaped epidote grains (A, B and C) showing signs of chemical dissolution (A and B). Clinozoisite (D) is distinguished by its perfect cleavage.

Scale: 200X

Table 5. Average chemical composition of selective minerals from Kleinzee. All values are in ppm, with the standard deviation given in brackets.

	Epidote series	**Aluminosilicates**	**Staurolite**	**Glauconite**	**Titanite**
	n=33	**n=25**	**n=10**	**n=10**	**n=3**
SiO_2	38.04 (0.41)	37.67 (0.44)	28.27 (0.33)	41.71 (3.38)	27.01 (3.93)
TiO_2	0.08 (0.04)	0.00 (0.02)	0.39 (0.10)	0.24 (0.18)	32.37 (5.90)
Al_2O_3	23.43 (1.40)	64.78 (0.81)	56.23 (0.64)	3.95 (0.75)	10.67 (8.92)
Cr_2O_3	0.01 (0.02)	0.01 (0.02)	0.02 (0.03)	0.06 (0.03)	0.00 (0.00)
Fe_2O_3	0.00 (0.00)	0.00 (0.00)	0.00 (0.00)	0.00 (0.00)	0.00 (0.00)
FeO	12.98 (1.43)	0.44 (0.34)	15.19 (0.69)	32.39 (3.07)	1.16 (0.97)
MnO	0.32 (0.24)	0.00 (0.00)	0.06 (0.04)	0.00 (0.00)	0.05 (0.09)
MgO	0.03 (0.03)	0.00 (0.00)	1.87 (0.05)	2.92 (0.55)	0.00 (0.00)
CaO	23.74 (0.52)	0.00 (0.00)	0.00 (0.00)	0.45 (0.26)	26.47 (3.50)
Na_2O	0.00 (0.00)	0.00 (0.00)	0.00 (0.00)	0.23 (0.19)	0.00 (0.00)
K_2O	0.00 (0.00)	0.00 (0.00)	0.00 (0.00)	6.64 (1.10)	0.00 (0.00)
Total	98.64 (0.75)	102.90 (0.94)	102.02 (0.65)	88.58 (3.05)	97.73 (0.61)

5.10. Other minerals

5.10.1. Aluminosilicates

Kyanite occurs as very large (~500 μm) elongated grains with marked prismatic (Plate 5.16A) or square shaped fragments. Grains are dominantly colourless or rarely blue. Strong cleavage is observed on the (100) face (Plate 5.16A) and the combination thereof with parting on (001) at right angles to the cleavage traces results in a conspicuous cross-cleavage. Weathering of these grains produces characteristic step-like facets at the grain edges. Most of the grains are clustered with inclusions that prove to be rutile, apatite, carbon, and fluid and gas phases.

Sillimanite is less commonly present and occurs as colourless, narrow perfect prisms, elongated on the c-axis (Plate 5.16B and 5.16C). Some grains are typically marked by longitudinal splitting and cleavage traces parallel to length (Plate 5.16C). The characteristic habit and brilliant interference colours provide an easy optical diagnosis.

The average chemical composition of kyanite is supplied in Table 5. Microprobe results indicate that kyanite is relatively pure and in addition to Al and Si, iron is the only substitute to occur in trace amounts. Significant iron staining of grains (Plate 5.16A and C) accounts for the presence of iron.

5.10.2. Monazite

Monazite grains occur as a minor component in the study area exhibiting well-rounded oval to round shapes (Plate 5.17A). The monazites are usually colourless and a rare pale yellow and greenish-yellow colour in the mineral is noticeable from the coarser grains. Distinctive interference colour bands and cross fracturing mark nearly all grains (Plate 5.17B). Frequent brown staining, prominent along fractures and severe surface pitting, aids to distinguish monazite from zircon. The majority of monazites are devoid of inclusions, but the larger grains contain inclusions that have not been identified.

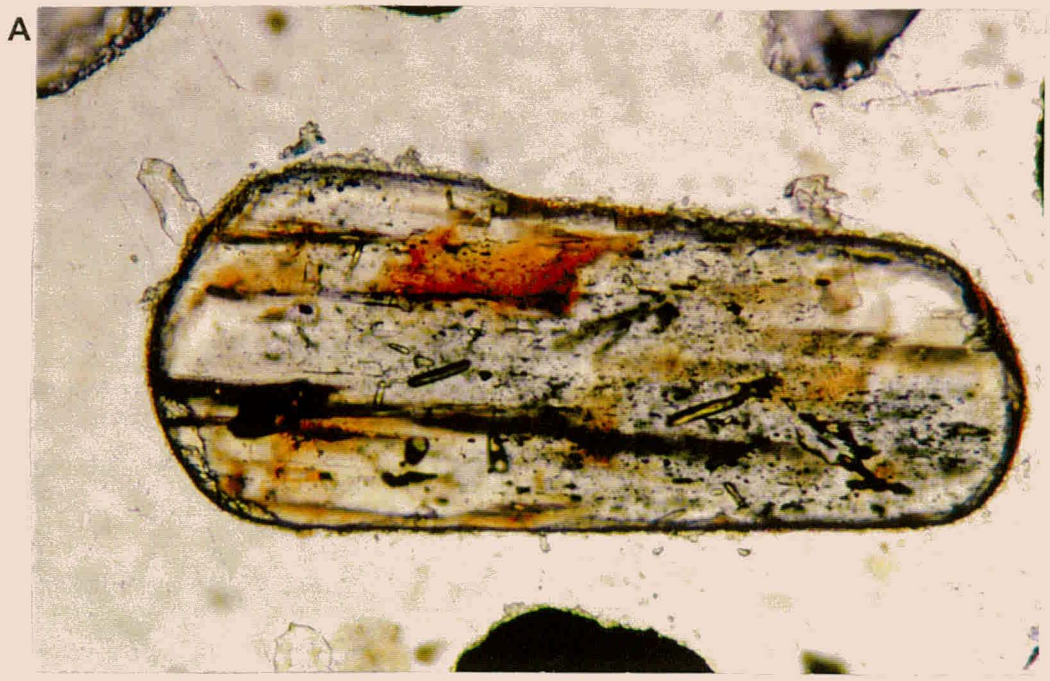

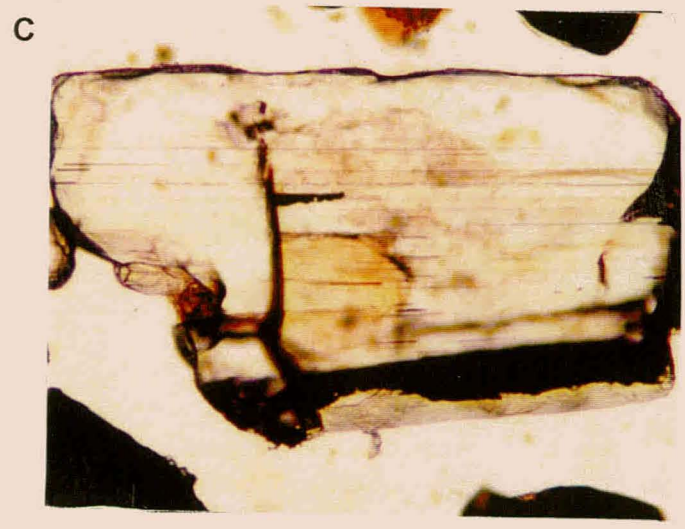

Plate 5.16. Selected aluminosilicates.

Prismatic kyanite (A), with perfect cleavage and cluttered with inclusions. Crystals of euhedral sillimanite (B and C).

Scale: 200X

Like zircons, the high roundness of monazite indicates considerable abrasion during the sedimentary cycle. Contrary to general belief, monazite can survive extensive transportation despite its phosphate composition and is not easily prone to weathering (Pettijohn, 1975). A Miocene palaeochannel in Annex Kleinzee contains in addition to ilmenite and zircon appreciable amounts of monazite, highlighting the significant chemical stability of this mineral.

5.10.3. Titanite (sphene)

Titanite occurs either as discrete euhedral squares and subrounded grains (Plate 5.17C and 17D) or in a lesser amount as an interlocked phase with magnetite (Plate 5.17C). Grains are colourless to greyish and usually display a high resinous lustre that is unmistakable. Characteristics that aided in the identification of titanite are very strong dispersion and abnormally high-order polarisation colours. Grains often host several inclusions of different types and composition (Plate 5.17D). Titanite is not very stable in a marine environment (Morton, 1991) and is generally weathered, manifested as etch grooves and hacksaw textures. The mineral is often altered to leucoxene giving the grains a dusky appearance. The composition of titanites are often non-stoichiometric (Table 5) and highly variable as these minerals are altered to leucoxene to varying degrees (Golding, 1961).

5.10.4. Staurolite

Staurolite occurs as irregular subangular or subrounded grains. It often shows hacky to subconchoidal fractures, distinctive vivid pleochroic golden yellow and brown colour, high index of refraction and numerous inclusions (Plate 5.18A). Staurolite is regarded as metastable (Velbel *et al.*, 1996) and evidence of staurolite dissolution in the study area includes ragged grain boundaries and etch patterns on the surface. Microprobe analyses (Table 5) indicate that staurolite in the study area is near stoichiometric and shows small compositional variation.

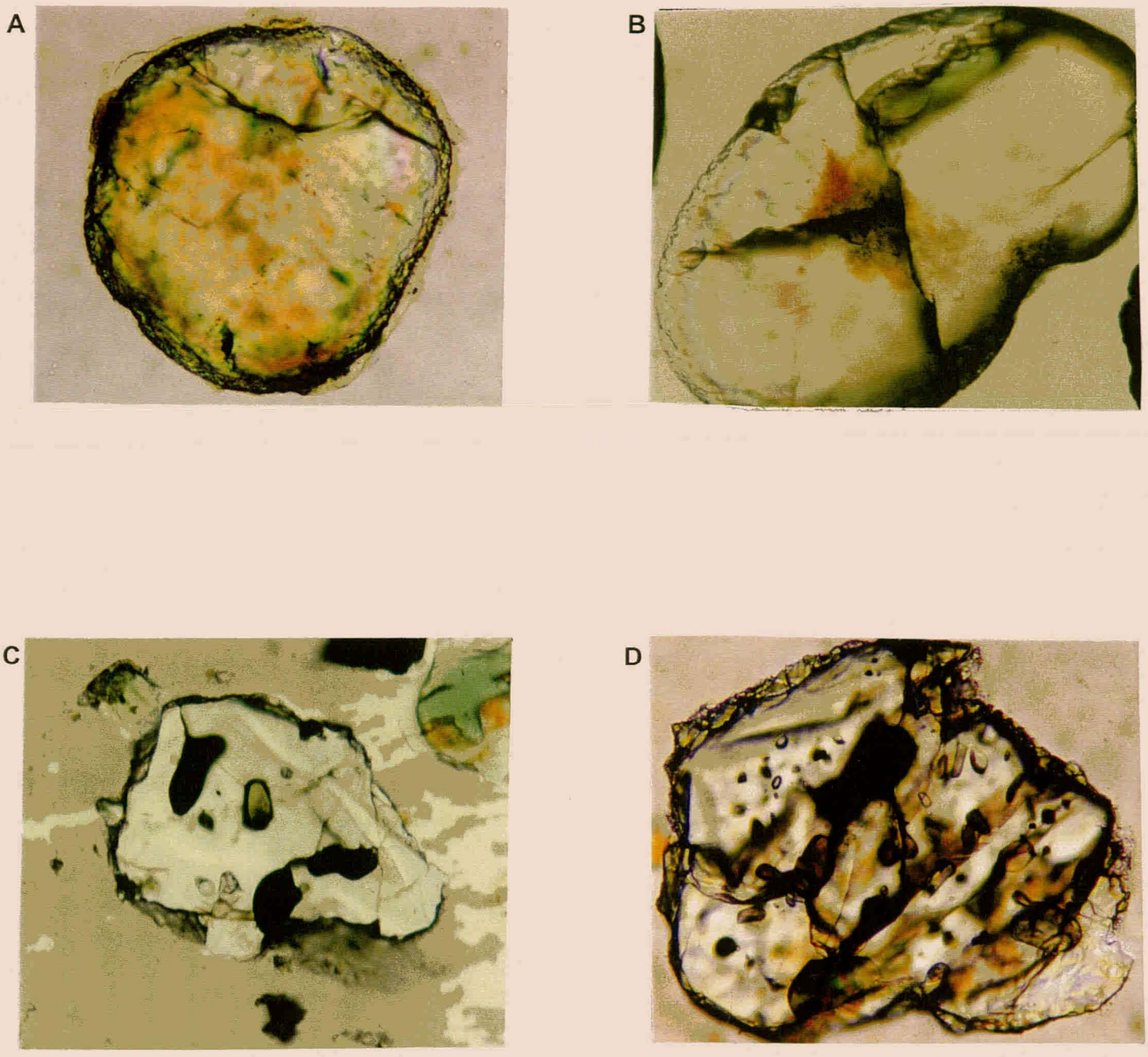

Plate 5.17. Grains of monazite (A and B) and titanite (C and D).

Scale: 200X

5.10.5. Glauconite

Glauconite occurs as large (300-500 μm) well-rounded, microcrystalline grains. It is characterised by a brilliant green (Plate 5.18B) or yellow-green colour with iron staining along cracks. Glauconite encountered in the study area did not form *in situ*, but is present as a detrital mineral recycled from pre-existing glauconitic sediments. The average chemical composition of glauconite grains is presented in Table 5. The results show that except for SiO_2 and FeO, these grains show minimal compositional variation. The very low totals are indicative of the presence of OH^- groups in the mineral structure.

5.10.6. Apatite

Apatite grains are generally concentrated in the finer grain-sizes and occur as yellow-brown, well-rounded, egg-shaped grains (Plate 5.18C). Grains are invariably cryptocrystalline and are nearly isotropic and judging from these features could be labelled collophane. A common feature is that nearly all the apatite grains are pitted somewhat, often iron-oxide pigmented and contain various inclusions.

5.10.7. Gorceixite

Gorceixite is a Ba-Al phosphate [$BaAl_3(PO_4)_2(OH)_5 \bullet H_2O$] that belongs to the candrallite series and forms *in situ* from solution during diagenesis (Wilson, 1985; Milton *et al.*, 1958). The presence of gorceixite is limited in the study area and it occurs almost exclusively in the palaeochannels (Kirtley, 1985). SEM-EDS indicated the minor presence of an Al-phosphate, but failed to establish the presence of Ba. The rather sparse information available on this uncommon mineral failed to aid in positive identification.

5.10.8. Marcasite

Marcasite is restricted to the palaeochannels and two distinctive types are discriminated by the SEM. It occurs either as an irregular crystallised grains or authigenic framboidal grains. The presence of marcasite in the palaeochannels indicates that it was formed *in situ* under reducing conditions, as they will not survive mechanical processes such as in a marine environment.

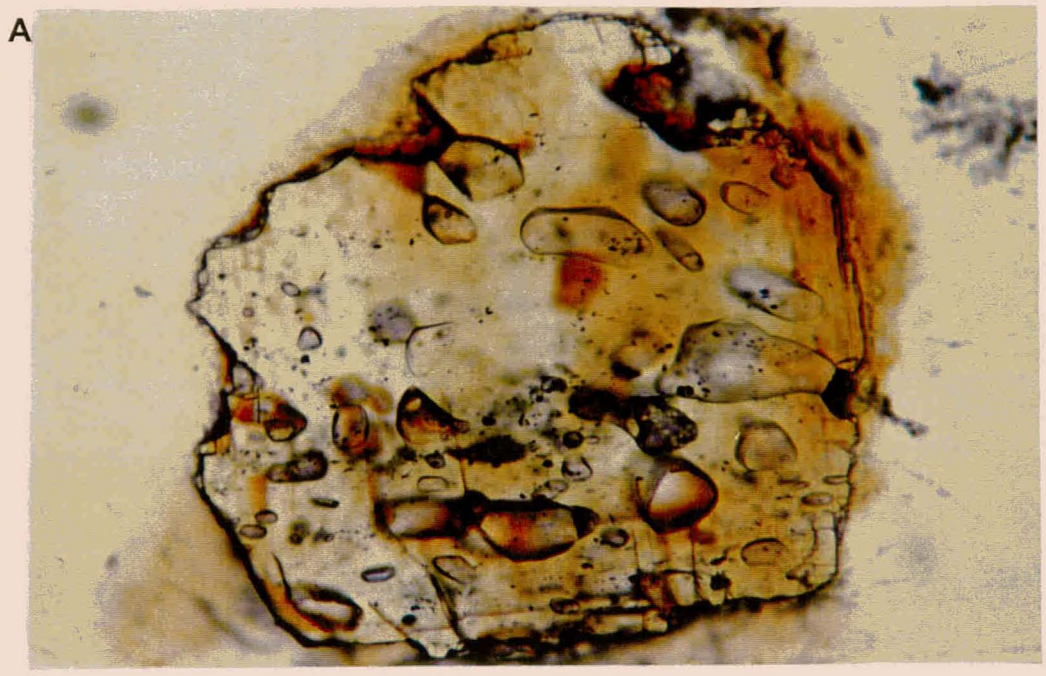

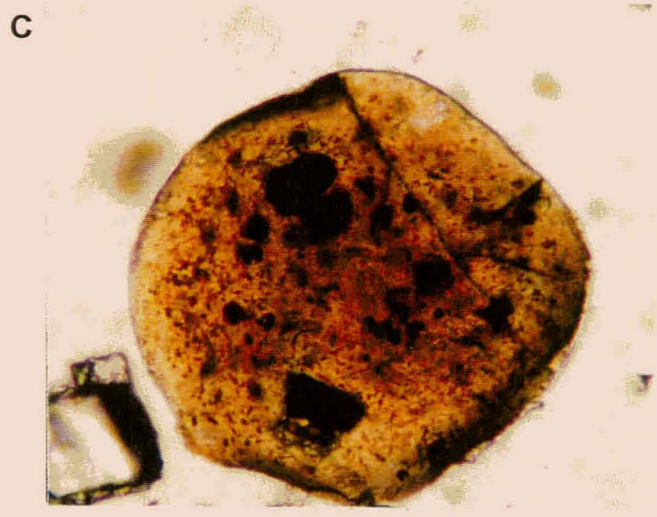

Plate 5.18. Staurolite (A) with numerous inclusions, well-rounded glauconite (B) and egg-shaped apatite (C).

Scale: 200X

5.10.9. Light minerals

The light mineral fraction consists mainly of quartz, feldspar (primarily orthoclase, microcline and plagioclase), shell fragments, Ca-rich carbonates, muscovite and biotite. Light minerals were often encountered in the heavy fraction, as they are iron-coated or interlocked with heavy minerals. Rock fragments of various parageneses, often with sutured grain contacts, were also observed, but in very low quantities (<1%). No detailed mineralogical investigation was performed on the light minerals.

CHAPTER 6
PROVENANCE INDICATORS

Heavy minerals are extremely provenance sensitive because of their diversity and characteristic parageneses. Considering this sensitivity in constraining source rocks, the characteristics of heavy minerals are widely applied in determining sediment provenance, but are also used to correlate and differentiate sediment bodies (Pettijohn, 1975; Morton *et al.*, 1991). However, heavy mineral suites are not controlled by provenance alone, but several other factors govern the mineral composition of sediments including (1) the climate in the source area, (2) the tectonic setting, (3) the effect of depositional environment and (4) diagenetic processes (Pettijohn, 1975; McLane, 1995). Hence, the interpretation of provenance by using heavy mineral assemblages is not always conducive and restricted by the effect of these factors.

In order to minimise the loss of provenance-related information induced by these processes, it is necessary to examine and quantify different features of a single mineral species. The usual method in achieving this is by performing varietal studies (Morton, 1985, 1991). These studies are usually conducted by utilising classical methods such as optical differentiation or more sophisticated analytical techniques including electron microprobe analysis, PIXE analysis, luminescence studies and radiometry. Not only do varietal studies provide additional information to corroborate the gross assumptions made about the source through the implementation of mineral assemblages and sediment characteristics, but they also make it possible to characterise the source rocks more distinctly. In theory, minerals like zircon, tourmaline, rutile and garnet offer the best means of discriminating provenance because of their relatively stable nature. However, minerals such as ilmenite, amphibole and even pyroxene, although less stable, might provide useful information regarding provenance.

Recent varietal studies that have been successfully applied using various heavy minerals include garnet (Morton, 1985, 1987; Morton and Hallsworth, 1994), zircon (Owen, 1987) and opaque minerals, in particular ilmenite (Basu and Moliranoli, 1989; Darby, 1984; Darby and Young, 1986; Grigsby, 1990, 1992; Mitra, *et al.*, 1992; Razjigaeva and Naumova, 1992; Schneiderman, 1992). Morton (1985, 1991) listed a whole range of other heavy minerals including amphibole, pyroxene, epidote and tourmaline that are less commonly implemented in varietal studies.

6.1. Mineral assemblages

It has been demonstrated in Chapter 4 that distinctive heavy mineral assemblages mark specific stratigraphic sequences in the study area. Since heavy mineral assemblages in a sedimentary unit reflect its source rocks (Morton and Hallsworth, 1994), it would suggest that various successions had different source areas. Mineral assemblages however, are greatly influenced by sedimentological conditions during deposition and post-depositional alteration. As a result, heavy mineral assemblages are controlled by (1) source rock mineralogy; (2) hydraulic conditions in the depositional environment during deposition and (3) diagenetic processes (Stapor, 1973; Pettijohn, 1975; Morton and Smale, 1990). The influences of these factors on the studied mineral assemblages were examined.

Source rock mineralogy

The predominance of opaque minerals, garnet and zircon indicates that the source rocks for the sediments are enriched in these minerals. The consistent distribution of these minerals in the entire study area also indicates a uniform source area. Local source rocks however, are also responsible for slight differences in heavy mineral proportions amongst particular successions. The consistent occurrence of epidote in RET and Lower Terrace sediments in the BMC area could be derived from greenschist facies rocks as observed in the Gariep Supergroup (Saggerson and Turner, 1995). Gariep Supergroup basement is prevalent northwards from Kleinzee (Kröner, 1971), but poorly represented in the KNC area, explaining the insignificant distribution of epidote in sediments of the latter. Similarly, the striking increase of pyroxene in the FGS sediments indicates a localised, relative proximal pyroxene-rich

source in the KNC terrain. It was also shown that the Upper CFS sediments in the KNC and the contemporaneous RET sediments in the BMC area are comparatively enriched in garnet. It is inferred that differential tectonic uplift or a minor sea-level drop during the Quaternary (Dingle and Hendey, 1984; De Decker, 1986) unroofed a garnetiferous source, which accounts for the increase in garnet content in these successions.

Hydraulic conditions during deposition

The hydraulic behaviour of minerals is controlled by grain size, density and shape (McLane, 1995). Any change in the hydraulic regime will cause fluctuations in the heavy mineral proportions of a sediment (Pye, 1994). The shape factor controls the relative abundance of minerals with different habits, so that minerals with equant habit (such as opaques and garnet) are hydraulically equivalent and mutually deposited, differing from those with a bladed habit such as hornblende (Morton, 1994). Fig. 4.11 illustrates that partial correlation analysis has yielded two distinctive mineral groups than could be related to mineral specific gravity. Opaques, zircon and garnet form one group whereas hornblende, pyroxene and epidote form the other. Selective sorting, entrainment and transport can be regarded as mechanisms responsible for the observed grouping of these minerals (Slingerland, 1977, 1984; Komar and Wang, 1984). These hydraulic processes were more effective in concentrating the more dense minerals like opaques, garnet and zircon to the expense of the less dense minerals like epidote and hornblende. Opaques will be most concentrated, followed by zircon and garnet in abundance (Guza and Thornton, 1982; Komar and Wang, 1984). Lower density minerals stay in suspension and are transported offshore or alongshore; only being deposited when hydraulic conditions become favourable. The predominance of opaques, zircon and garnet in sediments of Upper CFS and RET in the KNC area and the Middle and Upper Terraces in the BMC leaves little doubt that selective sorting, entrainment and transport might have been active in concentrating these minerals. This would imply that sediments of other successions such as the Lower Terrace and FGS were deposited under different hydraulic conditions.

Diagenetic processes

Diagenetic processes, especially chemical dissolution gradually modifies mineral composition and texture of a sediment (Pettijohn, 1975). Pettijohn (1975) formulated a chemical stability series where the minerals are sequentially ranked according to their chemical stability. Unstable minerals would successively be removed if the effect of diagenetic processes increases; resulting in increasing maturity of the sediment. The effect of weathering is usually shown by the decrease of the less stable component, such as augite, hornblende and epidote and a corresponding increase of the stable components such as opaque minerals, zircon and garnet (Morton and Smale, 1990).

Studied grains of hornblende, epidote and pyroxene as well as garnets are commonly ragged and slightly altered which is consistent with intrastratal etching and alteration. Even very stable minerals like opaques and zircon display some degree of alteration that could only be chemically induced. Undoubtedly, the very stable (mature) assemblage (opaques-zircon) of the palaeochannels is the result of extreme decay modifications by diagenetic processes following deposition. Ilmenite is very susceptible to alteration. The low degree of ilmenite alteration as well as the low proportion of altered ilmenites (~8%) confirm that chemical dissolution has not been extensive in the study area. In conclusion, although there are clear indications of diagenetic alteration, it played an insignificant role in modifying and forming the present heavy mineral assemblages in the study area.

Discussion

The consistent and predominant distribution of Fe-Ti oxides in all the stratigraphic successions undoubtedly indicates a uniform source area. A uniform provenance for the entire study area is also supported by the fact that no mineral is exclusive to a particular succession. It was demonstrated that the variation in heavy mineral proportions and assemblages are the interrelated result of mainly source rock mineralogy and hydraulic conditions during deposition. Post-depositional weathering played a subordinate role. The Swartlintjies and Buffels Rivers, which are regarded

as the main source rivers, contain similar mineral suites to the studied sediments, indicating that they carried sediment from similar if not the same provenance area.

Compared to marine deposits from Graauwduinen and Geelwal Karoo, heavy mineral assemblages of the study area are quite different since opaques, garnet and zircon dominate most of the studied assemblages. Graauwduinen marine successions are marked by a distinct heavy mineral assemblage (cpx-opaques-garnet-zircon; Cilliers, 1996) that is very similar to that of the Geelwal Karoo placer (garnet-opaques-cpx-zircon; Macdonald, 1996). FGS sediments have almost identical heavy mineral assemblages as encountered in these equivalent 50m Package sediments from the west coast. This would imply that during the Pliocene the coastal rivers providing the KNC area and similar localities with detritus had a similar drainage basin, indicating a common source area. Unlike the KNC, where only a small part of the FGS deposits was preserved, sedimentation of linear sheet-like aeolianites protected the sediments in the Geelwal Karoo and Graauwduinen areas (Cilliers, 1995; Macdonald, 1996). Low levels of *in situ* diagenetic alteration furthermore, aided in the preservation of the primarily unstable heavy mineral assemblage. Despite the difference between heavy mineral assemblages of the study area, Graauwduinen and Geelwal Karoo, similar suites of heavy minerals have been reported for Graauwduinen (Cilliers, 1995) and Geelwal Karoo (Macdonald, 1996). These workers designate the Namaqua Metamorphic Complex (NMC) as primary source terrain for the bulk of the heavy minerals. Considering the proximity of these localities with respect to Kleinzee, it would therefore be reasonable to assume that the majority of heavy minerals in the Kleinzee area were also derived from the NMC.

The Richards Bay Minerals deposit along the east coast of South Africa contains very similar heavy mineral suites to those from Graauwduinen and Geelwal Karoo. Opaque minerals dominate the heavy fraction, followed by pyriboles (pyroxene+amphibole), garnet and zircon (Hugo, 1993). Hugo (1993) also reported similar heavy mineral suites for sediments from the Eastern Cape, Zululand and Natal. The bulk of the opaque minerals were derived from the Kaap Igneous

Province and the pyriboles, garnet and zircon came from the Natal Metamorphic Province (Hugo, 1993). Although the heavy mineral suites for the east coast and west coast heavy mineral occurrences indicate some similarities, mineral chemistry unambiguously demonstrate their contrasting provenance (Hugo, 1993; Cilliers, 1995; Macdonald, 1996).

A characteristic that marks all the major heavy mineral deposits is that their ultimate source rocks are from a large metamorphic terrain (Force, 1991). Heavy mineral placers along the northeastern coast of the United States host very similar suites of ilmenite, zircon, staurolite and rutile. These deposits, which include Amelia, Altama, Green Cove Springs, Folkestone, Jacksonville, Trail Ridge and Yulee had a similar source which is postulated to be the high-grade Blue-Ridge and inner Piedmont terrain (Force, 1991). Coastal heavy mineral deposits in Eastern Australia have similar assemblages viz. ilmenite-rutile-zircon-tourmaline and their source rocks belong to a metamorphic belt in the interior of the Australian Craton (Rose, 1999). Eneabba, Bunbury and other western Australian heavy mineral deposits contain chiefly ilmenite followed by zircon and rutile. Their source rocks are believed to belong to the metamorphic Yilgarn and Leuwin blocks of central Australia (Force, 1991). The Travancore deposit in India contains mainly ilmenite and zircon with rutile and sillimanite in decreasing abundance. The ultimate sources of the heavy minerals are granulite-facies gneisses of the Indian interior (Force, 1991).

6.2. Varietal studies

In an attempt to unravel the provenance of the heavy minerals, no mineralogical investigation was undertaken for the country rocks in the study area or in the envisaged hinterland. Instead, provenance reconstruction in this sense relied on the voluminous studies consummated on the geology of western Namaqualand (Kröner, 1978; Theart, 1980; Jack, 1980; Zelt, 1980).

6.2.1. The Fe-Ti oxides

Ilmenite, hematite and magnetite are most commonly found as accessories in a wide range of igneous and metamorphic rocks. In metapelitic and metabasitic rocks ilmenite does not emerge until the mid-greenschist or lower amphibolite facies are reached (Philips and Griffen, 1982). Where hematite is closely associated with ilmenite it is found in metabasites and oxidised pelitic rocks (Deer *et al.*, 1992). Magnetite is found in a variety of metamorphic rocks including metabasites, iron-formations, quartzo-feldspathic gneisses and some metapelites.

Ilmenite

In recent years, the application of iron-titanium oxides in provenance determination has gained considerable popularity. Mainly two approaches are followed; some workers (Buddington and Lindsley, 1964; Grigsby, 1990; Basu and Molinaroli, 1989, Mitra *et al.*, 1992; Darby and Bischof, 1996) relate petrographic textures to distinct source lithologies, while other studies (Darby, 1984; Darby and Tsang, 1987; Basu and Molinaroli, 1991; Grigsby, 1992) demonstrated the usefulness of mineral chemistry to discriminate source rock paragenesis. Darby (1987) and Basu and Molinaroli (1989) stressed the insensitivity of detrital Fe-Ti oxide chemistry in provenance determination, stating that the use of it requires not only direct knowledge of mineral chemistry in the source areas, but the effects of weathering on element behaviour should be considered as well. In this approach, a dataset of ilmenite chemistry is usually compiled from possible source rocks and provenance discrimination in a sedimentary province is accomplished by comparing the chemical composition of these particular ilmenites with those obtained from the possible source rocks.

Fe-Ti oxides in the ilmenite-hematite series from plutonic igneous sources display exsolution or intergrowth features more commonly as contrasted to those from metamorphic sources (Basu and Molinaroli, 1989, 1991; Mitra *et al.*, 1992). Detrital Fe-Ti opaques in the study area display a diverse array of textures that is the result of primary crystallisation or oxidation-exsolution (Hugo, 1993). On average, more than 5% of the studied Fe-Ti population shows intergrowth or exsolution features. It is therefore inferred that these particular Fe-Ti intergrowths were predominantly derived from igneous parent rocks. Ilmenite-hematite exsolution is specifically more common in anorthosites and granites (Haggerty, 1976), but Riezebos (1979) also noted their presence in a variety of metamorphic rocks. Titanohematite may occur in any rocks that have been subjected to slow cooling or retrogressive metamorphism and those displaying the "blitz" texture (Plate 2.1F) are restricted to felsic igneous rocks (Haggerty, 1976).

Stoichiometric ilmenite contains 52-53 wt% TiO_2 and greater values reflect Fe depletion by weathering whilst lesser values indicate substitution mostly by divalent cations. Several workers (Basu and Molinaroli, 1989, 1991; Grigsby, 1992) have shown that ilmenites derived from mafic igneous and metamorphic sources are richer in titanium (~51-52% TiO_2) than ilmenites derived from felsic and intermediate igneous terrains (~47-48% TiO_2; Fig. 6.1.), where Ti depletion in the latter is explained by significant Mg and Mn substitution.

As previously mentioned, weathering may effect the composition of Fe-Ti oxides and consequently only chemical analyses from homogeneous, unaltered Fe-Ti oxides opaques have been considered in provenance discrimination. Ilmenites derived from the study area display a unimodal TiO_2 histogram that are positively skewed with a modal class of 52% TiO_2 (Fig. 6.1.) In view of previous findings, this clearly denotes metamorphic rocks as principal precursors for the ilmenite in the study area. Fig. 6.1. also illustrates that ilmenites from Graauwduinen and Geelwal Karoo show strikingly similar TiO_2 ranges and modal classes. This indicates that ilmenites from Graauwduinen, Geelwal and Kleinzee had a similar source area. Since both Graauwduinen and Geelwal ilmenites were derived from the Namaqua Metamorphic Complex (Cilliers, 1995; Macdonald, 1996), it is inferred that the bulk of the Kleinzee

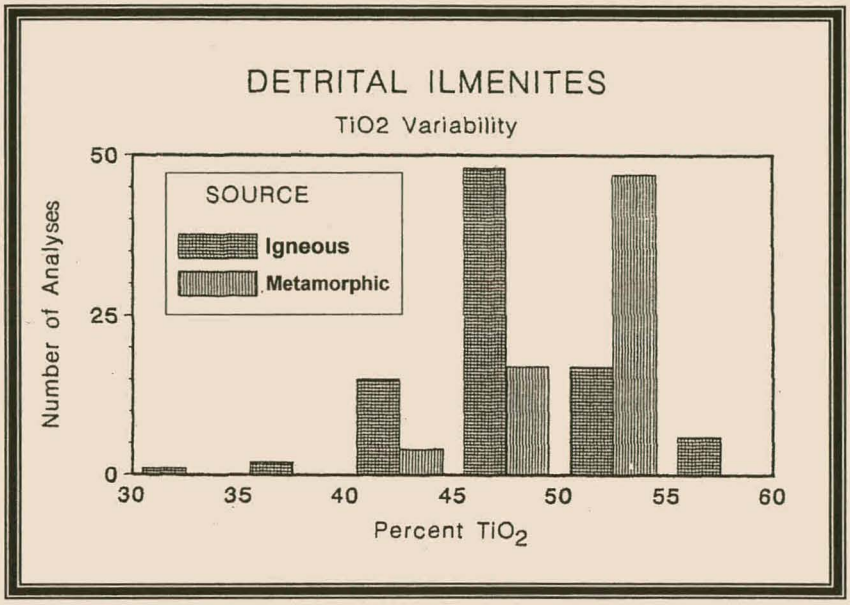

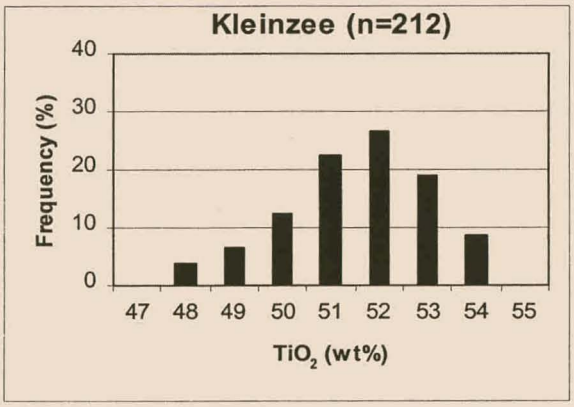

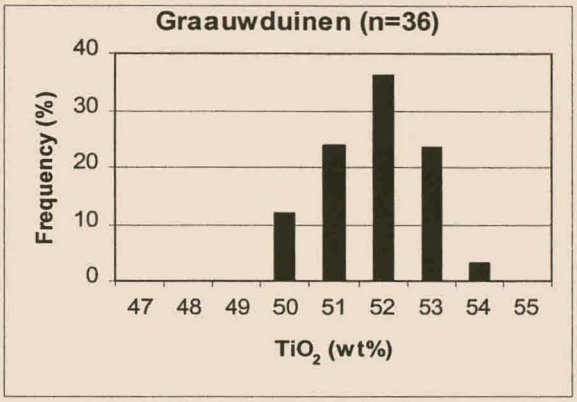

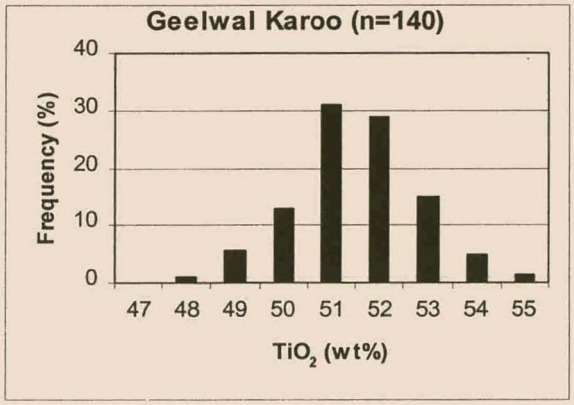

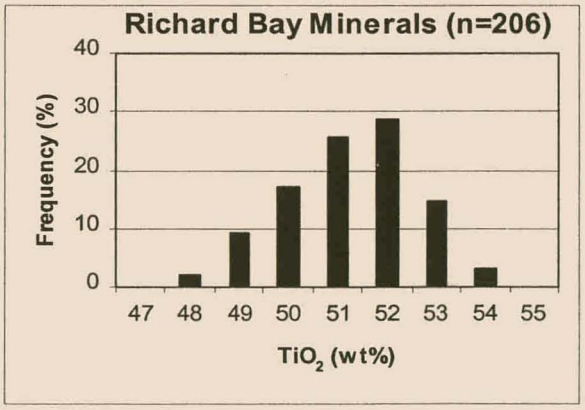

Figure 6.1. Distribution of titanium content in detrital ilmenites from Kleinzee, Graauwduinen (Cilliers, 1995), Geelwal Karoo (Macdonald, 1996) and Richards Bay Minerals (Hugo, 1993) compared to the ilmenite dataset of Basu and Moliranoli (1989).

ilmenites were also derived from metamorphic rocks of the NMC. Fig. 6.1. illustrates that ilmenites from the Richards Bay Minerals (RBM) deposit also have a metamorphic origin. Hugo (1993) however, used trace element chemistry of ilmenite to show that these particular ilmenites were derived from the Kaap Igneous Province with only minor contributions from the metamorphic Natal Basement. This indicates that TiO_2 histograms should be cautiously used in the interpretation of ilmenite provenance and conclusions should not be made without considering their trace element chemistry.

Previous studies have shown that the Mn, Mg, V and Cr content of ilmenites are provenance sensitive and that other minor elements do not indicate any specific source terrain (Basu and Moliranoli, 1989; Darby, 1984; Darby and Young, 1986; Grigsby, 1990, 1992; Mitra, *et al.*, 1992; Razjigaeva and Naumova, 1992; Schneiderman, 1992). It must be stressed however, that very low concentrations of these provenance diagnostic elements are not specific to any type of source rock (Basu and Molinaroli, 1989). Several of these workers (Darby, 1984; Darby and Young, 1986; Darby and Bischof, 1996) however analysed ilmenite concentrates, which compared to single ilmenite analyses, make their results less accurate since contamination by other minerals could influence the element measurements. Ilmenites from felsic rocks generally have high MnO (>2.0%) and low MgO contents (<1.5%) while those that crystallised in mafic and ultramafic rocks have elevated MgO values (>1.5%), with significant amounts of V and Cr (Cawthorn and Biggar, 1993; Buddington and Lindsley, 1964; Neumann, 1974; Haggerty, 1976; Basu and Moliranoli, 1989; Grigsby, 1992). Ilmenites from kimberlites and peridotites are significantly enriched in Cr (Moore *et al.*, 1992).

Kleinzee ilmenites have a variable MnO (0-12%) and very low MgO (0-1.6%) content and are depleted in Cr_2O_3 (~0.1%). Similar values were reported for ilmenites from Graauwduinen and Geelwal Karoo (Cilliers, 1995; Macdonald, 1996). The possibility of a mixed provenance for the Kleinzee ilmenites as indicated by mineral petrography, is further supported by a MnO-MgO scatterdiagram which in Hugo's (1993) opinion is a powerful provenance indicator. As demonstrated (Fig. 6.2.),

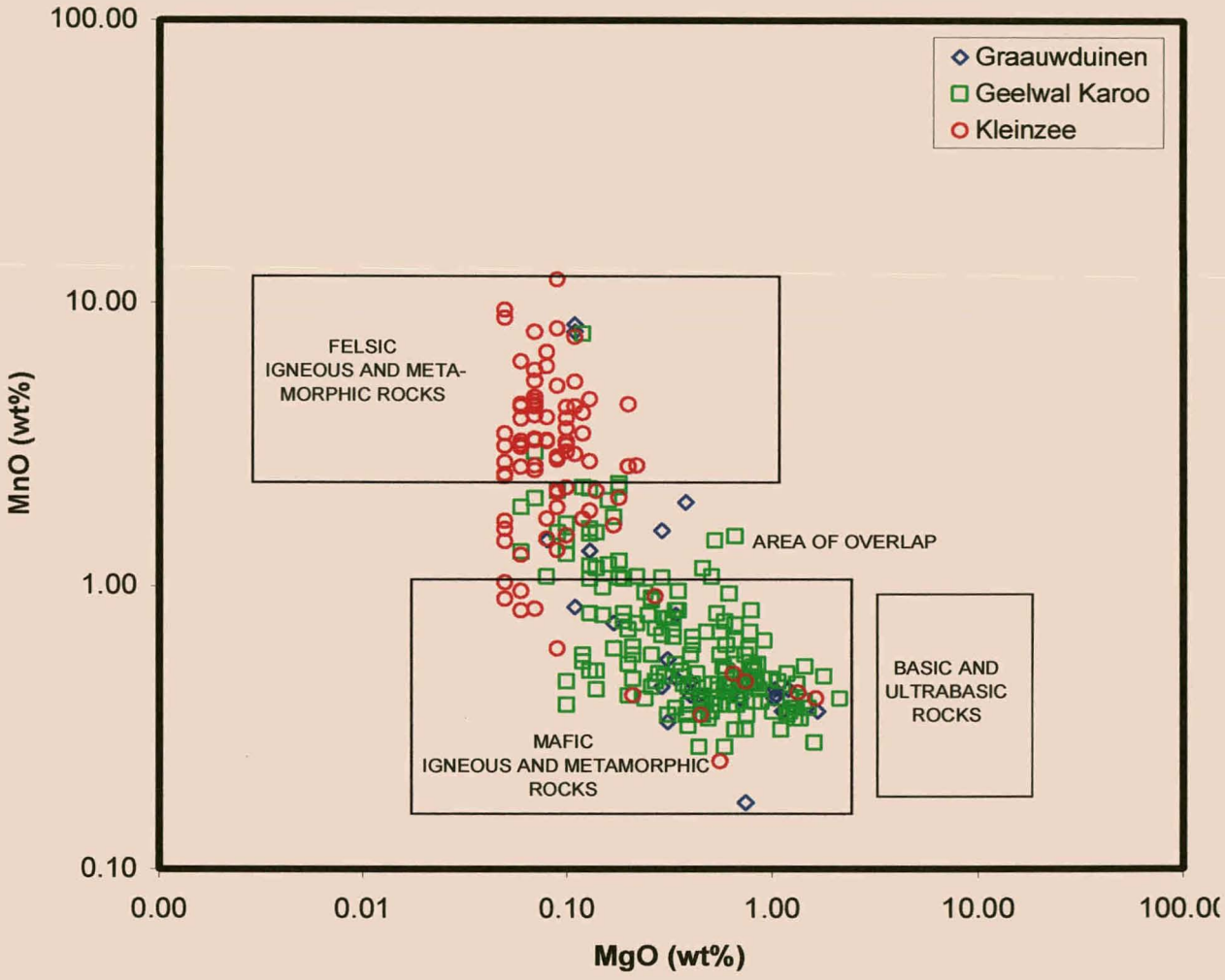

Figure 6.2. MnO-MgO variation diagram for ilmenite from Kleinzee, Graauwduinen (Cilliers, 1995) and Geelwal Karoo (Macdonald, 1996). Outlined fields demarcate ilmenite compositions from various wholerocks pertaining to the Kaap Igneous Province and Natal Basement (after Hugo, 1993).

Kleinzee ilmenites plot well into the demarcated fields designated by felsic and mafic igneous and metamorphic rocks. A large proportion of the analyses also plots in an area that is non-diagnostic of source rocks. Fig. 6.2. indicates that ilmenites from Graauwduinen and Geelwal mainly occupy the mafic field, whereas the bulk of the Kleinzee ilmenites (~60%) plot in the felsic field. This indicates that compared to Graauwduinen and Geelwal, the Kleinzee ilmenites were mainly derived from felsic igneous and metamorphic rocks. As mentioned previously, ilmenite petrography has indicated the low abundance of Fe-Ti intergrowths (<5%) in the study area, which suggests that compared to felsic metamorphites, felsic igneous rocks were minor ilmenite sources. Consequently, it signifies that the bulk of the ilmenites in the Kleinzee area came from felsic metamorphic rocks.

In conclusion, petrographic and chemical properties of detrital ilmenites in the study area indicate a mixed provenance demonstrating that felsic/mafic metamorphic and igneous rocks are the most probable sources. This perspective is corroborated by the ubiquitous distribution of ilmenites in granites, granitoids, gneisses, schists, amphibolites and granulites in western Namaqualand (Theart, 1980; Jack, 1980; Moore, 1986; Hartnady *et al.*, 1990). Although the trace elements of ilmenites indicate differences in source rock lithologies for Kleinzee and Geelwal Karoo as well Graauwduinen, it is postulated that the ilmenite along the west coast of South Africa came from the same metamorphic terrain, presumably the NMC, where felsic and mafic rock suites are interrelated.

Magnetite

Homogeneous magnetite could be equated to felsic or intermediate igneous and metamorphic rocks (Grigsby, 1990). Textures which include ilmenite-hematite exsolution, woven or cloth textures (Ramdohr, 1980), ulvöspinel and pleonaste exsolution suggest igneous mafic or metamorphosed mafic and ultramafic rocks as well as gneisses (Hugo, 1993). Discrimination diagrams based on textural proportions of magnetite as proposed by Grigsby (1990; Fig. 6.3.) have limited application and were not considered in this study because of the low abundance of these particular types of magnetite. Secondly, since magnetite is easily oxidised, magnetite abundance is modified with transport and weathering (Hugo, 1993)

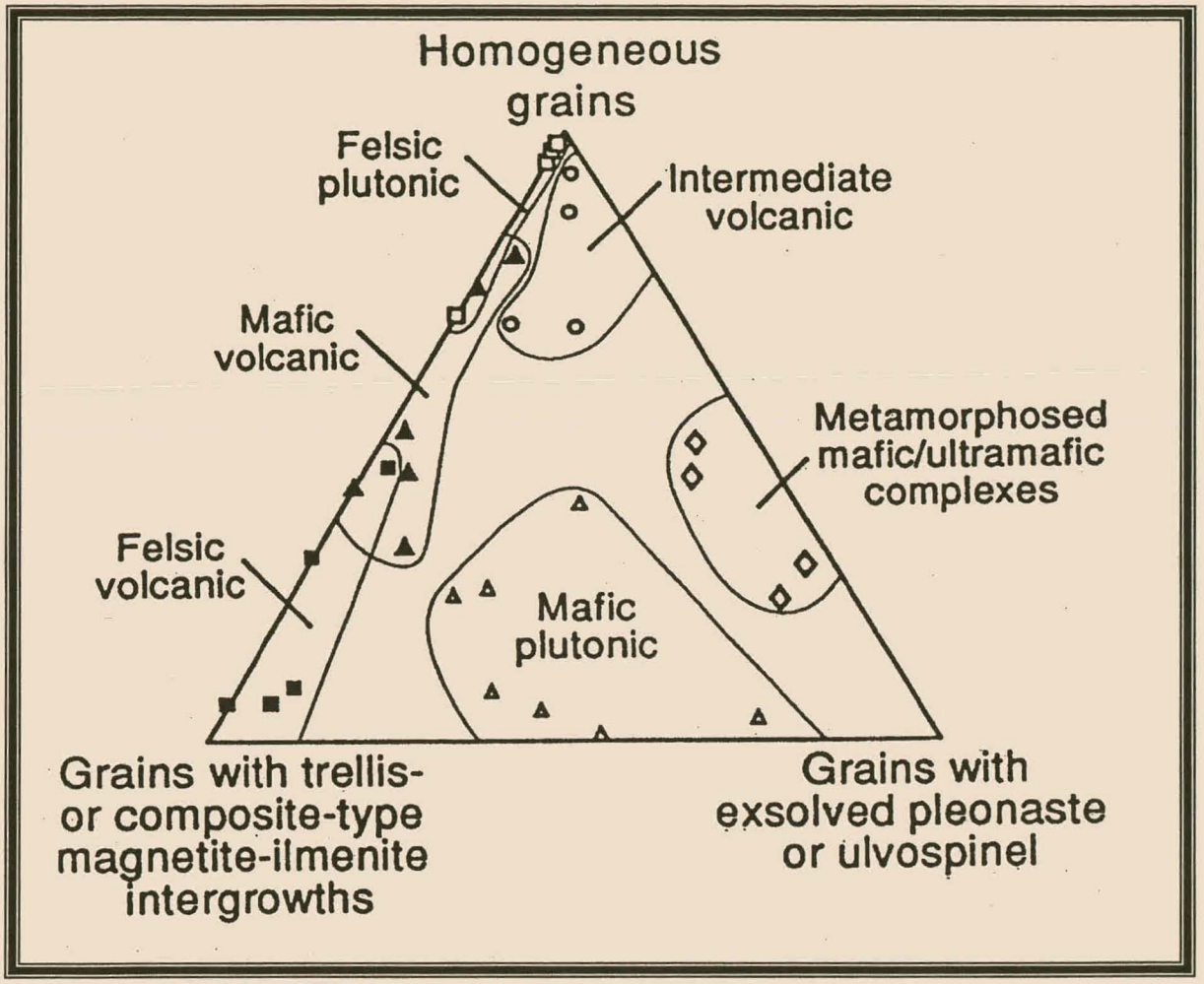

Figure 6.3. Magnetite discrimination diagram based on textural proportions (Grigsby, 1990).

making the application of this diagram in a magnetite provenance less useful. Exsolution features in magnetite present in the Kleinzee study area are less abundant than in ilmenite, and most of the magnetites manifests themselves as homogeneous grains, which indicate felsic or intermediate igneous and metamorphic rocks as sources.

Magnetites derived from felsic igneous and metamorphic rocks are generally Ti-poor compared to titanomagnetite and titaniferous magnetite that are indicative of more basic igneous rocks (Reynolds, 1978; Frost, 1991; Frost and Lindsley, 1991). Hugo (1993) concurred that homogeneous magnetites are virtually pure and contain stoichiometric proportions of Fe_3O_4 signifying both metamorphic and igneous origins. Felsic magnetites are generally depleted in Mg, Al, V and Cr compared to their intermediate and mafic counterparts (Grigsby, 1990; Razjigaeva and Naumova, 1992). Hugo (1993) suggested that a plot of Al_2O_3 against ($Fe_2O_3/Fe_2O_3+TiO_2$) is a good discriminator of magnetite provenance. Using this plot, magnetite analyses of Kleinzee (Fig. 6.4.) show that roughly equal proportions of magnetite could be ascribed to a metamorphic origin or alternatively were derived from basic igneous rocks. Only a small proportion of the analyses could not be classified with certainty. Magnetites from Geelwal Karoo plot mainly in the metamorphic field, indicating metamorphic rocks as sources. It is concluded that both magnetite and ilmenite chemistry indicates slight variations among probable source rocks for Fe-Ti oxides from Kleinzee, Geelwal and Graauwduinen. Nevertheless, it is assumed that these source lithologies are connected to a regional source terrain with a very strong metamorphic signature.

Rutile

Rutile is virtually absent in igneous rocks so that its presence as detrital grains in sediments is usually evidence of a high-grade metamorphic terrain (Mezger *et al.,* 1989). Under metamorphic conditions rutile is formed either in the kyanite or sillimanite facies of regional dynomathermal metamorphism or in the highest grade of burial metamorphism (Force, 1980). Because of its ultrastability, it is naturally subjected to sedimentary recycling (Deer *et al.*, 1992). Rutile in the study area was

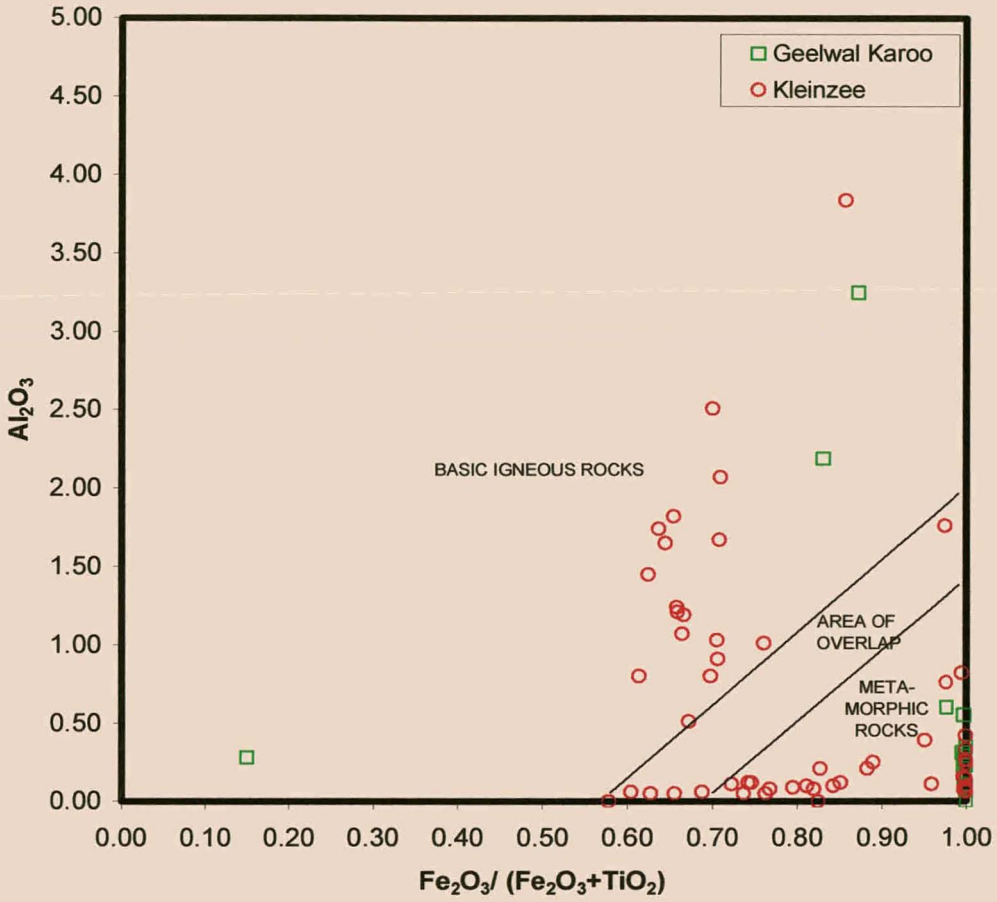

Figure 6.4. Plot of Al_2O_3 against (Fe_2O_3 /Fe_2O_3+TiO_2) for magnetite from Kleinzee and Geelwal Karoo (Macdonald, 1996). Outlined fields demarcate magnetite compositions from various wholerocks pertaining to the Kaap Igneous Province and Natal Basement (after Hugo, 1993).

probably derived from granite-gneisses as noted by Jack (1980) and Theart (1980) in their studies of western Namaqualand.

6.2.2. Zircon

The diverse effects that temperature, pressure, oxygen fugacity and initial magma composition could have on the chemistry of zircon, make elemental analysis of zircon an excellent tool to discriminate provenance. The ultrastability of zircon during sedimentary transport, diagenesis, metamorphism and anatexis further aids in the use of zircon as a provenance indicator. Previous studies utilising zircon as a provenance indicator concentrated on the physical properties of zircon such as crystal morphology and zoning patterns. Classification of zircons based on zoning facets (Pupin, 1980) is well known in igneous petrology studies, but, has limited application for zircons derived from sedimentary environments, due to secondary features such as overgrowths and abrasion that obliterate the primary morphological nature of the zircon.

Owen (1987) reasoned that Hf variability in a magma might lead to distinctive Hf compositions in a zircon population. Hf is furthermore immobile and the Hf content in a zircon is unaffected by sedimentary processes, making it a useful provenance indicator. Kinny *et al.* (1991) verified that the Hf content of a zircon population might be used to identify and distinguish between possible protoliths of rocks. Owen (1987) showed in his work that it is possible to discriminate provenance by plotting the Hf content of zircons as a frequency distribution. According to this model, the shape of the frequency distribution and the spread about the mean will reflect the variety of zircon populations present. Two genetically different zircon populations will yield a bimodal frequency distribution of Hf content, in contrast with a single zircon population that will plot as a unimodal distribution. Zircons from Kleinzee, Graauwduinen and Geelwal Karoo all have unimodal Hf frequency distributions (Fig. 6.5.), implicating that zircons from each area had a single source. Zircon populations from all these areas also have identical HfO_2 modal classes (1.2-1.4 wt%), indicating a single zircon source for all these localities. Considering the large area that the present study and those of Cilliers (1995) and Macdonald (1996) span, this suggests that the majority of zircons from the west coast of South Africa were mainly derived

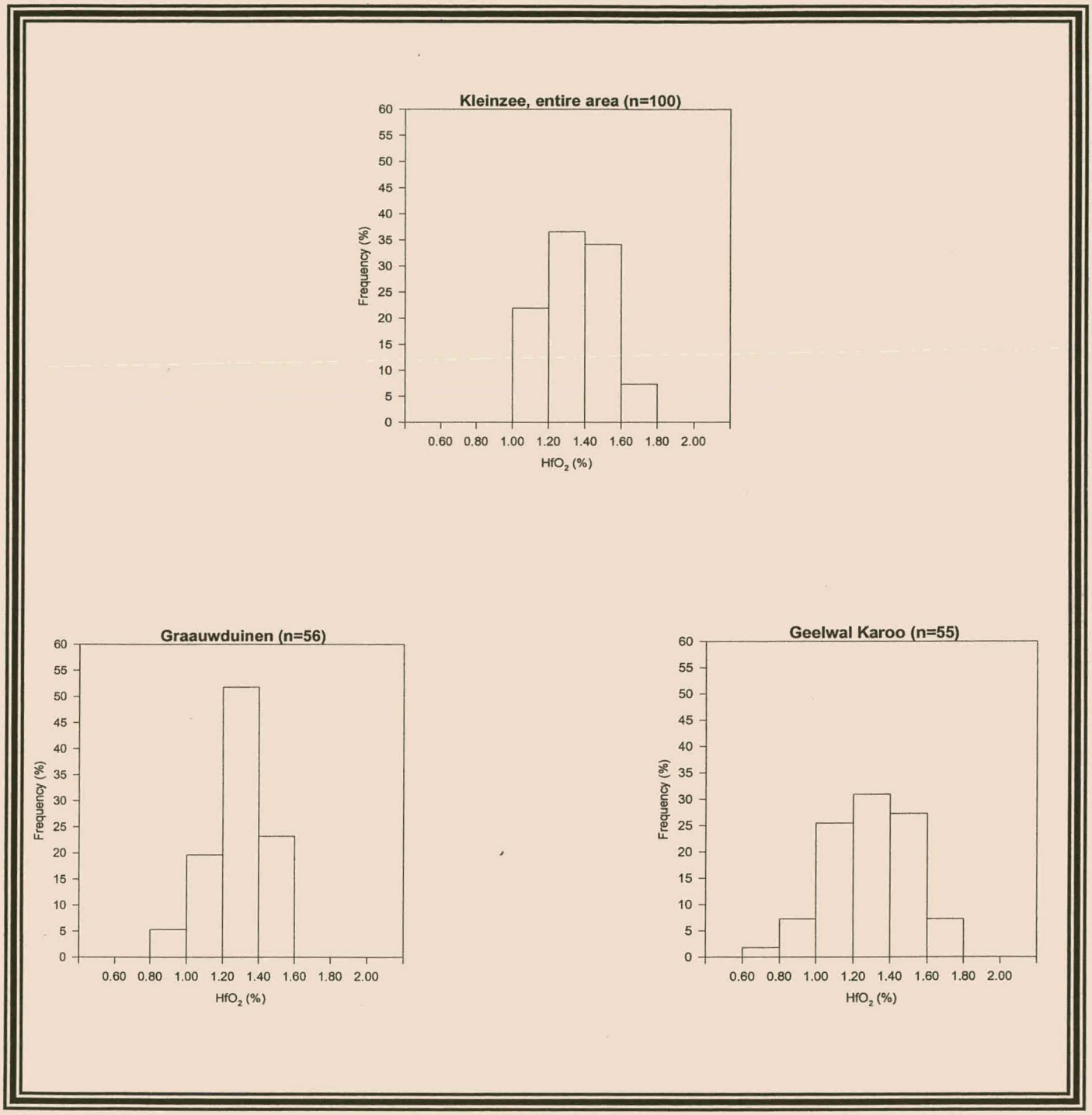

Figure 6.5. Frequency distribution of Hf content for zircons from Kleinzee, Graauwduinen (Cilliers, 1995) and Geelwal Karoo (Macdonald, 1996).

from a uniform source terrain, presumably the NMC. Although the primary source terrain (NMC) contains a diversity of rocks, present zircon chemistry indicates that the Hf signature of zircons from the regional rock suite is uniform.

REE chemistry as well as radiometry however, indicate that the zircon populations from Kleinzee, Graauwduinen and Geelwal are different. These differences are believed to be related to the composition (blend) of the zircon populations, which are ultimately connected to the temporal evolution of the coastal sediments. In their study of west coast zircons, Rozendaal (1998), Philander *et al.* (1998) and Rozendaal *et al.* (1999) have demonstrated that the colour of zircon is associated with distinctive chemistry. Concentration of the various grain-types is variable in different samples and contributes to the unique character of each population. This significant relationship is related to source rock composition and the stage of sedimentological evolution i.e. sediment maturity. The variable LREE character of representative zircon separates from these west coast localities confirms that the heterogeneity of their populations differ (Fig. 6.6).

In a similar manner, the radiometric character for a locality or depositional environment is distinctive. The zircon population from the Buffels River is heterogeneous, containing unstable zircons high in U and Th (Fig. 6.7.), indicating an immature host sediment. In comparison, zircons from Geelwal Karoo are present in more mature sediments from a beach environment, where consecutive marine processes were effective in removing unstable zircons, resulting in the much lower Bi activity of these particular samples (Fig. 6.7). Zircon populations from the palaeochannels are highly evolved as can be seen from their very low Bi activity, indicating a very low abundance of uraniferous, metamict zircons. Similarly, Graauwduinen zircon populations, which are mainly from an aeolian environment, indicate an intermediate stage in the evolution of west coast sediments. It is concluded that the difference in the geochemical and radiometric character of zircons from various west coast localities can be ascribed to the evolution of their host sediments.

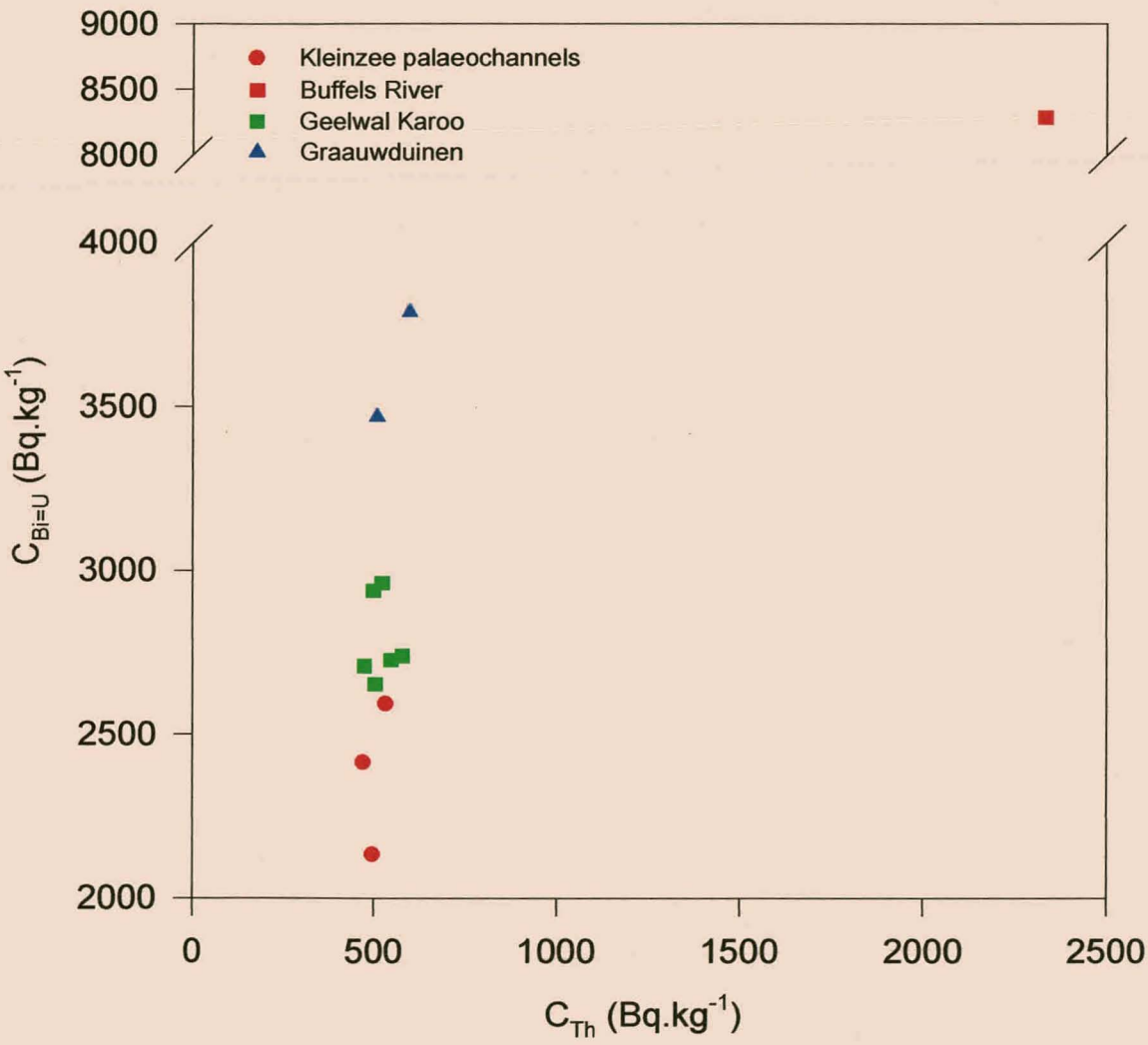

Figure 6.7. Radiometric activity plot of C_{Th} against C_{Bi} for zircon separates from Kleinzee palaeochannels, Geelwal Karoo and Graauwduinen.

It was stated that based on colour, a variety of zircons, which include colourless, pink, yellow, brown, purple and metamict types, have been identified in the study area as well as from other localities along the west coast of South Africa. In his study of the Richards Bay Mineral's zircon, Pietersen (1993) identified a similar range of zircon types and reasoned that these different zircon types belong to different source rocks. Using the REE profiles and calculated partition data of the various zircon types, he modelled REE profiles for potential source rocks. These calculated profiles of the possible source rocks were compared to a range of REE profiles of known lithology to determine the most probable source rocks for each zircon type. Pietersen (1993) showed that colourless zircons were derived from acid rocks, which include syenites, granites, granophyres, migmatites and rhyolites. Pink zircons were ascribed to granite-gneiss and pegmatites, whereas the brown, highly coloured and metamict zircons were presumably derived from mafic rocks, migmatites, carbonatites and pegmatites.

Fig. 6.8. illustrates that HREE profiles of the different zircon types from RBM are similar, but that their LREE profiles vary significantly (Pietersen, 1993). Rozendaal *et al.* (1999) demonstrated identical trends for various zircon types from the west coast of South Africa. Fig. 6.8. however shows that for a particular zircon type, the shape and shift of the LREE profiles are different for the two localities. This is most probably attributed to the difference in the method of REE analysis. Pietersen (1993) performed REE analysis by ICP-MS on zircon fractions and stated that the fractions could have been contaminated by monazite, resulting in the relatively high concentrations of the LREE and ΣREE. REE analysis of west zircons was performed on single grains by LA-ICP-MS (Rozendaal *et al.*, 1999), which is by comparison a much more accurate method. Recent, undocumented research on zircons from several world-wide localities indicate that the shape and shift of LREE profiles for a given colour type are constant, irrespective of their locality. This corroborates Pietersen's (1993) view that a specific zircon type is derived from a particular type of source rock. This suggests that the different zircon types in west coast sediments can be assigned to similar source lithologies as determined by Pietersen (1993).

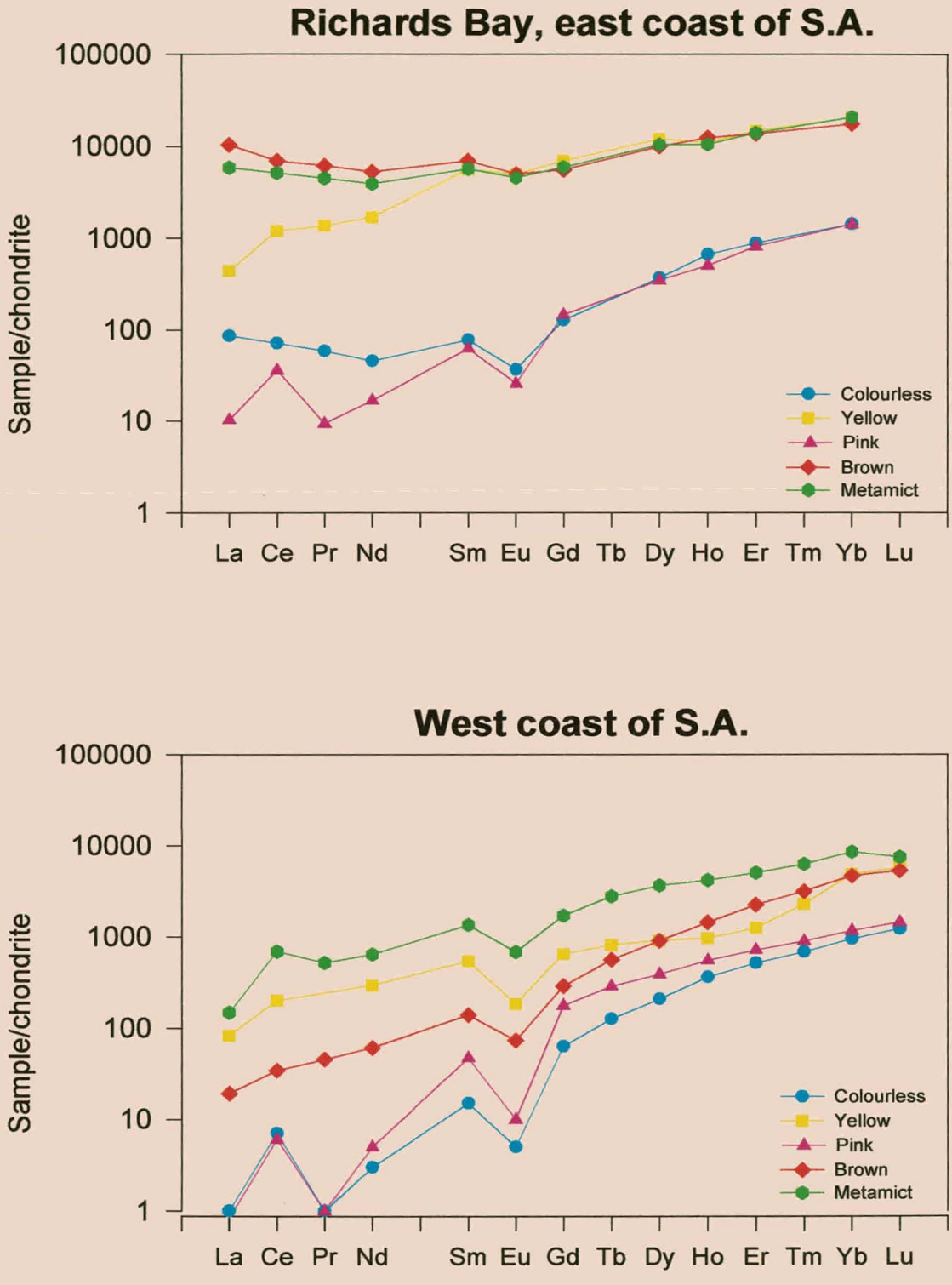

Figure 6.8. REE profiles for zircon separates from Richards Bay Minerals (from Pietersen, 1993) and single zircon grains representative of the west coast of South Africa (from Rozendaal *et al.*, 1999).

In conclusion, the studied zircons indicate mixed populations and are mainly derived from felsic metamorphic and felsic igneous rocks, presumably pertaining to the NMC. The high roundness of the majority of zircons unequivocally indicates that they were recycled. Cathodoluminescence has revealed a variety of zircon types each with inherited cores and intricate zone overgrowths, which are linked to distinctive trace element distribution. Comparison with other studies (Pidgeon, 1992; Campbell *et al.*, 1993; Hanchar and Miller, 1993; Koschek, 1993; Vavra *et al.*, 1996, 1999) verifies that the presently observed zircons are derived from igneous as well as metamorphic rocks. Robb *et al.* (1998) reported zircons with similar core and growth characteristics from various rocks belonging to the NMC, confirming the relationship between the studied zircon population and lithologies from the NMC. The postulation of the NMC as primary source for the studied zircons is also substantiated by Jack (1980) and Theart (1980) who reported the presence of zircons in granites-gneisses and schists from the West Coast Belt.

6.2.3. Garnet

Compositional variations shown by detrital garnets have proved particularly useful in provenance studies (Morton, 1985, 1987, 1991; Hutchison and Oliver, 1998), since there is a wide variety of potential garnet compositions in sediments, with seven principal garnet end-members (pyrope, almandine, spessartine, grossular, andradite, uvarovite and hydrogrossular). Garnets in most cases are associated with a wide range of metamorphic rocks, but are also characteristic of many igneous rocks. Blatt *et al.,* (1980) verified that garnets of different compositions belong to different parageneses. According to him, the garnets of granites and pegmatites are almandine and spessartine, the garnets of peridotites are pyrope and those of biotite-schists are almandine, and grossular and andradite are characteristic of calcareous contact metamorphic aureoles (Deer *et al.,* 1982).

Geochemistry indicates that the main garnet type in the Kleinzee sediments is almandine-pyrope. Macdonald (1996) and Cilliers (1995) also reported garnets with similar chemical composition from the Graauwduinen and Geelwal Karoo deposits (Fig. 6.9A.), which indicates a uniform source for Kleinzee, Geelwal Karoo and Graauwduinen garnets. Identical REE patterns of garnets from all these localities

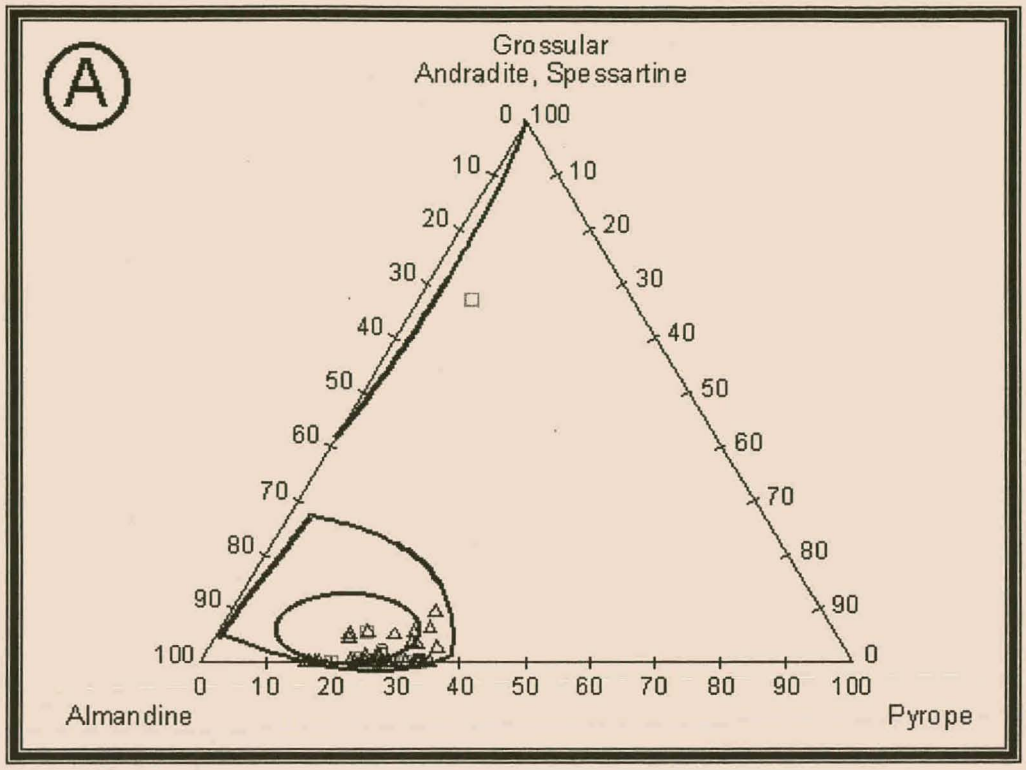

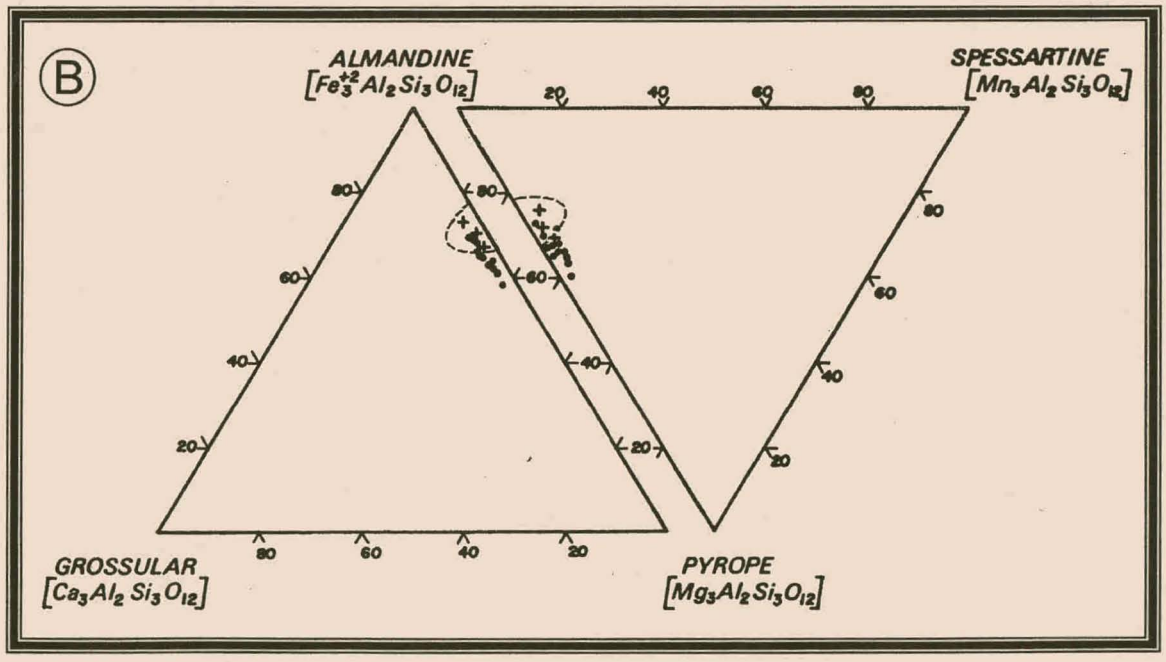

Figure 6.9. A) Chemical composition of garnet in the Kleinzee area. Outlined fields are for garnets from Graauwduinen (Cilliers, 1995) and Geelwal Karoo (Macdonald, 1996).
B) Chemical composition of garnet in pelitic gneisses from the Namaqualand Metamorphic Complex near Kliprand (after Albat, 1984). Outline fields are for garnets from pelitic gneisses from the NMC in the West Coast Belt (data from Jack, 1980; Theart, 1980; Zelt, 1980).

(Fig. 5.22.), substantiates a uniform garnet provenance. In addition to almandine, Macdonald (1996) reported significant amounts of grossular-andradite in the Geelwal Karoo sediments. The absence of grossular-andradite in the Kleinzee area either could be accounted for by a difference in garnet provenance or may be explained by the low stability of grossular in a high-energy sedimentary environment (Morton, 1985, 1991). Grossular-andradite garnet is considered to come from calc-silicate gneisses (Albat, 1984), which is absent from the West Coast Belt (Theart, 1980).

Garnets with an almandine-pyrope composition have also been reported mainly from aluminous (pelitic) gneisses (Fig. 6.9B.), with minor occurrences in schists and granites from western Namaqualand (Kröner, 1973; Zelt, 1975; Joubert, 1978; Jack, 1980; Albat, 1984). These studies show that almandine-pyrope initially appears in the epidote-amphibolite facies; is most diagnostic of the amphibolite facies and even continues to be stable in the lower part of the granulite facies. A single spessartine garnet was probably derived from a sillimanite bearing-gneiss (Theart, *op. cit*). Considering all the evidence, it seems reasonable therefore to ascribe the primary source of the studied garnet suite to pelitic rocks belonging to the NMC. This is in agreement with Cilliers (1995) and Macdonald (1996) who also proposed a high-grade metamorphic terrain as primary source for the Graauwduinen and Geelwal garnets.

6.2.4. Pyroxene

The chief pyroxenes in the study area are augite with subordinate amounts of pigeonite. Augite generally occurs in a variety of igneous rocks, but is more prevalent in amphibolites, granulites and other high-grade metamorphic rocks (Deer *et al.*, 1992). This is consistent with the work done by Theart (1980) and Jack (1980) in western Namaqualand who report pyroxenes with an augitic composition (Fig. 6.10A.) from mafic amphibolites and granulites.

Several studies in Namaqualand (Lipson and McCarthy, 1977; Zelt, 1978, 1980; Theart, 1980; Moore, 1986) have shown that augite may be more common in the amphibolite facies than in the granulite facies and when it occurs in the latter it is restricted to the lower part of the granulite facies. This indicates that the majority of

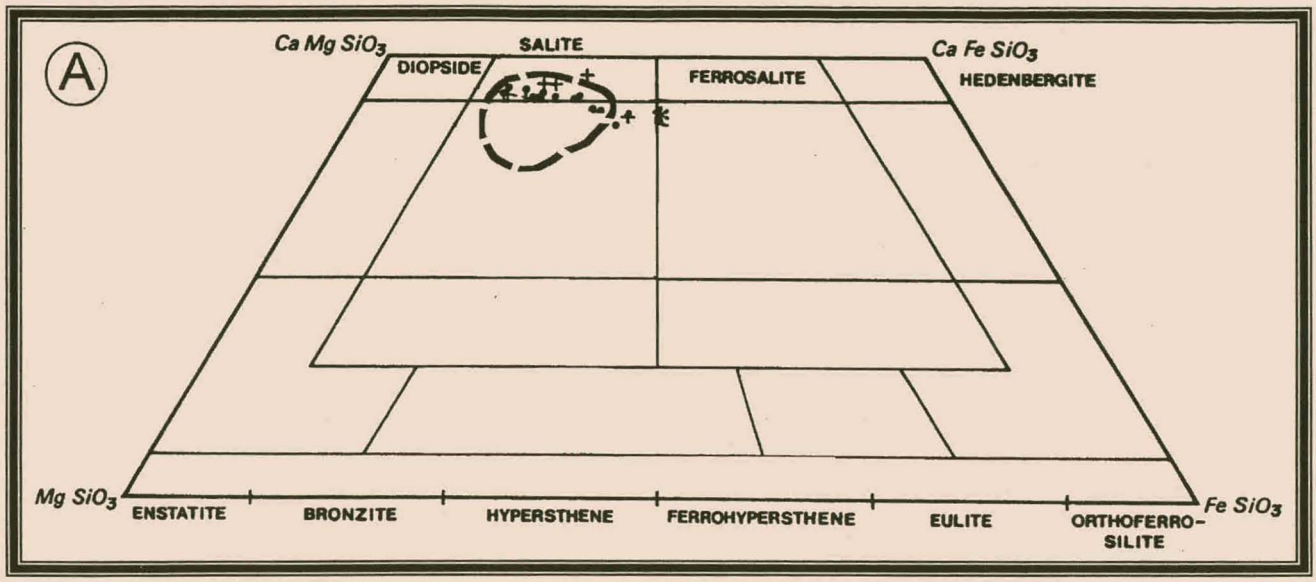

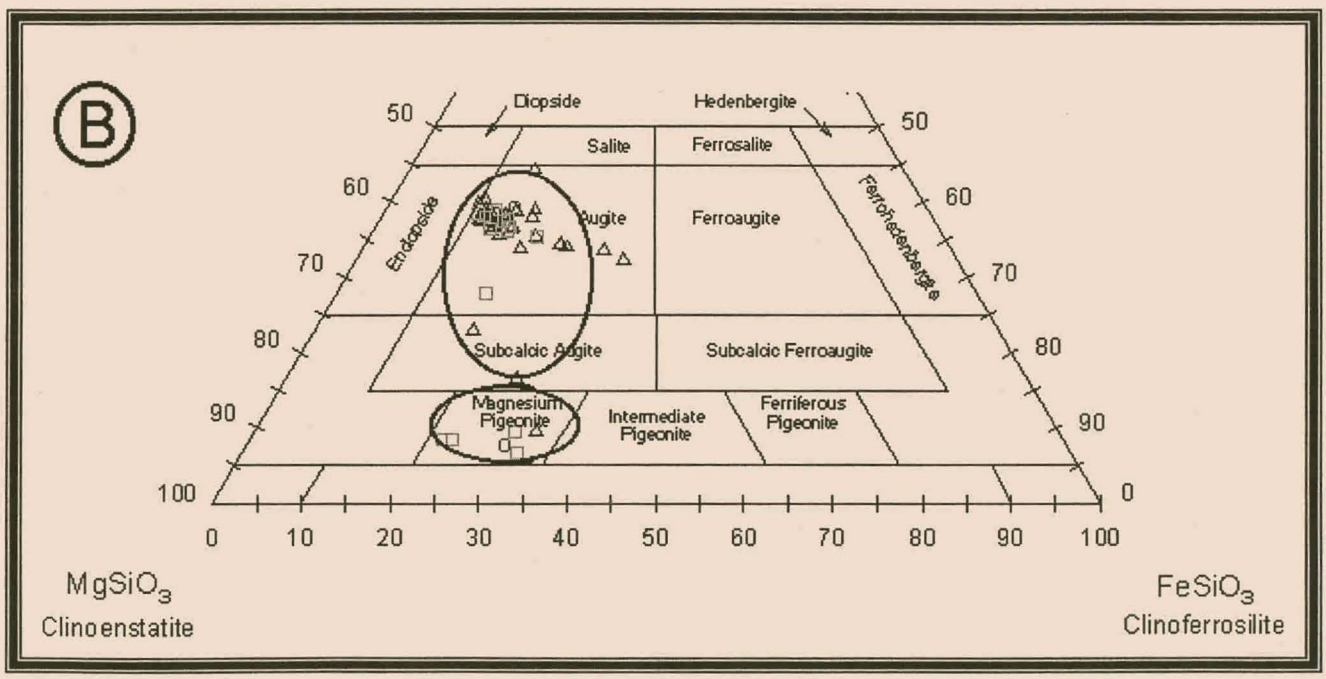

Figure 6.10. A) Chemical composition of augite from the Namaqualand Metamorphic Complex, West Coast Belt (Theart, 1980). Outline fields are for garnets from amphibolites in the West Coast Belt (data from Jack; Zelt, 1980).
B) Chemical composition of clinopyroxene in the Kleinzee area. Outlined fields are for clinopyroxenes from Graauwduinen (Cilliers, 1995) and Geelwal Karoo (Macdonald, 1996).

augite in the study area came from amphibolite facies (medium-grade) mafic rocks. Pyroxenes with strikingly similar chemical composition were also reported from Graauwduinen (Cilliers, 1995) and Geelwal Karoo sediments (Macdonald, 1996; Fig. 6.10B). It is therefore concluded that the majority of pyroxenes in Cainozoic west coast sediments were derived from mafic rocks that were metamorphosed to amphibolite facies (medium-grade) metamorphism.

6.2.5. Amphibole

The majority of studied amphiboles can generally be regarded as hornblende. Members of the hornblende series exhibit a continuous compositional range, denoting a wide range of P-T conditions giving rise to diverse parageneses (Hawthorne, 1981; Deer *et al.*, 1992). In igneous rocks, hornblende occurs in felsic and alkaline intrusives and is the most common ferro-magnesium mineral in intermediate plutonics (Deer *et al.*, 1992). Hornblende is also the most common mineral of regional metamorphism where it appears in schists, gneisses, amphibolites and granulites (Deer *et al.*, 1992). It is present in the rocks from the amphibolite to the lower granulite facies, forming the principal mineral in the amphibolite facies.

From the very high microprobe totals, it is deduced that no appreciable number of OH^- groups is present in the studied population, suggesting a metamorphic origin for the hornblende population. Several workers (Jack, 1980; Theart, 1980; Albat, 1984) which investigated western Namaqualand, reported hornblende from a variety of rocks which include granite-gneisses, medium to high-grade amphibolites, mafic gneisses and granulites. They concluded that hornblende is more prevalent in medium-grade metamorphic rocks than any other lithology. Compared to the hornblende chemistry of the Kleinzee area, these workers reported similar chemical compositions (Fig. 6.11A.), suggesting that the majority of hornblende in the study area can be equated to mafic medium-grade metamorphites.

The colour of hornblende in metamorphic rocks is diagnostic of the provenance, where amphibole colour seems to be related to the thermal grade of metamorphism (Leake, 1978; Deer *et al.*, 1992). High-grade metamorphic rocks usually host brown

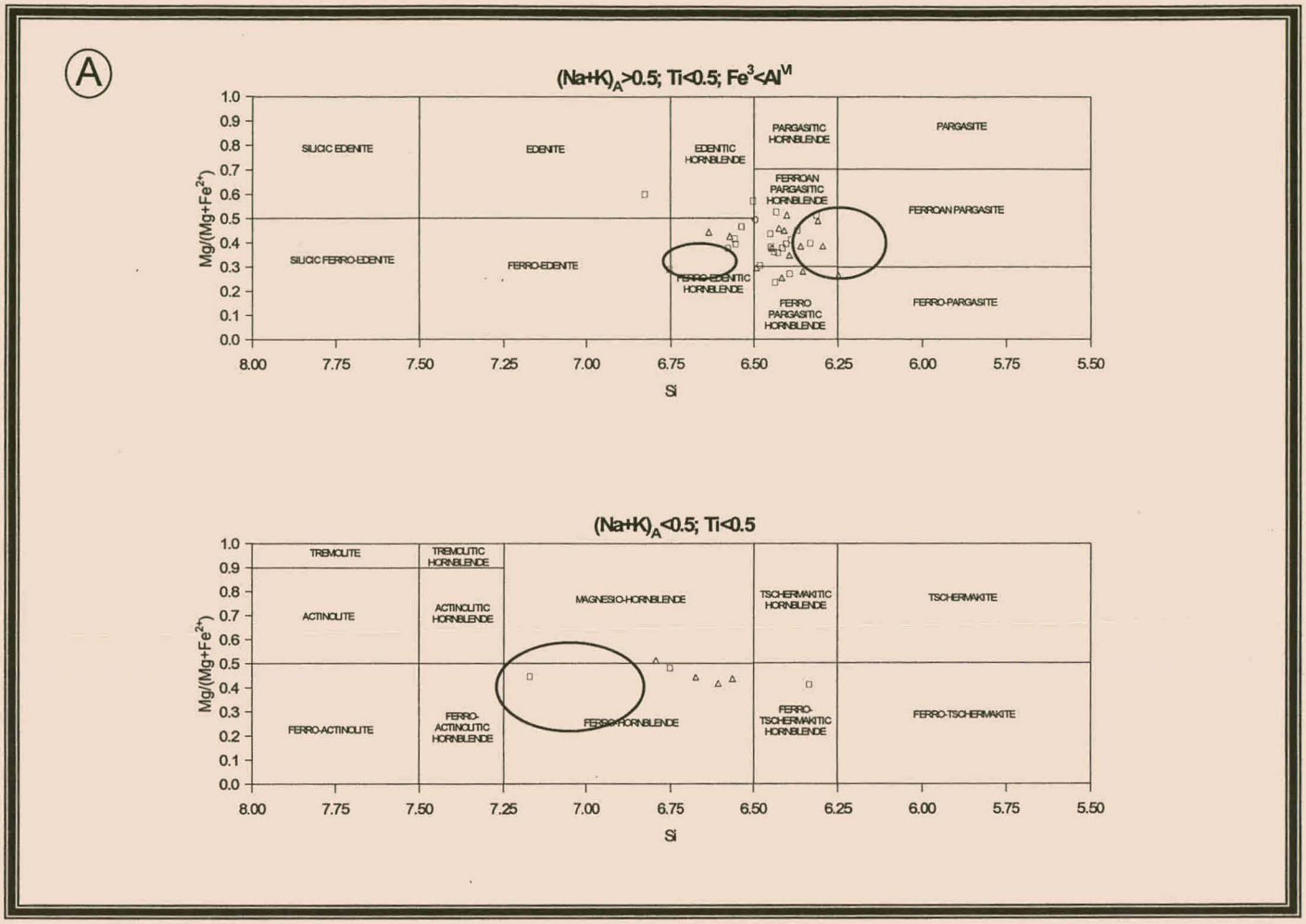

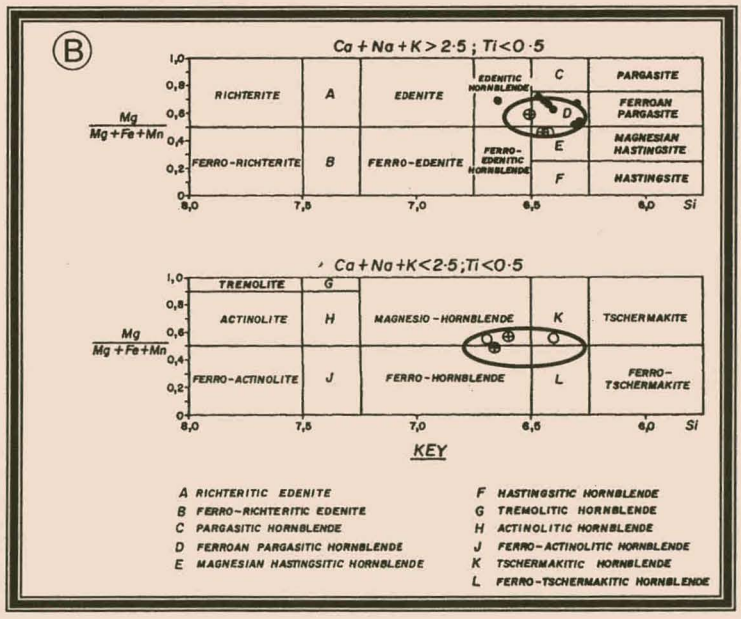

Figure 6.11. A) Chemical composition of amphiboles in the Kleinzee area. Outlined fields are for amphiboles from Graauwduinen (Cilliers, 1995) and Geelwal Karoo (Macdonald, 1996).
B) Chemical composition of amphiboles amphibolites from the West Coast Belt (Theart, 1980). Outline fields are for amphibolites near Kleinzee (from Jack, 1980).

or stronger shades of green compared to paler green hornblende that generally denotes medium-grade metamorphic rocks (Engel, 1961). Several workers (Jack, 1980; Theart, 1980; Albat, 1984) in western Namaqualand argued in a similar manner, equating the brown and olive-green amphiboles to the granulite facies and the green varieties to the amphibolite facies. Compared to the green variety, brown hornblende is poorly represented in the study area, which confirms that the majority of hornblende came from medium-grade metamorphites. Hornblende with similar chemical compositions has been reported from Graauwduinen and Geelwal Karoo (Cilliers, 1995; Macdonald, 1996; Fig 6.11B) which indicates a uniform source for hornblende along the west coast of South Africa.

6.2.6. Other minerals

Epidote

Clinozoisite and epidote show similar parageneses and are common in schists, phyllites and slates formed during medium-grade regional metamorphism (Deer *et al.*, 1992; Artioli *et al.*, 1995) and are particularly characteristic of rocks from the greenschist and epidote-amphibolite facies (Deer *et al.*, 1997). Epidote is almost exclusively hosted by mafic amphibolites in the West Coast Belt (Jack, 1980; Theart, 1980). In this region, epidote is also sparsely distributed in granite-gneiss, schist and calc-silicate metamorphic rocks.

Epidote is a prevalent mineral in the Gariep Supergroup of which outcrops are widespread north of Kleinzee (Kröner, 1974), explaining the uniform distribution of epidote in particular sediments in the BMC area. South of the Buffels River, Gariep rocks are poorly represented (Jack, 1980), which accounts for the very low abundance of epidote in sediments from the KNC area. A similar explanation is offered for the absence of epidote in sediments from Geelwal Karoo and Graauwduinen, which lie farther south. In conclusion, epidote from the study area had mafic amphibolites as its ultimate source.

Aluminosilicates

Kyanite is a high-pressure mineral of regional metamorphism forming in pelitic schists, gneisses, amphibolites and granulites (Deer *et al.*, 1982). Sillimanite has a

similar parageneses to kyanite, but the presence of sillimanite indicates high temperature regional or contact metamorphism (Deer et al, 1997). The presence of both sillimanite and kyanite in Kleinzee sediments indicate that the source rivers drained a region with rocks which were metamorphosed to different P-T conditions; viz. a medium and a high-grade metamorphic terrain. Within the boundaries of the study area kyanite and sillimanite occur almost exclusively in aluminous (pelitic) gneisses and to a minor degree in schists from the amphibolite facies (Joubert, 1971; Jack, 1980; Kirtley, 1985), making these lithologies the most likeable source for the aluminosilicates in the study area.

Staurolite

Staurolite is largely restricted to medium-grade regional metamorphic rocks such as mica schists and gneisses (Deer *et al.*, 1997). In pelitic schists and gneisses staurolite is associated with almandine, kyanite and micas indicating amphibolite facies metamorphism (Deer *et al.*, 1982) and in the lower grade metamorphics such as in schists and phyllites it appears with chlorite and chlorotoïd (Deer *et al.*, 1982). Albat (1984), Theart (1980) and Jack (1980) reported aluminous gneisses and to a lesser degree schists in western Namaqualand which contain mineral paragenesis of almandine-kyanite-staurolite, designating amphibolite facies metamorphism. This indicates that staurolite in the study area most probably came from medium-grade gneisses and schists from the NMC.

Titanite

The principal igneous parent rocks of titanite are intermediate and felsic plutonics (Philips and Griffin, 1981), but it is also widely distributed in rocks subjected to amphibolite facies metamorphism such as schists, granite-gneiss and amphibolites (Deer *et al.*, 1992). These particular titanites occur as grey cubes, a type that has been widely recognised in the study area. Titanite of similar habit has been reported in mafic amphibolites from the West Coast Belt, near Kleinzee (Jack, 1980). This mineral is restricted to a zone approximately 20-30 km from the present coastline near Kleinzee (Kröner, 1978; Jack, 1980). Its disappearance towards the east may indicate the start of the transition from an amphibolite facies terrain. It is concluded

that titanite in the Kleinzee sediments were eroded from mafic amphibolites in the near proximity.

Monazite

Monazite occurs mainly as an accessory mineral in granite, granodiorite, syenite and other similar plutonic rocks (Deer *et al.*, 1997). Neither Theart (1980) nor Jack (1980) mentioned any monazite in their petrographic investigation of the West Coast Belt. These workers probably confused monazite with zircon, as the characteristics of these minerals are very similar. This viewpoint is corroborated by Theart's (1980) description of "zircon-enriched" granites and gneisses along the coast near Kleinzee that are characterised by an unusual high radioactivity. It is concluded that monazite was probably derived from granites or felsic gneisses. Andreoli *et al.*, (1994) described fissures that host apatite-monazite at Steenkampskraal. Taking the high roundness of the observed monazite in account, it does not exclude the possibility that these minerals could have been eroded and transported from the Steenkampskraal or other similar deposits.

Apatite

Collophane (cryptocrystalline apatite) originates in sedimentary environments and is probably derived from skeletal material closely associated with phosphorites or as a biochemical precipitate (Pettijohn, 1975). Collophane occurs in the near-perfect spherical form and to a lesser extent as more irregular pieces. Fish teeth and other organic remnants in the study area have been identified to consist partially of collophane (Nicholas, 1995). The source of the collophane is probably the Pliocene phosphatic limestones occurring at elevations of 110m *amsl*

Glauconite

Glauconite probably originated from a sedimentary environment. Glauconite is deposited under quieter conditions usually in an offshore environment suggesting that the present glauconite was either reworked from older marine units or deposited in a sheltered sub-environment such as a J-bay. The former hypothesis is favoured, considering that the high roundness of the grains indicates extensive recycling.

6.3. Discussion

A brief discussion on the geology of the possible source terrain for the observed heavy minerals in the study area follows. The study area is underlain by the western part of the Namaqua Metamorphic Province that is divided into subprovinces, terrains and belts (Joubert, 1986; Fig. 6.12). Metamorphism in western Namaqualand ranges from greenschist facies in the Kheis Subprovince (Joubert, 1976) and central part of the Richtersveld Subprovince (Martin, 1975; Waters, 1986) to granulite facies southwards in the Bushmanland Subprovince (Zelt, 1980; Reid *et al.*, 1987) as well as along the spine of the Gordonia Subprovince (Watkeys, 1986). The extreme west of Namaqualand, comprising part of the Bushmanland Subprovince incorporating the West Coast Belt, is metamorphosed to amphibolite facies (Theart, 1980; Zelt, 1975, 1978). The Mid-Proterozoic Namaqua Metamorphic Complex which are locally referred to as the "basement", comprises diverse lithologies of polyphase deformed and metamorphosed sediments and volcanics intruded by various pre-, syn- and post-tectonic igneous rocks (De Villiers and Söhnge, 1959; Kröner, 1973; Lipson and McCarthy, 1977; Moore, 1986).

The basement has been overprinted by the Pan-African event (900-450 Ma) which is represented by the metavolcano-sedimentary Gariep Belt (Joubert and Kröner, 1971; Kröner, 1974; Germs and Gresse, 1991) and the sedimentary Nama Group (Germs, 1972; Gresse, 1992). In response to the Pan-African event the basement as well as the overlying Gariep Supergroup and Nama Group exhibit several thermotectonic phases which resulted in the intercalation of basement and supercrustals as well as the recrystallisation of new minerals through retrogression (Saggerson and Turner, 1995).

More specifically, the West Coast Belt portrays a polymetamorphic area where the Pan-African Gariep Complex overprints the Namaqua Metamorphic Complex. The southernmost outcrops of the Gariep Supergroup, represented by the Lower Stinkfontein "Formation", are exposed as overthrusted, tectonic slices with the basement just north of Kleinzee (Hartnady and Von Veh, 1990), whereas southwards from Kleinzee to the south of the Groen River outcrops are restricted to isolated

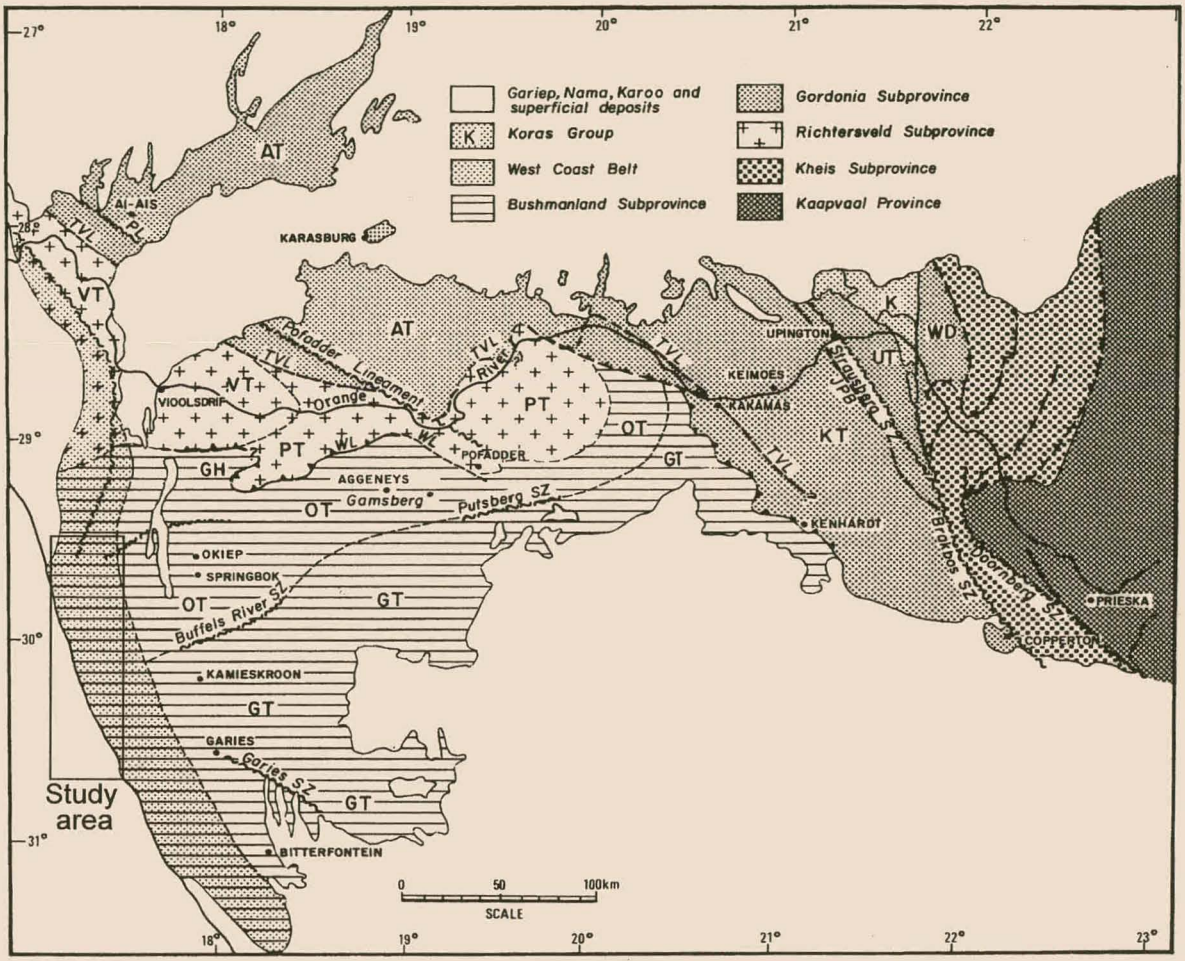

AT — Aus Terrane; GT — Garies Terrane; JPL — Jannelsepan Line; KT — Kakamas Terrane; OT — Okiep Terrane; PT — Pella Terrane; TVL — Tantalite Valley Line; UT — Upington Terrane; VT — Vioolsdrif Terrane; WL — Wortel Line; WD — Wilgenhoutsdrif Formation.

Figure 6.12. Division of subprovinces, terrains and belts in Namaqualand (after Joubert, 1986).

patches (Jack, 1980). Erratically distributed exposures of Nama Group rocks unconformably overlie the basement in the West Coast Belt (Jack, 1980).

The Plio-Pleistocene sediments in the Kleinzee area in general have similar heavy mineral assemblages. Some significant differences have been observed for the various successions, but could be satisfactorily explained by sedimentological factors such as source rock mineralogy and hydraulic sorting (see beginning of this chapter). No single mineral species or type is restricted to a particular area or a stratigraphic succession. Consequently, it is suggested that the provenance for the whole study area is uniform. Mineralogical characteristics supported by varietal geochemistry imply that these heavy mineral suites represent a mixture derived from several rock types. The data presented indicate two source types, a magmatic and a metamorphic suite in the provenance area. The association of rutile, staurolite, aluminosilicates, almandine-pyrope, epidote, augite, hornblende and titanite, mainly indicates their common metamorphic parentage whereas zircon, monazite and Fe-Ti oxides may have an igneous or metamorphic origin. Rounded heavy minerals imply that the source area was also composed of pre-existing sedimentary deposits. Heavy mineral data furthermore signals the predominance of metamorphic lithologies over igneous rocks in the provenance area.

Fe-Ti oxide and zircon chemistry indicates that the igneous sources include rocks from felsic to mafic composition, whereas the rest of the heavy mineral assemblages indicate a diversity of source rocks metamorphosed to various metamorphic grades. Epidote indicates low-grade (greenschist facies) metamorphism; staurolite, titanite, green hornblende and aluminosilicates denote medium-grade (amphibolite facies) metamorphism, whereas almandine-pyrope, Fe-Ti oxides, augite and brown hornblende could be stable from the amphibolite to the lower granulite facies (Bucher and Frey, 1994; Hess, 1989; Wilson, 1989). The studied heavy mineral suite indicates that the precursors of the metamorphic minerals, epidote, augite, hornblende, and titanite were mainly mafic rocks whereas the aluminosilicates, staurolite and almandine-pyrope represent pelitic rocks. The predominant occurrence of Fe-Ti oxide and zircon in the study area as well as their demonstrated felsic

signatures indicate that the source terrain for the Kleinzee sediments contain mainly felsic rocks.

It is reasonable to assume that the heavy minerals in the study area were derived from an area where metamorphic and interrelated igneous rocks were widely exposed. Considering the proximity of the comprehensive Namaqua Metamorphic Complex (NMC) it is therefore envisaged that diverse lithologies representative of the NMC can be regarded as the only principal and original sources that are consistent with the composition of the sands as well as with geological and physiographical conditions. The close relationship between the detrital mineral species in the study area and lithologies of the NMC as source rocks is confirmed by several studies in western Namaqualand that reported identical mineral species (Jack, 1980; Theart, 1980; Zelt, 1980; Albat, 1984). The striking similarity of mineral chemistry from Kleinzee sediments and lithologies from the NMC, unambiguously indicate the NMC as primary source terrain for the Kleinzee sediments. The possibility that lithologies of the Gariep Supergroup and Nama Group supplied source material cannot be excluded and it is reasonable to assume that the coastal sands could include recycled material derived from these complexes. Considering that the Pan-African complexes are metamorphosed maximally to greenschist facies in the north (Germs, 1972; Hartnady and Von Veh, 1990), contributions from these complexes would be minimal. This perspective is substantiated by the fact that diagnostic greenschist facies minerals, like epidote are poorly represented in the study area. Moreover, the smaller mass area of the Pan-African complexes compared to the NMC substantiates in part the fact that these Pan-African complexes did not supply significant amounts of material to the coastal deposits.

Some of the detrital material of the beach sands has been derived from intermediate sedimentary sources. Part of the marine sands is derived from direct erosion of beach and dune deposits, which are compositionally similar to coastal sands being deposited at the present-day beaches. Bimodal roundness distributions of both light and heavy minerals indicate that mixing of sediments of variable textural maturity occurred. Several grains bear abraded overgrowths, a characteristic, which suggests that these grains were recycled from a sedimentary source.

Heavy mineral compositions in the study area reflects the predominance of medium-grade (amphibolite facies) metamorphic rocks over low-grade (greenschist) and high-grade (granulite facies) rocks in the source area. The interpretation of metamorphic zonation in western Namaqualand (Zelt, 1978; Kröner, 1978; Jack, 1980; Theart, 1980) places an important constraint on the boundaries of the presumed source area (Fig. 6.13). Orthopyroxene as a specific indicator of the granulite zone first appears approximately 20-30 km from the coastline (Fig. 6.13.) and in view of its absence in the entire study area this could indicate a source area that lies very close to the present heavy mineral deposits. Evidence to substantiate this is reflected by the high angularity of the majority of minerals, verifying that they are juvenile material and were not transported over great distances. This is consistent with the moderate textural maturity of the sediments that suggests relatively little transport and reworking. These facts explain why the majority of detrital grains are of first cycle material that came directly from their primary sources. Furthermore, unstable minerals such as epidote, augite and hornblende indicate a relatively proximal source as these minerals could hardly survive prolonged abrasion or transport.

The local introduction of primary material is confirmed by the presence of etch pits on garnets, a feature that survives only short distances of transport and is only recognised close to the source (De Wit, 1993). Large gravel clasts are generally not found far from their source (McLane, 1995) and clasts of granite, amphibolite, gneiss and schist that closely resemble known bedrock formations emphasise the influence of close-by igneous and metamorphic sources. Zircons, especially those present in the palaeochannels, and an integral portion of the Fe-Ti oxides could be, if their durability is taken in consideration, transported over greater distances. These particular minerals could have come from as far as the Great Escarpment as it is known that the palaeochannels emerge from just east of this geomorphical feature. Otherwise, their physiochemical stability and continuous recycling could explain their roundness.

Judging from the presented evidence, it is hypothesised that the majority of heavy minerals in the study area were eroded and transported from an area situated in the West Coast Belt, approximately 20-30 km from the present coastline. The source

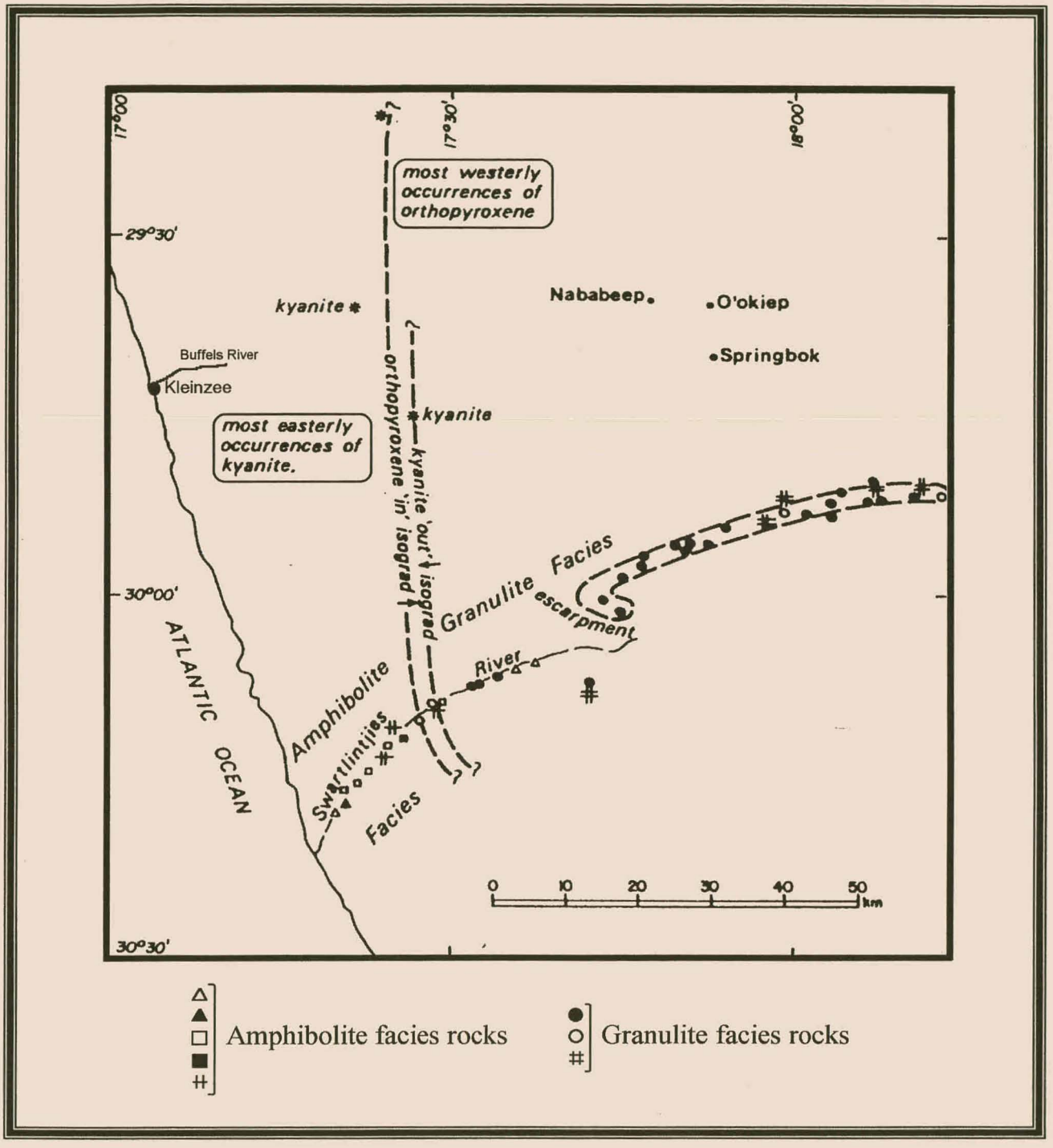

Figure 6.13. Metamorphic zonation along the West Coast Belt (after Kröner, 1978).

region also includes the Bushmanland Plateau. This conclusion indicates a relatively proximal source for the heavy minerals as well as the host sediments and has very important implications concerning diamond distribution. Heavy mineral populations, including diamonds, record the maturity of their host sediments, which is a function of the evolution of the latter. If a given diamond population is immature with respect to characteristics such as quality, textural sorting and grain-size and the heavy mineral assemblage of its host sediment is immature as well, this would indicate that both diamonds and the host sediments were minimally transported, indicating a very proximal, secondary diamondiferous reservoir. On the contrary, if the diamond population is mature, but its host sediment immature, it suggests that the diamonds were probably recycled from pre-existing deposits and mixed with sediment that was minimally transported and reworked. In this regard, little can be said about the proximity of secondary diamond sources. Similarly, if both the diamond population and its host sediment are highly evolved this would indicate that both diamond and heavy minerals were extensively recycled.

Although various palaeodrainage evolution models have been proposed for heavy mineral deposits along the west coast (Partridge and Maud, 1987; De Wit, 1993; De Wit, 1999), it is generally accepted that the coastal Orange, Olifants and Buffels Rivers acted as primary transporting mediums for sediment from the hinterland to the west coast. In this regard, the Swartlintjies, Spoeg, Groen and Sout Rivers played a subordinate part.

Several authors who studied west coast deposits (Cilliers, 1995; Macdonald, 1996; Rozendaal, 1998) reported strikingly similar heavy mineral suites and mineral chemistry; equating the provenance of heavy minerals along the west coast ultimately to the NMC. Realising the extended mass of the NMC, this accentuates the dominance of the NMC as a prime contributor of detritus to the coastal heavy mineral deposits, from the Late Cretaceous to the present. However, the specific type of source lithologies as well as the exact localities from which the heavy minerals were eroded and transported are at present enigmatic and must await a regional study of the rocks in the postulated hinterland.

CHAPTER 7
ECONOMIC EVALUATION OF HEAVY MINERAL DISTRIBUTION

In the reconnaissance phase of evaluating the economic potential of a heavy mineral deposit, several important factors have to be considered. These include:

- total heavy mineral content
- heavy mineral composition
- ore resources
- mineralogy and chemistry of ore minerals

Individually, none of these factors could indicate an economic prospect, but instead a favourable combination of these factors would signify a potentially economic deposit. The influence of these aspects on the economic potential of the heavy mineral distribution will be briefly addressed to whether a follow-up study is justified.

Compared to other major heavy mineral deposits, the heavy mineral distribution in the Kleinzee area cannot be regarded as significant (Table 7.1). On average, the studied sediments contain 6.4% total heavy minerals. This figure is highly exaggerated since more than 70% of the sediments in the Kleinzee area host <2.5 wt% of total heavy minerals. The rest of the sediments exhibit THM values that range between 5 and 60%. Table 7.1. shows that major heavy mineral-producing deposits such as Eneabba, Richards Bay, Trail Ridge and Travancore, generally have heavy mineral grades of 10-50% THM. Along the west coast of South Africa, the mega-placer at Graauwduinen has ore reserves of one billion tons at a grade of 13.8% THM. The very high-grade heavy mineral strandlines at Geelwal Karoo and Graauwduinen is the primary result of an effective concentrating mechanism in a J-bay environment (Macdonald, 1996). The Graauwduinen heavy mineral strandlines

Table 7.1. Comparison of the Kleinzee heavy mineral distribution with other selected heavy mineral deposits.

Deposit	Type	Age	Total heavy minerals (Mt)	THM (wt%)	Ilmenite wt% of THM	Zircon wt% of THM	Rutile wt% of THM	Ilmenite chemistry		
								TiO_2 (wt%)	FeO (wt%)	Fe_2O_3 (wt%)
Kleinzee, west coast of S.A.	palaeo-beach placer	Pliocene to Holocene	*	6.4	51	6	<1	53	37	5
Mine heaps; Kleinzee, west coast of S.A.	-	-	*	4.3	41	17	<1	*	*	*
[1]Geelwal Karoo, west coast of S.A.	palaeo-beach placer	Pleistocene	4	78	10	<1	<1	51	43	4
[2]Graauwduinen, west coast of S.A.	palaeo-aeolian placer	Pleistocene to Holocene	45	18	41	12	1	52	45	2
[3]Richards Bay, east coast of S.A.	aeolian placer	Pleistocene to Holocene	106	13.8	58	3	7	50	37	11
[4]Eneabba, west coast of Australia	palaeo-beach placer, aeolian	Tertiary to Pleistocene	27	50	60	18	10	56	14	26
[5]Bunbury, west coast of Australia	palaeo-beach placer	Pleistocene	22	10	>60	1	10	55	22	11
[6]Queensland, east coast of Australia	beach strandlines, coastal dunes	Pleistocene	26	<0.1	15	7	77	*	*	*
[7]WIM, south-east Australia	beach placer	Tertiary to Pleistocene	137	3	43	13	9	*	*	*
[8]Trail Ridge, Florida, USA	palaeo-shoreline	Pliocene to Pleistocene	14	50	*	15	3	58	12	25
[9]Lakehurst, New Jersey, USA	beach placer	Miocene	*	<2	86	7	<1	65	1	30
[10]Cabin Bluff, Georgia, USA	beach placer	Pleistocene	<2	<4	70	14	<1	61	*	*
[11]Coastal Plain, Virginia, USA	beach strandlines, coastal dunes	Pliocene	23	6	60	13	3	58	<1	38
[12]Travancore, coast of India	beach placer		*	50	75	5	4	61	9	24

*- not available

References

[1]Macdonald (1996)

[2]Palmer (1994)

[3]Fockema (1986)

[4]Force (1991)

[5]Force (1991)

[6]Force (1991)

[7]Williams (1990)

[8]Force (1991)

[9]Puffer and Cousminer (1982)

[10]Pirkle *et al* (1991)

[11]Carpenter and Carpenter (1991)

[12]Force (1991)

were subsequently upgraded by the development of large aeolian dunes (Cilliers, 1995). The absence of a J-bay as a major concentrating mechanism and the lack of substantial dune formation in the Kleinzee area explain the generally low concentration of heavy minerals in the area.

Namakwa Sands Ltd., which operates the Graauwduinen deposit, uses a 10% THM cut-off grade to delineate ore reserves. Consequently, it was decided to evaluate those sedimentary units in the Kleinzee area that has >10% THM. These particular sedimentary units that are potential prospects conform to stratigraphic successions from Langhoogte in the BIC, the Middle and Upper Terraces of the BMC and the FGS, Upper CFS and RET of the KNC (Table 7.2). The economic potential of these particular sedimentary units as well as the mine heaps will be discussed.

The economic importance of a heavy mineral deposit largely relies on the ore mineral composition. Conventionally, zircon, ilmenite and rutile are regarded as the main economical minerals with the remaining assemblage considered as gangue. Currently, monazite, which is valued for its REE, is not considered to be a commodity. The latest prices for ilmenite, zircon and rutile are quoted below (Mining Journal, 1999).

ilmenite (54% TiO_2)	\$95-110/t fob (bulk)
zircon (66-67% ZrO_2)	\$500-600/t fob (bulk)
rutile (95-97% TiO_2)	\$695-750/t fob (bulk)

The total economic fraction (TEF) of heavy minerals comprises the combined weight percentages of zircon, rutile and ilmenite in the heavy fraction. Table 7.2. indicates that the TEF constitutes a very large portion of the investigated heavy mineral suites. Generally, the TEF in the Kleinzee area is dominated by ilmenite (46-85%). Zircon (1-6%) and rutile (~1%) constitute the remainder of the economic fraction. Mine heaps on average contain fairly abundant zircon (17%). Regarding the significance of the economic fraction, major deposits such as Enabba, Queensland and WIM located along the Australian coast eclipse the present mineralisation, which are

relatively enriched in rutile and zircon (Table 7.1). Similarly, the South African situated Graauwduinen and Richards Bay deposits are of economic importance due to their elevated zircon and/or rutile content.

The strike and full extent of the investigated heavy mineral host sediments are not known at this time, but from exposures the measured thickness of the particular units was used to calculate the tonnage on a grid of 50m by 50m (Table 7.2). The tonnage is calculated by:

tonnage= [thickness of unit × 50m × 50m × $S.G._{sand}$] where the $S.G._{sand}$ was taken as 2 ton/m^3.

The *in situ* monetary value of the sands was determined by the following calculation.

$$\$/t = \Sigma[(THM_{ilmenite} \times TEF_{ilmenite} \times \$_{ilmenite}) + (THM_{zircon} \times TEF_{zircon} \times \$_{zircon}) + (THM_{rutile} \times TEF_{rutile} \times \$_{rutile})]$$

Table 7.2. THM, TEF, economic mineral abundance, tonnage and *in situ* monetary values for target areas.

Target area	Ilmenite (% of THM)	Zircon (% of THM)	Rutile (% of THM)	TEF	THM/t	Tonnage '000	$/t
DP127R	85.3	1.9		87.2	43.2	4	39
KN14	75.1	0.9		76.0	18.0	23	14
KV196R	79.6	1.5		81.1	14.5	26	12
KV198PR	64.6	5.5		70.1	11.3	2	10
LHC	78.3	1.4	0.2	79.9	23.5	4	19
LKC1-04	65.2	2.9	0.3	68.4	15.3	38	12
LKN8-03_3	45.8	6.0	2.8	54.5	11.0	21.5	10
SEA419	78.3	0.3		78.6	47.0	5	36
SNR1_3	58.6	4.7	0.3	63.6	12.0	4.5	10
TP262N_2	82.1	0.3		82.4	43.5	15.5	35
Mine heaps	60.0	17.0	0.5	77.6	3.6	5	5
Namakwa Sands	41.0	12.0	1.0	54.0	10	1 000 000	11

Weighted averages were calculated where units were successively mineralised. The relevant values were used to delineate possible target areas (Fig. 7). The intrinsic

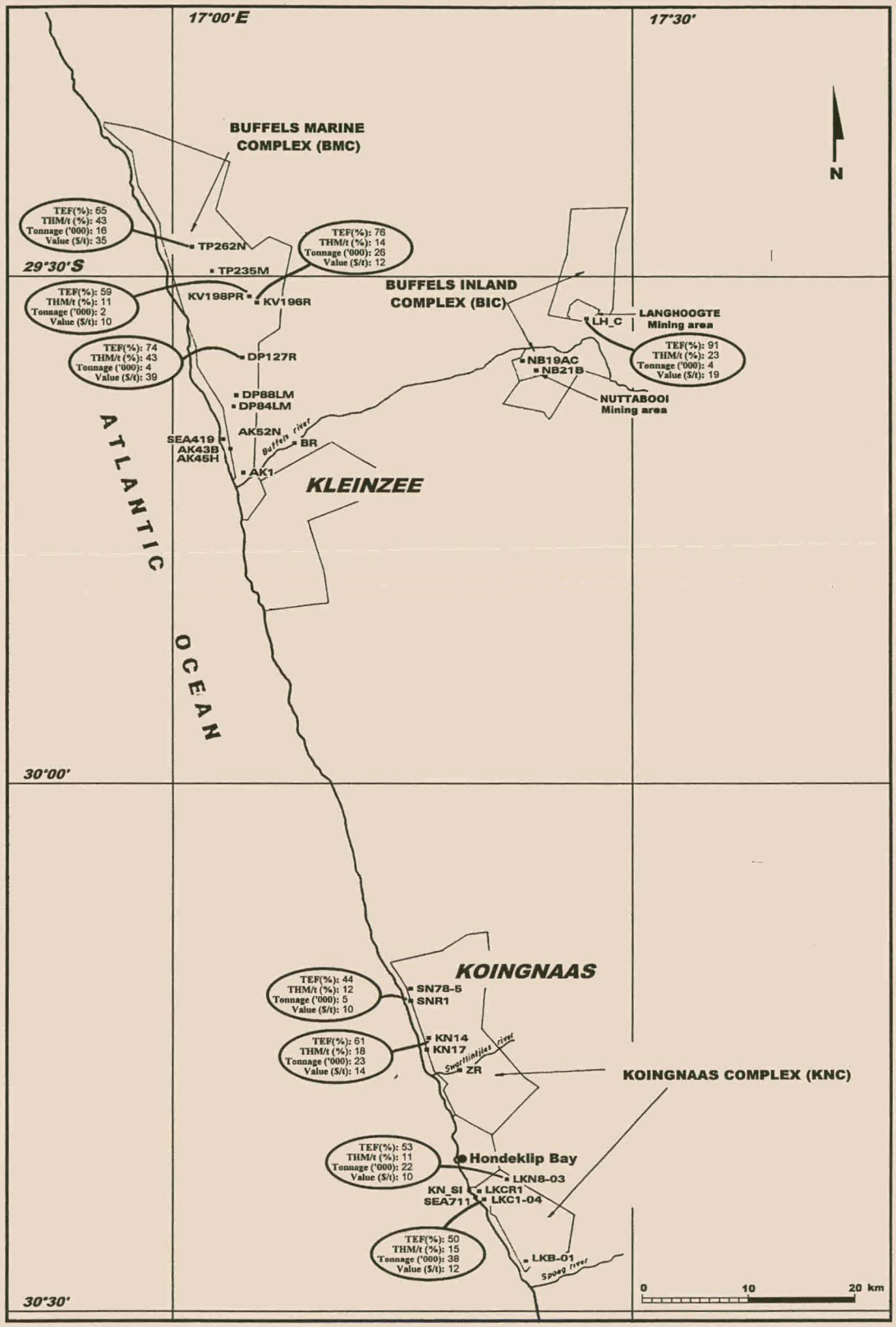

Figure 7. The economic potential of specific target areas in terms of total heavy mineral content (THM), total economic fraction (TEF), tonnage and intrinsic monetary value ($/t).

value of these unconsolidated sands ranges from 10 to 39 $/t (Table 7.2). Compared to a calculated intrinsic value of 11$/t for the Namakwa Sands deposit, most of the investigated sites are marginal and only a few areas indicate economic potential. These figures however sketch the most favourable scenario and penalties against mineral fractions that do not conform to set specifications could jeopardise the viability of the operation. Expected recovery losses of economic minerals during separation must also be taken into consideration and will greatly influence the economic potential of these occurrences. Although the mine heaps have a very low intrinsic value (5$/t), they are economically attractive, since production costs would be minimal to exploit this resource.

Heavy mineral producers usually define stringent specifications concerning the chemical composition of ilmenite, rutile and zircon. Generally, ilmenite feedstocks with less than 54% TiO_2 are not traded and additional beneficiation is required to market this product (Hugo, 1993). Table 7.1. indicates that deposits along the east coast of North America, Richards Bay and Australia are enhanced by their elevated TiO_2 content, which is greater than 55 wt%. Microprobe analysis indicates that the Kleinzee ilmenites contain on average 51 wt% TiO_2. The TiO_2 of the ilmenite as determined from microprobe analysis can however be regarded as exaggerated and may not be representative of the whole ilmenite population. TiO_2 abundance from single grain analyses are in all cases higher than those obtained from bulk analysis, because the ilmenite fraction can, aside from pure ilmenite, contain a suite of complex Fe-Ti oxides, minerals which often are intimately intergrown with the ilmenite. Non-titanium bearing inclusions and substitution elements can also lower the titanium grade. As a result, a bulk sample of the ilmenite fraction will have a lower TiO_2 content than pure ilmenite. XRF analysis of the ilmenite fractions may yield a more realistic figure. X-ray fluorescence analysis (XRF) was performed on magnetically separated ilmenite fractions from the study area (Table 7.3). Results indicate that the TiO_2 ranges from 45.9-51.5 % which is well below the specified content of 54% TiO_2.

Table 7.3. XRF results for selected, magnetically separated ilmenite concentrates.

Sample	SiO_2	TiO_2	Al_2O_3	Cr_2O_3	Fe_{Tot}	MnO	MgO	CaO	Na_2O	K_2O	P_2O5	H_2O-	LOI	Total
BMC: TP262N_3	0.1	44.9	0.2	0.0	51.8	3.0	0.1	0.1	0.0	0.0	0.0	0.0	0.0	100.3
KNC: KN14_3	0.1	45.8	0.1	0.0	52.9	3.0	0.1	0.0	0.0	0.0	0.0	0.0	0.0	102.1
BIC: LHC_1	0.1	51.6	0.1	0.0	43.0	3.3	0.2	0.0	0.0	0.0	0.0	0.0	0.0	101.4
Palaeochannels: SN78-5_1	0.2	55.2	0.8	0.1	37.3	1.7	0.1	0.0	0.0	0.0	0.1	0.0	0.0	98.3

The degree of *in situ* alteration has a beneficial effect on the TiO_2 content of the total ilmenite-related fraction and increases its metal grade. Ilmenites from the Kleinzee area display limited alteration and <8% of the ilmenite fraction is affected. Single grain analyses indicate that the titanium grade of the Kleinzee ilmenites is on average poor (51 wt% TiO_2) compared to other heavy mineral provinces in Australia, USA and India, which produce ilmenite containing 53-61 % TiO_2. Richards Bay ilmenites are also marked by TiO_2 enrichment (58% TiO_2) whereas the west coast Graauwduinen and Geelwal Karoo deposits contain low-grade ilmenite (51% TiO_2). Impurities such as Si, Al, P, Cr, Ca, Mg, Mn and V reduce the quality of titanium products and producers usually specify that their abundance should be less than a few tenths of a per cent. The ferric to ferrous ratio is also important since extra production cost is involved to reduce ferric iron to the ferrous state. It is obvious that the lower the content of the impurities the more marketable is the product. XRF analysis indicates that the impurity elements are very low and within the specified constraints. Despite their low TiO_2 content, the high purity of the South African ilmenites enhance their demand on the international market (Hugo, 1993).

Microprobe analysis has shown that rutile is essentially very pure and contains between 95-99 wt% TiO_2. Zircon on average contains 65 wt% ZrO_2 (excluding Hf) which is significantly lower than the specified 66-67 wt% and although they host a diversity of elements such as Fe, P, Al, Ca, U, Th and REE, their individual abundance is generally less than 0.2 wt%.

In conclusion, the present appraisal of the economic importance of the studied heavy mineral distribution indicates that it does not compare favourably with major

economic heavy mineral deposits. The economic viability of the area is greatly impaired by the generally low heavy mineral content as well as the composition of the economic fraction which is dominated by less valuable ilmenite. Bulk chemistry as well as single grain analysis also indicates that the TiO_2 content is low (<50%). Using a cut-off grade of 10% THM and an *in situ* monetary value of $11/t, several target areas have been delineated (Fig. 7). Several factors might however influence the final viability of these occurrences. These include production costs, loss of economic minerals during recovery as well as costly processing to produce a 54% TiO_2 concentrate.

Ore resources may also be the deciding factor in considering whether the Kleinzee area constitutes an economically viable deposit. In the author's opinion, specific target areas in the study region (Table 7.2.) indicate enticing prospects and deserve a follow-up study in order to evaluate their potential ore resources. It is recommended that large diameter auger (LDA) drilling is done on a 100 × 100m grid at the target areas to determine the dimensions of these heavy mineral concentrations. Bulk samples (~100kg) should be taken at grid intersections and from that heavy mineral concentrates should be obtained using Rickert cones or Humphreys spirals. These facilities are available at the Department of Engineering, University of Stellenbosch. Finally, these heavy mineral concentrates can be analysed by XRF to quantify their Ti and Zr content.

Considering that the development and exploitation of a new deposit requires large investments (Force, 1991), the economic feasibility of the Kleinzee area is more suited for the establishment of a small, subsidiary operation that supply heavy minerals to existing heavy mineral producers, such as Namakwa Sands. Heavy minerals can easily be separated in an on-site pilot plant and the upgraded heavy mineral product can be transported to Namakwa Sands. In addition, an attractive source of heavy minerals includes the mine heaps, which contain considerable amounts of zircon, and ilmenite, which can be cost-effectively, exploited.

CHAPTER 8

SUMMARY AND CONCLUSIONS

- A variety of Mid-Proterozoic rocks such as quartzites, schists, granitoids, gneisses and amphibolites of the Namaqua Metamorphic Complex and Pan-African Complexes constitute the basement rocks in the study area.
- Heavy mineral occurrences in the study area are associated with overlying Pliocene-Pleistocene unconsolidated marine successions as well as Miocene fluvial lithologies.
- In the KNC area, sediments are genetically related to characteristic sea-level elevations, whereas those from the BMC were deposited on a series of wave-cut terraces. It is inferred that the contrasting geomorphological nature of the two neighbouring mining areas is the result of variable bedrock competency.
- The BIC comprises a series of fluvial deposits that are related to the evolution of the proto-Buffels River. The oldest recognisable sediments in the study area form part of the kaolin-rich palaeochannels, which are linked to an imposing weathering episode correlated with the post-African surface.
- Grain-size analysis show that more than one source contributed detritus to the KNC area, compared to the BMC area which had a uniform source. The bimodal grain-size distribution of KNC sediments suggests unroofing in the hinterland of the KNC area, which is believed to be the result of large-scale regressions during the Pleistocene.
- Grain roundness studies revealed mixed populations implying a degree of sedimentary mixing or recycling.
- XRD analysis confirmed that kaolin is the main clay mineral in the palaeochannels. Relicts of partly kaolinised feldspar particles verify that the kaolin is mainly derived from the *in situ* weathering of a feldspar-rich (arkosic) source.

Extensive weathering of the bedrock indicates that the weathering predated the sedimentation of the channel sediments.

- The Kleinzee area contains on average 6.4 wt% total heavy minerals (THM). This figure is highly distorted since more than 70% of sediments in the study area contain on average ~2.5% THM. The rest of the sediments have a wide and variable range (5-60% THM) with local anomalies.
- In the BMC area, the stratigraphically older sediments of the Upper and Middle Terraces are marked by higher THM values (7-13%) compared to the much younger Lower Terrace and RET sediments that show no significant accumulation (1-2% THM). Conversely, the stratigraphically younger sediments from the RET and Upper CFS sediments in the KNC area feature high THM values (12-14%). The older, Pliocene FGS and Early Pleistocene Lower CFS sediments are generally depleted in heavy minerals (1-4%). Anomalous concentrations of heavy minerals (~12%) in the BIC suggests sedimentation on point bars. The palaeochannel sediments host very low amounts of heavy minerals (1-2%).
- The mechanism anticipated for the anomalous distribution of heavy minerals in particular marine deposits is believed to be a powerful wave-regime with favourable burial conditions considered essential in preserving the mineralisation. The low abundance of heavy minerals in the majority of studied sediments is ascribed to the absence of a favourable concentrating mechanism such as a J-bay as well as the lack of secondary upgrading by aeolian (deflation) processes. Both these factors significantly enhanced the heavy mineral concentration in the Graauwduinen mega-placer.
- A significant practical aspect is the fact that the total heavy mineral suite reports to 2-3ϕ (180-350μm) size fractions of the sand. This would allow upgrading of the heavy mineral suite by cost effective wet/dry screening.
- The mineralogical composition of the heavy mineral suites is qualitatively uniform throughout the entire study area, but the relative abundance of mineral species and groups varies regionally and spatially. Fe-Ti oxides generally predominate, followed by variable concentrations of zircon, garnet, hornblende, pyroxene and

epidote. Other minerals often present in minor or trace quantities include glauconite, aluminosilicates, staurolite, titanite, apatite (collophane), rutile and monazite.

- Principal component analysis performed on the heavy mineral compositions revealed that variance between samples is a function of mineral density and chemical stability. The dense and chemical stable mineral component is represented by the opaque minerals, zircon and garnet while hornblende, clinopyroxene and epidote depict the chemically less stable and less dense mineral component.

- Multivariate statistics identified the opaque minerals, zircon, garnet, pyroxene, hornblende and epidote as the prime contributors to variance of mineral abundance. A discriminant analysis using the significant factors discriminate six distinct mineral assemblages explaining the variance of mineral abundance amongst stratigraphic successions.

- A simple suite of weathering-resistant minerals (opaques and zircon) marks the palaeochannel and BIC sediments. Sediments of the BMC show that the Middle and Upper Terraces have mature assemblages in contrast with the RET and Lower Terrace that host a diverse, unstable assemblage. Immature assemblages are found in the FGS and Lower CFS in the KNC compared to mature assemblages of the RET and Upper CFS. Minor contrasts in source rock mineralogy and hydraulic sorting processes are interpreted to explain the difference in heavy mineral assemblages. For instance, the assemblage of opaques-garnet-zircon that marks the Upper CFS and RET sediments, contains the heaviest of heavy minerals, indicating that hydraulic sorting, entrainment and transport were effective in their concentration. The influence of local source rock mineralogy on the heavy mineral assemblages of the FGS sediments is demonstrated by the striking increase in clinopyroxene, which is the greatest in the entire study area.

- It is clear that mineralogical fingerprinting of litostratigraphic units can provide a valuable aid to geological mapping and provenance studies not only in the Kleinzee area, but also with careful analysis this could be extended to other west

coast deposits. Significant differences in grain-size, mineral roundness as well a heavy mineral assemblages between the Upper CFS and Lower CFS sediments, which Pether (1994) collectively perceived as a 30m Package equivalent, confirm that these marine successions should be considered as separate "packages". FGS sediments have almost identical heavy mineral assemblages as encountered in equivalent 50m Package sediments from Geelwal Karoo and Graauwduinen. This would imply that during the Pliocene the coastal rivers providing the KNC area and similar west coast localities with detritus had a similar drainage basin, indicating a common source area.

- Opaque minerals include ilmenite, hematite and magnetite. The titanium-bearing minerals comprise ilmenite plus its alteration products, rutile and complex, intimately intergrown phases of Fe-Ti oxides.
- On average ilmenites contain 51% TiO_2 with only trace amounts of impurities. Although the entire spectrum of ilmenite alteration is present in the Kleinzee area, only a small portion (~8%) of the ilmenite fraction is affected and in most cases alteration did not proceed past the hydrated stage. These results are remarkably consistent with previous studies conducted at other west coast localities, which indicates that climatic conditions during the Plio-Pleistocene were uniform along the entire west coast of South Africa.
- Zircon populations were found heterogeneous, displaying contrasting physical, geochemical, cathodoluminescent and radiometric properties.
- Zircon colour was found to extremely variable with the colourless to pink variety being most abundant. Some zircons display shades of yellow, brown, orange and purple. Zircon chemistry indicates that the colour is related to a distinctive trace-element distribution. Colourless-clear types were found to contain high Hf and very low U, Th and total REE concentrations compared to the zoned, coloured and metamict varieties. Brown and metamict zircons are enriched in Y-REE and may host U and Th up to percentage levels. Compared to colourless zircons, pink types contain similar amounts of REE, but are marked by a greater abundance of U and Th. Yellow zircons host a diversity of elements including Y-REE, Al, Fe, P,

U and Th in variable concentrations. Complex CL spectra demonstrated the variable trace-element chemistry and protracted evolution of single grains.

- It was shown that the composition of the zircon population and consequently each coloured variety differ proportionately for sediments from the marine, palaeochannel and fluvial environments.
- Geochemical and radiometric characteristics of zircon separates is a function of the heterogeneity of a given zircon population which reflects on the evolution (maturity) of its host sediments.
- Zircon chemistry and radiometry can be useful in diamond exploration. Geochemical and radiometric characteristics of zircon populations from known diamondiferous sediments can be used to locate sediments in the proximity with similar zircon attributes, which in all probability will also be diamond bearing. Zircon chemistry and radiometry of populations from diamondiferous sediments will indicate the relative maturity of their host sediments. From this information, the proximity of the precursors of these diamondiferous deposits can be tentatively determined.
- Heavy mineral assemblages of the study area indicate contributions from igneous and metamorphic as well as reworked sedimentary sources. Several of the components of the heavy mineral suite, including garnet, epidote, augite, hornblende, staurolite, titanite, rutile and aluminosilicates were demonstrated to be ultimately derived from metamorphic rocks. Other minerals such as the iron-titanium oxides, monazite and zircon could have come from igneous or metamorphic rocks. Collophane and glauconite are recognised as typical recycled minerals. Likewise, rounded heavy minerals imply recycled sedimentary sources. Heavy mineral data furthermore indicates the predominance of metamorphic (amphibolite facies) lithologies over igneous rocks in the inferred provenance area.
- Detailed petrography and geochemistry did not only confirm interpretations made from heavy mineral assemblages, but also indicated several possible source rocks. Yet, no single mineral species or type was totally exclusive to a particular

area or a stratigraphic succession, which could mean that the entire study area had a uniform provenance.

- The predominant occurrence of Fe-Ti oxide and zircon in the study area as well as their demonstrated felsic signatures indicate that the source terrain for the Kleinzee sediments contains mainly felsic rocks.
- Considering the proximity of the Namaqua Metamorphic Complex (NMC) it is therefore envisaged that the latter can be regarded as the principal source of the sediments and heavy minerals in the study area. The striking similarity of mineral chemistry from Kleinzee sediments and lithologies from the NMC unambiguously indicates the NMC as primary source terrain for the Kleinzee sediments. The possibility that the metasediments of the Gariep Belt and Nama Group and Table Mountain Sandstone supplied source material cannot be precluded, but their contributions would be subordinate and secondary.
- Mineralogical and textural evidence substantiates that the majority of heavy minerals were eroded and transported from a nearby area (~30 km). This conclusion indicates a relatively proximal source for the heavy minerals as well as the host sediments and has very important implications concerning diamond distribution. If a given diamond population is immature with respect to characteristics such as quality, textural sorting and grain size and the heavy mineral assemblage of its host sediment is immature as well, this would indicate that both diamonds and the host sediments were minimally transported, indicating a very proximal, secondary diamondiferous source. On the contrary, if the diamond population is mature, but its host sediment is immature, it would suggest that the diamonds were probably recycled from pre-existing deposits and mixed with sediment that was minimally transported and not reworked. In this regard, little can be deduced about the proximity of secondary diamond sources. Similarly, if both the diamond population and its host sediment are highly evolved this would indicate that both diamond and heavy minerals were extensively recycled.
- Heavy mineral suites from most west coast localities indicate the Namaqua Metamorphic Complex as being the major source.

- The present appraisal of the economic importance of heavy minerals in the Kleinzee area indicates that it does not compare favourably with major economic heavy mineral deposits in terms of heavy mineral content as well as the composition and mineral chemistry of the valuable heavy minerals.
- The economic viability of the area is greatly impaired by the generally low heavy mineral content as well as the composition of the economic fraction, which is dominated by less valuable ilmenite. Bulk chemistry as well as single grain analysis also indicate that the TiO_2 content is low (<50%).
- Using a cut-off grade of 10% THM, several target areas have been delineated which indicate an enticing prospect and deserves a follow-up study in order to evaluate their potential ore resources.
- The economic potential of the Kleinzee area is limited and is more suited for the establishment of a small, subsidiary operation that supplies heavy minerals to existing heavy mineral producers.

REFERENCES

Albat, A.M. (1984). The Proterozoic granulite facies terrain around Kliprand, Namaqua Metamorphic Complex. *Bull. Precambr. Res. Unit, Univ. Cape Town*, **33**, 382pp.

Anand, R.R. and Gilkes, R.J. (1985). Some alumina and silica in weathered ilmenite grains is present in clay minerals-a response to Frost *et al.* (1983). *Mineral. Mag.*, **49**, 141-145.

Andreoli, M.A.G., Smith, C.B., Watkeys, M., Moore, J.M., Ashwal, L.D. and Hart, R.J. (1994). The geology of the Steenkampskraal monazite deposit, South-Africa - implications for REE-Th-Cu mineralisation in charnockite-granulite terrains. *Bull. Soc. Econ. Geol.*, **89**, 994-1016.

Anon (1998). Oxide indicators. Mining Journal, September 1999.

Artioli, G., Quartieri, S. and Deriu, A. (1995). Spectroscopic data on coexisting prehnite-pumpellyite and epidote-pumpellyite. *Can. Mineral.*, **33**, 67-75.

Babu, D.S.S., Thomas, K.A., Das, P.N.M. and Damodaran, A.D. (1994). Alteration of Ilmenite in the Manavalakurichi Deposit, India. *Clays Clay Mineral.*, **42**, 567-571.

Bailey, S.W., Cameron, E.N., Spedden, H.R. and Weege R.J. (1956). The alteration of ilmenite in beach sands. *Econ. Geol.*, **51**, 263-279.

Barnes, R.M. (1981). ICP-AES: A review. *Trends Anal. Chem.*, **1**, 51-55.

Basu, A. and Molinaroli, E. (1989). Provenance characteristics of detrital opaque Fe-Ti oxide minerals. *J. Sed. Petrol.*, **59**, 922-934

Basu, A. and Molinaroli, E. (1991). Reliability of the application of detrital opaque Fe-Ti- oxide minerals in provenance determination. *In*: Morton, A.C., Todd, S. and Haughton, D.W. (eds). Developments in Sedimentary Provenance Studies. *Geol. Soc. Spec. Publ.*, **57**, 55-65.

Battey, M.H. (1981). *Mineralogy for Students*. Longman, London, 355pp.

Blatt, H., Middleton, G. and Murray, R. (1980). *Origin of Sedimentary Rocks*. Prentice-Hall Inc., New Jersey, 782pp.

Brooks, C.K. (1970). The concentrations of zirconium and hafnium in some igneous and metamorphic rocks and minerals. *Geochim. Cosmochim. Acta,* **34**, 411-416.

Brown, N.E., Navrotsky, A., Nord, G.L. and Banerjee, S.K. (1993). Hematite-ilmenite (Fe_2O_3-$FeTiO_3$) solid-solutions - determinations of Fe-Ti order from magnetic-properties. *Amer. Miner.*, **78**, 941-951.

Bucher, J. and Frey, M. (1994). *Petrogenesis of Metamorphic Rocks*. Springer, Berlin, 318pp.

Buddington, A.F. and Lindsley, D.H. (1964). Iron-titanium oxide minerals and synthetic equivalents. *J. Petrol.*, **5**, 310-357.

Campbell, J.L., Teesdale, W.J., Maxwell, J.A. and Higuchi, D. (1993). Chemical characteristics of oscillatory zoning and overgrowths in zircon using 3 MeV μ-PIXE. *Can. Mineral.*, **31**, 637-647.

Carpenter, R.H. and Carpenter, S.F. (1991). Heavy mineral deposits in the upper coastal plain of North Carolina and Virginia. *Econ. Geol.*, **86**, 1657-1671.

Carranza-Edwards, A. and Rosalez, L. (1994). Grains size trends and provenance of the southwestern Gulf of Mexico beach sands. *Can. J. Earth Sci.*, **32**, 2009-2014.

Carrington, A.J. and Kensley, B.F. (1969). Pleistocene Molluscs from the Namaqualand Coast. *Ann. S. Afr. Mus.*, **52**, 189-223.

Carver, R.E. (1971). *Procedures in Sedimentary Petrology*. Wiley-Interscience, New York, 653pp.

Cawthorn, R.G. and Biggar, G.M. (1993). Crystallisation of titaniferous chromite, magnesian ilmenite and armalcolite in tholeiitic suites in the Karoo Igneous Province. *Contrib. Mineral. Petrol.*, **114**, 221-235.

Cherniak, D.J., Hanchar, J.M. and Watson, E.B. (1993). Rare earth diffusion in zircon. *Eos Trans. Amer. Geophys. Union*, **74**, 651.

Cilliers, L.M. (1995). *The Geology of the Graauwduinen Heavy Mineral Sand Deposit, West Coast of South Africa.* M.Sc. thesis (unpubl.), Univ. Stellenbosch, 119pp.

Clowes, A. and Comfort, P. (1987). *Process and Landform*. Oliver and Boyd, London, 335pp.

Coetzee, J.A. and Rogers, J. (1982). Palynological and lithological evidence for the Miocene environment in the Saldanha region. *Palaeography, Palaeoclimatology, Palaeoecology,* **39**, 71-85.

Cole, D.I. and Roberts, D.L. (1996). Lignite from the western coastal plain of South Africa. *Afr. J. Earth Sci.*, **23**, 95-117.

Corbett, I.B. (1996). A review of diamondiferous marine deposits of western southern Africa. *Africa Geoscience Review*, **3**, 157-174.

Coward, B.D. (1981). A review of the geology of the Cape west coast (Orange to Berg River). *CSIR Res. Rept.,* **SEA8115**, 71pp.

Cygan, R.T. and Lasaga, A.C. (1982). Crystal growth and the formation of chemical zoning in garnet. *Contrib. Mineral. Petrol.*, **79**, 187-200

Darby, D.A. (1984). Trace elements in ilmenite: A way to discriminate provenance or age in coastal sands. *Geol. Soc. Amer. Bull.*, **95**, 1208-1218.

Darby, D.A. and Tsang, Y.W. (1986). Variation in ilmenite element composition within and among drainage basins: Implications for provenance. *J. Sed. Petrol.*, **57**, 831-838.

Darby, D.A. and Bischof, J.F. (1996). A statistical approach to source determination of lithic and Fe-oxide grains: An example from the Alpha Ridge, Arctic Ocean. *J. Sed. Petrol.*, **66**, 599-607.

De Decker, R.H.H. (1986). Surficial sediments on the inner shelf between the Orange River and Wreck Point. *Tech. Rept. Geol. Surv. Univ. Cape Town Mar. Geosci. Unit*, **15**, 135-156.

De Decker, R.H.H. (1987). The Geological Setting of Diamondiferous Deposits on the Inner Shelf between the Orange River and Wreck Point, Namaqualand. *Bull. Geol. Surv. S. Afr.,* **86**, 99pp.

De Meijer, R.J. Lesscher, H.M.E., Schuling, R.D. & Elburg, M.E. (1990). Estimate of the heavy mineral content in sand and its provenance by radiometric methods. *Nuclear Geophysics*, **4**, 455-460.

De Meijer, R.J., Stapel, C., Jones, D.G., Roberts, P.D., Rozendaal, A. and Macdonald, W.G. (1997). Improved and new uses of natural radioactivity in mineral exploration and processing. *Explor. Mining Geol.*, **6**, 105-117.

De Villiers, J. and Söhnge P.G. (1959). The geology of the Richtersveld. *Mem. Geol. Surv. S. Afr.*, **48**, 295pp.

De Wit, M.C.J. (1993). *Cainozoic Evolution of Drainage Systems in the Northwestern Cape.* Ph.D thesis (unpubl.), Univ. Cape Town, 371pp.

De Wit, M.C.J. (1999). Post-Gondwana drainage and the development of diamond placers in western South Africa. *Econ. Geol.*, **94**, 721-739.

Deer, W.A., Howie, R.A. and Zussman, J. (1963). *Rock Forming Minerals, Vol. 5: Non-silicates*. Longman, Hong Kong, 371pp.

Deer, W.A., Howie, R.A. and Zussman, J. (1978). *Rock Forming Minerals, Vol. 2A: Single-chain Silicates, 2nd Ed.* Longman, Hong Kong, 668pp.

Deer, W.A., Howie, R.A. and Zussman, J. (1986). *Rock Forming Minerals, Vol. 1B: Disilicates and Ring silicates, 2nd Ed.* Longman, Hong Kong, 629pp.

Deer, W.A., Howie, R.A. and Zussman, J. (1992). *An Introduction to the Rock Forming Minerals.* Longman, Hong Kong, 696pp.

Deer, W.A., Howie, R.A. and Zussman, J. (1997). *An Introduction to the Rock Forming Minerals.* Longman, Hong Kong, 629pp.

Dimanche, F. and Bartolomé, P. (1976). The alteration of ilmenite in sediments. *Mineral. Sci. Eng.*, **8**, 187-201.

Dingle, R.V., Siesser, W.G. and Newton, A.R. (1983). *Mesozoic and Tertiary Geology of Southern Africa.* Balkema, Rotterdam, 375pp.

Dixey, F. (1955). Some aspects of the geomorphology of central and southern Africa. *Trans. Geol. Soc. S. Afr.*, **58**, 1-58.

Droop, G.T.R. (1987). A general equation for estimating Fe^{3+} concentrations in ferromagnesium silicates and oxides from microprobe analyses, using stoichiometric criteria. *Mineral. Mag.*, **51**, 431-435.

Dyadchenko, M.G. and Khatuntseva, A. (1960). Mineralogy and petrology of the weathering process of ilmenite. *Doklady. Akad. Nauk. SSSR. Earth. Sci. Sect.*, **123**, 435-438.

Elsner, H. (1992). Granulometry and mineralogy of some northeastern Florida placers: a consequence of heavy mineral concentration in nearshore bars. *Sed. Geol.*, **76**, 233-255.

Engel, A.E.J., Engel, C.G. and Havens, R.G. (1961). Variations in properties of hornblende formed during progressive metamorphism of amphibolites, northwestern Adirondack Mountains, New York. *U.S. Geol. Surv. Prof. Prof. Paper,* **424-C**, 313-316.

Farrow, D.J. (1988). Re-evaluation of the Nuttabooi orebody NB19-21, Buffels Inland Complex. *De Beers Geol. Dept. Rept.*, 8pp.

Fielding, P.E. (1970). The distribution of uranium, rare earths and colour centres in a crystal of natural zircon. *Amer. Miner.*, **55**, 428-440.

Fockema, (1986). The heavy mineral deposits north of Richards Bay. *In*: Anhaeusser, C.R. and Maske, S. (eds). Mineral deposits of South Africa. *Geol. Soc. S. Afr.*, 2301-2307.

Folk, R.L. and Ward, W.C. (1957). Brazos River bar: a study in the significance of grain size parameters. *Sedimentology*, **6**, 3-26.

Force E.R. (1991). Geology of titanium mineral deposits. *Geol. Soc. Amer. Spec. Paper,* **259**, 199pp.

Force, E.R. (1980). The provenance of rutile. *J. Sed. Petrol.*, **50**, 485-488.

Friedman, G.M. (1961). Distinction between dune, beach and river sands from their textural characteristics. *J. Sed. Petrol.*, **31**, 514-529.

Friedman, G.M. (1967). Dynamic processes and statistical parameters compared for size frequency distribution of beach and river sands. *J. Sed. Petrol.*, **37**, 327-354.

Friedman, G.M. (1979). Address of the retiring president of the International Association of Sedimentologists: Differences in size distributions of populations of particles among sizes of various origin. *Sedimentology*, **26**, 1-32.

Friedman, G.M. and Johnson, K.G. (1982). *Exercises in Sedimentology*. John Wiley and Sons, Inc., New York, 208pp.

Frost, B.R. (1991). Stability of oxide minerals in metamorphic rocks. *Rev. Mineral.*, **25**, 469-487.

Frost, B.R. and Lindsley, D.H. (1991). Occurrence of iron-titanium oxides in igneous rocks. *Rev. Mineral.*, **25**, 433-467.

Frost, M.T., Grey, I.E., Harrowfield, I.R. and Mason, K. (1983). The dependence of alumina and silica contents on the extent of alteration of weathered ilmenites from Western Australia. *Mineral. Mag.*, **47**, 201-208.

Gale, S.J. and Hoare, P.G. (1991). *Quaternary Sediments: Petrographic Methods for the Study of Unlithified Rocks*. Belhaven Press, London, 327pp.

Germs, G.J.B. (1972). The stratigraphy and palaeontology of the Lower Nama Group, South West Africa. *Bull. Precambr. Res. Unit, Univ. Cape Town*, **12**, 250pp.

Germs, G.J.B. and Gresse, P.G. (1991). The foreland basin of the Damara and Gariep orogens in Namaqualand and southern Namibia: stratigraphic correlations and basin dynamics. *S. Afr. J. Geol.*, **94**, 159-169.

Ghosh, S.K. and Chatterjee, B.K. (1994). Depositional mechanisms as revealed from grain size measures of the Palaeoproterozoic Kolhan Siliciclastics, Keonjhar District, Orissa, India. *Sed. Geol.*, **89**, 181-196.

Golding, H.G. (1961). Leucoxene terminology and genesis. *Econ. Geol.*, **56**, 1138-1149.

Goto, A. and Banno, S.H. (1990). Hydration of basic granulite to garnet-epidote amphibolite in the Sambagawa Metamorphic Belt, Central Shikoku, Japan. *Chem. Geol.*, **85**, 247-263.

Greenfield, M.B., de Meijer, R.J., Put, L.W., Wiersma, J.F. and Donahue, J.F. (1989). Monitoring beach sand transport by use of radiometric heavy minerals. *Nuclear Geophysics*, **3**, 231-244.

Gresse, P.G. (1988). Washover boulder fans and reworked phosphorite in the Alexander Bay Formation. *S. Afr. J. Geol.*, **91**, 391-398.

Gresse, P.G. (1992). The tectono-sedimentary history of the Vanrhynsdorp Group. *Geol. Surv. S. Afr. Mem.*, **79**, 169pp.

Grey, I.E and Reid, A.F. (1975). The structure of pseudorutile and its role in the natural alteration of ilmenite. *Amer. Miner.*, **60**, 898-906.

Grigsby, J.D. (1990). Detrital magnetite as provenance indicator. *J. Sed. Petrol.*, **60**, 940-951.

Grigsby, J.D. (1992). Chemical fingerprinting detrital ilmenite: A viable alternative in provenance research? *J. Sed. Petrol.*, **62**, 331-337.

Guza R.T and Thornton, E.B. (1982). Swash oscillations on a natural beach. *J. Geophys. Res.*, **87**, 483-491.

Haggerty, S.E. (1976). Oxidation of opaque minerals in basalts. *Rev. Mineral.*, **3**, 1-98.

Hails, J.R. and Hoyt, J.H. (1972). The nature and occurrence of heavy minerals in Pleistocene and Holocene sediments of the lower Georgia coastal plain. *J. Sed. Petrol.*, **46**, 646-666.

Hallam, C.D. (1964). The geology of the coastal diamond deposits of Southern Africa. *In:* Haughton S.H. (ed). *The Geology of some Ore Deposits in Southern Africa. Geol. Soc. S. Afr.*, 671-728.

Hanchar, J.M. and Miller, C.F. (1993). Zircon zonation patterns as revealed by cathodoluminescence and back-scattered electron images: Implications for interpretation of complex crustal histories. *Chem. Geol.*, **110**, 1-13.

Hanchar, J.M. and Rudnick R.L. (1997). Revealing hidden structures: the application of cathodoluminescence and back-scattered electron imaging to dating zircons from lower crustal xenoliths. *Lithos*, **36**, 289-303.

Hartmann, L.A., Takehara, L., Leite, J.A.D., McNaughton, N.J. and Vasconcellos, M.A.Z. (1997). Fracture sealing in zircon as evaluated by electron microprobe analyses and backscattered electron imaging. *Chem. Geol.*, **141**, 67-72.

Hartnady, C.J.H and Von Veh, M.W. (1990) Tectonostratigraphic and structural history of the Late Proterozoic-Early Palaeozoic Gariep Belt, Cape Province, South Africa. *Guidebook Geocongress '90, Geol. Soc. S. Afr.*, **P01**, 1-49.

Haughton, S.H. (1928). The palaeontology of the Namaqualand coastal deposits. *In*: Wagner, P.A. and Merensky, H. (ed). The diamond deposits on the coast of Little Namaqualand. *Trans. Geol. Soc. S. Afr.*, **31**, 1-41.

Haughton, S.H. (1931). The Late Tertiary and Recent deposits of the west coast of South Africa. *Trans. Geol. Soc. S. Afr.*, **34**, 19-57.

Hawthorne, F.C. (1981). Crystal chemistry of the amphiboles. *In*: Veblen, D.R. (ed). Amphiboles and other hydrous pyribole-mineralogy. *Rev. Mineral.*, **9B**, 1-3.

Hemingway, B.S., Robie, R.A., Evans, H.T. and Kerrick, D.M. (1991). Heat-capacities and entropies of sillimanite, fibrolite, andalusite, kyanite, and quartz and the Al_2SiO_5 phase-diagram. *Amer. Miner.*, **76**, 1597-1613.

Hendey, Q.B. (1976). The Pliocene fossil occurrences in "E" Quarry, Langebaanweg, South Africa. *Ann. S. Afr., Mus.*, **69**, 215-247.

Hendey, Q.B. (1978). Preliminary report on the Miocene vertebrates from Arrisdrift, South West Africa. *Ann. S. Afr., Mus.*, **76**, 1-41.

Hendey, Q.B. (1981). Geological sequence at Langebaanweg, Cape Province and global events of the Late Tertiary. *S. Afr. J. Sci.*, **77**, 33-38.

Hendey, Q.B. (1982). *Langebaanweg, a Record of Past Life.* South African Museum, Cape Town, 71pp.

Herzberg, W. (1969). Investigation of aerial radiometric anomalies in Namaqualand, Areas A and B. *Geol. Surv. Rept.,* **13**.

Herzberg, W. (1970). The deposit of heavy minerals in dune sands near Soutfontein, in Namaqualand. *Geol. Surv. Rept.,* **219**.

Hess, P.C. (1989). *Origin of Igneous Rocks*. Harvard University Press, Cambridge, 336pp.

Heydorn, A.E.F. and Tinley, K.L. (1980). Estuaries of the Cape : Part I: Synopsis of the Cape Coast, natural features, dynamics and utilisation. *CSIR Res. Rept.*, **380**, 96pp.

Hickmott, D.D., Shimizu, N., Spear, F.S. and Selverstone, J. (1987). Trace-element zoning in metamorphic garnet. *Geology*, **15**, 573-576.

Hickmott, D. D. and Shimizu, N. (1990). Trace element zoning in garnet from the Kwoiek Area, British Colombia: disequilibrium partitioning during garnet growth? *Contrib. Mineral. Petrol.*, **104**, 619-630.

Hickmott, D. and Spear, F.S. (1992). Major and trace-element zoning in garnets from calcareous pelites in the NW Shelburne Falls Quadranglem Massachusetts: garnet growth histories in retrograde rocks. *J. Petrol.*, **33**, 965-1005.

Hinton, R.W. and Upton, B.G.J. (1991). The chemistry of zircon: variations within and between large crystals from syenite and alkali basal xenoliths. *Geochim. Cosmochim. Acta*, **55**, 3287-3302.

Hubert, J.F. (1962). A zircon-tourmaline-rutile maturity index and the interdependence of the composition of heavy mineral assemblages with the gross composition and texture of sandstones. *J. Sed. Petrol.*, **32**, 440-450.

Hugo, V.E. (1988). *A Mineralogical and Chemical Study of Titanium Losses at Richards Bay Minerals.* M.Sc. thesis (unpubl.), Univ. Natal, 201pp.

Hugo, V.E. (1993). *A Study of Titanium-Bearing Minerals in Heavy Mineral Deposits along the East Coast of Africa.* Ph.D thesis, Univ. Natal, 357pp.

Hugo, V.E. and Cornell, D.H. (1991). Altered ilmenites in Holocene dunes from Zululand, South Africa: petrographic evidence for multistage alteration. *S. Afr. J. Geol.*, **94**, 365-378.

Hutchison, A. R. and Oliver, G.J.H. (1998). Garnet provenance studies, juxtaposition of Laurentian marginal terrains and the timing of the Grampian Orogeny in Scotland. *J. Geol.* Soc., **155**, 541-550.

Irving, A. J. and Frey, F. A. (1978). Distribution of trace elements between garnet megacrysts and host volcanic liquids of kimberlitic to rhyolitic composition. *Geochim. Cosmochim. Acta,* **42**, 771-778.

Jack, A.M. (1980). The geology of western Namaqualand. *Bull. Precambr. Res. Unit, Univ, Cape Town*, **29**, 173pp.

Joubert, P. (1976). The relationship between the Namaqua Metamorphic Complex and the Kheis Group. *S. Afr. J. Sci.*, **72**, 312-313.

Joubert, P. (1986). Namaqualand - a model of Proterozoic accretion? *Trans. Geol. S. Afr.*, **89**, 79-96.

Joubert, P. and Kröner, A. (1971). The Stinkfontein Formation south of the Richtersveld. *Trans. Geol. Soc. S. Afr.*, **75**, 47-53.

Karkhanavala, M.D. and Momin, A.C. (1959). The alteration of ilmenite. *Econ. Geol.*, **54** 1095-1102.

Kensley, B. and Pether, J. (1986). Late Tertiary and Early Quaternary Mollusca of the Hondeklip Bay area, Cape Province, South Africa. *Ann. S. Afr. Mus.*, **97**, 141-225.

Keyser, U. (1972). The occurrence of diamonds along the coast between the Orange River estuary and the Port Nolloth reserve. *Geol. Surv. S. Afr. Bull.*, **54**, 1-23.

King, C.A.M. (1966). *Techniques in Geomorphology*. Arnold, London, 342pp.

King, L.C. (1951). *South African Scenery.* Oliver and Boyd, Edinburgh, 379pp.

Kinny, P.D., Compston, W. and Williams, I.S. (1991). A reconnaissance ion-probe study of hafnium isotopes in zircons. *Geochim. Cosmochim. Acta*, **55**, 849-859.

Kirtley, R. (1985). A geological study of the bedrock and sedimentary parameters on Dreyerspan and Annex Kleinzee. *De Beers Geol. Dept. Rept.*, 32pp.

Klovan, J.E. (1966). The use of factor analysis in determining depositional environments from grain-size distributions. *J. Sed. Petrol.*, **36**, 115-125.

Klute, A. (1990). *Methods of Soil Analysis, Part 1: Physical and Mineralogical Methods*. ASA Publications, Wisconson, 242pp.

Komar, P.D. and Wang, C. (1984). Processes of selective grain transport and the formation of placers on beaches. *J. Geol.*, **92**, 637-655.

Koschek, G. (1993). Origin and significance of the SEM cathodoluminescence from zircon. *J. Microscopy*, **171**, 223-232.

Krige, A.V. (1927). An examination of the Tertiary and Quaternary changes of sea-level in South Africa, with special stress on the evidence in favour of a recent world-wide sinking ocean level. *Ann. Univ. Stell. Sect.* **A**, 1-81.

Kröner, A. (1973). Metasomatism and granitisation in part of the Namaqualand Granite-gneiss complex- a comparison between petrologic evidence and geochemical data. *Spec. Publ. Geol. Soc. S. Afr.*, **3**, 411-417.

Kröner, A. (1974). The Gariep group. Part I: Late Precambrian formations in the western Richtersveld, Northern Cape Province. *Bull. Precambr. Res. Unit, Univ. Cape Town*, **13**, 115pp.

Leake, B.E. (1978). Nomenclature of amphiboles. *Amer. Miner.*, **63**, 1023-1052.

Lee, J.K.W. and Tromp, J. (1995). Self-induced fracture generation in zircon. *J. Geophys. Res.*, **100**, 17753-17770.

Leeder, M.R. (1982). *Sedimentology: Process and Landform*. Allen and Unwin, London. 344pp.

Lewis, D.W. (1984). *Practical Sedimentology*. Hutchinson Ross Publishing Company, 227pp.

Lipson R.D. and McCarthy, T.S. (1977). Geochemical correlation between some rock types of the Namaqualand Granite-gneiss Complex. *Trans. Geol. Soc. S. Afr.*, **80**, 177-181.

Macdonald, W.G. (1996). *The Geelwal Karoo Heavy Mineral Deposit: a Modern Day Beach Placer*. M.Sc. thesis (unpubl.), Univ. Stellenbosch, 214pp.

Macdonald, W.G. and Rozendaal, A. (1995). The Geelwal Karoo heavy mineral deposit: a modern day beach placer. *Afr. J. Earth Sci.*, **21**, 187-200.

Macdonald, W.G., Rozendaal, A. and De Meijer, R.J. (1997). Radiometric characteristics of heavy mineral deposits along the west coast of South Africa. *Mineral. Deposita*, **32**, 371-381.

Mange, M.A. and Maurer, H.F.W. (1991). *Heavy Minerals in Colour*. Chapman and Hall, London, 147pp.

Mariano, A.N. (1988). Some further geologic applications of cathodoluminescence. *In*: Marshall, D.J. (ed). Cathodoluminescence of Geologic Materials. Unwin Hyman, Boston, 94-123.

Mariano, A.N. (1989). Cathodoluminescence emission spectra of rare earth element activators in minerals. *Rev. Mineral.*, **21**, 339-348.

Marshall, D. (1988). *Cathodoluminescence of Geologic Materials*. Unwin Hyman, Boston, 146pp.

Martin, H. (1975). The Precambrian geology of S.W.A. and Namaqualand. *Bull. Precambr. Res. Unit, Univ. Cape Town*, 159pp.

Martins, L.R. (1964). Significance of skewness and kurtosis in environmental interpretation. *J. Sed. Petrol.*, **35**, 768-770.

Mason, C.C. and Folk, R.L. (1958). Differentiation of beach, dune and aeolian flat environments by size analysis, Mustang Island, Texas. *J. Sed. Petrol.*, **28**, 211-226.

Matumara, O. and Koga, H. (1962). On colour centres in $ZrSiO_4$. *J. Phys. Soc. Jap.*, **17**, 409.

McCormick, N.J. (1988). Geology of the Nuttabooi deposit, Buffels Inland Complex, Namaqualand, Northwestern Cape. *De Beers Geol. Dept. Rept.,* 24pp.

McLane, M. (1995). *Sedimentology.* Oxford University Press, Oxford, 423pp.

McManus, J. (1988). Grain size determination and interpretation. *In*: Tucker M. (ed). *Techniques in Sedimentology.* Blackwell Scientific Publications, Oxford, 63-85.

Mezger, K., Hanson, G.N. and Bohlen, S.R. (1989). High-precision U-Pb ages of metamorphic rutile- application to the cooling history of high-grade terrains. *Earth Planet. Sci. Lett.*, **96**, 106-118.

Millot, G. (1970). *Geology of Clays*. Springer-Verlag, New York, 429pp.

Milton, C., Axelrod, J.M., Carron, M.K. and Stearns, F. (1958). Gorceixite from Dale County, Alabama. *Amer. Miner.*, **43**, 688-694.

Mitra, S., Ahmed, S.S. and Moon, H. (1992). Mineralogy and chemistry of the opaques of Cox's Bazar (Bangladesh) beach sands and the oxygen fugacity of their provenance. *Sed. Geol.*, **77**, 235-247.

Moiola, R.J. and Weisser, D. (1968). Textural parameters: an evaluation. *J. Sed. Petrol.*, **38**, 45-53.

Moore, J.M. (1986). *A comparative study of metamorphic supercrustal rocks from the western Namaqua Metamorphic Complex.* Ph.D thesis, Univ. Cape Town, 376pp.

Moore, R.O., Griffin, W.L., Gurney, J.J., Kyan, C.G., Cousens, D.R., Sie, S.H. and Suter, G.F. (1992). Trace element geochemistry of ilmenite megacrysts from the Monastery kimberlite, South Africa. *Lithos*, **29**, 1-18.

Morad, S. and Aldaham, A.A. (1986). Alteration of detrital Fe-Ti oxides in sedimentary rocks. *Geol. Soc. Amer. Bull.*, **97**, 567-578.

Morton A.C. (1991). Geochemical studies of detrital heavy minerals and their application to provenance research. *In*: Morton, A.C., Todd, S. and Haughton, D.W.

(eds). Developments in Sedimentary Provenance Studies. *Geol. Soc. Spec. Publ.*, **57**, 31-45.

Morton, A.C. (1985). Heavy minerals in provenance studies. *In*: Zuffa, G.G. (ed). *Provenance of Arenites.* Riedel Publishing Co., 249-277.

Morton, A.C. (1987). Influences of provenance and diagenesis on detrital garnet suites in the Palaeocene Forties Sandstone, Central North Sea. *J. Sed. Petrol.*, **57**, 1027-1032.

Morton, A.C. and Hallsworth, C. (1994). Identifying provenance-specific features of detrital heavy mineral assemblages in sandstones. *Sed. Geol.*, **90**, 241-256.

Morton, A.C. and Smale, D. (1990). The effects of transport and weathering on heavy minerals from the Cascade River, New Zealand. *Sed. Geol.*, **68**, 117-123.

Morton, A.C., Todd, S.& Haughton, D.W. (eds). (1991). Developments in Sedimentary Provenance Studies. *Geol. Soc. Spec. Publ.*, **57**.

Mücke, A. and Chaudhuri, J.N. (1991). The continuous alteration of ilmenite through pseudorutile to leucoxene. *Ore Geology Reviews*, **6**, 25-44.

Nagasawa, H. (1970). Rare earth concentrations in zircons and apatites and their host dacites and granites. *Earth Planet. Sci. Lett.*, **9**, 359-364.

Nasdala, L., Götze, J., Pidgeon, R.T., Kemp, U. and Seifert, T. (1998). Constraining a SHRIMP U-Pb age: micro-scale characterisation of zircons from Saxonian Rotliegend rhyolites. *Contrib. Mineral. Petrol.*, **132**, 300-306.

Nassef, S. N. (1981). Distribution and properties of placer ilmenite in East Rosetta sands, Egypt. *Mineral. Deposita*, **16**, 259-267.

Nemchin, A.A. and Pidgeon, R.T. (1997). Evolution of the Darling Range Batholith, Yilcarn Craton, and Western Australia: a SHRIMP zircon study. *J. Petrol.*, **38**, 625-649.

Neumann, E.R. (1974). The distribution of Mn^{2+} and Fe^{2+} between ilmenites and magnetites in igneous rocks. *Amer. J. Sci.*, **274**, 1074-1088.

Nicholas, G. (1995). *Sedimentological study of the Main Marine Deposits at the Koingnaas Mining Area.* B.Sc. Hons. Rept. (unpubl.), Univ. Stellenbosch, 90pp.

Norrish, K. and Hutton, J.T. (1969). An accurate X-ray spectrographical method for the analysis of a wide range of geological samples. *Geochim. Cosmochim. Acta*, **33**, 431-435.

Ollier, C.D. (1969). *Weathering*. Oliver and Boyd, London, 304pp.

Ortleva, P., Merino, E., Moore, C. and Chadam, J. (1987). Geochemical self-organisation: Reaction transport feedbacks and modelling approach. *Amer. J. Sci.*, **287**, 979-1007.

Owen, M.R. (1987). Hafnium content of detrital zircons, a new tool in provenance studies. *J. Sed. Petrol*, **57**, 824-830.

Palmer, G.L. (1994). The discovery and delineation of heavy mineral sand orebodies at Graauwduinen, Namaqualand, Republic of South Africa. *Explor. Mining Geol.*, **3**, 399-405.

Palmer, J. (1909). Arizonite, ferric metatitanate. *Amer. J. Sci.*, **28**, 353-356.

Partridge, T.C. and Maude, R.R. (1987). Geomorphic evolution of southern Africa since the Mesozoic. *S. Afr. J. Geol.*, **90**, 179-208.

Pether, J. (1983). *The lithostratigraphy of Hondeklip Bay- a reconnaissance.* B.Sc. Hons. Rept. (unpubl.), Univ. Cape Town, 61pp.

Pether, J. (1986). Late Tertiary and Early Quaternary marine deposits of the Namaqualand Coast, Cape Province: new perspectives. *S. Afr. J. Sci.,* **82**, 464-470.

Pether, J. (1994). *The Sedimentology, Palaeontology and Stratigraphy of Coastal-Plain Deposits at Hondeklip Bay, Namaqualand, South Africa.* M.Sc. thesis, Univ. Cape Town, 307pp.

Pettijohn, F.J. (1975). *Sedimentary rocks*. Harper and Bros., New York, 718pp.

Philander, C., Rozendaal, A. and de Meijer, R.J. (1998). Characteristics of zircon in placer deposits along the west coast of South Africa. *S. Afr. J. Sci.,* **95**, 381-386.

Philips, Wm.R. and Griffen, D.T. (1981). *Optical Mineralogy*. W.H. Freeman and Co., San Francisco, 677pp.

Pidgeon, R.T. (1992). Recrystallisation of oscillatory zircon: some geochronological and petrological implications. *Contrib. Mineral. Petrol.*, **110**, 463-472.

Pidgeon, R.T. and Nemchin, A.A. and Hitchen, G.J. (1998). Internal structures of zircons from Archaean granites from the Darling Range batholith: implications for zircon stability and the interpretation of zircon U-Pb ages. *Contrib. Mineral. Petrol.*, **132**, 288-299.

Pietersen, K.J. (1993). *Richards Bay zircon*. M.Sc. thesis, Univ. Natal, 130pp.

Pirkle, F.L., Pirkle, E.C., Reynolds, J.G., Pirkle, W.A., Jones, D.S., Spangler, D. and Goodman, T.A. (1991). Cabin Bluff heavy mineral deposits of Southeastern Georgia. *Econ. Geol.*, **86**, 436-443.

Poldervaart, A. and Hess, H.H. (1951). Pyroxenes in the crystallisation of basaltic magma. *J. Geol.*, **59**, 472-489.

Powers, M. (1953). A new roundness scale for sedimentary particles. *J. Sed. Petrol.*, **23**, 117-119.

Puffer, J.H. and Cousminer, H.L. (1982). Factors controlling the accumulation of titanium-iron oxide-rich sands in the Cohansy Formation, Lakehurst Area, New Jersey. *Econ. Geol.*, **77**, 379-391.

Pye, K. (1994). *Sediment Transport and Depositional Processes*. Blackwell Scientific Publications, Oxford, 397pp.

Ramdohr, P. (1980). *The ore minerals and their intergrowths*. Pergamon, Oxford, 1174pp.

Razjigaeva, N.G. and Naumova, V.V. (1992). Trace element composition of detrital magnetite from coastal sediments of North-western Japan Sea for provenance study. *J. Sed. Petrol.*, **62**, 802-809.

Reid, D.L., Welke, H.J., Erlank, A.J. and Betton, P.J. (1987). Composition, age and setting of amphibolites in the central Bushmanland Group, western Namaqualand, Namaqua Province, Southern Africa. *Bull. Precambr. Res. Unit, Univ. Cape Town*, **36**, 99-126.

Remond, G., Ohnenstetter, D., Claude, J.M., Caruba, C. and RoquesCarmes, C. (1990). Cathodoluminescence of minerals with particular analysis of rare-earth element bearing crystals. *Scanning*, **12**, 113-114.

Reynolds, I.M. (1978). *A Mineralogical Investigation of Co-Existing Iron-Titanium Oxides from Various Igneous Rocks with Special Reference to some South African Titaniferous Ores.* Ph.D thesis (unpubl.), Rhodes Univ., 622pp.

Riezebos, P.A. (1979). Compositional downstream variation of opaque and translucent heavy residues in some modern Rio Magdalena sands (Colombia). *Sed. Geol.*, **24**, 197-225.

Robb, L. J., Armstrong, R. A. and Waters, D.J. (1998). Nature and duration of mid-crustal granulite facies metamorphism and crustal growth: evidence from single zircon U-Pb geochronology in Namaqualand South Africa. *Econ. Geol. Res. Unit, Univ. Wits. Inf. Circ.*, **323**, 38.

Rogers, J. (1977). Sedimentation on the Continental Margin off the Orange River and the Namib Desert. *Bull. Geol. Surv. S. Afr. Univ. Cape Town Mar. Geosci. Unit*, 210pp.

Rogers, J., Pether, J., Moleneux, R., Genis, G., Kilham, J.L.V., Cooper, G. and Corbett, I.B. (1990). Cainozoic geology and mineral deposits along the west coast of South Africa and the Sperrgebiet. *Guidebook Geocongress '90, Geol. Soc. S. Afr.*, **PR1**, 1-111.

Romans, P.A., Brown, L. and White, J.C. (1975). An electron microprobe study of yttrium, rare earth and phosphorus distribution in zoned and ordinary zircon. *Amer. Miner.*, **60**, 475-480.

Rose, R.S. (1999). Heavy mineral beaches in southeastern Australia: their nature and genesis. *Econ. Geol.*, **94**, 567-588.

Rozendaal, A and Gresse, P.G. and Scheepers, R. (1995). *Economic geology of the Western Cape.* Centennial conference, Nov. 1995, Field excursion guide book. Dept. Geol. Univ. Stellenbosch, South Africa.

Rozendaal, A. (1998). *Mineralogical characteristics of heavy mineral deposits along the west coast of South Africa.* Workshop For Mineral Processing Engineers, SAIMM, Western Cape, 17pp.

Rozendaal, A., Philander, C. and de Meijer, R.J. (1999). *Mineralogy of heavy mineral placers along the west coast of South Africa.* Heavy minerals 1999, Symposium S23, The South African Institute of Mining and Metallurgy, 63-66.

Rozendaal, A., Philander, C. and de Meijer, R.J. (1999). Mineralogical characteristics of large Ti-Zr heavy mineral deposits along the west coast of South Africa. *Journal of African Earth Sciences (submitted)*.

Rubatto, D., Gebauer, D. and Fanning M. (1998). Jurassic formation and Eocene subduction of the Zermatt-Saas-Fee ophiolites: implications for the geodynamic evolution of the Central and Western Alps. *Contrib. Mineral. Petrol.*, **132**, 269-287.

Saggerson, E.P. and Turner, L.M. (1995). *A review of metamorphism in the Republic of South Africa and the kingdoms of Lesotho and Swaziland.* Council for Geoscience, Pretoria, 285pp.

Schaltegger, U. and Krahenbuhl, U. (1990). Heavy rare-earth element enrichment in granites of the Aar Massif (Central Alps, Switzerland). *Chem. Geol.*, **89**, 49-63.

Scheiderman, J.S. (1995). Detrital opaque oxides as provenance indicators in River Nile sediments. *J. Sed. Res.*, **65A**, 668-674.

Semenov, E.I. and Barinskii, R.L. (1958). The composition characteristics of the rare earths in minerals. *Geochem.*, **4**, 398-419.

Shepard, F.P and Young, R. (1961). Distinguishing between beach and dune sands. *J. Sed. Petrol.*, **31**, 196-214.

Siesser, W.G. and Dingle, R.V.D. (1981). Tertiary sea-level movements around Southern Africa. *J. Geol.*, **89**, 83-96.

Sisson, T. W. and Bacon, C. R. (1992). Garnet/high-silica rhyolite trace element partitioning coefficients measured by ion microprobe. *Geochim. Cosmochim. Acta,* **56**, 2133-2136.

Slingerland, R.L. (1977). The effect of entrainment on the hydraulic equivalence relationships with light and heavy minerals in sand. *J. Sed. Petrol.*, **47**, 753-770.

Slingerland, R.L. (1984). Role of hydraulic sorting in the origin of fluvial placers. *J. Sed. Petrol.*, **54**, 137-150.

Sorenson, S.S. and Grossman, J.N. (1989). Enrichment of trace elements in garnet amphibolites from a palaeo-subduction zone: Catalina Schist, southern California. *Geochim. Cosmochim. Acta,* **53**, 3155-3177.

Speer, J.A. (1980). Zircon. *In*: Ribbe, P.H. (ed). Orthosilicates. *Rev. Mineral.*, **5**, 67-112.

Stapor, F.W. (1973). Heavy mineral concentrating processes. *J. Sed. Petrol.*, **43**, 396-407.

Sutherland, R.A. and Lee, C. (1994). Discrimination between coastal subenvironments using textural characteristics. *Sedimentology*, **41**, 1133-1145.

Tankard, A.J. (1966). *The Namaqualand Coastal Deposits with Special Reference to the Area between the Groen and Buffels Rivers.* B.Sc. Hons. Rept. (unpubl.), Univ. Natal, 40pp.

Tankard, A.J. (1975). Thermally anomalous Late Pleistocene Molluscs from the South-Western Cape Province, South Africa. *Ann. S. Afr. Mus.*, **69**, 17-45.

Tankard, A.J. (1976). *The Late Cainozoic History and Palaeoenvironments of the Coastal Margin of the South-Western Cape Province, South Africa.* Ph.D. thesis, Rhodes University.

Tankard, A.J. Jackson, M.P.A., Eriksson, K.A., Hobday, D.K., Hunter, D.R. and Minter, W.E.L. (1982). *Crustal Evolution of Southern Africa: 3.8 Billion Years of Earth History.* New York, Springer-Verlag, 523pp.

Taylor, S.R. and McLennan, S.M. (1985). *The Continental Crust: Its Composition and Evolution.* Blackwell Scientific, London, 312pp.

Temple, A.K. (1966). Alteration of ilmenite. *Econ. Geol.*, **61**, 695-714.

Teufer, G. and Temple, A.K. (1966). Pseudo-rutile-a new mineral intermediate between ilmenite and rutile in the alteration of ilmenite. *Nature*, **211**, 179-181.

Theart, H.F.J. (1980). The geology of the Precambrian terrain in parts of western Namaqualand. *Bull. Precambr. Res. Unit, Univ. Cape Town*, **30**, 103pp.

Toerien, D.K. and Groeneveld, D. (1957). *In*: Coetzee, C.B. (ed). Ilmeniet-houdende sand langs die Weskus in die distrik Vanrhynsdorp. *Geol. Surv. S. Afr. Bull.*, **25**, 17pp.

Truswell, J. (1977). *The Geological Evolution of South Africa.* Purnell, Cape Town, 218pp.

Tucker, M.E. (1988). *Techniques in Sedimentology*. Blackwell Scientific, Oxford, 394pp.

Vail, P.R. and Hardenbol, J. (1979). Sea-level changes during the Tertiary. *Oceanus*, **22**, 71-79.

Vasconcellos, M.A.Z., Chemale, L.T. and Steele, I.M. (1996). Zircon zonation: An experimental study using electron probe microanalysis, cathodoluminescence spectroscopy and synchrotron x-ray fluorescence. *International Conference on Cathodoluminescence and related techniques in Geosciences and Geomaterials*, 39-40.

Vavra, G. and Hansen, B.T. (1991). Cathodoluminescence studies and the U/Pb dating of zircons in pre-Mesozoic gneisses of the Tauern window: Implications for the Pennic basement evolution. *Geologische Rundshau*, **80**, 703-715.

Vavra, G., Gebauer, G., Schmid, R. and Compston, G. (1996). Multiple zircon growth and recrystallisation during polyphase Late Carboniferous to Triassic metamorphism in granulites in the Ivrea Zone (Southern Alps); an ion microprobe (SHRIMP) study. *Contrib. Mineral. Petrol.*, **122**, 337-358.

Vavra, G., Schmid, R. and Gebauer, D. (1999). Internal morphology, habit and U-Th-Pb microanalysis of amphibolite-to-granulite facies zircons: geochronology of the Ivrea Zone (Southern Alps). *Contrib. Mineral. Petrol.*, **134**, 380-404.

Wagner, P.A. and Merensky, H. (1928). The diamond deposits on the coast of Little Namaqualand. *Trans. Geol. Soc. S. Afr.* **31**, 1-41.

Waters, D.J. (1986). Metamorphic zonation and thermal history of pelitic gneisses from western Namaqualand, South Africa. *Trans. Geol. Soc. S. Afr.*, **89**, 97-102.

Watkeys, M.K. (1986). The Achab gneiss: a flaw in Bushmanland or a flaw in Namaqualand? *Trans. Geol. S. Afr.*, **89**, 103-116

Williams, V.A. (1990). WIM 150 detrital heavy mineral deposit. *In*: Hughes, F.E. (ed). Geology of the mineral deposits of Australia and Papua New Guinea, 1609-1614.

Wilson, J.A. (1985). Crandallite group minerals in the Helikian Athabasca Group in Alberta, Canada. *Can. J. Earth Sci.*, **22**, 637-641.

Wilson, M. (1989). *Igneous Petrogenesis.* Unwin Hyman, London, 466pp.

Woodborne, M.W. (1986). The seafloor geology of the Namaqualand inner shelf between White Point and Stompneus Bay (Diamond Concession Area No. 4). *S. Afr. Geol. Surv. Rept.,***1986-0077**, 1-21.

Woodborne, M.W. (1991). The geology of the diamondiferous inner shelf off Namaqualand between Stompneus Bay and White Point just north of the Buffels River. *S. Afr Geol. Surv. Rept.*, **99**, 68pp.

Wort, M.J. and Jones, M.P. (1980). X-ray diffraction and magnetic studies of altered ilmenites and pseudorutile. *Mineral. Mag.*, **43**, 659-663.

Yang, B., Luff, B.J. and Townsend, P.D. (1992). Cathodoluminescence of natural zircons. J. *Phys. Condens. Matter*, **4**, 5617-5624.

Zelt, G.A.D. (1975). Preliminary report on the petrochemistry of high grade metamorphic rocks in western Namaqualand. *Ann. Rept. Precambr. Res. Unit, Univ. Cape Town*, **13**, 83-88.

Zelt, G.A.D. (1978). Mafic populations and high-grade metamorphic zoning in western Namaqualand. *Ann. Rept. Precambr. Res. Unit, Univ. Cape Town*, **14/15**, 103-113.

Zelt, G.A.D. (1980). Granulite-facies metamorphism in Namaqualand, South Africa. *Precambr. Res.*, **13**, 253-274.

APPENDIX A

LIST OF SAMPLES COLLECTED IN THE STUDY AREA

Abbreviations

BMC- Buffels Marine Complex

KNC- Koingnaas Complex

BIC- Buffels Inland Complex

AK- Annex Kleinzee

DP- Dreyerspan

KN- Koingnaas

KV- Karreedoornvlei

LH- Langhoogte

LKB- Langklip, block B

LKC- Langklip, block C

NB- Nuttabooi

SEA- sea beacon

TP- Tweepad

GEOLOGICAL SAMPLES COLLECTED FROM THE BMC

Sample site	Y	X	Elevation (m)	Origin
AK1	-6412.23	78214.132	96.407	Upper Terrace
AK1_1				
AK1_2				
AK43B	-4222.45	79460.25	10.624	RET
AK43B_1				
AK43B_2				
AK45H	-4530.92	78649.614	15.062	RET
AK45H_1				
AK45H_2				
AK45H_3				
AK45H_4				
AK45H_5				
AK52N	-5657.84	78273.433	50.175	Lower Middle Terrace
AK52N_1				
AK52N_2				
DP127R	-6921.83	70590.728	84.519	Upper Terrace
DP127R_1				
DP127R_2				
DP127R_3				
DP127R_4				
DP68D1	-6386.34	76114.091	70.698	Upper Middle Terrace
DP68D1_1				
DP68D1_2				
DP68D1_3				
DP84LM	-5169.78	75301.407	35.843	Lower Terrace
DP84LM_1				
DP84LM_2				
DP88LM	-5630.13	74254.831	33.344	Lower Terrace
DP88LM_1				
DP88LM_2				
DP88LM_3				
KV196R	-6896.56	63654.285	90.667	Upper Terrace
KV196R_1				
KV196R_2				
KV196R_3				
KV196R_4				
KV198PR	-6483.38	63593.874	64.754	Upper Middle Terrace
KV198PR_1				
KV198PR_2				
TP235M	-3081.92	60074.925	51.574	Lower Middle Terrace
TP235M_1				
TP235M_2				
TP235M_3				
TP262N	-1622.53	57684.606	55.439	Lower Middle Terrace
TP262N_1				
TP262N_2				
TP262N_3				
TP262N_4				
SEA419	-3340.83	78272.41	3.858	Present-day beach
SEA419_1				
SEA419_2				
SEA419_3				

GEOLOGICAL SAMPLES COLLECTED FROM THE KNC

Sample site	Y	X	Elevation (m)	Origin
68/69F3-02	-25584.9	146961.58	2.289	channel
68/69F3-02_1				
68/69F3-02_2				
68/69F3-02_3				
KN14	-23312.4	144285.33	18.974	Upper CFS
KN14_1				
KN14_2				
KN14_3				
KN14_4				
KN17	-24682.9	145503.84	30.915	Lower CFS
KN17_1				
KN17_2				
KN17_3				
LKB-01	-33333.925	169251.022	-2.048	channel
LKB-01_1				
LKB-01_2				
LKB-01_3				
LKB-01_4				
LKC1-04	-29986.5	161560.09	5.068	Lower UCFS, RET
LKC1-04_1				
LKC1-04_2				
LKC1-04_3				
LKC1-04_4				
LKC1-04_5				
LKC1-04_6				
LKC1-04_7				
LKC1-04_8				
LKC1-04_9				
LKC1-04_10				
LKC1-04_11				
LKC1-04_12				
LKCR1				10m Terrace RET
LKCR1_1				
LKCR1_2				
LKN8-03	-31591	158737.68	25.445	Upper CFS
LKN8-03_1				
LKN8-03_2				
LKN8-03_3				
LKN8-03_4				
SN78-5	-22172.7	140893.533	3.574	channel
SN78-5_1				
SN78-5_2				
SN78-5_3				
SN78-5_4				
SN78-5_5				
SN78-5_6				
SNR1	-22858.9	138782.68	18.31	RET
SNR1_1				
SNR1_2				
SNR1_3				
KN_SI	25090	3348430		
SEA711	28715.473	160569.927		

GEOLOGICAL SAMPLES COLLECTED FROM THE BIC

Sample site	*Y*	*X*	*Elevation (m)*
LH_C	-41215.383	66807.533	145.120
LH_C_1			
LH_C_2			
LH_C_3			
LH_C_4			
LH_C_5			
NB19AC	-34281	72305.296	125.182
NB19AC_1			
NB19AC_2			
NB19AC_3			
NB19AC_4			
NB21B	-34509.5	72869.748	114.489
NB21B_1			
NB21B_2			
NB21B_3			
NB21B_4			
NB21B_5			

GEOLOGICAL SAMPLES COLLECTED FROM RIVERS

ZL	Swartlintjies River
BR	Buffels river

NON-GEOLOGICAL SAMPLES (MINE HEAPS)

BMC	
AK3P_SD_1	
AK3P_SD_2	
AK3P_SD_3	
AK3P_D	
TPP_SD	
TPP_D_1	
TPP_D_2	
BS_SD_1	
BS_SD_2	
BS_D_1	
BS_D_2	
BIC	
LH_SD	
KNC	
KNP_D_1	
KNP_D_2	
KNP_SD_1	
KNP_SD_2	

APPENDIX B

DETAILS OF SELECTIVE LABORATORY TECHNIQUES

Grain-size analysis

A split of the sand-size range of the sample was used in grain size analysis.

Where disaggregation was deemed necessary the sample was gently crushed with a rubber pestle in a dispersive solution.

Carbonates, iron oxides, organic matter and soluble salts were removed by hydrochloric and hydrogen peroxide as stated in Friedman and Johnson (1982).

The <63μm fraction was removed through wet sieving and retrieved onto filter paper.

The rest of the sample was dried in an oven at 20°C.

Samples were sieved for 15 min. with a mechanical shaker.

New sieves ranging from -2 to 4ϕ at 0.5 ϕ intervals were used.

The 14 different fractions were collected and the weights recorded.

All computations including processing of the raw data and the calculation of textural parameters based on the method of Folk and Ward (1957) were done by computer.

Frequency histograms were drawn using SigmaPlot®.

Heavy mineral separation

The initial weight of a raw sample intended for heavy mineral analysis was recorded.
The > 4 mm fraction was removed and the sample was treated with oxalic acid and sodium sulphite to remove iron coatings.
Samples were put in an ultrasonic bath for 10 min, washed with de-ionised water and dried.
Bromoform (s.g.=2.82 g/cm^3) has been used to separate the light from the heavy minerals.
Both the light fraction and heavy fraction were washed with acetone until bromoform free.

The light fraction was discarded and the heavy fraction was retained for mineralogical and chemical analysis.

The total heavy mineral content is calculated from the representative fraction weights.

Fraction separation

The main object of further separations was to obtain monomineralic fractions of garnet, ilmenite and zircon.

Magnetic grains were removed from the heavy mineral split using an ordinary hand magnet.

In the next stage, the Frantz isodynamic separator was used to separate the heavy fraction into semi-monomineralic fractions. The Frantz was set at 25° forward tilt and 15° side tilt.

Ilmenite was removed at 0.25-0.35A, garnet at 0.35-0.5A and zircon and rutile at +1.5A.

Since these fraction are not entirely monomineralic, but contain relative amounts of other minerals, a Superpanner was used to upgrade the mineral fraction.

The zircon fraction was powdered and treated with 8N HCl to remove any monazite. Excess HCl was removed by centrifuge.

Garnet and zircon fractions were subjected for REE analysis whereas the zircon fractions were radiometrically analysed.

XRD analysis

The >2mm fraction was removed by passing the samples through a sieve.

The rest of the sample was washed with de-ionised water through a 63μm sieve.

The <63μm fraction was collected, put in a sedimentation column and drained when all the sediment had settled.

Chemical pre-treatment methods used were after Klute (1990) and are discussed below.

Organic matter was removed by using a 30% H_2O_2 and 0.5M $MgCl_2$ solution.

The citrate-dithionite method was used to remove all soluble salts and free iron oxides.

The chemically treated sample was centrifuged with de-ionised water until the water was clear.

Approximately 50g of the wet sample was suspended in a sedimentation funnel.

The settling time for the 5-63μm fraction was determined under the relevant conditions.

Once the settling has been reached the <5μm fraction was siphoned from the top using an automatic pipette and transferred to a glass slide.

The 5-63μm fraction was simply drained from the sedimentation funnel onto a glass slide.

Both orientated fractions were subjected to XRD analysis.

APPENDIX C

DETAILS AND OPERATING CONDITIONS OF ANALYTICAL EQUIPMENT

XRD APPARATUS

MODEL:	Philips PW 1130/00
RADIATION:	Cu(K_α)
VOLTAGE:	50 kV
CURRENT:	40 mA
SCAN RATE:	1°/min
STEP SIZE:	0.1
DETECTION LIMIT:	~5%

XRF APPARATUS

MODEL:	Philips 1100/00 (Wavelength dispersive)
RADIATION:	Rh(K_α)
AQUIRE TIME:	Peak = 200s; background = 100s
DETECTION LIMIT:	~5%

ELECTRON MICROPROBE AT UCT

A). MODEL: Cameca Camebax Electron Probe Microanalyzer
VOLTAGE: 15 kV
CURRENT: 30 nA
BEAM APERATURE: 5 μm
AQUIRE TIME: Peak = 20s; background = 10s
DATA REDUCTION: Bench-Albi
STANDARDS AND DETECTION LIMITS

Element	Standard	Crystal	Lower limit of detection
Si	K-P	TAP	0.04
Ti	rutile	PET	0.05
Al	chromite	TAP	0.03
Cr	chromite	TAP	0.05
Fe	ilmenite	LiF	0.07
Mn	rhodonite	LiF	0.05
Mg	chromite	TAP	0.02
Ca	K-P	PET	0.04

ELECTRON MICROPROBE AT COUNCIL FOR GEOSCIENCE

B.) MODEL: JEOL Superprobe 733
VOLTAGE: 15 kV
CURRENT: 40 nA
BEAM APERATURE: 3 μm
AQUIRE TIME: Peak = 30s; background = 10s
DATA REDUCTION: Duncoumb and Reid (1968)
STANDARDS AND DETECTION LIMITS

Element	Standard	Crystal	Lower limit of detection
Si	pure	TAP	0.03
Ti	pure	PET	0.02
Al	spinel	TAP	0.02
Cr	chromite	TAP	0.03
Fe	ilmenite	LiF	0.02
Mn	rhodonite	LiF	0.01
Mg	spinel	TAP	0.02
Ca	pure	PET	0.02

ICP-AES at U.S. used for REE analysis

PLASMA GAS: 15.0 l/min
AUXILIARY GAS: 1.5 l/min
FORWARD POWER: 1.0 kW
INTEGRATION TIME: 3s

SEM at UCT used to identify mineral phases

MODEL: Leica Stereoscan S440
X-RAY ANALYZER: Kevex 7000 X-ráy analyser
DATA REDUCTION: Kevex Sigma™ Software
BEAM VOLTAGE: 20 kV
BEAM CURRENT: 40 μA
BEAM APERATURE: 5 μm
WORKING DISTANCE: 30 mm
TAKE-OFF ANGLE: 20°
AQUIRE TIME: 60s
DETECTION LIMIT: 0.2%

APPENDIX D

GRAIN-SIZE DATA

Abbreviations

Med median grain diameter

Mean mean grain diameter

Sort sorting

S_K skewness

K_G graphic kurtosis

Sample	Med	Mean	Sort	S_k	K_G
AK1_1	1.03	1.04	1.57	0.34	0.68
AK1_2	1.81	1.79	1.12	0.08	1.05
AK43B_1	2.23	1.88	1.15	-0.57	1.75
AK43B_2	2.08	1.55	1.63	-0.38	1.49
AK45H_1	2.02	1.96	0.90	-0.07	2.02
AK45H_2	0.40	0.51	1.31	0.56	0.51
AK45H_3	0.95	0.80	1.35	0.29	0.66
AK45H_4	1.30	1.02	1.65	-0.11	0.98
AK45H_5	1.46	1.16	1.40	0.10	0.69
AK52N_1	1.87	2.00	0.70	0.41	1.62
AK52N_2	1.85	2.12	1.12	0.36	1.61
BR	0.81	0.86	1.32	0.15	1.15
DP127R_1	1.06	0.91	1.02	-0.22	1.46
DP127R_2	1.21	1.08	1.04	-0.15	1.31
DP127R_3	1.50	1.44	0.71	-0.15	1.02
DP127R_4	1.36	1.36	0.60	0.09	1.17
DP68D1_1	1.85	1.78	1.87	-0.07	0.90
DP68D1_2	2.09	2.05	1.56	-0.05	1.05
DP68D1_3	2.57	2.65	0.95	0.12	1.10
DP84LM_1	-0.64	-0.18	1.20	1.01	0.54
DP84LM_2	1.52	1.46	1.14	-0.04	1.72
DP88LM_1	1.50	1.34	1.04	-0.03	1.39
DP88LM_2	0.27	0.60	1.45	0.45	1.71
DP88LM_3	1.49	1.49	0.60	0.09	1.34
KV196R_1	1.51	1.54	0.73	0.26	1.75
KV196R_2	1.23	1.32	1.20	0.23	1.68
KV196R_3	1.51	1.59	0.67	0.27	1.41
KV196R_4	1.94	2.07	0.85	0.25	1.20
KV198PR_1	1.38	1.38	0.55	0.08	1.13
KV198PR_2	1.27	1.30	0.46	0.17	1.61
TP235M_1	1.44	1.32	0.84	-0.30	0.93
TP235M_2	1.32	1.31	1.06	0.10	1.01
TP235M_3	0.98	0.85	0.77	0.12	0.95
TP262N_1	-0.04	0.04	0.87	0.32	1.33
TP262N_2	1.29	1.32	0.89	0.02	0.55
TP262N_3	1.86	1.76	0.88	-0.03	1.27
TP262N_4	1.39	1.55	1.02	0.30	1.69
SEA419_1	0.66	0.64	0.81	-0.04	0.90
SEA419_2	1.28	1.24	0.60	-0.12	1.38
SEA419_3	0.47	0.53	0.76	0.12	1.15
LH_C_1	0.40	0.49	1.29	0.31	1.77
LH_C_2	0.21	0.32	1.27	0.59	0.77
LH_C_3	-0.04	0.12	1.22	0.68	0.74
LH_C_4	1.01	1.01	1.00	0.15	1.88
LH_C_5	0.79	0.69	1.42	0.02	1.27
NB19AC_1	0.87	0.76	1.38	0.28	0.52
NB19AC_2	-0.60	-0.01	1.21	1.14	0.79
NB19AC_3	1.74	1.92	1.24	0.21	1.24
NB19AC_4	1.75	1.77	0.88	0.01	1.53
NB21B_1	0.04	0.16	0.99	0.72	0.66
NB21B_2	0.35	0.32	1.05	0.47	0.52
NB21B_3	1.34	1.46	1.06	0.20	1.31
NB21B_4	2.37	2.37	1.02	0.01	1.27
NB21B_5	1.46	1.50	0.38	0.22	0.90
68/69_1	1.72	1.53	1.37	-0.23	0.97
68/69_2	1.10	1.18	1.20	0.13	1.01
68/69_3	1.68	1.69	0.67	0.01	1.33
KN14_1	0.50	0.35	0.82	0.38	0.34
KN14_2	-0.04	0.15	0.97	0.31	1.04
KN14_3	-0.80	-0.60	0.75	1.20	0.65
KN14_4	0.95	0.95	1.32	0.17	1.21
KN17_1	0.05	0.68	0.59	1.34	0.30
KN17_2	2.57	2.45	0.69	-0.45	1.73
KN17_3	-0.08	0.23	1.18	0.44	1.63
LKB01_1	1.64	1.47	1.46	-0.16	0.95
LKB01_2	1.92	1.83	1.08	-0.03	0.85
LKB01_3	1.79	1.81	0.42	0.03	1.11
LKB01_4	2.30	2.32	0.48	0.06	1.11
LKC1-04_1	1.15	1.06	1.72	0.00	0.80
LKC1-04_2	1.11	0.89	1.22	-0.23	1.47
LKC1-04_3	2.59	2.55	0.45	-0.12	1.05
LKC1-04_4	0.21	0.40	0.90	0.46	1.72
LKC1-04_5	1.69	1.68	0.62	-0.04	0.98
LKC1-04_6	1.23	1.19	0.69	-0.19	1.24
LKC1-04_7	-0.03	0.22	1.14	0.26	0.70
LKC1-04_8	1.19	1.16	0.45	-0.06	1.21
LKC1-04_9	0.72	0.96	1.25	0.31	0.83
LKC1-04_10	1.36	1.36	0.82	0.19	1.46
LKC1-04_11	1.42	1.38	0.99	0.01	1.13
LKC1-04_12	1.58	1.56	0.39	0.03	0.95
LKCR1_1	1.33	1.31	0.58	-0.08	1.16
LKCR1_2	0.39	0.53	0.82	0.33	1.35
LKN803_1	1.19	1.18	0.53	-0.03	1.16
LKN803_2	-1.02	0.66	0.98	2.06	0.34
LKN803_3	2.56	2.28	0.84	-0.40	0.87
LKN803_4	1.68	1.68	0.62	-0.04	0.98
SN785_1	0.25	0.43	1.24	0.62	0.52
SN785_2	1.63	1.58	1.40	-0.08	0.96
SN785_3	0.66	1.22	0.99	0.76	0.39
SN785_4	2.49	2.51	0.39	0.18	0.97
SN785_5	-0.03	0.16	0.99	0.31	1.06
SN785_6	1.89	1.75	0.88	-0.34	1.57
SNR1_1	0.69	0.67	1.32	0.00	1.01
SNR1_2	-0.59	-0.06	1.15	1.08	0.42
SNR1_3	1.65	1.65	0.59	-0.03	1.22
KN_SI	1.98	1.97	0.46	-0.05	1.04
SEA711	2.15	2.10	0.30	-0.22	0.86
ZL	2.53	2.66	1.22	0.09	1.03

APPENDIX E

ROUNDNESS ESTIMATION

ACCORDING TO SHEPARD AND YOUNG (1961)

Ilmenite

Stratigraphic package	Sample	Very angular	Angular	Sub-angular	Sub-rounded	Rounded	Well-rounded	
BMC								
RET	AK43B_1	0	0	0	51	140	22	
	AK52_2	0	0	0	38	122	45	
Lower Terrace	DP84LM_1	0	0	0	23	133	43	
	DP88LM_3	0	0	0	45	122	54	
Lower Middle Terrace	TP235M_2	0	0	0	50	166	10	
	TP235M_4	0	0	0	33	120	23	
Upper Middle Terrace	KV198PR_1	0	0	0	37	109	78	
	KV198PR_2	0	0	0	40	135	31	
Upper Terrace	DP127R_3	0	0	0	42	119	48	
	KV196R_2	0	0	0	60	108	30	
	Total	0	0	0	419	1274	384	Total grains
	Avg. (%)	0.0	0.0	0.0	20.2	61.3	18.5	2077
BIC								
Langhoogte	LH_C_2	0	0	19	48	111	2	
	LH_C_5	0	0	15	70	126	3	
Nuttabooi	NB19AC_3	0	0	12	56	132	9	
	NB21B_2	0	0	23	67	115	7	
	Total	0	0	69	241	484	21	Total grains
	Avg. (%)	0.0	0.0	8.5	29.6	59.4	2.6	815
KNC								
RET	LKC1-04_11	0	0	0	34	108	42	
	SNR1_3	0	0	0	49	123	32	
UCFS	KN14_2	0	0	0	53	151	54	
	LKC1-04_9	0	0	0	23	133	36	
LCFS	LKB01_3	0	0	0	37	141	47	
	SN78-5_4	0	0	0	28	111	15	
FGS	LKN8-03_2	0	0	0	19	108	27	
	LKN8-03_3	0	0	0	44	132	30	
	Total	0	0	0	287	1007	283	Total grains

Stratigraphic package	Sample	Very angular	Angular	Sub-angular	Sub-rounded	Rounded	Well-rounded	
	Avg. (%)	0.0	0.0	0.0	18.2	63.9	17.9	1577
Palaeochannels								
	6869F3-02_1	0	0	21	107	52	1	
	LKB-01_1	0	0	13	122	39	2	
	SN78-5_2	0	0	19	103	48	0	
	SNR1_1	0	0	34	132	58	4	
	Total	0	0	87	464	197	7	Total grains
	Avg. (%)	0.0	0.0	11.6	62.0	26.3	0.9	748

Garnet

Stratigraphic package	Sample	Very angular	Angular	Sub-angular	Sub-rounded	Rounded	Well-rounded	
BMC								
RET	AK43B_1	2	44	119	3	0	0	
	AK52_2	3	33	136	5	0	0	
Lower Terrace	DP84LM_1	3	18	124	7	0	0	
	DP88LM_3	1	42	130	8	0	0	
Lower Middle Terrace	TP235M_2	0	34	152	3	0	0	
	TP235M_4	0	51	110	1	0	0	
Upper Middle Terrace	KV198PR_1	2	36	119	6	0	0	
	KV198PR_2	3	42	127	3	0	0	
Upper Terrace	DP127R_3	7	29	103	4	0	0	
	KV196R_2	3	54	111	0	0	0	
	Total	24	383	1231	40	0	0	Total grains
	Avg. (%)	1.4	22.8	73.4	2.4	0.0	0.0	1678
BIC								
Langhoogte	LH_C_2	53	145	58	0	0	0	
	LH_C_5	39	137	27	0	0	0	
Nuttabooi	NB19AC_3	67	119	46	0	0	0	

Stratigraphic package	Sample	Very angular	Angular	Sub-angular	Sub-rounded	Rounded	Well-rounded	
	NB21B_2	80	160	50	0	0	0	
	Total	239	561	181	0	0	0	Total grains
	Avg. (%)	24.4	57.2	18.5	0.0	0.0	0.0	981
KNC								
RET	LKC1-04_11	8	34	109	4			
	SNR1_3	6	51	156	8			
UCFS	KN14_2	2	23	143	6			
	LKC1-04_9	0	17	135	3			
LCFS	LKB01_3	2	36	117	0			
	SN78-5_4	0	49	108	3			
FGS	LKN8-03_2	2	58	125	9			
	LKN8-03_3	6	29	122	11			
	Total	26	297	1015	44	0	0	Total grains
	Avg. (%)	1.9	21.5	73.4	3.2	0.0	0.0	1382
Palaeochannels								
	6869F3-02_1	29	112	37	0	0	0	
	LKB-01_1	24	101	27	0	0	0	
	SN78-5_2	63	98	46	0	0	0	
	SNR1_1	22	119	23	0	0	0	
	Total	138	430	133	0	0	0	Total grains
	Avg. (%)	19.7	61.3	19.0	0.0	0.0	0.0	701

APPENDIX F

X-RAY DIFFRACTOMETRY

Sample	Mineralogy			
	5-63 μm fraction		*<5 μm fraction*	
AK1_1	Kaolinite	99%	Kaolinite	100%
	Quartz	1%		
6869F3-02_1	Kaolinite	87%	Kaolinite	100%
	Quartz	13%		
6869F3-02_2	Kaolinite	52%	Kaolinite	100%
	Quartz	48%		
LKB-01_1	Kaolinite	79%	Kaolinite	100%
	Quartz	21%		
LKB-01_2	Kaolinite	60%	Kaolinite	100%
	Quartz	40%		
SN78-5_1	Kaolinite	80%	Kaolinite	100%
	Quartz	20%		
SN78-5_2	Kaolinite	78%	Kaolinite	100%
	Quartz	22%		
SNR1_1	Kaolinite	95%	Kaolinite	100%
	Quartz	5%		

detection limit ± 5%

error on calculation < 0.8%

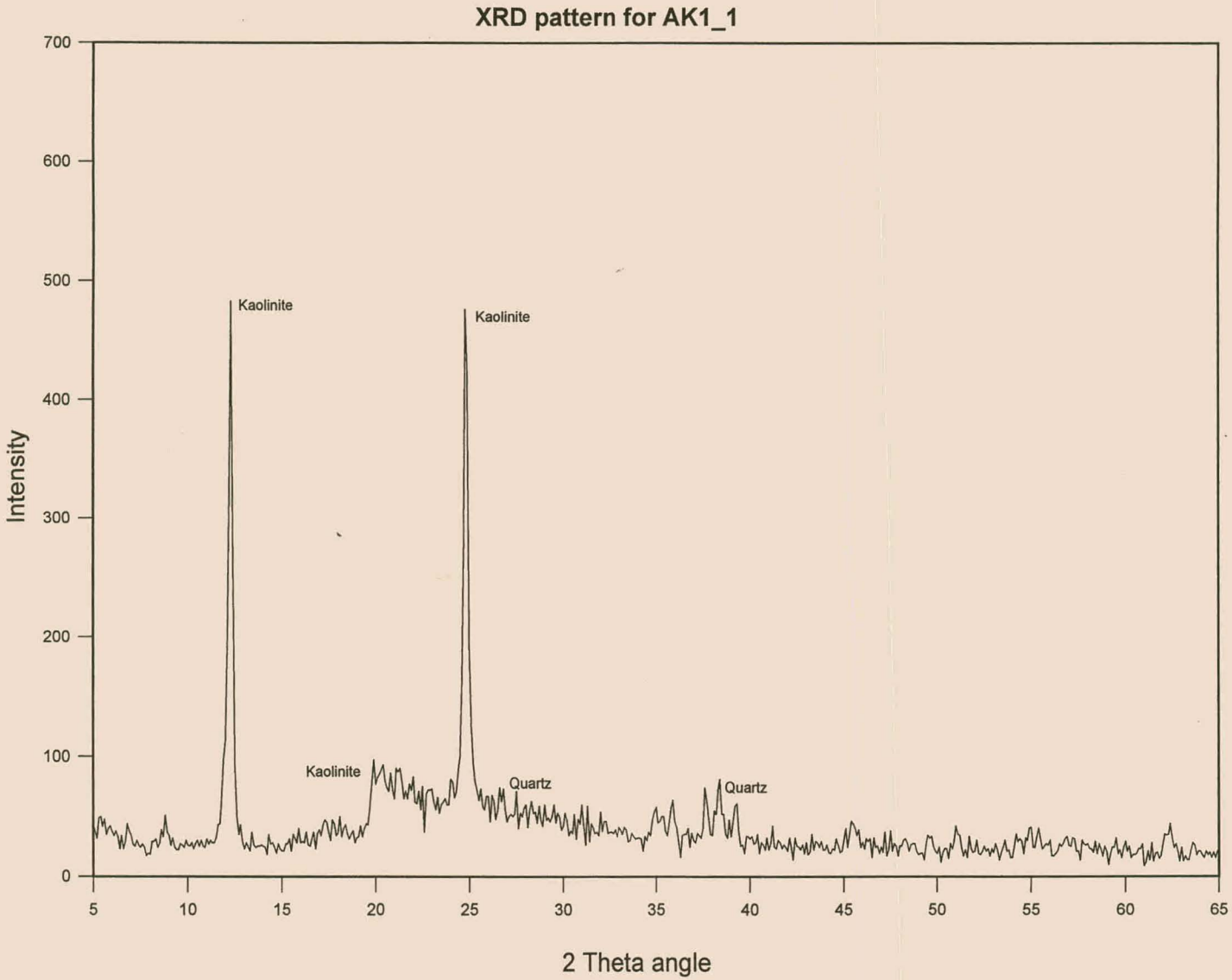

Figure 1. X-ray diffractogram of clay sample AK1_1.

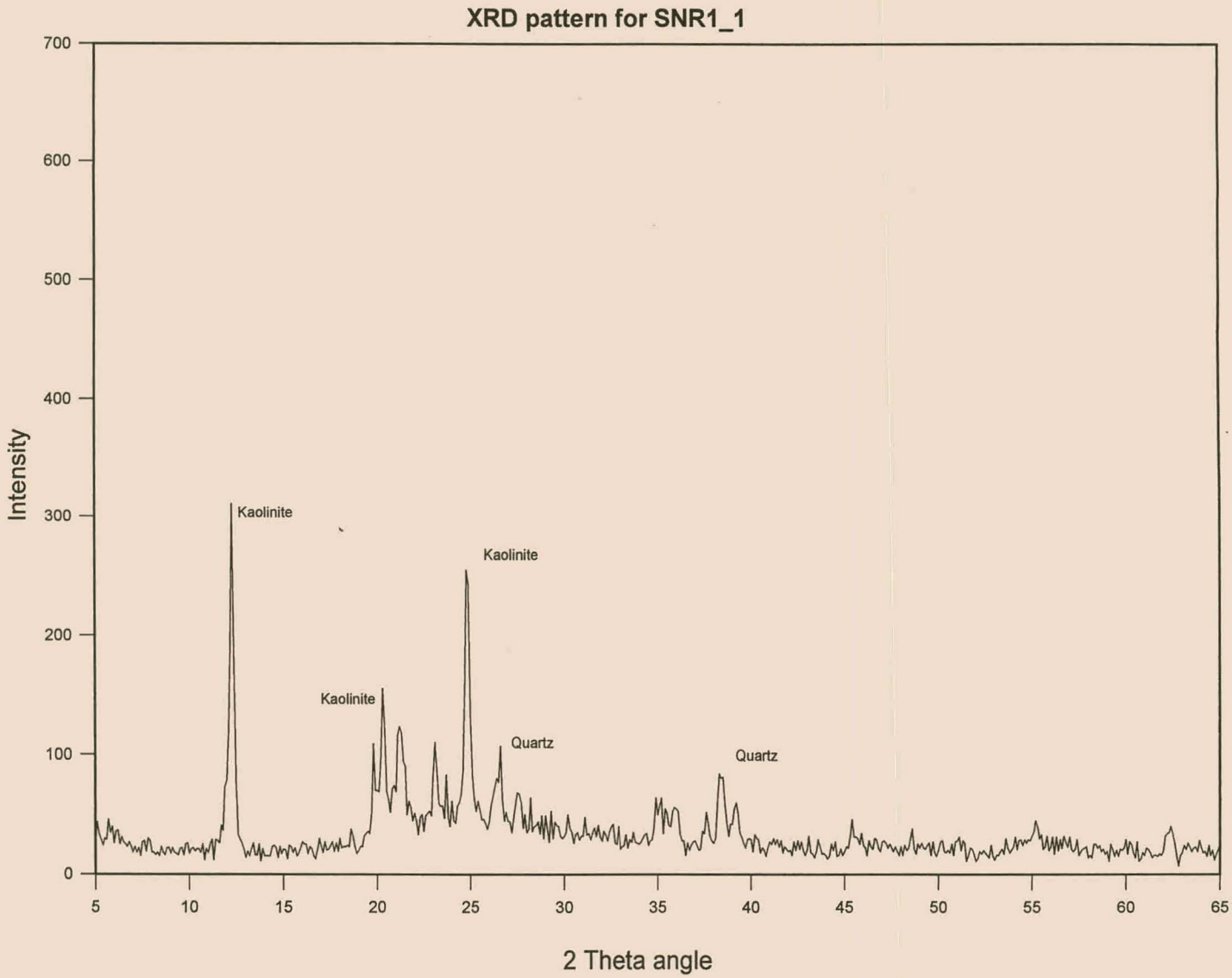

Figure 2. X-ray diffractogram of clay sample SNR1_1.

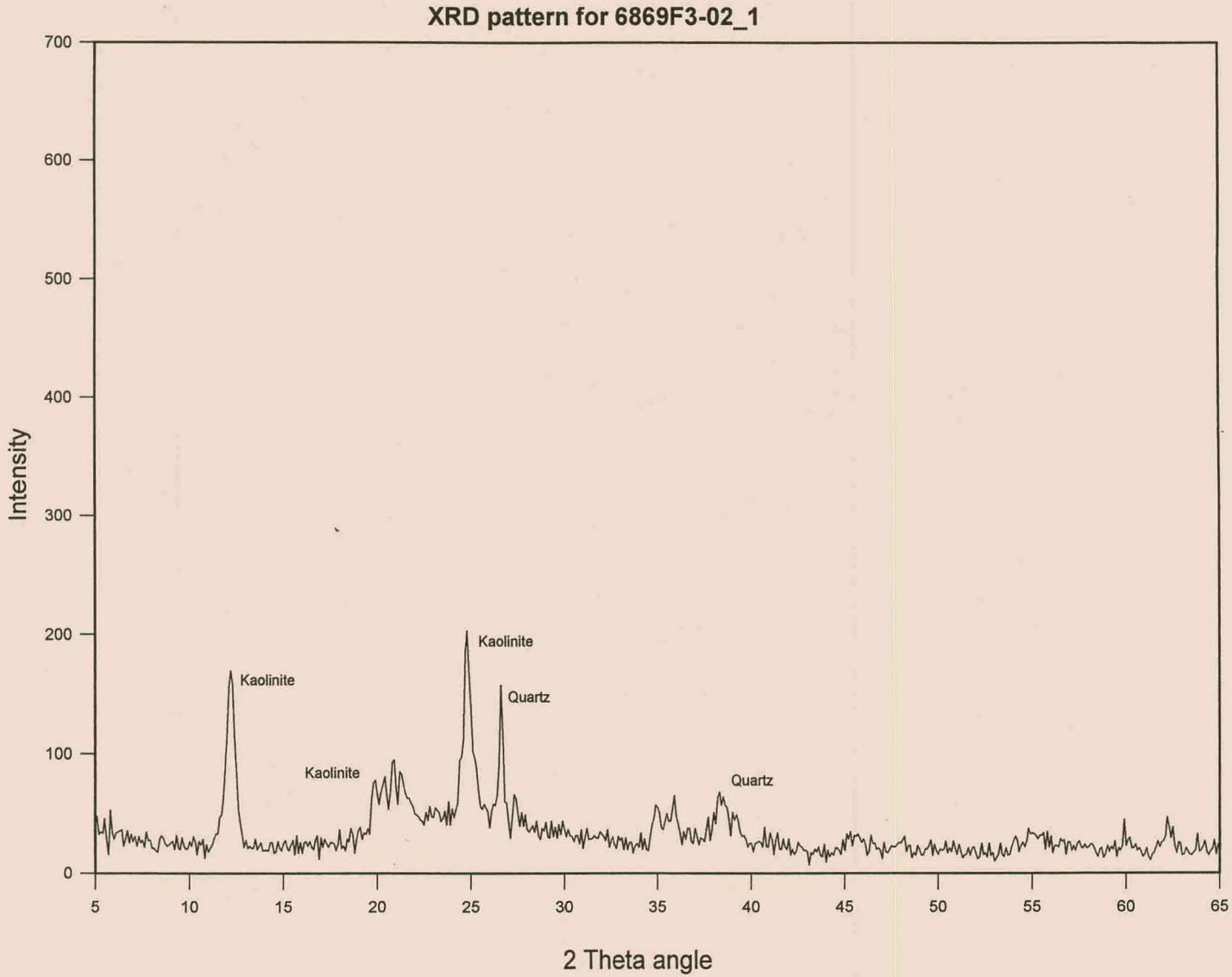

Figure 3. X-ray diffractogram of clay sample 6869F3-02_1.

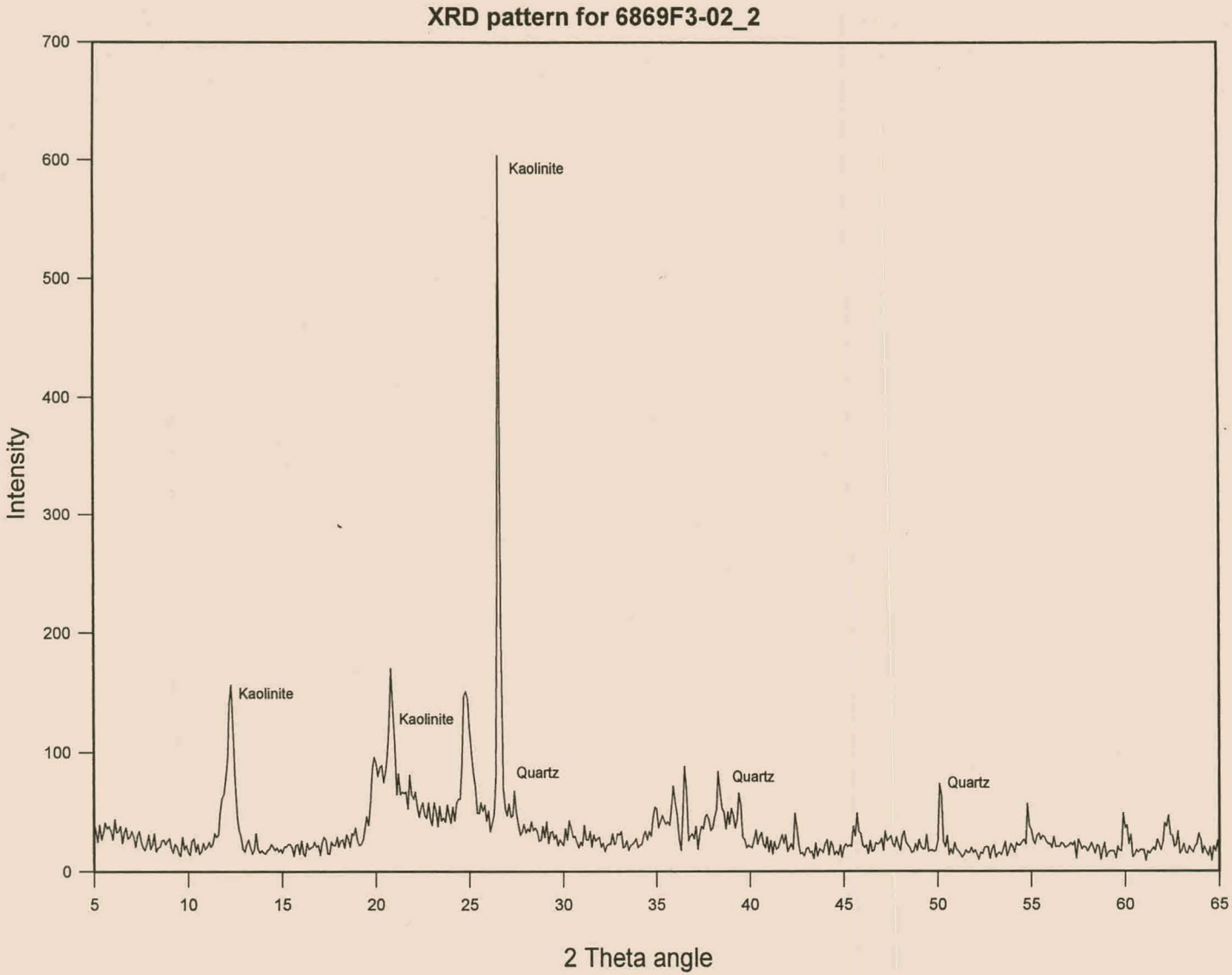

Figure 4. X-ray diffractogram of clay sample 6869F3-02_2.

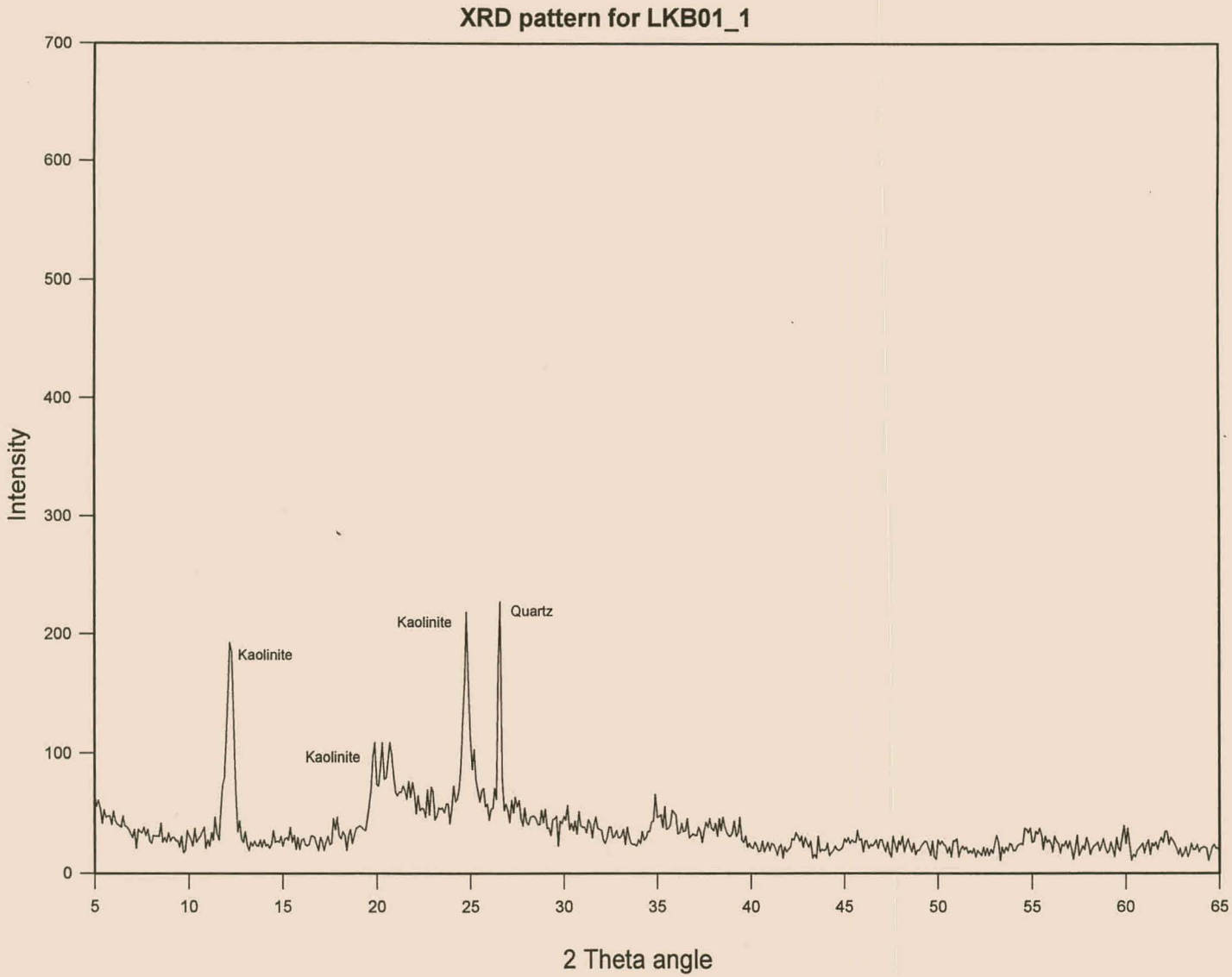

Figure 5. X-ray diffractogram of clay sample LKB-01_1.

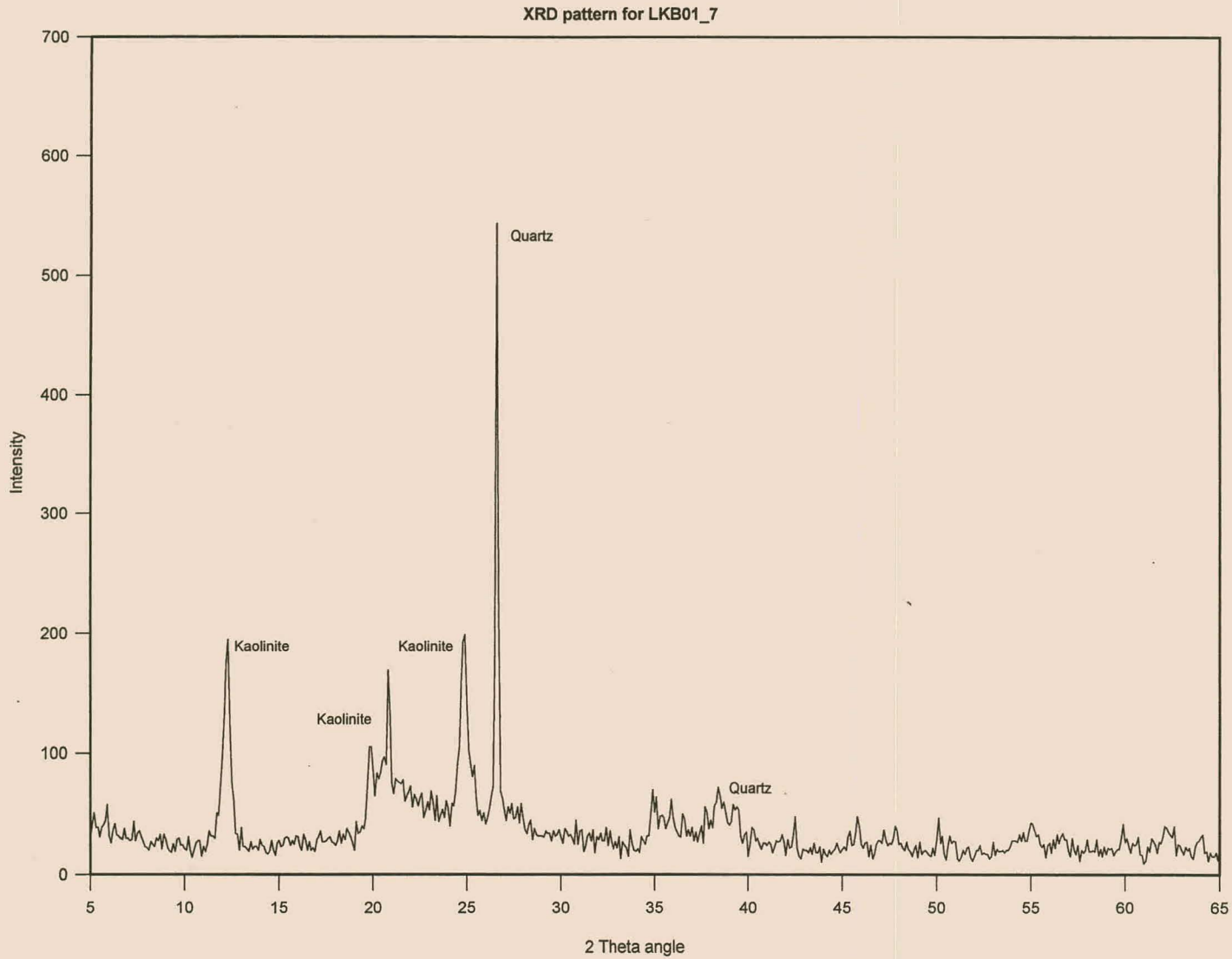

Figure 6. X-ray diffractogram of clay sample LKB-01_2.

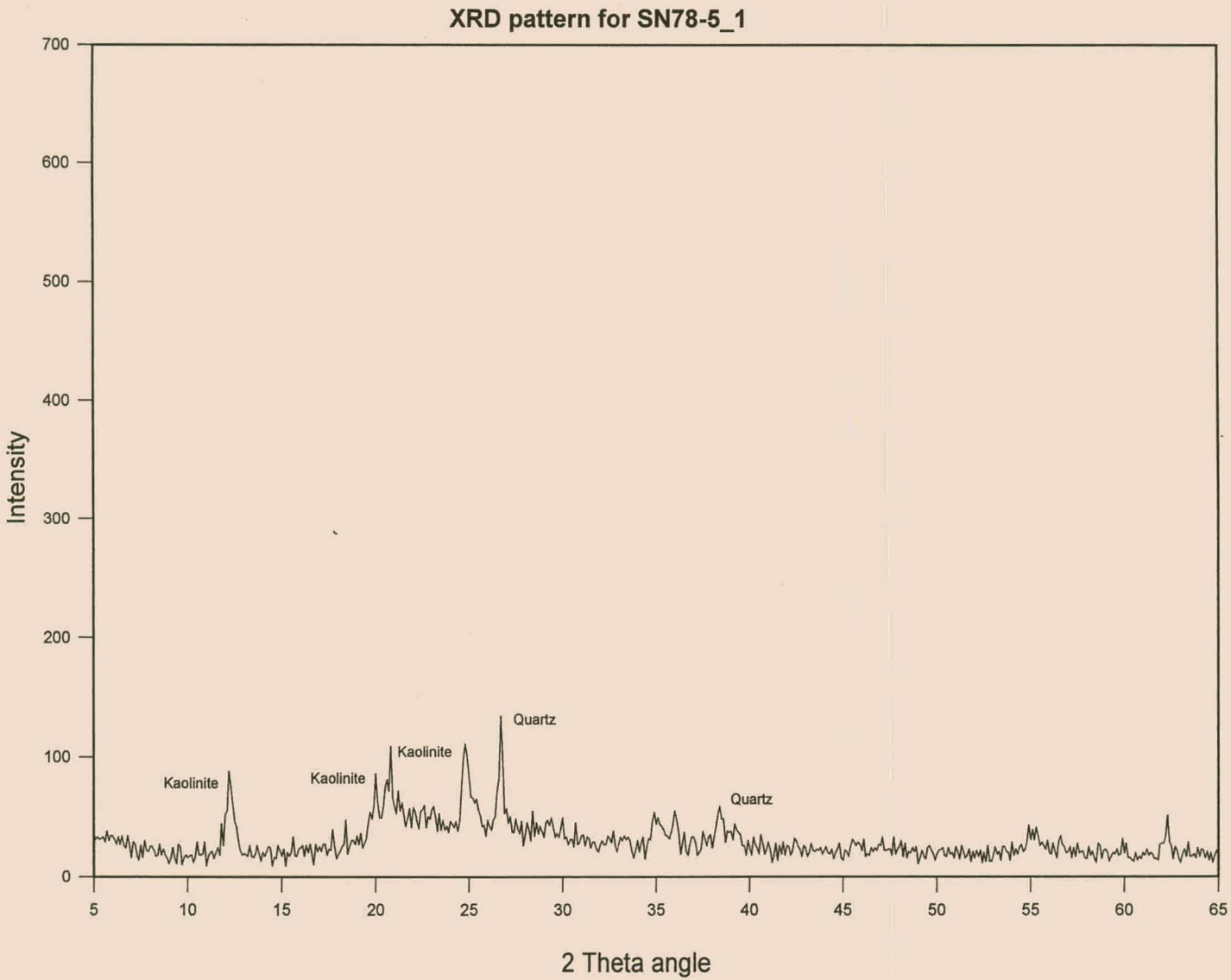

Figure 7. X-ray diffractogram of clay sample SN78-5_1.

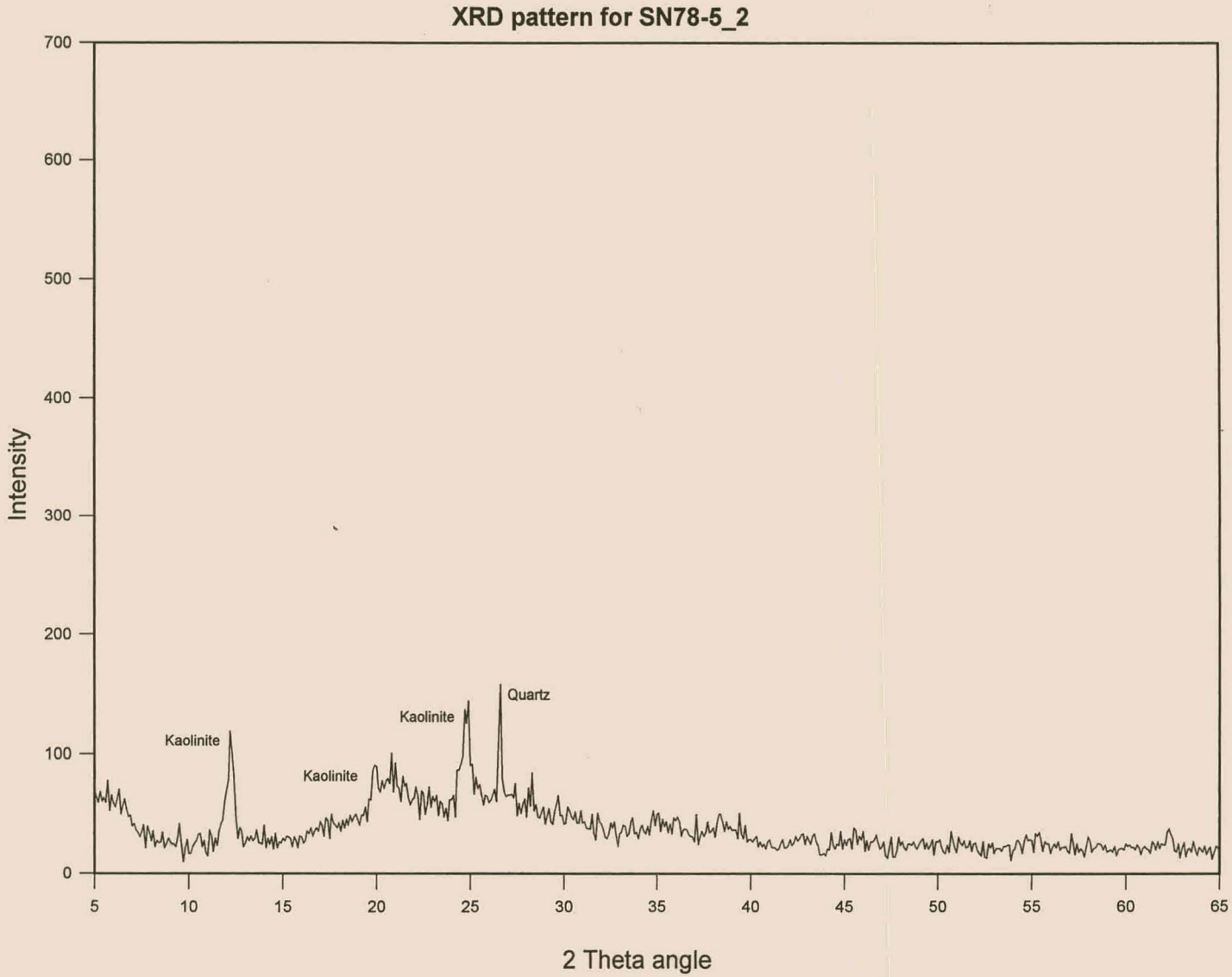

Figure 8. X-ray diffractogram of clay sample SN78-5_2.

APPENDIX G

HEAVY MINERAL PROPORTIONS

Abbreviations

THM	total heavy minerals
unalt-Ilm	unaltered ilmenite
alt-Ilm	altered ilmenite (excluding leucoxene)
ΣIlm	sum of altered and unaltered ilmenites
Lcx	leucoxene
Hm	hematite
Fe-Ti Int	Fe-Ti intergrown minerals; includes hemo-ilmenite and ilmo-hematite
Mt	magnetite, including martite
Grt	garnet
Zrn	zircon
Cpx	clinopyroxene (augite)
Ap	apatite (collophane)
Hbl	hornblende
Ep	epidote
Mz	monazite
Rt	rutile
Ky-Si	kyanite + sillimanite
St	staurolite
Tt	titanite
TEF	total economic fraction; calculated as (ΣIlm+Lcx+Zrn+Rt)
Alt (%)	percentage of altered grains; calculated by $\frac{\text{alt - Ilm} + \text{Lcx}}{\Sigma\text{Ilm} + \text{Lcx}}$

Data presented as modal percentages.

Sample	THM (wt%)	unalt-Ilm	alt-Ilm	ΣIlm	Lcx	Hm	Fe-Ti Int	Mt	ΣOPQ	Grt	Zrn	Cpx	Ap	Hbl	Ep	Mz	Rt	Ky	St	Tt	TEF	Alt (%)
BMC: RET																						
AK43B_1	0.3	42.7	3.0	45.7	3.0	8.6	7.7	0.3	65.3	12.2	8.9	0.3	0.6	2.4	4.7	3.3	0.6	1.2		0.6	58.2	12.2
AK43B_2	0.1	56.2	0.9	57.0	2.0	6.0	3.7	0.9	69.6	10.9	4.9	5.2	2.0	1.7	2.9	0.6	0.6	1.1	0.3	0.3	64.5	4.9
AK45H_1	1.1	38.6	1.6	40.2	2.4	8.2	1.4		52.2	10.6	11.4	10.9	1.1	6.5	4.1	1.4	1.1		0.3	0.5	55.2	9.6
AK45H_2	0.3	42.0	2.4	44.4			2.0	0.4	46.8	15.2	16.0	1.6	1.6	10.4	4.4	1.2	1.6		0.4	0.8	62.0	5.4
AK45H_3	0.3	49.8	1.8	51.7	0.4	15.1	3.7	1.1	72.0	11.1	8.5	0.4	1.1	1.5	3.0	1.5	0.4		0.4	0.4	60.9	4.3
AK45H_4	0.2	35.2	2.4	37.6	0.3	15.9	8.0	1.5	63.3	10.7	7.0	0.9		11.0	3.1	2.1	0.9	0.6	0.3		45.9	7.3
AK45H_5	0.4	40.8	1.9	42.7	1.0	23.8	3.4	1.5	72.3	6.8	5.8		1.0	4.9	4.4	2.9	0.5	0.5	0.5	0.5	50.0	6.7
AK52N_1	0.4	32.9	1.0	33.9	2.6	12.3	2.3	0.3	51.3	8.1	9.0	2.3	2.9	14.8	5.5	1.6	1.3	1.0	0.6	1.6	46.8	9.7
AK52N_2	0.8	36.1		36.1	0.9	12.8	2.2	0.4	52.4	4.4	5.3	1.8	2.6	19.8	9.7			1.3	0.9	1.8	42.3	2.4
n= 9																						
Avg.	0.4	41.6	1.7	43.3	1.4	11.4	3.8	0.7	60.6	10.0	8.5	2.6	1.4	8.1	4.6	1.6	0.8	0.6	0.4	0.7	54.0	6.9
BMC: Lower Terrace																						
DP84LM_1	0.3	15.8		15.8	0.9	11.6	0.5	1.9	30.7	2.8	6.0	4.7	14.9	5.1	34.0			1.9			19.5	5.6
DP84LM_2	0.9	30.2	1.9	32.1	0.4	13.1	7.5	3.0	56.0	8.2	5.2	6.0	4.5	5.6	9.3	2.6	0.7	0.7	0.7	0.4	41.4	6.9
DP88LM_1	3.0	52.9	3.1	56.1	0.4	9.8	2.4	1.6	70.2	7.8	2.0	0.4	8.2	3.1	4.3	1.2	2.0			0.8	66.3	6.3
DP88LM_2	3.6	62.2	2.6	64.8	0.5	10.9	4.7	1.6	82.4	4.1	3.1	1.6	4.1	0.5	3.6			0.5			69.4	4.8
DP88LM_3	1.9	48.4	3.2	51.6	2.5	10.4	3.6		68.1	3.9	6.1	1.4	5.0	10.0	2.5		0.4	1.8	0.7		58.4	10.6
n= 5																						
Avg.	1.9	41.9	2.2	44.1	0.9	11.2	3.7	1.6	61.5	5.4	4.5	2.8	7.4	4.9	10.7	0.8	0.6	1.0	0.3	0.2	51.0	6.8
BMC: Lower Middle Terrace																						
TP235M_1	0.3	42.4	6.6	49.1	2.2	17.1	5.1	1.9	75.3	1.9	9.8	0.6	3.2	0.6	1.3	1.9		0.9	2.5	1.9	61.1	17.3
TP235M_2	0.3	52.8	4.0	56.9	1.7	14.4	4.3	2.3	79.6	5.0	7.4	0.7		1.7	1.0	2.3	1.0	0.3		1.0	66.9	9.7
TP235M_3	1.6	51.4	1.0	52.4	1.0	15.3	4.2	1.0	74.0	3.5	2.1	2.4		6.9	2.4	2.1		1.7	3.8	1.0	55.6	3.9
TP262N_1	1.2	70.0	1.5	71.5	0.6	6.5	10.5	0.3	89.5	3.4	2.5		0.6	0.6		1.9	0.3	0.9	0.3		74.9	3.0
TP262N_2	19.6	64.1	1.0	65.1		11.2	13.6	1.7	91.5	5.4	0.3	0.7	0.3		1.0	0.7					65.4	1.6
TP262N_3	58.4	68.1	3.2	71.3	0.3	4.8	13.9	1.6	91.9	6.1	0.3	0.3				0.6		0.3		0.3	71.9	5.0
TP262N_4	9.0	41.5	2.9	44.4	0.4	30.7	5.1		80.5	2.9	5.8	0.7	1.4	4.7	1.1	1.4	1.1			0.4	51.6	7.3
n= 7																						
Avg.	12.9	55.8	2.9	58.7	0.9	14.3	8.1	1.3	83.2	4.0	4.0	0.8	0.8	2.1	1.0	1.6	0.3	0.6	1.0	0.7	63.9	6.8

Sample	THM (wt%)	unalt-Ilm	alt-Ilm	ΣIlm	Lcx	Hm	Fe-Ti Int	Mt	ΣOPQ	Grt	Zrn	Cpx	Ap	Hbl	Ep	Mz	Rt	Ky	St	Tt	TEF	Alt (%)
BMC: Upper MiddleTerrace																						
KV198PR_1	3.1	58.8	4.3	63.1	0.9	7.6	16.2	0.6	88.4	7.6	0.9	0.3	0.9					0.6	0.9	0.3	64.9	8.1
KV198PR_2	11.3	50.8	2.0	52.8	1.2	8.7	10.6	1.6	74.8	5.5	5.5	1.6	2.0	5.5	0.8	0.8		0.8	2.8		59.4	5.8
n= 2																						
Avg.	7.2	54.8	3.1	57.9	1.0	8.1	13.4	1.1	81.6	6.6	3.2	0.9	1.4	2.8	0.4	0.4		0.7	1.8	0.2	62.2	7.0
BMC: Upper Terrace																						
AK1_2	0.4	41.8	5.7	47.5	1.6	27.4	1.0		77.5	7.3	3.1		0.5	1.6	1.6	7.0	0.3	0.3	0.8		58.2	14.9
DP127R_1	2.3	64.3	3.9	68.2	0.6	7.7	7.7		84.2	1.0	3.2	1.6	3.2	1.3	1.6	3.2			0.6		71.7	6.5
DP127R_2	7.5	69.4	1.0	70.4	1.7	8.8	7.4		88.2	1.0	4.0	1.3	1.0	0.3	1.7	1.0	0.3	1.0			76.1	3.7
DP127R_3	43.2	71.5	0.6	72.1		9.0	13.1		94.2	1.6	1.9		0.6			1.6					74.0	0.9
DP127R_4	1.0	48.7	0.7	49.5	2.2	19.7	6.8	1.4	79.6	5.0	3.9	0.7	1.8	3.2	2.5	0.7		1.4	1.1		58.1	5.6
KV196R_1	0.4	53.7	4.7	58.4	1.9	7.5	4.3		72.0	1.2	6.2	1.2	1.9	8.7	5.0	0.9	0.3	1.6		0.9	64.3	10.8
KV196R_2	0.3	47.4	2.3	49.7	3.6	15.4	3.9	0.3	72.9	3.9	5.2	0.7	2.0	1.3	8.5	1.3	0.3	1.6		2.3	59.5	11.0
KV196R_3	14.5	68.6	4.4	73.1	1.2	11.5	5.3	1.8	92.9	1.5	0.9	0.6	1.2		0.9	1.2		0.9			75.7	7.6
KV196R_4	1.4	41.3	2.1	43.4	0.9	20.8	3.1		68.2	10.1	4.0	0.3	2.8	5.5	0.9	1.2	1.8	1.5	3.7		57.5	6.9
n= 9																						
Avg.	7.9	56.3	2.8	59.1	1.5	14.2	5.9	0.4	81.1	3.6	3.6	0.7	1.7	2.4	2.5	2.0	0.3	0.9	0.7	0.4	66.1	7.6
BMC: Present-day beach																						
SEA419_1	35.9	52.8	3.7	56.5		12.0	20.4	1.4	90.3	4.6				3.7		0.5			0.9		56.5	6.6
SEA419_2	51.2	48.0	3.0	51.0		12.0	22.5	1.5	87.0	7.0	0.5	1.5		1.0		0.5			2.5		51.5	5.9
SEA419_3	54.0	57.8	2.0	59.7	0.3	8.3	24.4	1.0	93.7	5.0	0.3	0.3							0.7		60.4	3.8
n= 3																						
Avg.	47.0	52.8	2.9	55.7	0.1	10.8	22.4	1.3	90.3	5.5	0.3	0.6		1.6		0.3			1.4		56.1	5.4
BIC: Langhoogte																						
LHC_1	1.2	82.7	3.0	85.7	2.4	2.4	3.0	4.8	98.2		1.2					0.6					89.3	6.1
LHC_2	7.7	59.4	5.9	65.4	0.5	22.2	2.3	2.6	93.0	1.0	3.9					1.3	0.8				70.5	9.8
LHC_3	0.8	79.9	2.3	82.2	0.7	4.0	0.3	5.9	93.1	1.3	3.6					1.3			0.3	0.3	86.5	3.6
LHC_4	26.2	79.8	9.0	88.9		3.6	2.1	2.7	97.3	0.3	2.1						0.3				91.3	10.2
LHC_5	21.8	60.4	4.3	64.7		28.7	1.0	2.0	96.4	0.7	0.7					2.0			0.3		65.3	6.6
n= 5																						
Avg.	11.5	72.5	4.9	77.4	0.7	12.2	1.7	3.6	95.6	0.7	2.3					1.0	0.2		0.1	0.1	80.6	7.3

Sample	THM (wt%)	unalt-Ilm	alt-Ilm	ΣIlm	Lcx	Hm	Fe-Ti Int	Mt	ΣOPQ	Grt	Zrn	Cpx	Ap	Hbl	Ep	Mz	Rt	Ky	St	Tt	TEF	Alt (%)
BIC: Nuttabooi																						
NB19AC_1	2.4	67.4	9.5	76.9	0.6			0.8	78.3	0.3	18.9			0.8		0.6	1.1				97.5	12.9
NB19AC_2	0.1	26.7	4.3	31.0	1.3	0.8	3.2	1.3	37.7	5.1	53.9	0.3		1.1		1.3	0.5				86.8	17.5
NB19AC_3	1.1	75.6	6.4	82.0		1.3	1.9		85.2	1.0	8.4	0.3				3.2	0.6	1.3			91.0	7.8
NB19AC_4	0.7	60.1	1.4	61.5	1.0	5.6	5.6	2.8	76.6	1.4	14.3	0.3		3.1		1.7	0.3	1.0	1.0		77.3	3.9
NB21B_1	3.0	78.2	7.6	85.8	1.6	0.3	0.9	1.3	89.9	0.9	3.2				0.6	5.0	0.3				90.9	10.5
NB21B_2	6.6	67.0		67.0	3.5		1.3		71.8		8.8	9.3			8.4	1.3	0.4				79.7	5.0
NB21B_3	2.4	62.4	5.5	67.9	3.1	0.3	0.3	0.9	72.5	0.3	22.0				0.3	3.4	0.9	0.3		0.3	93.9	12.1
NB21B_4	1.4	64.4	5.8	70.1	1.6	1.1	0.8	0.3	74.0	0.8	22.7					2.2	0.3				94.8	10.3
NB21B_5	0.2	65.7	3.4	69.0	0.7	6.4	4.7	1.7	82.5	3.7	5.7			0.7		1.3	0.3	2.0	3.0	0.7	75.8	5.8
n= 9																						
Avg.	2.0	63.0	4.9	67.9	1.5	1.8	2.1	1.0	74.3	1.5	17.6	1.1		0.6	1.0	2.2	0.5	0.5	0.5	0.1	87.5	9.5
KNC: RET																						
LKC1-04_11	9.8	70.7	3.3	74.0	1.2	3.6	1.8	3.0	83.4	4.7	6.5		0.3	0.6		3.3	0.9			0.3	82.5	5.9
LKC1-04_12	32.9	39.5	1.2	40.7		7.3	10.9	3.2	62.1	24.6	3.6	0.4		1.2		7.7			0.4		44.4	3.0
LKCR1_1	1.0	55.9	4.5	60.4	1.5	7.9	12.1	2.4	84.3	7.3	1.2	0.6	1.2	2.1		1.2	1.2	0.6	0.3		64.4	9.8
LKCR1_2	8.5	53.3	2.4	55.7	1.0	5.5	18.3	6.2	86.9	6.6	0.3	0.7		1.7		2.1	0.3	1.4			57.4	6.1
SNR1_3	12.0	37.4	1.7	39.1	0.3	12.5	19.2	4.4	75.4	9.4	4.7	3.7	0.3	4.0	1.0		0.3	0.3		0.7	44.4	5.1
n= 5																						
Avg.	12.8	51.4	2.6	54.0	0.8	7.3	12.5	3.8	78.4	10.5	3.3	1.1	0.4	1.9	0.2	2.8	0.6	0.5	0.1	0.2	58.6	6.0
KNC: Upper CFS																						
KN14_1	0.7	45.8	2.6	48.3	0.7	8.5	5.9	1.5	64.9	9.2	4.4	3.7	4.1	8.9	2.2	0.4	0.7	1.1	0.4		54.2	6.8
KN14_2	3.1	42.7	2.4	45.1	1.7	9.6	7.5	5.5	69.3	4.8	5.1	5.5	1.0	8.9	1.7	0.7	1.4	0.3	0.3	1.0	53.2	8.8
KN14_3	22.2	55.1	4.8	59.9		7.0	13.2	7.0	87.1	9.2	1.1	1.1			0.7				0.7		61.0	8.0
KN14_4	17.5	54.7	3.1	57.8	0.3	12.1	18.9	2.5	91.6	5.3	0.6	1.2		1.2							58.7	5.9
LKC1-04_8	3.1	61.6	2.5	64.1	1.2	10.8	4.3	0.9	81.4	6.5	5.6	0.6	0.9	1.2		1.5	0.9	0.6	0.6		71.8	5.7
LKC1-04_9	21.8	48.3	0.7	49.0		16.3	17.4	7.3	89.9	5.6	1.0	1.7		0.3		1.4					50.0	1.4
LKC1-04_10	32.2	46.4	2.0	48.3	0.7	18.5	16.9	5.0	89.4	6.3	0.3	0.3		1.0		2.0	0.3	0.3			49.7	5.4
n= 7																						
Avg.	14.4	50.6	2.6	53.2	0.7	11.8	12.0	4.2	82.0	6.7	2.6	2.0	0.9	3.1	0.7	0.9	0.5	0.3	0.3	0.1	57.0	6.0

Sample	THM (wt%)	unalt-Ilm	alt-Ilm	ΣIlm	Lcx	Hm	Fe-Ti Int	Mt	ΣOPQ	Grt	Zrn	Cpx	Ap	Hbl	Ep	Mz	Rt	Ky	St	Tt	TEF	Alt (%)
KNC: Lower CFS																						
KN17_1	0.1	53.3	3.1	56.4		16.7	3.1	0.8	77.0	5.4	2.7	1.2	1.2	2.7	7.8		0.4	0.8		0.8	59.5	5.5
KN17_2	0.1	38.3	1.3	39.6		7.1	3.2	1.0	51.0	4.2	11.4	1.3	8.1	15.9	2.6		2.6		2.6	0.3	53.6	3.3
KN17_3	0.1	48.2	0.6	48.8			1.5	1.2	51.5	8.1	15.7	4.5	4.8	4.2	4.8	0.3	1.2	0.9	1.2	2.7	65.7	1.2
LKB01_3	0.8	44.1	1.8	45.8		7.5	20.7	1.3	75.3	16.3	0.9	0.9	1.8	0.4			0.4	0.9	3.1		47.1	3.8
LKB01_4	0.8	46.3	3.7	50.0	0.3	4.3	1.2	0.6	56.4	14.1	12.0	0.6	6.7	4.0	0.6		2.8	0.9	1.8		65.0	7.9
LKC1-04_2	1.1	41.6	1.7	43.3	1.3	3.7	4.0	3.4	55.7	12.1	7.0	0.3	11.7	7.4	1.3	1.0	0.3	1.3	1.7		52.0	6.8
LKC1-04_3	2.3	37.7	2.0	39.7	2.3	3.6	2.0	0.7	48.3	20.9	7.9	6.6	5.0	2.6	3.0	1.0	4.0	0.7			54.0	10.2
LKC1-04_4	3.9	23.9	0.7	24.6	6.3	11.3	8.5	2.8	53.5	27.5	2.1	3.5	2.8	7.0		2.1	1.4				34.5	22.7
LKC1-04_5	0.6	39.5	2.3	41.8	2.0	3.7	1.4	2.0	50.9	22.2	10.5	3.1	2.3	4.3	0.9	0.3	3.7	1.1		0.9	58.0	9.7
LKC1-04_6	0.5	32.2	1.7	33.9	4.8	8.9	4.5	1.7	53.8	22.3	9.2		0.3	6.5	4.1	1.7	0.3	1.4		0.3	48.3	16.8
LKC1-04_7	0.1	47.7	5.7	53.5	3.6	1.5		1.2	59.8	4.8	22.8		3.3	2.7	0.3	1.8	2.1	1.2	0.3	0.9	82.0	16.3
SN78-5_3	0.4	36.4	1.6	38.0	0.6	5.7	1.9	3.5	49.7	8.5	6.6		1.6	15.2	3.5	4.4	0.9	1.6		7.9	46.2	5.7
SN78-5_4	2.9	48.0	0.9	48.8	2.9	2.6	1.8	1.2	57.3	15.8	10.8	0.9	2.3	6.4	0.9	0.9	2.6	0.9		1.2	65.2	7.3
SN78-5_5	1.0	48.7	1.3	50.0	4.3	3.0	4.3	0.3	61.9	19.5	11.3		0.3	2.3	0.7	1.0	1.3	0.7		1.0	66.9	10.4
SN78-5_6	0.5	77.8	1.4	79.2	4.2	2.8	0.9	0.9	88.2	3.3	2.4	0.9		2.4	0.5	0.5	0.9			0.9	86.8	6.8
SNR1_2	0.3	61.8	2.4	64.2	1.4	7.4	2.1	1.7	76.8	4.5	10.5	1.2	2.4	1.9	1.2	0.2	1.2				77.3	5.8
n= 16																						
Avg.	1.0	45.3	2.0	47.4	2.1	5.6	3.8	1.5	60.5	13.1	9.0	1.6	3.4	5.4	2.0	1.0	1.6	0.8	0.7	1.1	60.1	8.8
KNC: FGS																						
LKN8-03_1	6.0	49.2	0.7	49.9	0.7	1.6	0.2	0.5	52.9	9.1	6.5	18.6	1.6	2.8	1.2	0.9	2.1	1.9	1.9	0.5	59.2	2.8
LKN8-03_2	0.4	20.7	2.1	22.8	6.8	4.2	2.1		35.9	17.3	19.0	16.0	4.6	3.0	0.8	1.3	0.4	0.8	0.8		48.9	30.0
LKN8-03_3	11.0	42.3	0.6	42.9	1.3	0.6	1.6		46.4	8.8	6.0	20.7	8.2	2.5	2.2		2.8	1.6	0.9		53.0	4.3
LKN8-03_4	1.6	41.2	2.3	43.5	2.0	6.2	3.3		54.9	7.5	14.1	7.2	3.9	6.2	2.0		1.0	1.0	2.3		60.5	9.4
n= 4																						
Avg.	4.8	38.3	1.4	39.8	2.7	3.2	1.8	0.1	47.5	10.7	11.4	15.6	4.6	3.6	1.5	0.5	1.6	1.3	1.5	0.1	55.4	11.6
KNC: Present-day beach																						
KN_SI	3.1	52.0	0.3	52.3	2.2	1.4	0.8	0.3	56.9	6.5	13.4	19.6		1.6		0.8	0.3	0.3		0.5	68.1	4.5
SEA711	3.5	12.8		12.8	0.9	0.6	0.6	0.9	15.7	11.0	2.7	63.2	2.4	4.5		0.3	0.3				16.6	6.5
n= 2																						
Avg.	3.3	32.4	0.1	32.5	1.5	1.0	0.7	0.6	36.3	8.8	8.0	41.4	1.2	3.0		0.6	0.3	0.1		0.3	42.4	5.5

Sample	THM (wt%)	unalt-Ilm	alt-Ilm	ΣIlm	Lcx	Hm	Fe-Ti Int	Mt	ΣOPQ	Grt	Zrn	Cpx	Ap	Hbl	Ep	Mz	Rt	Ky	St	Tt	TEF	Alt (%)
Palaeochannels																						
AK1_1	0.9		39.8	39.8	2.4				42.3		21.1		4.9	0.8	10.6	9.8	4.9		4.9	0.8	68.3	5.8
6969_1	1.9	7.5	33.3	40.9	5.7				46.6		53.0						0.4				100.0	28.5
6869_2	0.8	2.7	23.3	26.0	2.0				28.0		71.7						0.3				100.0	16.7
6869_3	1.9	6.6	43.0	49.6		0.9			50.4		49.6										99.1	13.3
LKB01_1	1.7	3.6	33.5	37.1	2.7	8.4	5.4	0.3	53.9	5.1	34.4			1.8	1.5		1.8	0.6	0.3	0.6	76.0	15.8
LKB01_2	1.7	0.7	11.3	11.9	1.1	5.1	0.9	0.2	19.2	0.4	79.6			0.7							92.7	13.6
LKC1-04_1	0.8	1.0	25.1	26.1	1.6	4.7	0.5		32.9	2.9	43.3		9.4	8.4	0.5		1.3	1.3			72.3	9.4
SN78-5_1	2.1	0.8	17.9	18.7		2.4		0.5	21.7		76.2			0.3		0.8	0.8	0.3			95.7	4.3
SN78-5_2	0.1	2.0	48.7	50.7	2.0	1.4	0.6	0.3	55.0	4.3	37.8			0.3		1.4	1.2				91.6	7.7
SNR1_1	0.9	2.9	26.8	29.7	1.4	14.5	2.2	3.6	51.4	3.6	42.0			0.7			0.7			1.4	73.9	14.0
n= 10																						
Avg.	1.3	30.3	2.8	33.1	1.9	3.7	1.0	0.5	40.2	1.6	50.9		1.4	1.3	1.3	1.2	1.1	0.2	0.5	0.3	87.0	12.9
Rivers																						
BR	0.9	42.9	1.1	44.0	2.9	3.7	2.9	3.3	56.8	9.9	4.0	2.6	0.7	19.8	2.9	0.7		0.7	0.7	1.1	50.9	8.6
ZL		21.9	0.2	22.1	0.6	6.0	0.2	2.6	31.5	1.9	15.5	3.2	7.9	23.0	14.9			1.9		0.2	38.3	3.7
DP68D1_1	0.5	21.5	0.6	22.1	0.6	35.5	5.0		63.2	1.6	5.0		16.5	5.3	2.8	1.6	1.2	0.6		2.2	29.0	5.5
DP68D1_2	1.0	29.2	1.5	30.7	0.6	21.3	1.8		54.4	5.6	11.4		4.4	12.0	6.4	0.3	0.9	0.3	0.9	3.5	43.6	6.5
DP68D1_3	1.0	29.7		29.7	1.5	23.9	4.4	0.9	60.3	2.0	5.0	1.2	11.4	12.0	4.7	0.6	0.6	1.5		0.9	36.7	4.7
n= 3																						
Avg.	0.8	26.8	0.7	27.5	0.9	26.9	3.7	0.3	59.3	3.1	7.1	0.4	10.8	9.7	4.6	0.8	0.9	0.8	0.3	2.2	36.4	4.8

Sample	THM	unalt-Ilm	alt-Ilm	ΣIlm	Lcx	Hm	Fe-Ti Int	Mt	ΣOPQ	Grt	Zrn	Cpx	Ap	Hbl	Ep	Mz	Rt	Ky	St	Tt	TEF
Heaped tailings																					
AK_SD1	0.9	22.8	0.9	24.6	0.0	21.9	6.3	3.6	56.3	4.9	12.1	1.8	1.8	14.7	5.8	0.4	0.9	0.0	0.9	0.4	37.5
AK_SD2	3.4	46.3	3.7	50.3	0.3	18.5	4.0	1.9	75.0	4.9	6.2	0.0	0.6	5.9	5.6	0.3	0.0	0.6	0.9	0.0	56.8
AK_SD3	4.3	41.6	0.7	42.3	0.3	15.4	3.8	5.9	67.8	7.7	7.7	0.3	2.1	7.7	4.9	0.3	0.3	0.7	0.3	0.0	50.7
AK3P_D	4.1	30.6	2.5	33.1	0.6	20.8	0.6	3.5	58.7	6.6	9.5	0.9	2.8	13.6	5.0	0.9	0.3	0.3	0.9	0.3	43.5
BS_SD1	16.3	42.8	2.6	45.4	0.4	17.5	3.7	1.1	68.0	2.6	11.9	0.0	1.5	11.9	1.5	0.4	1.1	0.4	0.7	0.0	58.7
BS_SD2	1.1	36.8	1.6	39.5	3.0	21.7	1.0	3.6	68.8	2.6	12.8	0.3	1.3	10.2	2.6	0.3	0.3	0.0	0.7	0.0	55.6
BS_D1	5.3	52.2	1.3	56.9	0.6	6.6	4.1	2.8	71.1	1.6	14.2	0.0	0.6	8.5	1.6	0.3	0.9	0.3	0.0	0.9	72.6
BS_D2	2.8	25.2	0.9	26.2	0.0	21.0	1.9	5.6	54.7	3.7	14.0	0.5	4.2	16.8	2.8	0.0	1.9	0.5	0.5	0.5	42.1
TPP_D1	3.5	39.3	1.5	42.9	0.3	19.0	3.4	1.2	66.9	2.1	13.2	0.3	0.9	12.0	4.0	0.0	0.6	0.0	0.0	0.0	57.1
TPP_D2	2.1	51.2	0.3	51.5	0.3	23.5	6.5	1.0	82.9	1.0	6.1	0.0	0.7	3.1	4.8	0.0	0.7	0.7	0.0	0.0	58.7
TPP_SD	5.8	42.5	2.8	45.2	0.8	23.4	7.9	1.6	79.0	2.0	13.1	0.4	0.8	2.4	1.2	0.0	1.2	0.0	0.0	0.0	60.3
LH_SD	0.3	29.1	12.5	41.6	2.0	30.1	0.0	5.4	79.1	0.3	19.3	1.4	0.0	0.0	0.0	0.0	0.0	0.0	0.0	0.0	62.8
KNP_SD1	2.3	45.8	1.2	47.1	1.2	7.1	1.8	1.5	58.8	3.4	26.2	0.3	1.8	4.3	3.4	0.3	0.3	0.0	0.6	0.6	74.8
KNP_SD2	2.3	31.2	1.6	32.8	1.2	28.3	4.0	2.0	68.4	4.0	16.6	0.4	1.2	5.7	1.2	1.6	0.0	0.0	0.4	0.4	50.6
KNP_D1	0.8	30.8	4.0	34.9	1.9	5.9	0.3	0.6	43.6	2.2	46.7	0.3	0.6	5.3	0.6	0.0	0.0	0.3	0.0	0.0	83.5
KNP_D2	1.6	42.9	4.1	47.1	1.8	3.8	1.2	0.6	54.4	1.5	42.1	0.0	1.2	0.3	0.3	0.3	0.0	0.0	0.0	0.0	90.9
n= 16																					
Avg.	3.6	38.2	2.7	41.3	0.9	17.8	3.2	2.6	65.8	3.2	17.0	0.4	1.4	7.6	2.8	0.3	0.5	0.2	0.4	0.2	59.8

APPENDIX H

MICROPROBE ANALYSIS

1. **Unaltered ilmenite**
2. **Altered ilmenite**
3. **Hematite**
4. **Titanohematite**
5. **Magnetite**
6. **Rutile**
7. **Zircon**
8. **Garnet**
9. **Pyroxene**
10. **Amphibole**
11. **Epidote**
12. **Aluminosilicates**
13. **Staurolite**
14. **Glauconite**
15. **Titanite**

FeO and Fe_2O_3 calculations were performed at the Council for Geoscience using the method of Droop (1987).

1. UNALTERED ILMENITE

Sample	No.	SiO_2	TiO_2	Al_2O_3	Cr_2O_3	Fe_2O_3	FeO	MnO	MgO	CaO	Total
AK43B_1	2	0.00	50.89	0.00	0.00	3.27	43.26	2.47	0.00	0.00	99.89
AK43B_1	4	0.11	52.85	0.52	0.00	0.00	41.11	0.61	0.19	0.08	95.47
AK43B_1	5	0.00	49.87	0.00	0.22	4.99	42.99	1.83	0.00	0.00	99.90
AK43B_1	7	0.00	51.20	0.00	0.00	2.96	41.64	3.92	0.17	0.10	99.99
AK45H_4	1	0.00	49.16	0.00	0.00	6.21	42.94	1.25	0.00	0.00	99.56
AK45H_4	2	0.00	46.03	0.00	0.05	12.41	39.22	1.95	0.11	0.00	99.77
AK45H_4	5	0.00	49.45	0.00	0.00	6.00	40.68	3.63	0.06	0.00	99.82
AK45H_4	7	0.09	48.06	0.07	0.00	8.75	39.02	3.85	0.23	0.00	100.07
AK45H_4	8	0.00	52.12	0.19	0.00	0.93	43.16	3.39	0.06	0.13	99.98
AK45H_4	10	0.00	51.80	0.00	0.00	1.33	44.28	2.27	0.00	0.00	99.68
AK52N_2	5	0.00	51.46	0.05	0.00	0.62	43.96	0.40	1.07	0.00	97.56
AK52N_2	6	0.00	49.42	0.00	0.00	5.59	39.13	5.24	0.00	0.00	99.38
AK52N_2	8	0.00	51.13	0.00	0.00	3.34	44.13	0.40	0.81	0.00	99.82
AK52N_2	9	0.00	47.44	0.05	0.00	9.17	41.22	1.42	0.00	0.00	99.30
AK52N_2	10	0.00	51.17	0.00	0.00	2.02	43.16	2.74	0.00	0.06	99.15
DP127R_2	2	0.00	51.17	0.00	0.00	2.39	40.83	5.12	0.00	0.00	99.51
DP127R_2	3	0.00	50.51	0.00	0.00	4.47	42.54	2.74	0.06	0.00	100.32
DP127R_2	4	0.00	50.96	0.00	0.00	3.94	42.75	3.04	0.00	0.00	100.68
DP127R_2	5	0.00	52.65	0.05	0.00	0.00	43.86	1.55	0.72	0.00	98.83
DP127R_2	8	0.00	49.06	0.00	0.00	7.03	39.26	4.71	0.00	0.07	100.12
DP127R_2	9	0.00	49.45	0.00	0.00	6.11	41.70	2.42	0.18	0.00	99.85
DP127R_2	10	0.00	51.26	0.00	0.00	2.33	42.13	3.92	0.00	0.00	99.63
DP127R_2	11	0.00	51.47	0.00	0.00	2.47	40.84	5.13	0.14	0.00	100.05
DP127R_2	14	0.00	50.38	0.00	0.06	4.47	40.16	5.08	0.00	0.00	100.15
DP88LM_2	1	0.00	50.25	0.17	0.00	3.26	40.19	4.93	0.00	0.00	98.81
DP88LM_2	2	0.00	49.87	0.00	0.00	3.46	36.71	8.03	0.00	0.00	98.08
DP88LM_2	3	0.91	50.88	0.10	0.00	0.00	40.07	2.97	0.12	1.27	96.42
DP88LM_2	6	0.00	48.18	0.00	0.00	4.51	40.92	2.38	0.00	0.00	95.98
DP88LM_2	7	0.35	51.42	0.62	0.00	0.00	38.57	3.90	0.11	0.19	95.16
DP88LM_2	8	0.00	51.41	0.00	0.00	2.67	43.07	3.12	0.00	0.00	100.27
DP88LM_2	10	0.00	52.16	0.00	0.00	0.95	45.09	1.79	0.00	0.00	100.00
DP88LM_2	11	0.00	50.83	0.00	0.00	3.00	44.21	1.39	0.05	0.00	99.48
DP88LM_2	12	0.34	51.69	0.65	0.00	0.00	39.16	0.66	0.05	0.07	92.62
DP88LM_2	15	0.00	50.14	0.00	0.00	4.33	43.61	1.37	0.05	0.00	99.50
KV196R_1	1	0.00	50.81	0.00	0.00	0.75	40.29	5.17	0.09	0.00	97.12
KV196R_1	2	0.00	52.65	0.00	0.00	0.00	39.59	5.85	0.00	0.00	98.09
KV196R_1	8	0.00	49.36	0.00	0.00	5.56	37.88	6.42	0.00	0.00	99.23
KV196R_1	9	0.06	51.87	0.05	0.00	0.00	40.67	3.58	0.00	0.00	96.23
KV196R_1	15	0.00	52.09	0.00	0.05	0.00	38.99	5.93	0.07	0.00	97.13
KV196R_1	16	0.00	50.46	0.00	0.00	0.09	40.14	5.08	0.00	0.07	95.84
KV198PR_3	2	0.00	50.29	0.00	0.00	3.75	43.00	2.20	0.00	0.00	99.24
KV198PR_3	3	0.00	48.73	0.00	0.00	5.34	37.16	6.45	0.07	0.00	97.76
KV198PR_3	4	0.00	50.91	0.00	0.00	1.19	43.20	2.55	0.00	0.00	97.85
KV198PR_3	6	0.00	47.60	0.00	0.00	7.57	35.23	7.34	0.08	0.00	97.82
KV198PR_3	8	0.00	48.85	0.00	0.00	4.56	42.42	1.49	0.00	0.00	97.32
KV198PR_3	9	0.00	47.14	0.00	0.00	9.07	41.09	1.28	0.00	0.00	98.59
KV198PR_3	10	0.00	49.26	0.00	0.00	5.02	39.11	5.02	0.06	0.00	98.46
KV198PR_3	14	0.00	50.40	0.00	0.00	2.91	41.13	4.14	0.00	0.00	98.58
KV198PR_3	15	0.00	49.67	0.00	0.00	3.38	37.01	7.56	0.00	0.00	97.62
KV198PR_3	16	0.00	50.26	0.00	0.00	3.64	41.52	3.51	0.07	0.00	98.99
KV198PR_3	17	0.00	50.03	0.00	0.00	2.64	39.16	5.76	0.00	0.00	97.58
KV198PR_3	18	0.00	49.97	0.00	0.00	0.00	43.88	0.33	0.00	0.25	94.43
TP235M_3	3	0.00	49.06	0.00	0.00	6.35	39.45	4.52	0.05	0.00	99.43
TP235M_3	4	0.00	52.45	0.06	0.11	0.54	45.84	0.57	0.42	0.00	99.99
TP235M_3	5	0.00	50.00	0.00	0.00	2.83	41.25	3.56	0.06	0.00	97.70
TP235M_3	6	0.00	51.26	0.00	0.00	2.91	42.29	3.76	0.00	0.00	100.22
TP235M_3	7	0.00	49.59	0.00	0.00	3.41	40.04	4.41	0.05	0.00	97.50

1. UNALTERED ILMENITE

Sample	No.	SiO_2	TiO_2	Al_2O_3	Cr_2O_3	Fe_2O_3	FeO	MnO	MgO	CaO	Total
TP235M_3	9	0.00	51.12	0.00	0.00	2.67	43.56	2.38	0.00	0.00	99.73
TP235M_3	10	0.00	51.31	0.00	0.00	1.50	41.67	4.31	0.06	0.00	98.85
TP235M_3	11	0.00	50.50	0.00	0.00	4.49	40.79	4.56	0.00	0.00	100.34
TP235M_3	12	0.00	48.84	0.05	0.00	5.53	40.66	3.13	0.05	0.00	98.26
TP235M_3	13	0.00	50.08	0.00	0.05	4.83	40.19	4.66	0.07	0.00	99.88
TP235M_3	14	0.00	51.67	0.00	0.00	2.04	42.30	4.11	0.00	0.00	100.12
TP235M_3	15	0.00	47.95	0.00	0.00	7.74	39.44	3.63	0.00	0.00	98.77
TP235M_3	16	0.00	50.69	0.00	0.00	5.17	42.72	2.74	0.05	0.00	101.37
TP235M_3	17	0.00	49.84	0.00	0.00	3.73	40.26	4.38	0.07	0.00	98.27
TP235M_3	18	0.00	50.83	0.00	0.00	2.87	41.06	4.59	0.00	0.00	99.35
TP235M_3	19	0.06	50.96	0.10	0.07	0.00	44.08	1.59	0.05	0.00	96.91
TP235M_3	20	0.00	50.80	0.00	0.00	3.60	41.87	3.76	0.00	0.00	100.03
TP235M_3	22	0.00	47.81	0.14	0.00	6.52	38.67	4.01	0.07	0.11	97.32
TP235M_3	23	0.00	52.46	0.00	0.00	1.04	42.65	4.47	0.00	0.00	100.61
TP235M_3	24	0.00	50.59	0.00	0.00	3.72	39.44	5.98	0.00	0.00	99.72
TP235M_3	25	0.00	52.11	0.00	0.00	0.00	43.64	0.00	0.00	0.00	95.75
TP235M_3	26	0.00	50.20	0.00	0.00	4.71	41.77	3.15	0.10	0.00	99.93
TP235M_3	29	0.00	52.31	0.00	0.00	0.79	45.21	1.81	0.00	0.00	100.12
TP235M_3	30	0.00	52.17	0.00	0.00	0.72	39.95	6.88	0.00	0.00	99.71
TP262N_2	1	0.00	50.23	0.00	0.00	2.67	42.56	2.49	0.05	0.00	98.00
TP262N_2	3	0.00	49.46	0.00	0.00	4.80	40.86	3.57	0.00	0.00	98.69
TP262N_2	4	0.00	49.70	0.00	0.00	4.71	40.17	4.29	0.10	0.00	98.97
TP262N_2	5	0.00	51.80	0.00	0.00	0.00	44.40	2.01	0.00	0.00	98.21
TP262N_2	6	0.00	50.45	0.00	0.00	2.27	42.30	2.87	0.09	0.00	97.98
TP262N_2	8	0.00	50.67	0.00	0.00	3.52	33.12	12.13	0.09	0.00	99.53
TP262N_2	9	0.14	53.57	0.94	0.00	0.00	38.94	2.84	0.09	0.08	96.60
TP262N_2	10	0.00	50.87	0.00	0.00	0.17	43.89	1.83	0.00	0.00	96.76
TP262N_2	11	0.00	49.65	0.00	0.00	2.78	41.98	2.63	0.00	0.00	97.05
TP262N_2	12	0.00	49.61	0.00	0.00	2.78	42.65	1.73	0.12	0.00	96.89
TP262N_2	13	0.00	51.05	0.00	0.00	1.43	41.34	4.40	0.06	0.00	98.28
TP262N_2	14	0.00	49.75	0.20	0.00	1.67	40.18	4.50	0.00	0.00	96.30
TP262N_2	17	0.00	49.01	0.00	0.00	5.81	41.62	2.17	0.14	0.00	98.75
TP262N_2	18	0.00	49.92	0.00	0.00	2.81	41.24	3.60	0.00	0.00	97.57
LH_C_1	2	0.07	51.29	0.15	0.00	0.00	43.57	1.47	0.08	0.00	96.63
LH_C_1	4	0.00	51.17	0.00	0.00	2.39	43.33	2.65	0.00	0.00	99.54
LH_C_1	5	0.00	51.82	0.00	0.00	0.26	42.04	4.31	0.11	0.00	98.54
LH_C_1	7	0.00	50.46	0.00	0.00	3.85	41.32	3.90	0.06	0.00	99.59
LH_C_1	8	0.00	47.87	0.16	0.00	4.99	43.05	0.00	0.00	0.00	96.07
LH_C_1	10	0.00	50.53	0.00	0.00	3.86	41.73	3.66	0.00	0.00	99.79
LH_C_1	11	0.07	51.55	0.07	0.00	0.00	43.01	3.16	0.06	0.00	97.92
LH_C_1	13	0.19	53.95	0.08	0.00	0.00	35.55	6.23	0.06	0.06	96.12
LH_C_1	16	0.00	51.80	0.00	0.00	0.00	42.62	3.74	0.00	0.00	98.16
LH_C_1	19	0.00	52.58	0.00	0.00	0.00	40.94	4.69	0.00	0.00	98.21
LH_C_1	20	0.00	50.48	0.00	0.00	3.27	39.13	6.18	0.00	0.00	99.07
LH_C_1	22	0.00	52.36	0.00	0.00	0.00	42.11	3.95	0.08	0.00	98.50
LH_C_4	5	0.00	52.46	0.00	0.00	0.26	42.30	4.58	0.13	0.00	99.74
LH_C_4	18	0.07	50.28	0.00	0.00	1.51	41.86	3.25	0.08	0.00	97.05
LH_C_4	19	0.00	49.02	0.00	0.00	6.66	40.25	3.61	0.10	0.00	99.64
LH_C_4	20	0.00	48.43	0.00	0.00	7.98	39.40	3.92	0.10	0.00	99.83
NB19AC_1	2	0.00	51.52	0.00	0.00	0.63	41.62	4.65	0.00	0.00	98.42
NB19AC_1	10	0.06	51.47	0.00	0.06	0.00	35.39	8.13	0.09	0.00	95.20
NB21B_3	3	0.00	52.08	0.00	0.00	0.00	43.79	1.95	0.00	0.00	97.82
NB21B_3	4	0.00	50.74	0.00	0.00	2.44	40.63	4.93	0.00	0.00	98.74
NB21B_3	6	0.05	51.06	0.00	0.00	2.55	42.12	3.81	0.00	0.00	99.59
NB21B_3	7	0.00	52.43	0.00	0.00	0.00	40.02	2.78	0.00	0.00	95.23
NB21B_3	10	0.05	52.18	0.00	0.00	0.00	40.63	4.83	0.00	0.00	97.69
NB21B_3	13	0.00	47.14	0.00	0.00	7.28	39.61	2.64	0.06	0.00	96.73

1. UNALTERED ILMENITE

Sample	No.	SiO_2	TiO_2	Al_2O_3	Cr_2O_3	Fe_2O_3	FeO	MnO	MgO	CaO	Total
NB21B_3	16	0.00	48.43	0.00	0.08	8.37	39.88	3.46	0.05	0.06	100.33
NB21B_3	18	0.00	50.37	0.00	0.00	3.29	36.22	8.87	0.05	0.00	98.80
NB21B_5	2	0.07	49.34	0.16	0.00	3.26	39.80	4.59	0.00	0.00	97.23
NB21B_5	3	0.05	46.09	0.00	0.00	12.34	36.70	4.39	0.20	0.00	99.78
NB21B_5	6	0.00	50.69	0.00	0.00	2.65	41.11	4.42	0.00	0.00	98.87
NB21B_5	9	0.00	50.40	0.33	0.00	2.54	35.63	9.48	0.05	0.00	98.43
NB21B_5	14	0.00	49.56	0.00	0.00	4.68	41.74	2.67	0.07	0.00	98.72
NB21B_5	16	0.20	52.73	0.11	0.00	0.00	41.36	2.23	0.10	0.00	96.73
NB21B_5	17	0.23	53.00	0.53	0.00	0.00	40.96	1.34	0.09	0.00	96.15
NB21B_5	18	0.10	51.10	0.00	0.00	0.00	41.30	3.36	0.00	0.00	95.86
NB21B_5	19	0.00	52.50	0.00	0.00	0.00	42.92	3.83	0.00	0.00	99.25
NB21B_5	21	0.00	46.05	0.00	0.08	10.64	40.45	0.83	0.07	0.00	98.12
KN14_3	1	0.00	47.75	0.00	0.00	8.20	39.90	2.65	0.20	0.00	98.70
KN14_3	4	0.00	49.62	0.00	0.15	7.17	42.08	2.14	0.09	0.17	101.42
KN14_3	13	0.00	49.94	0.00	0.00	4.95	41.26	3.60	0.00	0.00	99.76
KN14_3	14	0.18	51.29	0.10	0.00	0.24	45.40	0.82	0.06	0.00	98.09
KN14_3	15	0.00	46.20	0.00	0.00	12.59	37.19	4.09	0.12	0.00	100.19
KN14_3	16	0.00	52.47	0.00	0.00	1.40	41.72	5.10	0.09	0.11	100.89
KN14_3	17	0.00	47.06	0.00	0.00	10.42	41.11	1.19	0.00	0.00	99.78
KN14_3	19	0.00	48.35	0.14	0.09	6.30	42.71	0.60	0.09	0.00	98.28
KN14_3	20	0.00	50.44	0.00	0.00	3.78	43.81	1.44	0.05	0.00	99.52
LKC1-04_11	2	0.06	50.65	0.00	0.00	3.26	41.50	4.07	0.00	0.00	99.54
LKC1-04_11	5	0.00	47.81	0.00	0.00	8.62	41.58	1.29	0.06	0.00	99.36
LKC1-04_11	6	0.00	51.94	0.00	0.00	1.65	41.48	5.16	0.00	0.00	100.24
LKC1-04_11	7	0.05	48.99	0.00	0.00	6.16	41.39	2.57	0.07	0.00	99.23
LKC1-04_11	12	0.00	50.55	0.00	0.00	4.94	42.29	2.93	0.11	0.00	100.82
LKC1-04_11	13	0.00	49.37	0.00	0.00	2.98	40.91	3.32	0.07	0.00	96.65
LKC1-04_11	15	0.99	50.90	0.00	0.00	0.53	44.91	2.02	0.00	0.00	99.35
LKC1-04_11	17	0.65	49.84	0.95	0.00	0.00	42.32	2.05	0.18	0.17	96.16
LKC1-04_11	18	0.06	49.21	0.00	0.00	6.11	40.78	2.76	0.13	0.40	99.45
LKC1-04_11	21	0.00	50.17	0.00	0.00	3.96	43.22	1.73	0.08	0.00	99.16
LKC1-04_2	6	0.05	47.61	0.00	0.00	8.59	39.15	3.46	0.12	0.00	98.98
LKC1-04_2	8	0.00	51.60	0.00	0.05	1.33	42.93	3.29	0.08	0.00	99.27
LKC1-04_2	10	0.15	52.24	0.18	0.00	0.00	43.12	2.99	0.10	0.00	98.78
LKC1-04_2	11	0.00	51.23	0.00	0.00	0.00	41.20	3.53	0.00	0.00	95.96
LKC1-04_2	12	0.00	51.91	0.00	0.00	1.40	42.50	4.13	0.00	0.00	99.94
LKC1-04_2	13	0.00	52.38	0.12	0.00	0.00	43.21	3.67	0.00	0.00	99.38
LKC1-04_2	14	0.00	49.07	0.00	0.00	6.06	39.71	4.36	0.00	0.00	99.20
LKC1-04_2	15	0.00	49.68	0.07	0.00	5.01	39.98	4.51	0.07	0.00	99.32
LKC1-04_9	1	0.00	52.00	0.00	0.00	1.52	43.56	3.16	0.00	0.00	100.24
LKC1-04_9	4	0.00	52.63	0.00	0.00	0.00	44.27	3.01	0.00	0.00	99.91
LKC1-04_9	5	0.00	48.07	0.00	0.05	8.70	42.15	0.96	0.06	0.00	99.99
LKC1-04_9	7	0.63	51.09	0.52	0.00	0.00	40.58	5.31	0.07	0.00	98.20
LKC1-04_9	8	0.00	51.71	0.00	0.00	0.39	42.60	3.85	0.00	0.00	98.55
LKC1-04_9	9	0.00	47.42	0.00	0.00	8.26	41.76	0.87	0.00	0.00	98.31
LKC1-04_9	10	0.00	51.75	0.00	0.00	0.70	38.40	7.91	0.07	0.00	98.83
LKC1-04_9	12	0.00	49.18	0.00	0.00	6.84	41.13	2.67	0.22	0.00	100.03
LKC1-04_9	13	0.05	49.81	0.00	0.00	2.69	41.33	3.48	0.00	0.00	97.36
LKC1-04_9	14	0.00	49.15	0.00	0.00	3.69	41.20	2.80	0.09	0.00	96.93
LKC1-04_9	15	0.00	49.51	0.00	0.05	6.18	41.22	3.26	0.00	0.00	100.22
LKC1-04_9	16	0.00	50.81	0.00	0.00	2.86	43.88	1.70	0.05	0.00	99.30
LKC1-04_9	17	0.48	52.04	0.45	0.06	0.00	37.83	2.19	0.09	0.00	93.14
LKC1-04_9	18	0.00	47.59	0.00	0.00	7.40	40.94	1.83	0.00	0.00	97.76
LKC1-04_9	19	0.00	49.56	0.09	0.00	5.58	42.48	1.90	0.09	0.00	99.70
LKN8-03_1	1	0.00	49.20	0.00	0.00	4.92	38.03	5.99	0.08	0.00	98.22
LKN8-03_1	2	0.00	51.13	0.00	0.00	2.03	42.57	3.26	0.06	0.00	99.05
LKN8-03_1	3	0.00	51.09	0.06	0.00	3.02	43.98	1.64	0.17	0.00	99.96

1. UNALTERED ILMENITE

Sample	No.	SiO_2	TiO_2	Al_2O_3	Cr_2O_3	Fe_2O_3	FeO	MnO	MgO	CaO	Total
LKN8-03_1	4	0.00	51.12	0.06	0.00	1.53	44.81	0.35	0.45	0.00	98.32
LKN8-03_1	5	0.00	50.88	0.06	0.00	1.40	44.05	1.51	0.10	0.00	98.00
LKN8-03_1	6	0.00	51.57	0.00	0.00	0.56	44.32	2.03	0.00	0.00	98.48
LKN8-03_1	8	0.00	52.35	0.07	0.00	0.90	41.53	5.28	0.11	0.00	100.24
LKN8-03_1	10	0.00	50.79	0.00	0.00	1.34	38.70	6.88	0.00	0.00	97.71
LKN8-03_1	11	0.00	50.85	0.00	0.00	3.41	44.64	1.07	0.00	0.00	99.97
LKN8-03_3	1	0.00	50.56	0.00	0.06	4.20	42.16	0.40	1.63	0.00	99.01
LKN8-03_3	2	0.00	48.96	0.00	0.00	6.49	43.25	0.77	0.00	0.00	99.47
LKN8-03_3	4	0.00	52.00	0.00	0.00	0.00	42.25	3.08	0.00	0.00	97.33
LKN8-03_3	5	0.00	50.65	0.00	0.00	1.26	44.75	0.79	0.00	0.00	97.45
LKN8-03_3	9	0.00	50.46	0.00	0.00	3.83	43.59	0.46	0.74	0.00	99.08
LKN8-03_3	10	0.00	49.22	0.10	0.00	6.12	43.02	0.24	0.56	0.00	99.26
LKN8-03_3	11	0.00	51.25	0.00	0.00	1.70	43.53	2.44	0.05	0.00	98.97
LKN8-03_3	13	0.00	47.46	0.00	0.00	9.60	39.12	3.51	0.00	0.00	99.69
LKN8-03_3	17	0.00	50.04	0.00	0.00	3.82	43.41	1.57	0.00	0.00	98.84
SN78-5_6	1	0.00	49.80	0.00	0.07	3.25	42.73	2.03	0.00	0.00	97.88
SN78-5_6	4	0.00	49.76	0.00	0.10	4.53	43.20	1.53	0.00	0.00	99.11
SN78-5_6	5	0.00	50.45	0.00	0.07	2.57	43.55	1.79	0.00	0.00	98.44
LKB01_1	2	0.00	46.69	0.00	0.00	10.65	39.82	1.85	0.13	0.05	99.19
LKB01_1	3	0.00	49.77	0.00	0.00	5.69	43.03	1.70	0.00	0.00	100.19
LKB01_1	4	0.00	51.12	0.00	0.00	2.78	41.48	4.31	0.07	0.00	99.76
LKB01_1	8	0.00	49.94	0.00	0.00	4.58	41.12	3.74	0.00	0.00	99.38
LKB01_1	9	0.00	52.00	0.00	0.00	1.23	43.22	3.24	0.10	0.06	99.85
LKB01_1	11	0.00	49.94	0.00	0.00	5.26	43.91	0.90	0.05	0.00	100.06
LKB01_1	12	0.94	50.69	0.00	0.00	0.78	40.00	6.72	0.08	0.00	98.31
LKB01_1	13	0.00	49.49	0.00	0.00	4.12	40.53	3.92	0.00	0.00	98.06
LKB01_1	14	0.00	50.27	0.00	0.00	4.51	41.77	3.27	0.07	0.00	99.89
LKB01_1	17	0.00	49.33	0.00	0.00	6.27	43.23	1.03	0.05	0.00	99.91
LKB01_1	20	0.00	51.54	0.00	0.00	2.42	38.44	7.61	0.11	0.00	100.12
LKB01_1	22	0.00	51.41	0.00	0.00	1.69	42.89	3.30	0.00	0.00	99.29
LKB01_1	24	0.00	52.62	0.00	0.00	0.00	41.23	5.81	0.07	0.00	99.73
SN78-5_1	3	0.00	51.14	0.00	0.00	3.37	42.74	3.10	0.06	0.00	100.41
SN78-5_1	11	0.00	51.09	0.05	0.00	4.19	43.13	0.42	1.34	0.00	100.22
SN78-5_1	13	0.00	46.58	0.00	0.00	6.37	38.79	3.06	0.00	0.00	94.80
SN78-5_1	18	0.00	52.57	0.00	0.00	2.14	46.48	0.41	0.21	0.00	101.81
SN78-5_1	25	0.00	53.39	0.05	0.00	1.52	46.29	0.49	0.65	0.05	102.44
SN78-5_1	26	0.00	52.27	0.00	0.00	1.88	42.09	4.85	0.00	0.00	101.09
SN78-5_1	27	0.00	52.15	0.00	0.00	3.65	45.48	0.92	0.27	0.00	102.48
SN78-5_1	28	0.00	52.13	0.00	0.00	3.35	44.79	2.06	0.00	0.00	102.34
SN78-5_1	29	0.00	52.32	0.00	0.00	2.26	44.43	2.59	0.00	0.00	101.60
SN78-5_1	30	0.00	52.90	0.00	0.00	1.48	45.04	2.50	0.00	0.00	101.92
	n= 212										
	Avg.	0.04	50.44	0.04	0.01	3.32	41.52	3.30	0.08	0.02	98.76

2. ALTERED ILMENITE

Sample	No.	SiO_2	TiO_2	Al_2O_3	Cr_2O_3	Fe_2O_3	FeO	MnO	MgO	CaO	Total
AK43B_1	6	6.18	82.98	1.51	0.11	3.01	0.00	0.00	0.57	0.19	94.55
AK43B_1	8	0.30	59.70	0.33	0.05	26.88	6.80	0.71	0.20	0.14	95.10
AK43B_1	9	0.90	94.39	0.43	0.15	1.21	0.00	0.09	0.06	0.25	97.48
AK45H_4	9	1.32	83.34	6.31	0.00	5.55	0.00	0.14	0.18	0.40	97.25
DP127R_2	1	0.40	56.90	0.39	0.00	21.01	16.58	2.59	0.17	0.00	98.05
DP127R_2	13	0.20	57.50	0.16	0.00	21.98	15.54	2.18	0.07	0.00	97.63
DP88LM_2	4	0.09	54.18	0.08	0.00	0.27	41.76	3.05	0.00	0.00	99.43
DP88LM_2	14	0.00	55.41	0.00	0.00	0.00	44.22	0.27	0.00	0.00	99.90
KV196R_1	4	0.00	55.17	0.25	0.00	12.55	27.22	5.07	0.11	0.00	100.37
KV196R_1	6	0.13	59.16	0.16	0.00	26.02	9.08	0.87	0.31	0.05	95.79
KV196R_1	7	6.70	77.59	1.40	0.00	4.73	0.00	0.00	0.00	6.50	96.92
KV196R_1	12	0.00	53.47	0.21	0.00	0.00	41.62	4.02	0.09	0.07	99.48
KV196R_1	13	0.06	55.66	0.00	0.00	13.37	26.52	4.11	0.00	0.00	99.73
KV196R_1	14	0.16	59.79	0.21	0.06	27.00	6.12	0.29	0.00	0.10	93.73
KV196R_1	17	0.06	55.02	0.07	0.00	0.00	43.15	2.13	0.00	0.00	100.43
KV196R_1	19	0.31	54.93	0.34	0.00	14.62	24.27	2.45	0.00	0.00	96.91
KV198PR_3	13	0.10	56.27	0.10	0.05	16.70	22.47	1.77	0.00	0.00	97.46
TP262N_2	9	0.14	53.57	0.94	0.00	0.00	43.27	2.84	0.09	0.08	100.93
TP262N_2	16	0.00	79.11	0.00	0.00	21.11	0.18	0.16	0.00	0.00	100.56
LH_C_1	1	0.00	56.54	0.07	0.00	10.48	31.00	1.84	0.00	0.00	99.92
LH_C_1	6	0.07	57.94	0.07	0.00	22.56	14.96	1.55	0.00	0.00	97.15
LH_C_1	9	0.00	53.16	0.00	0.00	0.00	46.39	3.97	0.08	0.00	103.60
LH_C_1	12	0.00	55.45	0.00	0.00	18.79	18.77	8.12	0.00	0.00	101.13
LH_C_1	13	0.19	53.95	0.08	0.00	10.23	29.27	6.23	0.06	0.06	100.08
LH_C_1	14	0.07	55.37	0.05	0.00	9.53	31.29	3.19	0.16	0.00	99.66
LH_C_1	18	0.07	56.01	0.00	0.00	11.97	28.65	2.81	0.00	0.00	99.51
LH_C_1	21	0.00	55.26	0.00	0.00	4.32	37.70	2.57	0.00	0.00	99.85
LH_C_1	23	0.08	57.18	0.06	0.00	18.95	19.99	2.52	0.00	0.05	98.83
LH_C_1	24	0.16	57.87	0.09	0.00	21.09	17.32	1.57	0.10	0.00	98.20
LH_C_1	25	0.06	53.91	0.35	0.05	9.53	30.15	4.74	0.14	0.00	98.92
LH_C_4	1	0.08	56.23	0.05	0.00	12.68	27.90	1.62	0.00	0.00	98.55
LH_C_4	2	0.10	56.27	0.25	0.00	16.65	22.55	2.66	0.08	0.00	98.56
LH_C_4	3	0.11	56.67	0.28	0.00	22.55	13.78	4.02	0.09	0.00	97.50
LH_C_4	6	0.06	55.36	0.13	0.00	7.10	34.34	4.14	0.13	0.00	101.26
LH_C_4	7	0.14	54.73	0.23	0.00	16.61	21.34	3.46	0.10	0.05	96.66
LH_C_4	8	0.17	57.94	0.17	0.00	23.48	13.31	2.94	0.07	0.07	98.16
LH_C_4	9	0.20	59.12	0.17	0.00	25.96	9.20	3.14	0.00	0.00	97.79
LH_C_4	10	0.11	56.92	0.11	0.00	21.74	15.41	3.43	0.06	0.00	97.78
LH_C_4	11	0.16	56.79	0.18	0.00	18.25	20.69	2.71	0.06	0.00	98.84
LH_C_4	12	0.12	54.85	0.00	0.00	4.97	36.58	2.72	0.07	0.00	99.31
LH_C_4	13	0.07	54.86	0.07	0.00	0.00	42.71	2.29	0.00	0.00	100.00
LH_C_4	15	0.14	55.39	1.03	0.00	20.57	15.96	7.54	0.12	0.06	100.81
NB19AC_1	1	0.23	55.83	0.06	0.06	12.62	27.65	0.80	0.25	0.00	97.50
NB19AC_1	3	0.21	56.48	0.00	0.00	24.10	10.54	3.99	0.05	0.00	95.37
NB19AC_1	4	0.26	57.12	0.58	0.00	24.40	10.60	4.14	0.09	0.07	97.25
NB19AC_1	5	0.08	55.28	0.00	0.00	5.50	36.26	3.68	0.00	0.00	100.80
NB19AC_1	6	0.12	56.10	0.17	0.00	19.86	17.71	3.36	0.11	0.00	97.42
NB19AC_1	7	0.18	57.50	0.18	0.00	25.66	7.61	5.21	0.13	0.00	96.47
NB19AC_1	8	0.13	55.21	0.07	0.00	19.40	17.64	4.01	0.05	0.00	96.51
NB19AC_1	9	0.21	53.64	0.08	0.00	15.17	22.47	3.68	0.09	0.05	95.39
NB19AC_1	11	0.13	57.03	0.00	0.00	22.97	13.37	3.63	0.06	0.00	97.19
NB19AC_1	12	0.19	57.00	0.52	0.00	23.21	12.90	2.43	0.07	0.05	96.37
NB19AC_1	13	0.19	57.01	0.07	0.00	23.44	12.47	2.81	0.12	0.00	96.11
NB19AC_1	14	0.24	55.68	0.06	0.00	21.29	15.04	3.45	0.06	0.00	95.82
NB19AC_1	16	0.20	56.99	0.00	0.00	23.18	12.94	3.34	0.11	0.00	96.76
NB19AC_1	17	0.17	57.96	0.00	0.00	25.73	8.16	4.75	0.09	0.00	96.86
NB21B_3	1	0.09	55.84	0.00	0.00	9.94	31.13	2.08	0.00	0.00	99.08

2. ALTERED ILMENITE

Sample	No.	SiO_2	TiO_2	Al_2O_3	Cr_2O_3	Fe_2O_3	FeO	MnO	MgO	CaO	Total
NB21B_3	2	0.31	57.81	0.16	0.00	22.97	14.11	2.11	0.00	0.00	97.47
NB21B_3	5	0.07	57.59	0.09	0.00	18.78	20.58	2.38	0.00	0.00	99.49
NB21B_3	8	0.12	58.01	0.08	0.00	21.82	16.27	1.84	0.00	0.00	98.13
NB21B_3	9	0.21	57.64	0.12	0.00	24.00	12.00	2.77	0.00	0.08	96.83
NB21B_3	11	0.06	54.71	0.08	0.00	15.28	23.18	2.05	0.05	0.00	95.41
NB21B_3	12	0.53	59.31	0.63	0.00	26.32	8.38	1.51	0.07	0.08	96.84
NB21B_3	14	0.22	58.37	0.25	0.00	25.42	9.67	2.13	0.10	0.00	96.15
NB21B_3	17	0.05	53.97	0.06	0.00	0.00	42.47	4.30	0.00	0.05	100.90
NB21B_5	4	1.60	57.27	1.13	0.00	24.29	11.00	1.84	0.13	0.07	97.33
NB21B_5	5	1.81	70.09	1.61	0.00	22.62	0.41	0.09	0.05	0.13	96.82
NB21B_5	7	0.05	53.64	0.00	0.00	0.00	46.70	1.90	0.00	0.00	102.29
NB21B_5	12	0.18	58.22	0.14	0.00	23.93	12.74	2.88	0.00	0.00	98.09
NB21B_5	15	2.06	54.26	3.18	0.00	22.68	11.12	3.53	0.14	0.17	97.15
NB21B_5	25	0.34	54.31	0.26	0.00	6.39	34.40	4.35	0.10	0.00	100.16
LKC1-04_2	3	8.00	79.62	1.41	0.13	0.88	0.00	0.00	0.17	3.51	93.72
LKC1-04_2	4	0.61	57.49	4.55	0.00	25.90	6.44	2.27	0.13	0.20	97.59
LKC1-04_2	7	4.17	59.77	2.64	0.00	22.20	0.80	6.23	0.36	0.21	96.38
LKN8-03_1	7	0.47	61.27	0.21	0.05	27.66	5.17	1.26	0.09	0.19	96.37
LKN8-03_3	7	0.42	59.33	0.19	0.00	23.81	14.06	0.49	0.27	0.05	98.62
LKN8-03_3	12	0.37	53.91	0.14	0.06	0.00	44.56	1.39	0.11	0.00	100.54
SN78-5_6	2	1.25	65.88	1.07	0.08	25.49	1.15	0.57	0.17	0.12	95.78
SN78-5_6	3	0.49	54.59	1.36	0.08	11.31	28.38	0.95	0.15	0.11	97.43
SN78-5_6	6	0.30	58.18	0.29	0.00	25.88	8.03	2.32	0.28	0.10	95.38
SN78-5_6	7	0.32	57.76	0.33	0.00	25.12	9.66	2.37	0.33	0.06	95.94
SN78-5_6	8	1.66	62.96	2.17	0.00	24.23	1.06	1.70	0.43	0.19	94.40
SN78-5_6	9	0.33	58.85	0.33	0.00	26.58	5.93	3.36	0.42	0.05	95.85
SN78-5_6	11	1.44	85.42	1.49	0.00	7.26	0.00	0.84	0.22	0.07	96.75
6869F3-02_2	1	0.13	55.90	6.66	0.05	22.89	12.41	2.20	0.05	0.10	100.38
6869F3-02_2	2	0.13	57.29	0.16	0.00	21.50	16.14	1.97	0.05	0.06	97.30
6869F3-02_2	3	0.21	58.02	0.78	0.06	24.04	12.32	1.74	0.00	0.07	97.24
6869F3-02_2	4	0.14	56.83	0.21	0.14	20.80	16.86	0.45	0.50	0.09	96.02
6869F3-02_2	5	0.11	57.23	0.09	0.07	23.87	11.83	1.41	0.05	0.10	94.77
6869F3-02_2	6	0.13	58.93	0.16	0.00	26.51	6.86	2.61	0.06	0.00	95.25
6869F3-02_2	7	0.17	57.84	0.95	0.00	24.17	11.86	2.29	0.05	0.06	97.40
6869F3-02_2	8	0.14	57.73	0.21	0.00	22.99	14.00	1.62	0.05	0.00	96.75
6869F3-02_2	9	0.29	56.65	0.45	0.06	18.21	20.63	1.79	0.09	0.00	98.17
6869F3-02_2	10	7.52	94.31	0.00	0.00	0.23	0.00	0.00	0.00	0.23	102.29
6869F3-02_2	12	0.12	55.39	0.18	0.00	20.89	15.44	2.20	0.06	0.06	94.34
6869F3-02_2	14	0.13	57.10	0.13	0.08	19.90	18.49	0.40	0.08	0.00	96.32
6869F3-02_2	15	0.13	57.59	0.18	0.06	21.47	16.46	0.43	0.91	0.00	97.23
6869F3-02_2	16	0.17	54.58	4.09	0.00	18.42	18.58	1.17	0.06	0.08	97.16
6869F3-02_2	17	0.12	59.02	0.95	0.00	26.63	6.27	3.52	0.00	0.07	96.57
6869F3-02_2	18	0.10	57.65	0.09	0.05	24.32	11.37	2.80	0.07	0.09	96.53
AK1_2	1	0.17	61.14	0.10	0.00	27.52	4.61	1.76	0.17	0.07	95.54
AK1_2	2	0.20	63.29	0.15	0.00	26.27	1.84	1.56	0.10	0.16	93.56
AK1_2	3	0.12	59.60	0.18	0.05	26.90	4.94	1.60	0.00	0.09	93.48
AK1_2	4	0.12	59.94	0.06	0.00	26.77	3.81	4.65	0.00	0.09	95.44
AK1_2	5	0.12	61.58	0.08	0.00	27.49	3.88	1.49	0.10	0.06	94.80
AK1_2	7	0.17	63.34	0.08	0.00	26.70	2.10	1.04	0.12	0.10	93.65
AK1_2	8	0.15	59.80	0.12	0.00	27.01	6.00	1.67	0.09	0.00	94.84
AK1_2	9	0.09	58.26	0.10	0.00	24.84	10.91	0.39	0.05	0.08	94.72
AK1_2	10	0.13	56.67	0.15	0.00	22.37	14.11	0.96	0.07	0.06	94.51
AK1_2	11	0.14	59.40	0.10	0.00	26.83	5.86	1.12	0.05	0.07	93.57
AK1_2	12	0.19	59.73	0.14	0.05	26.71	7.69	1.51	0.07	0.05	96.15
AK1_2	13	0.11	59.83	0.08	0.05	26.50	8.64	1.55	0.07	0.00	96.83
AK1_2	14	0.30	60.40	0.15	0.00	27.28	5.36	1.22	0.09	0.08	94.88
AK1_2	15	0.20	60.22	0.20	0.00	26.99	7.49	1.27	0.12	0.07	96.56

2. ALTERED ILMENITE

Sample	No.	SiO_2	TiO_2	Al_2O_3	Cr_2O_3	Fe_2O_3	FeO	MnO	MgO	CaO	Total
AK1_2	16	0.20	62.25	0.15	0.05	27.84	4.06	0.99	0.16	0.14	95.83
AK1_2	17	0.18	61.12	0.15	0.08	27.62	5.67	1.67	0.00	0.00	96.48
AK1_2	18	0.13	59.60	0.18	0.06	26.41	8.56	1.28	0.09	0.00	96.31
AK1_2	19	0.19	59.60	0.17	0.00	26.83	6.80	0.96	0.17	0.08	94.80
AK1_2	20	0.18	59.92	0.11	0.00	26.02	10.11	0.99	0.09	0.09	97.51
AK1_2	21	0.16	60.63	0.13	0.00	27.18	4.14	2.91	0.23	0.09	95.47
AK1_2	22	0.16	60.86	0.20	0.00	27.49	5.37	1.43	0.06	0.06	95.63
LKB01_1	1	0.42	58.86	0.11	0.00	25.22	10.74	1.40	0.16	0.00	96.91
LKB01_1	15	0.06	54.49	0.00	0.00	0.00	46.60	1.66	0.00	0.00	102.81
LKB01_1	18	0.19	53.22	0.09	0.00	0.00	44.15	2.15	0.00	0.00	99.80
LKB01_1	19	0.23	56.80	0.05	0.00	17.59	21.65	1.84	0.00	0.00	98.16
LKB01_1	21	0.00	53.78	0.00	0.00	0.00	48.31	2.18	0.00	0.00	104.27
SN78-5_1	1	0.17	54.34	0.09	0.00	24.54	4.75	8.97	0.00	0.05	92.91
SN78-5_1	2	0.11	58.51	0.11	0.00	22.82	15.05	0.91	0.05	0.00	97.55
SN78-5_1	5	0.23	58.44	0.08	0.00	23.41	13.93	1.60	0.06	0.06	97.81
SN78-5_1	7	0.19	57.68	0.06	0.00	21.24	16.92	1.50	0.07	0.00	97.65
SN78-5_1	8	0.11	57.86	0.07	0.00	22.15	15.58	3.67	0.13	0.00	99.57
SN78-5_1	9	0.11	59.17	0.07	0.00	26.46	7.64	5.01	0.05	0.00	98.50
SN78-5_1	14	0.22	56.83	0.12	0.00	25.67	5.04	4.85	0.09	0.09	92.92
SN78-5_1	15	0.17	57.81	0.08	0.00	23.88	12.43	2.12	0.11	0.00	96.60
SN78-5_1	16	0.13	58.21	0.10	0.00	23.83	12.92	1.81	0.07	0.00	97.07
SN78-5_1	17	0.00	55.24	0.07	0.00	19.91	16.87	2.24	0.07	0.00	94.40
SN78-5_1	19	0.19	58.40	0.13	0.00	24.10	12.59	1.09	0.09	0.09	96.69
SN78-5_1	21	0.19	59.70	0.23	0.05	26.94	4.99	1.99	0.10	0.08	94.28
SN78-5_1	23	0.10	61.17	0.00	0.00	27.64	5.71	2.68	0.05	0.00	97.35
SN78-5_1	24	0.08	59.38	0.06	0.00	25.67	10.30	3.48	0.11	0.00	99.08
	n= 140										
	Avg.	0.47	59.04	0.44	0.01	18.71	16.15	2.36	0.10	0.12	97.39

3. HEMATITE

Sample	No.	SiO_2	TiO_2	Al_2O_3	Cr_2O_3	Fe_2O_3	FeO	MnO	MgO	CaO	Total
KV196R_1	4	0.00	0.00	0.25	0.00	98.25	0.00	0.00	0.00	0.00	98.50
KV196R_1	6	0.13	0.00	0.16	0.00	96.45	0.00	0.00	0.00	0.00	96.74
KV196R_1	7	0.07	0.20	0.40	0.00	96.90	0.00	0.00	0.00	0.00	97.57
KV196R_1	12	0.00	0.50	0.21	0.00	95.98	0.00	0.00	0.00	0.00	96.69
LH_C_1	9	0.00	0.00	0.00	0.00	99.89	0.00	0.00	0.00	0.00	99.89
LH_C_1	12	0.00	0.00	0.00	0.00	98.23	0.02	0.01	0.00	0.01	98.27
LH_C_1	13	0.12	0.00	0.08	0.00	97.23	0.02	0.00	0.00	0.00	97.45
LH_C_1	14	0.07	0.00	0.05	0.00	99.65	0.53	0.00	0.00	0.00	100.30
SN78-5_6	6	0.03	0.00	0.29	0.00	97.64	0.00	0.00	0.00	0.00	97.96
SN78-5_6	7	0.02	0.76	0.33	0.00	96.74	0.00	0.02	0.00	0.02	97.89
SN78-5_6	8	0.06	0.00	0.17	0.00	99.26	0.23	0.00	0.00	0.00	99.72
SN78-5_6	9	0.03	0.42	0.33	0.00	99.86	0.08	0.00	0.00	0.00	100.72
SN78-5_6	11	0.04	0.05	0.49	0.00	99.01	0.26	0.00	0.00	0.00	99.85
	n= 13										
	Avg.	0.04	0.15	0.21	0.00	98.08	0.09	0.00	0.00	0.00	98.58

4. TITANOHEMATITE

Sample	No.	SiO_2	TiO_2	Al_2O_3	Cr_2O_3	Fe_2O_3	FeO	MnO	MgO	CaO	Total
AK45H_4	6	0.00	24.38	0.05	0.07	17.58	50.27	1.38	0.09	0.00	93.82
AK45H_4	12	0.00	32.45	0.00	0.00	38.16	28.30	0.55	0.18	0.00	99.64
KV196R_1	11	0.00	39.73	0.00	0.00	23.02	32.54	3.15	0.00	0.00	98.44
KV198PR_3	1	0.00	25.45	0.00	0.00	49.03	21.28	1.51	0.00	0.06	97.33
TP235M_3	28	0.00	41.55	0.00	0.00	20.47	34.71	2.62	0.00	0.00	99.35
TP262N_2	7	0.00	36.44	0.21	0.00	25.55	32.60	0.17	0.00	0.00	94.97
TP262N_2	15	0.00	33.32	0.00	0.05	33.03	28.17	1.59	0.10	0.00	96.27
KN14_3	11	0.00	22.50	0.00	0.00	22.22	48.78	1.66	0.00	0.00	95.17
LKC1-04_11	9	0.06	45.09	0.00	0.00	14.29	32.20	8.31	0.00	0.00	99.95
LKC1-04_11	16	0.06	39.58	0.05	0.08	21.66	33.90	1.74	0.00	0.00	97.07
LKC1-04_2	2	0.00	33.85	0.00	0.00	34.75	24.92	5.36	0.05	0.00	98.93
LKC1-04_2	5	0.00	43.88	0.00	0.07	16.59	38.63	0.61	0.12	0.00	99.90
LKN8-03_3	14	0.00	43.70	0.00	0.17	16.50	35.65	3.32	0.16	0.00	99.50
LKB01_1	6	0.00	38.59	0.00	0.00	24.75	32.20	2.36	0.06	0.00	97.97
LKB01_1	7	0.00	44.46	0.00	0.00	13.67	36.01	3.81	0.06	0.00	98.02
	n= 15										
	Avg.	0.01	36.33	0.02	0.03	24.75	34.01	2.54	0.05	0.00	97.76

5. MAGNETITE

Sample	No.	SiO_2	TiO_2	Al_2O_3	Cr_2O_3	Fe_2O_3	FeO	MnO	MgO	CaO	Total
AK43B_1	3	0.00	0.05	0.27	0.00	63.25	28.49	0.18	0.00	0.05	92.29
AK43B_1	10	0.00	15.79	0.06	0.21	34.78	42.70	1.47	0.00	0.00	95.01
AK45H_4	3	0.00	9.82	0.00	0.10	46.15	38.19	0.28	0.00	0.00	94.54
AK45H_4	4	0.08	0.00	0.24	0.00	63.89	28.93	0.10	0.00	0.06	93.30
AK45H_4	11	0.06	0.00	0.26	0.07	63.95	29.07	0.00	0.00	0.05	93.47
AK45H_4	13	0.17	1.52	0.76	0.06	61.04	30.81	0.35	0.00	0.00	94.71
AK45H_4	14	0.16	0.06	0.14	0.00	64.70	29.70	0.00	0.00	0.00	94.76
AK52N_2	3	0.00	2.61	0.11	0.00	59.65	31.13	0.27	0.06	0.08	93.90
DP127R_2	15	0.00	3.05	0.39	0.00	58.38	31.91	0.12	0.00	0.00	93.85
DP88LM_2	9	0.19	0.05	0.42	0.14	64.23	29.80	0.00	0.00	0.00	94.83
DP88LM_2	13	1.61	11.66	1.01	0.00	37.08	41.63	0.00	0.33	0.00	93.31
KV196R_1	5	0.00	13.24	0.12	0.00	38.16	40.98	0.00	0.05	0.00	92.55
KV198PR_3	5	0.00	16.47	0.05	1.42	31.32	43.88	0.15	0.22	0.00	93.51
KV198PR_3	12	0.19	0.06	0.10	0.09	64.98	29.91	0.00	0.00	0.00	95.33
TP262N_2	2	0.00	9.61	0.21	0.00	46.03	37.68	0.45	0.00	0.00	93.98

5. MAGNETITE

Sample	No.	SiO_2	TiO_2	Al_2O_3	Cr_2O_3	Fe_2O_3	FeO	MnO	MgO	CaO	Total
NB21B_5	8	0.08	0.21	0.16	0.00	62.77	28.92	0.00	0.00	0.00	92.15
NB21B_5	13	0.00	18.92	0.06	0.00	28.92	47.08	0.00	0.00	0.00	94.98
NB21B_5	22	0.06	19.63	0.00	0.00	26.89	46.68	0.85	0.00	0.00	94.11
KN14_3	2	0.00	12.68	0.05	0.07	40.73	41.03	0.17	0.00	0.00	94.73
KN14_3	5	0.05	18.13	0.05	0.00	30.54	43.96	2.42	0.05	0.00	95.20
KN14_3	9	0.00	6.87	0.21	0.05	51.57	35.73	0.00	0.00	0.00	94.42
LKC1-04_11	3	0.05	9.97	0.08	0.13	45.34	38.42	0.14	0.00	0.00	94.13
LKC1-04_11	4	0.00	13.90	0.05	0.08	38.86	41.74	0.81	0.00	0.00	95.44
LKC1-04_11	8	0.00	10.51	0.10	0.07	45.19	38.70	0.63	0.00	0.00	95.20
LKC1-04_11	10	0.00	12.24	0.08	0.13	40.44	40.13	0.19	0.00	0.00	93.21
LKC1-04_11	11	0.00	6.52	0.25	0.25	52.45	35.48	0.14	0.00	0.00	95.08
LKC1-04_11	14	0.06	8.47	0.12	0.27	48.52	37.26	0.16	0.00	0.00	94.86
LKC1-04_11	19	0.05	9.07	0.10	0.10	48.59	38.24	0.17	0.00	0.00	96.32
LKC1-04_11	20	0.05	9.07	0.10	0.10	48.59	38.24	0.17	0.00	0.00	96.32
LKC1-04_11	22	0.06	11.17	0.09	0.10	43.30	39.61	0.21	0.00	0.00	94.55
LKC1-04_9	3	0.06	13.13	0.12	0.00	38.61	40.47	0.35	0.08	0.19	93.01
KV198PR_1	1	0.07	16.96	1.65	0.08	30.76	44.89	0.28	0.26	0.06	95.01
KV198PR_1	2	0.92	14.12	2.51	0.05	32.97	42.96	0.65	0.26	0.11	94.55
KV198PR_1	3	0.31	18.17	0.80	0.00	28.88	46.30	0.39	0.07	0.12	95.04
KV198PR_1	4	0.19	16.68	1.82	0.05	31.58	45.27	0.35	0.19	0.00	96.13
KV198PR_1	5	1.29	0.33	0.82	0.53	62.22	32.41	0.00	0.05	0.00	97.65
KV198PR_1	6	0.25	16.18	1.07	0.07	32.07	44.42	0.35	0.08	0.00	94.49
KV198PR_1	7	0.00	0.15	0.07	0.00	68.07	30.95	0.00	0.00	0.00	99.24
KV198PR_1	8	0.12	16.75	1.21	0.06	32.35	45.33	0.37	0.08	0.00	96.27
KV198PR_1	9	0.07	14.66	2.07	0.09	35.76	43.22	0.31	0.33	0.00	96.51
KV198PR_1	10	0.21	16.23	1.19	0.10	32.42	44.68	0.32	0.09	0.00	95.24
KV198PR_1	11	0.25	14.93	0.80	0.08	34.46	43.05	0.24	0.15	0.00	93.96
KV198PR_1	13	0.05	8.29	3.84	0.00	49.75	31.95	0.29	4.42	0.00	98.59
KV198PR_1	14	0.00	0.05	0.06	0.00	67.47	30.40	0.09	0.00	0.00	98.07
LHC_3	15	0.00	1.71	1.76	0.00	64.76	25.81	0.37	4.03	0.07	98.51
LHC_3	16	0.07	15.12	1.03	0.08	36.18	44.04	0.25	0.06	0.00	96.83
LHC_3	17	0.00	0.09	0.15	0.00	67.02	30.10	0.32	0.00	0.00	97.67
LHC_3	18	0.00	0.16	0.09	0.00	66.69	30.19	0.17	0.00	0.00	97.30
LHC_3	19	0.00	0.00	0.06	0.00	67.45	30.39	0.00	0.00	0.00	97.89
LHC_3	20	0.00	14.29	0.11	0.24	37.21	41.93	0.61	0.05	0.00	94.44
LHC_3	21	0.12	17.12	1.74	0.08	30.01	44.81	0.49	0.26	0.06	94.69
LHC_3	22	0.00	0.05	0.33	0.00	67.57	30.73	0.00	0.00	0.00	98.68
LHC_3	23	0.13	16.54	0.51	0.08	33.95	45.27	0.37	0.05	0.00	96.90
LHC_3	24	0.06	15.18	0.91	0.08	36.45	44.06	0.30	0.09	0.00	97.13
LHC_3	25	0.00	14.73	1.67	0.20	35.73	43.10	0.36	0.21	0.00	96.00
LHC_3	26	0.07	16.75	1.24	0.10	32.28	45.24	0.30	0.11	0.00	96.09
LHC_3	29	0.45	17.01	1.45	0.09	28.30	44.75	0.32	0.22	0.00	92.59
LHC_3	30	0.00	0.00	0.00	0.00	67.84	30.35	0.17	0.00	0.00	98.36
	n= 58										
	Avg.	0.13	9.43	0.60	0.09	46.54	37.98	0.30	0.20	0.01	95.29

6. RUTILE

Sample	No.	SiO_2	TiO_2	Al_2O_3	Cr_2O_3	Fe_2O_3	FeO	MnO	MgO	CaO	Total
AK43B_1	6	0.00	99.74	0.00	0.00	0.00	0.39	0.00	0.00	0.00	100.13
AK43B_1	8	0.00	99.59	0.00	0.00	0.00	0.51	0.00	0.00	0.00	100.10
AK43B_1	9	0.00	99.33	0.00	0.00	0.00	0.42	0.00	0.00	0.00	99.75
AK52N_2	5	0.00	99.37	0.00	0.01	0.00	0.00	0.00	0.00	0.05	99.43
AK52N_2	6	0.00	99.37	0.00	0.01	0.00	0.00	0.00	0.00	0.05	99.43
AK52N_2	8	0.00	99.37	0.00	0.01	0.00	0.33	0.00	0.00	0.05	99.76
NB19AC_1	2	0.02	97.77	0.00	0.00	0.00	0.89	0.00	0.00	0.00	98.68
NB19AC_1	10	0.00	96.98	0.00	0.00	0.00	0.71	0.00	0.00	0.00	97.69
NB21B_5	3	0.02	99.03	0.00	0.00	0.00	0.45	0.00	0.00	0.00	99.50
NB21B_5	4	0.00	98.83	0.00	0.00	0.00	0.23	0.00	0.00	0.00	99.06
LKC1-04_9	8	0.00	99.00	0.00	0.00	0.00	0.00	0.00	0.00	0.00	99.00
LKC1-04_9	9	0.00	99.00	0.00	0.00	0.00	0.00	0.00	0.00	0.00	99.00
LKC1-04_9	10	0.00	99.00	0.00	0.00	0.00	0.00	0.00	0.00	0.00	99.00
LKN8-03_3	1	0.00	99.41	0.00	0.00	0.00	0.40	0.00	0.00	0.00	99.81
LKN8-03_3	2	0.01	99.30	0.00	0.00	0.00	0.56	0.00	0.00	0.00	99.87
LKN8-03_3	3	0.00	98.33	0.00	0.00	0.00	0.00	0.00	0.00	0.00	98.33
LKN8-03_3	4	0.00	99.25	0.00	0.00	0.00	0.00	0.00	0.00	0.00	99.25
LKN8-03_3	5	0.00	98.99	0.00	0.00	0.00	0.00	0.00	0.00	0.00	98.99
LKN8-03_3	6	0.01	98.33	0.00	0.00	0.00	0.00	0.00	0.00	0.00	98.34
	n= 19										
	Avg.	0.00	98.95	0.00	0.00	0.00	0.26	0.00	0.00	0.01	99.22

7. ZIRCON

Sample	No.	SiO_2	ZrO_2	HfO_2	Al_2O_3	Y_2O_3	P_2O_5	ThO_2	UO_2	K_2O	CaO	MgO	FeO	Total
AK45H_1	1	33.90	63.25	1.33	0.02	0.23	0.04	0.04	0.00	0.00	0.01	0.00	0.07	98.91
AK45H_1	2	34.50	64.61	1.19	0.02	0.19	0.12	0.00	0.00	0.00	0.01	0.00	0.09	100.72
AK45H_1	3	34.11	62.74	1.47	0.03	0.29	0.23	0.00	0.00	0.00	0.01	0.00	0.13	99.00
AK45H_1	4	34.03	63.68	1.21	0.02	0.10	0.00	0.04	0.00	0.00	0.01	0.00	0.12	99.23
AK52N_1	1	34.15	64.64	1.09	0.01	0.00	0.00	0.00	0.00	0.00	0.02	0.00	0.08	99.99
AK52N_1	2	34.03	64.21	1.42	0.02	0.00	0.05	0.00	0.01	0.00	0.00	0.00	0.19	99.93
AK52N_1	3	33.94	65.29	1.29	0.01	0.53	0.09	0.02	0.00	0.00	0.01	0.00	0.07	101.26
TP262N_4	1	34.13	65.50	1.09	0.00	0.29	0.19	0.00	0.00	0.00	0.01	0.00	0.07	101.28
TP262N_4	2	34.25	64.94	1.43	0.01	0.25	0.10	0.02	0.00	0.00	0.01	0.00	0.08	101.09
TP262N_4	3	34.09	65.47	1.53	0.02	0.09	0.03	0.04	0.06	0.00	0.00	0.00	0.12	101.86
TP262N_4	4	34.46	65.13	1.40	0.00	0.13	0.03	0.07	0.00	0.00	0.02	0.00	0.00	101.24
NB19AC_1	1	32.08	66.89	1.55	0.00	0.09	0.10	0.00	0.00	0.00	0.00	0.00	0.04	100.75
NB19AC_1	2	31.99	65.32	1.57	0.03	0.34	0.21	0.06	0.02	0.01	0.02	0.00	0.05	99.60
NB19AC_1	3	31.78	65.33	1.72	0.00	0.25	0.10	0.07	0.07	0.00	0.01	0.01	0.10	99.43
NB19AC_1	5	32.65	66.16	1.41	0.00	0.13	0.05	0.04	0.00	0.00	0.00	0.00	0.05	100.48
NB19AC_1	6	32.58	65.87	1.72	0.00	0.10	0.05	0.05	0.00	0.00	0.01	0.01	0.03	100.42
NB19AC_1	7	32.24	65.68	1.60	0.00	0.08	0.04	0.01	0.01	0.01	0.00	0.02	0.05	99.75
NB19AC_1	8	32.42	66.01	1.60	0.03	0.45	0.17	0.00	0.00	0.01	0.00	0.00	0.13	100.83
NB19AC_1	9	32.34	68.45	1.42	0.00	0.13	0.00	0.04	0.00	0.00	0.00	0.00	0.04	102.44
NB19AC_1	10	32.10	66.17	1.62	0.00	0.12	0.07	0.04	0.00	0.04	0.01	0.01	0.07	100.25
NB19AC_1	11	32.54	66.32	1.54	0.01	0.29	0.17	0.07	0.00	0.01	0.01	0.02	0.04	101.02
NB21B_4	1	31.92	67.15	1.15	0.00	0.25	0.00	0.00	0.00	0.00	0.01	0.00	0.02	100.49
NB21B_4	2	31.19	66.57	1.57	0.01	0.26	0.07	0.09	0.00	0.00	0.01	0.00	0.04	99.82
NB21B_4	3	32.08	66.20	1.28	0.00	0.40	0.07	0.10	0.00	0.00	0.00	0.01	0.05	100.19
NB21B_4	4	31.86	67.45	1.26	0.00	0.03	0.00	0.01	0.00	0.01	0.00	0.00	0.05	100.67
NB21B_4	6	31.08	66.10	1.60	0.00	0.32	0.03	0.00	0.00	0.01	0.01	0.01	0.02	99.18
NB21B_4	7	32.31	66.10	1.57	0.00	0.16	0.13	0.00	0.00	0.00	0.00	0.00	0.04	100.31
KN17_2	1	32.43	65.48	1.49	0.00	0.33	0.22	0.01	0.00	0.00	0.01	0.00	0.04	99.99
KN17_2	2	32.45	63.77	1.26	0.13	0.02	0.14	0.06	0.00	0.00	0.04	0.00	0.23	98.11
KN17_2	3	32.08	64.88	1.44	0.01	0.32	0.24	0.00	0.02	0.00	0.01	0.00	0.07	99.05
KN17_2	4	31.25	65.29	1.35	0.00	0.06	0.03	0.05	0.00	0.00	0.00	0.00	0.03	98.06
KN17_2	5	32.46	65.71	1.67	0.01	0.20	0.01	0.03	0.00	0.00	0.01	0.00	0.09	100.17
LKB01_4	1	32.62	66.84	1.35	0.03	0.11	0.06	0.05	0.05	0.01	0.01	0.02	0.13	101.28
LKB01_4	2	32.61	67.76	1.12	0.01	0.18	0.02	0.00	0.00	0.00	0.02	0.02	0.11	101.85
LKB01_4	4	31.86	66.02	1.22	0.01	0.23	0.08	0.01	0.00	0.00	0.00	0.00	0.09	99.51
LKB01_4	5	32.98	66.85	1.09	0.01	0.09	0.06	0.08	0.00	0.00	0.00	0.00	0.09	101.24
LKB01_4	6	32.86	66.22	1.25	0.02	0.00	0.04	0.03	0.00	0.00	0.00	0.00	0.07	100.48
LKB01_4	7	32.92	65.41	1.22	0.02	0.11	0.02	0.01	0.00	0.00	0.00	0.00	0.03	99.72
LKN8-03_3	1	31.87	66.96	1.43	0.00	0.05	0.10	0.00	0.00	0.00	0.00	0.00	0.07	100.49
LKN8-03_3	2	32.24	66.46	1.15	0.00	0.11	0.04	0.01	0.01	0.00	0.02	0.00	0.09	100.12
LKN8-03_3	3	32.60	65.48	1.30	0.00	0.30	0.05	0.00	0.00	0.00	0.00	0.00	0.14	99.87
LKN8-03_3	4	32.19	67.14	1.16	0.00	0.27	0.10	0.06	0.00	0.00	0.02	0.00	0.05	100.99
LKN8-03_3	5	32.27	65.67	1.56	0.00	0.04	0.00	0.00	0.00	0.00	0.02	0.00	0.06	99.62
SN78-5_5	1	34.17	63.64	1.23	0.04	0.08	0.05	0.00	0.00	0.00	0.01	0.00	0.12	99.34
SN78-5_5	2	34.01	64.48	1.21	0.00	0.17	0.07	0.03	0.00	0.00	0.00	0.00	0.07	100.03
SN78-5_5	3	33.70	64.51	1.21	0.00	0.17	0.01	0.02	0.02	0.00	0.01	0.00	0.04	99.69
SN78-5_5	4	33.73	63.36	1.27	0.01	0.21	0.01	0.05	0.00	0.00	0.01	0.00	0.06	98.72
SN78-5_5	5	33.84	63.50	1.16	0.00	0.23	0.01	0.06	0.00	0.00	0.01	0.00	0.10	98.93
6869F3-02_1	2	32.89	64.01	1.32	0.00	0.07	0.00	0.06	0.00	0.00	0.01	0.00	0.02	98.38
6869F3-02_1	3	32.50	65.43	1.34	0.01	0.02	0.03	0.05	0.00	0.01	0.01	0.00	0.05	99.44
6869F3-02_1	4	32.32	64.64	1.43	0.00	0.02	0.00	0.03	0.05	0.00	0.02	0.01	0.02	98.55
6869F3-02_1	5	32.49	63.91	1.41	0.00	0.12	0.14	0.04	0.00	0.00	0.00	0.00	0.06	98.18
6869F3-02_1	7	32.64	64.40	1.21	0.00	0.10	0.02	0.02	0.00	0.00	0.00	0.00	0.02	98.42
6869F3-02_3	1	32.35	65.57	1.59	0.00	0.16	0.00	0.14	0.02	0.01	0.00	0.00	0.02	99.87
6869F3-02_3	2	32.60	64.20	1.14	0.00	0.28	0.00	0.05	0.00	0.00	0.01	0.00	0.04	98.33
6869F3-02_3	3	32.60	65.26	1.15	0.01	0.47	0.01	0.07	0.00	0.00	0.01	0.00	0.03	99.60
6869F3-02_3	4	32.55	65.82	1.34	0.01	0.11	0.02	0.02	0.00	0.00	0.01	0.00	0.00	99.89

7. ZIRCON

Sample	No.	SiO_2	ZrO_2	HfO_2	Al_2O_3	Y_2O_3	P_2O_5	ThO_2	UO_2	K_2O	CaO	MgO	FeO	Total
6869F3-02_3	5	32.37	65.83	1.24	0.03	0.05	0.03	0.00	0.00	0.01	0.00	0.00	0.00	99.56
6869F3-02_3	6	32.09	64.88	1.32	0.00	0.14	0.03	0.00	0.00	0.01	0.01	0.00	0.01	98.48
LKB-01_2	1	32.33	65.04	1.19	0.03	0.03	0.05	0.02	0.00	0.00	0.00	0.00	0.04	98.71
LKB-01_2	2	32.42	64.95	1.19	0.03	0.03	0.04	0.02	0.00	0.00	0.00	0.01	0.01	98.71
LKB-01_2	3	32.37	66.09	1.23	0.00	0.19	0.03	0.02	0.00	0.01	0.01	0.00	0.00	99.95
LKB-01_2	4	32.01	65.45	1.26	0.00	0.05	0.09	0.00	0.00	0.00	0.00	0.01	0.00	98.87
LKB-01_2	5	32.55	65.57	1.19	0.00	0.24	0.10	0.00	0.00	0.01	0.00	0.00	0.01	99.68
LKB-01_2	6	32.28	65.96	1.29	0.00	0.24	0.12	0.03	0.00	0.01	0.01	0.01	0.00	99.94
LKC1-04_1	1	31.97	67.30	1.12	0.00	0.13	0.07	0.01	0.00	0.01	0.01	0.00	0.12	100.74
LKC1-04_1	2	31.78	65.58	1.42	0.01	0.08	0.00	0.01	0.00	0.00	0.00	0.00	0.11	98.97
LKC1-04_1	4	32.26	64.83	1.41	0.11	0.38	0.07	0.13	0.00	0.00	0.03	0.01	0.08	99.30
LKC1-04_1	5	32.29	64.92	1.24	0.00	0.00	0.02	0.08	0.00	0.00	0.01	0.01	0.03	98.60
LKC1-04_1	6	33.07	65.99	1.16	0.03	0.29	0.11	0.00	0.00	0.03	0.01	0.00	0.01	100.70
LKC1-04_1	8	32.05	67.03	1.14	0.01	0.14	0.02	0.00	0.03	0.00	0.01	0.01	0.06	100.50
SN78-5_2	1	32.35	65.16	1.29	0.00	0.01	0.02	0.00	0.00	0.01	0.00	0.01	0.07	98.94
SN78-5_2	2	32.35	63.07	1.43	0.09	0.07	0.04	0.01	0.03	0.05	0.01	0.00	0.06	97.20
SN78-5_2	3	31.45	65.26	1.17	0.02	0.33	0.12	0.00	0.00	0.01	0.00	0.00	0.06	98.42
SN78-5_2	4	32.14	66.09	1.58	0.00	0.16	0.06	0.03	0.00	0.02	0.00	0.02	0.08	100.19
SN78-5_2	5	32.10	64.54	1.23	0.02	0.23	0.03	0.07	0.04	0.01	0.01	0.00	0.06	98.36
SN78-5_2	6	31.55	64.62	1.51	0.01	0.13	0.01	0.02	0.00	0.02	0.00	0.00	0.15	98.02
SNR1_1	1	32.65	64.21	1.39	0.00	0.03	0.00	0.00	0.00	0.00	0.01	0.00	0.00	98.30
SNR1_1	2	31.88	63.49	1.29	0.00	0.26	0.07	0.05	0.00	0.01	0.00	0.00	0.03	97.09
SNR1_1	3	34.27	63.37	1.41	0.01	0.25	0.01	0.00	0.00	0.02	0.02	0.01	0.03	99.40
SNR1_1	4	32.11	64.53	1.43	0.00	0.08	0.03	0.01	0.00	0.00	0.01	0.00	0.01	98.21
BR	1	32.08	66.55	1.51	0.01	0.00	0.07	0.04	0.00	0.00	0.01	0.00	0.06	100.32
BR	2	32.43	65.44	1.21	0.02	0.08	0.02	0.03	0.00	0.00	0.02	0.00	0.06	99.29
BR	3	31.05	64.81	1.36	0.00	0.13	0.00	0.02	0.00	0.00	0.01	0.00	0.02	97.40
BR	4	32.09	64.58	1.41	0.01	0.10	0.00	0.05	0.04	0.00	0.01	0.00	0.04	98.32
BR	5	31.96	66.81	1.57	0.00	0.00	0.04	0.02	0.00	0.00	0.00	0.00	0.02	100.42
BR	6	32.08	65.24	1.14	0.00	0.33	0.13	0.05	0.00	0.00	0.01	0.00	0.02	99.00
BR	7	32.31	64.35	1.33	0.01	0.00	0.00	0.00	0.00	0.00	0.01	0.00	0.04	98.05
BR	8	32.44	64.23	1.18	0.00	0.28	0.13	0.13	0.00	0.00	0.01	0.00	0.09	98.49
BR	9	32.60	64.17	1.15	0.00	0.12	0.05	0.04	0.00	0.00	0.00	0.00	0.10	98.23
DP68D1_2	1	32.82	63.90	1.12	0.24	0.26	0.06	0.00	0.00	0.00	0.02	0.00	0.29	98.71
DP68D1_2	2	31.90	64.44	1.53	0.06	0.07	0.27	0.05	0.11	0.00	0.18	0.00	0.37	98.98
DP68D1_2	3	34.10	64.75	1.38	0.00	0.15	0.04	0.00	0.00	0.02	0.04	0.02	0.12	100.63
DP68D1_2	5	34.05	64.69	1.50	0.00	0.20	0.12	0.08	0.04	0.00	0.02	0.00	0.13	100.83
DP68D1_2	6	34.30	65.08	1.35	0.01	0.16	0.04	0.06	0.00	0.00	0.02	0.00	0.07	101.07
ZL	1	32.50	65.26	1.09	0.00	0.13	0.08	0.00	0.00	0.00	0.01	0.00	0.14	99.20
ZL	2	32.49	65.19	1.43	0.00	0.19	0.16	0.06	0.00	0.00	0.01	0.00	0.32	99.86
ZL	3	32.45	64.95	1.30	0.01	0.11	0.10	0.04	0.00	0.00	0.01	0.00	0.08	99.02
ZL	4	32.50	64.13	1.15	0.02	0.30	0.14	0.03	0.00	0.00	0.03	0.00	0.10	98.40
ZL	5	33.01	63.41	1.57	0.02	0.18	0.11	0.09	0.01	0.00	0.02	0.00	0.15	98.56
	n=	100												
	Avg.	32.63	65.26	1.34	0.01	0.16	0.06	0.03	0.01	0.00	0.01	0.00	0.07	99.60

8. GARNET

Sample	No.	SiO_2	TiO_2	Al_2O_3	Cr_2O_3	Fe_2O_3	FeO	MnO	MgO	CaO	Na_2O	Total	Pyrope	Almandine	Grossular	Spessartine	Uvarovite	Andradite
AH45H_4	1	38.19	0.00	22.24	0.00	0.00	31.15	0.74	7.89	0.93	0.00	101.14	30.79	68.22	0.99	0.00	0.00	0.00
AH45H_4	2	37.86	0.00	21.94	0.00	0.00	30.65	2.00	7.04	1.69	0.00	101.18	27.91	68.20	3.89	0.00	0.00	0.00
AH45H_4	3	37.96	0.00	22.17	0.00	0.00	31.79	1.02	7.47	1.12	0.00	101.53	29.39	70.19	0.42	0.00	0.00	0.00
AH45H_4	4	37.90	0.00	22.02	0.00	0.00	32.88	0.69	5.94	1.90	0.00	101.33	23.36	72.56	4.09	0.00	0.00	0.00
AH45H_4	5	37.57	0.00	22.01	0.00	0.00	30.36	0.52	8.52	1.08	0.00	100.06	32.13	67.87	0.00	0.00	0.00	0.00
AH45H_4	6	36.70	0.00	19.40	0.00	2.69	10.46	24.52	2.02	4.26	0.00	100.05	8.20	23.83	3.09	56.59	0.00	8.29
AH45H_4	7	38.08	0.00	22.47	0.00	0.00	33.78	0.58	6.48	0.75	0.00	102.14	25.36	74.19	0.45	0.00	0.00	0.00
AH45H_4	8	38.22	0.00	22.49	0.00	0.00	30.94	0.71	7.99	0.85	0.00	101.20	31.16	67.70	1.14	0.00	0.00	0.00
AH45H_4	9	37.73	0.00	22.03	0.00	0.00	31.45	1.50	6.98	1.23	0.00	100.92	27.57	69.71	2.72	0.00	0.00	0.00
AH45H_4	10	37.90	0.00	22.06	0.00	0.00	30.92	0.91	7.57	1.47	0.00	100.83	29.81	68.32	1.87	0.00	0.00	0.00
AH45H_4	11	37.73	0.00	22.18	0.00	0.00	31.65	2.54	5.62	1.60	0.00	101.32	22.20	70.16	1.94	5.70	0.00	0.00
AH45H_4	12	37.80	0.06	22.06	0.05	0.00	32.37	1.60	5.66	1.97	0.00	101.57	22.29	71.53	5.24	0.60	0.16	0.00
AH45H_4	14	37.66	0.00	21.93	0.00	0.00	35.41	0.86	4.99	0.90	0.00	101.75	19.75	78.64	1.62	0.00	0.00	0.00
AH45H_4	15	38.75	0.00	23.00	0.00	0.00	30.03	0.68	8.65	0.90	0.00	102.01	33.27	64.81	1.92	0.00	0.00	0.00
AH45H_4	16	38.65	0.05	22.50	0.00	0.00	31.10	0.85	7.60	1.48	0.00	102.23	29.28	67.23	3.35	0.00	0.00	0.00
AH45H_4	17	38.77	0.00	22.80	0.00	0.00	30.61	0.69	8.61	0.84	0.00	102.32	33.10	66.03	0.87	0.00	0.00	0.00
NB19AC_1	1	37.57	0.06	21.99	0.00	0.00	31.31	1.56	6.64	1.51	0.00	100.64	26.31	69.61	3.90	0.00	0.00	0.00
NB19AC_1	2	38.01	0.07	21.72	0.00	0.00	30.88	1.72	6.58	1.49	0.00	100.47	25.82	68.00	4.00	1.97	0.00	0.00
NB19AC_1	3	37.71	0.00	21.73	0.00	0.00	31.11	1.57	6.53	1.54	0.00	100.19	25.83	69.05	4.38	0.74	0.00	0.00
NB19AC_1	4	37.78	0.05	21.61	0.00	0.00	31.48	1.64	6.53	1.57	0.00	100.66	26.02	70.40	3.43	0.00	0.00	0.00
NB19AC_1	5	38.18	0.00	21.66	0.00	0.00	30.98	1.60	6.59	1.54	0.00	100.55	25.87	68.24	4.35	1.55	0.00	0.00
LKC1-04_4	1	36.83	0.00	22.15	0.00	0.00	31.41	1.03	7.53	0.93	0.00	99.88	28.68	71.32	0.00	0.00	0.00	0.00
LKC1-04_4	2	37.58	0.00	22.29	0.00	0.00	30.35	0.86	7.89	1.01	0.00	99.98	31.29	67.54	1.17	0.00	0.00	0.00
LKC1-04_4	3	36.28	0.05	21.59	0.00	0.00	35.00	1.03	4.32	1.78	0.00	100.05	17.73	80.60	1.52	0.00	0.00	0.00
LKC1-04_4	4	36.89	0.00	22.06	0.00	0.00	32.38	0.69	6.70	1.13	0.00	99.85	26.59	73.41	0.00	0.00	0.00	0.00
LKC1-04_4	5	36.03	0.00	21.63	0.00	0.00	35.63	1.05	3.99	1.74	0.00	100.07	16.64	83.36	0.00	0.00	0.00	0.00
LKC1-04_4	6	37.52	0.00	22.34	0.00	0.00	31.82	0.58	7.27	1.29	0.00	100.82	28.93	71.07	0.00	0.00	0.00	0.00
LKC1-04_4	7	38.14	0.08	22.51	0.00	0.00	30.58	0.73	8.69	0.98	0.00	101.71	32.81	66.95	0.00	0.00	0.00	0.00
LKC1-04_4	8	37.98	0.00	22.45	0.00	0.00	29.67	1.10	8.34	0.97	0.00	100.51	32.73	65.33	1.94	0.00	0.00	0.00
LKC1-04_11	1	37.80	0.00	22.19	0.00	0.00	30.71	1.51	7.05	1.37	0.00	100.63	27.90	68.20	3.90	0.00	0.00	0.00
LKC1-04_11	2	37.66	0.00	22.06	0.06	0.00	33.04	1.32	5.48	1.64	0.00	101.26	21.69	73.37	4.48	0.27	0.19	0.00
LKC1-04_11	3	37.86	0.00	22.22	0.00	0.00	32.71	0.72	6.53	0.94	0.00	100.98	25.70	72.26	2.04	0.00	0.00	0.00
LKC1-04_11	4	37.62	0.00	21.84	0.00	0.00	31.56	1.51	5.87	1.89	0.00	100.29	23.25	70.16	5.38	1.20	0.00	0.00
LKC1-04_11	5	37.63	0.00	22.13	0.00	0.00	31.03	2.46	5.52	1.85	0.00	100.62	22.69	71.57	0.00	5.75	0.00	0.00
LKC1-04_11	6	38.43	0.07	22.54	0.00	0.00	29.63	0.39	8.60	1.26	0.00	100.92	34.02	65.77	0.00	0.00	0.00	0.00
LKC1-04_11	7	37.71	0.00	22.16	0.00	0.00	33.82	2.04	5.17	1.06	0.00	101.96	20.43	75.01	0.00	4.56	0.00	0.00
LKC1-04_11	8	37.49	0.06	21.85	0.00	0.00	32.72	2.28	4.96	1.60	0.00	100.96	19.69	72.90	2.08	5.15	0.00	0.00
LKC1-04_11	9	38.04	0.00	22.15	0.00	0.00	31.88	0.80	7.16	1.03	0.00	101.06	28.05	70.09	1.86	0.00	0.00	0.00

8. GARNET

Sample	No.	SiO_2	TiO_2	Al_2O_3	Cr_2O_3	Fe_2O_3	FeO	MnO	MgO	CaO	Na_2O	Total	Pyrope	Almandine	Grossular	Spessartine	Uvarovite	Andradite
LKC1-04_13	1	38.29	0.00	22.62	0.00	0.00	28.49	1.29	9.04	0.90	0.00	100.63	35.19	62.23	0.00	2.59	0.00	0.00
LKC1-04_13	2	37.98	0.00	22.31	0.00	0.00	26.36	4.13	7.91	1.31	0.00	100.00	31.58	59.05	0.00	9.37	0.00	0.00
LKC1-04_13	3	36.91	0.00	21.45	0.00	0.00	33.48	2.03	3.98	2.05	0.00	99.90	16.42	77.50	6.08	0.00	0.00	0.00
LKC1-04_13	4	37.19	0.05	21.80	0.05	0.00	32.48	0.75	6.16	0.96	0.00	99.44	24.66	72.97	2.06	0.00	0.16	0.00
LKC1-04_13	5	38.36	0.00	22.30	0.00	0.00	28.74	1.47	8.80	1.19	0.00	100.86	34.19	62.66	3.15	0.00	0.00	0.00
LKC1-04_13	6	38.07	0.00	21.97	0.00	0.00	29.45	1.52	8.03	0.86	0.00	99.90	31.44	64.70	0.49	3.38	0.00	0.00
LKC1-04_13	7	37.54	0.00	21.88	0.06	0.00	31.68	1.14	6.38	1.83	0.00	100.51	25.33	70.58	3.90	0.00	0.19	0.00
LKC1-04_13	8	37.81	0.07	22.23	0.00	0.00	31.71	0.59	7.46	0.97	0.00	100.84	29.36	70.04	0.39	0.00	0.00	0.00
LKC1-04_13	9	38.04	0.00	22.19	0.00	0.00	29.88	0.44	8.70	1.14	0.00	100.39	34.16	65.84	0.00	0.00	0.00	0.00
LKC1-04_13	10	37.27	0.00	22.10	0.00	0.00	33.19	1.06	5.74	1.67	0.00	101.03	22.95	74.48	2.57	0.00	0.00	0.00
LKC1-04_13	11	38.25	0.00	22.30	0.00	0.00	27.74	2.92	8.17	0.92	0.00	100.30	31.83	60.65	1.05	6.47	0.00	0.00
LKC1-04_13	12	37.23	0.00	21.94	0.00	0.00	30.07	2.52	6.83	1.18	0.00	99.77	27.34	67.55	0.00	5.11	0.00	0.00
LKC1-04_13	13	37.84	0.00	22.20	0.00	0.00	31.71	0.72	6.87	1.43	0.00	100.77	27.06	70.08	2.86	0.00	0.00	0.00
LKC1-04_13	15	37.68	0.00	22.24	0.07	0.00	29.45	1.64	7.70	1.09	0.00	99.87	30.46	65.37	0.27	3.69	0.22	0.00
LKC1-04_13	16	38.29	0.00	22.27	0.00	0.00	29.45	0.77	8.39	1.07	0.00	100.24	32.66	64.32	2.99	0.03	0.00	0.00
LKC1-04_13	17	36.56	0.00	21.41	0.00	0.00	34.72	1.16	3.72	1.90	0.00	99.47	15.16	79.42	5.41	0.00	0.00	0.00
LKN8-03_3	1	37.02	0.00	21.77	0.00	0.00	31.39	1.32	5.74	2.41	0.00	99.65	23.11	70.91	5.98	0.00	0.00	0.00
LKN8-03_3	2	37.95	0.07	22.18	0.09	0.00	28.94	0.36	8.51	1.43	0.00	99.53	33.37	63.69	2.45	0.00	0.28	0.00
LKN8-03_3	3	37.13	0.00	21.85	0.00	0.00	32.36	0.61	6.12	1.09	0.00	99.16	24.56	72.89	2.55	0.00	0.00	0.00
LKN8-03_3	4	37.42	0.00	22.00	0.00	0.00	29.10	0.69	8.13	1.32	0.00	98.66	32.38	65.04	2.58	0.00	0.00	0.00
LKN8-03_3	5	37.38	0.00	21.84	0.00	0.00	28.26	2.40	7.41	1.77	0.00	99.06	29.54	63.23	1.79	5.44	0.00	0.00
LKN8-03_3	6	37.37	0.07	21.88	0.00	0.00	30.35	0.79	6.64	2.08	0.00	99.18	26.44	67.83	5.52	0.00	0.00	0.00
LKN8-03_3	7	36.91	0.00	21.75	0.00	0.00	30.08	1.40	6.31	1.80	0.00	98.25	25.48	68.16	5.23	1.14	0.00	0.00
	n= 61																	
	Avg.	37.68	0.01	22.04	0.01	0.04	30.89	1.64	6.81	1.40	0.00	100.54	26.87	68.73	2.22	1.99	0.02	0.14

9. PYROXENE

Sample	No.	SiO_2	TiO_2	Al_2O_3	Cr_2O_3	Fe_2O_3	FeO	MnO	MgO	CaO	Na_2O	K_2O	Total	Wo	En	Fs
Pigeonite																
AK43B_1	7	54.05	0.18	0.84	0.00	0.00	19.78	0.42	22.62	3.39	0.00	0.00	101.28	6.70	62.16	31.15
NB19AC_1	19	54.35	0.22	0.91	0.00	0.00	18.33	0.44	22.68	3.78	0.05	0.00	100.76	7.56	63.12	29.32
LKN8-03_1	17	51.32	0.25	0.85	0.09	0.00	23.64	0.34	19.73	3.80	0.00	0.00	100.02	7.60	54.93	37.46
DP84LM_2	16	54.92	0.21	1.11	0.08	0.00	14.09	0.34	26.24	4.38	0.08	0.00	101.45	8.40	70.00	21.60
DP84LM_2	13	54.89	0.23	0.86	0.16	0.00	14.65	0.38	25.49	4.41	0.08	0.00	101.15	8.55	68.72	22.74
DP84LM_2	10	53.94	0.34	0.84	0.00	0.00	18.90	0.37	22.50	4.86	0.08	0.00	101.83	9.49	61.13	29.38
LKN8-03_3	12	52.82	0.30	0.83	0.00	0.00	20.17	0.41	21.27	4.79	0.05	0.00	100.64	9.49	58.66	31.85
LKC1-04_2	14	53.28	0.27	1.12	0.00	0.00	15.75	0.44	21.49	8.04	0.09	0.00	100.48	15.90	59.11	24.99
	n= 8															
	Avg.	53.70	0.25	0.92	0.04	0.00	18.16	0.39	22.75	4.68	0.05	0.00	100.95	9.21	62.23	28.56
Augite																
AK43B_1	5	53.46	0.42	1.75	0.20	0.00	8.62	0.24	17.15	18.50	0.17	0.00	100.51	37.54	48.42	14.04
AK43B_1	6	52.67	0.36	2.47	0.81	0.00	7.88	0.20	17.63	17.71	0.24	0.00	99.97	36.48	50.53	13.00
AK45H_3	1	53.17	0.32	2.17	0.59	0.00	6.49	0.20	17.93	18.93	0.25	0.00	100.05	38.55	50.81	10.64
AK45H_3	2	52.99	0.42	1.74	0.00	0.00	9.35	0.19	17.11	17.66	0.19	0.00	99.65	36.10	48.67	15.23
AK45H_3	3	52.65	0.37	2.54	0.43	0.00	7.58	0.25	16.93	18.98	0.22	0.00	99.95	39.01	48.42	12.57
AK45H_3	7	52.52	0.38	1.61	0.11	0.00	8.35	0.31	17.66	18.78	0.21	0.00	99.93	37.47	49.03	13.49
AK45H_3	12	51.27	0.51	1.76	0.10	0.00	11.62	0.29	16.01	17.26	0.19	0.00	99.01	35.34	45.62	19.04
DP84LM_2	9	53.10	0.33	1.77	0.17	0.00	9.42	0.23	17.01	18.11	0.19	0.00	100.33	36.73	48.00	15.28
DP84LM_2	12	52.50	0.42	2.00	0.28	0.00	8.86	0.18	16.93	18.56	0.22	0.00	99.95	37.74	47.90	14.35
DP84LM_2	17	53.93	0.33	1.71	0.16	0.00	10.59	0.30	19.86	13.94	0.14	0.00	100.96	27.84	55.18	16.98
DP84LM_2	18	52.68	0.41	2.18	0.58	0.00	7.16	0.18	17.73	18.74	0.24	0.00	99.90	38.14	50.20	11.66
LKC1-04_2	8	50.58	0.33	2.02	0.42	0.00	9.81	0.24	14.67	18.02	0.25	0.00	96.34	38.94	44.11	16.96
LKC1-04_2	11	52.75	0.54	3.10	0.71	0.00	7.51	0.16	17.40	18.51	0.26	0.00	100.94	38.00	49.70	12.29
LKN8-03_1	1	51.49	0.52	1.70	0.00	0.00	11.56	0.33	16.23	17.48	0.20	0.00	99.51	35.42	45.76	18.81
LKN8-03_1	4	50.53	0.80	1.88	0.00	0.00	10.28	0.29	15.52	18.31	0.27	0.00	97.88	38.02	44.84	17.14
LKN8-03_1	5	51.83	0.42	2.14	0.35	0.00	7.55	0.17	17.66	18.79	0.19	0.00	99.10	38.05	49.75	12.20
LKN8-03_1	6	51.86	0.34	1.91	0.30	0.00	8.14	0.20	17.58	18.56	0.18	0.00	99.07	37.47	49.38	13.15
LKN8-03_1	8	52.27	0.44	2.06	0.18	0.00	8.12	0.23	17.86	17.81	0.17	0.00	99.14	36.21	50.53	13.26
LKN8-03_1	9	54.51	0.57	2.12	0.14	0.00	8.75	0.26	15.77	18.40	0.18	0.00	100.70	38.84	46.31	14.85
LKN8-03_1	13	52.45	0.33	1.68	0.29	0.00	7.28	0.19	17.85	19.03	0.21	0.00	99.31	38.29	49.97	11.74
LKN8-03_1	14	51.34	0.39	3.14	1.12	0.00	6.89	0.21	17.69	18.59	0.28	0.00	99.65	38.14	50.49	11.37
LKN8-03_1	15	51.77	0.41	1.61	0.06	0.00	9.71	0.23	17.16	18.37	0.23	0.00	99.55	36.74	47.75	15.52
LKN8-03_1	16	51.95	0.44	2.14	0.43	0.00	6.83	0.21	17.48	19.09	0.25	0.00	98.82	39.03	49.73	11.24

9. PYROXENE

Sample	No.	SiO_2	TiO_2	Al_2O_3	Cr_2O_3	Fe_2O_3	FeO	MnO	MgO	CaO	Na_2O	K_2O	Total	Wo	En	Fs
LKN8-03_1	18	52.55	0.34	1.71	0.29	0.00	7.85	0.16	17.57	18.83	0.21	0.00	99.51	38.02	49.36	12.63
LKN8-03_1	19	51.97	0.45	2.67	0.86	0.00	6.09	0.18	17.51	19.42	0.23	0.00	99.38	39.89	50.05	10.06
LKN8-03_1	20	51.73	0.45	2.98	0.92	0.00	7.02	0.20	18.07	18.43	0.24	0.00	100.04	37.45	51.09	11.46
LKN8-03_1	21	50.82	0.58	1.61	0.00	0.00	14.10	0.36	15.19	16.68	0.23	0.00	99.57	33.97	43.04	22.99
LKN8-03_1	22	52.96	0.33	1.59	0.17	0.00	8.32	0.27	18.06	18.42	0.18	0.00	100.30	36.65	50.00	13.35
LKN8-03_3	1	51.76	0.46	1.72	0.09	0.00	8.39	0.23	17.13	18.93	0.20	0.00	98.91	38.25	48.16	13.60
LKN8-03_3	2	52.25	0.32	2.04	0.49	0.00	7.16	0.19	18.06	19.06	0.20	0.00	99.77	38.18	50.33	11.50
LKN8-03_3	4	51.08	0.53	1.53	0.00	0.00	13.29	0.32	15.09	16.63	0.21	0.00	98.68	34.47	43.51	22.02
LKN8-03_3	5	51.87	0.36	2.29	0.60	0.00	8.46	0.20	16.70	18.62	0.21	0.00	99.31	38.30	47.79	13.91
LKN8-03_3	6	50.27	0.75	1.61	0.00	0.00	16.57	0.36	13.55	16.18	0.23	0.00	99.52	33.53	39.07	27.39
LKN8-03_3	7	52.54	0.29	1.76	0.19	0.00	8.24	0.23	17.28	18.27	0.17	0.00	98.97	37.34	49.14	13.52
LKN8-03_3	8	51.07	0.62	2.67	0.39	0.00	10.73	0.27	16.79	16.41	0.19	0.00	99.14	33.93	48.31	17.76
LKN8-03_3	9	51.29	0.48	3.16	1.14	0.00	6.47	0.14	16.95	19.39	0.26	0.00	99.28	40.28	49.00	10.72
LKN8-03_3	10	52.46	0.38	2.27	0.31	0.00	8.80	0.25	17.47	17.47	0.22	0.00	99.63	35.77	49.77	14.47
LKN8-03_3	11	52.32	0.35	2.48	0.97	0.00	6.70	0.23	17.85	18.42	0.23	0.00	99.55	37.85	51.03	11.12
LKN8-03_3	13	52.68	0.39	2.01	0.42	0.00	9.40	0.22	16.93	17.76	0.22	0.00	100.03	36.37	48.24	15.38
LKN8-03_3	14	50.01	1.02	2.33	0.00	0.00	18.01	0.36	12.80	15.40	0.20	0.00	100.13	32.39	37.45	30.16
LKN8-03_3	15	52.63	0.39	2.16	0.39	0.00	7.85	0.19	13.23	19.66	0.29	0.00	96.79	44.33	41.51	14.16
NB19AC_1	2	51.21	0.43	2.58	0.80	0.00	8.61	0.17	16.53	18.38	0.23	0.00	98.94	38.11	47.68	14.21
NB19AC_1	3	50.97	0.46	2.47	0.47	0.00	8.81	0.15	15.93	18.78	0.23	0.00	98.27	39.17	46.24	14.59
NB19AC_1	10	52.33	0.31	2.01	0.57	0.00	7.82	0.18	17.22	18.82	0.24	0.00	99.50	38.39	48.87	12.74
NB19AC_1	11	52.14	0.34	1.99	0.36	0.00	7.97	0.24	17.73	18.49	0.22	0.00	99.48	37.30	49.77	12.93
	n= 45															
	Avg.	52.07	0.44	2.11	0.37	0.00	9.00	0.23	16.85	18.15	0.22	0.00	99.44	37.20	48.01	14.79

10. AMPHIBOLE

Sample	No.	SiO_2	TiO_2	Al_2O_3	Cr_2O_3	Fe_2O_3	FeO	MnO	MgO	CaO	Na_2O	K_2O	Total
Green hornblende													
AK45H_4	12	44.64	0.38	13.85	0.00	0.00	14.58	0.29	11.62	11.67	1.62	0.32	98.97
SN78-5_6	1	46.02	0.44	10.61	0.00	0.00	13.69	0.30	12.70	12.22	1.25	0.56	97.79
SEA711	8	45.49	0.46	11.07	0.00	0.00	15.47	0.27	12.13	12.47	1.30	0.90	99.56
SEA711	6	43.26	0.47	11.95	0.00	0.00	17.15	0.36	10.65	12.00	1.59	1.60	99.03
SN78-5_6	11	48.71	0.48	6.87	0.00	0.00	15.44	0.31	12.40	12.15	0.98	0.53	97.87
KV196R_1	2	43.42	0.52	15.41	0.00	0.00	15.06	0.18	10.55	11.80	1.42	0.42	98.78
KV196R_1	9	42.73	0.55	11.92	0.00	0.00	17.93	0.26	10.01	12.13	1.47	1.53	98.53
AK52N_2	1	45.87	0.62	12.06	0.00	0.00	14.95	0.20	11.69	11.94	1.10	0.23	98.66
KV196R_1	5	44.63	0.64	11.95	0.00	0.00	15.62	0.24	11.00	12.07	1.20	0.42	97.77
KV196R_1	6	41.39	0.67	14.15	0.00	0.00	21.37	0.37	7.49	11.23	1.70	0.78	99.15
KV196R_1	3	42.59	0.68	10.59	0.00	0.00	20.87	0.52	9.18	11.40	1.84	1.00	98.67
SN78-5_6	14	43.10	0.68	12.00	0.00	0.00	17.26	0.34	10.33	12.18	1.31	1.40	98.60
SEA711	1	45.09	0.68	11.60	0.00	0.00	15.75	0.34	11.50	12.59	1.26	1.20	100.01
SEA711	2	44.07	0.69	11.05	0.05	0.00	16.62	0.36	10.77	12.30	1.58	1.44	98.93
KV196R_1	7	42.61	0.71	14.96	0.00	0.00	16.08	0.30	9.93	11.85	1.42	0.58	98.44
KV196R_1	10	44.97	0.73	12.25	0.00	0.00	15.44	0.22	11.81	11.75	1.42	0.35	98.94
SEA711	7	48.15	0.75	9.98	0.14	0.00	10.43	0.20	15.66	11.98	1.49	0.71	99.49
SEA711	12	43.36	0.75	11.97	0.00	0.00	18.33	0.12	9.38	12.21	1.19	1.40	98.71
KV196R_1	8	42.85	0.79	11.46	0.00	0.00	20.59	0.39	8.46	11.85	1.42	0.65	98.46
KV196R_1	4	43.36	0.81	13.51	0.00	0.00	16.63	0.28	10.12	11.58	1.69	0.54	98.52
AK52N_2	5	41.80	0.82	12.00	0.00	0.00	21.29	0.61	8.14	11.76	1.36	1.35	99.13
KV196R_1	1	43.19	0.86	12.53	0.00	0.00	16.69	0.31	10.91	11.87	1.89	0.38	98.63
AK52N_2	2	42.71	0.89	13.10	0.00	0.00	20.68	0.32	7.69	11.74	1.61	0.84	99.58
AK45H_4	2	44.36	0.95	10.43	0.11	0.00	16.49	0.68	11.75	11.78	1.52	1.43	99.50
SEA711	9	44.61	0.96	9.77	0.05	0.00	20.00	0.36	8.09	11.87	1.48	1.05	98.24
AK52N_2	4	42.43	1.03	11.02	0.06	0.00	23.68	0.50	7.26	11.36	1.85	1.00	100.19
SEA711	10	44.51	1.32	11.50	0.00	0.00	17.24	0.27	10.38	11.46	1.74	0.35	98.77
SEA711	5	46.64	1.35	9.89	0.05	0.00	12.75	0.25	13.22	12.15	1.00	0.73	98.03
	n= 28												
	Avg.	44.16	.74	11.77	0.02	0.00	17.07	0.33	10.53	11.91	1.45	0.85	98.82
Brown Hornblende													
AK45H_4	11	43.12	1.52	12.65	0.13	0.00	12.75	0.14	13.40	11.85	1.76	1.39	98.71
AK45H_4	1	43.43	1.63	11.56	0.00	0.00	15.23	0.23	12.45	11.82	1.77	1.81	99.93
AK45H_4	8	44.02	1.69	12.04	0.18	0.00	12.88	0.12	13.40	11.83	1.69	1.42	99.27
AK45H_4	5	44.23	1.70	11.90	0.19	0.00	14.91	0.18	12.43	11.58	1.81	1.15	100.08
AK45H_4	13	44.31	1.75	10.37	0.00	0.00	14.41	0.54	12.57	11.65	1.71	1.50	98.81
AK45H_4	3	43.00	1.79	11.50	0.00	0.00	16.22	0.27	11.37	11.52	1.75	1.55	98.97
SEA711	11	44.61	1.81	10.63	0.14	0.00	11.00	0.21	14.71	12.12	1.52	1.78	98.53
AK45H_4	7	42.03	1.94	10.53	0.00	0.00	22.52	0.52	7.56	10.72	2.10	1.52	99.44
SN78-5_6	12	44.07	2.02	9.82	0.00	0.00	14.34	0.57	12.50	11.86	1.83	1.45	98.46
SN78-5_6	2	42.49	2.03	10.63	0.00	0.00	17.57	0.21	9.95	11.51	1.88	1.71	97.98
AK45H_4	4	44.31	2.12	11.25	0.23	0.00	12.36	0.14	13.72	12.13	1.66	1.50	99.42
SN78-5_6	15	42.88	2.16	11.32	0.17	0.00	14.31	0.10	11.54	12.11	1.35	1.71	97.65
AK45H_4	10	44.77	2.20	11.18	0.06	0.00	13.25	0.14	13.00	11.99	1.72	1.20	99.51
SN78-5_6	4	43.23	2.23	10.75	0.00	0.00	14.89	0.15	11.51	12.00	1.66	1.77	98.19
AK45H_4	6	42.78	2.33	11.60	0.00	0.00	16.68	0.30	10.97	11.62	1.89	1.52	99.69
SN78-5_6	5	43.19	2.35	12.75	0.07	0.00	13.47	0.20	12.76	11.17	2.21	0.55	98.72
AK52N_2	3	42.91	2.48	11.18	0.00	0.00	18.28	0.28	9.55	11.58	1.81	1.69	99.76
AK45H_4	9	42.66	2.75	11.43	0.00	0.00	16.70	0.34	10.29	11.44	1.65	1.77	99.03
	n= 18												
	Avg.	43.45	2.03	11.28	0.07	0.00	15.10	0.26	11.87	11.69	1.77	1.55	99.01

11. EPIDOTE SERIES

Sample	No.	SiO_2	TiO_2	Al_2O_3	Cr_2O_3	Fe_2O_3	FeO	MnO	MgO	CaO	Na_2O	K_2O	Total
AK52N_2	1	37.91	0.08	23.14	0.00	0.00	13.04	0.19	0.00	21.34	0.00	0.00	95.70
AK52N_2	2	38.85	0.00	25.68	0.08	0.00	11.60	0.11	0.00	23.66	0.00	0.00	99.98
AK52N_2	3	39.19	0.00	26.98	0.00	0.00	10.10	0.00	0.00	24.14	0.00	0.00	100.41
AK52N_2	4	37.67	0.09	22.06	0.00	0.00	14.32	0.57	0.05	23.41	0.00	0.00	98.17
AK52N_2	5	37.66	0.07	21.84	0.00	0.00	14.77	0.59	0.05	23.40	0.00	0.00	98.38
AK52N_2	6	37.31	0.07	21.87	0.00	0.00	14.88	0.71	0.00	23.46	0.00	0.00	98.30
AK52N_2	7	37.69	0.07	21.69	0.00	0.00	14.99	0.75	0.00	23.51	0.00	0.00	98.70
AK52N_2	8	37.21	0.08	21.79	0.00	0.00	14.89	0.66	0.06	23.42	0.00	0.00	98.11
AK52N_2	9	37.51	0.06	21.62	0.00	0.00	14.77	0.72	0.00	23.55	0.00	0.00	98.23
AK52N_2	10	37.68	0.08	21.34	0.00	0.00	15.11	0.73	0.06	23.58	0.00	0.00	98.58
AK52N_2	11	37.83	0.07	21.56	0.00	0.00	14.72	0.58	0.05	23.18	0.00	0.00	97.99
AK52N_2	12	37.63	0.08	21.18	0.00	0.00	14.82	0.63	0.07	23.52	0.00	0.00	97.93
AK52N_2	13	37.79	0.07	21.80	0.00	0.00	14.60	0.74	0.06	23.64	0.00	0.00	98.70
AK52N_2	14	37.84	0.14	23.47	0.00	0.00	12.99	0.21	0.07	23.85	0.00	0.00	98.57
AK52N_2	15	38.10	0.08	23.71	0.07	0.00	12.30	0.21	0.06	23.85	0.00	0.00	98.38
LKN8-03_3	1	37.95	0.11	23.62	0.00	0.00	12.60	0.26	0.09	24.01	0.00	0.00	98.64
LKN8-03_3	2	38.43	0.10	25.22	0.00	0.00	10.78	0.22	0.05	24.14	0.00	0.00	98.94
LKN8-03_3	3	38.39	0.06	25.38	0.05	0.00	10.37	0.19	0.07	24.27	0.00	0.00	98.78
LKN8-03_3	4	38.12	0.12	23.65	0.00	0.00	13.21	0.00	0.00	24.12	0.00	0.00	99.22
LKN8-03_3	5	38.42	0.10	23.87	0.00	0.00	12.68	0.28	0.00	23.96	0.00	0.00	99.31
LKN8-03_3	6	38.11	0.00	23.75	0.00	0.00	12.66	0.19	0.08	23.73	0.00	0.00	98.52
LKN8-03_3	7	38.29	0.07	23.64	0.00	0.00	13.08	0.14	0.00	23.99	0.00	0.00	99.21
LKN8-03_3	8	38.00	0.05	23.66	0.00	0.00	12.88	0.14	0.00	24.05	0.00	0.00	98.78
LKN8-03_3	9	38.18	0.13	23.61	0.00	0.00	12.66	0.17	0.00	24.17	0.00	0.00	98.92
LKN8-03_3	10	38.38	0.10	23.73	0.00	0.00	12.37	0.24	0.00	23.66	0.00	0.00	98.48
LKN8-03_3	11	38.30	0.11	23.83	0.00	0.00	13.20	0.18	0.00	23.82	0.00	0.00	99.44
LKN8-03_3	12	37.99	0.00	23.51	0.00	0.00	13.00	0.09	0.00	23.97	0.00	0.00	98.56
LKN8-03_3	13	38.15	0.06	23.81	0.00	0.00	12.47	0.11	0.00	23.90	0.00	0.00	98.50
LKN8-03_3	14	38.41	0.13	24.56	0.00	0.00	11.46	0.21	0.05	23.90	0.00	0.00	98.72
LKN8-03_3	15	38.10	0.10	24.14	0.00	0.00	11.94	0.21	0.07	23.90	0.00	0.00	98.46
LKN8-03_3	16	38.18	0.13	24.47	0.00	0.00	11.62	0.21	0.05	23.95	0.00	0.00	98.61
LKN8-03_3	17	38.31	0.09	24.78	0.00	0.00	11.66	0.17	0.06	24.34	0.00	0.00	99.41
LKN8-03_3	18	37.90	0.12	24.20	0.00	0.00	11.73	0.24	0.06	24.14	0.00	0.00	98.39
	n= 33												
	Avg.	38.04	0.08	23.43	0.01	0.00	12.98	0.32	0.03	23.74	0.00	0.00	98.64

12. ALUMINOSILICATES

Sample	No.	SiO_2	TiO_2	Al_2O_3	Cr_2O_3	Fe_2O_3	FeO	MnO	MgO	CaO	Na_2O	K_2O	Total
KV196R_4	1	37.21	0.00	63.58	0.00	0.00	0.89	0.00	0.00	0.00	0.00	0.00	101.68
KV196R_4	2	37.65	0.00	64.51	0.00	0.00	0.86	0.00	0.00	0.00	0.00	0.00	103.02
KV196R_4	3	37.71	0.00	64.65	0.00	0.00	0.79	0.00	0.00	0.00	0.00	0.00	103.15
KV196R_4	4	37.65	0.00	64.56	0.00	0.00	0.84	0.00	0.00	0.00	0.00	0.00	103.05
KV196R_4	5	37.98	0.00	63.63	0.00	0.00	0.81	0.00	0.00	0.00	0.00	0.00	102.42
KV196R_4	6	37.49	0.00	64.52	0.00	0.00	0.74	0.00	0.00	0.00	0.00	0.00	102.75
KV196R_4	7	37.58	0.00	64.50	0.00	0.00	0.79	0.00	0.00	0.00	0.00	0.00	102.87
KV196R_4	8	37.47	0.00	64.23	0.00	0.00	0.86	0.00	0.00	0.00	0.00	0.00	102.56
KV196R_4	9	37.59	0.00	64.49	0.00	0.00	0.82	0.00	0.00	0.00	0.00	0.00	102.90
KV196R_4	10	37.47	0.00	64.27	0.00	0.00	0.76	0.00	0.00	0.00	0.00	0.00	102.50
NB21B_5	1	38.08	0.00	65.78	0.07	0.00	0.12	0.00	0.00	0.00	0.00	0.00	104.05
NB21B_5	2	38.06	0.00	65.41	0.00	0.00	0.19	0.00	0.00	0.00	0.00	0.00	103.66
NB21B_5	3	37.62	0.00	65.43	0.00	0.00	0.19	0.00	0.00	0.00	0.00	0.00	103.24
NB21B_5	4	37.68	0.00	65.51	0.00	0.00	0.17	0.00	0.00	0.00	0.00	0.00	103.36
NB21B_5	5	37.82	0.00	65.49	0.05	0.00	0.12	0.00	0.00	0.00	0.00	0.00	103.48
NB21B_5	6	36.37	0.00	64.82	0.00	0.00	0.14	0.00	0.00	0.00	0.10	0.08	101.51
LKN8-03_3	1	36.96	0.00	62.34	0.06	0.00	0.71	0.00	0.00	0.00	0.00	0.00	100.07
LKN8-03_3	7	37.41	0.00	64.89	0.00	0.00	0.17	0.00	0.00	0.00	0.00	0.00	102.47
LKN8-03_3	8	37.32	0.07	64.49	0.00	0.00	0.00	0.00	0.00	0.00	0.00	0.00	101.88
LKN8-03_3	9	38.44	0.00	65.82	0.05	0.00	0.13	0.00	0.00	0.00	0.00	0.00	104.44
LKN8-03_3	10	37.98	0.00	65.65	0.00	0.00	0.13	0.00	0.00	0.00	0.00	0.00	103.76
SN78-5_1	22	38.24	0.00	65.73	0.00	0.00	0.15	0.00	0.00	0.00	0.00	0.00	104.12
SN78-5_1	23	38.20	0.05	65.20	0.00	0.00	0.19	0.00	0.00	0.00	0.00	0.00	103.64
SN78-5_1	24	37.97	0.00	64.85	0.00	0.00	0.12	0.00	0.00	0.00	0.00	0.00	102.94
SN78-5_1	25	37.69	0.00	65.18	0.00	0.00	0.20	0.00	0.00	0.00	0.00	0.00	103.07
	n= 25												
	Avg.	37.67	0.00	64.78	0.01	0.00	0.44	0.00	0.00	0.00	0.00	0.00	102.90

13. STAUROLITE

Sample	No.	SiO_2	TiO_2	Al_2O_3	Cr_2O_3	Fe_2O_3	FeO	MnO	MgO	CaO	Total
DP127R_1	1	28.32	0.33	55.81	0.02	0.00	14.99	0.08	1.89	0.00	101.44
DP127R_2	2	28.45	0.41	55.86	0.00	0.00	15.17	0.03	1.94	0.00	101.86
NB19AC_1	1	27.96	0.47	56.68	0.05	0.00	15.80	0.04	1.78	0.00	102.78
NB19AC_1	2	28.03	0.37	56.03	0.00	0.00	15.01	0.09	1.84	0.00	101.37
NB19AC_1	3	27.66	0.23	57.39	0.00	0.00	14.09	0.00	1.87	0.00	101.24
NB19AC_1	4	28.25	0.53	56.21	0.06	0.00	15.75	0.09	1.86	0.00	102.75
NB19AC_1	5	28.18	0.49	56.52	0.00	0.00	15.87	0.09	1.86	0.00	103.01
NB19AC_1	6	28.38	0.47	55.68	0.05	0.00	15.71	0.09	1.91	0.00	102.29
LKC1-04_2	1	28.76	0.37	55.23	0.00	0.00	15.51	0.09	1.91	0.00	101.87
LKC1-04_2	2	28.66	0.23	56.85	0.05	0.00	13.99	0.00	1.80	0.00	101.58
	n=	10									
	Avg.	28.27	0.39	56.23	0.02	0.00	15.19	0.06	1.87	0.00	102.02

14. GLAUCONITE

Sample	No.	SiO_2	TiO_2	Al_2O_3	Cr_2O_3	Fe_2O_3	FeO	MnO	MgO	CaO	Na_2O	K_2O	Total
DP127R_2	1	38.24	0.44	3.79	0.06	0.00	35.97	0.00	3.07	0.70	0.32	5.95	88.54
DP127R_2	2	42.98	0.10	4.05	0.07	0.00	31.87	0.00	3.25	0.06	0.61	7.49	90.46
DP127R_2	3	45.27	0.22	4.45	0.07	0.00	28.82	0.00	2.77	0.61	0.13	7.37	89.72
DP127R_2	4	37.42	0.20	2.87	0.09	0.00	35.34	0.00	2.54	0.10	0.26	5.28	84.10
DP127R_2	5	42.47	0.31	3.44	0.02	0.00	31.11	0.00	2.95	0.77	0.51	6.82	88.41
DP127R_2	6	45.00	0.62	3.91	0.05	0.00	28.20	0.00	1.85	0.50	0.09	7.01	87.23
DP127R_2	7	37.42	0.05	2.87	0.07	0.00	35.11	0.00	2.43	0.60	0.17	4.43	83.13
SN78-5_6	1	38.99	0.22	4.30	0.11	0.00	36.18	0.00	3.18	0.29	0.09	6.63	89.99
SN78-5_6	2	43.26	0.12	4.55	0.00	0.00	31.96	0.00	3.61	0.64	0.08	7.50	91.72
SN78-5_6	3	46.02	0.10	5.23	0.08	0.00	29.35	0.00	3.59	0.21	0.08	7.88	92.54
	n=	10											
	Avg.	41.71	0.24	3.95	0.06	0.00	32.39	0.00	2.92	0.45	0.23	6.64	88.58

15. TITANITE

Sample	No.	SiO_2	TiO_2	Al_2O_3	Cr_2O_3	Fe_2O_3	FeO	MnO	MgO	CaO	Total
AK52N_2	4	22.91	30.50	20.28	0.00	0.00	0.43	0.15	0.00	22.77	97.04
NB21B_5	23	27.37	38.98	2.67	0.00	0.00	2.26	0.00	0.00	26.90	98.18
LKC1-04_2	9	30.74	27.64	9.05	0.00	0.00	0.80	0.00	0.00	29.74	97.97
	n=	3									
	Avg.	27.01	32.37	10.67	0.00	0.00	1.16	0.05	0.00	26.47	97.73

APPENDIX I

REE ANALYSIS DATA

Zircon

Raw data

Sample	La	Ce	Pr	Nd	Sm	Eu	Gd	Dy	Ho	Er	Yb	ΣREE	La/Yb
68/69F3-02_1	352	833	74	179	26	3	46	116	25	165	223	2042	1.17
68/69F3-02_3	94	136	12	31	8	3	48	124	26	176	227	886	0.23
SN78-5_1	200	345	22	111	30	4	58	132	26	170	215	1313	0.56
SN78-5_2	79	113	2	22	9	5	46	152	29	205	257	919	0.15
LKB-01_1	280	429	41	97	20	4	41	124	25	173	235	1467	0.72
LKB-01_2	118	171	15	39	14	5	58	136	27	185	232	1001	0.28

Normalised Data

Sample	La	Ce	Pr	Nd	Sm	Eu	Gd	Dy	Ho	Er	Yb	ΣREE
68/69F3-02_1	1438	1306	767	378	171	60	223	458	433	995	1351	2042
68/69F3-02_3	383	213	129	65	54	55	233	490	460	1061	1377	886
SN78-5_1	818	541	231	234	192	74	286	520	453	1023	1300	1313
SN78-5_2	324	178	20	47	59	79	224	596	517	1232	1557	919
LKB-01_1	1144	672	421	205	130	67	199	486	438	1044	1421	1467
LKB-01_2	483	269	153	82	91	91	284	534	481	1115	1407	1001

Garnet

Raw data

Sample	La	Ce	Pr	Nd	Sm	Eu	Gd	Dy	Ho	Er	Yb	ΣREE	La/Yb
DP127R_1	4	13	2	7	11	0	37	121	35	123	127	480	0.05
LKC1-04_1	4	13	2	6	9	1	31	114	35	127	144	485	0.04
LHC_1	4	13	2	6	9	0	34	118	25	126	141	479	0.05

Normalised Data

Sample	La	Ce	Pr	Nd	Sm	Eu	Gd	Dy	Ho	Er	Yb	ΣREE
DP127R_1	18	21	25	14	68	7	180	474	626	741	767	919
LKC1-04_1	16	20	22	12	57	9	153	447	614	768	872	1467

All data in ppm.

APPENDIX J

RADIOMETRIC RESULTS OF ZIRCON FRACTIONS

Sample	$C_{Bi=U}$ $Bq.kg^{-1}$	C_{Th} $Bq.kg^{-1}$	$C_{Th/U}$
BR (Buffels River)	8286	2333	0.28
68/69F3-02_1	3117	1324	0.42
68/69F3-02_2	3132	1275	0.41
68/69F3-02_3	2132	497	0.23
SN78-5_1	3609	1028	0.28
SN78-5_2	2592	533	0.21
LKB-01_1	3211	900	0.28
LKB-01_2	2413	471	0.20

ADDENDUM A
GEOLOGICAL CROSS-SECTIONS AND GRAIN-SIZE DISTRIBUTIONS

Section descriptions

The lithological samples carry the name of the mining block as a prefix and are numbered upward from the bedrock. For example, AK1_1 is the (first) unit overlying the bedrock in mining block AK1. The thickness of samples was measured with a tape. A detailed sedimentological investigation was beyond the scope of the study and only a general description of each lithological unit is given. Grain size and sorting were determined by sieving, with the grain size described by the Udden-Wentworth scale. The composition of the samples was determined with a hand lens and the colour of the sediments estimated in terms of Munsell colours. The description of sedimentary features was aided by the work of Lewis (1976). Window sections were compiled from these observations in conjunction with field sketches and photographs and presented hereafter. In addition the total heavy mineral content (THM), total economic fraction (TEF) and individual mineral proportions are supplied.

BUFFELS MARINE COMPLEX

Sample site AK1 (Fig. 1A).

Unit AK1_1

This unit consists of a poorly sorted, clast-supported pebble gravel. Clasts are angular to subangular grey quartz that range in size from 2-5 cm. The matrix is a muddy, quartzose sand that gives the unit a very light grey (N8) colour. The sand portion of the matrix is medium-grained and poorly sorted. This unit appears to be similar to the channel gravels of the KNC.

Unit AK1_2

This unit forms a sharp contact with the underlying gravel and consists of a poorly sorted, bimodal medium to coarse quartzo-feldspathic sand. The sand has an orange hue (10YR 6/6) and is generally structureless, semi-compacted and calcretized of the top.

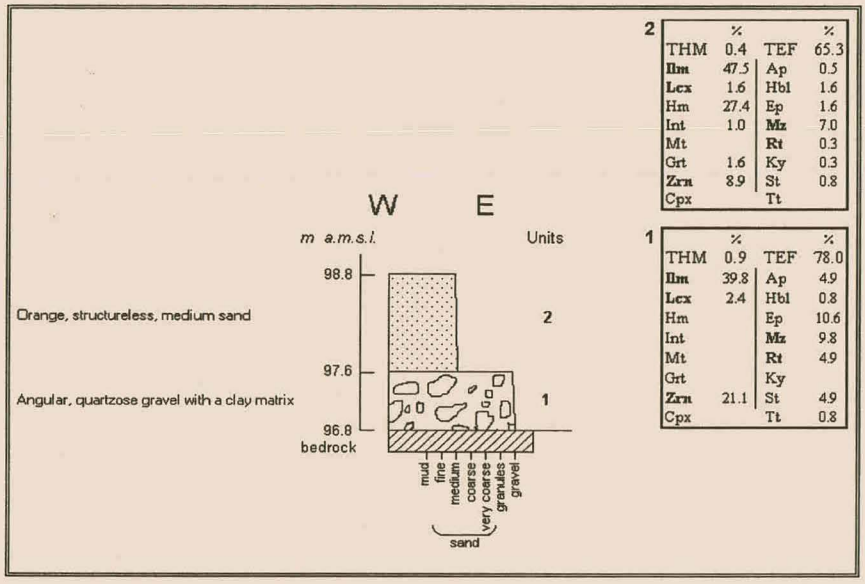

Figure 1A. Geological cross-section of AK1.

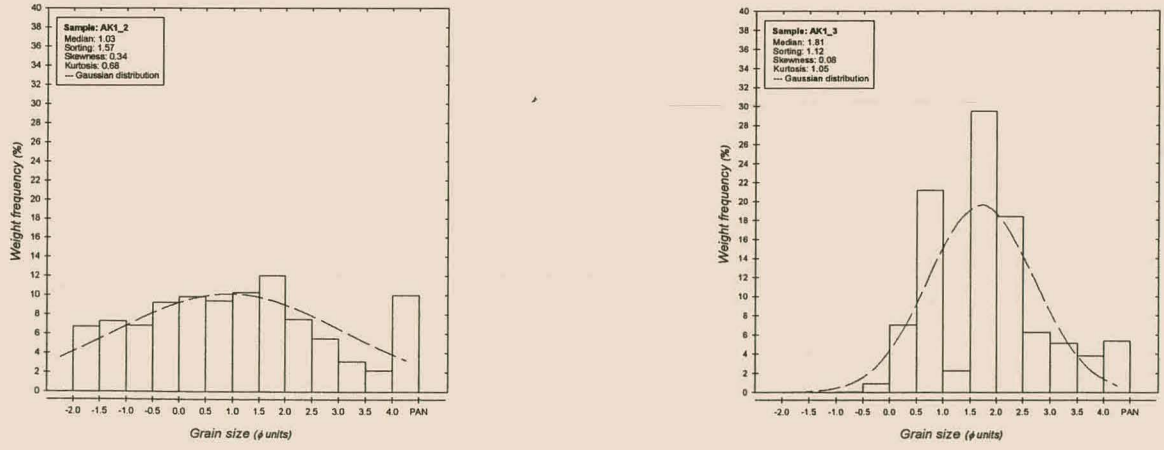

Figure 1B. Grain-size distributions of AK1 samples.

Sample site AK43B (Fig. 2A).

Unit AK43B_1

Bedrock is overlain by a clast-supported pebble gravel unconformably overlying the preceding unit. The clasts are sub-horizontally aligned. Gravel clasts are mainly schist and quartzite and the matrix comprises a poorly sorted, fine-grained quartzo-feldspathic sand. Abundant plant roots and shell debris with a well-defined calcrete layer mark the upper part of the unit.

Unit AK43B_2

This unit consists of an orange (10YR 6/6), fine quartzo-feldspathic sand that shows poor sorting. The sand is heavily bioturbated with cross-bedding faintly visible. The unit is overlain by a calcrete layer.

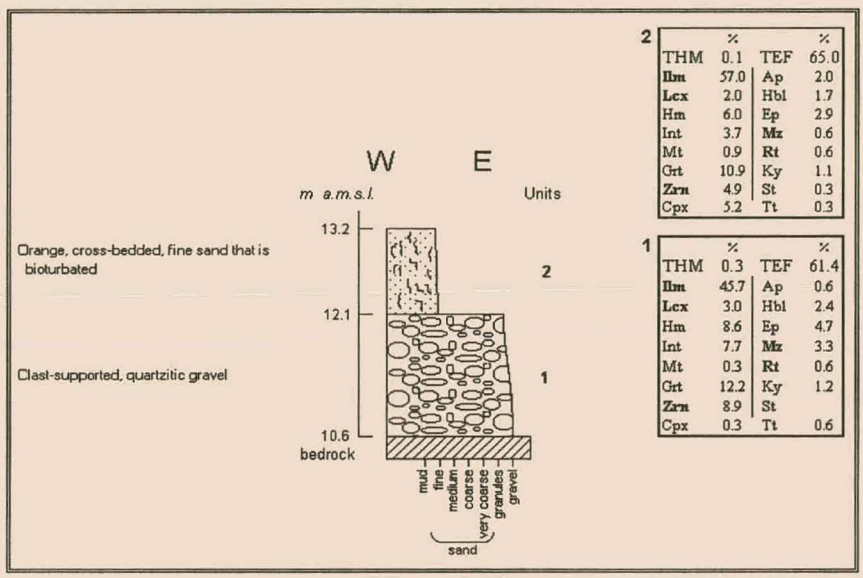

Figure 2A. Geological cross-section of AK43B.

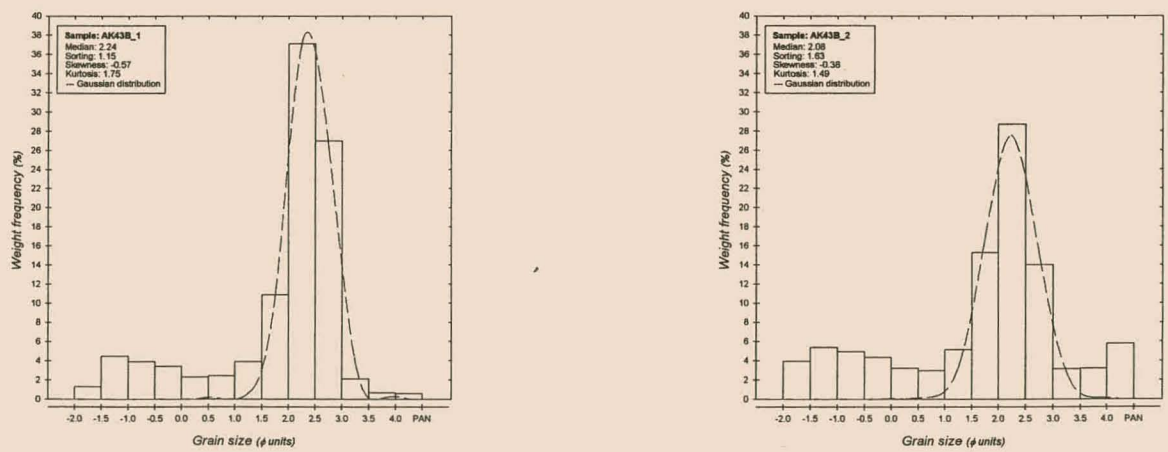

Figure 2B. Grain-size distributions of AK43B samples.

Sample site AK45H (Fig. 3A).

Unit AK45H_1
Orange (10YR 6/6), cross-bedded, fine quartzo-feldspathic sand that is poorly sorted.

Unit AK45H_2
Clast-supported cobble gravel with a poorly sorted quartzo-feldspathic sand as matrix. Clasts consist of well-rounded schist that dip slightly seaward. Clast size varies from 10-30 cm.

Unit AK45H_3
The unit consists of an orange (10YR 6/6), cross-bedded, poorly sorted, bimodal, very coarse and medium sand.

Unit AK45H_4
Clast-supported pebble gravel with poorly sorted medium sand as a matrix. Clasts consist of rounded quartzite and schist ranging from 2-6 cm in size and which dip sub-horizontally.

Unit AK45H_5
Orange (10YR 6/6), poorly sorted, compacted, medium, quartzo-feldspathic sand. A well-defined calcrete layer marks the sand's top.

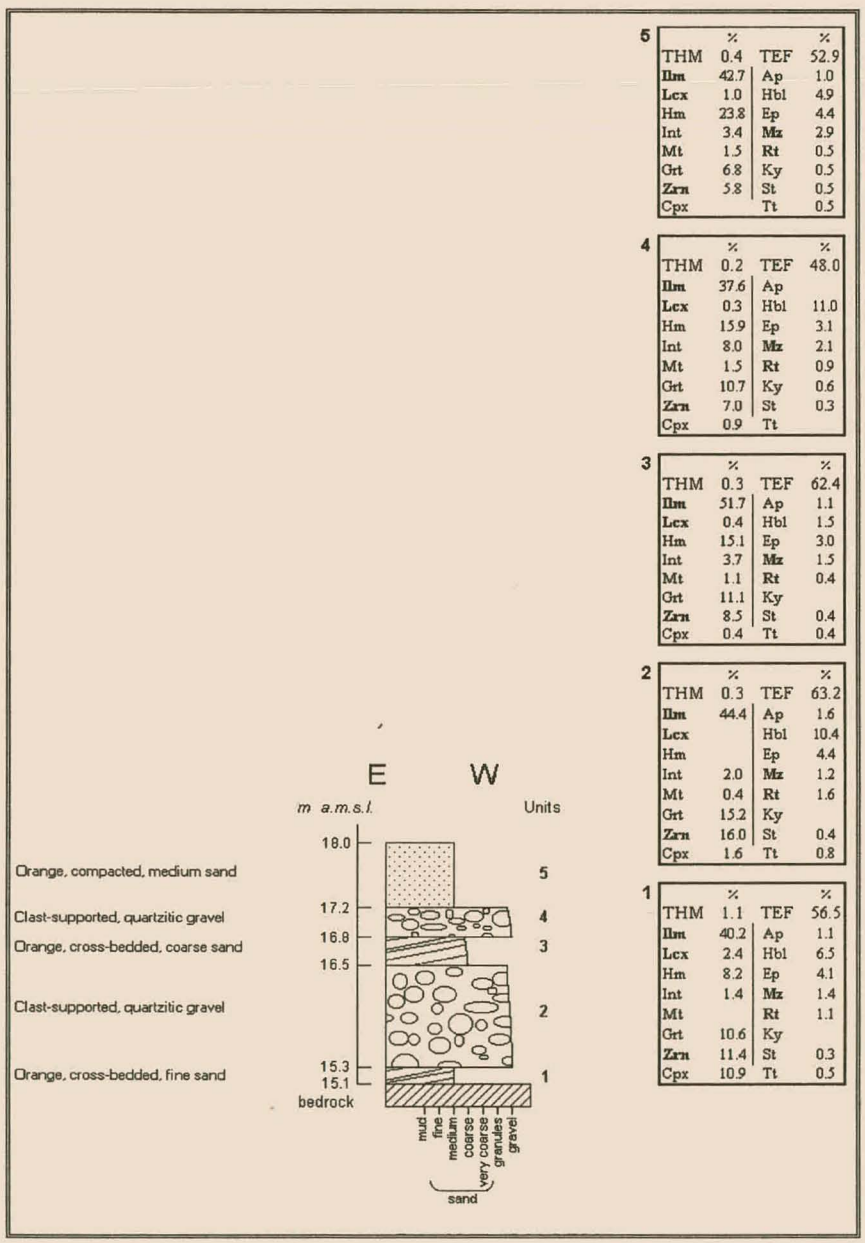

5	%		%
THM	0.4	TEF	52.9
Ilm	42.7	Ap	1.0
Lcx	1.0	Hbl	4.9
Hm	23.8	Ep	4.4
Int	3.4	Mz	2.9
Mt	1.5	Rt	0.5
Grt	6.8	Ky	0.5
Zrn	5.8	St	0.5
Cpx		Tt	0.5

4	%		%
THM	0.2	TEF	48.0
Ilm	37.6	Ap	
Lcx	0.3	Hbl	11.0
Hm	15.9	Ep	3.1
Int	8.0	Mz	2.1
Mt	1.5	Rt	0.9
Grt	10.7	Ky	0.6
Zrn	7.0	St	0.3
Cpx	0.9	Tt	

3	%		%
THM	0.3	TEF	62.4
Ilm	51.7	Ap	1.1
Lcx	0.4	Hbl	1.5
Hm	15.1	Ep	3.0
Int	3.7	Mz	1.5
Mt	1.1	Rt	0.4
Grt	11.1	Ky	
Zrn	8.5	St	0.4
Cpx	0.4	Tt	0.4

2	%		%
THM	0.3	TEF	63.2
Ilm	44.4	Ap	1.6
Lcx		Hbl	10.4
Hm		Ep	4.4
Int	2.0	Mz	1.2
Mt	0.4	Rt	1.6
Grt	15.2	Ky	
Zrn	16.0	St	0.4
Cpx	1.6	Tt	0.8

1	%		%
THM	1.1	TEF	56.5
Ilm	40.2	Ap	1.1
Lcx	2.4	Hbl	6.5
Hm	8.2	Ep	4.1
Int	1.4	Mz	1.4
Mt		Rt	1.1
Grt	10.6	Ky	
Zrn	11.4	St	0.3
Cpx	10.9	Tt	0.5

Figure 3A. Geological cross-section of AK45H.

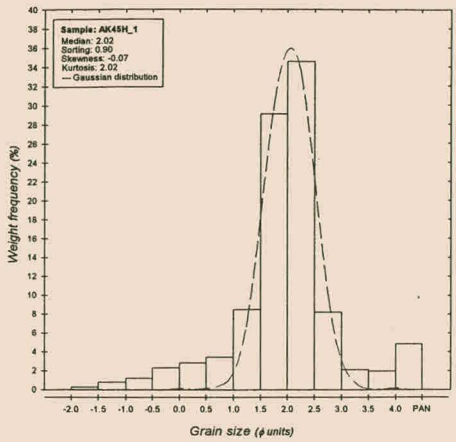

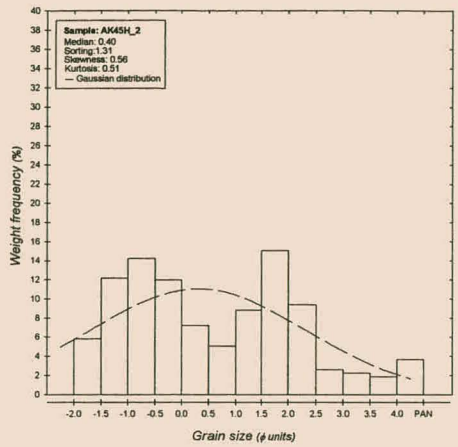

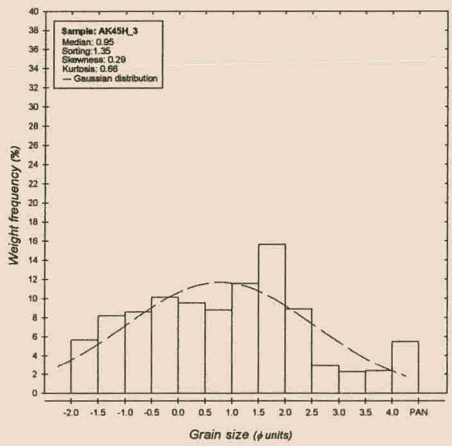

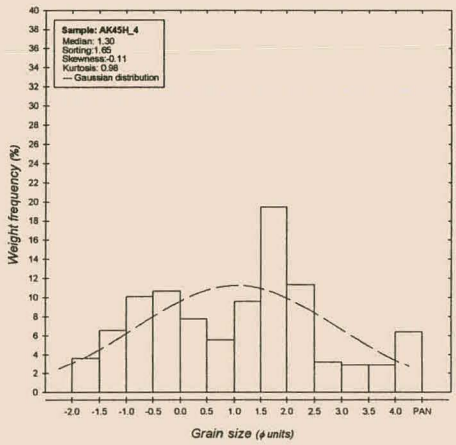

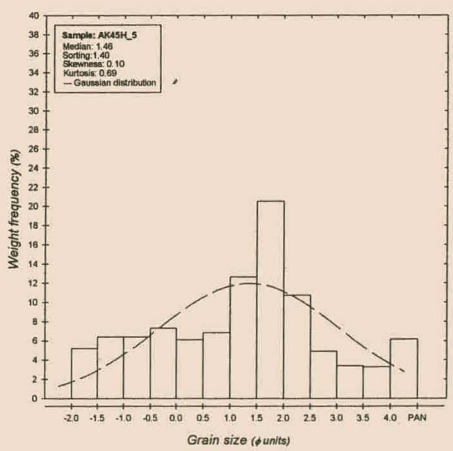

Figure 3B. Grain-size distributions of AH45H samples.

Sample site AK52N (Fig. 4A).

Unit AK52N_1

Cross-laminated, light brown (5YR 5/6), medium quartzo-feldspathic sand that is poorly sorted.

Unit AK52N_2

Orange (10YR 7/4), quartzo-feldspathic, medium sand that is poorly sorted. The unit is essentially structureless; partly calcretized throughout with distinct calcrete bands near the top.

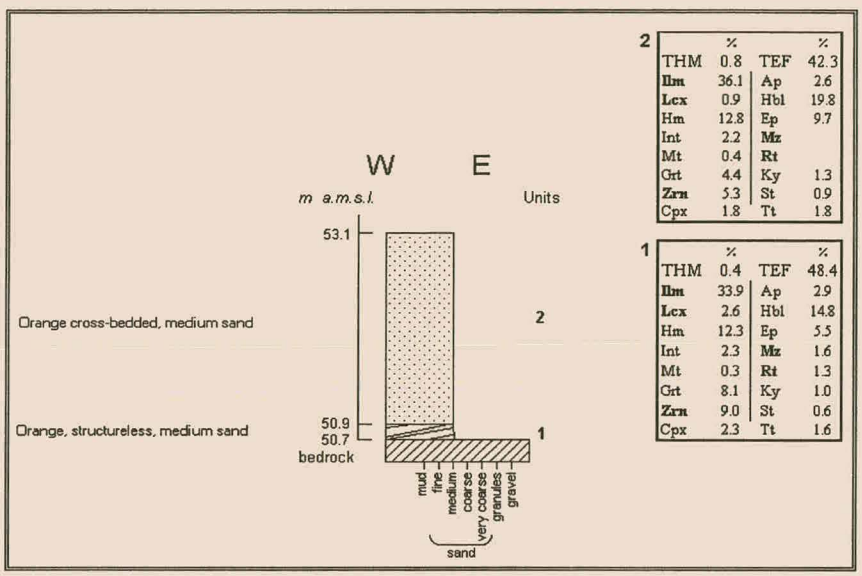

2	%		%
THM	0.8	TEF	42.3
Ilm	36.1	Ap	2.6
Lcx	0.9	Hbl	19.8
Hm	12.8	Ep	9.7
Int	2.2	**Mz**	
Mt	0.4	**Rt**	
Grt	4.4	Ky	1.3
Zrn	5.3	St	0.9
Cpx	1.8	Tt	1.8

1	%		%
THM	0.4	TEF	48.4
Ilm	33.9	Ap	2.9
Lcx	2.6	Hbl	14.8
Hm	12.3	Ep	5.5
Int	2.3	**Mz**	1.6
Mt	0.3	**Rt**	1.3
Grt	8.1	Ky	1.0
Zrn	9.0	St	0.6
Cpx	2.3	Tt	1.6

Figure 4A. Geological cross-section of AK52N.

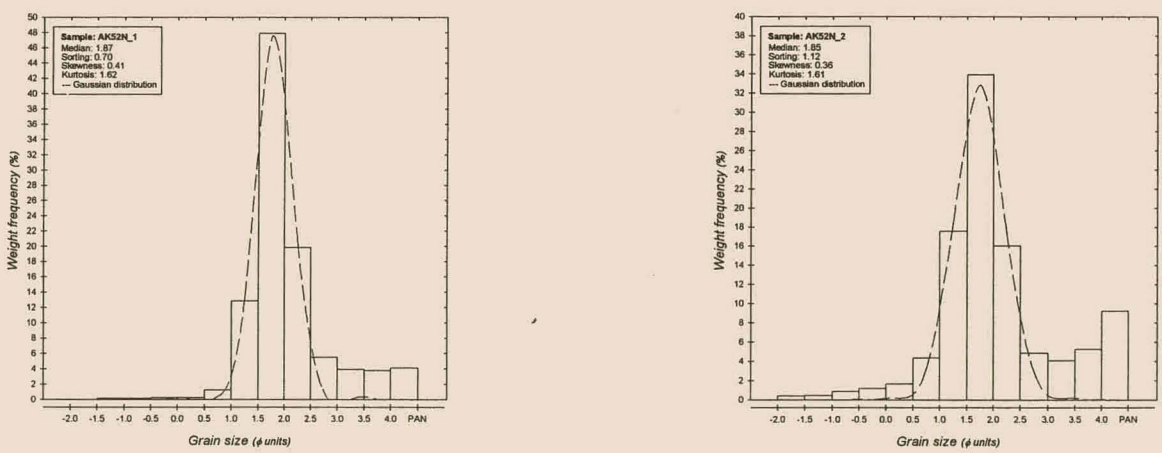

Figure 4B. Grain-size distributions of AK52N samples.

Sample site DP127R (Fig. 5A).

Unit DP127R_1

Moderately sorted, orange (10YR 6/6), cross-bedded, medium quartzo-feldspathic sand forms the basal unit. Sedimentary structures seem to be destroyed by intense bioturbation.

Unit DP127R_2

A cobble gravel with a moderately sorted, medium quartzo-feldspathic sand as matrix. Clasts vary from 5-15 cm and are mainly schist and quartzite. The gravel bed dips slightly seaward.

Unit DP127R_3

The gravel grades into orange, cross-bedded, medium, quartzo-feldspathic sand that displays moderate sorting. This unit hosts a range of well developed, horizontal laminated heavy mineral beds that dip seaward at 15°. Primary sedimentary features are often destroyed due to intense bioturbation.

Unit DP127R_4

The top unit consists of a lighter orange (10 YR 8/6), medium, quartzo-feldspathic sand that is compacted. Sorting is moderate, despite the presence of gritty quartz granules.

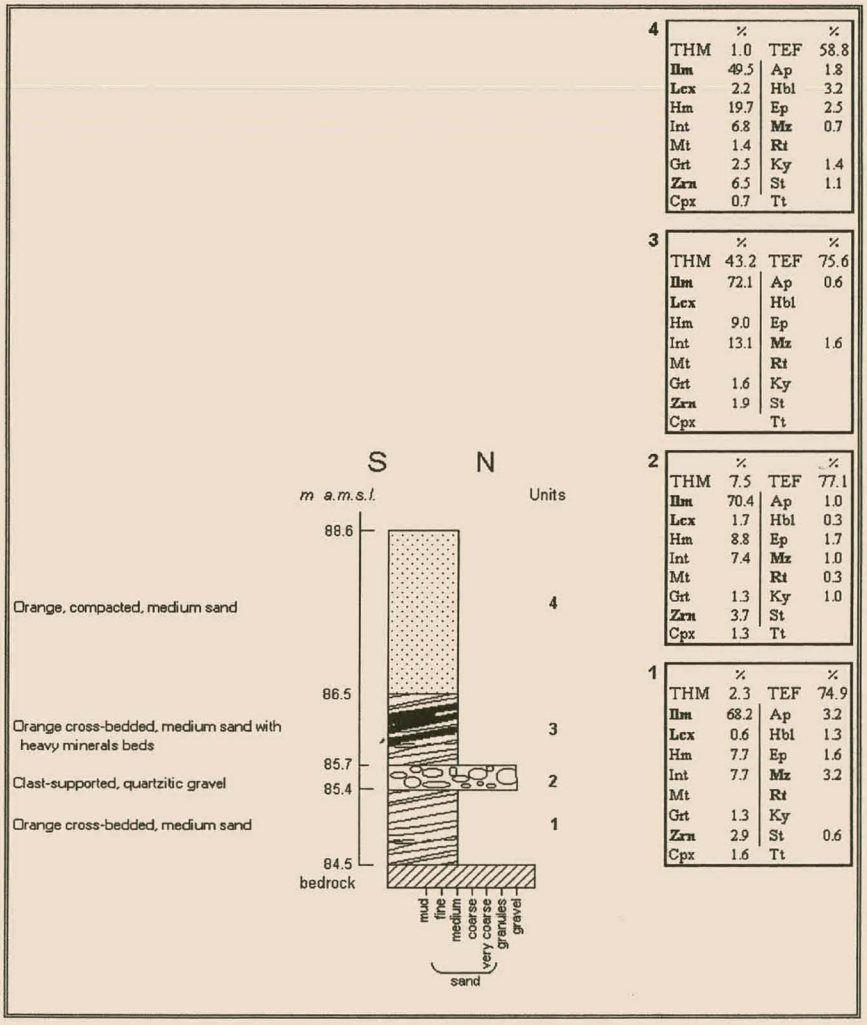

4	%		%
THM	1.0	TEF	58.8
Ilm	49.5	Ap	1.8
Lcx	2.2	Hbl	3.2
Hm	19.7	Ep	2.5
Int	6.8	Mz	0.7
Mt	1.4	Rt	
Grt	2.5	Ky	1.4
Zrn	6.5	St	1.1
Cpx	0.7	Tt	

3	%		%
THM	43.2	TEF	75.6
Ilm	72.1	Ap	0.6
Lcx		Hbl	
Hm	9.0	Ep	
Int	13.1	Mz	1.6
Mt		Rt	
Grt	1.6	Ky	
Zrn	1.9	St	
Cpx		Tt	

2	%		%
THM	7.5	TEF	77.1
Ilm	70.4	Ap	1.0
Lcx	1.7	Hbl	0.3
Hm	8.8	Ep	1.7
Int	7.4	Mz	1.0
Mt		Rt	0.3
Grt	1.3	Ky	1.0
Zrn	3.7	St	
Cpx	1.3	Tt	

1	%		%
THM	2.3	TEF	74.9
Ilm	68.2	Ap	3.2
Lcx	0.6	Hbl	1.3
Hm	7.7	Ep	1.6
Int	7.7	Mz	3.2
Mt		Rt	
Grt	1.3	Ky	
Zrn	2.9	St	0.6
Cpx	1.6	Tt	

Figure 5A. Geological cross-section of DP127R.

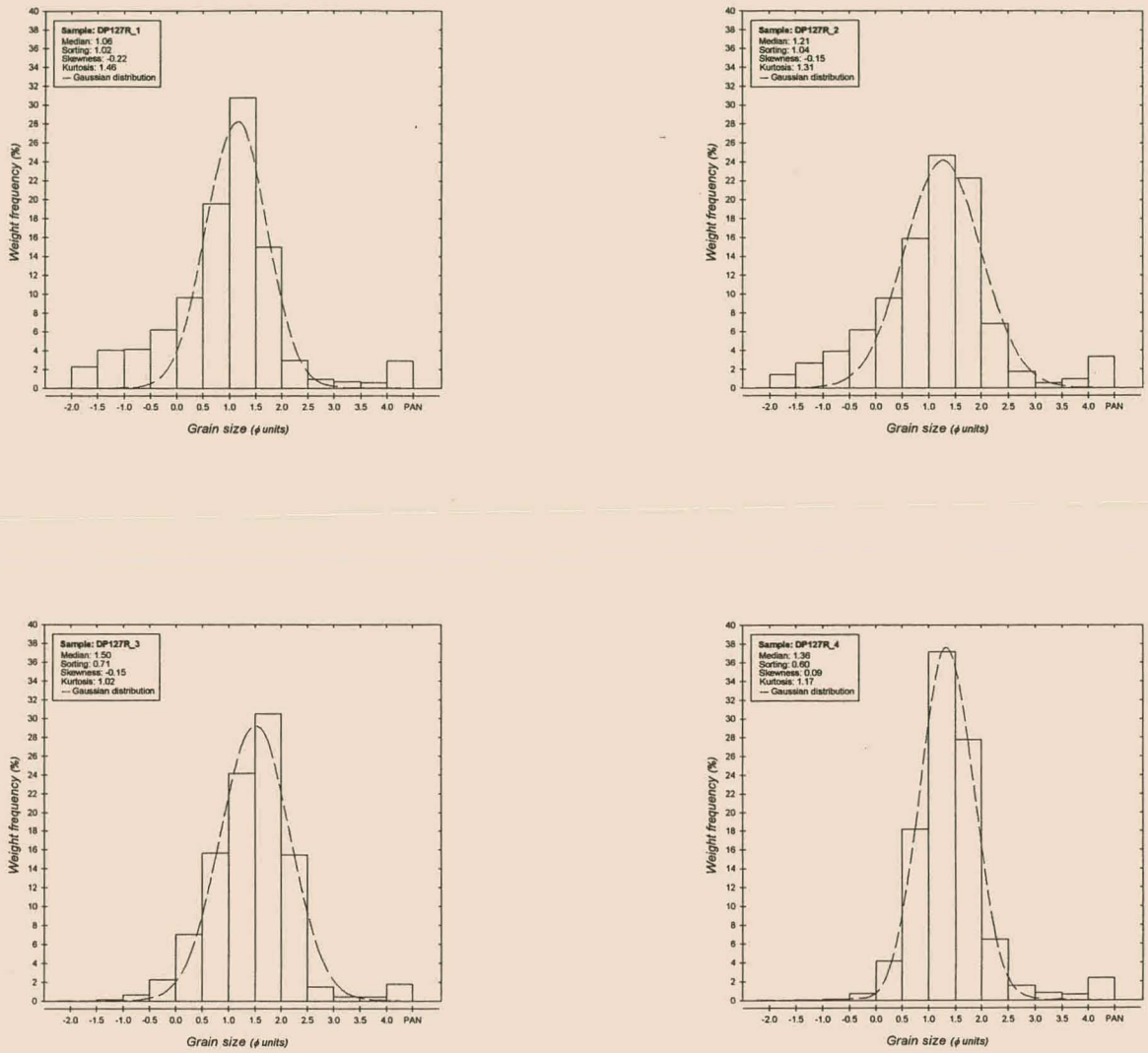

Figure 5B. Grain-size distributions of DP127R samples.

Sample site DP68D1 (Fig. 6A).

Unit DP68D1_1
Cobble gravel consisting of angular quartz and schist in a poorly sorted, medium sand.

Unit DP68D1_2
Light brown (5YR 5/6), muddy, fine, poorly sorted sand. Sedimentary structures are obscured by the muddy character of the unit.

Unit DP68D1_3
Muddy light brown (5YR 5/6), planar-bedded, fine sand that displays moderate sorting.

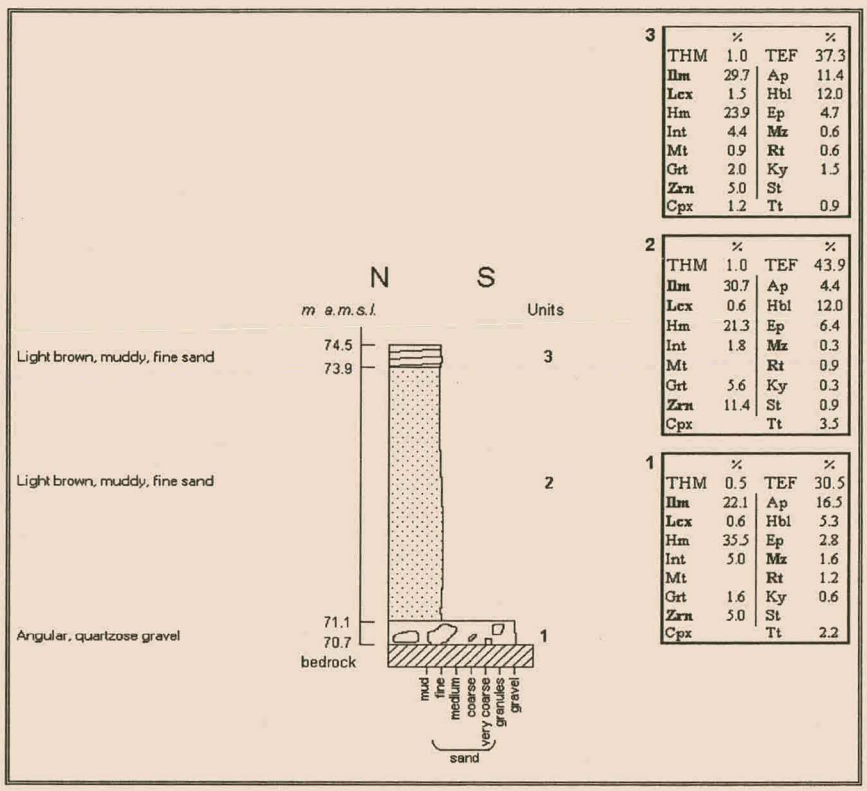

3	%		%
THM	1.0	TEF	37.3
Ilm	29.7	Ap	11.4
Lcx	1.5	Hbl	12.0
Hm	23.9	Ep	4.7
Int	4.4	Mz	0.6
Mt	0.9	Rt	0.6
Grt	2.0	Ky	1.5
Zrn	5.0	St	
Cpx	1.2	Tt	0.9

2	%		%
THM	1.0	TEF	43.9
Ilm	30.7	Ap	4.4
Lcx	0.6	Hbl	12.0
Hm	21.3	Ep	6.4
Int	1.8	Mz	0.3
Mt		Rt	0.9
Grt	5.6	Ky	0.3
Zrn	11.4	St	0.9
Cpx		Tt	3.5

1	%		%
THM	0.5	TEF	30.5
Ilm	22.1	Ap	16.5
Lcx	0.6	Hbl	5.3
Hm	35.5	Ep	2.8
Int	5.0	Mz	1.6
Mt		Rt	1.2
Grt	1.6	Ky	0.6
Zrn	5.0	St	
Cpx		Tt	2.2

Figure 6A. Geological cross-section of DP68D1.

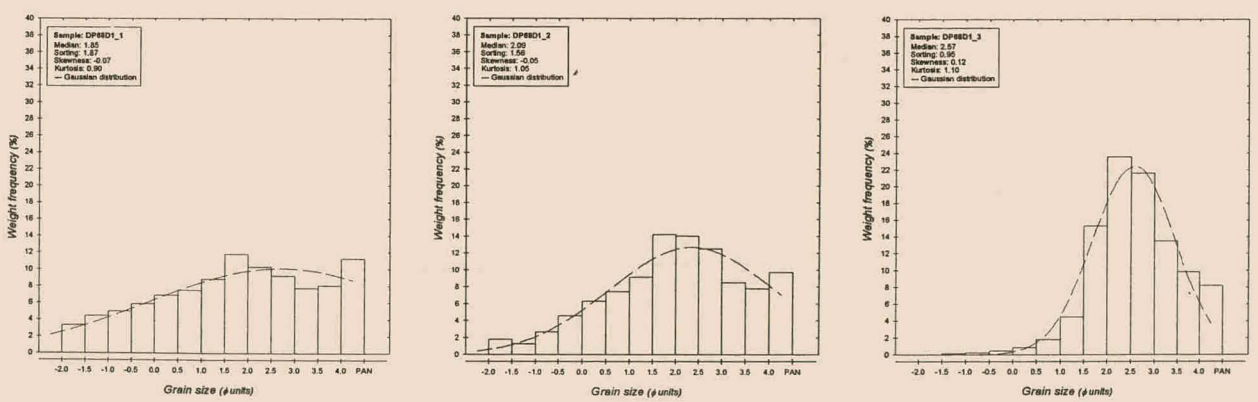

Figure 6B. Grain-size distributions of DP68D1 samples.

Sample site DP84LM (Fig. 7A).

Unit DP84LM_1

Matrix-supported pebble gravel with matrix of poorly sorted, granular quartzo-feldspathic sand. Clasts comprise quartzite of which the size rarely exceeds 1 cm.

Unit DP84LM_2

Poorly sorted, medium quartzo-feldspathic sand, with an orange (10YR 7/4) hue. The unit appears to be structureless and is capped by a calcrete layer.

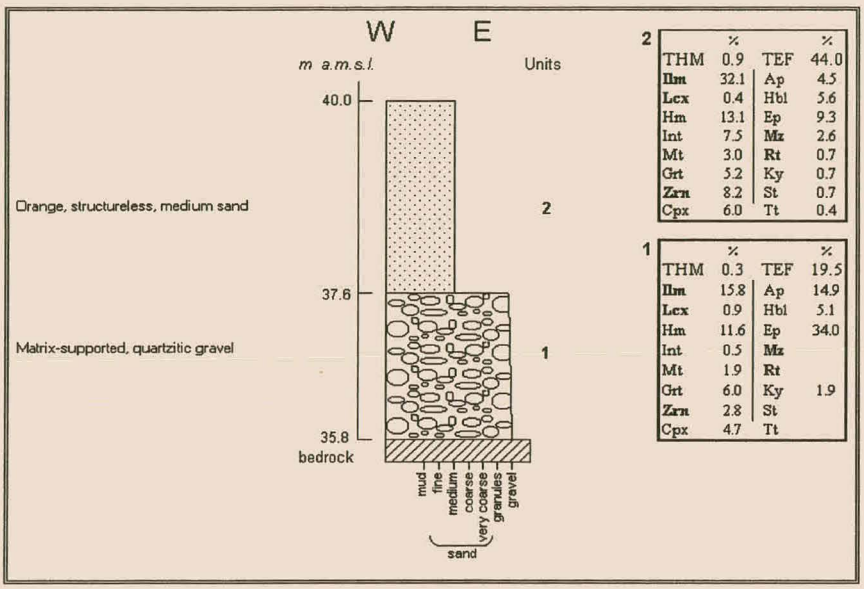

Figure 7A. Geological cross-section of DP84LM.

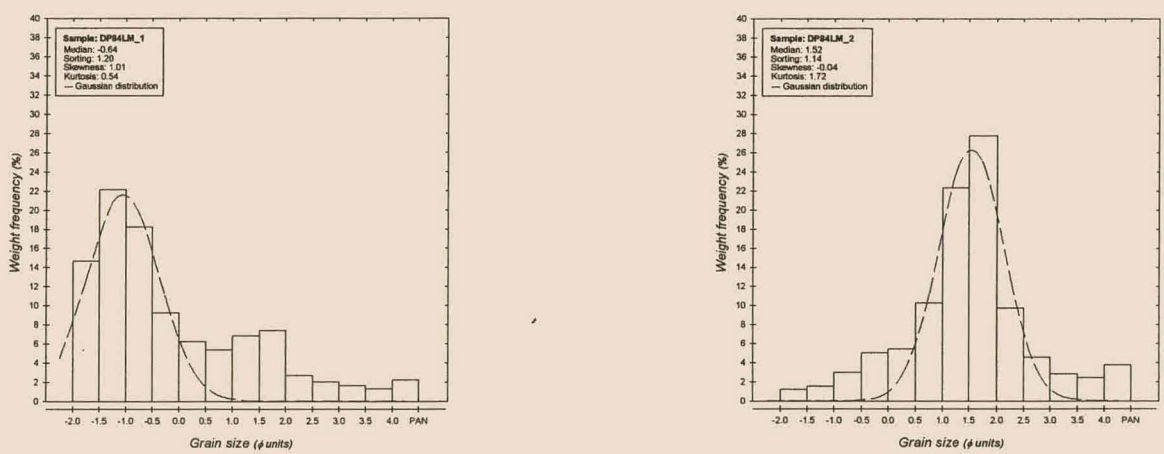

Figure 7B. Grain-size distributions of DP84LM samples.

Sample site DP88LM (Fig. 8A).

Unit DP88LM_1
Muddy, cross-bedded, dark brown (5YR 4/4), medium-grained quartzo-feldspathic sand. Sorting is poor and grains often display manganese staining.

Unit DP88LM_2
Muddy, poorly sorted, coarse to granular dark brown (5YR 4/4), quartzo-feldspathic sand with scattered quartz pebbles. Trough cross-bedding marks the bottom of the unit and grades into simple cross-bedding. Calcretized trace fossils and roots are abundant of the top of the unit.

Unit DP88LM_3
Structureless, compacted, dark brown (5YR 4/4), medium quartzo-feldspathic sand.

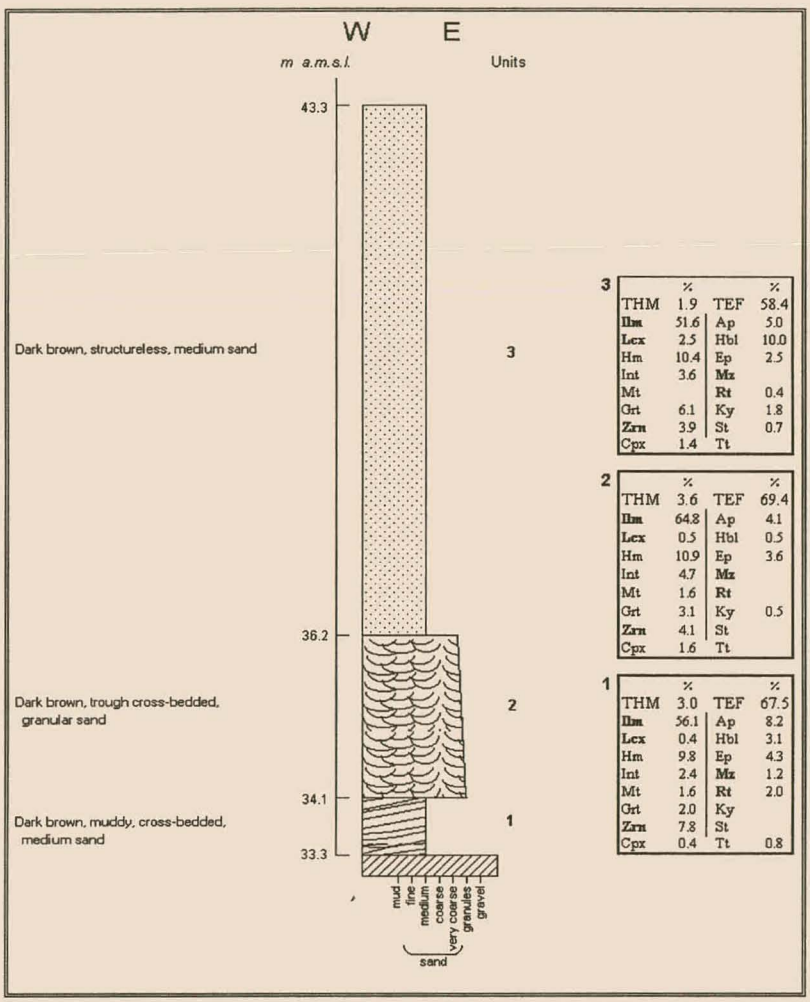

Figure 8A. Geological cross-section of DP88LM.

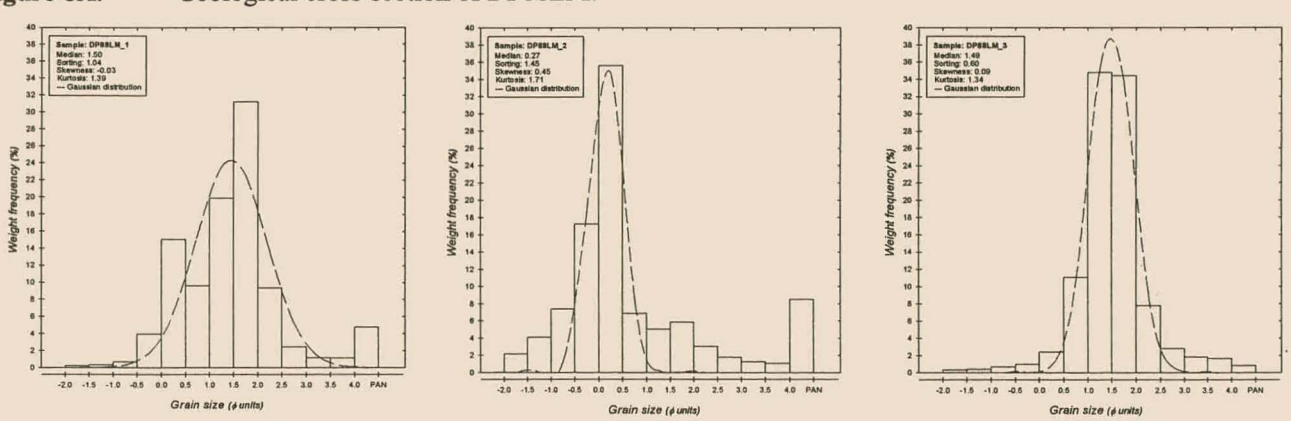

Figure 8B. Grain-size distributions of DP88LM samples.

Sample site KV196R (Fig. 9A).

Unit KV196R_1
Orange, moderately sorted, cross-bedded medium sand with faint, parallel heavy mineral laminae.

Unit KV196R_2
Clast-supported pebble gravel with poorly sorted, medium, quartzo-feldspathic sand as matrix. The packing of the clasts is chaotic. The bottom of the unit consists of rounded schist and quartzite cobbles which grade upwards into more flattened pebbles.

Unit KV196R_3
Medium-grained, moderately sorted low-angle cross-bedded quartzo-feldspathic sand with parallel heavy mineral laminae which dip approximately 2° seaward and are localised in the top of the unit.

Unit KV196R_4
Red (5YR 4/6), structureless, medium quartzose sand that displays moderate sorting.

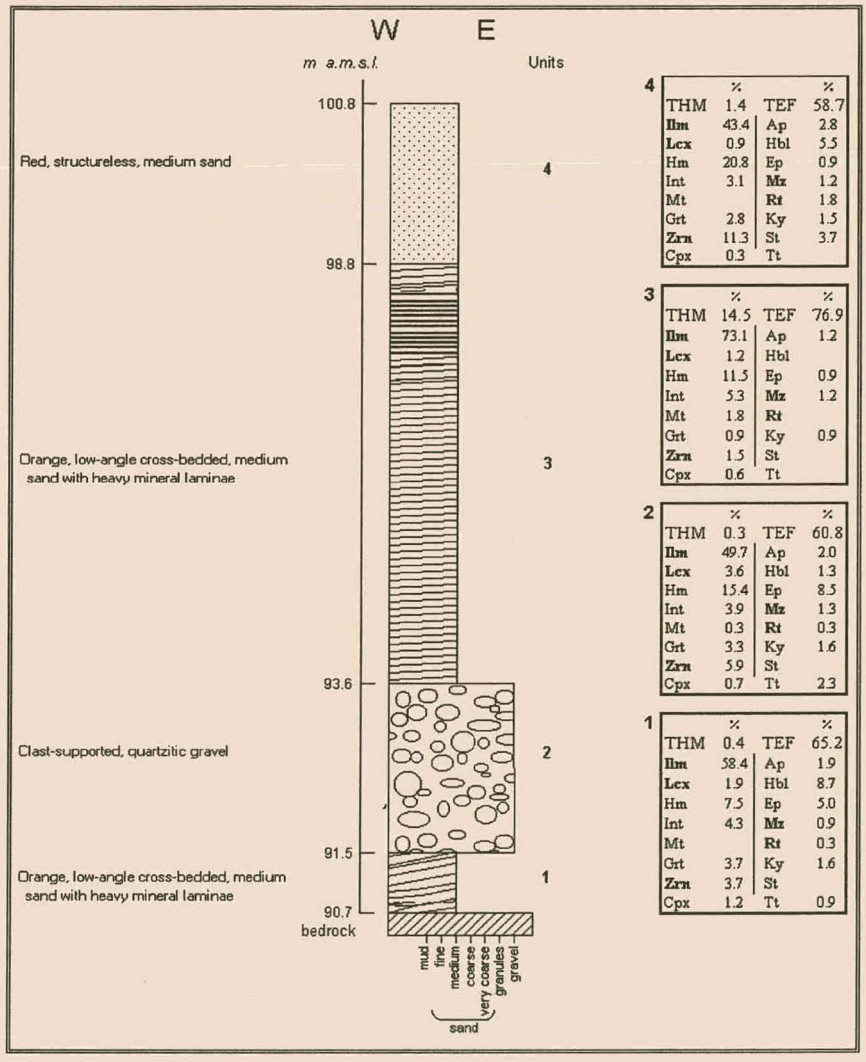

Figure 9A. Geological cross-section of KV196R.

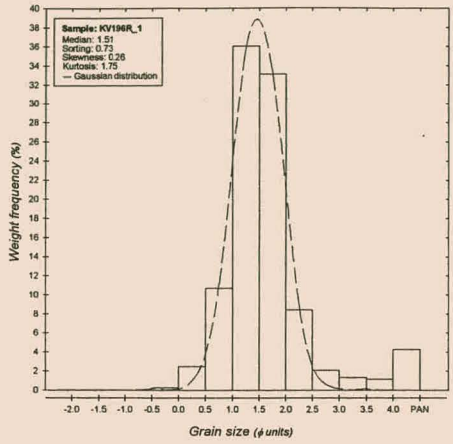

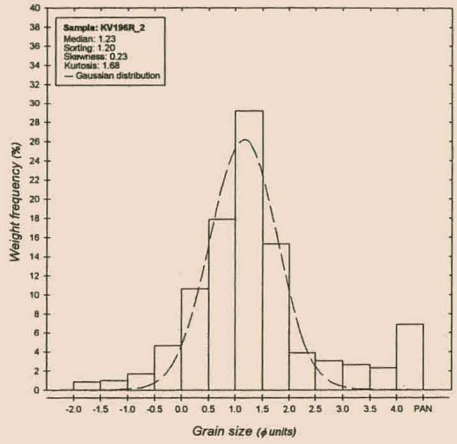

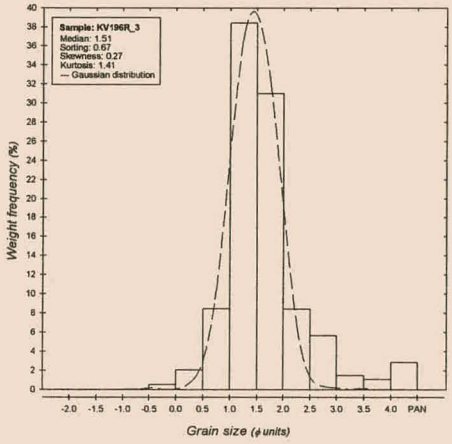

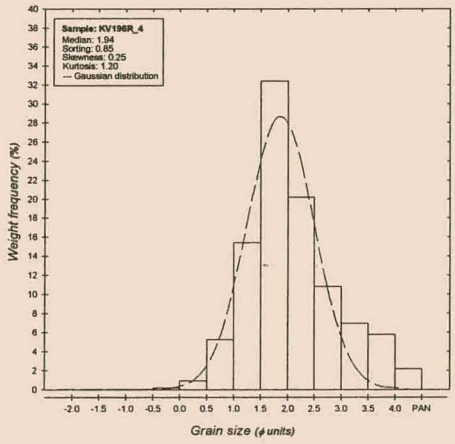

Figure 9B. Grain-size distributions of KV196R samples.

Sample site KV198PR (Fig. 10A).

Unit KV198PR_1

Pale yellow (10YR 8/6), cross-bedded, medium-grained quartzo-feldspathic sand with heavy mineral band of 15 cm. This unit displays moderate sorting and is consolidated due to calcretization.

Unit KV198PR_2

Well sorted, low-angle cross-bedded, medium quartzo-feldspathic sand with parallel heavy mineral laminae.

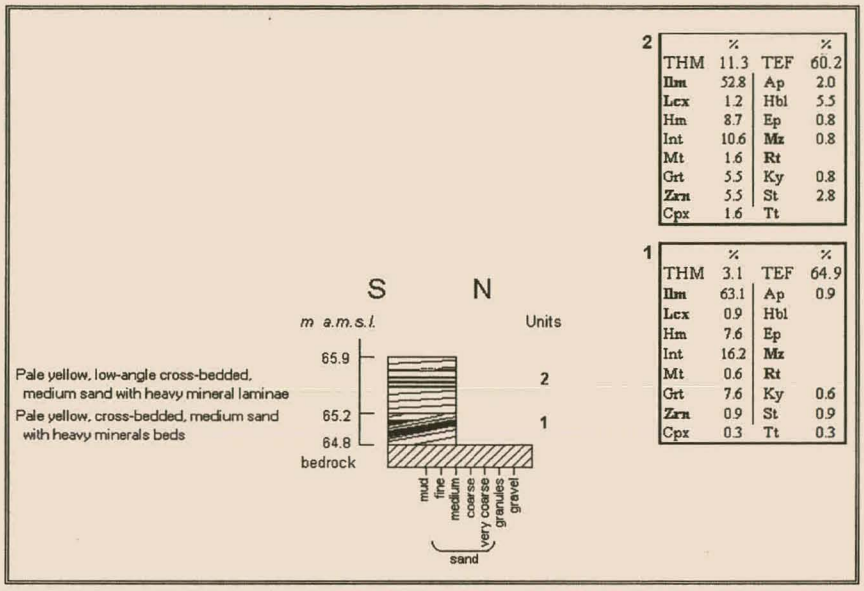

Figure 10A. Geological cross-section of KV198PR.

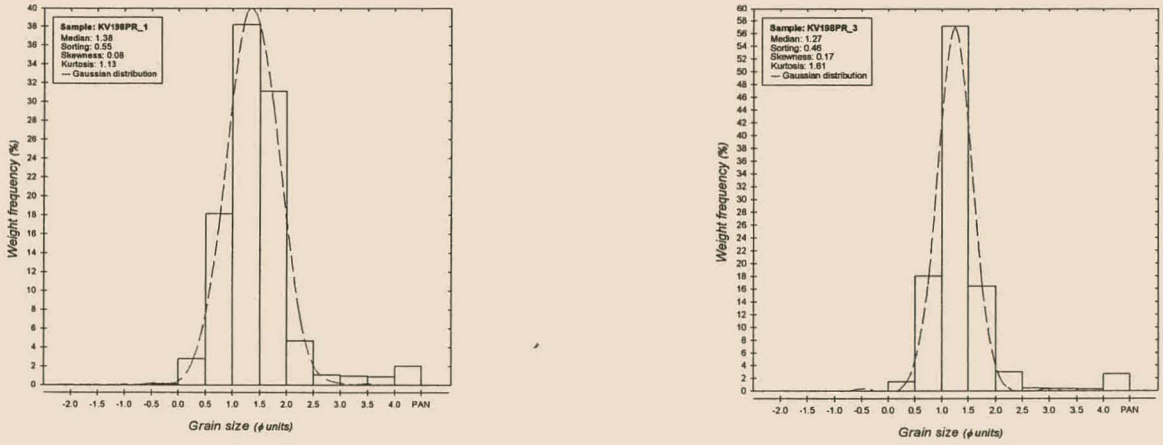

Figure 10B. Grain-size distributions of KV198PR samples.

Sample site TP235M (Fig. 11A).

Unit TP235M_1

Clast-supported cobble gravel with matrix of moderately sorted quartzo-feldspathic sand. Clasts comprise rounded schist and quartzite ranging in size from 5-15 cm. Packing is generally chaotic.

Unit TP235M_2

Yellow (10YR 8/6), cross-bedded, moderately sorted, medium quartzo-feldspathic sand. Trace fossils are abundant.

Unit TP235M_3

Orange, structureless, compacted, medium quartzo-feldspathic sand that displays poor sorting.

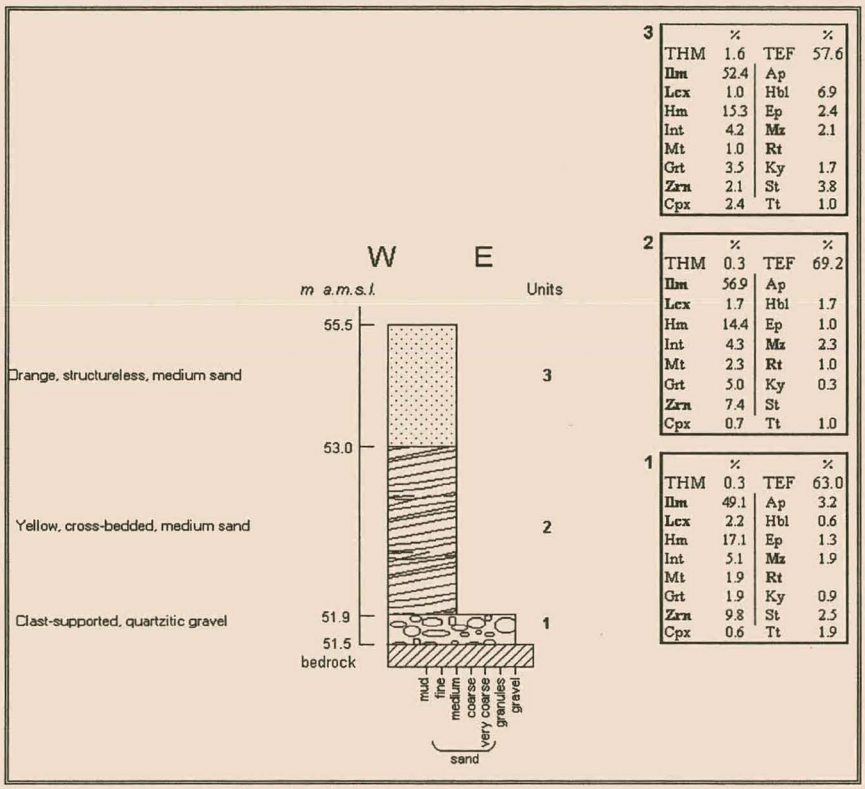

Figure 11A. Geological cross-section of TP235M.

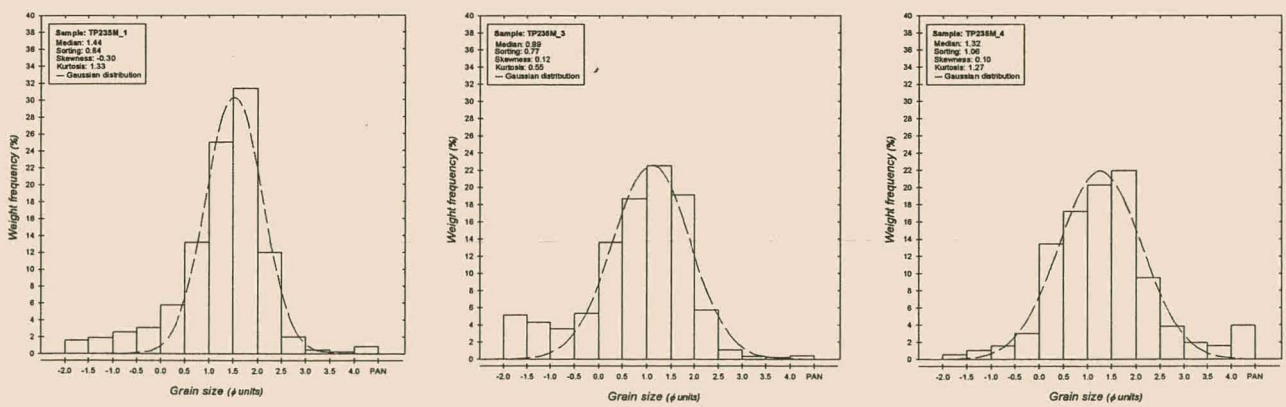

Figure 11B. Grain-size distributions of TP235M samples.

Sample site TP262N (Fig. 12A).

Unit TP262N_1
Yellow (10YR 5/4), cross-bedded, very coarse quartzo-feldspathic sand that is moderately sorted. This unit is partly consolidated due to calcretization.

Unit TP262N_2
Matrix-supported pebble gravel, matrix-supported with moderately sorted medium sand that contains disseminated heavy minerals. Clasts are randomly distributed and comprise rounded quartzite and schist.

Unit TP262N_3
Yellow (10YR 5/4), low-angle cross-bedded, medium-grained quartzo-feldspathic sand with parallel-laminated heavy mineral layers. Sorting is moderate

Unit TP262N_4
The top unit is a structureless, pale orange (10YR 8/2), poorly sorted, medium quartzo-feldspathic sand.

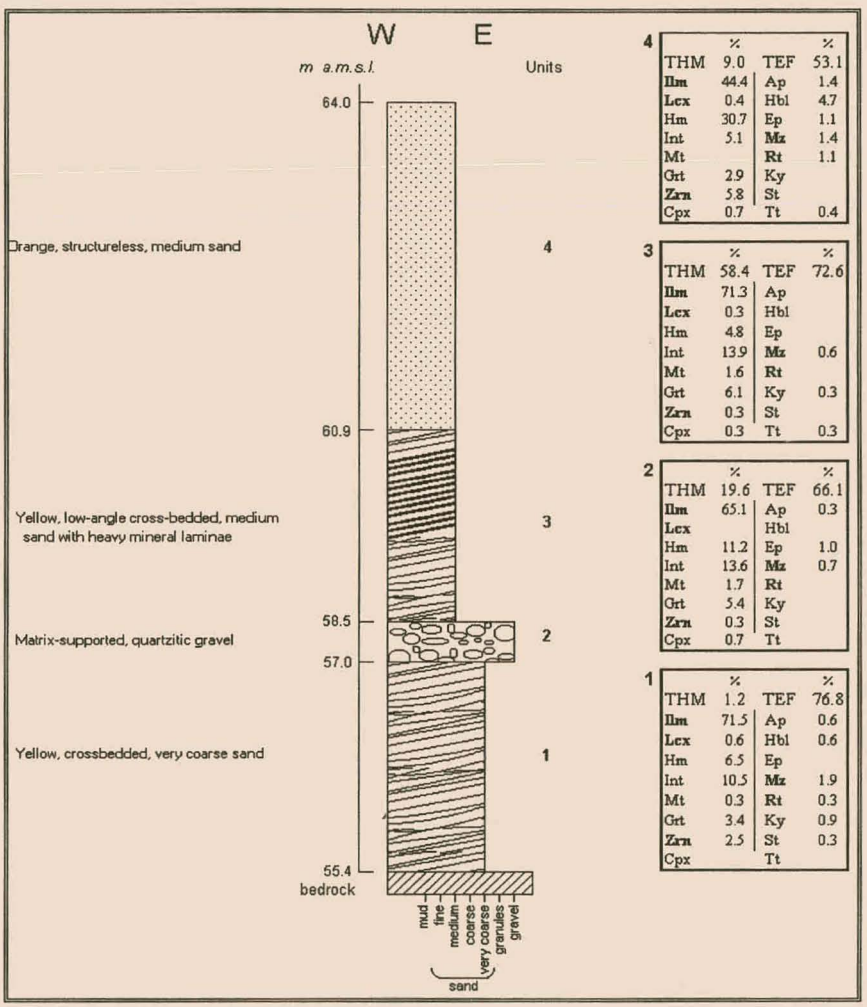

Figure 12A. Geological cross-section of TP262N.

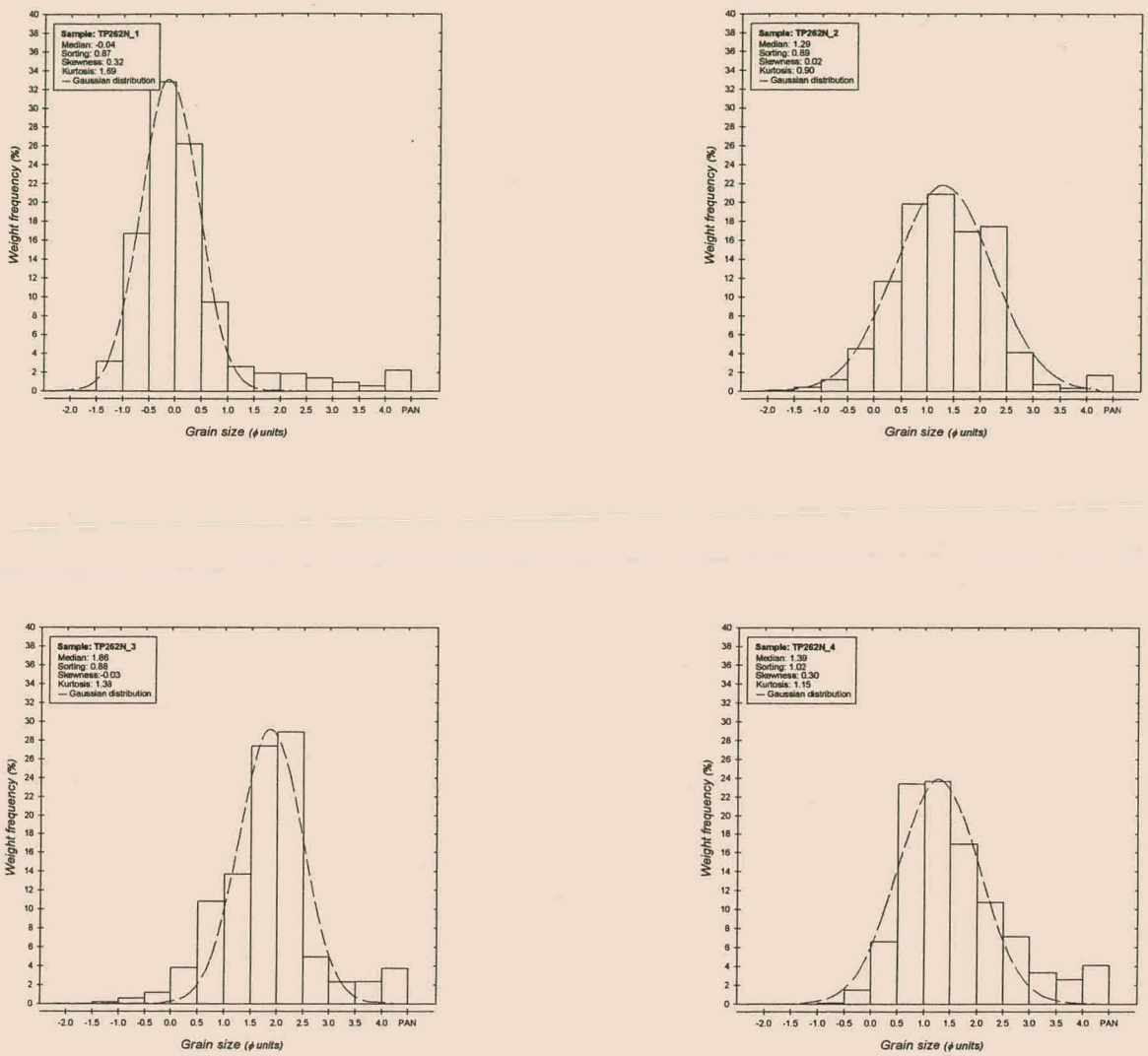

Figure 12B. Grain-size distributions of TP262N samples.

Sample site SEA419 (Fig. 13A).

Unit SEA419_1
Moderately sorted, coarse quartzose sand

Unit SEA419_2
Moderately sorted, medium quartzose sand

Unit SEA419_3
Moderately sorted, coarse quartzose sand

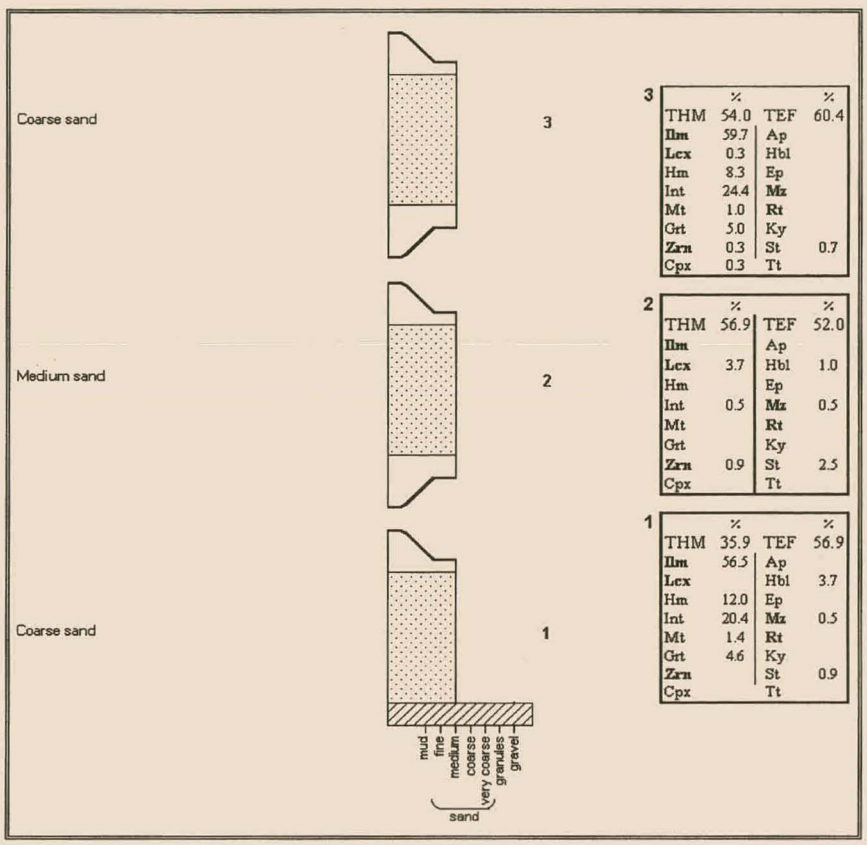

Figure 13A. Geological cross-section of SEA419.

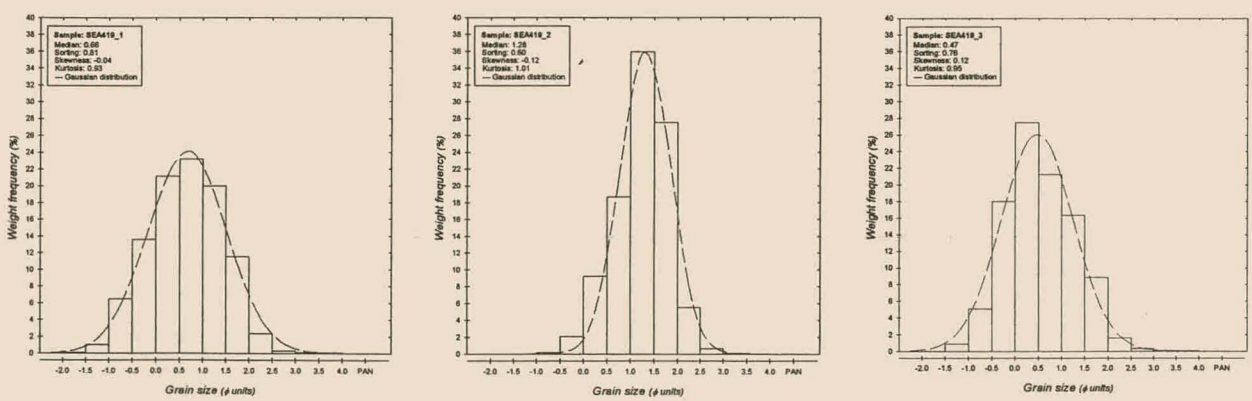

Figure 13B. Grain-size distributions of SEA419 samples.

BUFFELS INLAND COMPLEX

Sample site LH_C (Fig. 14A).

Unit LH_C_1
Reddish brown (10YR 4/6), cross-bedded, coarse sand that is poorly sorted.

Unit LH_C_2

Matrix-supported pebble gravel within a poorly sorted, very coarse sand matrix. Pebbles consist of angular quartz and schist that range from 2-5 cm.

Unit LH_C_3
Orange (10YR 6/6), poorly sorted, trough cross-bedded bimodal quartzo-feldspathic sand.

Unit LH_C_4
Orange, cross-bedded, coarse quartzo-feldspathic sand that is poorly sorted.

Unit LH_C_5
Matrix-supported pebble gravel with poorly sorted medium-grained matrix. A poorly sorted, gritty sandstone overlies this unit.

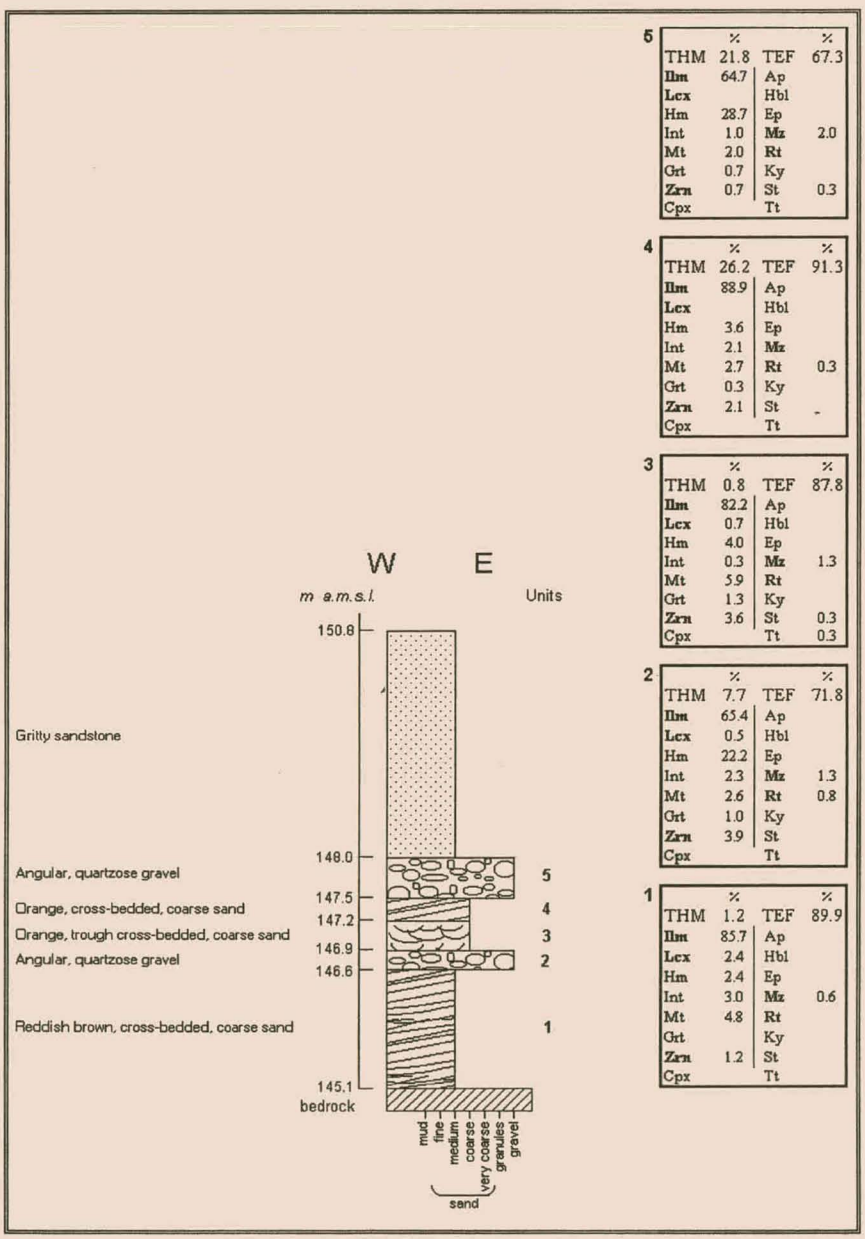

Figure 14A. Geological cross-section of LH_C.

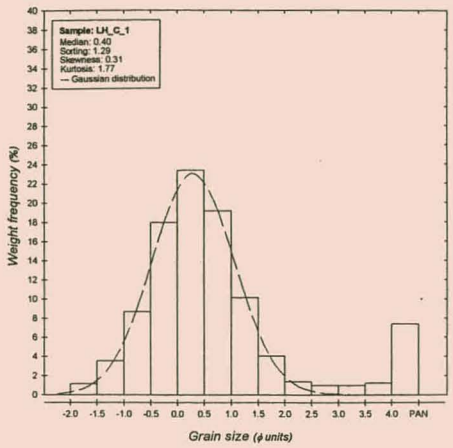

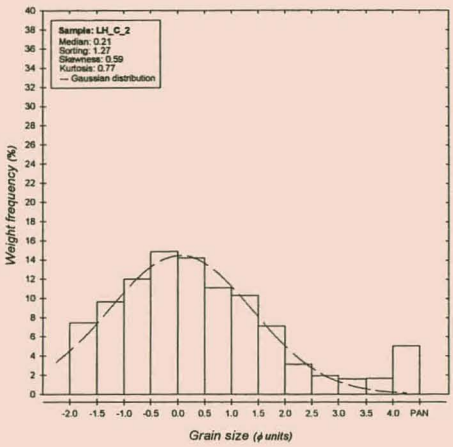

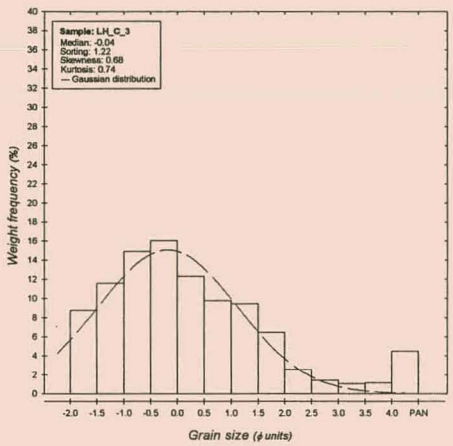

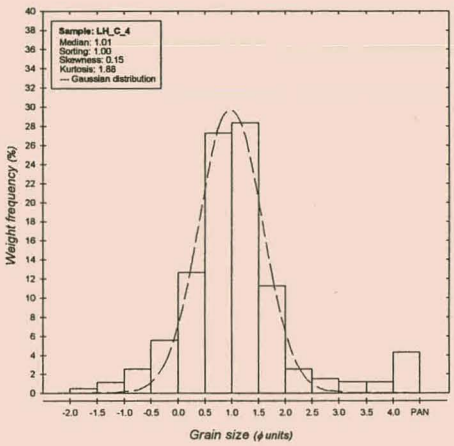

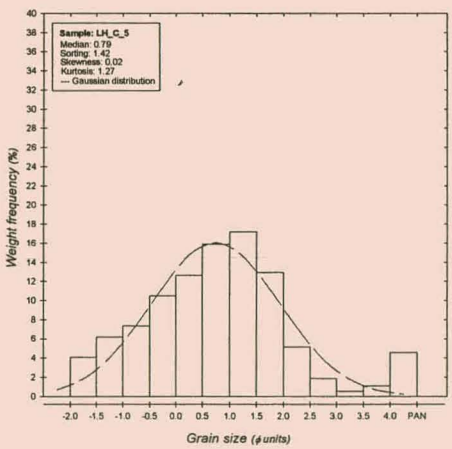

Figure 14B. Grain-size distributions of LH_C samples.

Sample site NB19AC (Fig. 15A).

Unit NB19AC_1

Clast-supported pebble gravel with a matrix of poorly sorted, argillaceous sand. Clasts vary from angular to subangular ranging in size from 1 to 5 cm. Clasts are predominantly quartz with minor proportion derived from the bedrock.

Unit NB19AC_2

The basal gravel grades upward into a very coarse, poorly sorted sand. The sand is semi-consolidated by a greenish mud giving the unit a green hue (10GY 7/2).

Unit NB19AC_3

Consolidated, greyish green (5 GY 8/1), poorly sorted, medium quartzo-feldspathic sand.

Unit NB19AC_4

Red (5R 4/6), moderately sorted, medium quartzose sand.

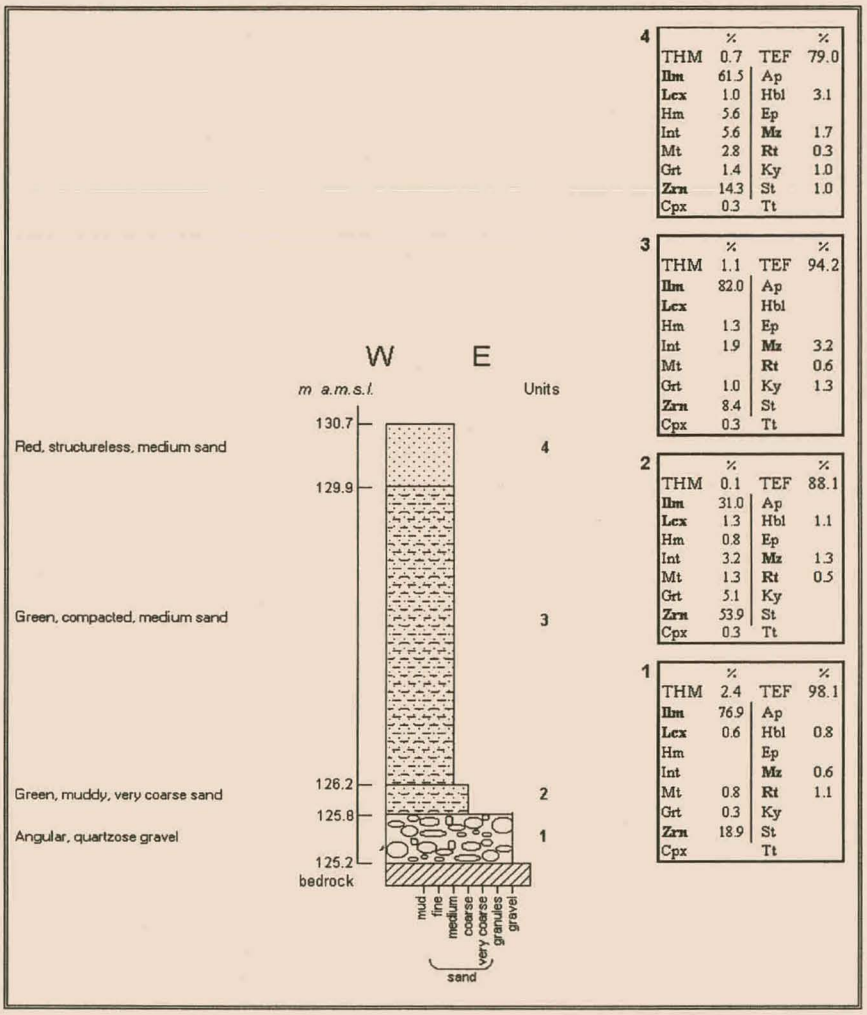

4	%		%
THM	0.7	TEF	79.0
Ilm	61.5	Ap	
Lcx	1.0	Hbl	3.1
Hm	5.6	Ep	
Int	5.6	**Mz**	1.7
Mt	2.8	**Rt**	0.3
Grt	1.4	Ky	1.0
Zrn	14.3	St	1.0
Cpx	0.3	Tt	

3	%		%
THM	1.1	TEF	94.2
Ilm	82.0	Ap	
Lcx		Hbl	
Hm	1.3	Ep	
Int	1.9	**Mz**	3.2
Mt		**Rt**	0.6
Grt	1.0	Ky	1.3
Zrn	8.4	St	
Cpx	0.3	Tt	

2	%		%
THM	0.1	TEF	88.1
Ilm	31.0	Ap	
Lcx	1.3	Hbl	1.1
Hm	0.8	Ep	
Int	3.2	**Mz**	1.3
Mt	1.3	**Rt**	0.5
Grt	5.1	Ky	
Zrn	53.9	St	
Cpx	0.3	Tt	

1	%		%
THM	2.4	TEF	98.1
Ilm	76.9	Ap	
Lcx	0.6	Hbl	0.8
Hm		Ep	
Int		**Mz**	0.6
Mt	0.8	**Rt**	1.1
Grt	0.3	Ky	
Zrn	18.9	St	
Cpx		Tt	

Figure 15A. Geological cross-section of NB19AC.

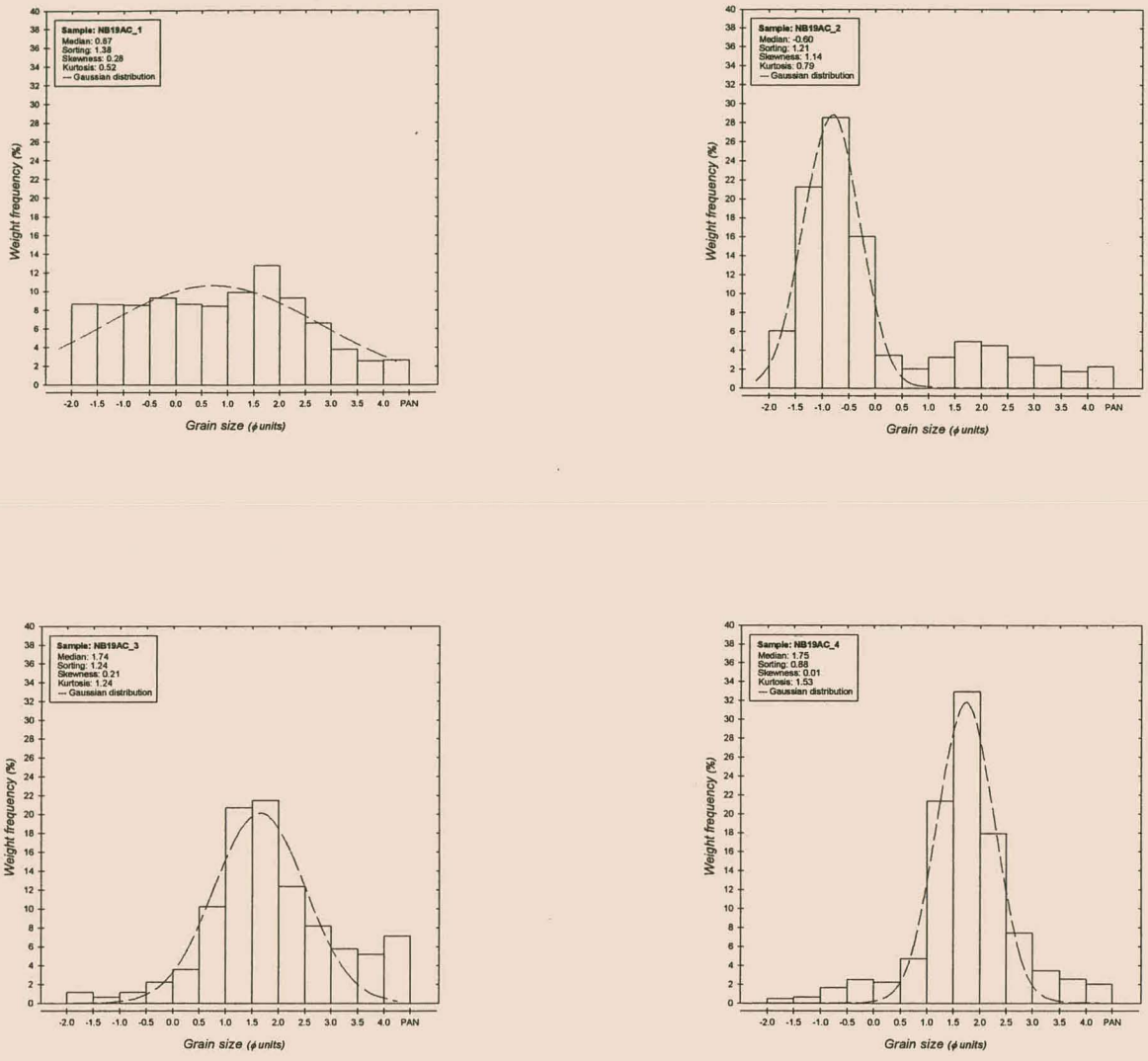

Figure 15B. Grain-size distributions of NB19AC samples.

Sample site NB21B (Fig. 16A).

Unit NB21B_1
Bedrock is overlain by yellow-grey (5Y 8/1), moderately sorted, very coarse quartzose sand.

Unit NB21B_2
Normal-graded, clast-supported cobble gravel within a coarse quartzose matrix. Clasts vary from 2-15 cm and consist mainly of angular grey quartz.

Unit NB21B_3
The gravel grades into a yellow-grey (5Y 8/1), medium, poorly sorted cross-bedded quartzose sand.

Unit NB21B_4
Muddy, cross-bedded, medium argillaceous sand. Sorting is poor and interfingering coarser sand is common in this unit.

Unit NB21B_5
Structureless, well-sorted medium quartzose sand with a red (5R 4/6) colour.

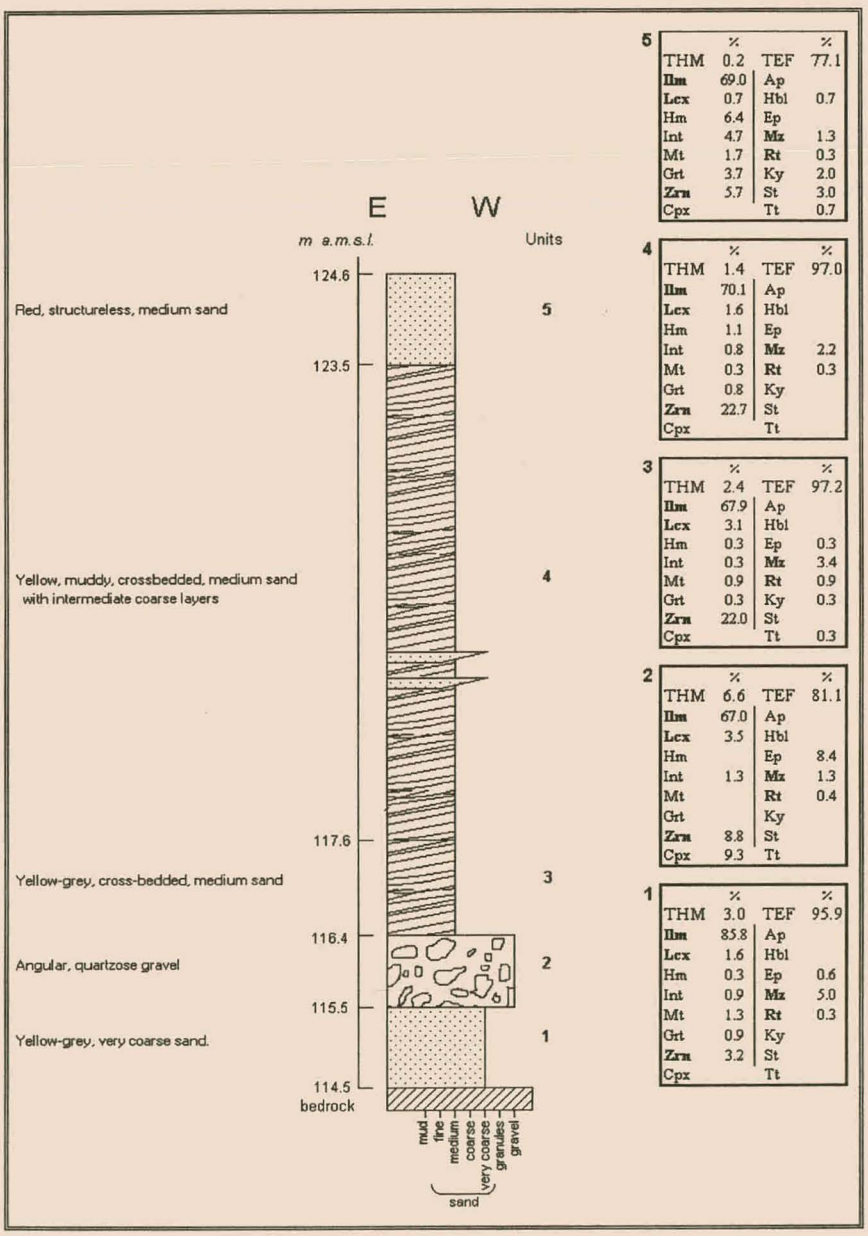

Figure 16A. Geological cross-section of NB21B.

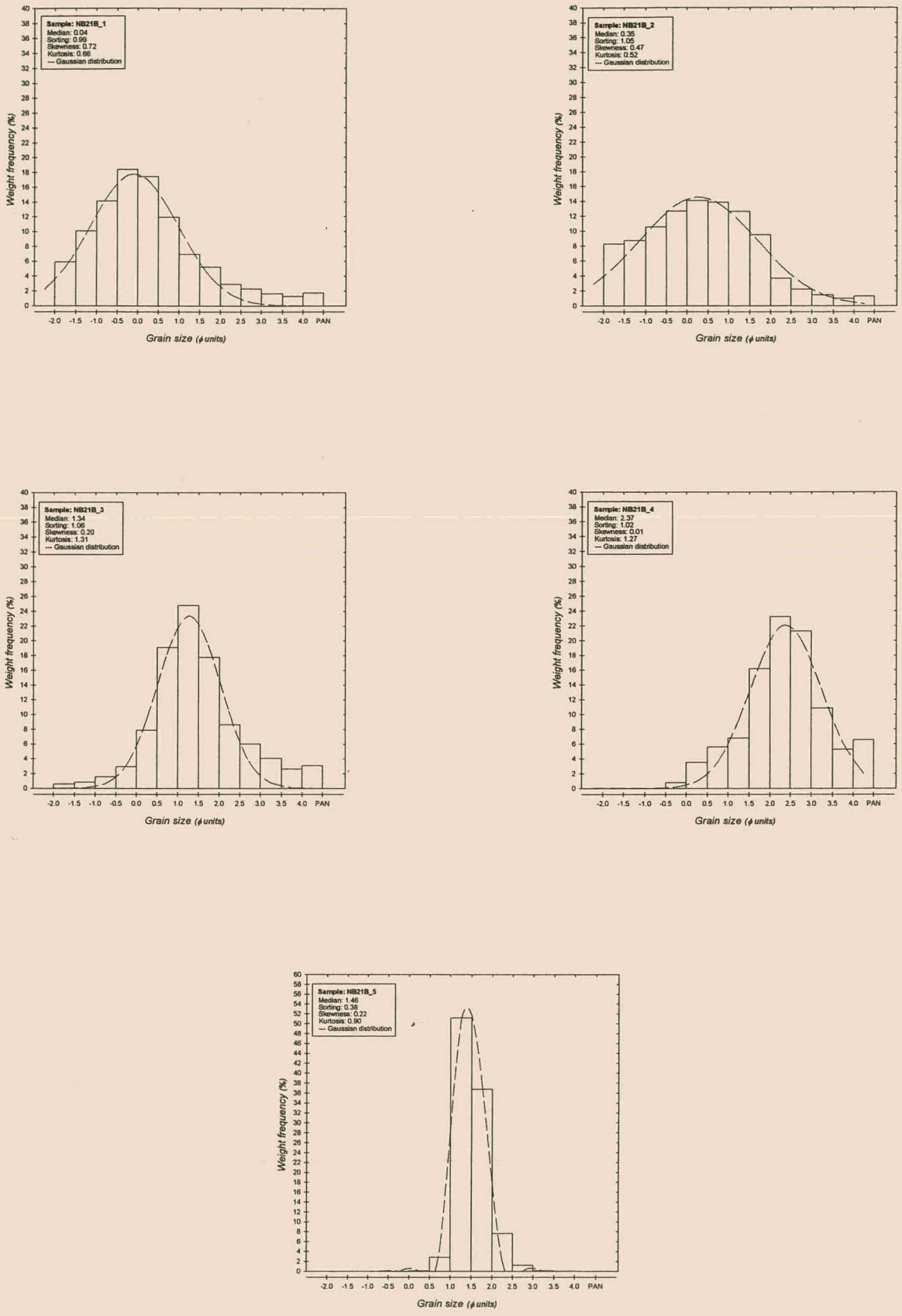

Figure 16B. Grain-size distributions of NB21B samples.

Sample site 68/69F3-02 (Fig. 17A).

Unit 68/69_1

Matrix-supported, poorly sorted channel gravel in a poorly sorted, muddy sand matrix. The clasts consist of angular and subangular grey quartz ranging in size from pebbles to cobbles. The matrix is poorly sorted, white to grey (5Y 8/1), with the sand size portion being mainly quartzose whereas the mud is kaolinitic. Poorly sorted, fine matrix.

Unit 68/69_2

The lithology of this unit is essentially the same as that of the previous sample, although this gravel does not overlie bedrock but occurs higher up in the channel sequence.

Unit 68/69_3

This unit was taken from a woody horizon in the channel gravel and comprises a grey medium, moderately sorted, muddy quartzose sand.

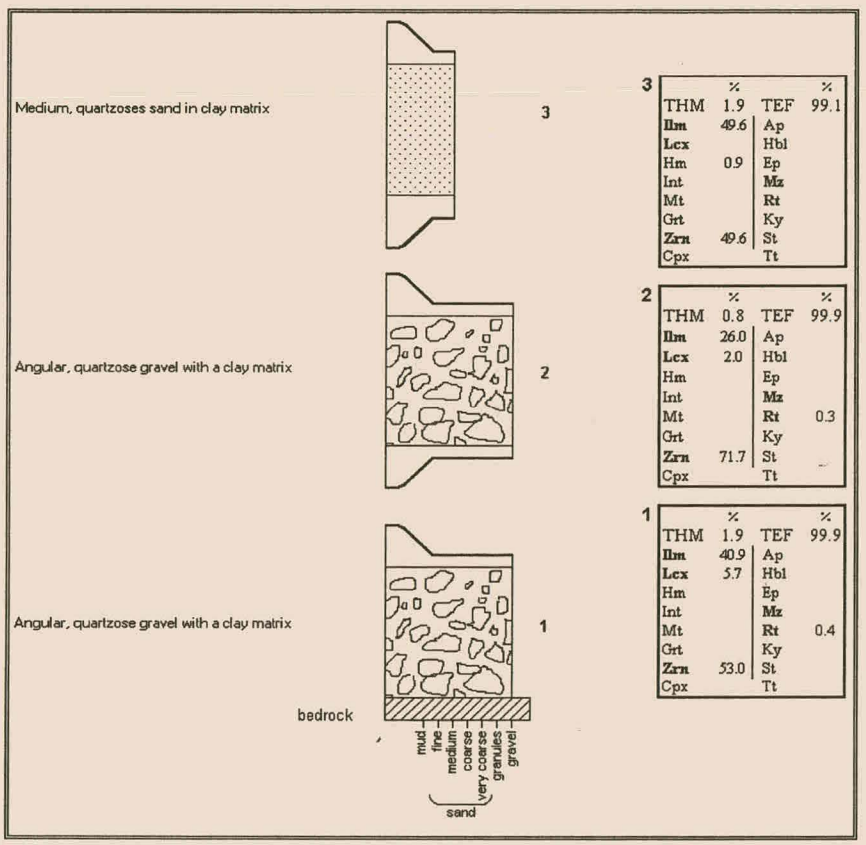

Figure 17A. Geological cross-section of 68/69F3-02.

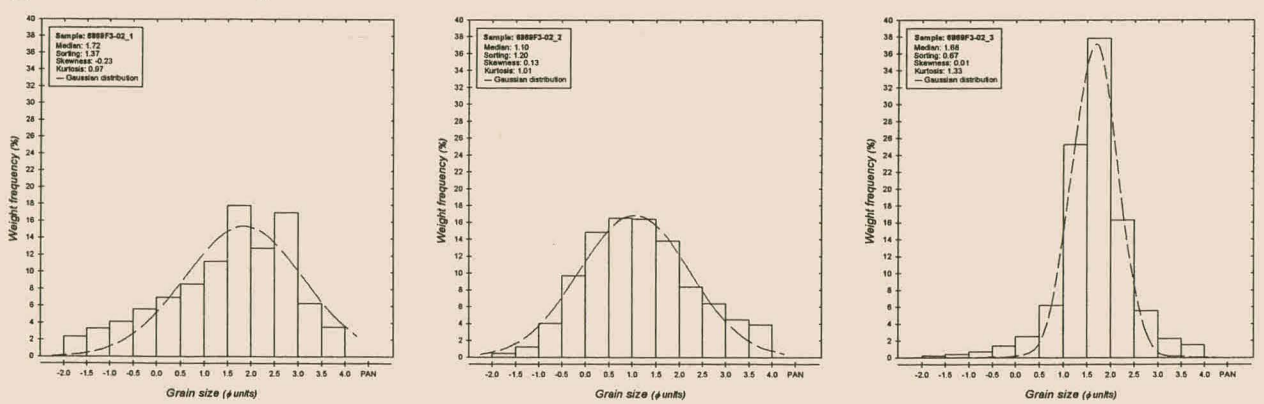

Figure 17B. Grain-size distributions of 68/69F3-02 samples.

Sample site KN14 (Fig. 18A).

Unit KN14_1

An angular gneissic cobble gravel within a quartzo-feldspathic matrix overlies the bedrock.

Unit KN14_2

The basal gravel is overlain by a dark brown (5R 4/4), trough cross-bedded, very coarse, quartzo-feldspathic sand with intermediate granular layers.

Unit KN14_3

Dark brown, cross-bedded, very coarse quartzo-feldspathic sand, that displays moderate sorting. The unit is marked by a succession of heavy mineral layers with a thickness of 15 cm. The heavy mineral layers dip slightly to the west.

Unit KN14_4

Compacted, brown (5YR 5/6), structureless, medium sand that is poorly sorted.

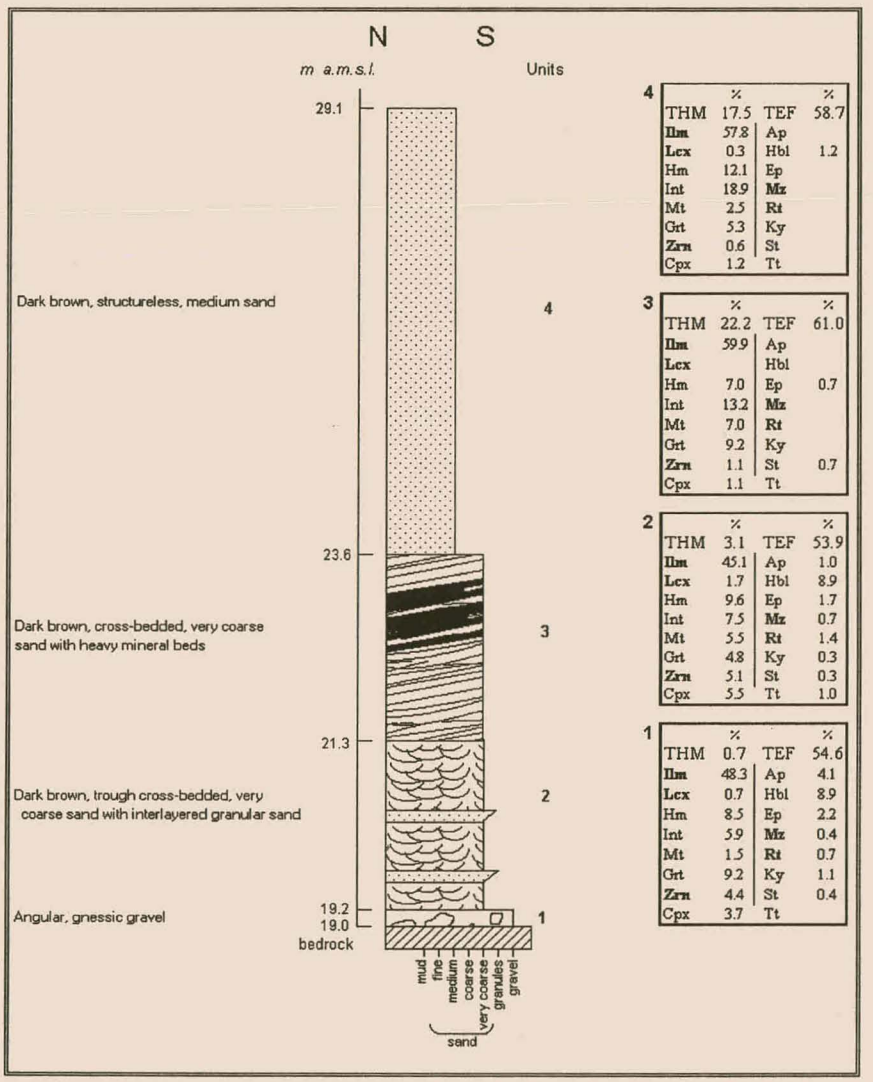

Figure 18A. Geological cross-section of KN14.

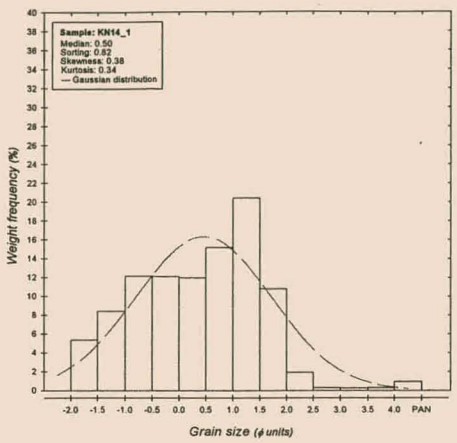

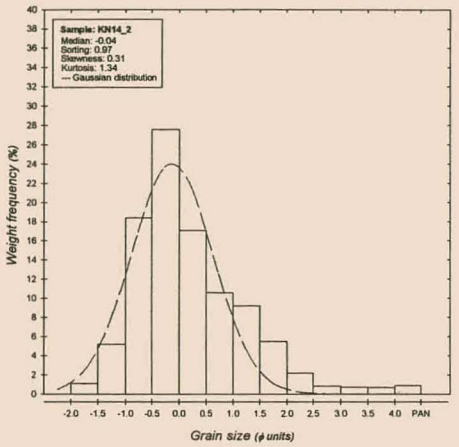

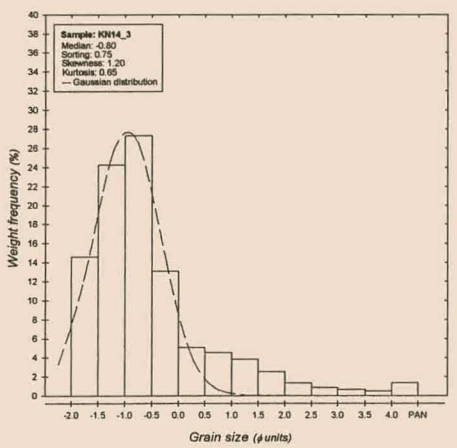

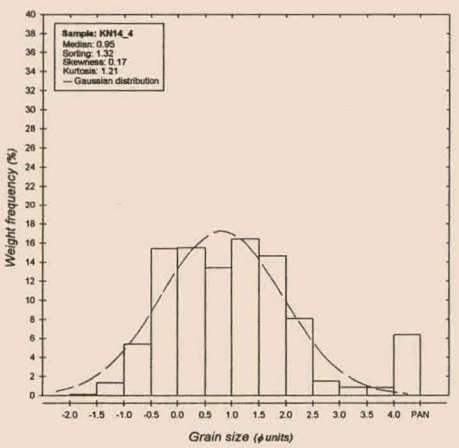

Figure 18B. Grain-size distributions of KN14 samples.

Sample site KN17 (Fig. 19A).

Unit KN17_1
Clast-supported pebble gravel with a moderately sorted granular sandy matrix. Clasts consist of well-rounded quartz and gneiss.

Unit KN17_2
Pale yellow (10YR 8/6), fine-grained, low-angle cross-bedded, moderately sorted quartzo-feldspathic sand with interlayered coarser sand.

Unit KN17_3
Dark brown (5R 4/4), poorly sorted, trough cross-bedded, very coarse quartzo-feldspathic sand. A pedogenic calcrete layer marks the top of the unit.

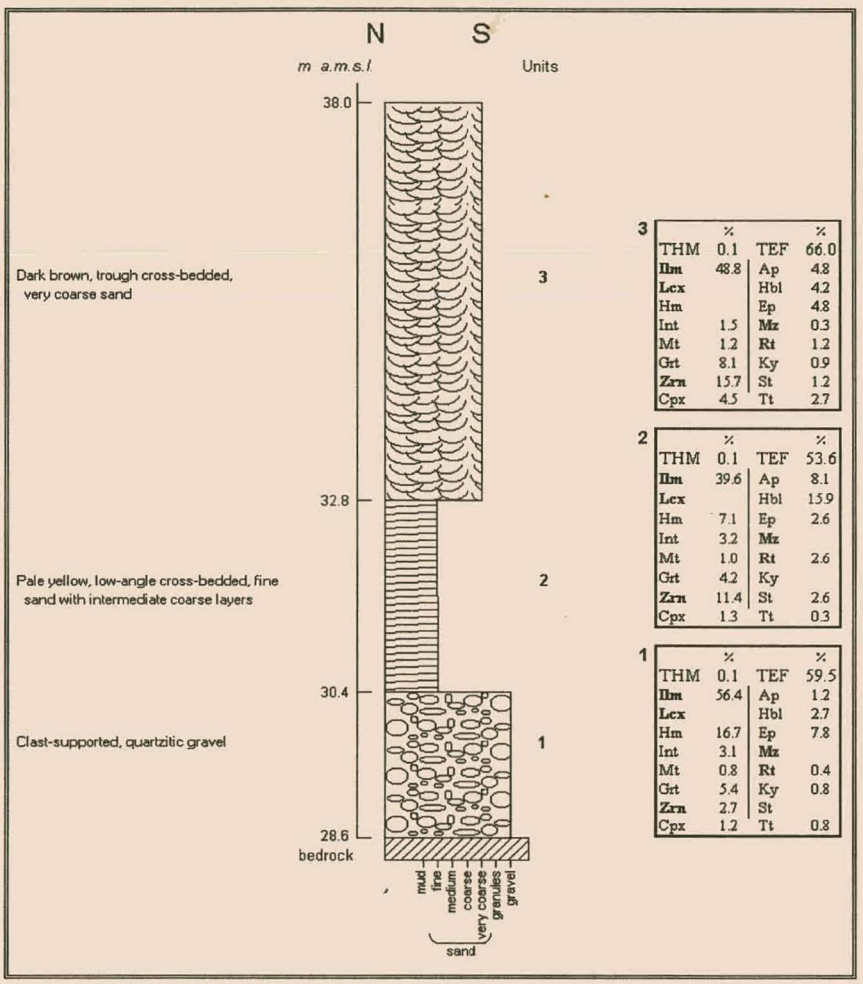

Figure 19A. Geological cross-section of KN17.

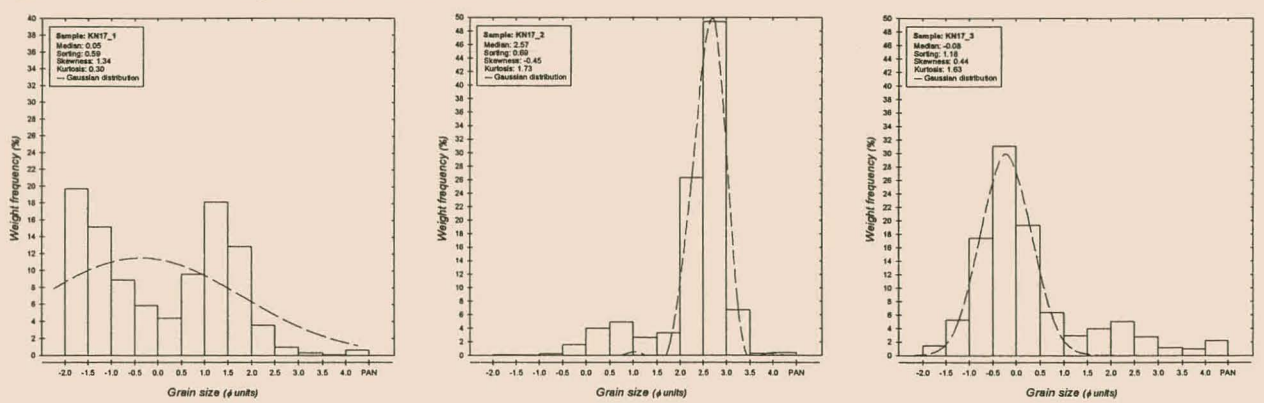

Figure 19B. Grain-size distributions of KN17 samples.

Sample site LKB-01 (Fig. 20A).

Unit LKB01_1
Basal channel gravel within a kaolinitic sand matrix. Clasts consist of grey quartz cobbles and pebbles.

Unit LKB01_2
The channel gravel grades upward into a grey muddy, poorly sorted quartzose sand.

Unit LKB01_3
Pale yellow (10YR 8/6), medium, well sorted, low-angle cross-bedded quartzo-feldspathic sand with interbedded coarser sand layers.

Unit LKB01_4
Semi-compacted, pale yellow (10YR 8/6), cross-bedded, fine sand that displays good sorting.

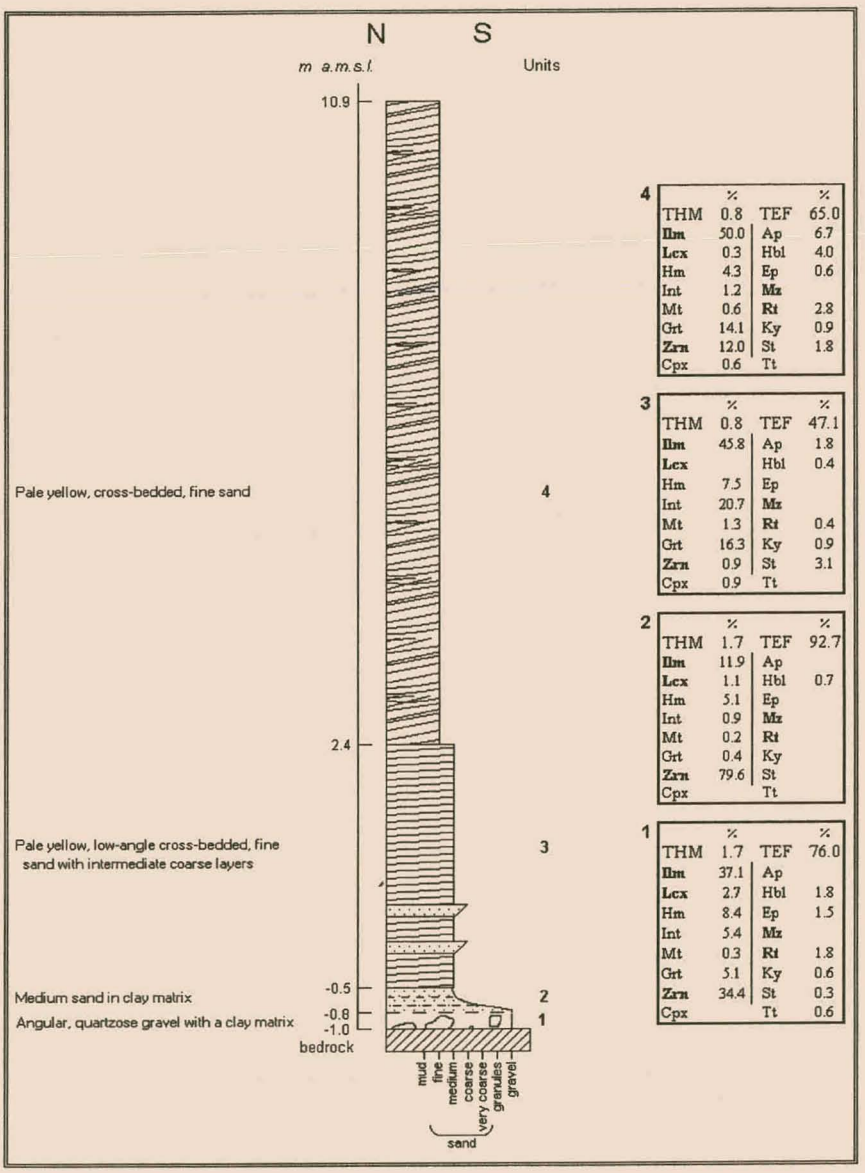

Figure 20A. Geological cross-section of LKB-01.

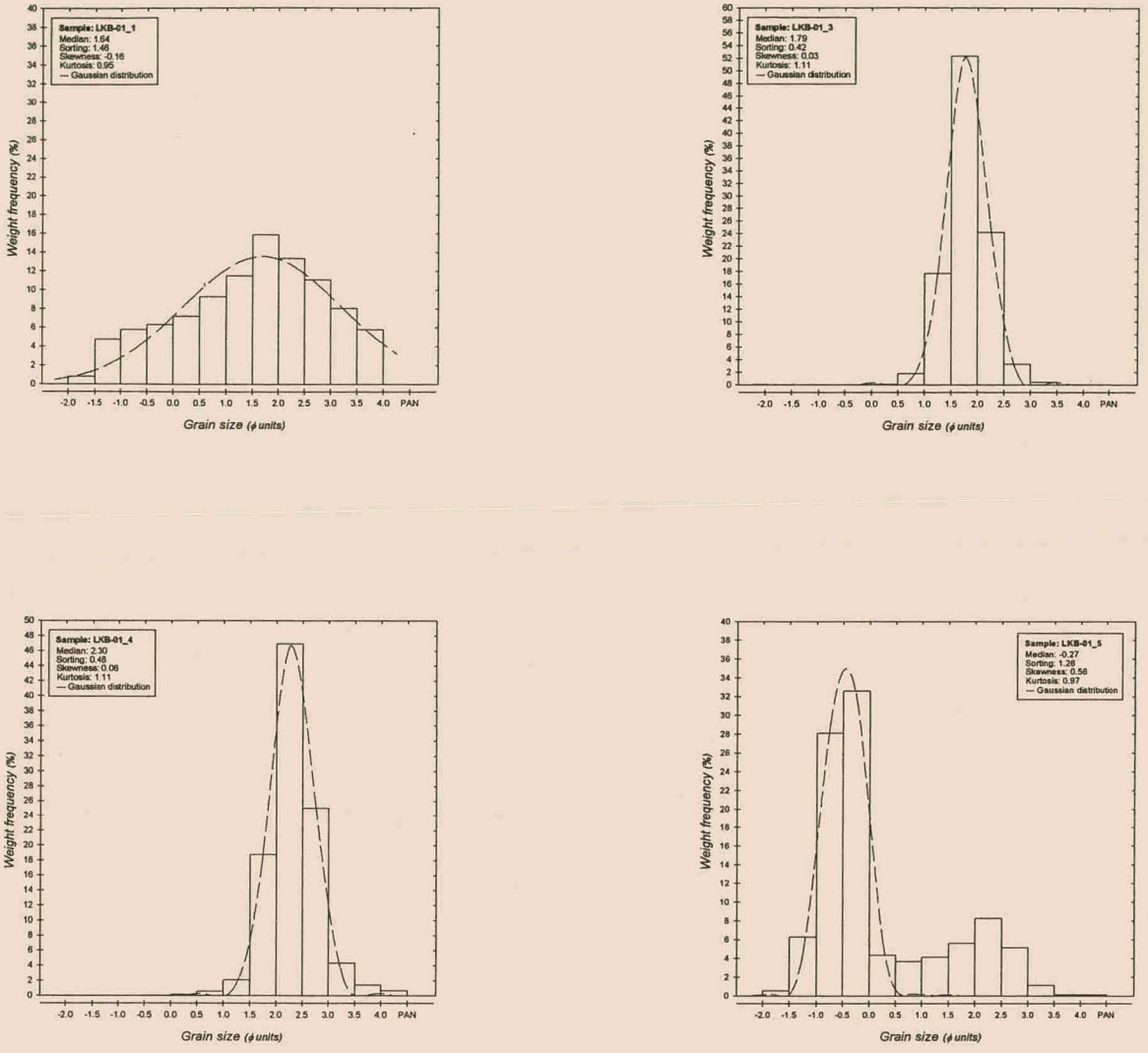

Figure 20B. Grain-size distributions of LKB-01 samples.

Sample site LKC1-04 (Fig 21A).

Unit LKC1-04_1
White (N9), bimodal, poorly sorted, fine and medium sand with a muddy matrix. This unit is most probably kaolinized bedrock.

Unit LKC1-04_2
Clast-supported cobble gravel within a medium sand matrix. The clasts comprise polished quartzite, gneiss and phosphorite.

Unit LKC1-04_3
Pale yellow (10YR 8/6) well sorted, low-angle cross-bedded with interfingering coarser sand. The unit is also marked by sub-horizontal heavy mineral laminae.

Unit LKC1-04_4
This unit consists of a dark yellow (5Y 6/4), moderately sorted, coarse quartzo-feldspathic sand that occasionally interfingers with unit LKC1-04_3.

Unit LKC1-04_5
Orange (10YR 6/6), moderately sorted, medium quartzo-feldspathic cross-bedded sand.

Unit LKC1-04_6
Light brown (5YR 5/6), trough cross-bedded, moderately sorted, medium quartzo-feldspathic sand.

Unit LKC1-04_7
Yellow brown (10YR 5/4), trough cross-bedded, poorly sorted, very coarse quartzo-feldspathic sand.

Unit LKC1-04_8
Cross-bedded, dark green (10GY 6/4), well-sorted, medium quartzo-feldspathic sand.

Unit LKC1-04_9
Dark brown (5R 4/4), trough cross-bedded, coarse quartzo-feldspathic sand with poor sorting.

Unit LKC1-04_10
Dark brown (5R 4/4), cross-bedded, medium quartzo-feldspathic sand with moderate sorting. Heavy mineral bands are conspicuously present and dip slightly seaward. Disseminated heavy minerals are distributed throughout the unit due to bioturbation.

Unit LKC1-04_11
Light orange (10YR 5/6), cross-bedded, moderately sorted, medium quartzo-feldspathic sand with seaward dipping heavy mineral laminae.

Unit LKC1-04_12
Pale yellow (10YR 8/6), well sorted, cross-bedded, medium quartzo-feldspathic quartzose sand with a distinct heavy mineral band.

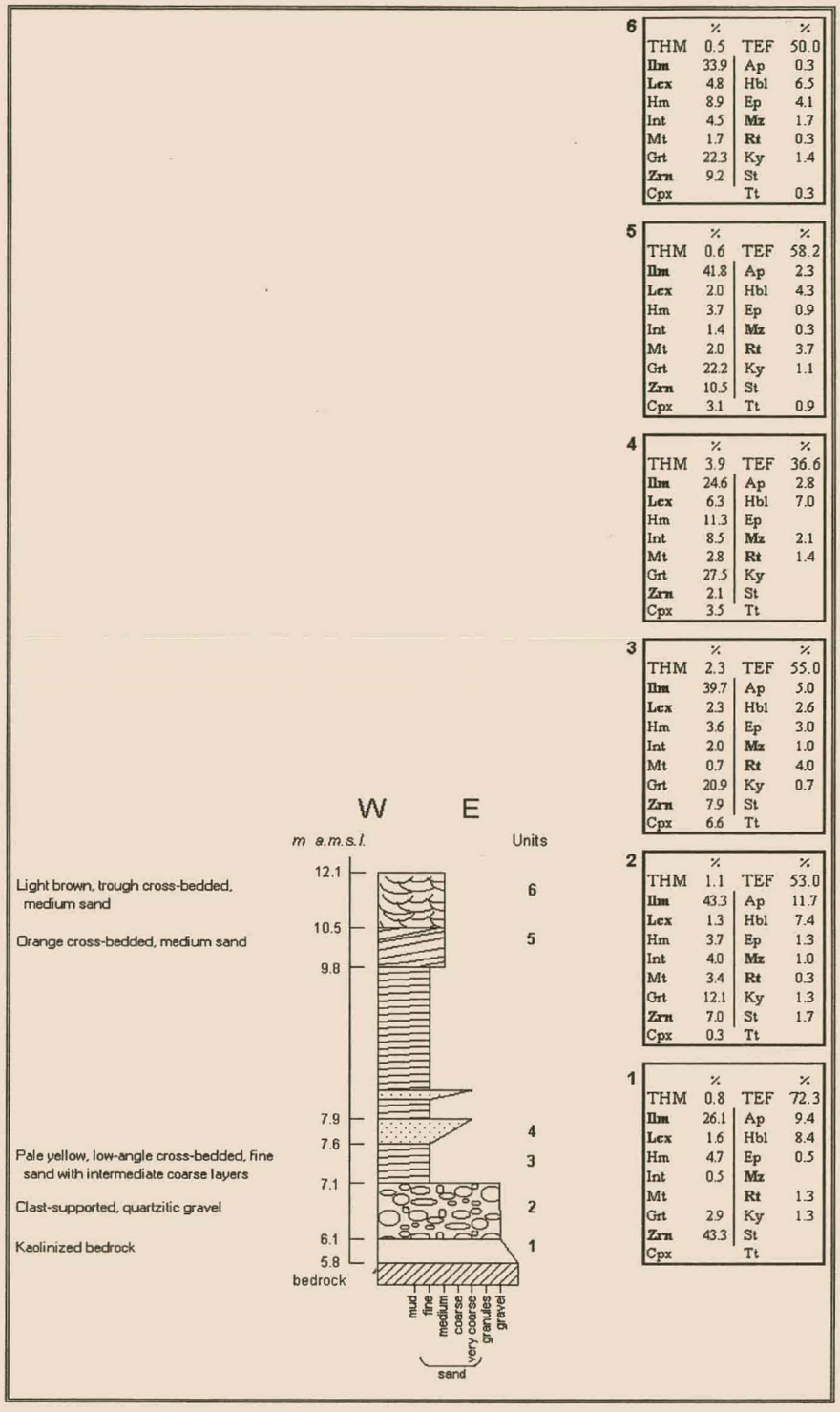

6	%		%
THM	0.5	TEF	50.0
Ilm	33.9	Ap	0.3
Lcx	4.8	Hbl	6.5
Hm	8.9	Ep	4.1
Int	4.5	**Mz**	1.7
Mt	1.7	**Rt**	0.3
Grt	22.3	Ky	1.4
Zrn	9.2	St	
Cpx		Tt	0.3

5	%		%
THM	0.6	TEF	58.2
Ilm	41.8	Ap	2.3
Lcx	2.0	Hbl	4.3
Hm	3.7	Ep	0.9
Int	1.4	**Mz**	0.3
Mt	2.0	**Rt**	3.7
Grt	22.2	Ky	1.1
Zrn	10.5	St	
Cpx	3.1	Tt	0.9

4	%		%
THM	3.9	TEF	36.6
Ilm	24.6	Ap	2.8
Lcx	6.3	Hbl	7.0
Hm	11.3	Ep	
Int	8.5	**Mz**	2.1
Mt	2.8	**Rt**	1.4
Grt	27.5	Ky	
Zrn	2.1	St	
Cpx	3.5	Tt	

3	%		%
THM	2.3	TEF	55.0
Ilm	39.7	Ap	5.0
Lcx	2.3	Hbl	2.6
Hm	3.6	Ep	3.0
Int	2.0	**Mz**	1.0
Mt	0.7	**Rt**	4.0
Grt	20.9	Ky	0.7
Zrn	7.9	St	
Cpx	6.6	Tt	

2	%		%
THM	1.1	TEF	53.0
Ilm	43.3	Ap	11.7
Lcx	1.3	Hbl	7.4
Hm	3.7	Ep	1.3
Int	4.0	**Mz**	1.0
Mt	3.4	**Rt**	0.3
Grt	12.1	Ky	1.3
Zrn	7.0	St	1.7
Cpx	0.3	Tt	

1	%		%
THM	0.8	TEF	72.3
Ilm	26.1	Ap	9.4
Lcx	1.6	Hbl	8.4
Hm	4.7	Ep	0.5
Int	0.5	**Mz**	
Mt		**Rt**	1.3
Grt	2.9	Ky	1.3
Zrn	43.3	St	
Cpx		Tt	

Figure 21A. Geological cross-section of LKC1-04.

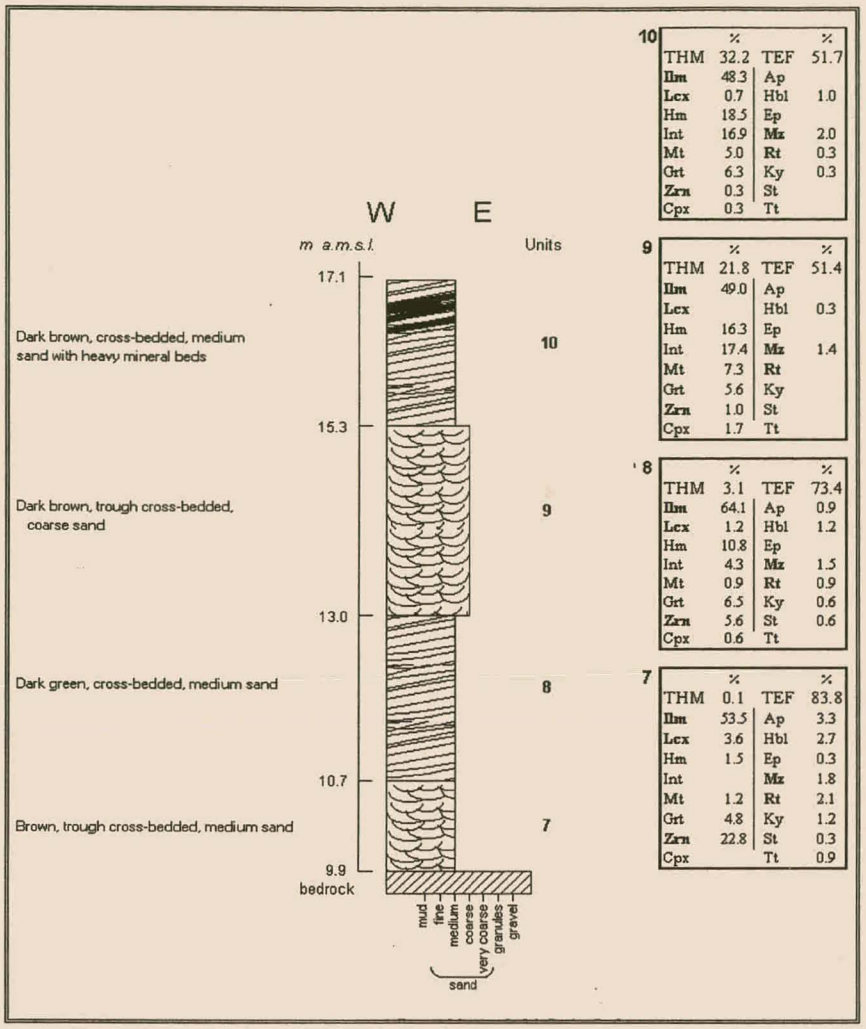

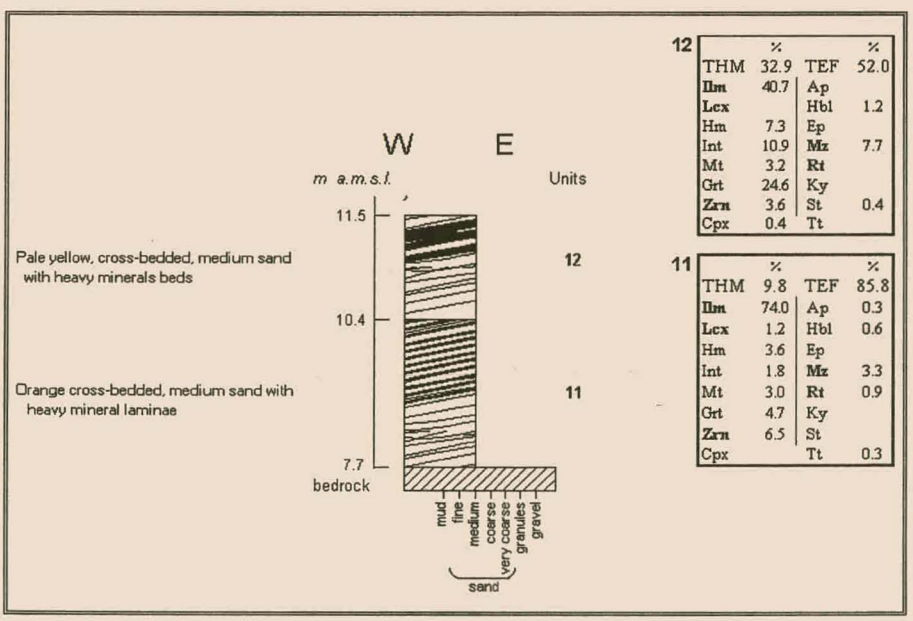

Figure 21A (cont). Geological cross-sections of LKC1-04.

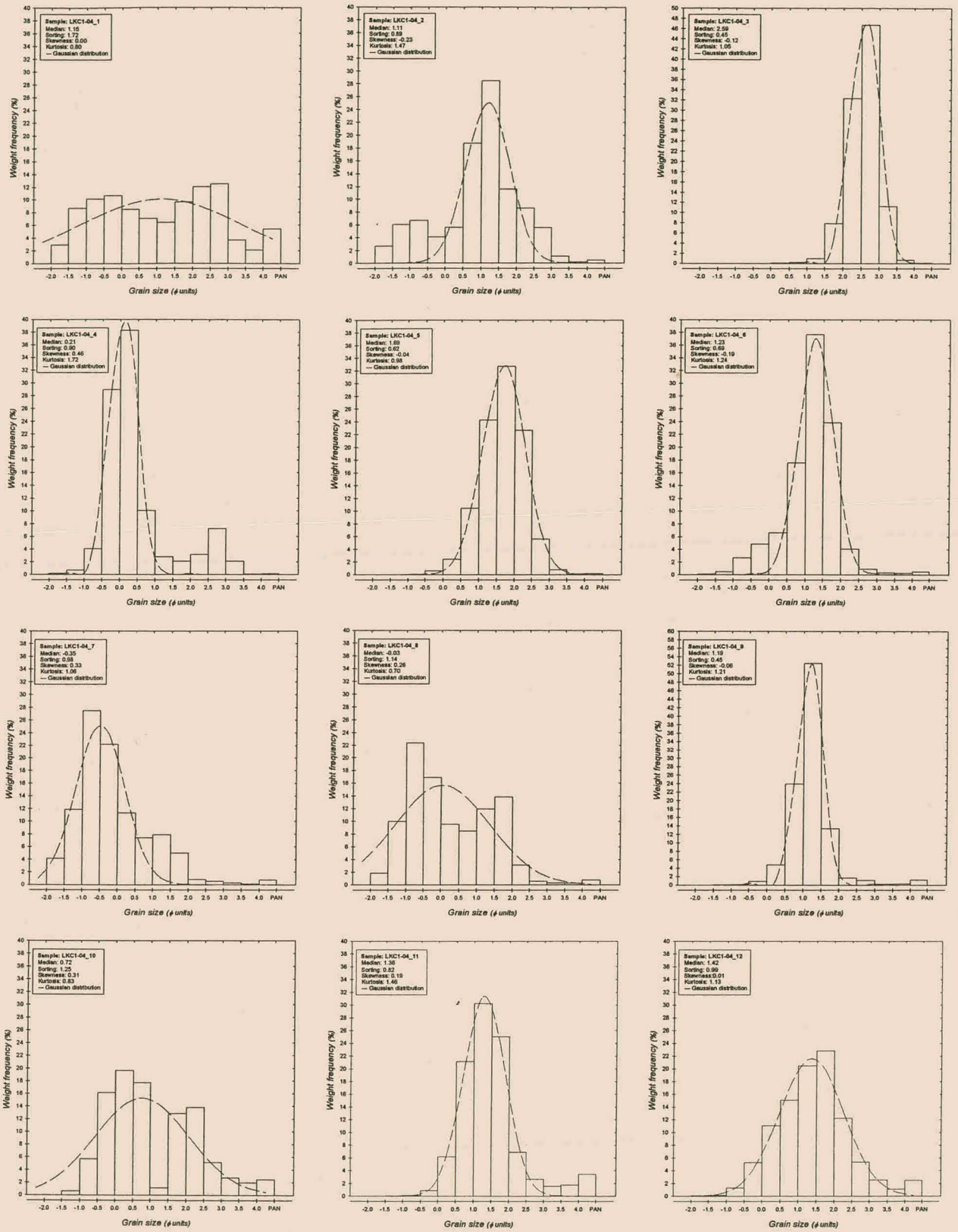

Figure 21B. Grain-size distributions of LKC1-04 samples.

Sample site LKCR1 (Fig. 22A).

Unit LKCR1_1

Matrix-supported gravel with a moderately sorted medium sand as matrix. Clasts of rounded, flattened quartzite dip seaward.

Unit LKCR1_2

Orange (10YR 6/6), cross-bedded, medium quartzo-feldspathic sand with seaward-dipping heavy mineral laminae.

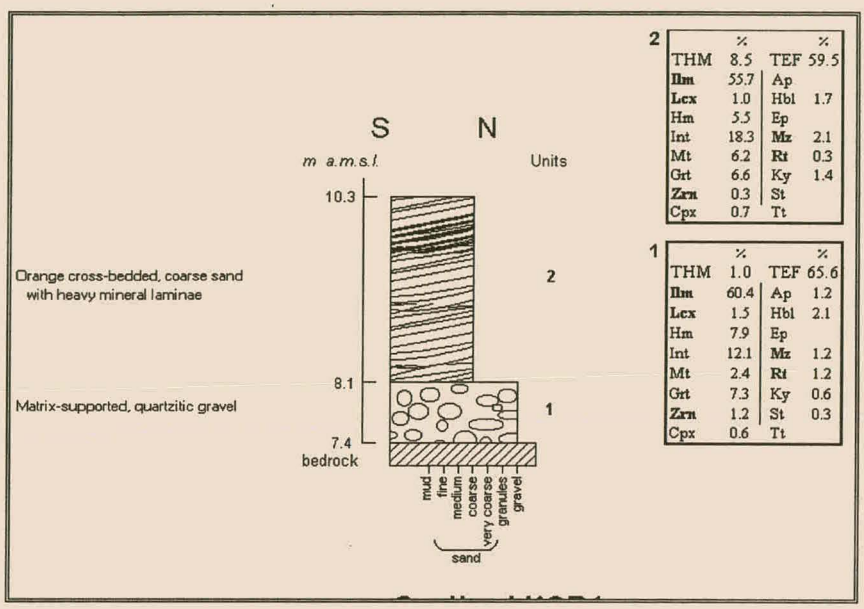

Figure 22A. Geological cross-section of LKCR1.

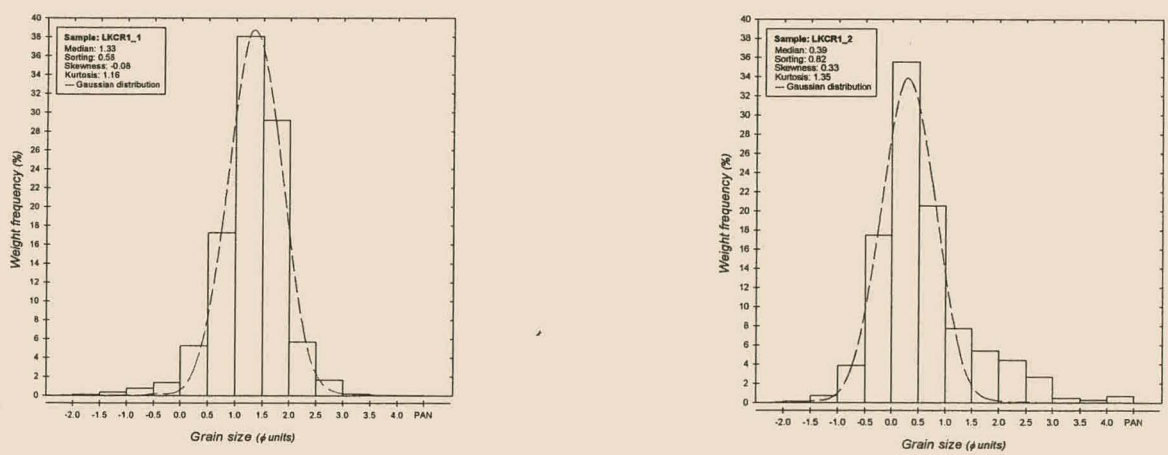

Figure 22B. Grain-size distributions of LKCR1 samples.

Sample site LKN8-03 (Fig. 23A).

Unit LKN803_1
Orange (10YR 6/6), trough cross-bedded, medium sand with moderate sorting. Disseminated dark minerals and gritty shell pieces are distributed throughout the unit.

Unit LKN803_2
Matrix-supported pebble gravel with granular sand as matrix. Clasts are mainly subangular and sub-rounded quartz, gneiss and schist.

Unit LKN803_3
Pale yellow (10YR 8/6), low-angle cross-bedded, fine sands overlie gravel alternating with coarser sand. Heavy minerals form laminations parallel to bedding. An extensive shell bed in a matrix of coarse shell fragments overlies the top of the unit.

Unit LKN803_4
Light brown (5YR 5/6), compacted, highly bioturbated, medium sand with poor sorting.

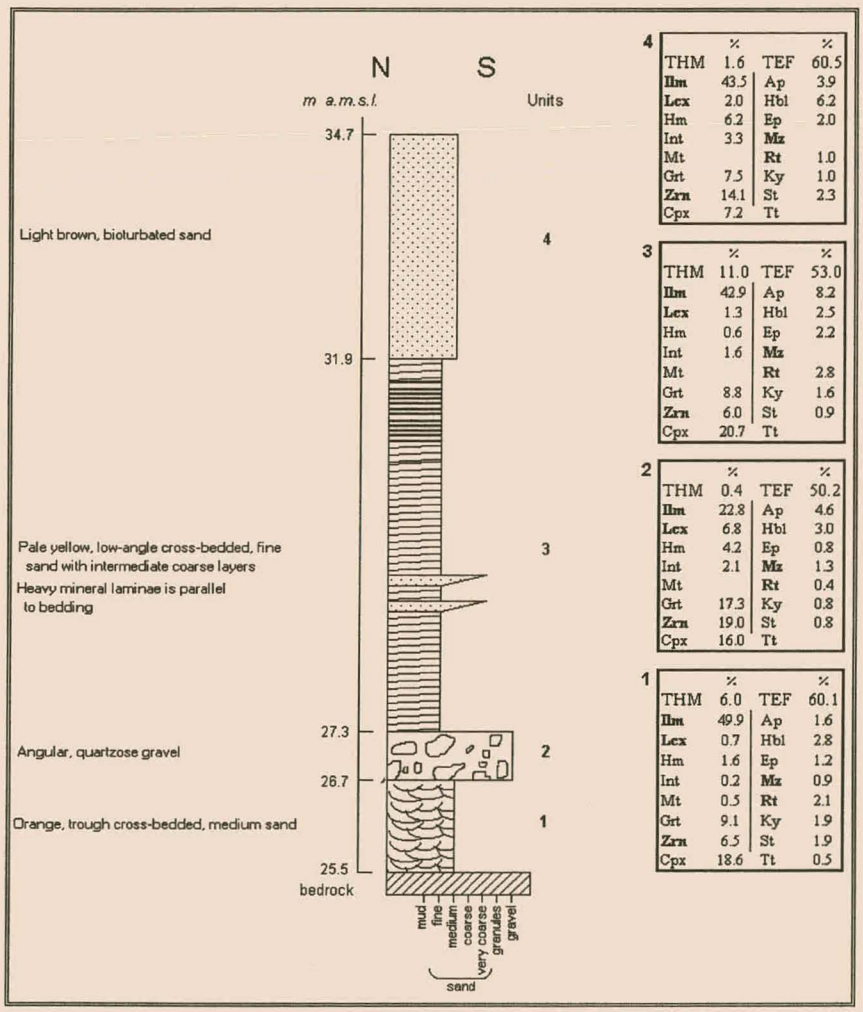

Figure 23A. Geological cross-section of LKN8-03.

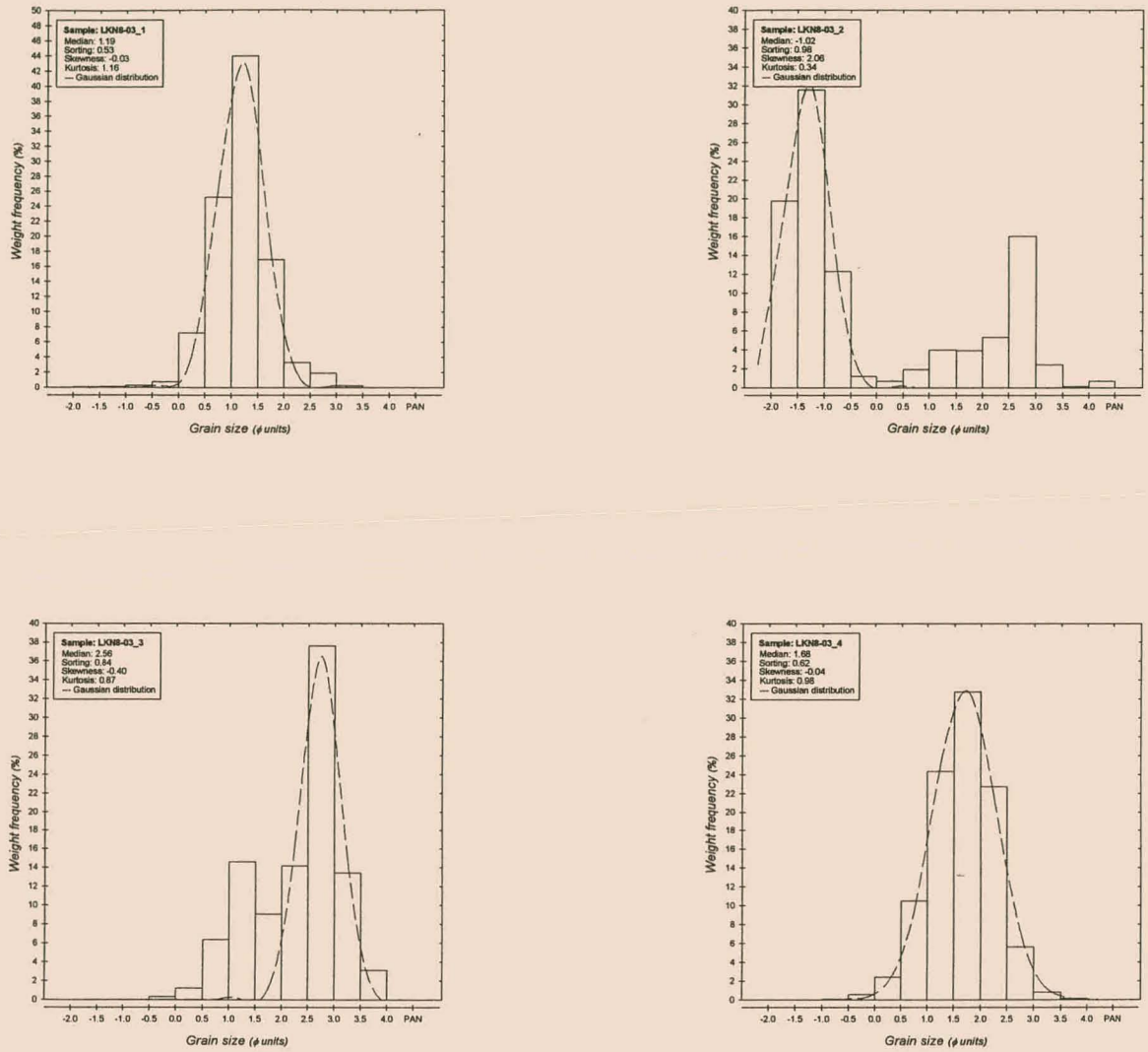

Figure 23B. Grain-size distributions of LKN8-03 samples.

Sample site SN78-5 (Fig. 24A).

Unit SN785_1
Poorly sorted channel gravel in a muddy, quartzose sand matrix. The clasts consist of angular and subangular, grey quartz.

Unit SN785_2
The gravel grades into a poorly sorted kaolinitic quartzose sand.

Unit SN785_3
Clast-supported cobble gravel in granular sand matrix. Clasts are flattened, rounded quartzite sub-horizontally orientated with respect to the bedding plane.

Unit SN785_4
Pale yellow (10YR 8/6), low-angle cross-bedded, fine sand that is very well sorted.

Unit SN785_5
Orange (10YR 6/6), trough cross-bedded, very coarse, poorly sorted sand.

Unit SN785_6
Light brown (5YR 5/6), moderately sorted, medium, low-angle cross-bedded sand with interlayered coarser sand.

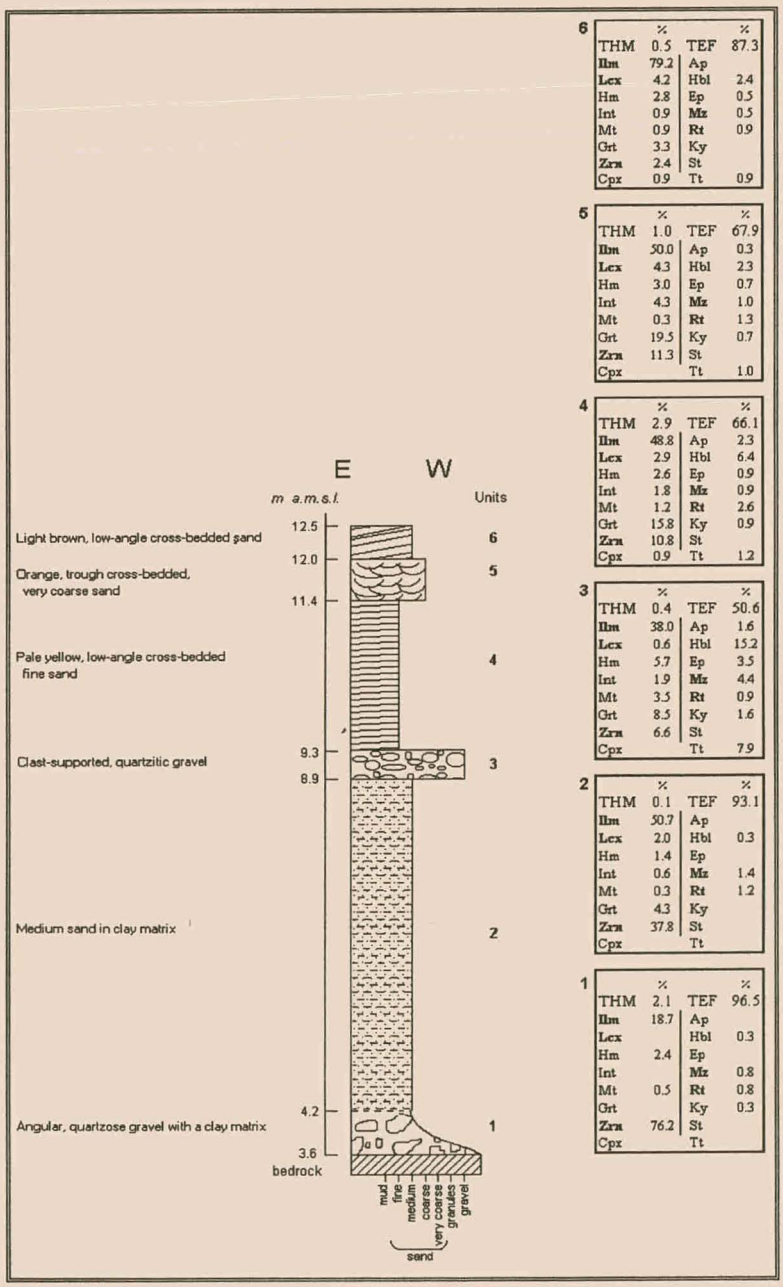

Figure 24A. Geological cross-section of SN78-5.

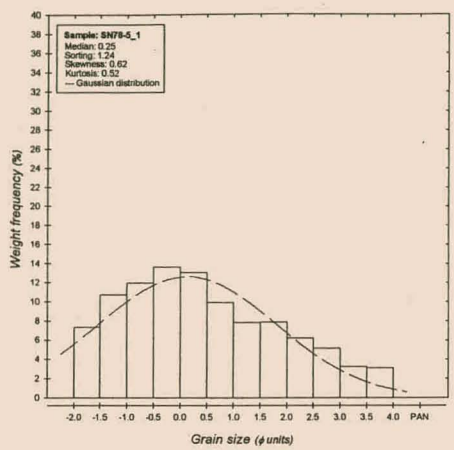

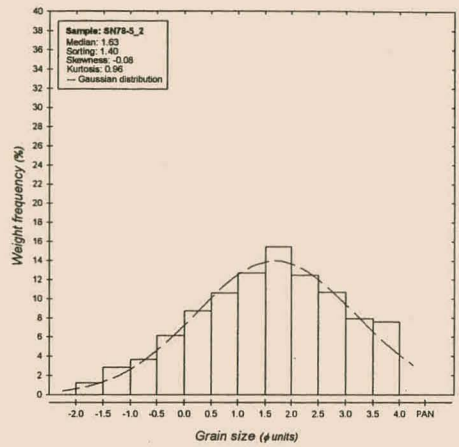

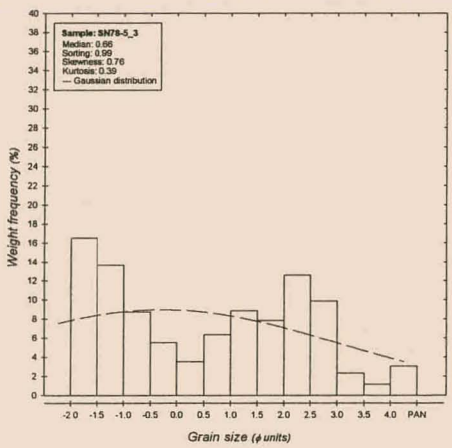

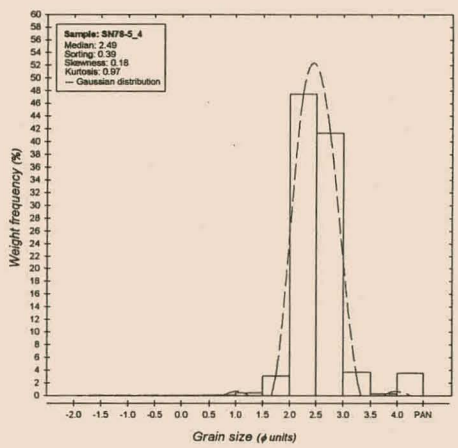

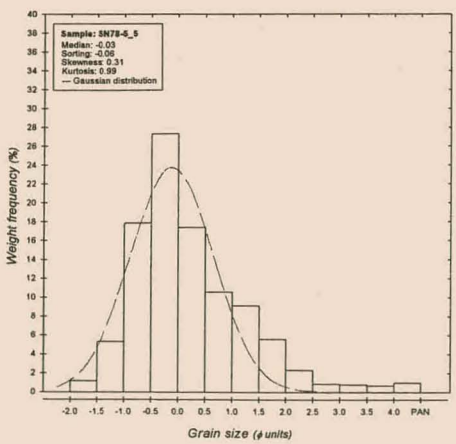

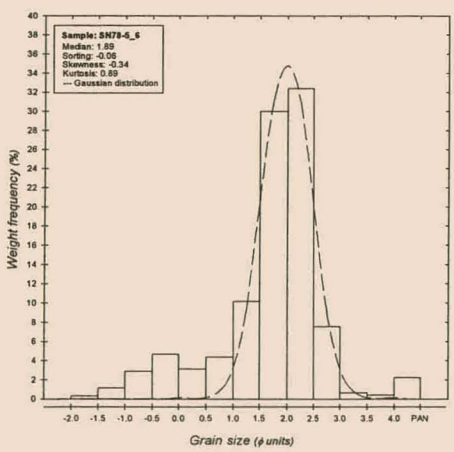

Figure 24B. Grain-size distributions of SN78-5 samples.

Sample site SNR1 (Fig. 25A).

Unit SNR1_1
Poorly sorted channel gravel in kaolinitic matrix.

Unit SNR1_2
Dark brown (5YR 4/4), trough cross-bedded, very coarse sand that is poorly sorted. Calcretization and manganese staining mark the unit.

Unit SNR1_3
Orange (10YR 6/6), cross-bedded, poorly sorted, medium sand with parallel heavy mineral laminae.

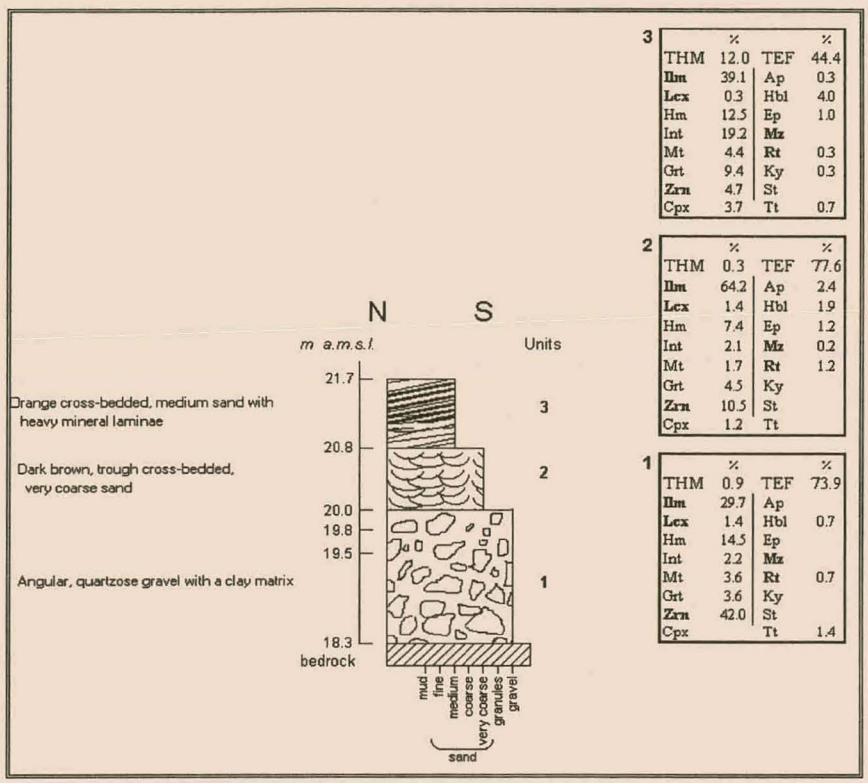

3	%		%
THM	12.0	TEF	44.4
Ilm	39.1	Ap	0.3
Lcx	0.3	Hbl	4.0
Hm	12.5	Ep	1.0
Int	19.2	**Mz**	
Mt	4.4	**Rt**	0.3
Grt	9.4	Ky	0.3
Zrn	4.7	St	
Cpx	3.7	Tt	0.7

2	%		%
THM	0.3	TEF	77.6
Ilm	64.2	Ap	2.4
Lcx	1.4	Hbl	1.9
Hm	7.4	Ep	1.2
Int	2.1	**Mz**	0.2
Mt	1.7	**Rt**	1.2
Grt	4.5	Ky	
Zrn	10.5	St	
Cpx	1.2	Tt	

1	%		%
THM	0.9	TEF	73.9
Ilm	29.7	Ap	
Lcx	1.4	Hbl	0.7
Hm	14.5	Ep	
Int	2.2	**Mz**	
Mt	3.6	**Rt**	0.7
Grt	3.6	Ky	
Zrn	42.0	St	
Cpx		Tt	1.4

Figure 25A. Geological cross-section of SNR1.

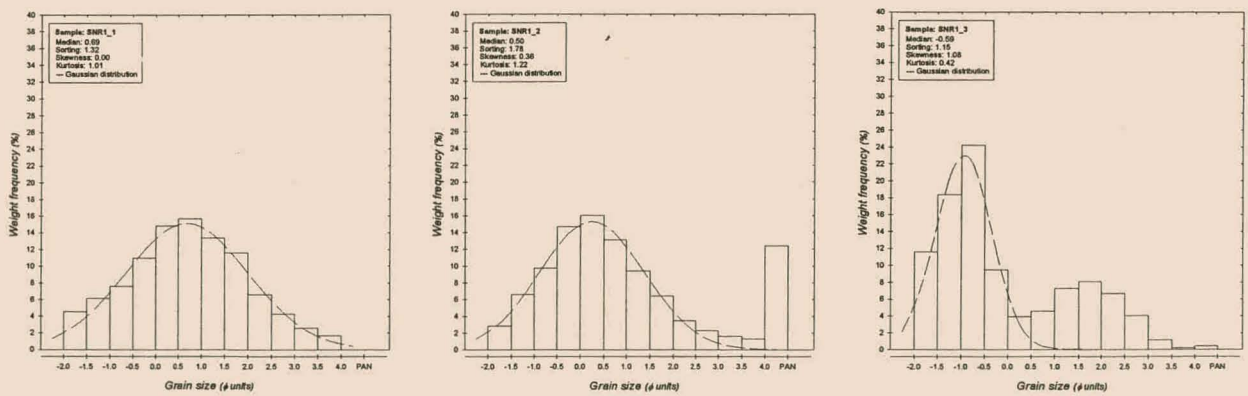

Figure 25B. Grain-size distributions of SNR1 samples.

Sample site KN_SI (Fig. 26A).

Unit KN_SI
Well sorted, medium sand.

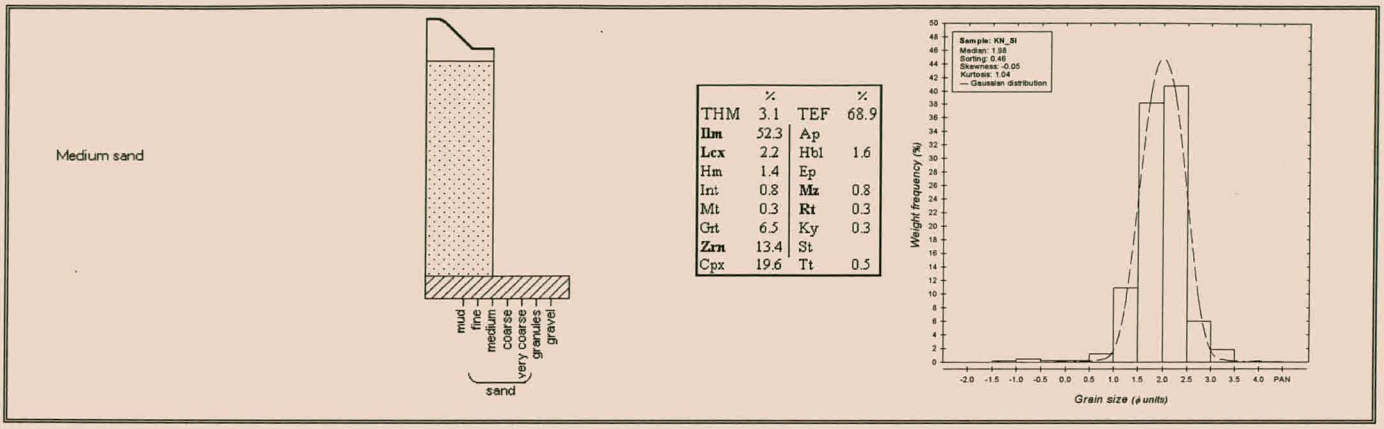

	%		%
THM	3.1	TEF	68.9
Ilm	52.3	Ap	
Lcx	2.2	Hbl	1.6
Hm	1.4	Ep	
Int	0.8	**Mz**	0.8
Mt	0.3	**Rt**	0.3
Grt	6.5	Ky	0.3
Zrn	13.4	St	
Cpx	19.6	Tt	0.5

Figure 26A. Geological cross-section and grain-size distribution of sample KN_SI.

Sample site SEA711 (Fig. 26B).

Unit SEA711
Very well sorted, fine sand

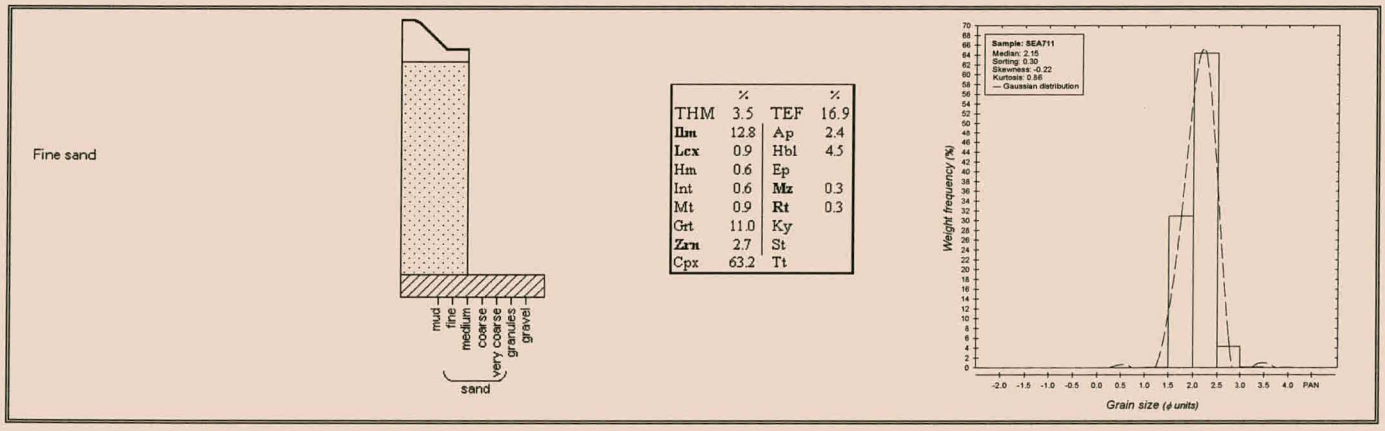

	%		%
THM	3.5	TEF	16.9
Ilm	12.8	Ap	2.4
Lcx	0.9	Hbl	4.5
Hm	0.6	Ep	
Int	0.6	**Mz**	0.3
Mt	0.9	**Rt**	0.3
Grt	11.0	Ky	
Zrn	2.7	St	
Cpx	63.2	Tt	

Figure 26B. Geological cross-section and grain-size distribution of sample SEA711.

Unit BR (Buffels River) (Fig. 27A).

Moderately sorted, brown (5YR 4/4) coarse sand.

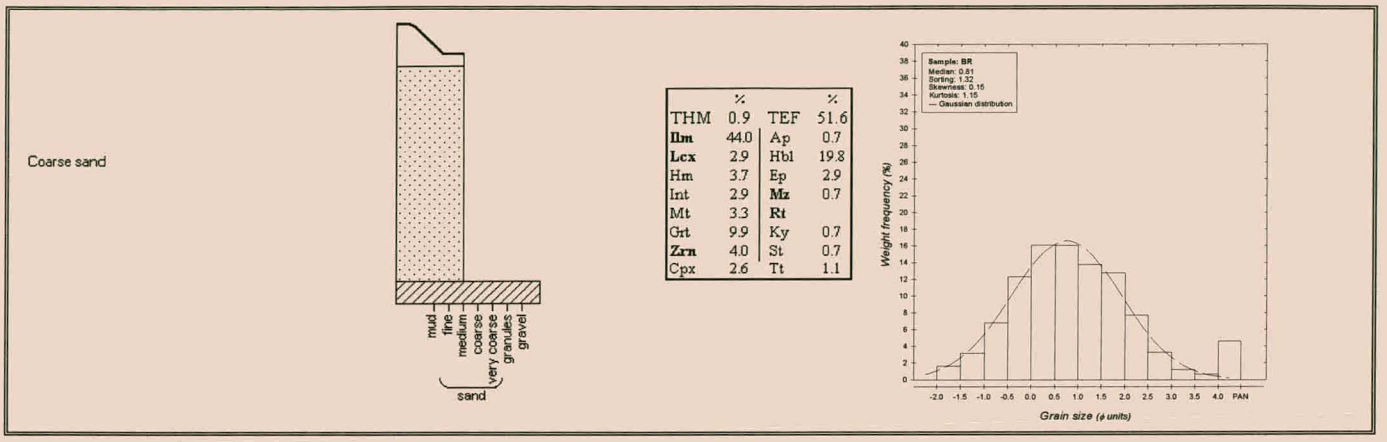

	%		%
THM	0.9	TEF	51.6
Ilm	44.0	Ap	0.7
Lcx	2.9	Hbl	19.8
Hm	3.7	Ep	2.9
Int	2.9	**Mz**	0.7
Mt	3.3	**Rt**	
Grt	9.9	Ky	0.7
Zrn	4.0	St	0.7
Cpx	2.6	Tt	1.1

Figure 27A. Geological cross-section and grain-size distribution of sample BR.

Unit ZL (Swartlintjies River) (Fig. 27B).

Fine, poorly sorted sand with a significant mud content.

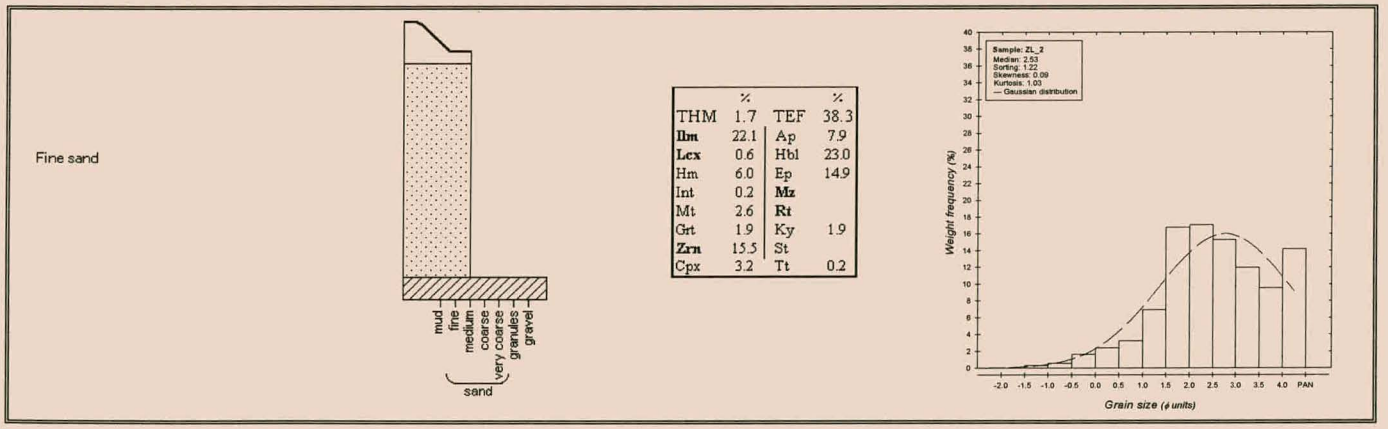

	%		%
THM	1.7	TEF	38.3
Ilm	22.1	Ap	7.9
Lcx	0.6	Hbl	23.0
Hm	6.0	Ep	14.9
Int	0.2	**Mz**	
Mt	2.6	**Rt**	
Grt	1.9	Ky	1.9
Zrn	15.5	St	
Cpx	3.2	Tt	0.2

Figure 27B. Geological cross-section and grain-size distribution of sample ZL.